NIST NCSTAR 1-9

Federal Building and Fire Safety Investigation of the World Trade Center Disaster

Structural Fire Response and Probable Collapse Sequence of World Trade Center Building 7

VOLUME 2

National Institute of Standards and Technology
U.S. Department of Commerce

TABLE OF CONTENTS

LIST OF FIGURES

This page intentionally left blank.

LIST OF TABLES

Chapter 9
FIRE SIMULATIONS

9.1 OVERVIEW

9.1.1 Approach

The major fires in WTC 7 were simulated using the Fire Dynamics Simulator, version 4, the same software that NIST used to simulate the fires in the World Trade Center towers (NIST NCSTAR 1-5F). (McGrattan 2004) These simulations were part of a sequence of estimates that included the debris damage from WTC 1, the subsequent fires, the heating of the structural elements, the structural response, and the eventual collapse. Temperature predictions from the fire model were passed to the structural model via the Fire Structure Interface, again using the same process as in the reconstruction of the collapse of the World Trade Center towers (NIST NCSTAR 1-5G).

As described in Chapter 5, sustained and/or late fires were observed on Floors 7 through 9 and 11 through 13 of WTC 7. There was a single observation of a late, small fire on floor 14. In addition, there might have been concealed fires in the mechanical spaces on floors 5 and 6. No fire was observed on the 10th floor. The fires on the upper floors (19, 22, 29, and 30) died out well before the collapse of WTC 7.

The fire simulations for WTC 7 were conducted for each floor individually. Chapter 3 showed that there were no pathways for the flames and heat to pass from one floor to another, aside from the debris-damaged area in the southwest of the building. The only floor-to-floor connection within the tenant spaces was a flight of convenience stairs connecting the 11th and 12th floors. It was located near the southwest corner of the building, near the multi-floor debris damage zone, and essentially acted as an enlargement of the debris damage zone. The stairs were thus not included in the FDS simulation. The analysis described in Section 9.1.2 found that any late developing floor breaches would not have had a major effect on the structural heating.

It would have been difficult to observe fires on the 5th and 6th floors, due to the partitions just behind the various windows or louvers (Chapter 3). Thus, the Investigation Team simulated a variety of fire scenarios and examined the outcome of each to determine whether it would have produced a visible telltale or whether it would have been severe enough to weaken any structural elements on those floors.

The actual fires on floors 7 through 9 and 11 through 13 were likely initiated when WTC 1 collapsed (Chapter 5). However, there is limited photographic evidence or on-site personal observation upon which to base simulation of the early development of these fires. While use was made of the appearance of flames and window breakage in photographs and videos in formulating the simulations, the Investigation Team realized that the absolute timing of the simulations might not align exactly with the timing of the fires on September 11, 2001.

Using a timeline reconstructed from the limited photographic evidence and eyewitness testimony, fire simulations were conducted for floors 7 and 8. For the simulations, the fires on these two floors were assumed to have initiated at a time designated as noon. There was no evidence of visible fire growth on

these floors during the morning; and, even at 2:00 p.m., the fire on the 7th floor was still in the southwest section of the building. The computations were continued for six hours, since the time in the structural simulations at which the building would become structurally unstable was not yet known.

The fire on the 9th floor was not observed until about 4:00 p.m., approximately one hour after fire was first observed on the 8th floor. Since there was no information about the history of the 9th floor fire prior to 4:00 p.m., and since there was limited knowledge of the layout of combustible materials on this floor, this fire was approximated by displacing the 8th floor fire one hour later.

The layouts of the 11th and 12th floors were essentially identical. The observation of fires on the 11th floor indicated that they were similar to those on the 12th floor, but lagged about an hour in reaching equivalent positions along the building perimeter. The intense fires on the 13th floor appeared after about 2:30 p.m. on the east face and the east side of the north face. These fires also appeared similar to those on the 12th floor, but lagged behind them by about a half hour. Thus, these fires were simulated using the 12th floor fires, suitably offset in time.

On the 14th floor, a small fire was observed at the far east of the north face at about 5:03 p.m. It was not observed at 4:52 p.m., nor at 5:09 p.m. On September 11, 2001, the 14th floor was unoccupied and should have had a very small combustible fuel load. From this evidence, the Investigation Team deduced that it was unlikely that there had been a sustained fire of appreciable heat output. Thus, no fire simulation was performed for this floor.

The calculations were very similar to those conducted for WTC 1 and WTC 2 (NIST NCSTAR 1-5F), and therefore only a brief description of the major assumptions is included. It should be remembered that there are far fewer photographs of WTC 7 than of the towers. Thus, while the severity of the simulated WTC 7 fires (as established from the visual evidence) is reasonable, the details of these fires are not as precise as for the fires in the towers.

9.1.2 Fire Spread

Ventilation Effects

If each floor of WTC 7 had been airtight (i.e., no broken windows or breach in the exterior from debris impact damage), a fire starting on a particular floor would have been limited to a size that would not likely have threatened the building for the following reasons:

- The volume of a floor was approximately 1×10^4 m^3 (4×10^5 ft^3). The mass of air contained in that volume was 1.7×10^4 kg; the mass of oxygen was 3×10^3 kg. The heat release from combustion of typical combustibles is 13.1 MJ per kg of oxygen consumed (Huggett 1980). Only about half the oxygen could have been consumed, since that would have resulted in an oxygen level below which flame spread would slow considerably and soon halt. Thus, a fire on this airtight floor would have generated about 2×10^4 MJ.

- If the density of combustible materials able to burn were 20 kg/m^2 (4 lb/ft^2), there would have been approximately 6×10^4 kg of combustibles on a given floor. Were they wood-like in heat of combustion (heat of combustion approximately 20 kJ/g (Drysdale 2002)), they would have generated 1×10^6 MJ, given sufficient oxygen. Since an airtight floor would have only

enough usable oxygen to generate 2×10^4 MJ, only about 2 percent of the combustibles would have burned.

- Even if this had happened over as short a duration as 1 h (3,600 s), the fire would have averaged only about 6 MW in intensity. This would not have been sufficient to heat enough of the insulated structural steel or the concrete floor slab to a temperature that would have led to significant weakening or thermal expansion.

The fires burned longer than this and, on some floors, had sustained intensities estimated to have exceeded 100 MW (Section 9.4). Thus, the rate at which fresh air became available played a major role in determining the intensity and duration of the fires. The locations from which air became available determined the direction of fire growth.

Initially, the intake air supply for the fires came from the south side of the building. As noted in Chapter 5, the debris from the collapse of WTC 1 created a gash in the west side of the south face of the building that stretched from the 17th floor down to the 5th floor. Photographs also show that windows in this vicinity were broken by the percussion and debris impact (Chapter 5). Fires on the interior of the tenant spaces would have had to draw and vent air through these openings. Chapter 5 also documents additional window breakage by the fires as they reached the building façade. Only a very few (about three) windows were known to have been broken by building occupants,[1] and these occurred well before fires reached these locations, and were too few to affect the fire ventilation or spread rate significantly.

Floor-to-floor Fire Spread

Initially, the Investigation Team hypothesized that it was unlikely that fires, once ignited on a given floor but prior to the initiation of the total building collapse, would have spread to an adjacent floor once they had moved past the gash in the south face. There were several bases for this reasoning:

- There was only one constructed opening connecting adjacent fire floors in the tenant spaces, which was for the convenience stair between the 11th and 12th floors in the southwest corner. This was in the immediate vicinity of the gash created by debris impact and would have been little more than an extension of the debris-caused opening between these two floors.

- There was no visual evidence of floors collapsing prior to the beginning of the building collapse itself.

- There were no photographs or videos indicating flames had emanated from a window and ignited a fire on the floor above through the windows located directly above.

Subsequently, thermostructural calculations (Chapter 11) indicated that approximately 15 min prior to the total building collapse, it was likely that the following floor sections had failed:

- 10th and 11th floors: a section of the north side, east of center.

- 12th and 14th floors: the same section as on the two lower floors, plus the southeast corner.

[1] NYC Housing Authority Interview 8, April 2004.

- 13th floor: the full east section of the floor.

In addition, the thermostructural simulations indicated that a small section east of center on the north side of the 8th floor had failed approximately 20 min to 45 min before the building collapse.

These support failures would have led to openings in the floor and could have altered the thermal profiles as follows.

- Hot gases from the lower floor would have vented to the upper floor. This would have slowed further heating of the ceiling of the lower floor. The hot gases would have increased the heating of the upper floor.

- Had a sizable hole opened in the floor slab, some combustibles from the upper floor could have fallen to the lower floor. Flames from the lower floor could have ignited combustibles adjacent to the hole on the upper floor. If portions of the floor slab actually separated and fell, they would have smothered some of the burning combustibles on the floor below.

The breaches in floors 10 through 14 would have only had a modest effect on the heating of the steel and concrete, since the holes would have been there for only a relatively short time. In addition:

- Prior to the breaches in the 8th, 12th and 13th floor slabs, there had been significant burning above and below the vicinity of the breach. Thus, the combustibles on the upper floors had already been ignited, and only a small fraction of the combustibles remained, potentially to fall to the floor below. In about 15 min, hot gas penetration to the already hot upper floor would not likely have had a major effect on the fire intensity or duration there.

- There were essentially no combustibles on the 14th floor. Thus, the only effect of the breach in the 14th floor slab would have been the short-term decrease in the heating of the 13th floor ceiling. The separation of this floor might have allowed for flames from the 13th floor to appear in the 14th floor windows, explaining the brief, late fire observed in the east end of the north face at 5:03 p.m.

- The floor collapses on the 10th and 11th floors resulted from thermal expansion of the support girders due to prolonged exposure to the hot gases from fires on the floors above and below.

    - No fire was observed on the 10th floor, and the fire on the 9th floor had just reached the area of the floor breach. Thus, the effects of the breach in the 10th floor would have been the short-term decrease in the heating of the 9th floor ceiling and the addition of (unignited) combustibles to the 9th floor fire, which had no shortage of fuel already.

    - There had already been a prominent fire on the east side of the 11th floor. Thus, a breach of its floor would not have affected the fire on the 11th floor significantly. Since no fire was observed on the 10th floor, there had been no significant effect of any combustibles falling from the floor above.

In light of the lack of visual evidence with which to validate the highly complex coupling of the fire and thermostructural models, the Investigation Team did not pursue simulating the modest effect of these late floor failures on the progress of the fires.

9.2 HYPOTHETICAL FIRES INVOLVING DIESEL FUEL

9.2.1 Floors 5 and 6

Fire Conditions and Limits to Fire Intensity

Figure 9–1and Figure 9–2 are schematic diagrams of the layout of the 5th and 6th floors, respectively. They include the locations of the diesel generators, the fuel lines that fed them, the intake and exhaust ports, and any interior partitions. These figures show that Column 79 was located in the same space as

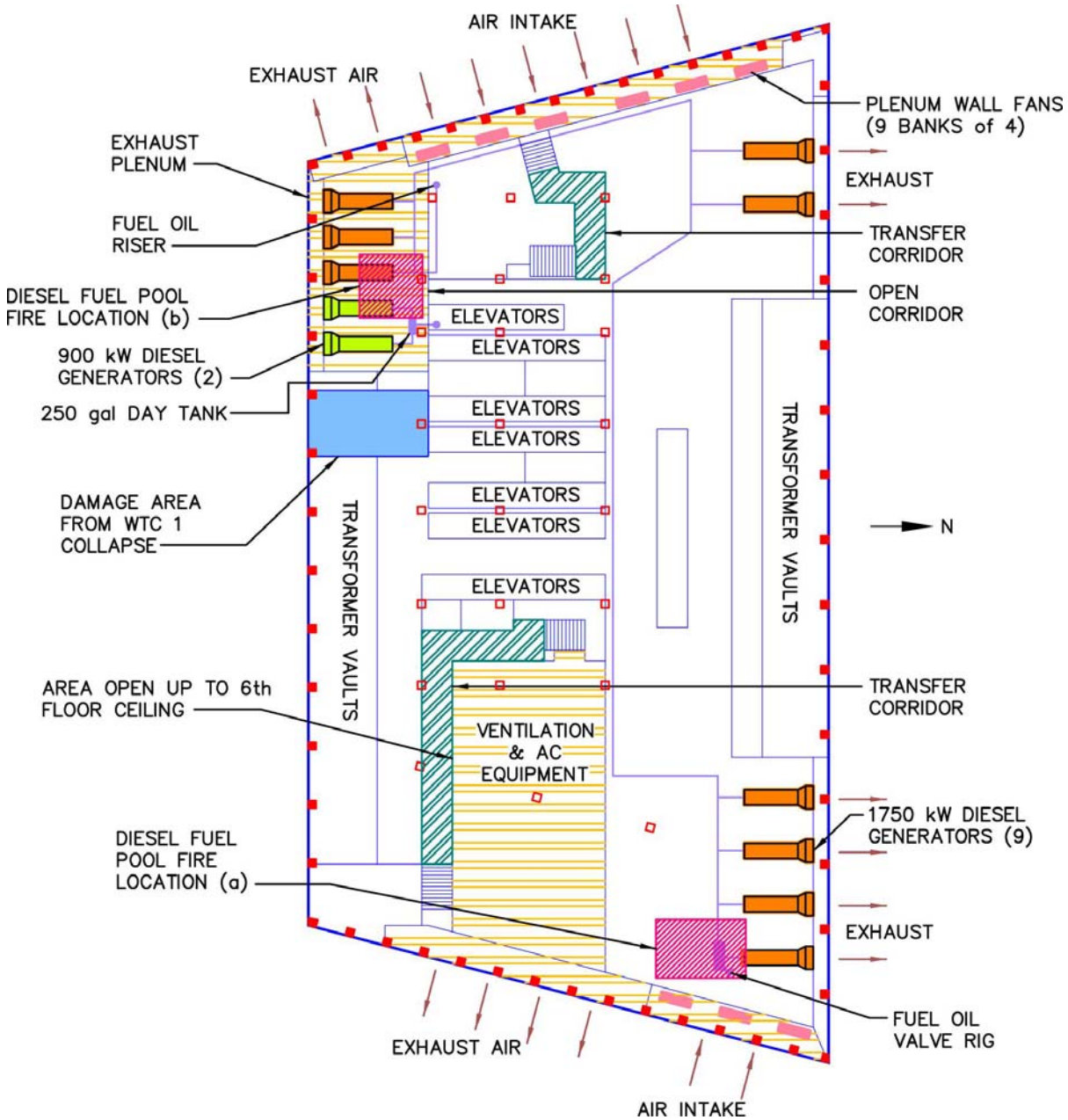

Figure 9–1. Plan view of the 5th floor, including estimated debris damage from WTC 1.

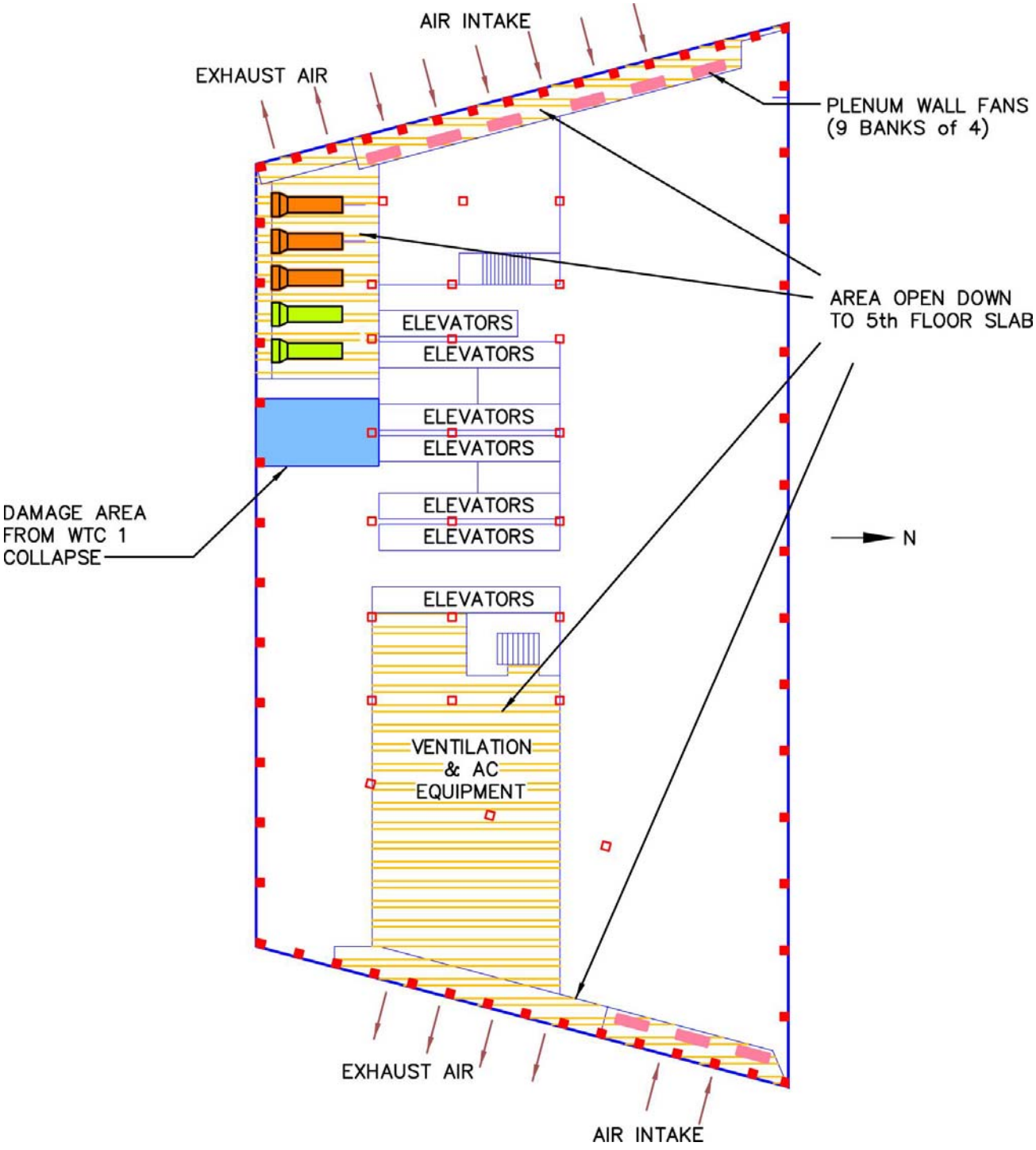

Figure 9–2. Plan view of the 6th floor, including estimated debris damage from WTC 1.

the four generators in the northeast quadrant. Column 80, Truss 1, and Truss 2 were located in the Ventilation and AC Equipment space, which was enclosed with masonry walls. Column 81 was located within the transfer corridor. Thus, of these critical structural components, only Column 79 could have been exposed to heating from a fuel oil fire on Floor 5.

As presented in Chapter 5 of this report, there was no visual evidence of a fire in this space. However, as presented in Section 3.3.2, louvers and blocked windows would have obscured views of a fire on the 5th floor from the north, east, and west. A fire on the north or west side of the core on the 6th floor would have been visible through the 6th floor windows; the two story louvers that extended up from the 5th floor would have obscured a fire on the 6th floor viewed from the east. Had a large, sustained fire occurred on the 5th floor, the partitions separating the exhaust and air intake plenums could have been breached, discharging visible smoke through the louvers to the west, east or north.

Chapter 8 suggests that the initial effect of a fire weakening the building structure would have occurred toward the east side of the building. The interior columns that might have been affected were Columns 79, 80, and/or 81. Figure 9–3 shows the developing thermal conditions for these heavy columns, insulated with 9/16 in. of thermal insulation[2], when exposed to a uniform temperature of 1100 ºC. It would have required a continuous, fully developed fire at the location of a column for approximately 7 h for a 50 percent reduction in its strength to occur (Section 4.1.2, NIST NCSTAR 1-6).

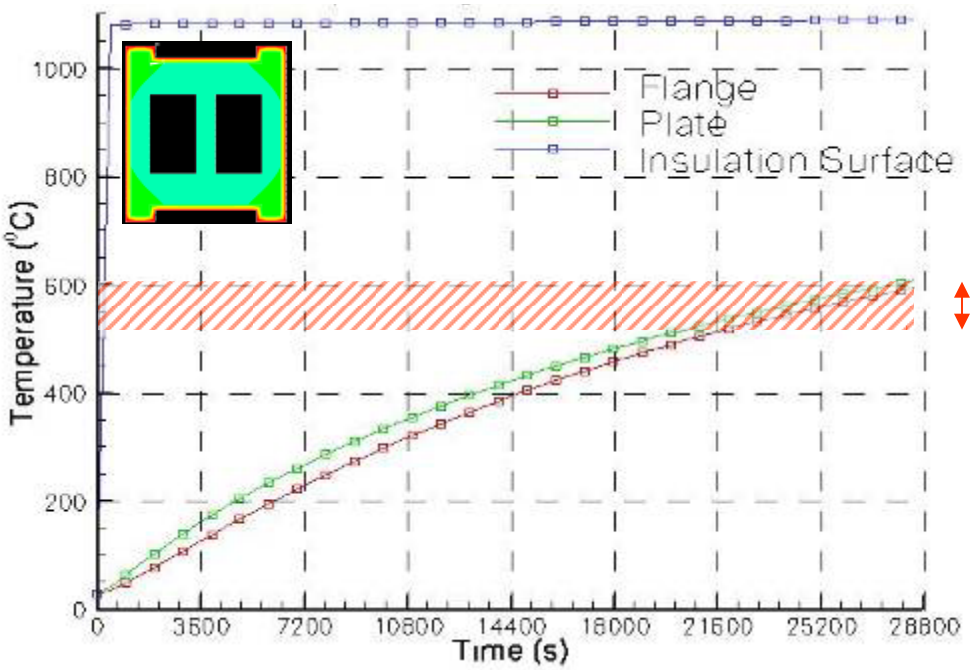

Figure 9–3. Minimum heating of reinforced heavy columns to initiate global collapse. The column modeled is a W14x730 with 9/16 in. of thermal insulation.

There was very little in the way of solid combustibles on the 5th and 6th floors. Therefore, any sizable fires would have had to involve the fuel oil that could have been delivered to the floor by the fuel pumps

[2] The nominal column insulation thickness for columns larger than a W14x228 was nominally 7/8 in. (Chapter 2). As part of determining the rate of heating in Column 79, a reduced thickness was evaluated.

(Section 3.4.2). NIST evaluated a set of hypothetical, extreme fire scenarios to determine whether the outcomes could have contributed to the weakening of the WTC 7 structure and whether the outcomes were consistent with the available evidence.

Hypothetical Fire Scenarios and Results

Fire Scenario Set 1

The fires in scenario set 1 would have originated in the northeast quadrant of the 5th floor (Figure 9–1). The scenarios presumed a rupture of the fuel oil supply piping, possibly where it was rigidly attached to the ceiling-mounted valve rig (refer to Figure 9–1 for location and Section 12.3 of NIST NCSTAR 1-1 for a fuller description of the piping), as the building responded to being struck by debris from the collapse of WTC 1 at 10:20 a.m. The maximum total fuel supply for the fires would have been the 55 m^3 (12,000 gal) from the SSB system (Section 4.3.2). The maximum flow from the circulating pump was 4.4 L/s (70 gal/min). Ignition of the fuel would have occurred at approximately the same time as the pipe rupture.

Scenario 1.a, maximum duration, over-ventilated fire: To be sustained for the approximately 7 h between the collapse of WTC 1 and the collapse of WTC 7, the fuel would have had to be pumped at about 1.8 L/s (29 gal/min), which was well within the capacity of the pumps. A large open pool of diesel fuel burns at a surface regression rate of about 4 mm/min (Gottuk and White 2002). A pool fire that burned the fuel at the same rate as it was being pumped would have had a surface area of about 30 m^2. For the purpose of the simulation, the pool was assumed to be a square, 6 m on a side, sited underneath the valve rig at location (a) in Figure 9-1. The needed air would have been supplied by continuously operating fans (95 m^3/s, 200,000 ft^3/min) and through breached partitions at elevator lobbies and the large gap on the south face. The steady state heat release rate from the over-ventilated fire would have been 50 MW to 60 MW. As suggested by the FEMA Building Performance Study Report (McAllister 2002), this fire scenario could have heated critical structural elements to high enough temperatures that the structural elements would have become incapable of maintaining the required load.

Result: Figure 9–4 shows the gas temperatures near the ceiling after 7 h for Scenario 1.a., as predicted by the FDS computer model. Maximum gas temperatures of approximately 1000 ºC are indicated in the vicinity of Column 79 (Figure 9–1). These temperatures, had they existed the entire 7 h, would have been sufficient to weaken this column substantially. However, the simulation also indicated that the gas temperatures above all of the nine water-cooled diesel generators would have exceeded their operating limit of about 100 ºC (the boiling point of water) in the northeast, northwest, and southwest quadrants in less than an hour. The emergency electrical distribution cables, which connected the various transformer vaults and the diesel generators, were protected by 2 h fire resistance rated partitions (Flack and Kurtz 1987). These cables would have been threatened by a sustained fire. Thus, with all nine generators and/or the electrical distribution system out of commission, there would have been no power to operate the fuel pumps for more than an hour or two, and the fires would have burned out well before the column experienced significant loss of strength or the 8 in. composite floor system at the 7th floor was damaged by the fire.

Scenario 1.b, maximum intensity, over-ventilated fire: This northeast fire location was the same as in Scenario 1.a. However, the fuel flow was doubled, which cut the possible fire duration in half, to

3.5 h. The forced air flow remained the same (95 m^3/s, 200,000 ft^3/min), which was more than enough to maintain an over-ventilated fire.

Result: The predicted temperatures of the upper layer of the 5th floor about 3.5 h into the fire are shown in Figure 9–5. The temperatures were somewhat higher across the floor as compared to Scenario 1.a, even though the total energy content was the same (that is, 100 MW to 120 MW heat release rate for half the time). The higher temperatures were due to the reduced amount of time for heat to be lost through the walls. The outcomes for Scenarios 1.a and 1.b were the same: the high temperatures near Column 79 could not be sustained because the environment around all the diesel generators and the electrical distribution system would likely have caused the electrical power to the fuel pumps to fail. Neither Column 79 nor the 7th floor composite floor system would have been thermally weakened.

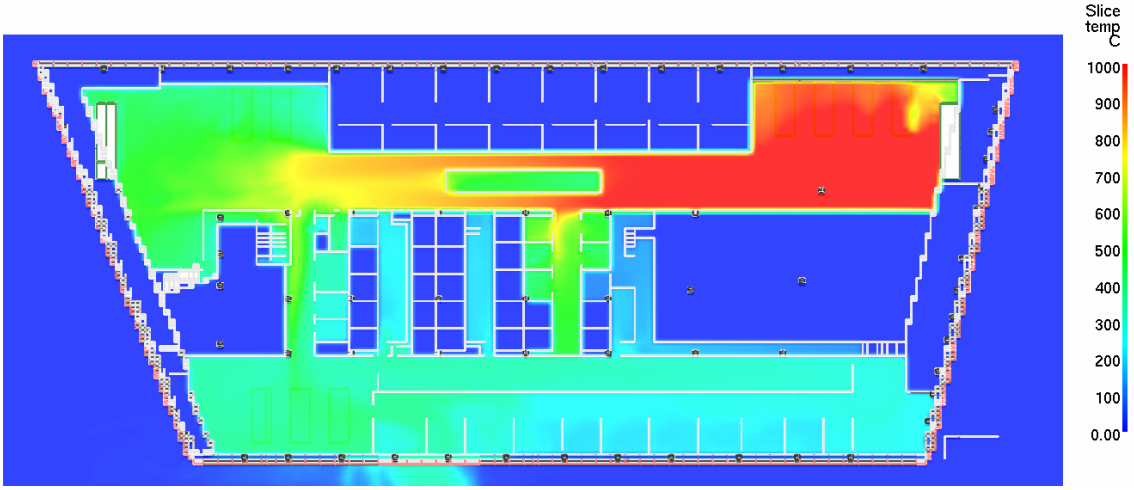

Figure 9–4. Temperatures near the 5th floor ceiling for the hypothetical maximum duration, over-ventilated diesel fuel pool fire after 7 h (Scenario 1.a).

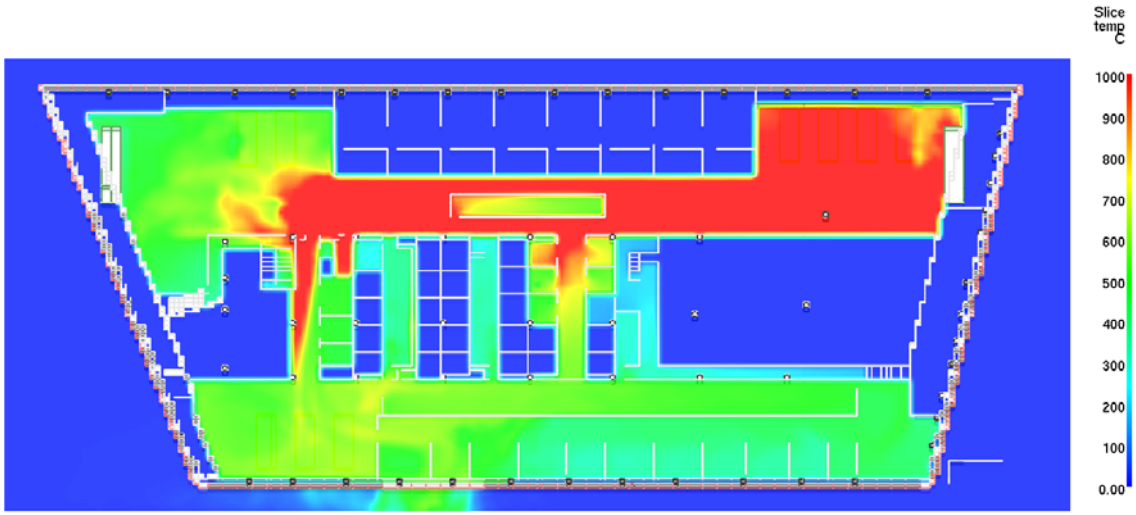

Figure 9–5. Temperatures near the 5th floor ceiling for the hypothetical maximum intensity, over-ventilated diesel fuel pool fire after 3.5 h (Scenario 1.b).

Scenario 1.c, maximum duration, under-ventilated fire: This fire location and pool size were the same as in Scenario 1.a. The louvers were assumed to be closed on the east and west sides of the 5th and 6th floors (preventing flames and smoke from escaping either side). Hence, air flow was limited to what could be entrained through breached partitions and the large gap in the south wall created when WTC 1 collapsed. The fuel flow was assumed to be 1 L/s (16.4 gal/min), which led to an underventilated fire. (Note that that this was a bit less than the fuel flow in scenario 1.a; however, additional fuel would only have served to cool the interior of the 5th floor because it would have been in excess of what the available air could burn.). The fire was located at the fuel source until the oxygen in that vicinity was consumed. It then traveled around the floor in search of a sufficient fresh supply of oxygen. The fire intensity in the vicinity of Column 79, about 40 MW initially, would have decreased with time.

Result: An FDS simulation showed gas temperatures near the ceiling ranging between 300 ºC and 400 ºC after about 15 min. A map of the temperatures near the ceiling for this time is shown in Figure 9–6a. Figure 9–6b shows the estimated gas temperatures near the ceiling more than two hours later,

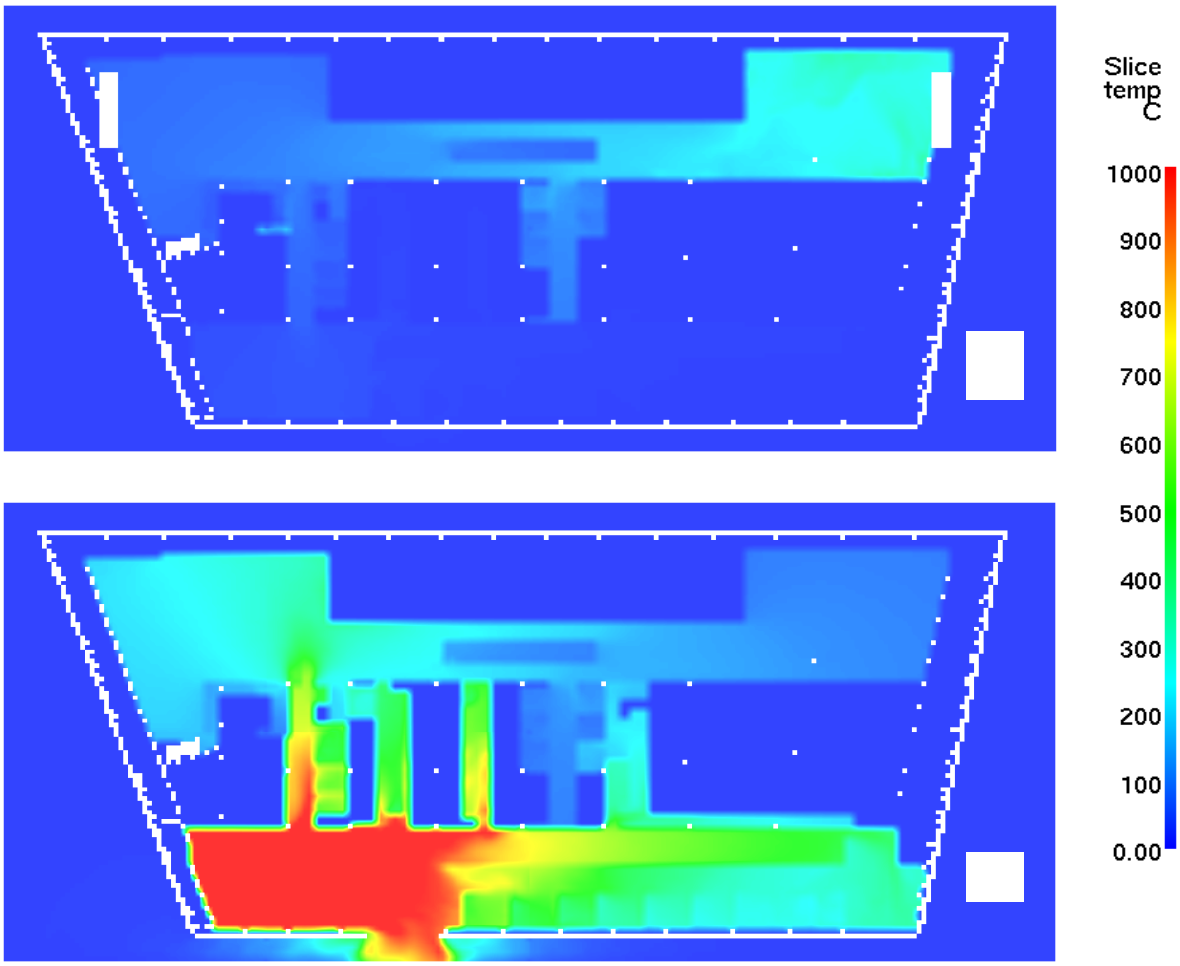

Figure 9–6. Estimated gas temperatures near the 5th floor ceiling for a hypothetical under-ventilated diesel fuel pool fire with the louvers closed (Scenario 1.c); (a) after 15 min; (b) after 3 h.

when the oxygen in the vicinity of the liquid fuel had been consumed and the flames were forced to find a fresh supply in the southwest corner of the building. This stage of the fire was highly speculative since the flames were no longer available to provide the heat needed to vaporize the diesel fuel in the pool. At any rate, the sustained temperature in the vicinity of Columns 79 did not exceed 400 ºC. Thus, the column temperature would not have risen to the point where significant loss of strength could have occurred. The generators in the northeast, northwest, and southwest sections would likely have all ceased to operate at these temperatures. Neither Column 79 nor the 7th floor composite floor system would have been thermally weakened.

Scenario 1.d, louvers open, fans inoperable: This fire was similar to Scenario 1.c, in that there was no forced air from the fans, but the louvers were open, augmenting the convection. The steady fire intensity would have been about 30 MW to 40 MW.

Result: The FDS simulation showed that the natural flow from the fire plume would have been out of the louvered openings on the east side of the building in a very short time. Significant plumes of smoke would have been seen emerging from the building within a few minutes of ignition, contradicting the visual evidence.

Fire Scenario 2

The pool was located in the southwest generator room (location (b) in Figure 9-1) and assumed to be about the same size as in Scenario 1.a: 6 m square, with a fuel flow of 1.8 L/s. The corridor on the west side of the core is assumed to be open, along with the louvers on the east and west sides of the 5th floor; the ventilation fans were assumed to be off.

Result: The air flow through the breach in the south wall was sufficient to consume the fuel and support an approximately 60 MW fire. The temperatures near the ceiling of the 5th floor above the southwest corner generator room quickly exceed 1000 ºC, which would have caused the generators in this corner to fail soon after the fires would have begun. The generators on the north side would not have been able to operate after their fuel supply line was broken. However, if, somehow, enough fuel were able to keep at least one generator operating, the temperatures near the ceiling of the 5th floor might have reached the close-to-steady state shown in Figure 9–7. Note that the ceiling in the generator room was the bottom of the 7th floor slab. The plume from the fire was predicted to extend well outside the breach on the south wall. There was no photographic evidence of fires originating from this area; however, the actual fire would have been difficult to distinguish from the plumes of other fires and dust on the south side of WTC 7. The nearby columns, especially those whose insulation was damaged by the debris from WTC 1, likely would have reached temperatures high enough to decrease their strength substantially. However, this scenario provided no open path for the hot gases to reach Columns 79. Any weakening of the 7th floor composite floor system would have been on the south side of the building, in the same region as the debris damage from the collapse of WTC 1.

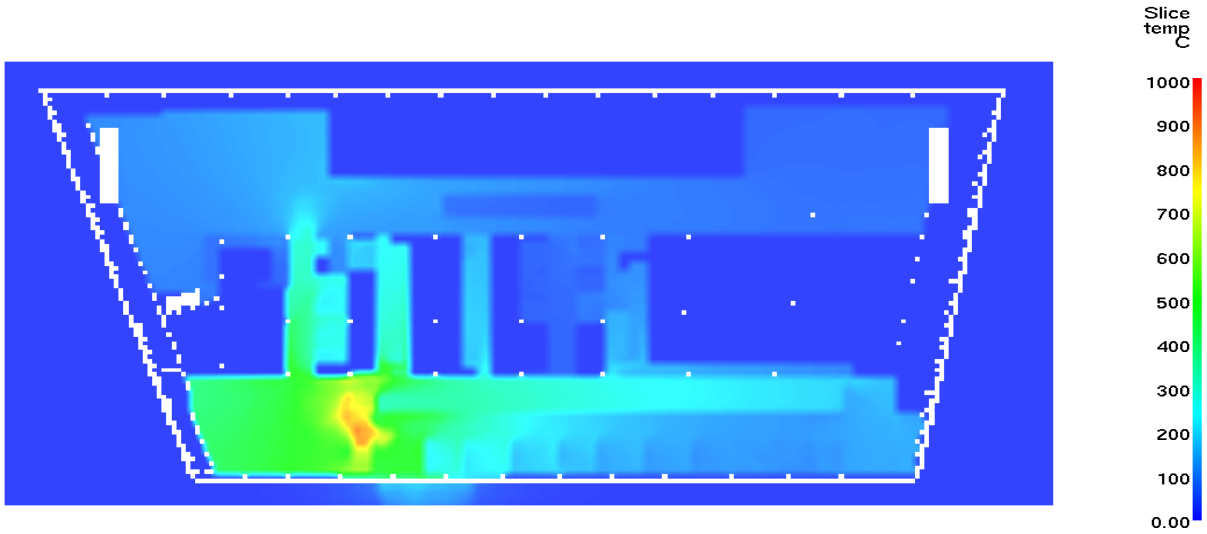

Figure 9–7. Temperatures near the 5th floor ceiling for a hypothetical diesel fuel pool fire in the southeast generator room in steady-state (Scenario 2).

9.2.2 Floors 7 through 9

Diesel generators were also located on the 7th, 8th and 9th floors of WTC 7 (Figure 3-11). Had the base emergency generators on the 5th floor operated as designed following loss of power to the building, the fuel pumps located on the first floor and the large storage tanks located underground could have continued for many hours to replenish the day tanks on Floors 7 through 9.

Three 500 kW generators were located on the south side of Floor 7 to support the OEM in an emergency. The 27 m^3 (6,000 gal) storage tank on the 1st floor was kept full by an automatic pump connected to the below-ground base storage tanks. The 1.25 m^3 (275 gal) day tank, located within a 2.5 m^3 (550 gal) rupture basin, was supplied through a riser by two 0.9 L/s (11.7 gal/min), 50 psi pumps. There was a horizontal run of the fuel oil return line along the south and west sides of the core on the 7th floor. The collapse of WTC 1 might have damaged the horizontal run in a way that allowed fuel oil to be pumped onto the 7th floor (and somehow didn't trigger the leak alarm), contributing to the severity of the fires in the southwest portion of these floors. The maximum pumping rate (which could have been maintained for over 4 h) would have been sufficient for a steady 50 MW fire along the south side of Floor 7. Smoke and flames from a fire in this region might not have been noticeable within the massive smoke and dust plume that shrouded the south side of WTC 7 for most of the day; however, the heat on Floor 7 from such a fire would have been isolated from the north and east side of the core.

The two 55 m^3 (12,000) gal, below grade storage tanks that were used to supply the base emergency power generators were also used to supply the 1.25 m^3 (275 gal) day tank for a single 350 kW generator on the west side of Floor 8, which served American Express. Two 0.2 L/s (2.8 gal/min), 100 psi pumps were located on the 1st floor, and the risers ran in the same enclosures as the risers supplying base building emergency power. There was a horizontal run of the fuel oil return line along the south and west sides of the core on the 7th floor, and a fuel oil supply run external to the core on the 8th floor. The generator room was sprinklered; however, since the primary and back-up supplies for the sprinkler system were both tied to the street water main, no water would have been available following the collapse of

WTC 1. The collapse of WTC 1 might have damaged the horizontal runs in a way that allowed fuel oil to be pumped onto the 7th and/or 8th floor (without triggering the leak alarm), increasing the severity of the fires in the southwest portion of these floors by as much as 12 MW. Sustained fires on the west side of Floor 8 were not captured in the video or photographic images collected by the Investigation Team.

The 125 kW emergency generator in the northwest corner of the 9th floor supplied power to the U.S. Secret Service. A 0.23 m^3 (50 gal) tank was mounted on the diesel engine. It was replenished with two 0.17 L/s (2.4 gal/min), 100 psi pumps, connected to the base fuel storage system. The fuel oil supply and return risers were located in the same shaft as the American Express risers. A horizontal pipe ran along the outside of the core on the 9th floor from the diesel engine to the riser shaft, and could have been vulnerable to debris from the collapse of WTC 1, contributing up to 10 MW to the fire along the west side of Floor 9; however, there was no evidence of a fire on Floor 9 until late in the day.

The day tanks themselves on Floors 7 through 9 contained a total of 600 gal of diesel fuel, roughly equivalent to 1800 kg (4,000 lb) of combustible furnishings. If spread evenly over the areas of the three floors, this amount of fuel was equivalent to only one percent of the estimated combustible material on these floors.

9.2.3 Summary

A broad range of hypothetical, extreme fires on the 5th floor did not produce a fire scenario that was consistent with the visual evidence that would have threatened the load bearing capacity of Columns 79, 80, or 81. Additionally, these hypothetical fires were likely to have caused collateral damage to the electrical and fuel supplies. This conclusion was also consistent with the information from interviews that sometime after 1:00 p.m., OEM and FDNY staff climbed the east stairway of WTC 7 and did not see much damage on the lower floors from their viewing location (Chapter 6). They made no mention of fire, heat or smoke.

The possible contribution of diesel fuel to the fires that were observed on Floors 7 through 9 was also considered. The amount of fuel available within the day tanks was insignificant compared to the normal combustible load on these floors, but the diesel fuel could have contributed to the initial ignition and spread of the fires on the south side of Floor 7 and on the west side of Floors 8 and 9. Had a rupture occurred in the horizontal runs of the fuel supply line, and had the base emergency generators on the 5th floor operated as designed, a significant fire on the south side of Floor 7 could have occurred without being distinguishable within the smoke and dust plume. Lesser fires on the west and southwest portions of the 8th and 9th floors might also have been possible under very special circumstances. All of these fires would have been well away from critical structural systems on the east side of WTC 7.

Based on the result of these analyses and the review of the numerous interview transcripts, the Investigation Team concluded that it was highly unlikely that any fires on the 5th floor contributed significantly to the collapse of WTC 7. Accordingly, in the structural modeling of the collapse initiation (Chapter 11), it was assumed that the temperatures on Floors 5 and 6 began at ambient values and only rose due to conductive heating from the fires on the floors above. For the different sets of reasons discussed above, the Investigation Team concluded that it was appropriate not to include diesel fuel explicitly in the simulation of the fires on Floors 7 through 9.

9.3 SIMULATION OF FIRES ON FLOORS 7 THROUGH 13

9.3.1 Model Input

Numerical Grid

As discussed in Section 9.1, independent fire simulations were carried out for the 7th, 8th, and 12th floors. The layouts of these floors can be found in Chapter 3 of this report.

The numerical grid dimensions for each floor of WTC 7 were the same as for the WTC towers. Grid cells of 0.5 m by 0.5 m by 0.4 m (vertical) were used, with a slab-to-slab height of 3.6 m. Although this grid was relatively coarse for a computational fluid dynamics (CFD) calculation, it was determined from validation experiments (NIST NCSTAR 1-5E) that it could adequately capture the peak temperatures, heat release rate, and burning duration of a fully engulfing workstation fire. The coarse grid would not be appropriate to describing the very early stages of the fires on each floor, nor would it help determine how the fires started. Much of this is unknown anyway, because it occurred in the damaged and heavily smoke-shrouded southern portion of the building. For this reason, the simulated fires were specified as having originated near the southern face of the building with a size of about 2 MW. This is roughly the equivalent of a single office workstation burning. As the fires grew and spread to other workstations, the coarse grid did reproduce qualitatively the observed fire activity.

Floor Layouts and Combustible Load

Once the spatial resolution of the numerical grid was chosen, architectural drawings were needed at a level of detail consistent with the underlying numerical grid. These were generally obtained from the tenants and augmented with interviews (Chapter 3).

Most of the drawings indicated large areas of open landscaping, mainly occupied by workstations, also referred to as cubicles. These were assumed to be similar to those in WTC 1 and WTC 2. Figure 9–8 shows a typical office environment in the WTC. (This photograph was taken in WTC 1, but the array is typical of the layout in the open spaces of WTC 7.) Despite varying appearances, these workstations typically contained about 250 kg of combustible material, mostly a mix of wood products, paper, and plastic (NIST NCSTAR 1-5C). In the numerical simulations, the modeled workstations were distributed on each floor, following the architectural plans.

Source: The Port Authority of New York and New Jersey.

Figure 9–8. Photograph of a work area in WTC 1.

For the simulation of fires in the WTC towers, NIST had estimated the combustible fuel load that was accessible to the fires in the cubicle-dominated tenant spaces to have been approximately 20 kg/m^2 (4 lb/ft^2) (NIST NCSTAR 1-5).[3] There was little information on the specific types of workstations in WTC 7, and the combustible mass had been found to vary only modestly among several types of workstations. Thus, the FDS simulations of the fires on the 7th and 8th floors of WTC 7 (which were mostly populated by cubicles) assumed similar fuel loads. As discussed in Chapter 3, the 11th and 12th floors of WTC 7 were mainly partitioned into offices. The combustible loading of office furnishings was estimated as follows. There were approximately 150 cubicles on the 8th floor and about 120 offices on the 12th floor. NIST assumed that the combustible mass of the furniture was about the same in an office as in a cubicle. Since the loading of other combustibles was reported to have been high on the 11th and 12th floors (Chapter 3), NIST assumed that the total combustible mass in an office was about double that of a cubicle. Thus, the average combustible fuel load on the 11th and 12th floors was estimated as 32 kg/m^2 (6.4 lb/ft^2). The density of combustibles on the 13th floor was varied and not well known. The average value was assumed to be the same as on the 12th floor. As noted later in this chapter, calculations were performed to estimate the sensitivity of the fire simulations to the combustible mass loading.

The core area contained elevator and HVAC shafts, stairwells, storage rooms, toilets, and various other support facilities. The magnitude of the combustible load in the various core areas was unclear, although it was likely to have been small. As a first approximation, the carpet that was assumed to be spread over

[3] As discussed in NIST NCSTAR 1-5, this fuel loading may appear to be lower than that in the surveys of actual offices. In this Investigation, the combustible mass cited in the FDS simulations is the fully burned mass. However, in the multi-cubicle tests reported in NIST NCSTAR 1-5E, a sizable fraction of the paper in file cabinets, shelves, and desk drawers did not combust fully.

the floor of the tenant spaces was extended into the core area. This was not necessarily meant to imply that the core was carpeted, but was to represent some light load of combustible objects that might have been found there.

The best information available was that the ceiling tile systems were similar to those in the towers. It was assumed that, except for the immediate damage area in the south of the building, the tile systems were intact following the debris impact. The tiles were assigned the same thermal properties as those for the systems in the WTC towers, and it was assumed that a tile became dislodged from its supports when its surface temperature reached 400 °C.

Exterior Damage

An important component of the fire simulations was the damage to the exterior of the building, both from the debris impact from WTC 1 and from the heat of the fires breaking windows. Exterior damage was input directly into the model from the assessment in Chapter 5. There were no attempts to predict window breakage with the model, nor was there any effort to assess the sensitivity of the calculations to the degree of exterior damage.

Ignition

For the simulations of the WTC 1 and WTC 2 fires, the initial ignition of furnishings was clearly a result of flaming jet fuel, and this effect was reproduced in the simulations using evaporating liquid droplets. For WTC 7, however, the ignition and early course of the fires were unknown because they were presumed to have occurred in the damaged and heavily smoke-shrouded southern portion of the building. For this reason, on each floor, a specified fire of 2 MW was positioned near the southern face of the building. This was roughly the equivalent of a small, single office workstation burning. Furnishings near the originally specified fire were assigned thermal properties obtained from small scale experiments (NIST NCSTAR 1-5F). Fire spread was predicted by the model as a natural consequence of surrounding objects heating and burning. The exception was that, for the simulation of the 8th floor, a second specified fire was needed to spread the fire to the north face of the building, where it was observed from about 3 p.m. until as late as 4:40 p.m. All of the simulations were carried out for six hours of elapsed time.

9.3.2 Results of the Simulations

The aim of the fire simulations for WTC 7 was to replicate the major features of the fires, given the limited knowledge of the debris impact damage and interior contents, while exploiting as much as possible the visual evidence contained within the few photographs and videotapes taken of WTC 7 following the collapse of the towers. As noted in the discussion of the individual floors below, the simulations generally replicated the major fire features, including the rate of spread of the fires at the building perimeter (the photographs could not show interior burning) and the overall burn time for each of the affected floors. There was some variability in simulation of the duration of fire activity in a given perimeter location on some highly partitioned floors. The descriptions of the actual fires are from Chapter 5 of this report.

Note that only the window glass breaking times were prescribed in the fire model. The observed fire activity gleaned from the photographs and videos was not a model input, and thus one should not expect a perfect correspondence between predicted high temperatures and observed fire activity.

Floor 7

A cubicle fire was observed on Floor 7 at about 12:15 p.m., near the southwest corner of the building. The fire spread north along the west face. By 3:00 p.m., the fire had progressed from the west side of the building past the halfway point of the north face. Shortly after this time, the fire on the north face appeared to stop and was not observed to progress further. About 4:25 p.m., a fire flared just east of this and died down within about another 15 min. As late as 4:45 p.m., fire was observed near the middle of the north face on Floor 7.

To simulate the fire on Floor 7, a 2 MW fire was prescribed near the southwest corner at an assigned time of 12:00 noon, which became the starting "time" of the simulation. This fire was chosen to initiate spread along the west face of the building. No other fires were prescribed, and the spread of this fire beyond its point of origin was predicted by the model. Windows were removed from the calculation at times observed in the (infrequent) photographs and videos. For the time periods between photographs, windows were removed in a linear fashion, consistent with the assumption that the fires spread at a nearly constant rate.

Figure 9–9 displays hourly snapshots of the upper layer temperatures predicted by the model. The simulations indicated that the clusters of workstations burned out in about 20 min to 30 min. The cold, rectilinear areas along the south wall and the east wall are the mechanical areas described in Chapter 3. Their fire-rated walls would have effectively resisted any significant heating of the contained space. The walls also impeded fire spread along the south face, explaining the clockwise movement of the fire. Figure 9–1 shows the location of columns 79, 80, and 81 relative to the mechanical area on the east side of the building.

The spread rate and intensity of the observed fire and the simulated fire were similar. The simulated fire reached the north face of the building a little later and spread a little more slowly to the east than the visuals indicated. (Note that the start time of the simulated fires was defined as 12:00 p.m., for lack of visual evidence, and that the visuals only indicated burning near the windows, not in the building interior.) The principal difference between the photographs and the simulation was that, unlike the actual fire on Floor 7, which stopped and then flared up to the east, the simulated fire slowed briefly near the middle of the north face and then continued toward the east. (There were office walls in this vicinity, but doors were left open in the simulation, and the fire eventually passed through the middle section of the building and moved to the east face, where it finally consumed the remainder of the furnishings.) The effect of these differences on the thermal environment would have been small.

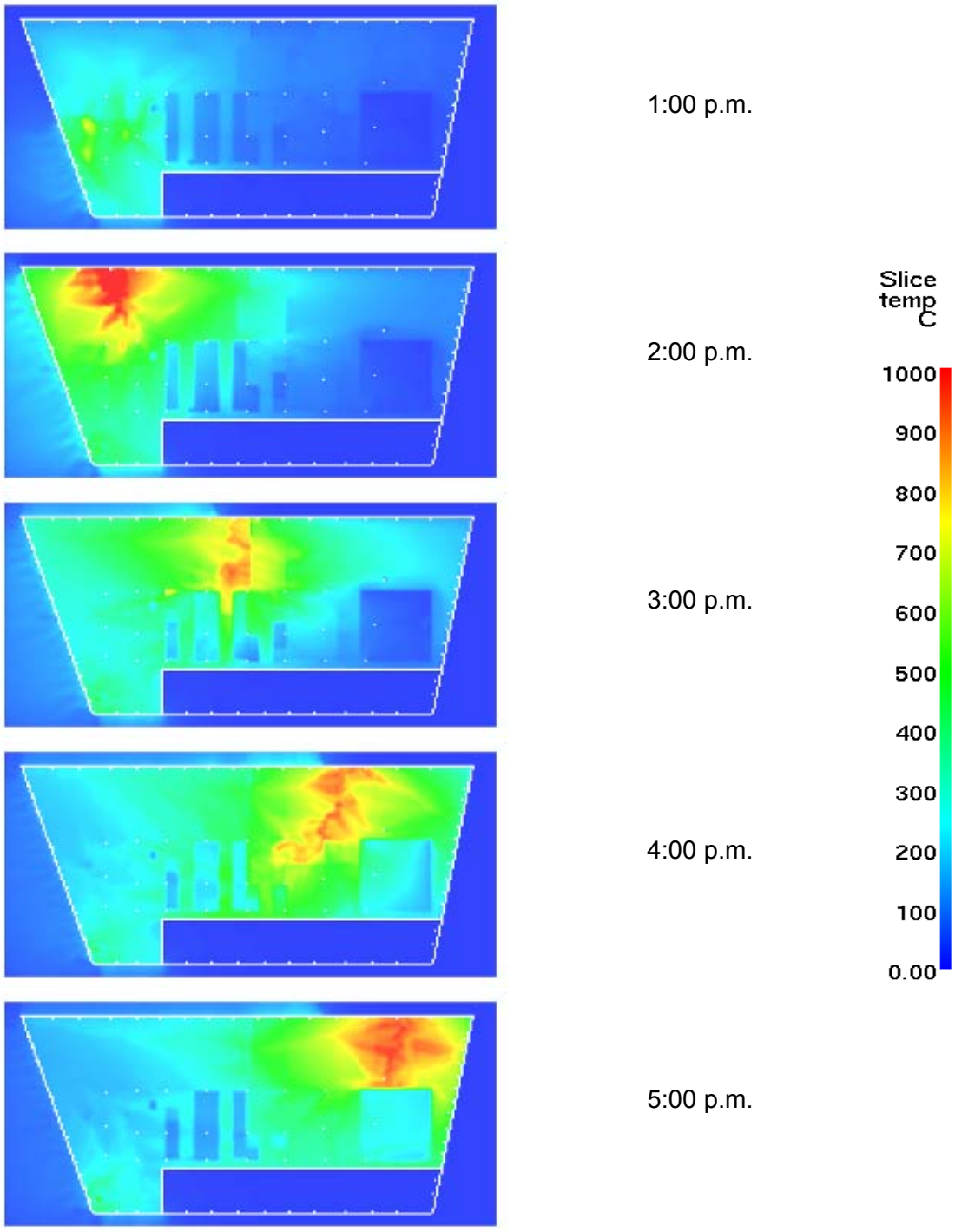

Figure 9–9. Progression of simulated fire on Floor 7 of WTC 7.
Shown are upper layer temperatures.

Floor 8

At 12:15 p.m., when the cubicle fire was observed on Floor 7, people being led from Floors 7 and 8 out of the building reported no fires, heavy dust, or smoke on Floor 8. Between 12:15 p.m. and 2:30 p.m., fire activity on Floor 8 was observed at the south face by eyewitnesses near the southwest corner of the building. At 3:15 p.m., fire was observed on Floors 7 and 12 at the north face, but not Floor 8. At about 3:40 p.m., fire was observed near the center of the north face of Floor 8 at roughly the same time fires were burning on the west face and in the northeast corner. Earlier fires between the western edge and the center of the north face appeared to have died down. Unlike the fire on Floor 7, the fire on Floor 8 continued to move east on the north face fairly steadily, reaching the northeast corner and moving to the east face around 4:00 pm and moving onto the east face. Low intensity interior fires were still present to the east of the center of the north face of Floor 8 around 4:45 p.m.

In the simulation, a 2 MW fire was prescribed near the middle of the south face at about 12: 30 p.m., 30 min after the start of the fire on Floor 7. Although there is no direct photographic evidence for it, in the model, windows were intentionally broken out along the west face, starting from the southwest corner, as a means of directing the simulated fire spread in the observed clockwise direction.

This fire did not spread to the north face in preliminary simulations. The cause was a partition (shown in the architectural drawing of the floor) that partially blocked the path from the southwest corner to the northwest corner. Thus, a second 2 MW fire was prescribed near the northwest corner at 3:00 p.m., based on the photographic evidence.

Figure 9–10 displays hourly snapshots of the upper layer temperatures predicted by the model. As with the fires on the 7th floor, the burning time and spread rate of the 8th floor fires were similar in the photographs and the simulation. The fire spread rate over the clusters of workstations was the same as on Floor 7. The principal difference between the simulations and the observations was that the simulated fires spread from the western edge to the east, while the imagery suggested the fire first appeared somewhere on the western side of the north face and then spread both west and east, first burning to the western edge and along the west side and reaching the eastern edge at a later time. In other words, the difference was the order in which the northwest corner and the west end of the north face burned. Since all the fuel in this region was consumed in about a half hour, the order of burning was not likely to have had a significant effect on the heating of the structure in that vicinity.

Floor 9

The first observations of fire on the 9th floor were soon after 4:00 p.m., on the west side of the north face. The fire spread eastward, reaching four-fifths of the way across the face by 4:15 p.m. Images showing further progress to the east were not available. The intensity of the fire had decreased markedly by 4:40 p.m. Since these observations of fire on the 9th floor were at times similar to those on the 8th floor about one hour earlier, the 9th floor fire was simulated by transposing the 8th floor fire one hour later.

Between 4:00 p.m. and 4:40 p.m., the progress of the simulated fire matched the visual evidence. The simulation added descriptions of the fires prior to and subsequent to this period. Since the fire physics should have been similar to that on the 7th and 8th floors, the overall fire progress on the 9th floor was assumed to be of the same accuracy as the fires on the two floors immediately below, despite the lack of visual corroboration.

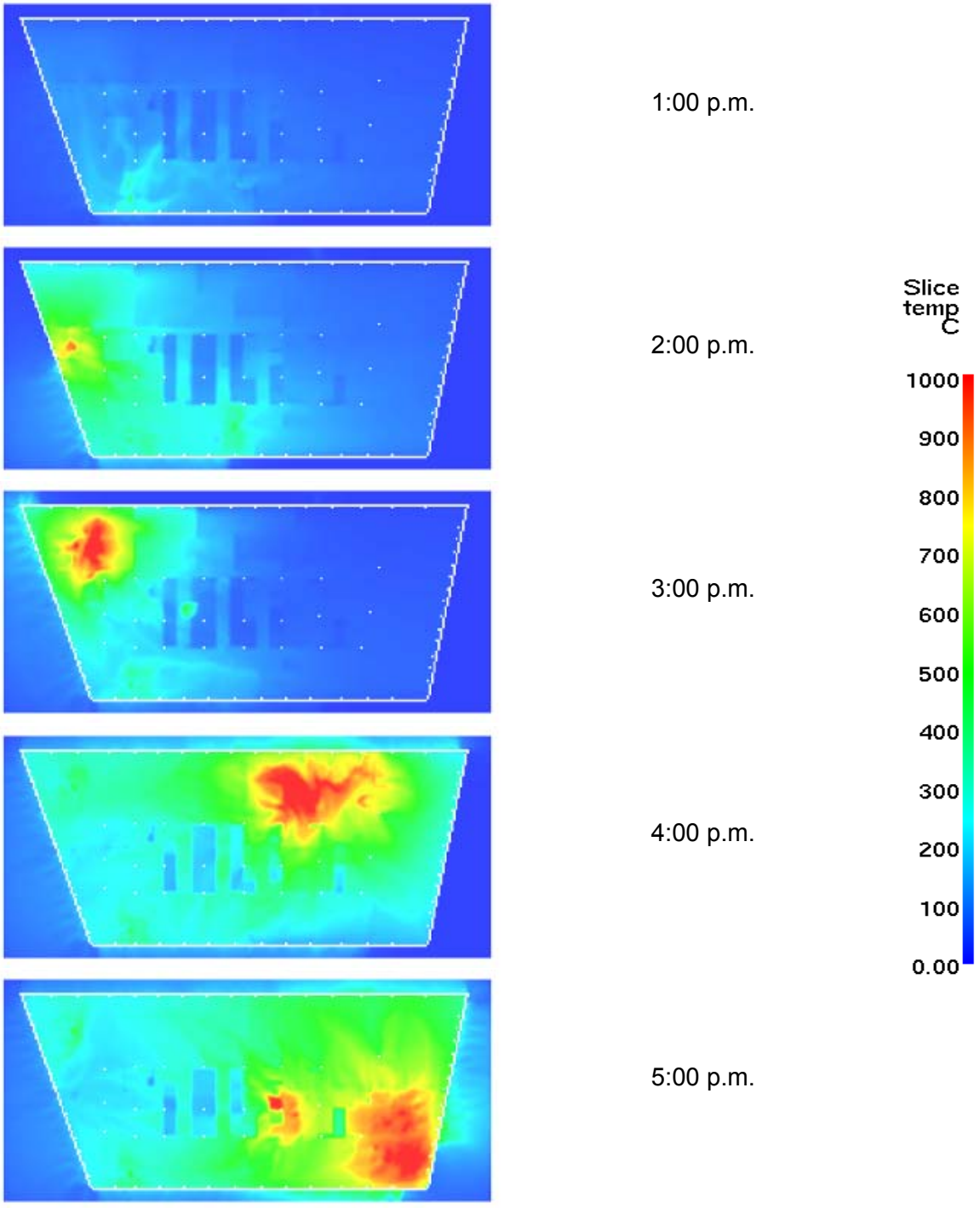

Figure 9–10. Progression of simulated fire on Floor 8 of WTC 7.
Shown are upper layer temperatures.

Floor 12

Fire was first observed on the 12th floor, on the south side of the east face, at about 2:10 p.m. Intact windows at the south edge indicated that the fire likely had bypassed the southeast corner as it moved from the south face onto the east. By around 2:30 p.m., the intense flames originally seen on the east face were dying down, while the fire had spread both south into the southeast corner and two-thirds of the way to the northeast corner. Just before 3:00 p.m., there were flames east of center on the north face. The fire had apparently bypassed the northeast corner of the floor and spread internally to the north face. By 3:15 p.m., the fire had spread to the east to engulf the northeast corner and to the west, reaching near the center of the face. By around 3:55 p.m., flames had reached west of the center of the north face. Around 5:00 p.m., the fire had continued spreading west to the northwest corner.

The simulation reflected the high partitioned floor layout and higher estimated fuel load, compared to Floors 7 and 8 (Chapter 3). In the simulation, a 2 MW fire was prescribed near the center of the south face at an assigned time of 12:00 noon. No other fires were prescribed, and the spread of this fire beyond its point of origin was predicted by the model. Windows were removed from the calculation at times observed in the photographs and videos, which were well spaced from about 2:30 p.m. until about 5:00 p.m. For the time periods between photographs, windows were removed in a linear fashion, consistent with the assumption that the fires spread at a nearly constant rate. Figure 9–11 displays hourly snapshots of the upper layer temperatures predicted by the model for the 12th floor.

The prescribed window breakage pattern in the model drove the fires in a counter-clockwise direction, consistent with the visual evidence. The fires also spread along the south face in the simulation, although there is no evidence to confirm this observation. The spread rate was about one-third to one-half slower than that on the lower floors due to the higher fuel load. The burning time near the north face was longer in the simulation than in the visual evidence, suggesting that (a) additional gasified fuel from the building interior was burning near the windows in the simulation, (b) the input fuel load was too high, and/or (c) the office partitions were more effective at slowing the fire progress in the simulation than in the actual fires. The first possibility would lead to overestimated temperatures near the north curtain wall, but not necessarily between the curtain wall and the building core. The second possibility would imply reduced heat release, which, in turn, would lead to overestimates of structural temperatures throughout the area between the north curtain wall and the building core. The third possibility would lead to heating of the northeast corner slightly earlier than in the actual fires. Explanations (a) and (c) are more likely the cause of longer apparent burning time than (b). (See Section 9.3.3.)

Floor 11

Fire on the 11th floor was first observed at about 2:10 p.m. near the southeast corner on the east face. The smoke patterns suggested intense flames prior to this time. The fires reached the midpoint of the east face about 2:30 p.m. There had been no indication of burning along the entire north face as late as 4:00 p.m. The next images of fire on this floor were about 4:40 p.m., showing burning just east of the center of the north face. By around 4:52 p.m., the flames in the original fire area had apparently died down. The fire continued to spread slowly across the north face toward the west until WTC 7 collapsed, having reached about 60 percent of the distance across the face.

The fire behavior on Floor 11 followed the pattern on Floor 12. The fires on the two floors occurred at similar times on the east face, prior to 2:30 p.m. The appearance times of the fires on the north face of the 11th floor were about 1½ h later than those on the 12th floor. Since the floor layouts were the same arrays of partitioned offices, and since it was unknown which office doors were open or closed, the Investigation Team decided that additional simulations of Floor 11 would not have provided any more meaningful results than time-offsetting the temperatures predicted for Floor 12. The Floor 11 fires were represented by the Floor 12 fires delayed by 1 h. This resulted in a westward fire spread rate along the north face that was faster and a burn duration that was longer than observed in the photographs. Combined, these could have led to a mild overestimate of the heating on the north side of the floor.

Floor 13

The visual evidence suggests that the fire, first seen about 2:30 p.m., burned along the east face, turned at the northeast corner, and was east of the center of the north face about 3:40 p.m. Around 4:00 p.m., flames had reached the center of the north face. Forty minutes later, any fires on the east side of the north face were no longer visible. At about 5:00 p.m., the fires had extended west of the center of the north face and were still there just prior to the building collapse.

The fire on this floor generally followed the pattern of the fire that was observed for the 12th floor. The timing of the fire on the east side was roughly one-half hour behind that of the fire on the 12th floor. The 13th floor fire arrived in the northeast corner about one-half hour later than the 12th floor fire and was about one-half hour slower in approaching the west section of the north face. Since the floor layout and fuel load on the east side of the 13th floor were highly uncertain, the Investigation Team decided that additional simulations of Floor 13 would not have provided any more meaningful results than time-offsetting the temperatures predicted for Floor 12. The Floor 13 fires were represented by the Floor 12 fires delayed by one-half hour. The westward fire rate along the north face was moderately faster, and the burn duration was longer than in the visual evidence. Combined, these could have led to a mild overestimate of the heating on the north side of the floor.

9.3.3 Sensitivity Tests

The paucity of visual evidence did not support an extensive series of tests of the sensitivity of the simulations to the various assumptions noted above. However, a small number of checks of important input parameters were performed to improve confidence in the fire behavior obtained from the initial simulations. The following are the result of those sensitivity checks.

- Doubling the combustible load on the 8th floor from 20 kg/m^2 to 40 kg/m^2. This caused the fires to burn in place longer, until the fuel was consumed, before advancing. As a result, the fires moved distinctly more slowly than in the visual evidence.

- Decreasing the combustible load on the 12th floor from 32 kg/m^2 to 20 kg/m^2, the value used for the floors whose combustible load was not described as high (Chapter 3). This showed little effect on the rate of fire progression. This suggests that the input combustible fuel load was not the principal factor in the longer burn duration (see above).

- Decreasing the combustible load on the 12th floor from 32 kg/m^2 to 20 kg/m^2 and doubling the strength of the ceiling tiles (Figure 9–12). This floor was heavily segmented into individual offices, and this change effectively slowed the fire movement past the walls and into adjacent offices. This fire spread rate was lower than in the visual evidence.

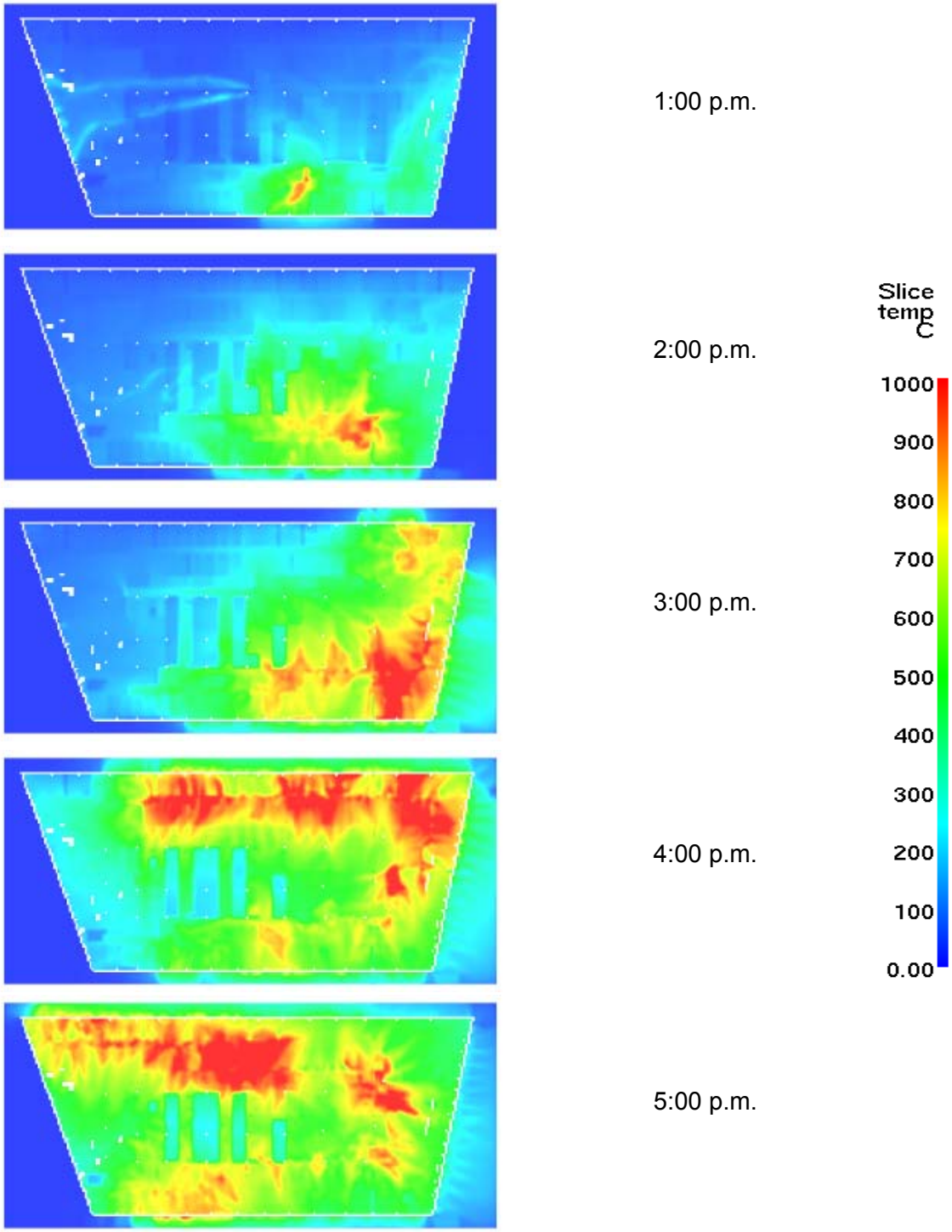

Figure 9–11. Progression of simulated fire on Floor 12 of WTC 7.
Shown are upper layer temperatures.

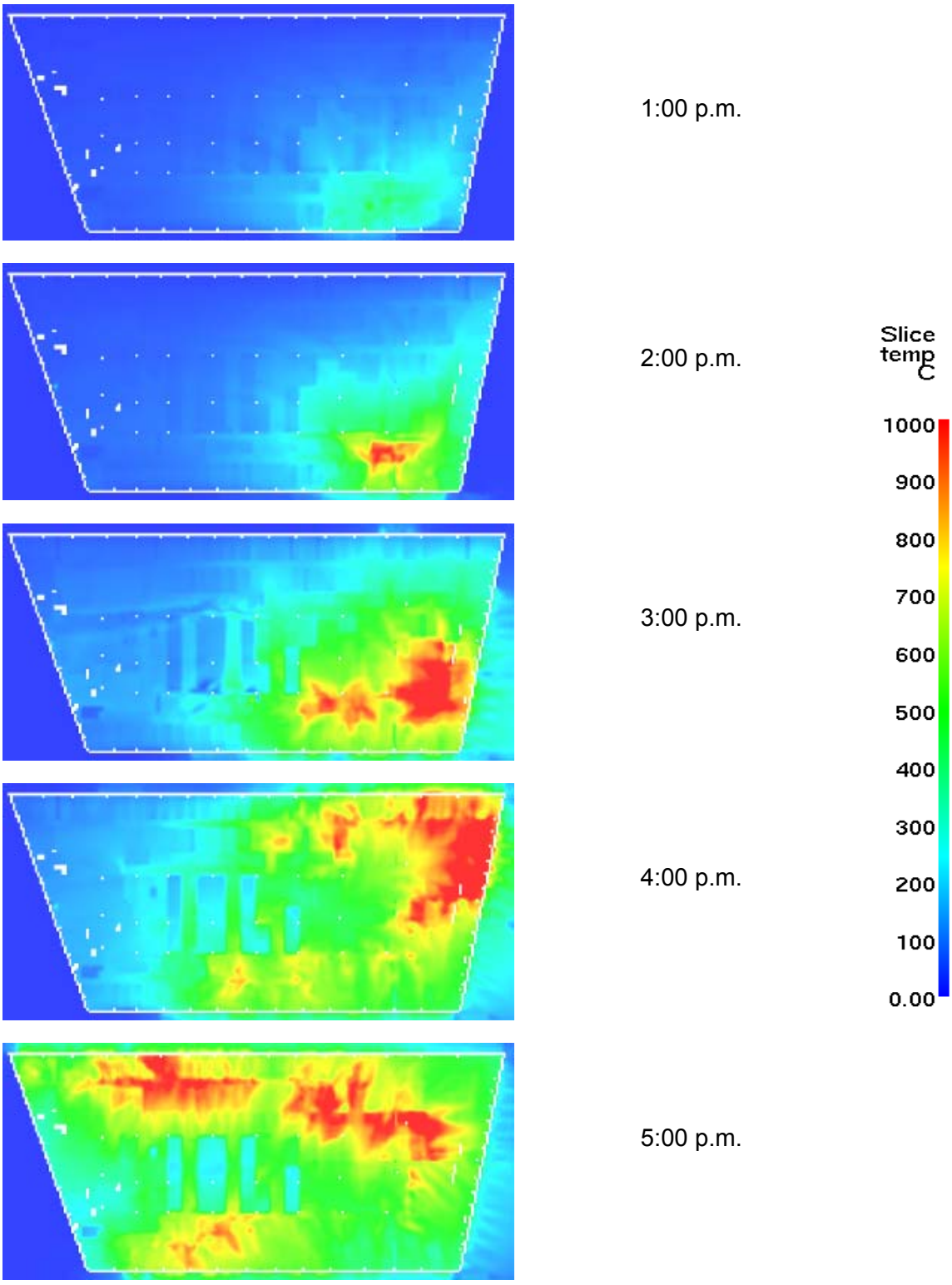

Figure 9–12. Progression of simulated fire on Floor 12 of WTC 7, with more durable ceiling tile system.

9.4 FIRE INTENSITIES

Figure 9–13 shows the rates of heat release for the simulated fires on the 7th, 8th, and 12th floors. The time of 0 h corresponds roughly to noon on September 11, 2001. There was only a single observation of a (small) fire on Floors 7 through 13 from 10:20 a.m., when it is likely that the actual fires started, until about 2:00 p.m. Thus, it is probable that the fires were no more intense during that interval than the early intensities in Figure 9–13.

The simulated fires on the 7th and 8th floors occurred in open landscaped areas, with free access to fresh air. Thus, the shapes of the heat release curves do not reflect the additional window breakage. The jump in heat release rate for the 8th floor at 3 h is a result of the second fire having been started in the already heated northwest section of the floor.

In the computations, the fire on the 12th floor, and thus the derivative fires on the 11th and 13 floors, generated significantly more heat than the fire on the 7th or 8th floor. This was in large part due to the higher fuel load in the simulations and the larger burning area of the Floor 12 fires.

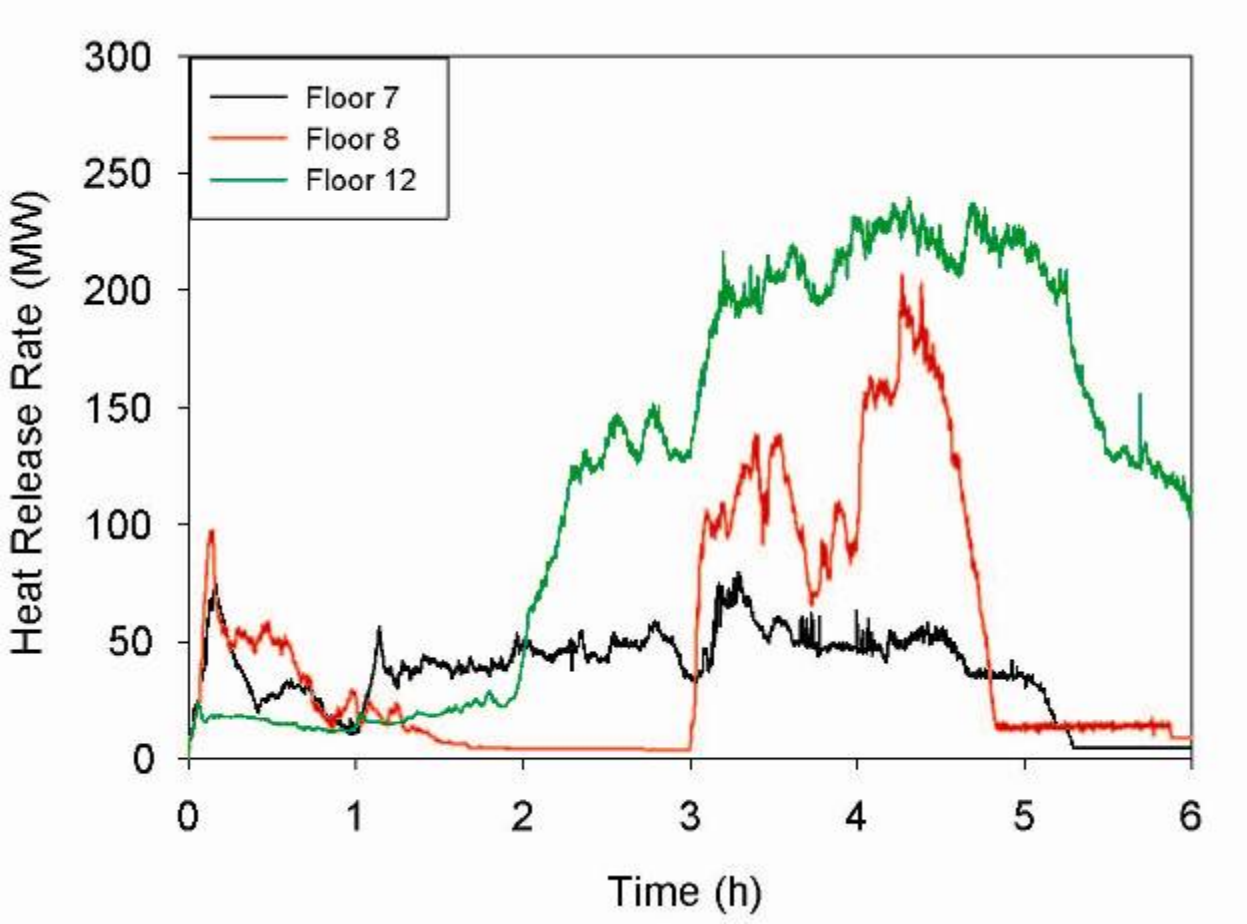

Figure 9–13. Rates of heat release of simulated fires in WTC 7.

9.5 SUMMARY OF THE SIMULATIONS OF FIRES IN WTC 7

The Investigation Team concluded that possible diesel fuel fires on the 5th or 6th floors were not likely to have been significant contributors to the eventual collapse of the building. The worst-case scenarios associated with ruptured fuel lines generated fires that could not be sustained long enough, or generated too little heat, to raise the temperatures of the steel and concrete structure to the point of significant loss of strength or stiffness, or these fires would have exhausted smoke from the exhaust louvers. No such emanation was observed.

Although the visual evidence for WTC 7 was not nearly as rich as for WTC 1 and WTC 2, the fire simulations did exploit as much as possible the few photographs showing the location of severe fire activity in WTC 7 at various times during the afternoon of September 11, 2001. Compared to the actual fires, the simulated fires followed the same general paths and, as evidenced by the validation experiments reported in NIST NCSTAR 1-5E, generated comparable temperatures to those in the fire tests. The simulations of the 12th floor fires (and thus the derivative 11th and 13th floor fires) may have mildly overestimated the duration of the fires and the fraction of the burning near the north face windows, relative to the burning in the interior of the tenant space.

The output from the fire simulations of the 7th, 8th, and 12th floors, along with the time-shifted output for the 9th, 11th, and 13th floors, was used as the input for the building thermal response calculations presented in the next chapter.

9.6 REFERENCES

Drysdale, D.D. 2002. Thermochemistry, in DiNenno, ed., The SFPE Handbook of Fire Protection Engineering, NFPA International, Quincy, MA, p. 1-93.

Flack and Kurtz. 1987. Design Criteria for Mechanical, Electrical, Plumbing, April 20.

Gottuk, D.T., and White, D.A. Liquid Pool Fires, in DiNenno, ed., The SFPE Handbook of Fire Protection Engineering, NFPA International, Quincy, MA, p. 2-309.

Huggett, C. 1980. Estimation of the Rate of Heat release by Means of Oxygen Consumption, Fire and Materials, vol. 12, pp. 61-65.

McAllister, T. ed. 2002. World Trade Center Building performance Study: Data Collection, Preliminary Observations, and Recommendations, FEMA 403, Federal Emergency Management Agency, Washington, DC. May.

McGrattan, K.B. (Ed.). 2004. Fire Dynamics Simulator (Version 4), Technical Reference Guide, NIST Special Publication 1018. National Institute of Standards and Technology, Gaithersburg, MD, July.

Chapter 10
STRUCTURAL HEATING

10.1 THE FIRE STRUCTURE INTERFACE

The Fire Structure Interface (FSI) was used to impose the air temperatures from the FDS simulations (Chapter 9) on the structural components of WTC 7 (Chapter 2) to predict the evolving thermal state of the building. The FSI also linked the thermal analysis and structural analysis by creating thermal loading data in a format that was consistent with the structural models that were used to predict the collapse of the building (Chapters 11 and 12). The structural response analysis of WTC 7 to understand the collapse initiation mechanism was performed using the thermal data presented in this section. The approach was similar to that used to predict the fire induced thermal response of WTC 1 and WTC 2 described in NCSTAR 1-5G, and therefore only a brief description of the major assumptions is included.

The FSI converts the rapidly changing, three-dimensional FDS gas temperature profiles into slowly varying upper gas layer and lower gas layer temperatures. These temperatures were time averaged over 100 s and spatially averaged over 1 m (3.3 ft). The upper layer temperatures were taken 0.4 m (1.3 ft) (one grid cell) below the ceiling. The lower layer temperatures were taken 0.4 m (1.3) ft above the floor. Under this plane layer approximation, a simplified form of the radiative transport equation was solved to predict the radiative fluxes incident on the sub-grid scale structural elements. The incident radiative fluxes are functions of space and time and depend on the location and orientation of the structural elements. The radiative fluxes were also related to the local instantaneous properties of the hot layer as defined by the upper and lower layer temperature, absorption coefficient, and depth of the hot layer as computed in the fire simulations.

10.2 MODEL INPUT

As indicated in the preceding chapter, the fire simulations for the 7^{th} and 8^{th} and 12^{th} floors were used to create thermal environments on Floors 7 through 13. The simulated fire on the 8^{th} floor was transposed one hour later and used to represent the fire on the 9^{th} floor. Similarly, the simulated fire on the 12^{th} floor was transposed one hour later to represent the fire on the 11^{th} floor and one-half hour later to represent the fire on the 13^{th} floor. The FSI source term for the remaining floors in the building was ambient temperature.

The thermal analysis performed for the reconstruction of the WTC 1 and WTC 2 fires indicated that significant heat transport from a floor with a flashed over fire did not extend past the adjacent floor. As indicated in Chapter 9, no fires were simulated on the 14^{th} floor, and the analysis in Chapter 9 indicated that there was no significant fire on the 5^{th} or 6^{th} floor. Thus, it was expected that the output from the FSI would indicate heating extending only from the 6^{th} floor to the 14^{th} floor.

The dimensions and structural formulation of the perimeter and core columns and the concrete floor slabs were those provided for WTC 7 (Chapter 2). The exterior surfaces of the perimeter and core columns were covered with a mean Monokote MK-5 insulation thickness of 22 mm (7/8 in.); the concrete slabs

were protected by 9.5 mm (3/8 in.) thick Monokote 5 on their bottom face only; the beams and girders were protected by 13 mm (0.5 in.) of Monokote MK-5 (Chapter 2). The damage from the debris from the collapse of the towers was not included in the simulations. This was because (a) little of the structure appeared to have been removed, and so the thermal capacity of the damaged steel and concrete probably was similar to that of the undamaged building; and (b) the thermal effect of the damage would have been local to the southwest portion of the building, while the eventual collapse initiated toward the northeast. Otherwise, the thermal response modeling of WTC 7 was identical to that performed for the WTC towers.

10.3 SIMULATED FIRE-INDUCED THERMAL RESPONSE OF WTC 7

10.3.1 General

It was assumed that the structure was initially at 23 ºC. The thermal analysis covered the approximately 21,600 s (6 h) period over which the FDS fires were present on these six floors. The minimum time step for the thermal analysis was 1 ms, while the maximum time step was limited to 50 s. As was done for the towers, the output file for use in the structural analysis contained thermal data at 12 instants in time, spaced at 30 min (1,800 s) intervals, beginning at 12:30 p.m.

The modeling of the steel elements was similar to that in NIST NCSTAR 1-5G. However, in WTC 7, there was no evidence of damage to the thermal insulation (away from the immediate impact area of debris from WTC 1). Since heat transport across the insulation layer was much slower than heat transport into the depth of the steel, temperature gradients across the thickness of even the heaviest structural steel columns were less than 1 °C.

As described in Chapter 2, the floor systems consisted of poured concrete over a corrugated steel deck. For floors 8 and above, the overall concrete thickness was 140 mm (5.5 in.), with the corrugations being 63 mm deep. The FSI simulated these slabs as uniformly 100 mm (4 in.) thick. The thickness was subdivided into eight elements, each 12.7 mm (0.5 in.) thick. For the 7th floor, the overall concrete thickness was 200 mm (8 in.), with the corrugations being 75 mm deep. The FSI simulated this slab as uniformly 200 mm (8 in.) thick. This thickness was also subdivided into eight elements, each 25 mm (1 in.) thick.

For each step, a set of thermal loading data was generated to completely specify the thermal state of the lower 16 stories of the building. The thermal loading data were in a format that was consistent with the structural models and could be readily read with the ANSYS finite element software to specify body loads (temperature and temperature gradient information) on the entire structure, for use in the simulations recounted in Chapter 11. ANSYS performed a linear interpolation between two consecutive load steps for convergence and stability of the numerical procedure. A second set of thermal loading data was generated as input to the LS-DYNA simulations of the building collapse (Chapter 12).

The Investigation Team estimated the sensitivity of the thermostructural simulations to the temperatures developed from the fires. Accordingly, three different thermal response computations were performed that were consistent with a realistic and reasonable range of expected fires. Case A used the temperature data just as obtained from the FDS simulation. Case B incremented the rise in gas temperature above ambient by 10 percent. This increased the severity of the fire in three ways. It increased the local heat transfer to the structural components, it increased the area over which the structural elements reached

temperatures where weakening of the steel or concrete could occur, and it increased the chance of hot zone overlap on adjacent floors. Given the limited guidance from the visual evidence, the Investigation Team estimated that a 10 percent change was within the uncertainty in the extent and intensity of the fires. In Case C, the gas temperature rise above ambient was decreased by 10 percent, again consistent with the expected range of realistic and reasonable fires in WTC 7 on September 11, 2001.

10.3.2 Case A

Two visualizations of the results were developed: with and without the opaque concrete floor slabs. Note that the simulations themselves always included the slabs.

Figure 10–1 is an example of a rendition of WTC 7, (viewed from the southeast corner), showing the thermal data generated with FSI and subsequently transferred to the ANSYS and LS-DYNA structural models for analysis (Chapters 11 and 12). The figure shows the perimeter and core columns extending from the ground level to Floor 16. The figure also shows the beams that support the concrete floor slabs. Only a fraction of the entire model is visible because of the concrete slabs. As noted above, the simulations showed essentially no thermal gradient across the thickness of the steel components. The depicted slab temperatures are in the midpoint of the uppermost thermal element. For the 7th floor slab, this was approximately 12.5 mm (0.5 in.) below the top surface; for the other floors, this was approximately 6 mm (0.25 in.) below the top surface.

Figure 10–2 shows a view of the same 16 floor simulation from the northeast corner. Here, the concrete slabs have been removed in the image to allow a better view of the heating of the internal floor beams and columns.

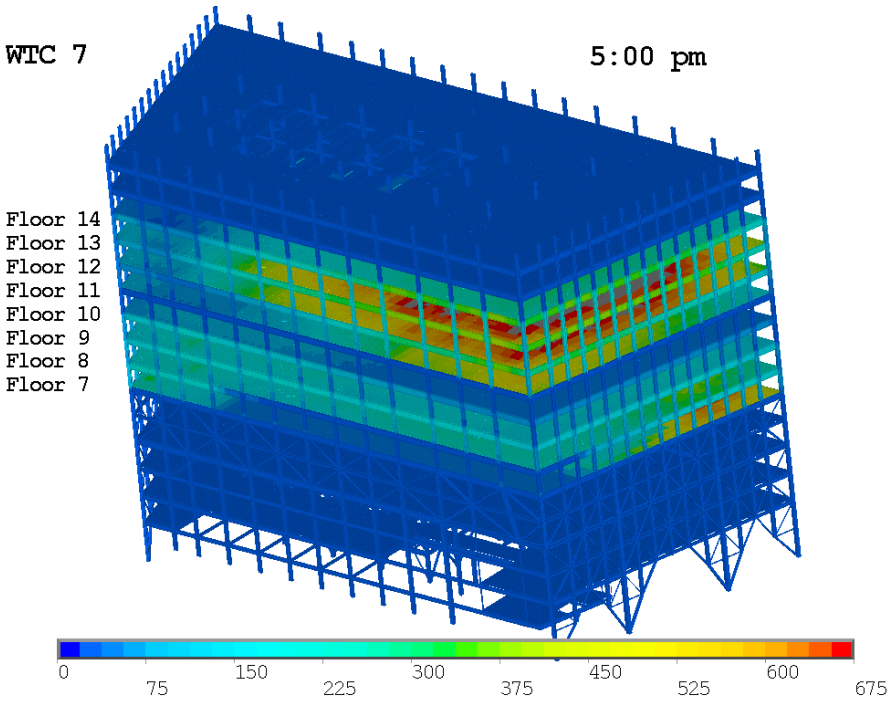

Figure 10–1. View from the southeast of the computed thermal loading of the 16 lower floors of WTC 7 at 5:00 p.m. (Case A).

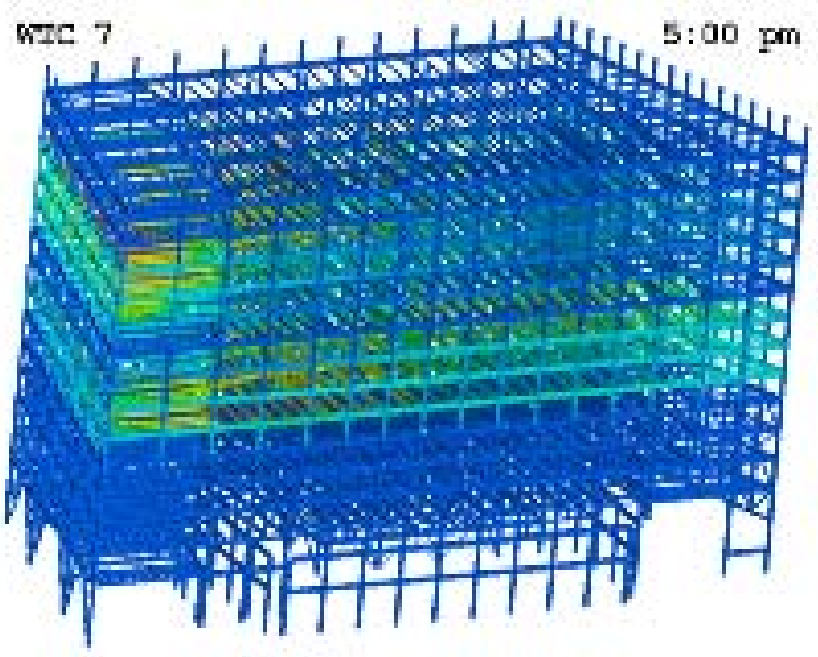

Figure 10–2. View from the northeast of the computed thermal loading of the 16 lower floors of WTC 7 at 5:00 p.m. (Case A, floor slabs removed).

Figure 10–3 shows the thermal loading on the 16 floor WTC 7 model at 12 different instants in time. Each sub-figure shows a view of the WTC 7 model from the southeast corner, similar to that shown in Figure 10–1. Each sub-figure shows the thermal state of WTC 7 at the time stamp noted in the top right hand corner. The results are presented at half hour intervals, with the first sub-figure showing the thermal loading at 12:30 p.m.

Figure 10–4 shows the thermal loading on the 16 floor WTC 7 model as viewed from the northeast corner. Each sub-figure is similar to that shown in Figure 10–2. Thermal loading data are visually shown at half hour intervals, starting at 12:30 p.m. The concrete slab has been removed from the images to allow a more detailed view of the heating of the interior beams and columns.

The simulation results shown in Figure 10–3 and Figure 10–4 indicate that there was significant heating of the floor systems on Floors 7, 8, 9, 11, 12, 13 and 14.[1] The floors below Floor 7, on Floor 10, and on the floors above Floor 14 did not heat significantly due to the absence of fire activity. The perimeter columns and core columns also did not heat significantly on the fire floors. The results indicated that there was intense heating of the ceiling beams in the northeast corner after 3:30 pm, especially those on floors 7, 8, 11, 12 and 13.

In the following sections, FSI results are described on a floor-by-floor basis. The figures in each of the following sections are visual representations of the thermal state of that floor at specific instants in time.

[1] In the graphics, a concrete floor slab is labeled with the number of its floor. The beams that support t he slab are labeled with the number of the floor below. Thus, e.g., the 11th floor beams stay cool because there was no fire on the 10th floor, while the 11th floor slab is heated by the fire on the 11th floor.

Floor 7

Figure 10–5 and Figure 10–6 show the thermal response of Floor 7 at 12 different instants in time ranging from 12:30 p.m. to 6:00 p.m. at half hour intervals. The perimeter and core columns above the 7th floor were subjected to fires on the 7th floor, while the columns below the 7th floor were subjected to the thermal environment on the 6th floor. The floor beams were also subject to the thermal environment on the 6th floor. As indicated earlier in this Chapter, it is unlikely that there was a significant fire on the 6th floor, so the floor beams and the columns below the 7th floor would have been at about ambient temperature, and the concrete slab would have been subjected to heating only from a fire on the 7th floor on its top face.

Late in the day, the most intense heating was in the northeast sector and the center of the south wall, just east of where there was extensive debris damage.

The thermal response of the perimeter and core columns was highly dependent on the thickness of the insulation, the shape and size of the column, and, to a lesser extent, on the fire growth and spread pattern. The simulated perimeter and core columns were covered with a mean insulation thickness of 22 mm (7/8 in.), which results in only a very moderate increase in the temperature of the columns. The maximum temperature in the perimeter and core column simulations at 6:00 p.m. was 100 ºC to 200 ºC.

The 100 mm (4 in.) thick concrete slab was protected by 9.5 mm (3/8 in.) thick insulation on its bottom face. The top surface of the concrete slab indicated very high temperatures, above 675 ºC, during the course of the simulation. Since the concrete slab had very low thermal conductivity, there was a sharp temperature gradient through the thickness of the concrete slab. The computed temperatures on the bottom of the slab and in the floor beams were barely above ambient.

Floor 8

Figure 10–7 and Figure 10–8 show the analogous thermal response of Floor 8 at 12 different instants in time ranging from 12:30 p.m. to 6:00 p.m. at half hour intervals. The pattern of the spread of heated structural components was similar to the 7th floor, but the temperature increases were much smaller. This was a result of the fire on the west side of the 8th floor being less intense until mid-afternoon.

During the course of the simulation, the floor beams heated up significantly due to the fire on the 7th floor. Initial heating of the floor beams was observed in the southwest corner at 1:00 p.m. At approximately 2:00 p.m., the floor beams in the northwest corner exhibited temperatures in the range of 500 º to 550 ºC. As the fires evolved and spread on Floor 7, the central portion of the floor beams heated up as observed at 4:00 p.m. Toward the end of the simulation, the fires were concentrated in the northeast corner, in the vicinity of column 79.

The increased temperatures on the top of the floor slab followed the fire as it moved across the north face from west to east. The temperatures in the northeast corner were above 675 ºC near 5:00 p.m.

The insulation on the interior and exterior columns functioned as intended. The steel temperatures rose by less than 100 ºC in the simulation.

Floor 9

Figure 10–9 and Figure 10–10 show the thermal response of Floor 9. The timing and intensity of the floor slab heating relative to the 8th floor heating were consistent with the FDS simulation of the 9th floor fire being the same as for the 8th floor, but delayed by one hour. The column temperatures rose less than 100 ºC. The temperature rise in the floor beams was lower than that on the 8th floor, reflecting the shorter duration 8th floor fire having less time to heat the steel through the insulation layer.

Floor 10

Figure 10–11 and Figure 10–12 show the thermal response of the 10th floor. Due to the absence of a fire on this floor, the floor slab and the columns were heated only by conduction and remain relatively cool. The peak floor beam temperatures, resulting from the fire on the 9th floor, did not exceed about 400 ºC.

Floor 11

Figure 10–13 and Figure 10–14 show the thermal response of the 11th floor. In Figure 10–14, the cold floor beams reflected the absence of a fire on the 10th floor. The fire on the 11th floor caused only a modest temperature rise in the insulated columns. The temperature on the top of the floor slab approached 600 ºC on the east side of the floor.

Floor 12

Figure 10–15 shows that the intense fire on this floor resulted in the most severe heating of a floor slab. Peak temperatures reached over 675 ºC on much of the east side and the east portion of the south side of the floor. These temperatures remained high for about 2 h. Figure 10–16 shows that the floor beams, heated by the fire on the 11th floor below, reached similar temperatures in these same locations.

Floor 13

Figure 10–17 shows the severe heating of the top of the 13th floor slab. The temperature pattern was similar to that on the 12th floor slab one-half hour earlier, as expected from the manner in which the 13th floor fire was simulated. The highest column temperatures were about 300 ºC, reflecting the effectiveness of the insulation. Figure 10–18 shows that many of the floor beams in the southeast half of the floor reached temperatures around 600 ºC and remained that hot for over an hour.

The computed thermal response of the perimeter and core columns was highly dependent on the thickness of the insulation, the shape and size of the column, and to a lesser extent, on the fire growth and spread pattern. The perimeter and core columns were covered with a mean fireproofing thickness of 7/8 in., which resulted in only a very moderate increase in the temperature of the columns. The maximum perimeter and core column temperature at 5:00 p.m. was between 100 ºC to 200 ºC, depending on its location.

Floor 14

Figure 10–19 provides an example of the degree of conductive heat transfer through the floor slab. With no fire on the 14th floor, but a severe fire on the 13th floor, the temperature on the top of the slab rose only about 100 ºC by the end of the simulation. The temperature rise in the floor beams in Figure 10–20 was as expected from a fire on the 13th floor that was equal to the 12th floor fire displaced one-half hour earlier.

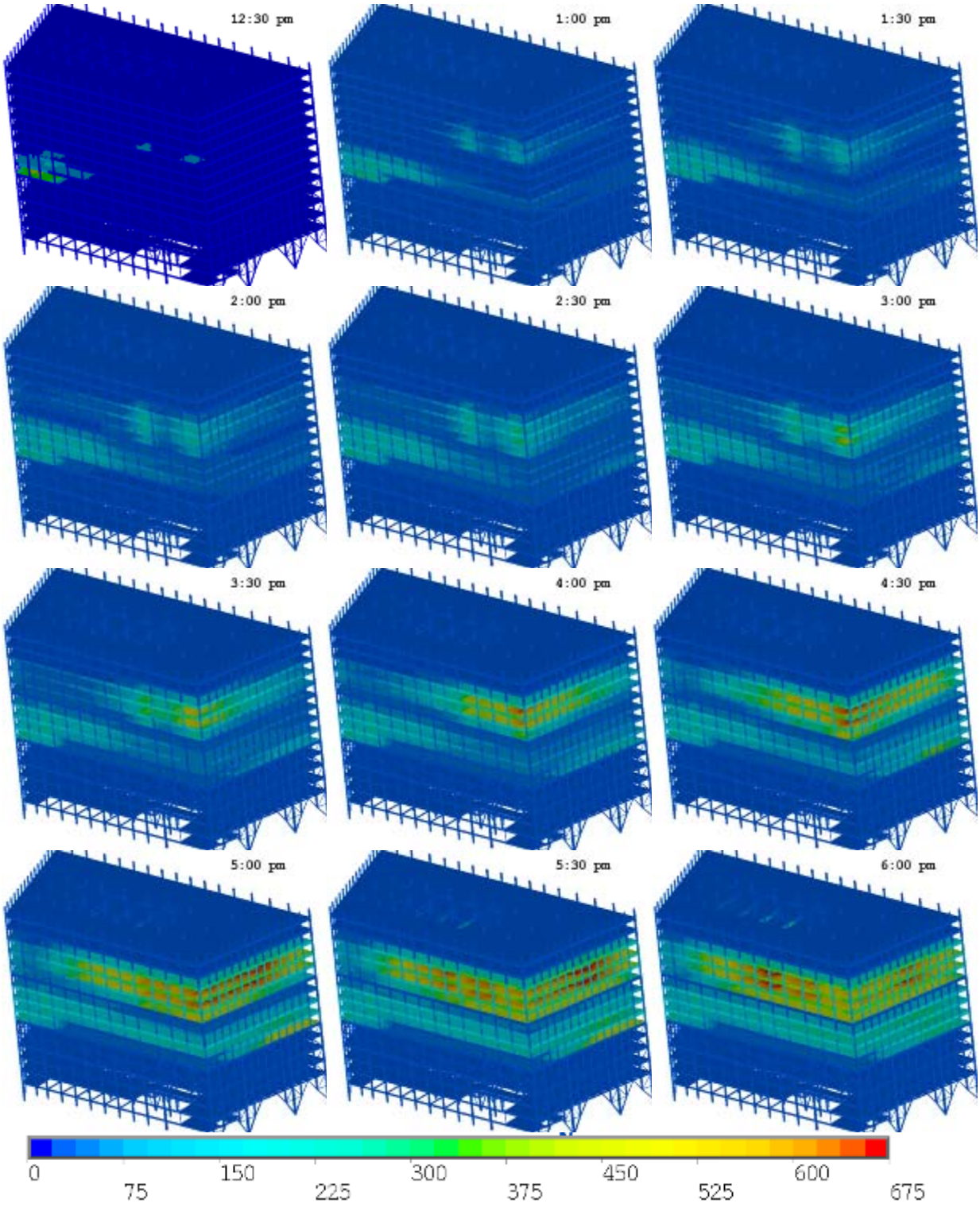

Figure 10–3. View from the southeast of the computed thermal loading of the lower 16 floors of WTC 7 at 12 different instants in time (Case A).

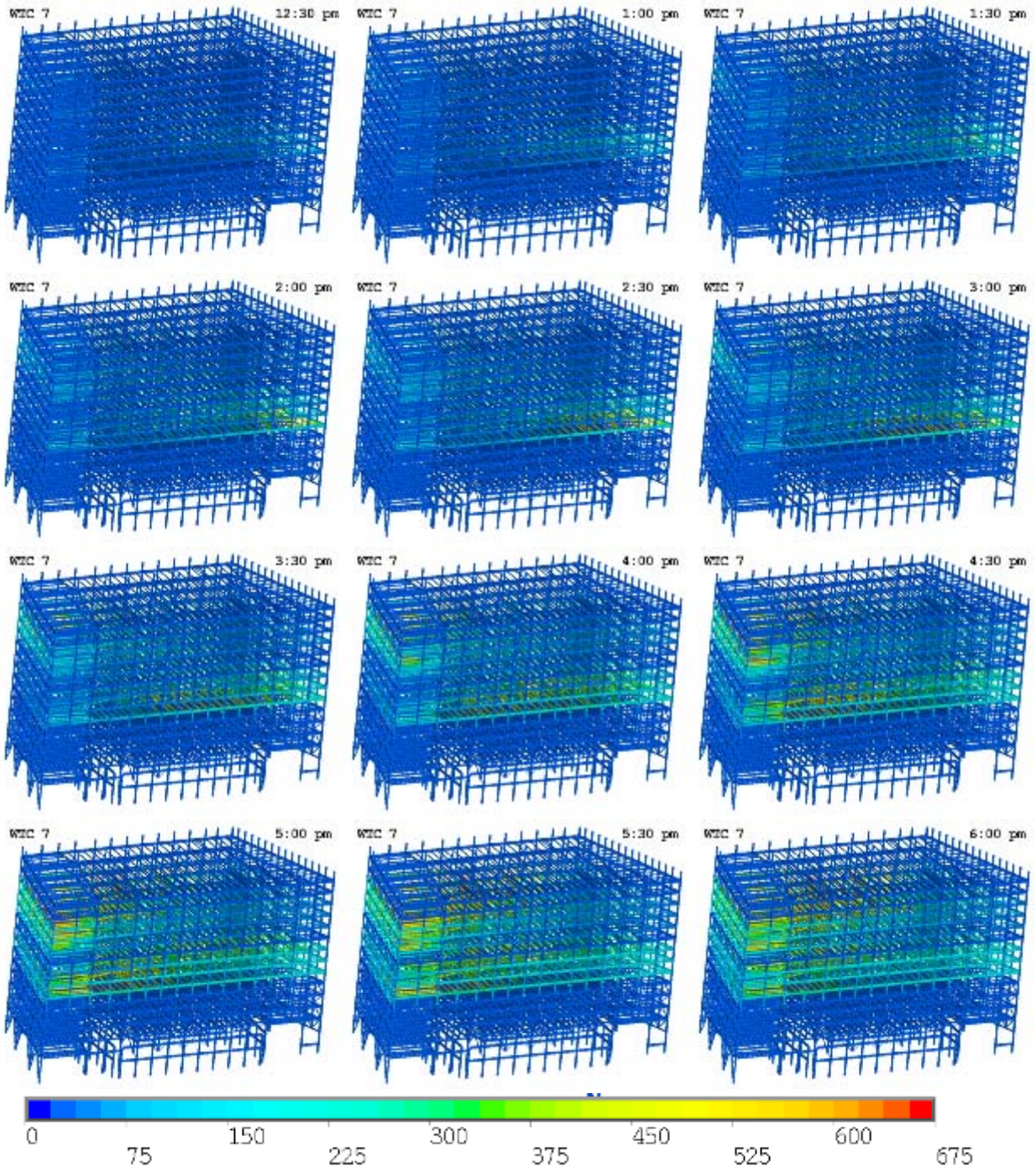

Figure 10–4. View from the northeast of the computed thermal loading of the lower 16 floors of WTC 7 at 12 different instants in time (Case A, floor slabs removed).

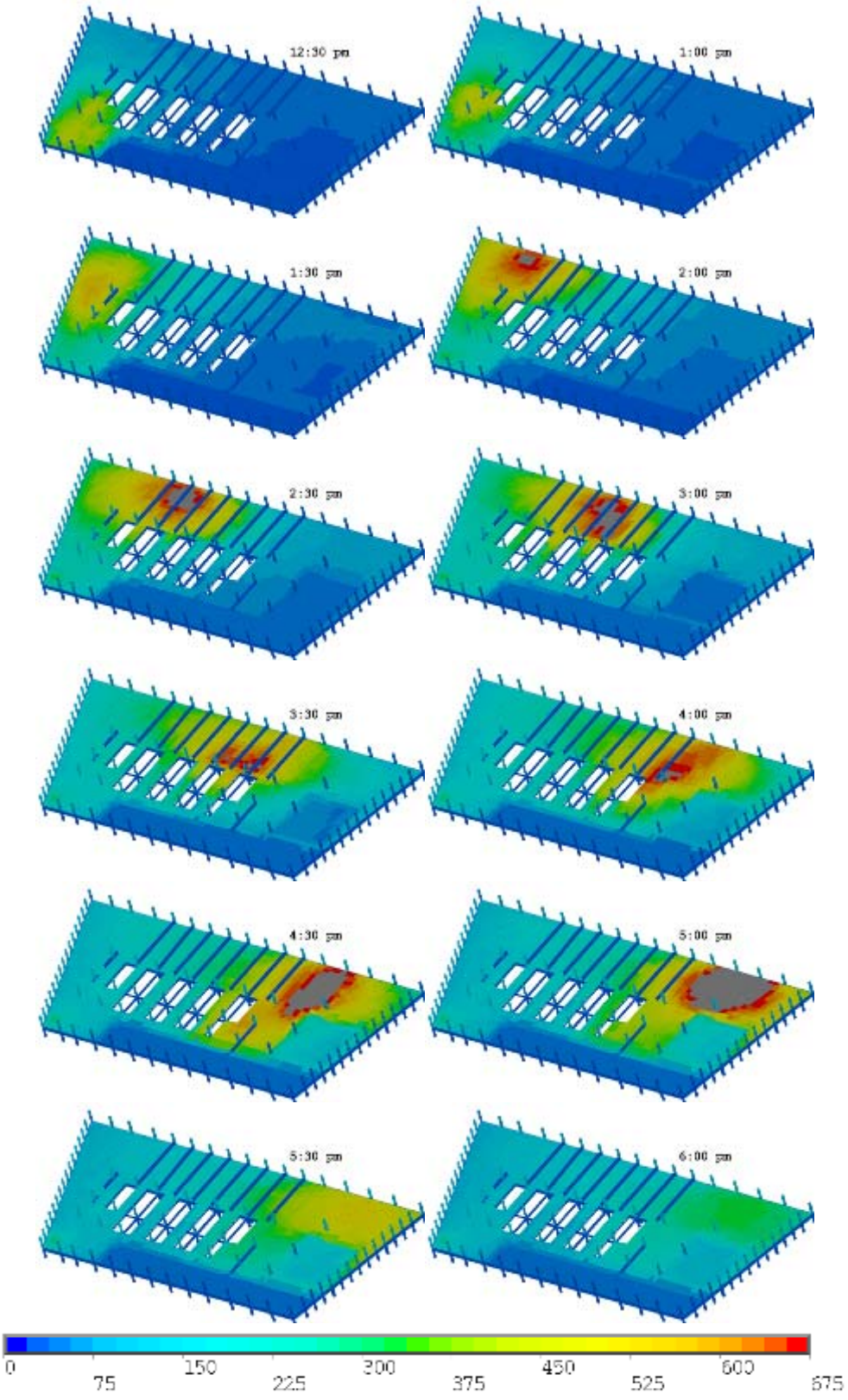

Figure 10–5. Computed temperature distribution (ºC) in the top layer of the concrete slab of Floor 7 at 12 different instants in time (Case A).

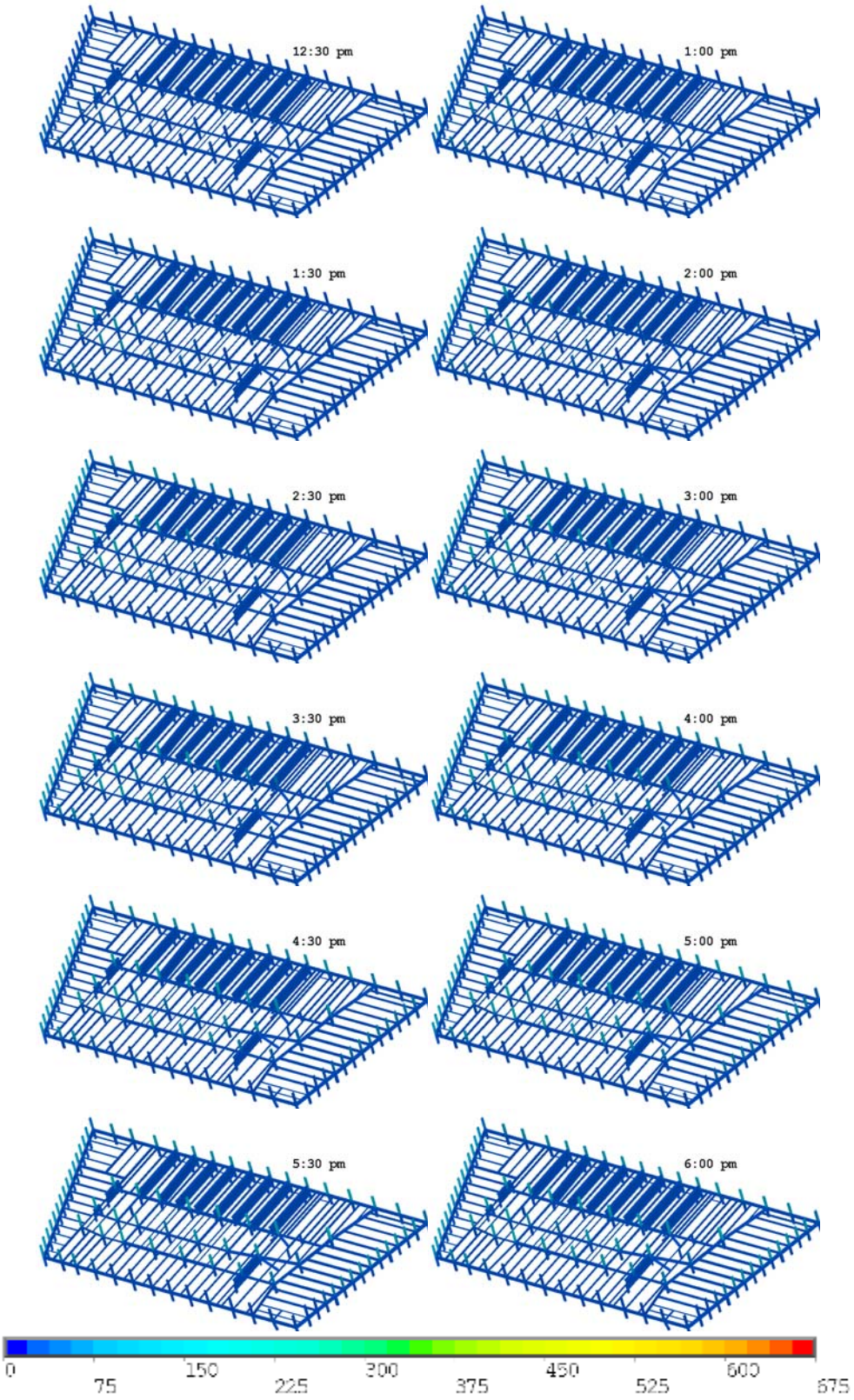

Figure 10–6. Computed temperature distribution (ºC) on the floor beams of Floor 7 at 12 different instants in time (Case A, floor slab removed).

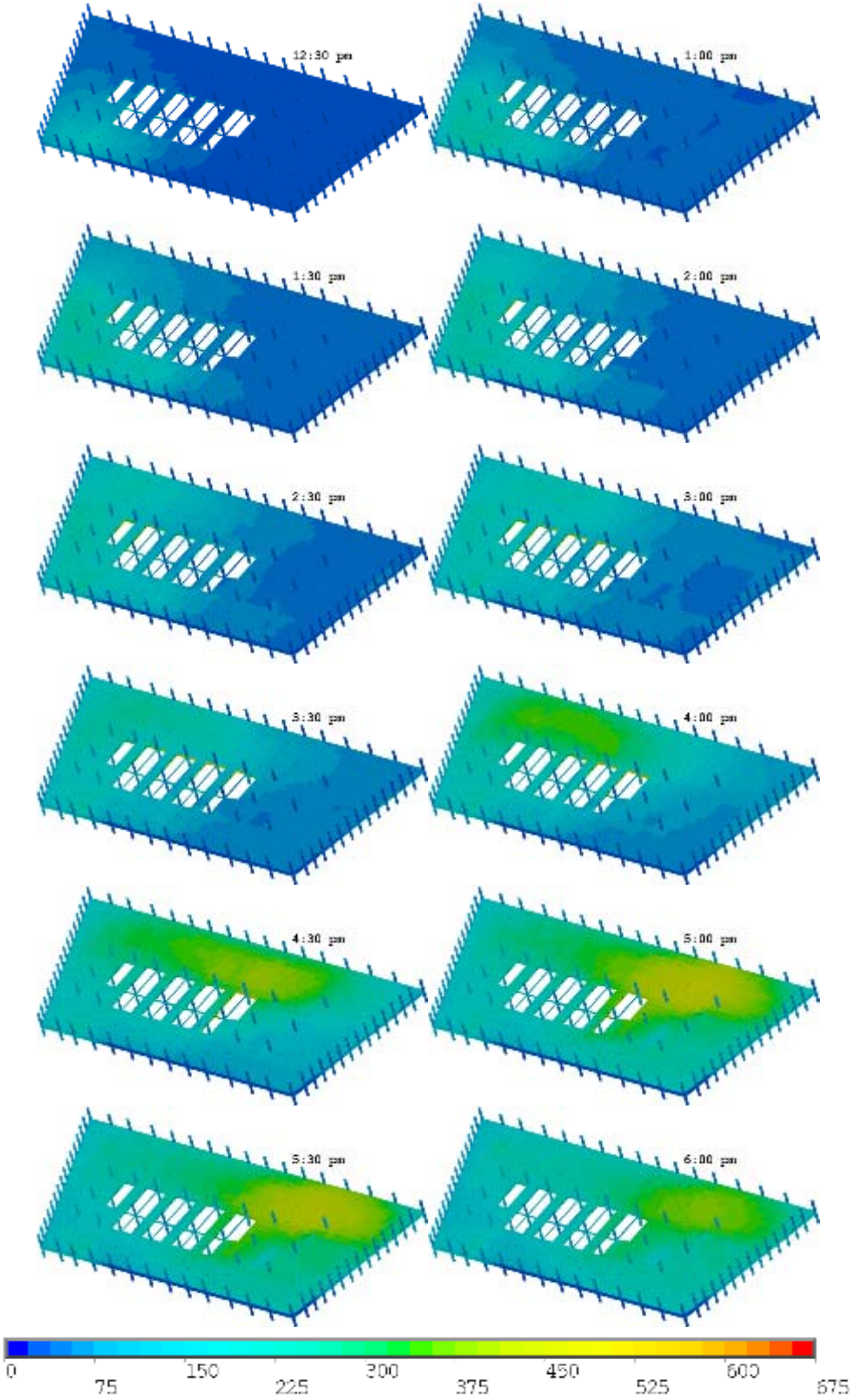

Figure 10–7. Computed temperature distribution (ºC) in the top layer of the concrete slab of floor 8 at 12 different instants in time (Case A).

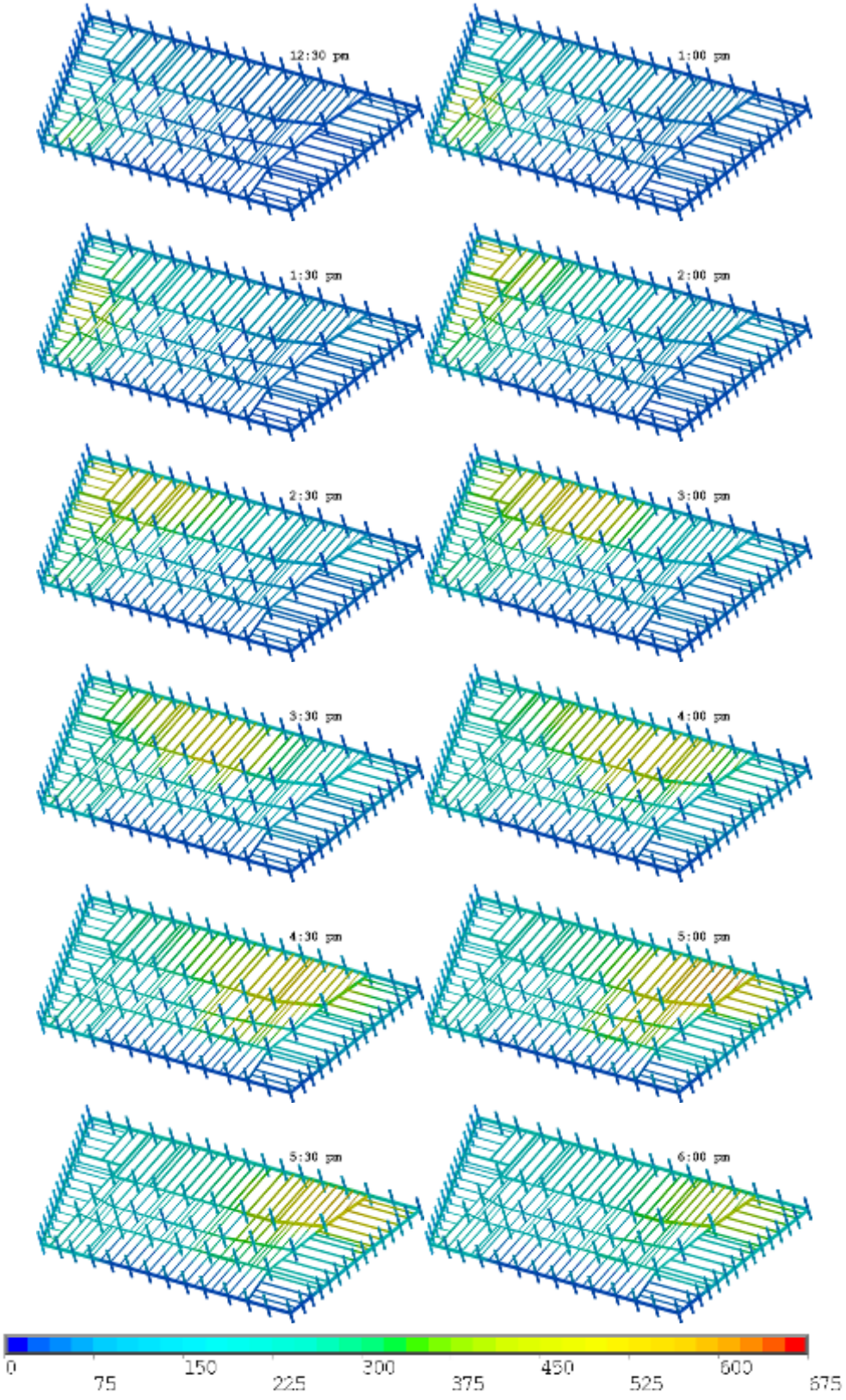

Figure 10–8. Computed temperature distribution (ºC) on the floor beams of floor 8 at 12 different instants in time (Case A, floor slab removed).

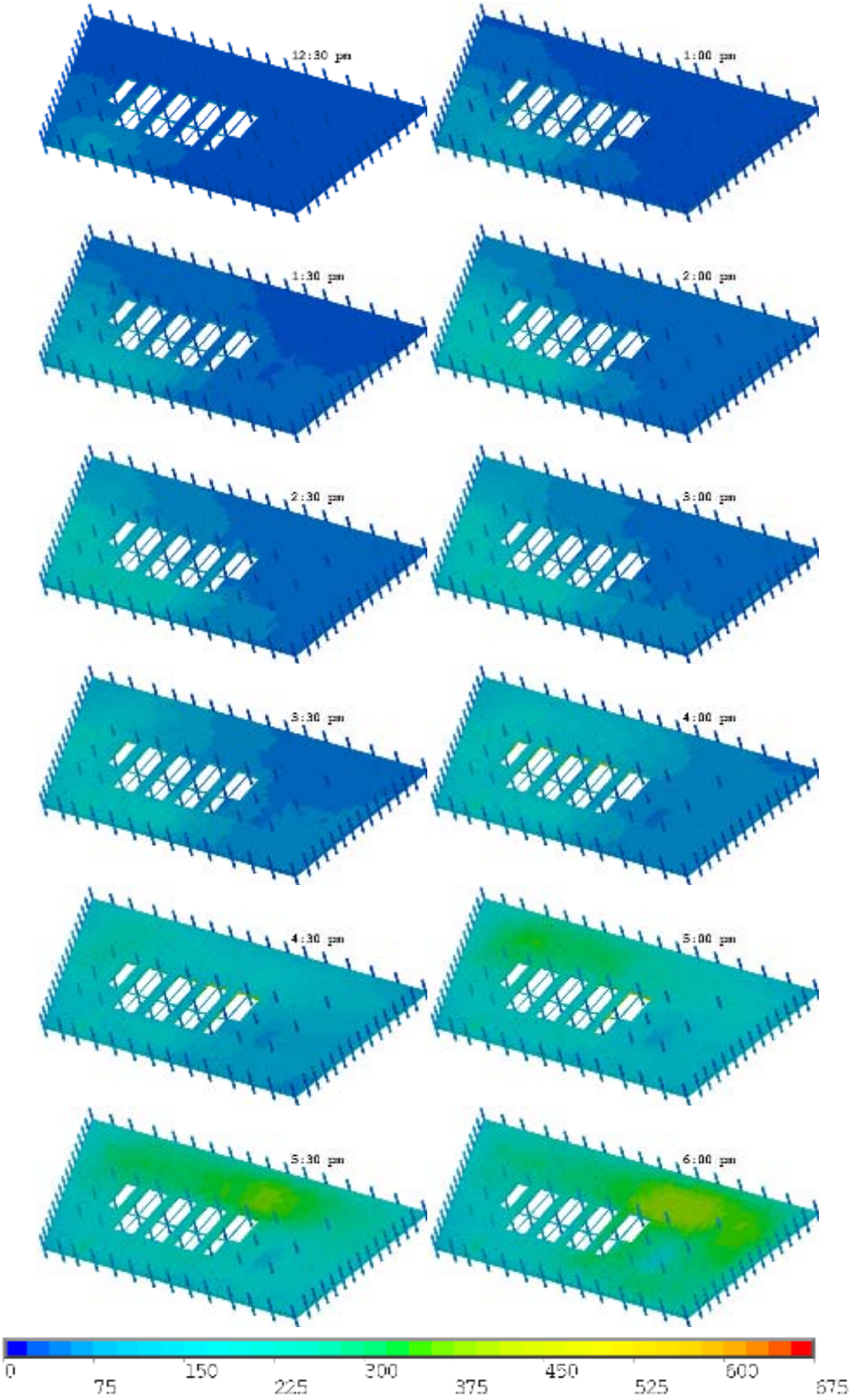

Figure 10–9. Computed temperature distribution (ºC) in the top layer of the concrete slab of floor 9 at 12 different instants in time (Case A).

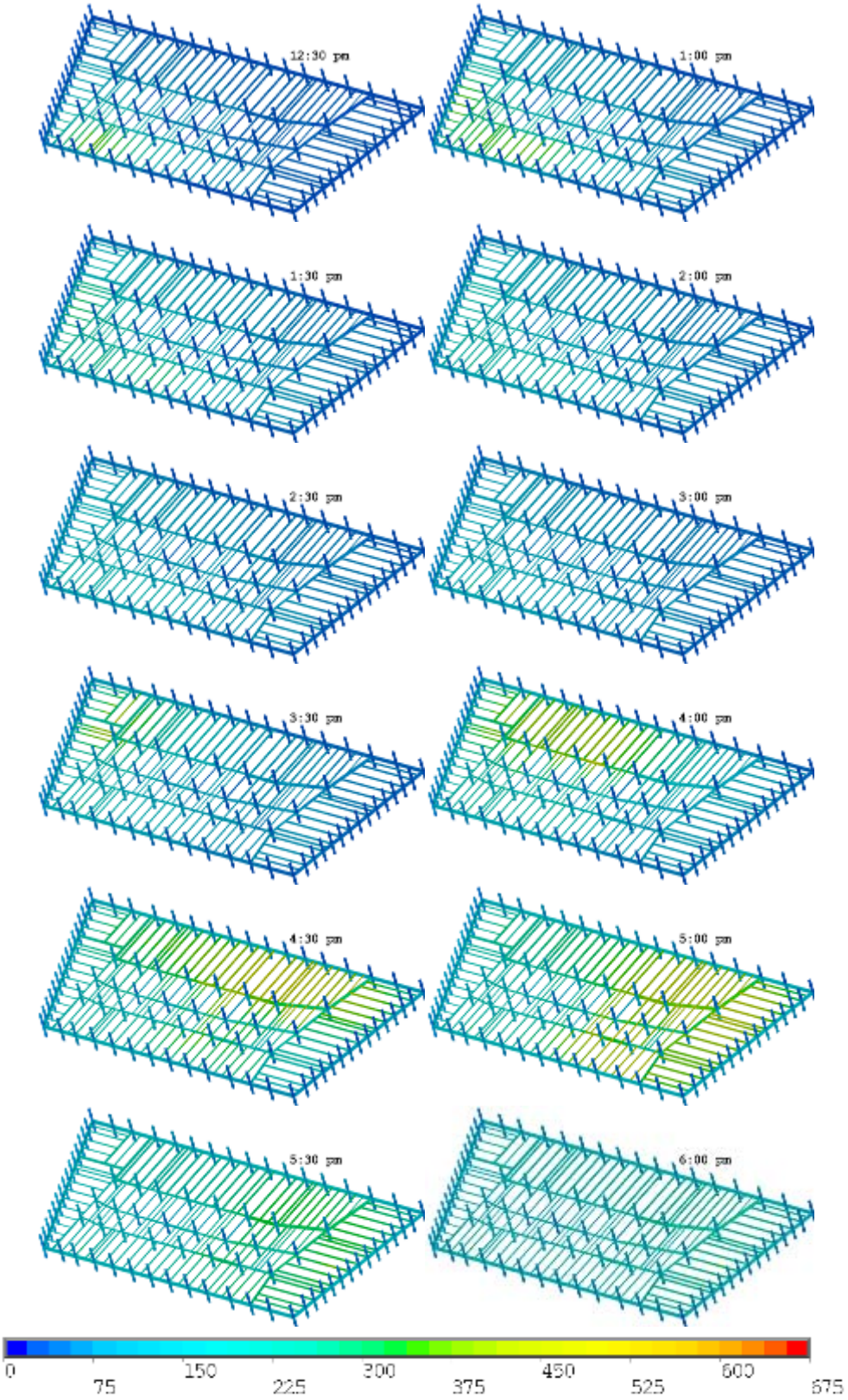

Figure 10–10. Computed temperature distribution (ºC) on the floor beams of floor 9 of WTC 7 at 12 different instants in time (Case A, floor slab removed).

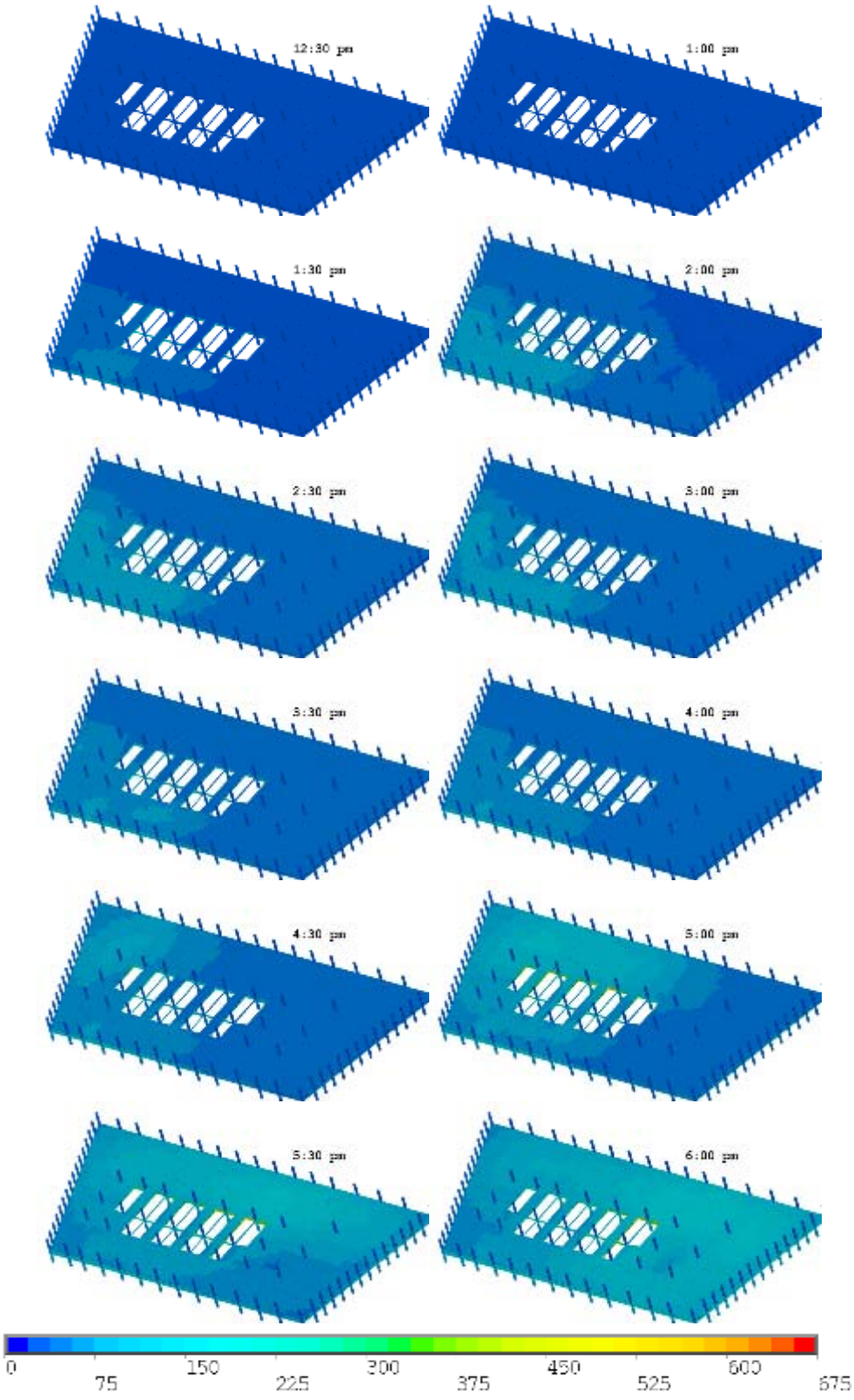

Figure 10–11. Computed temperature distribution (ºC) in the top layer of the concrete slab of floor 10 at 12 different instants in time (Case A).

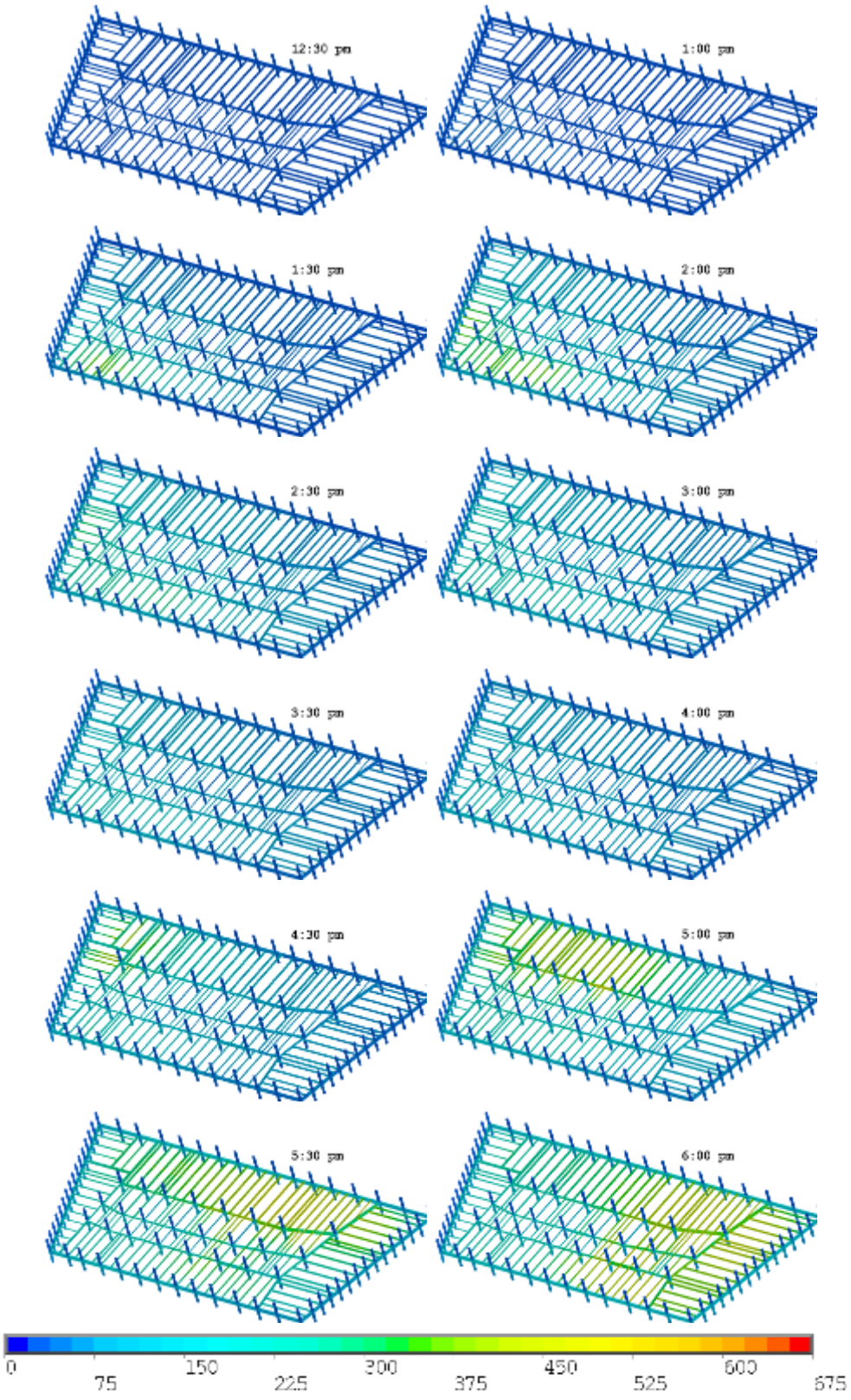

Figure 10–12. Computed temperature distribution (ºC) on the floor beams of floor 10 of WTC 7 at 12 different instants in time (Case A, floor slab removed).

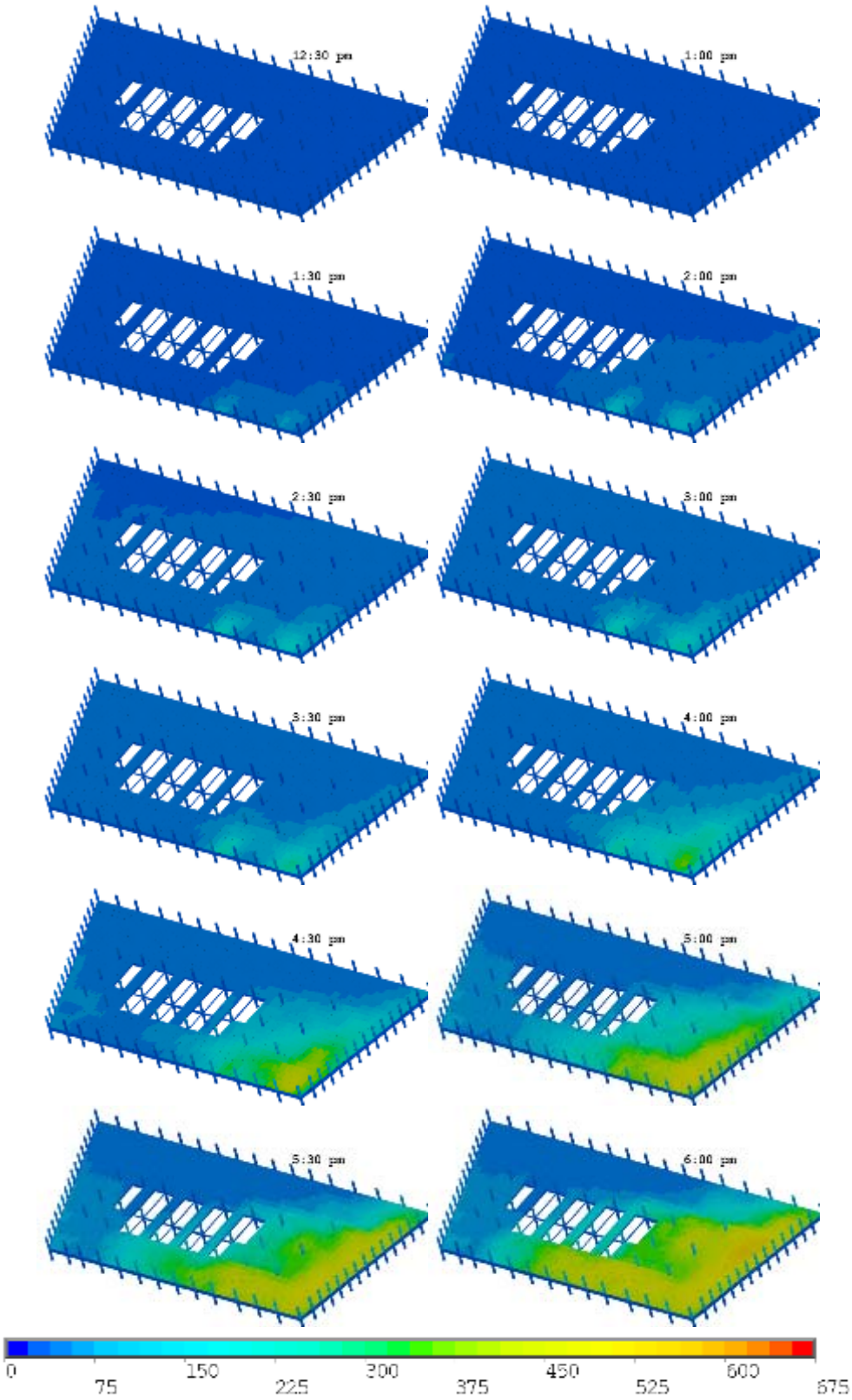

Figure 10–13. Computed temperature distribution (ºC) in the top layer of the concrete slab of floor 11 at 12 different instants in time (Case A).

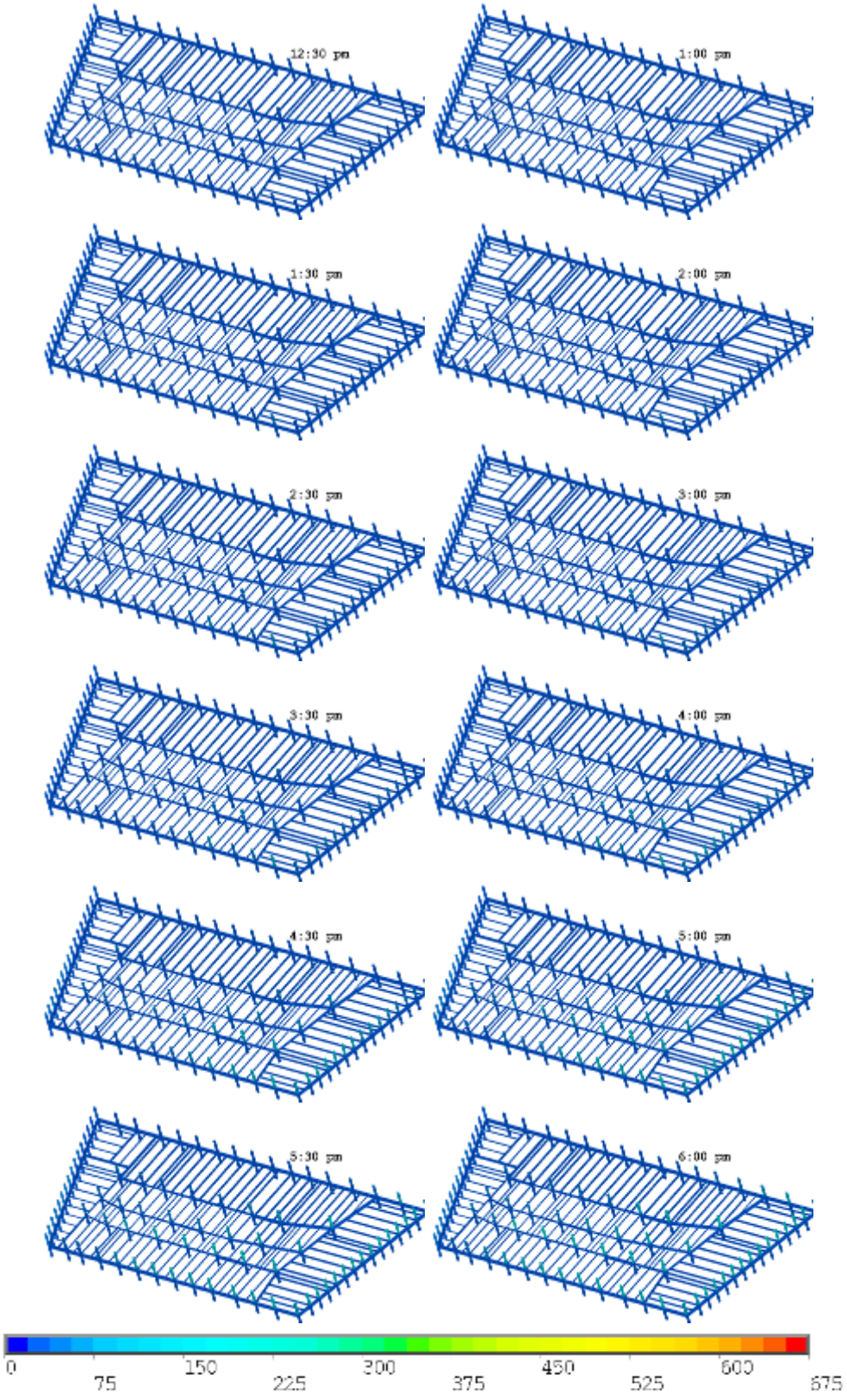

Figure 10–14. Computed temperature distribution (ºC) on the floor beams of floor 11 at 12 different instants in time (Case A, floor slab removed).

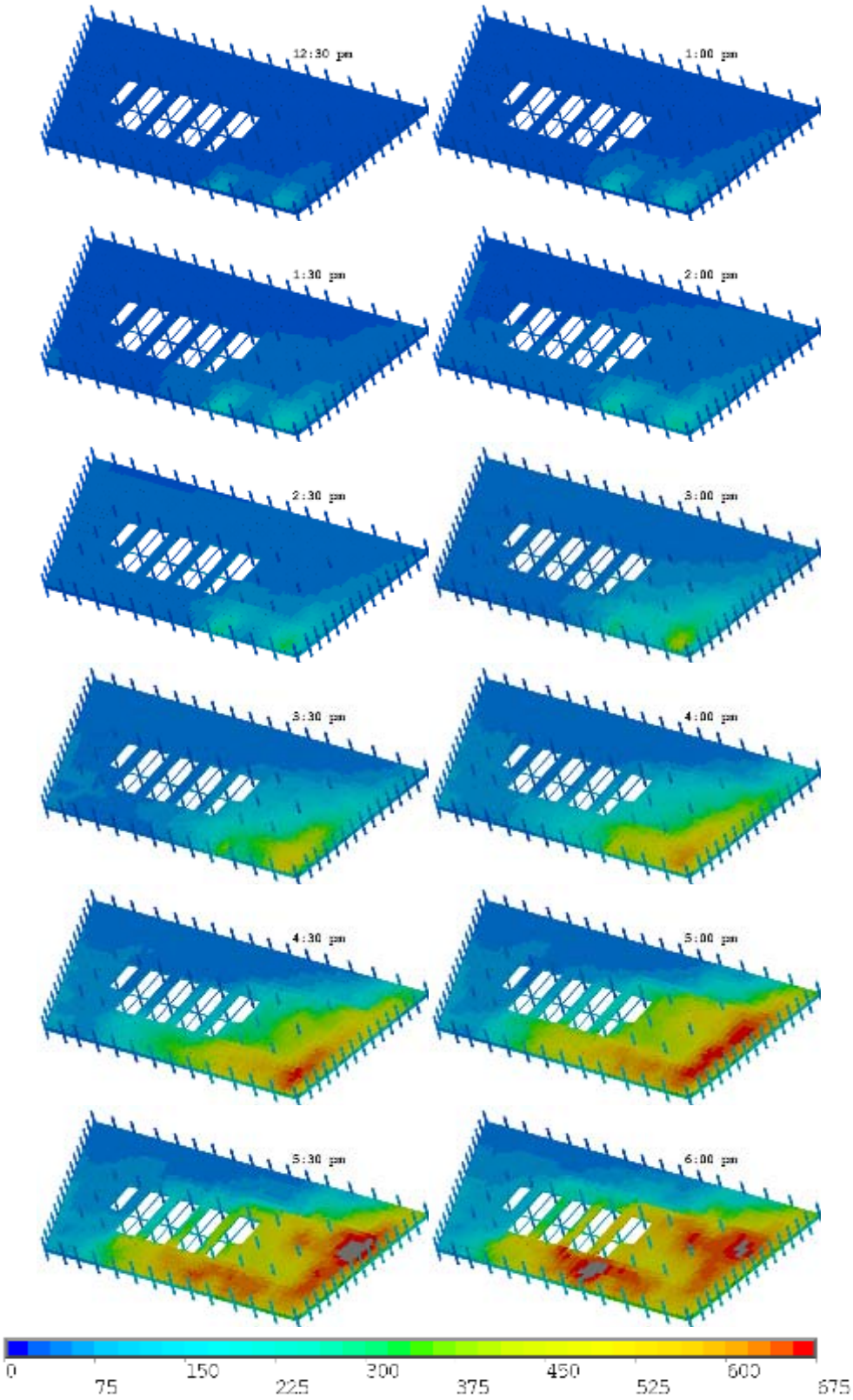

Figure 10–15. Computed temperature distribution (ºC) in the top layer of the concrete slab of floor 12 at 12 different instants in time (Case A).

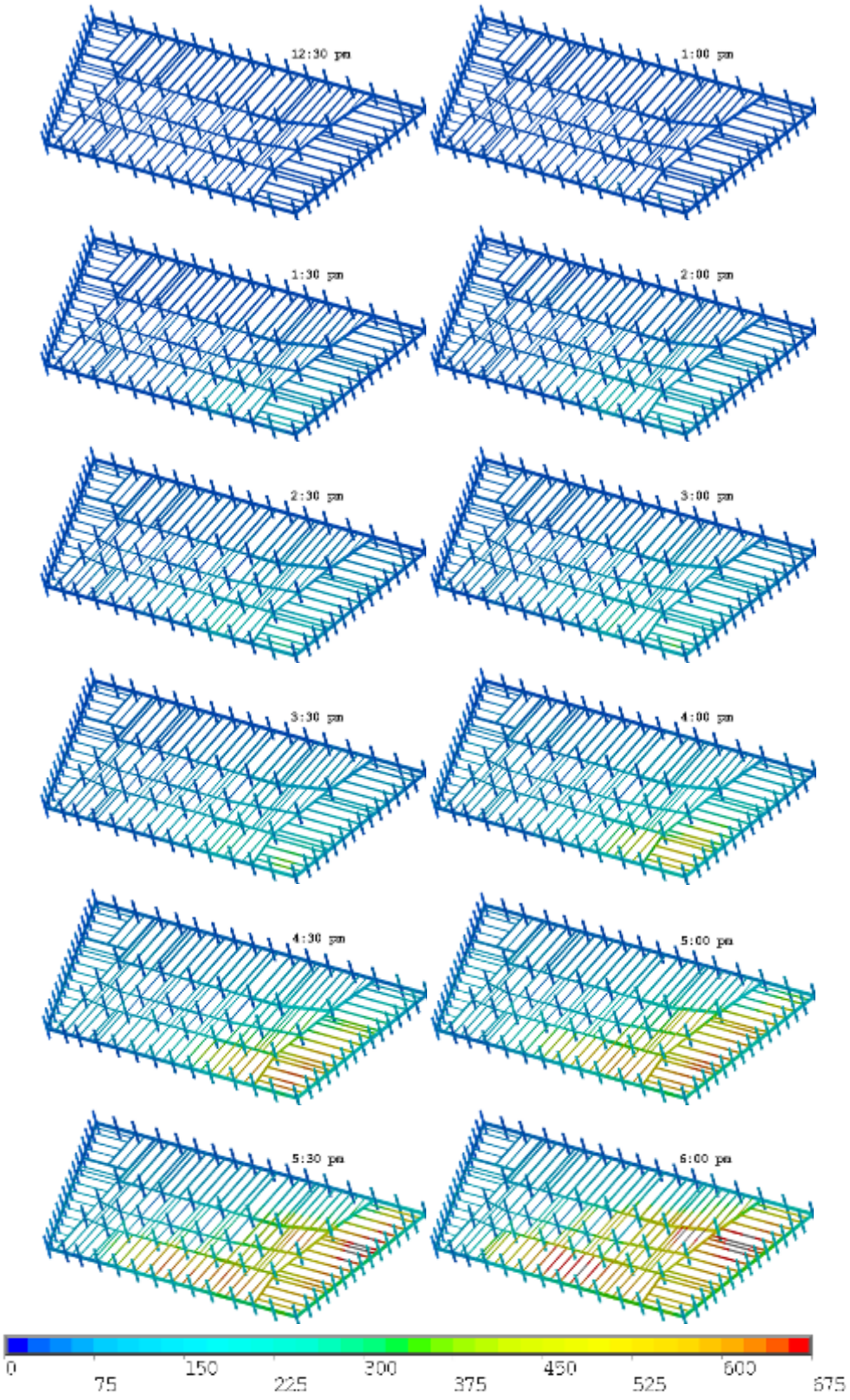

Figure 10–16. Computed temperature distribution (ºC) on the floor beams of floor 12 at 12 different instants in time (Case A, floor slab removed).

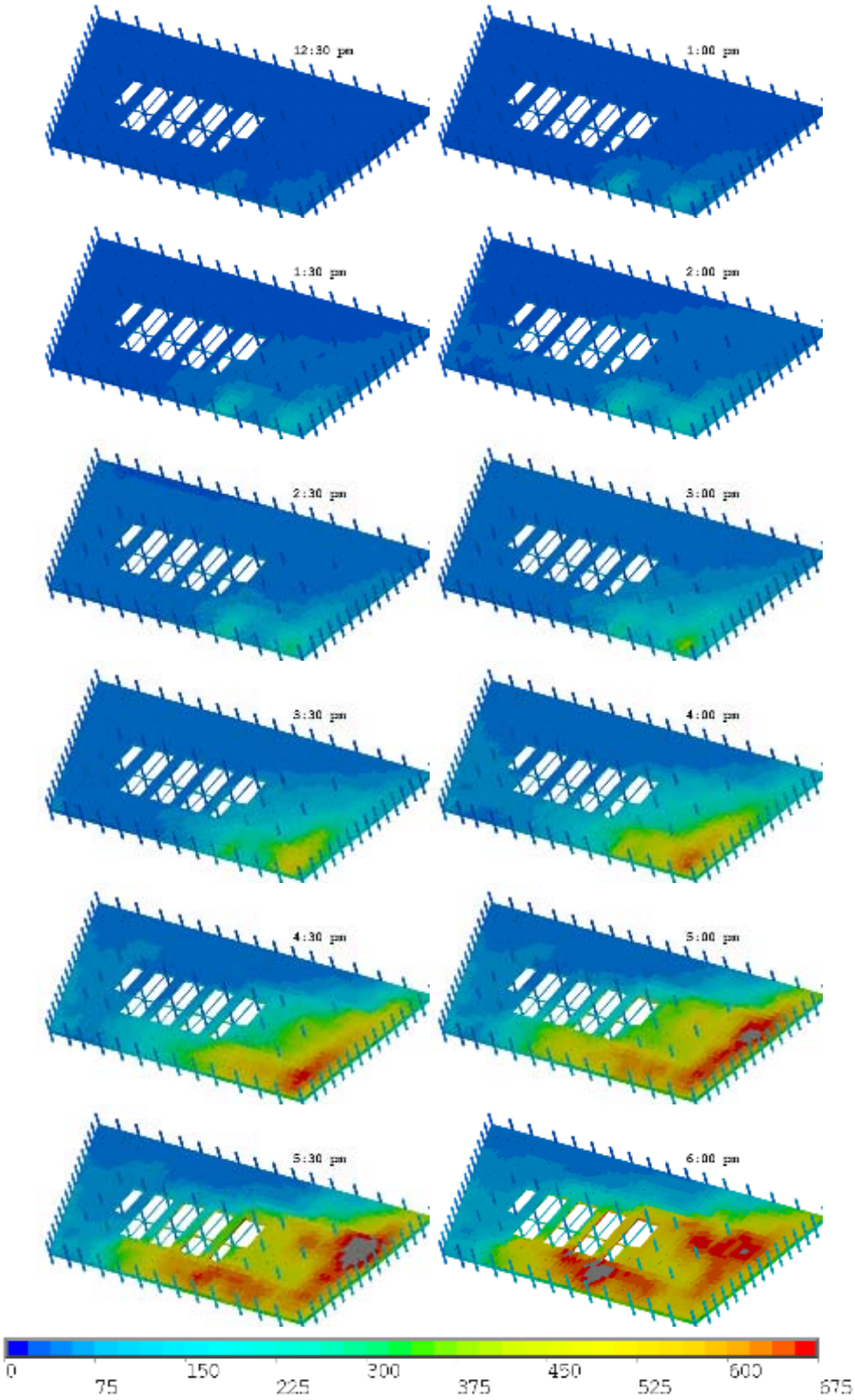

Figure 10–17. Computed temperature distribution (ºC) in the top layer of the concrete slab of floor 13 at 12 different instants in time (Case A).

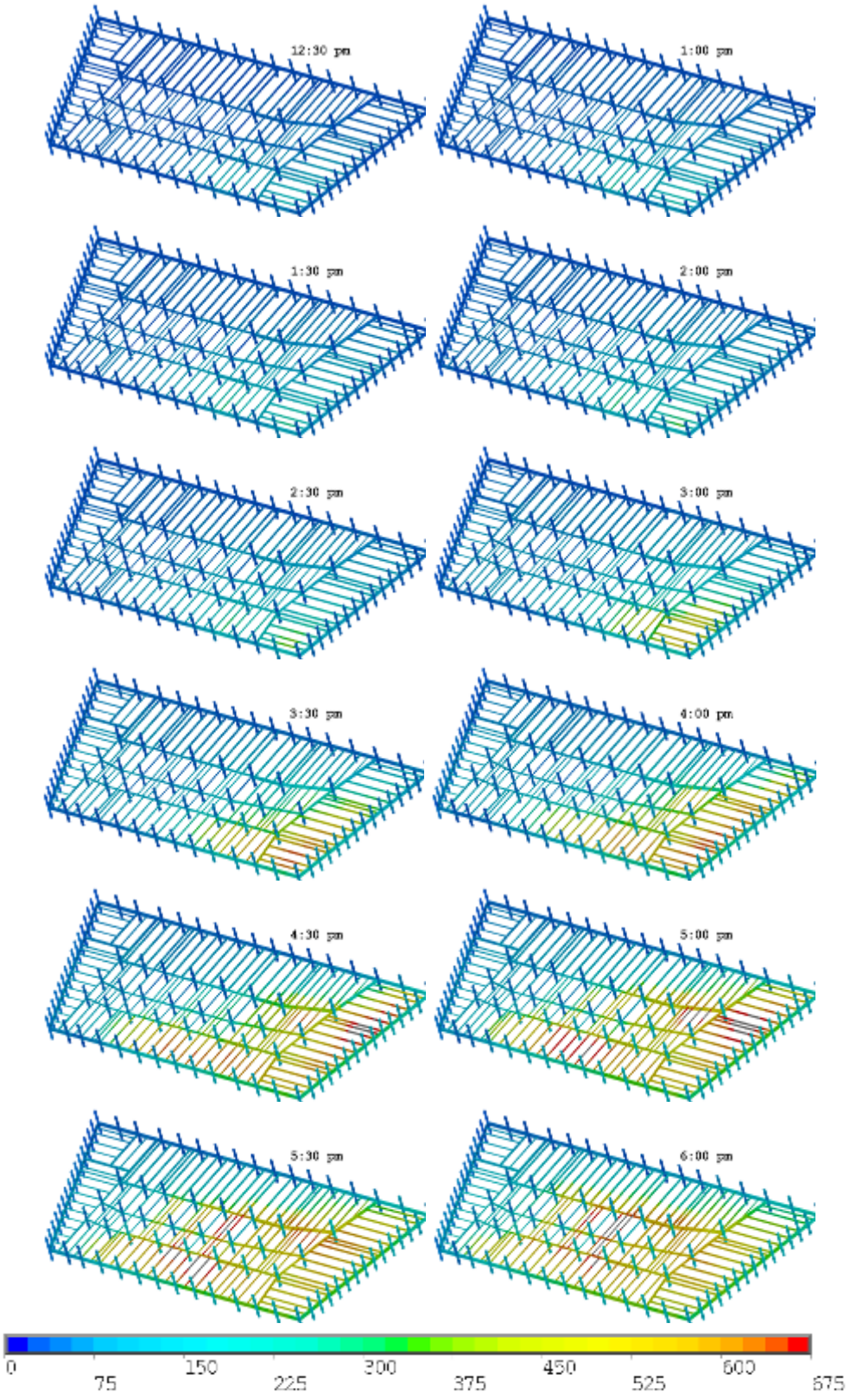

Figure 10–18. Computed temperature distribution (ºC) on the floor beams of floor 13 at 12 different instants in time (Case A, floor slab removed).

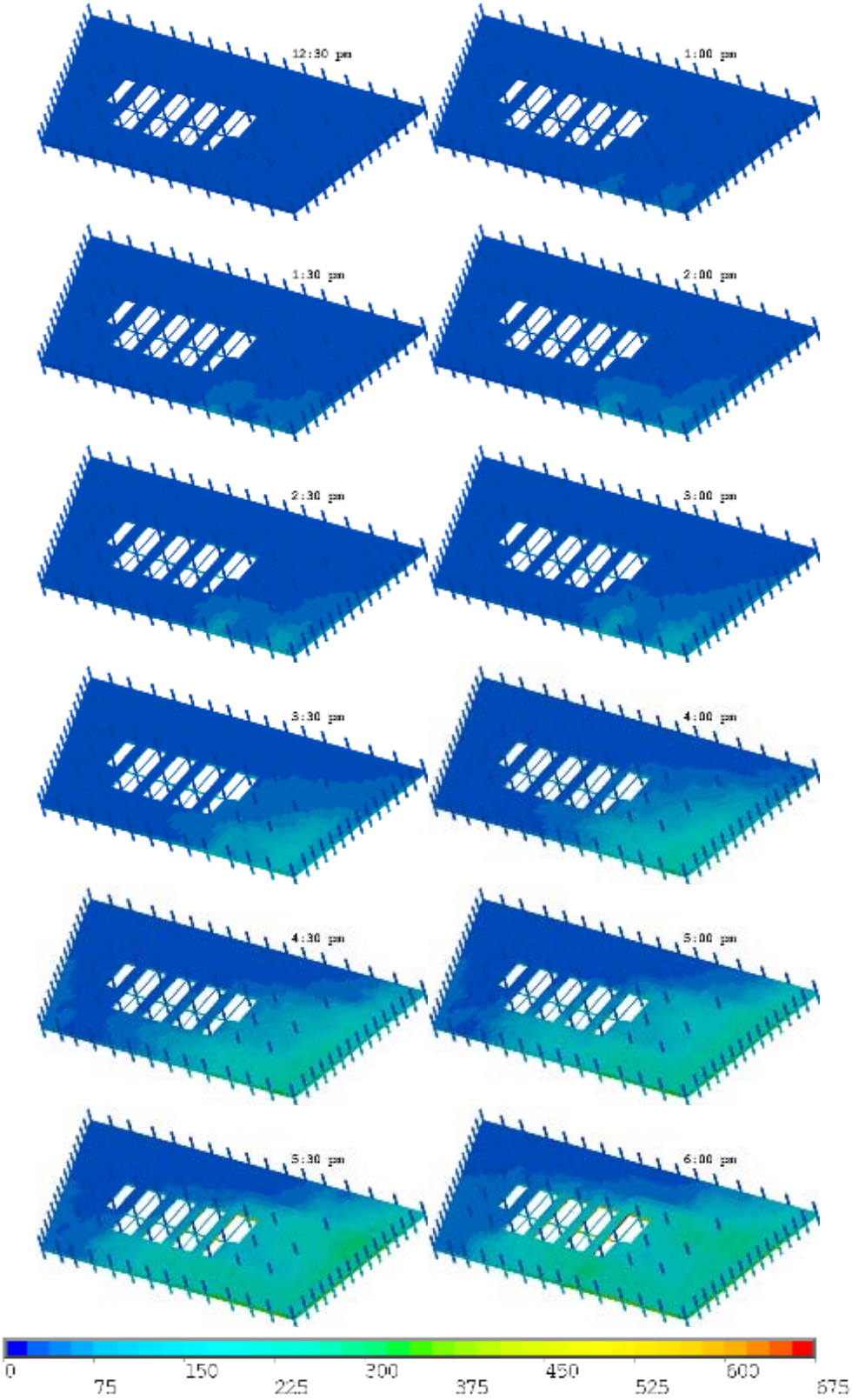

Figure 10–19. Computed temperature distribution (ºC) in the top layer of the concrete slab of floor 14 at 12 different instants in time (Case A).

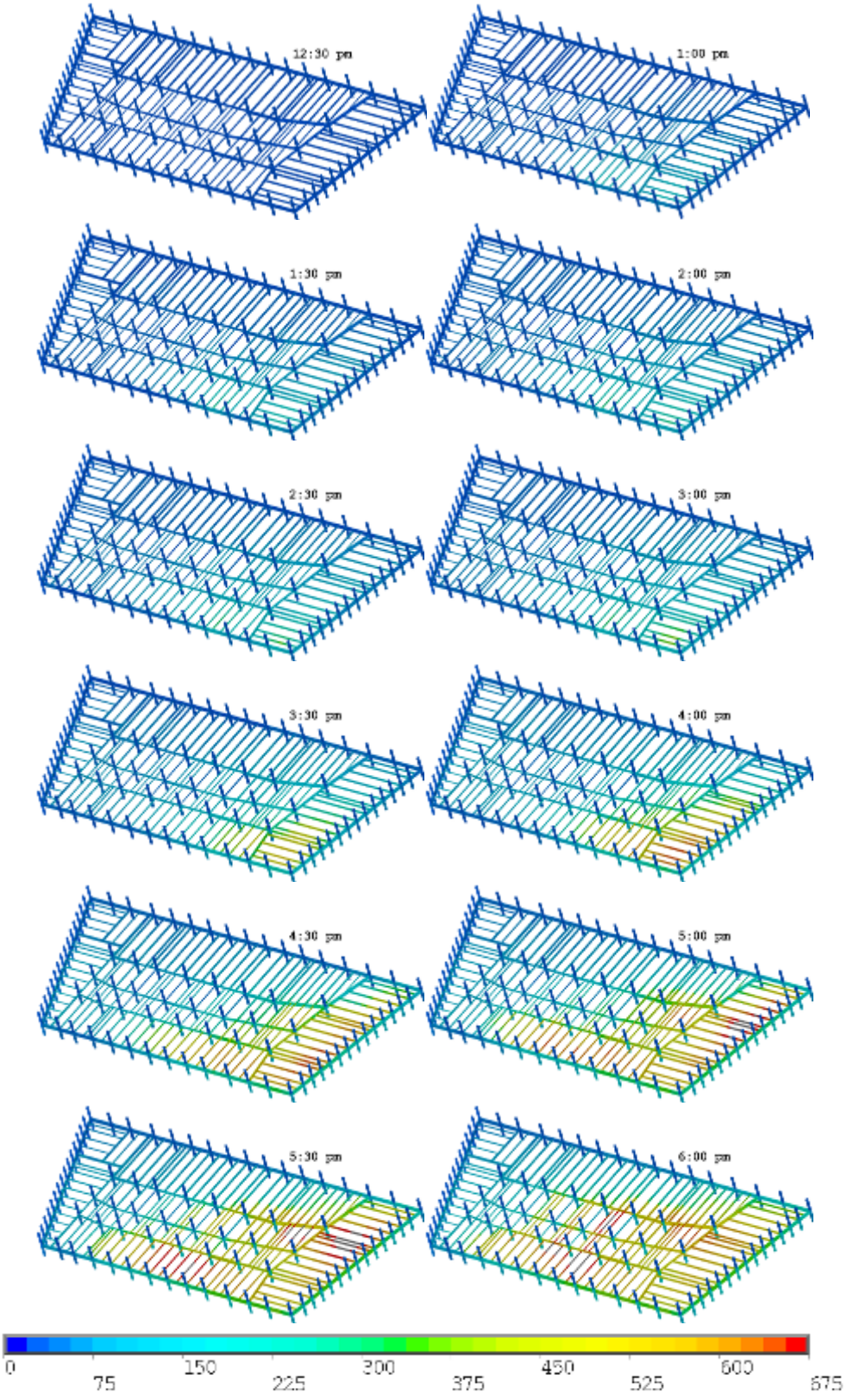

Figure 10–20. Computed temperature distribution (ºC) on the floor beams of floor 14 at 12 different instants in time (Case A, floor slab removed).

10.3.3 Case B

For Case B, the temperature increase at each location on Floors 7 through 14 was assumed to be 10 percent higher than that computed from the FDS simulation of Case A, which was within the expected range of reasonable and realistic fire-generated temperatures. Figure 10–21 and Figure 10–22 compare the temperatures of the building at two times for these two cases. Case A is on the left, and Case B is on the right. As expected, Case B resulted in mildly higher temperatures in the steel and concrete, wider hot zones, and greater overlap of hot zones between adjacent floors.

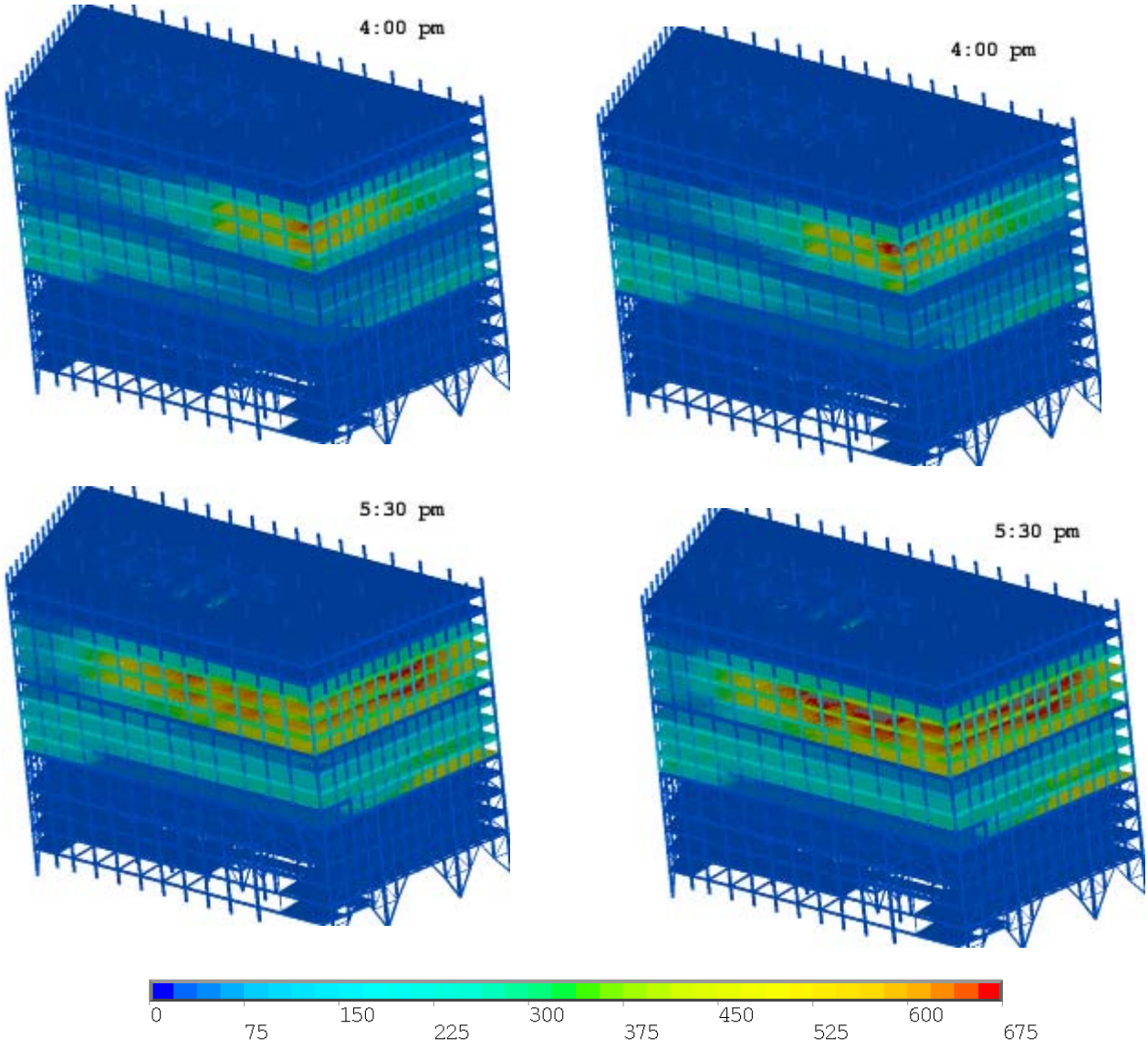

Figure 10–21. View from the southeast of the 16 lower floors of WTC 7, comparing Case A (left) and Case B (right) temperatures at two different times.

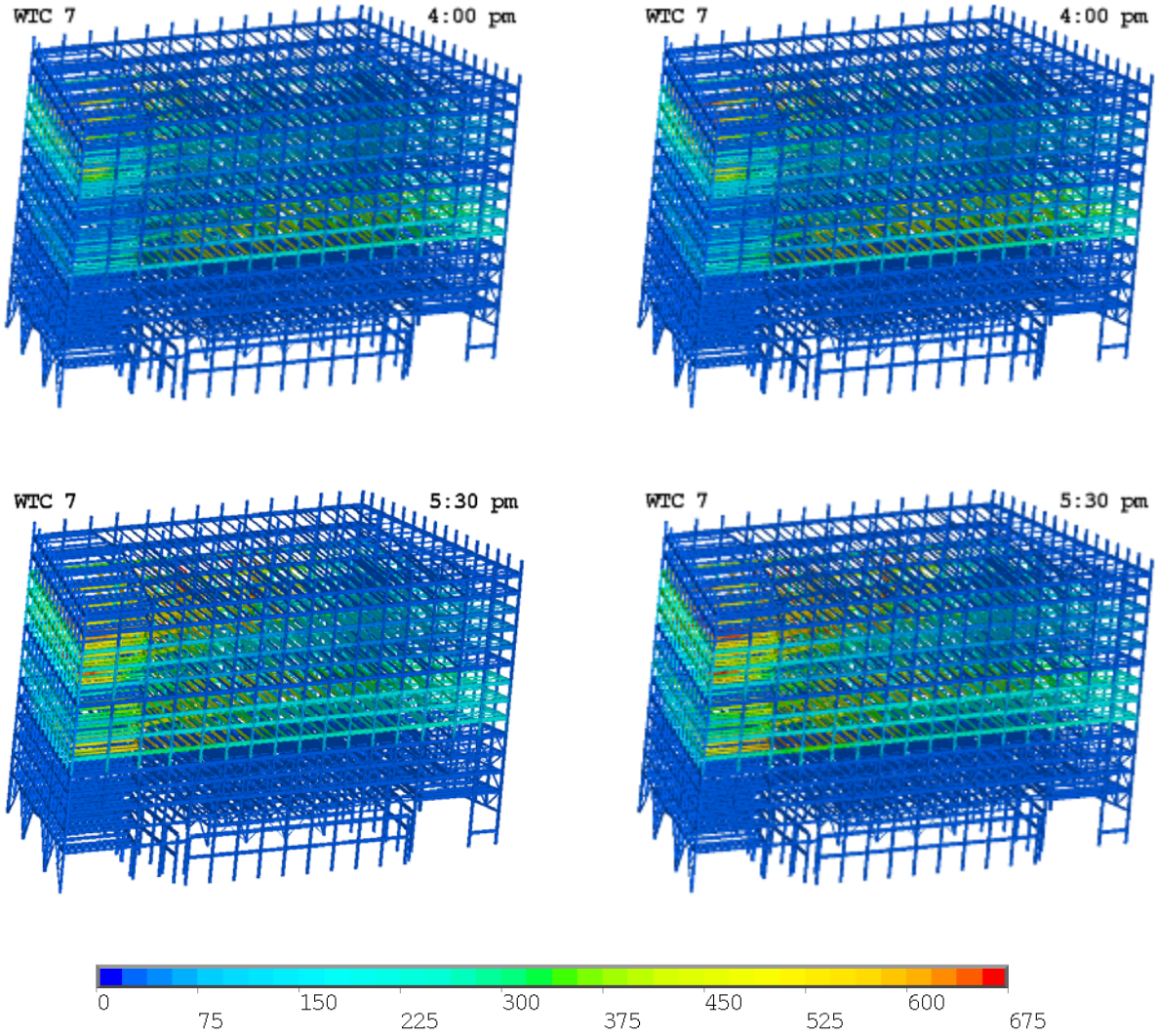

Figure 10–22. View from the northeast of the 16 lower floors of WTC 7, comparing Case A (left) and Case B (right) temperatures at two different times (floor slabs removed).

Figure 10–23 and Figure 10–24 show the full timed Case B sequence from which these examples were drawn. (The Case A sequences were shown in Figure 10–3 and Figure 10–4.) Figure 10–25 through Figure 10–40 show the floor-by-floor heating for Case B.

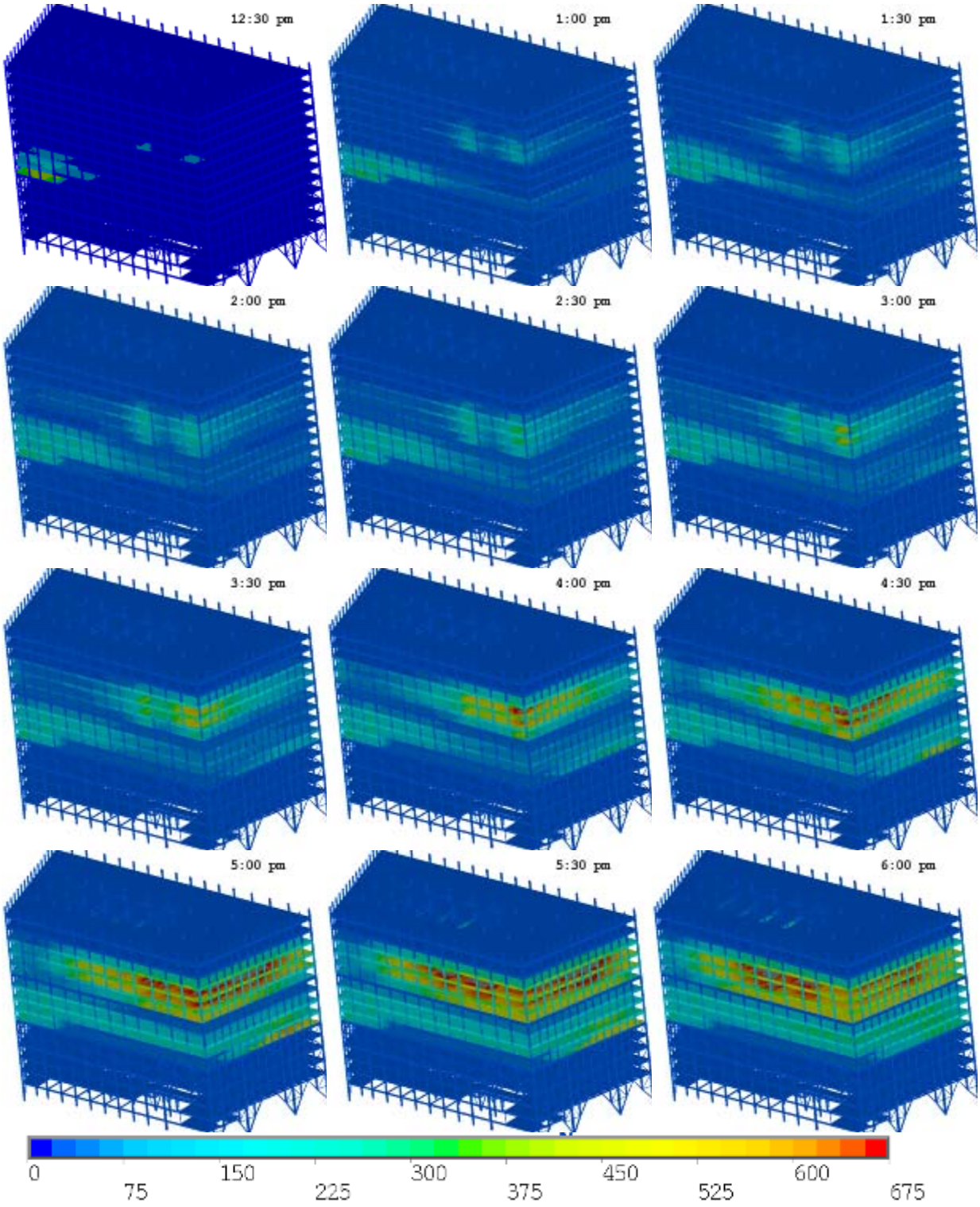

Figure 10–23. View from the southeast of the computed thermal loading of the lower 16 floors of WTC 7 at 12 instants in time (Case B).

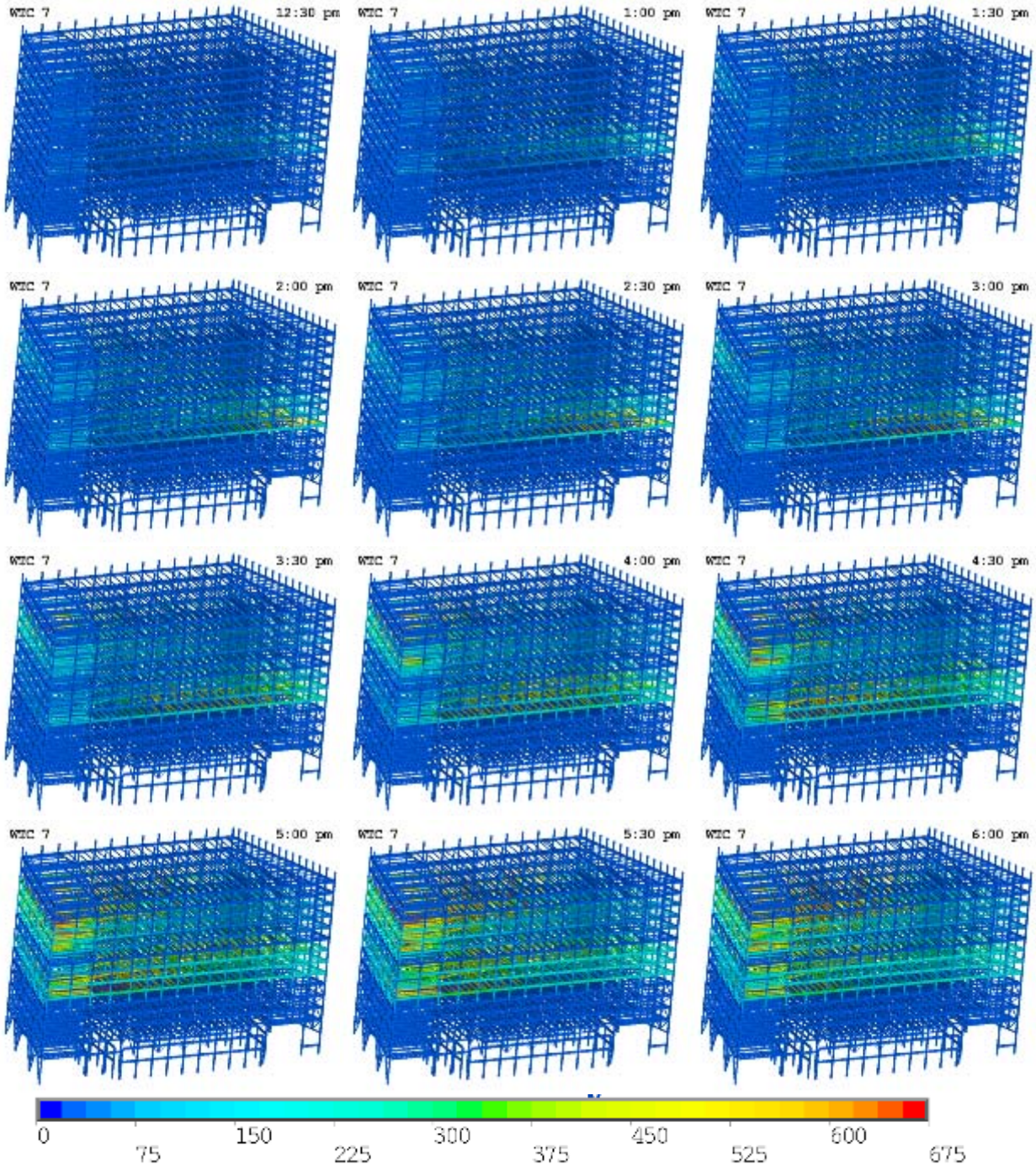

Figure 10–24. View from the northeast of the computed thermal loading of the lower 16 floors of WTC 7 at 12 different instants in time (Case B, floor slabs removed).

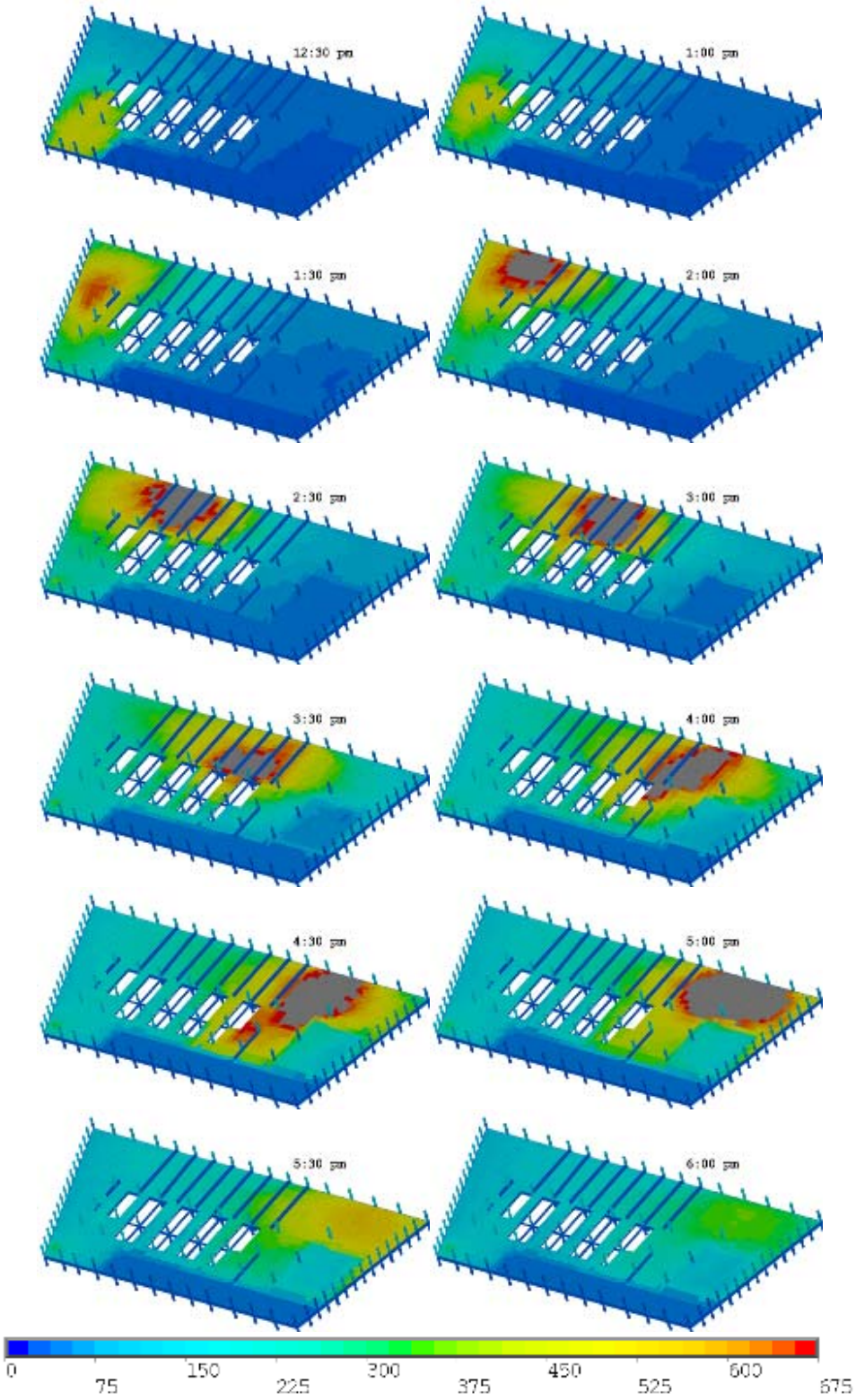

Figure 10–25. Computed temperature distribution (ºC) in the top layer of the concrete slab on floor 7 at 12 instants in time (Case B).

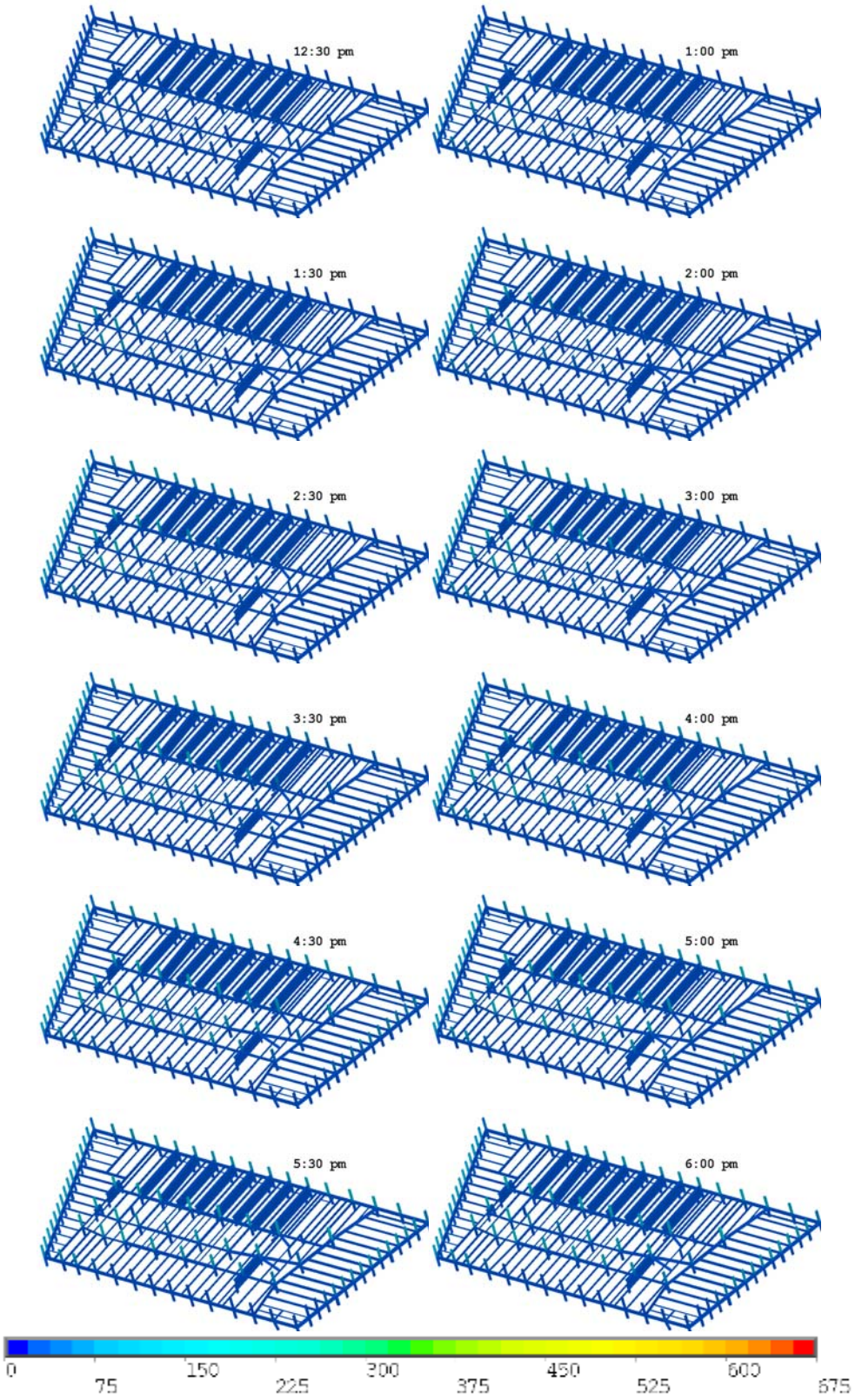

Figure 10–26. Computed temperature distribution (ºC) on the floor beams of floor 7 at 12 different instants in time (Case B, floor slab removed).

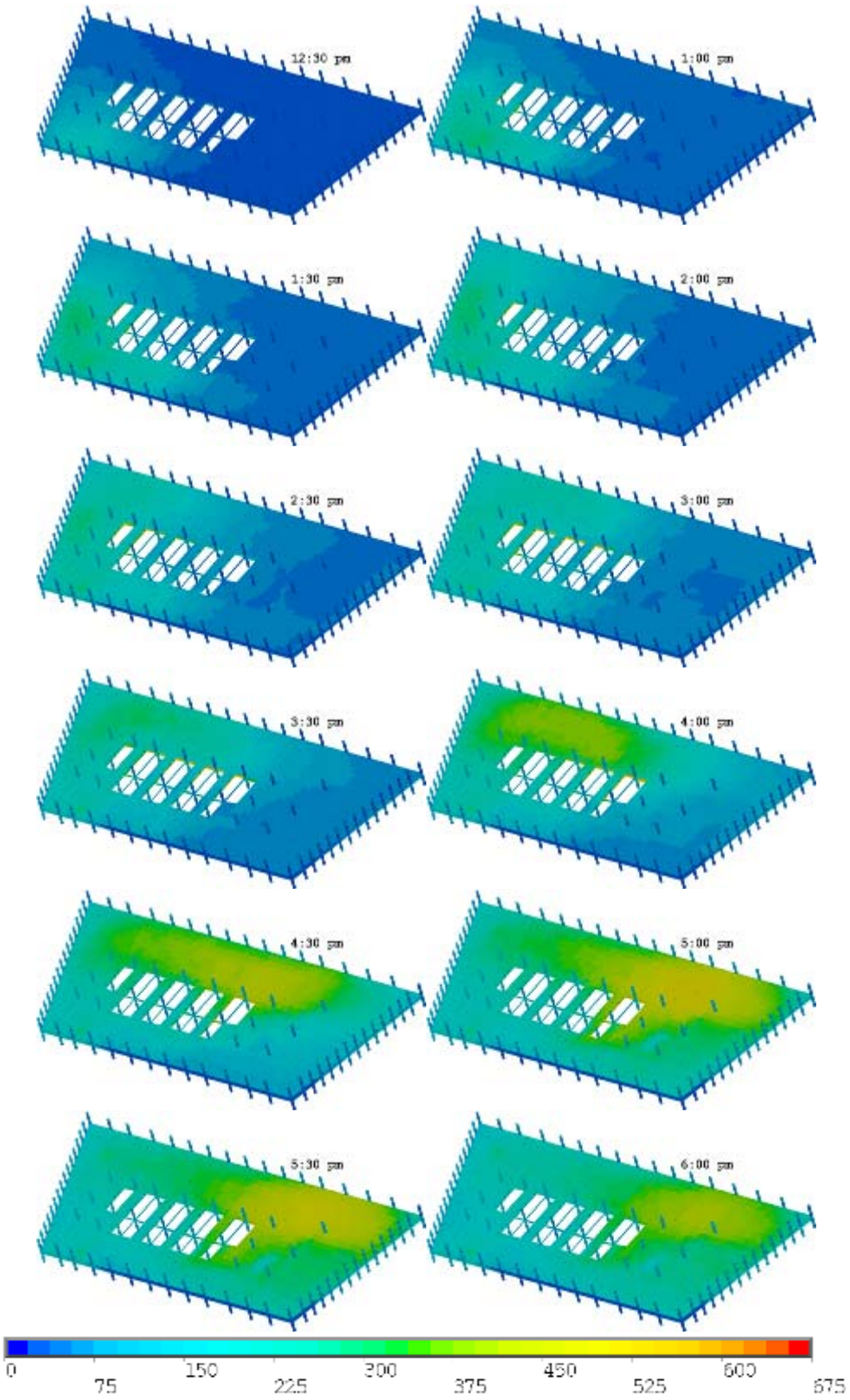

Figure 10–27. Computed temperature distribution (ºC) in the top layer of the concrete slab on floor 8 at 12 instants in time (Case B).

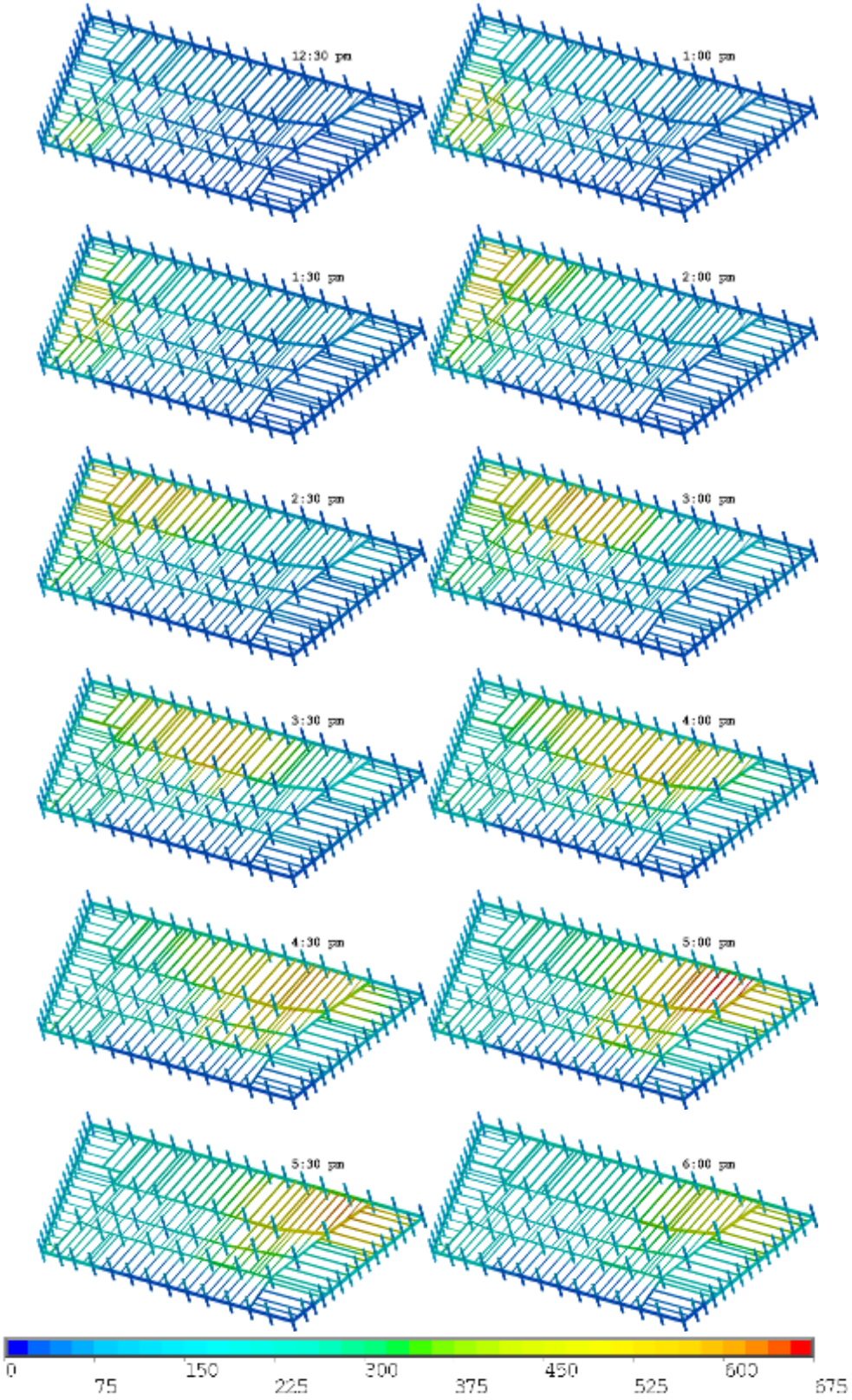

Figure 10–28. Computed temperature distribution (ºC) on the floor beams of floor 8 at 12 different instants in time (Case B, floor slabs removed).

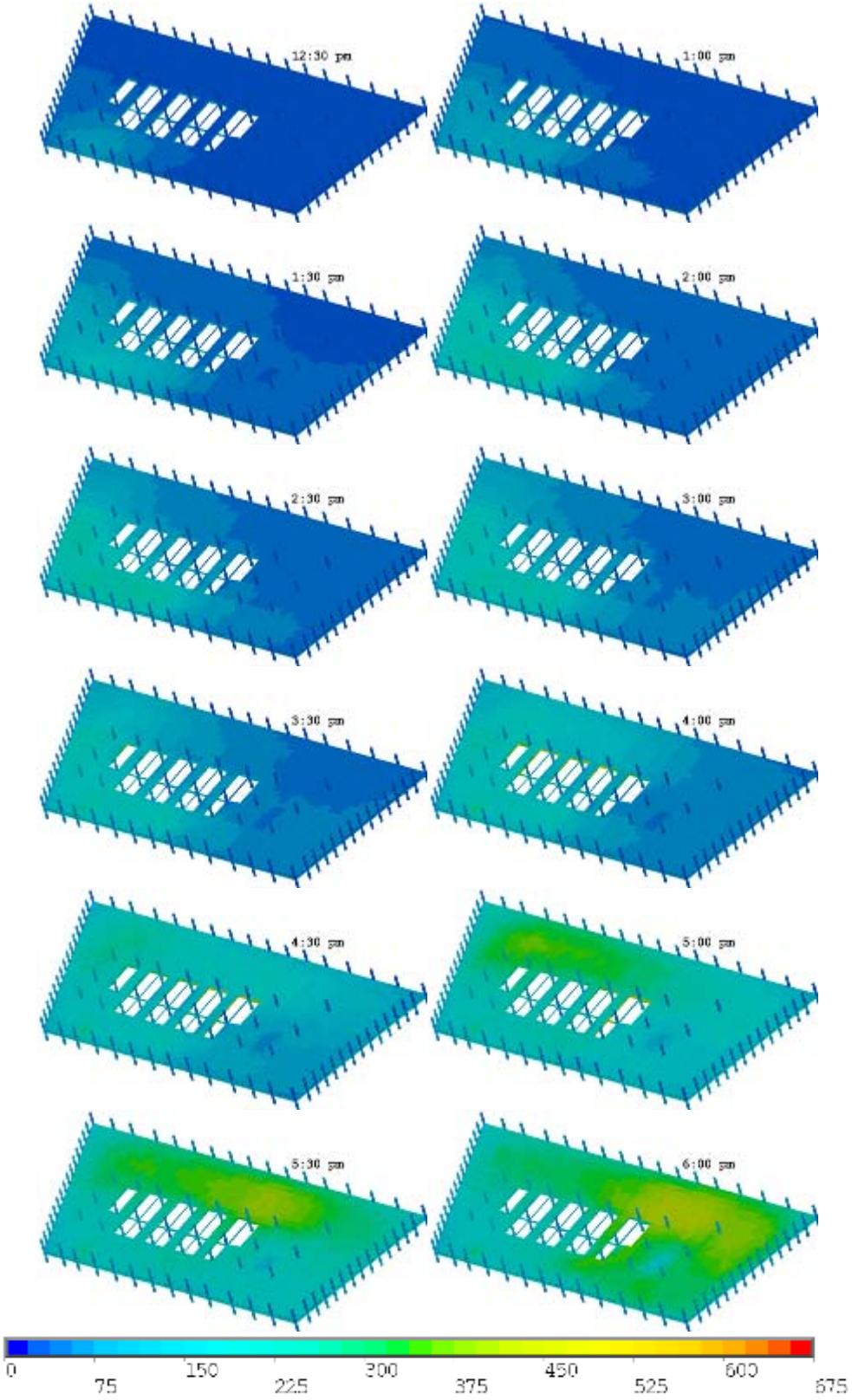

Figure 10–29. Computed temperature distribution (ºC) in the top layer of the concrete slab of floor 9 at 12 different instants in time (Case B).

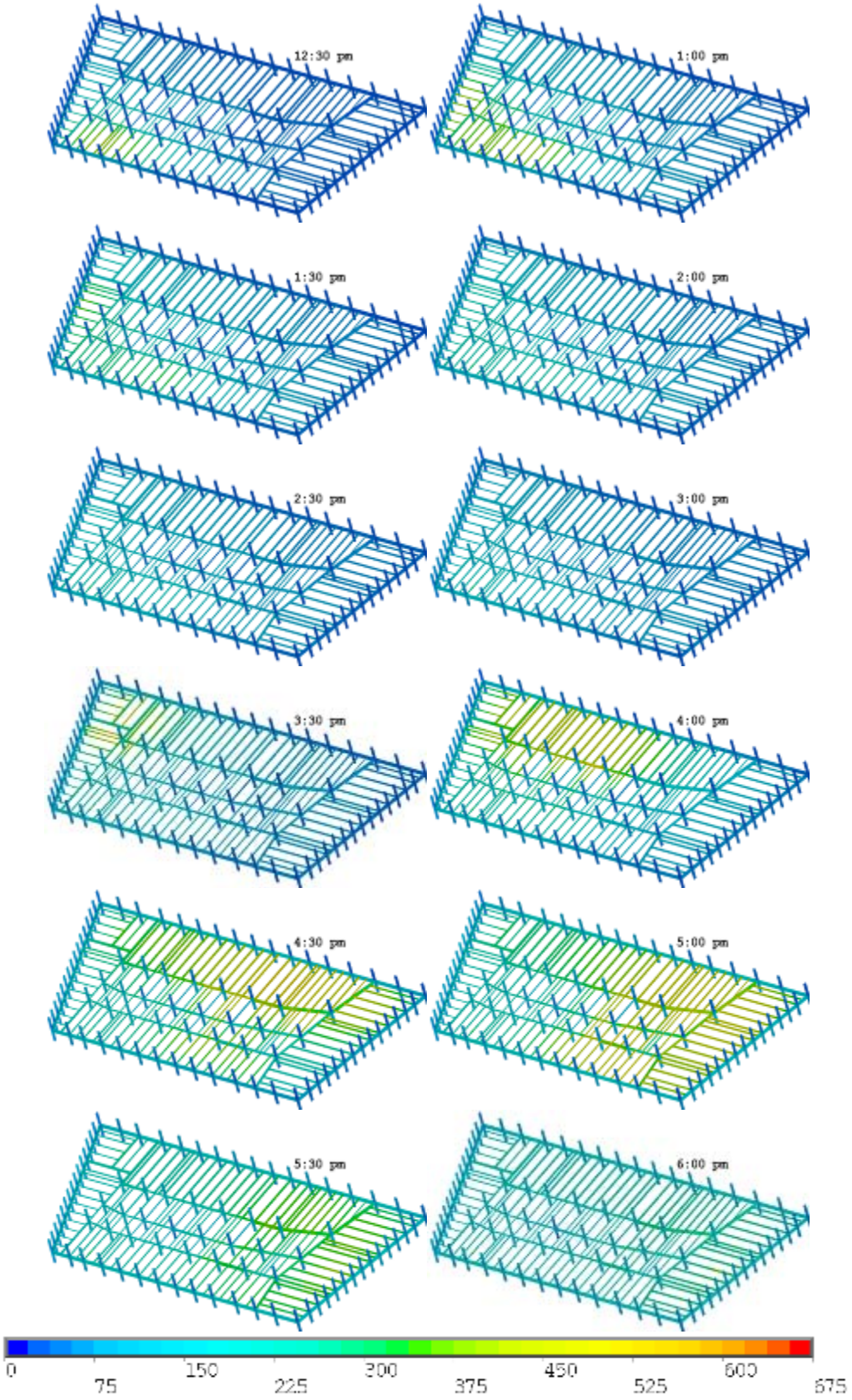

Figure 10–30. Computed temperature distribution (ºC) on the floor beams of floor 9 at 12 different instants in time (Case B, floor slabs removed).

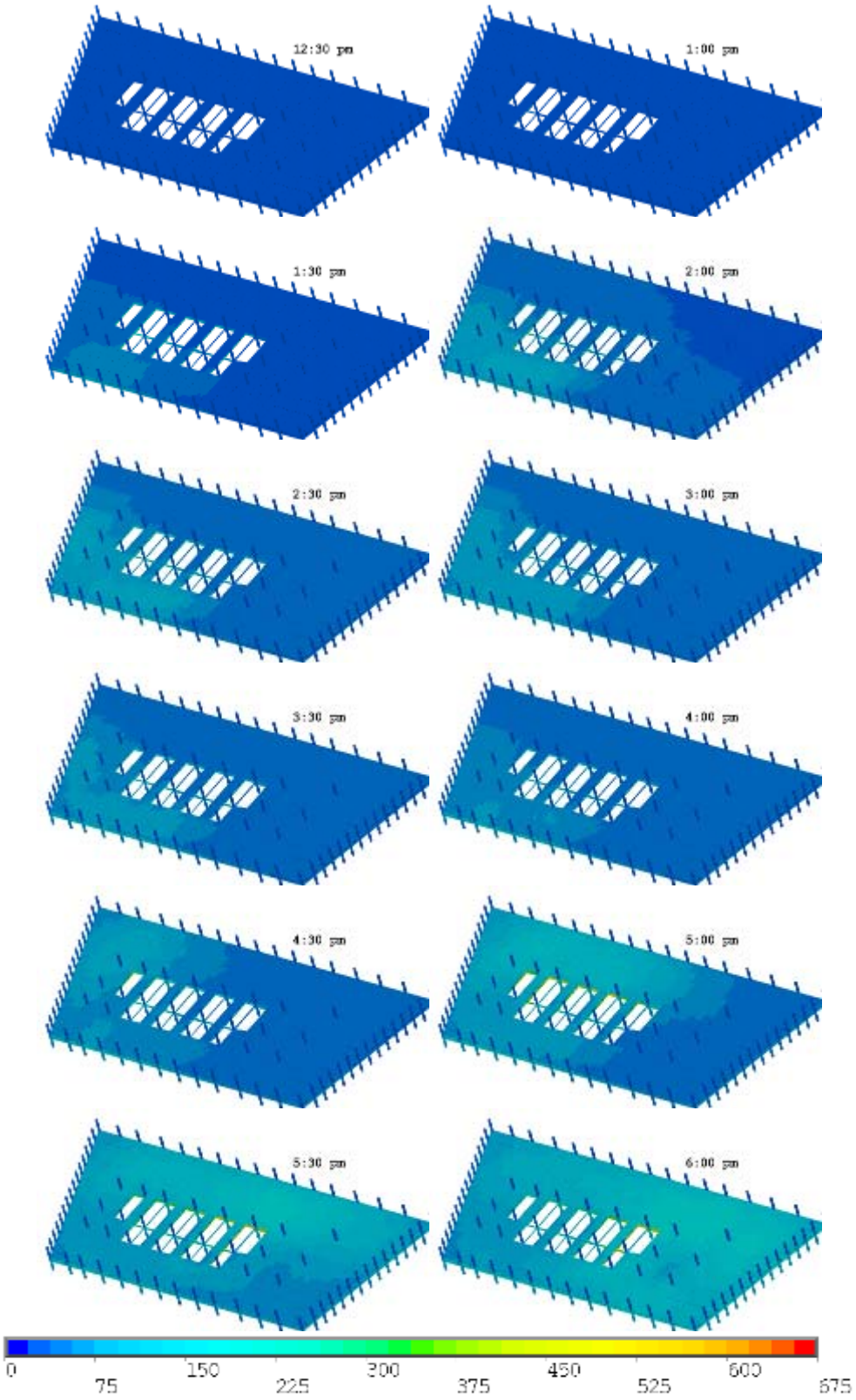

Figure 10–31. Computed temperature distribution (ºC) in the top layer of the concrete slab of floor 10 at 12 different instants in time (Case B).

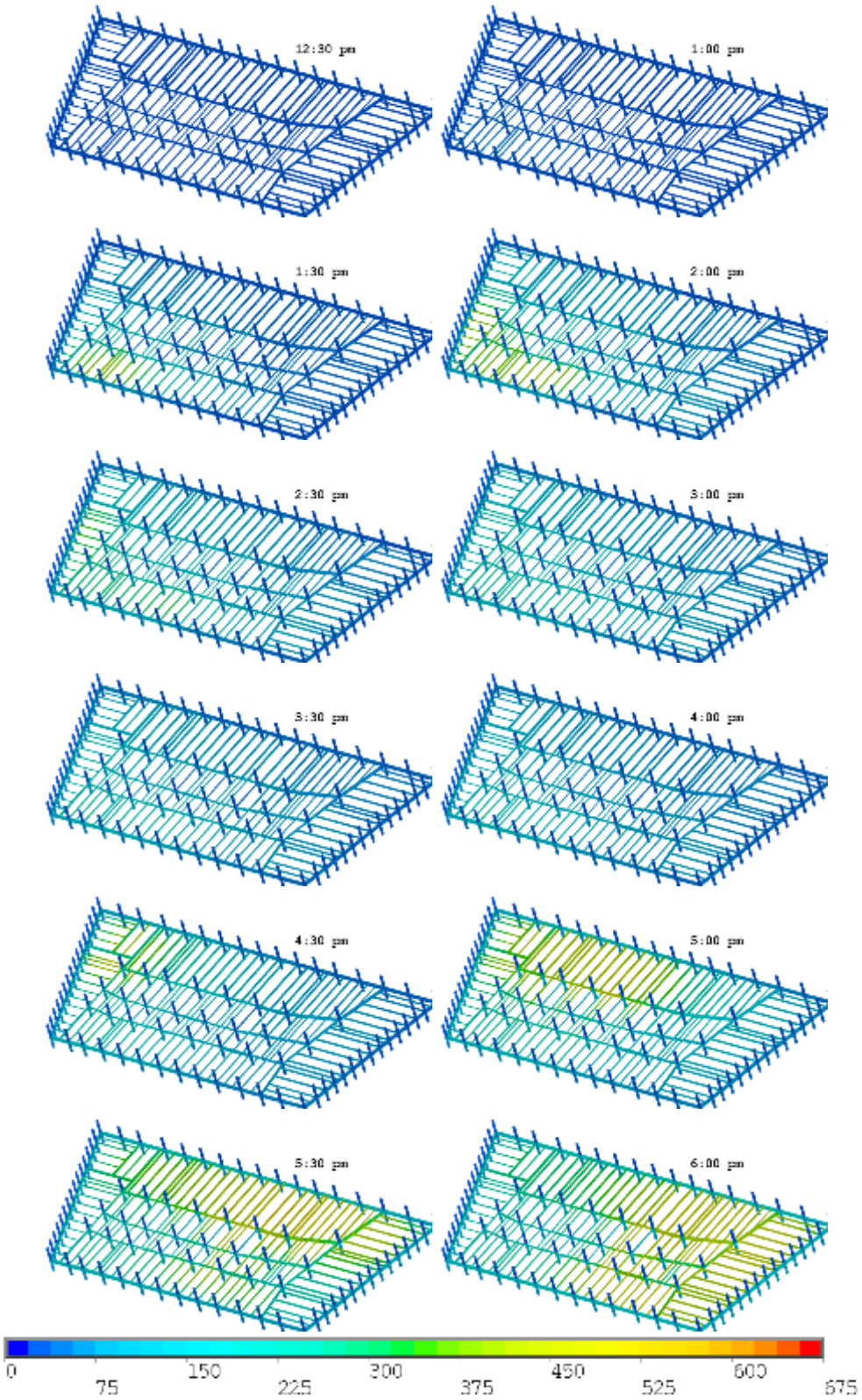

Figure 10–32. Computed temperature distribution (ºC) on floor beams of Floor 10 of WTC 7 at 12 different instants in time (Case B, floor slabs removed).

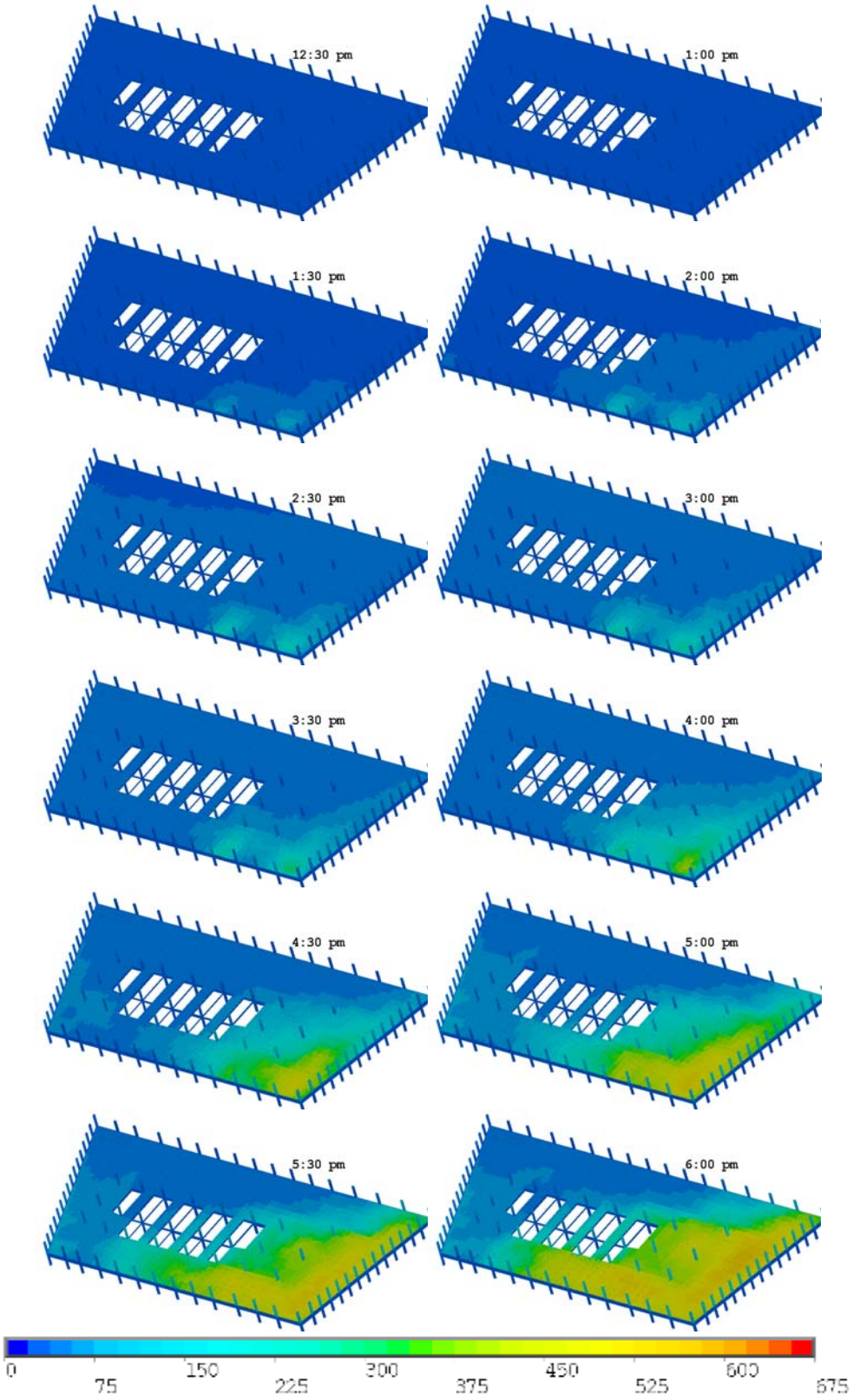

Figure 10–33. Computed temperature distribution (ºC) in the top layer of the concrete slab of floor 11 at 12 different instants in time (Case B).

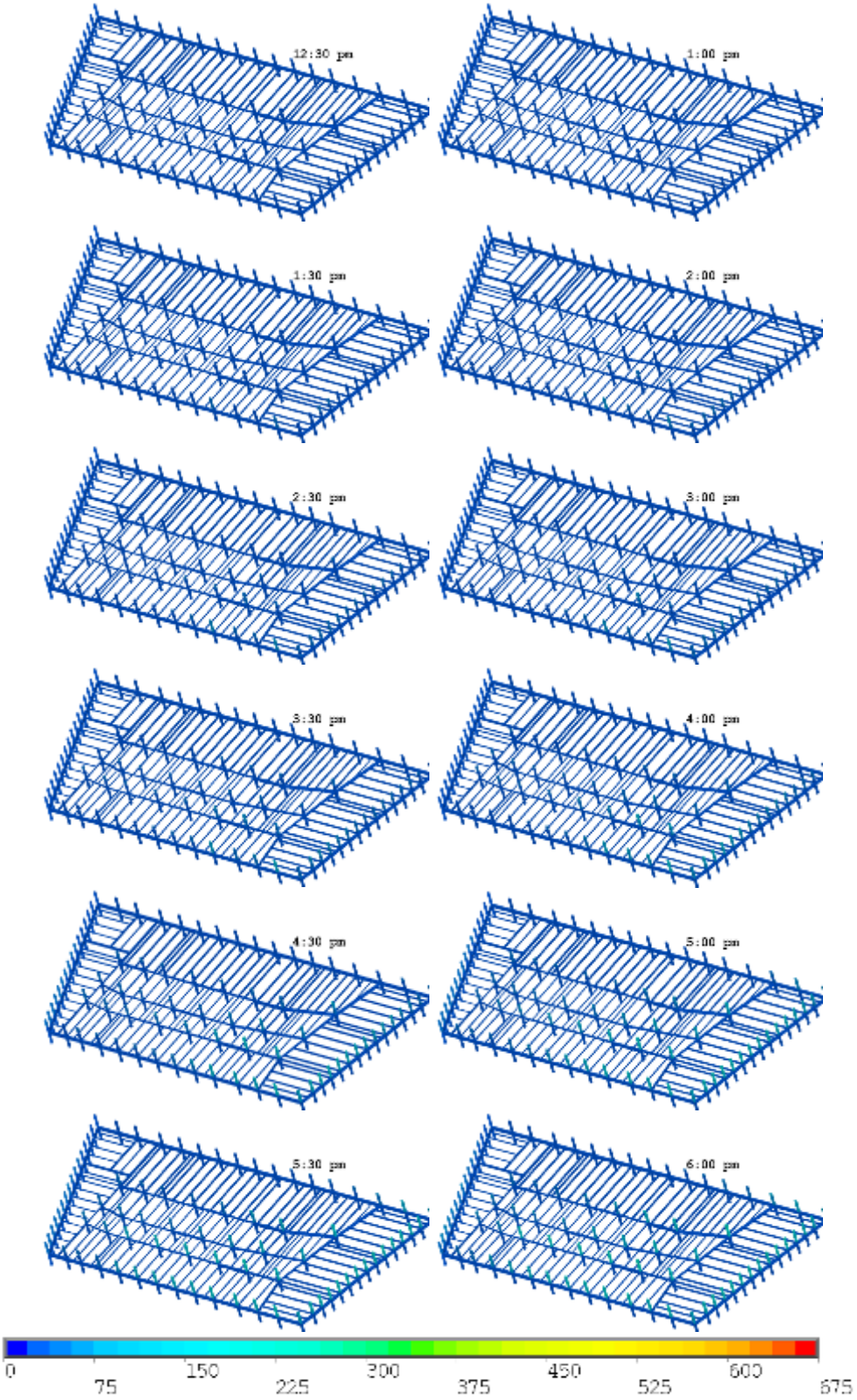

Figure 10–34. Computed temperature distribution (ºC) on the floor beams of floor 11 at 12 different instants in time (Case B, floor slabs removed).

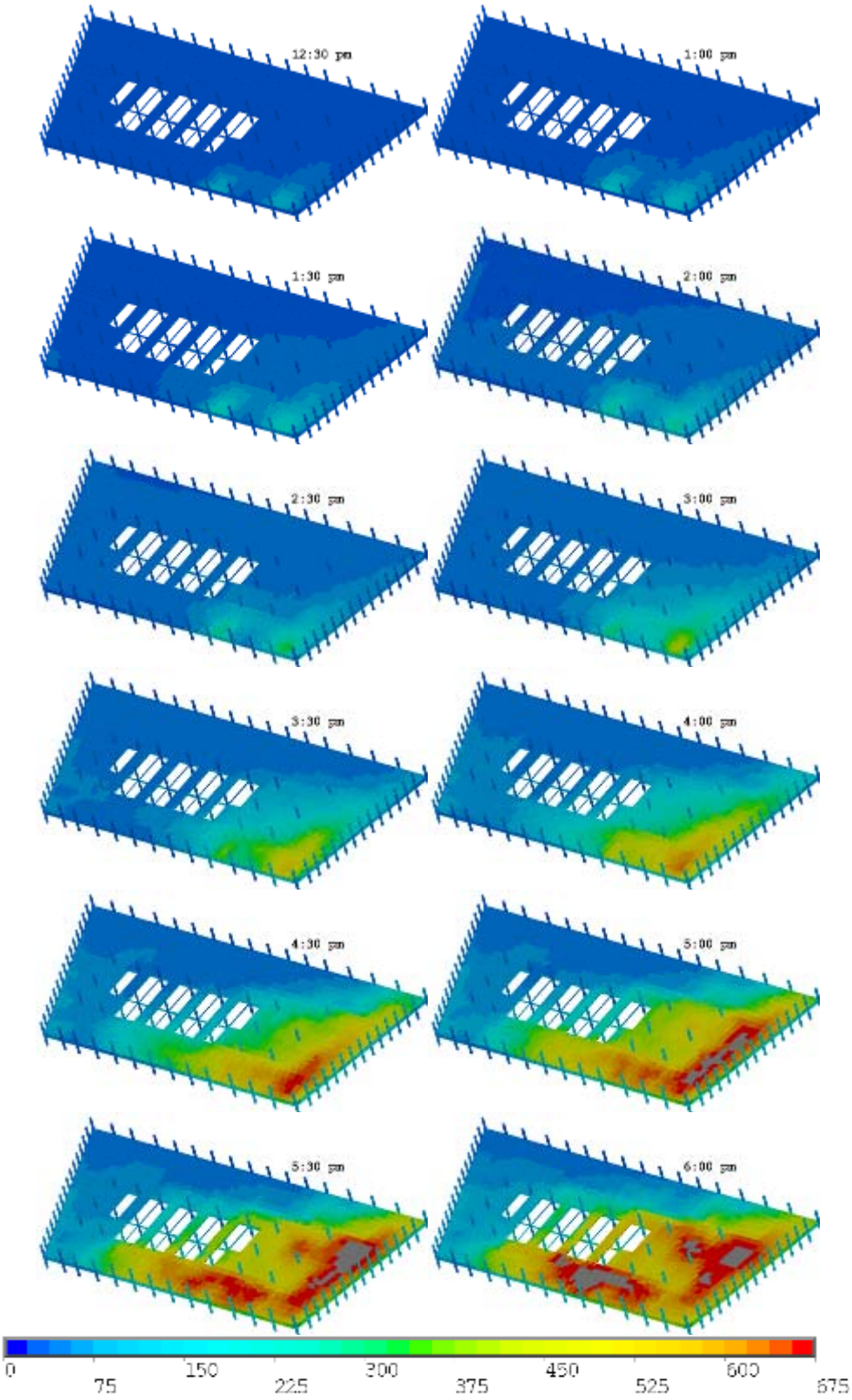

Figure 10–35. Computed temperature distribution (ºC) in the top layer of the concrete slab of floor 12 at 12 different instants in time (Case B).

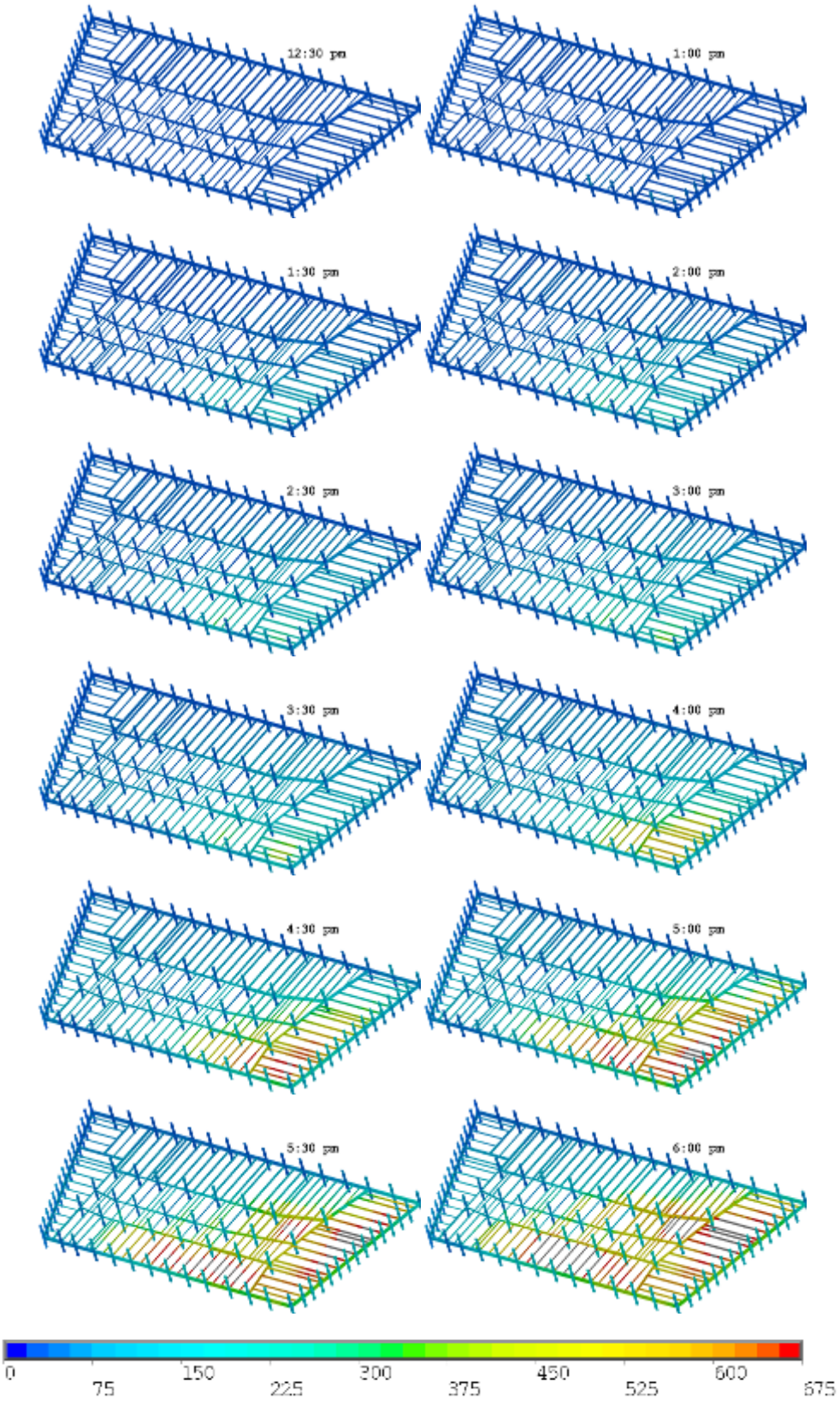

Figure 10–36. Computed temperature distribution (ºC) on the floor beams of floor 12 of WTC 7 at 12 different instants in time (Case B, floor slabs removed).

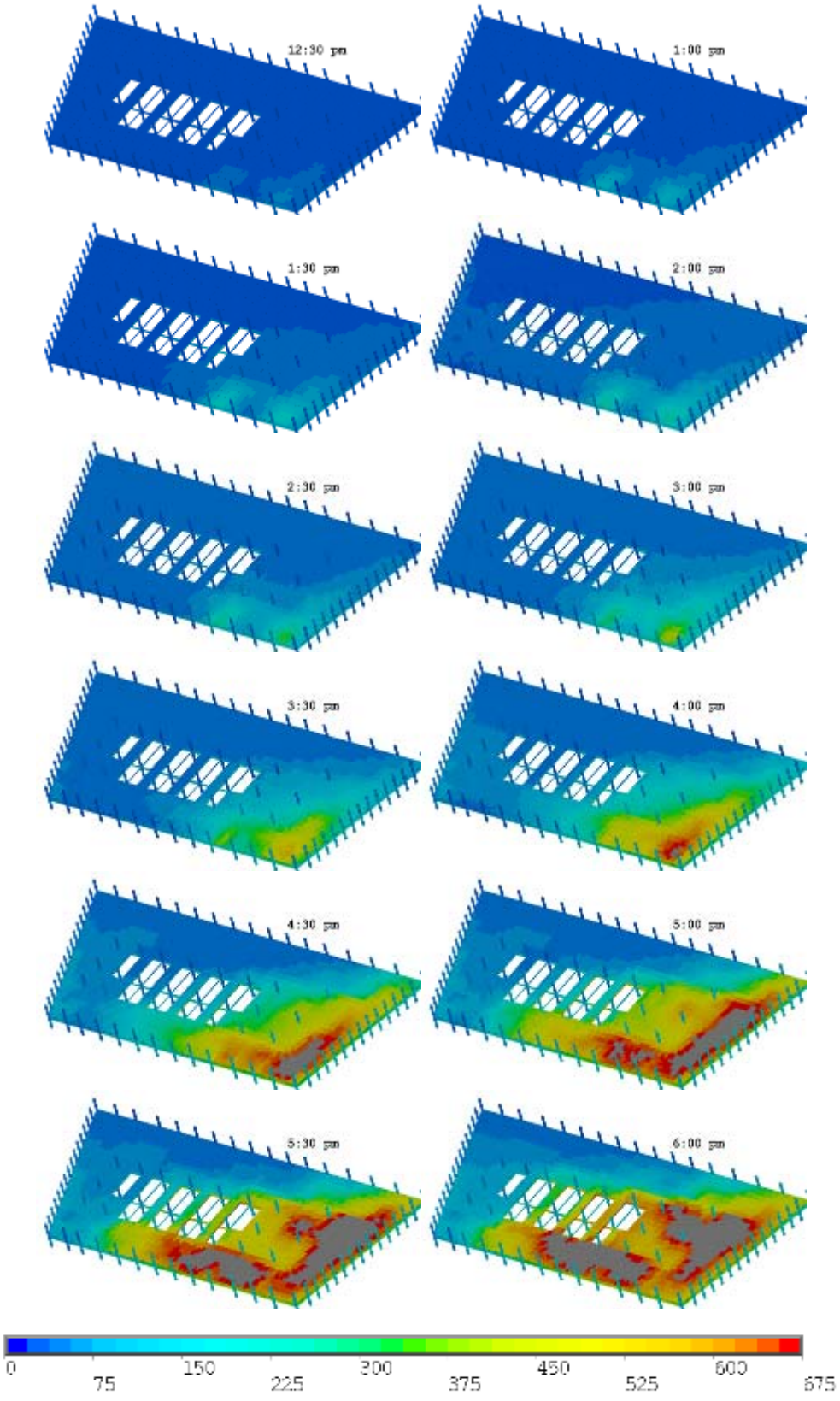

Figure 10–37. Computed temperature distribution (ºC) in the top layer of the concrete slab of floor 13 at 12 different instants in time (Case B).

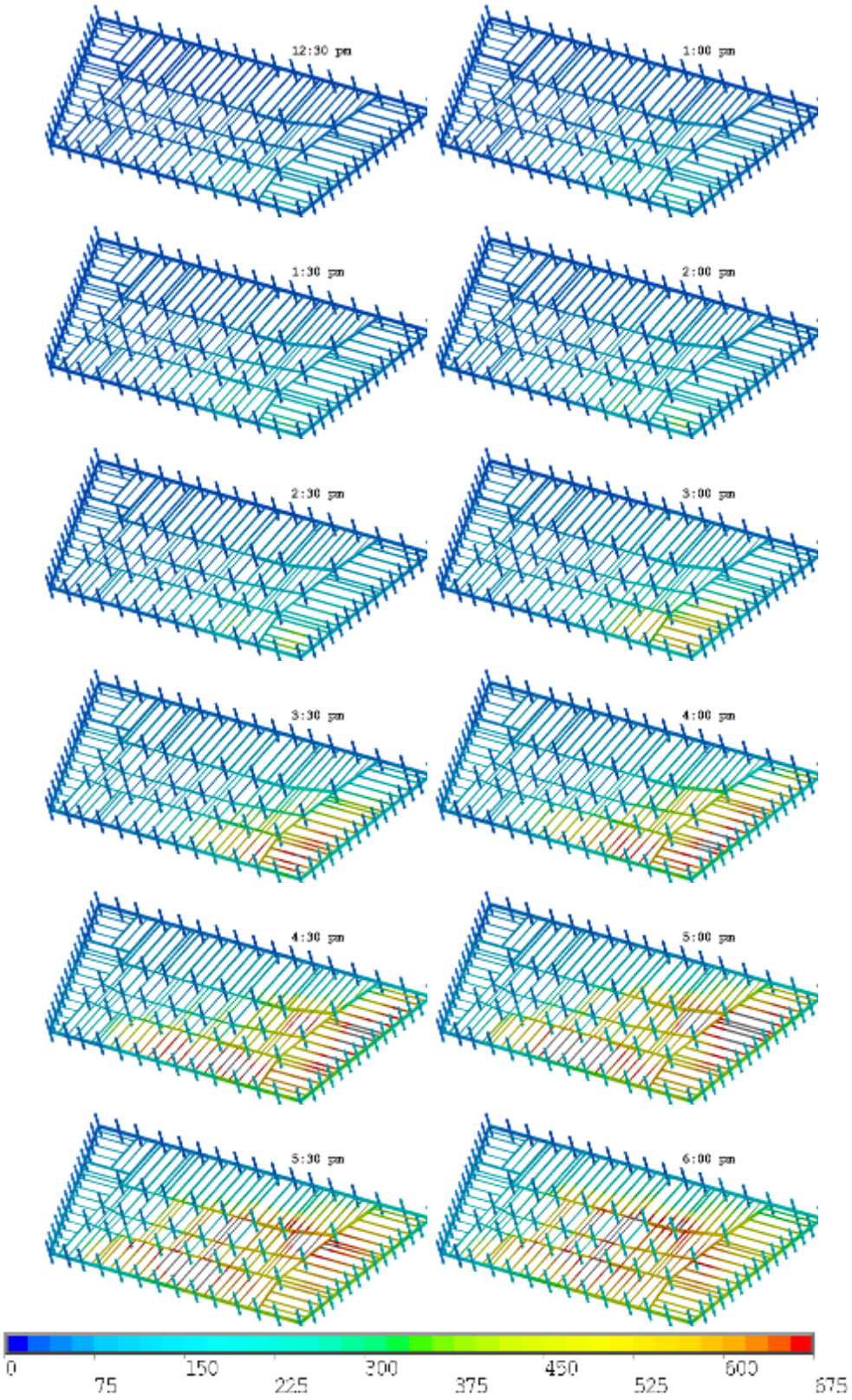

Figure 10–38. Computed temperature distribution (ºC) on the floor beams of floor 13 at 12 different instants in time (Case B, floor slabs removed).

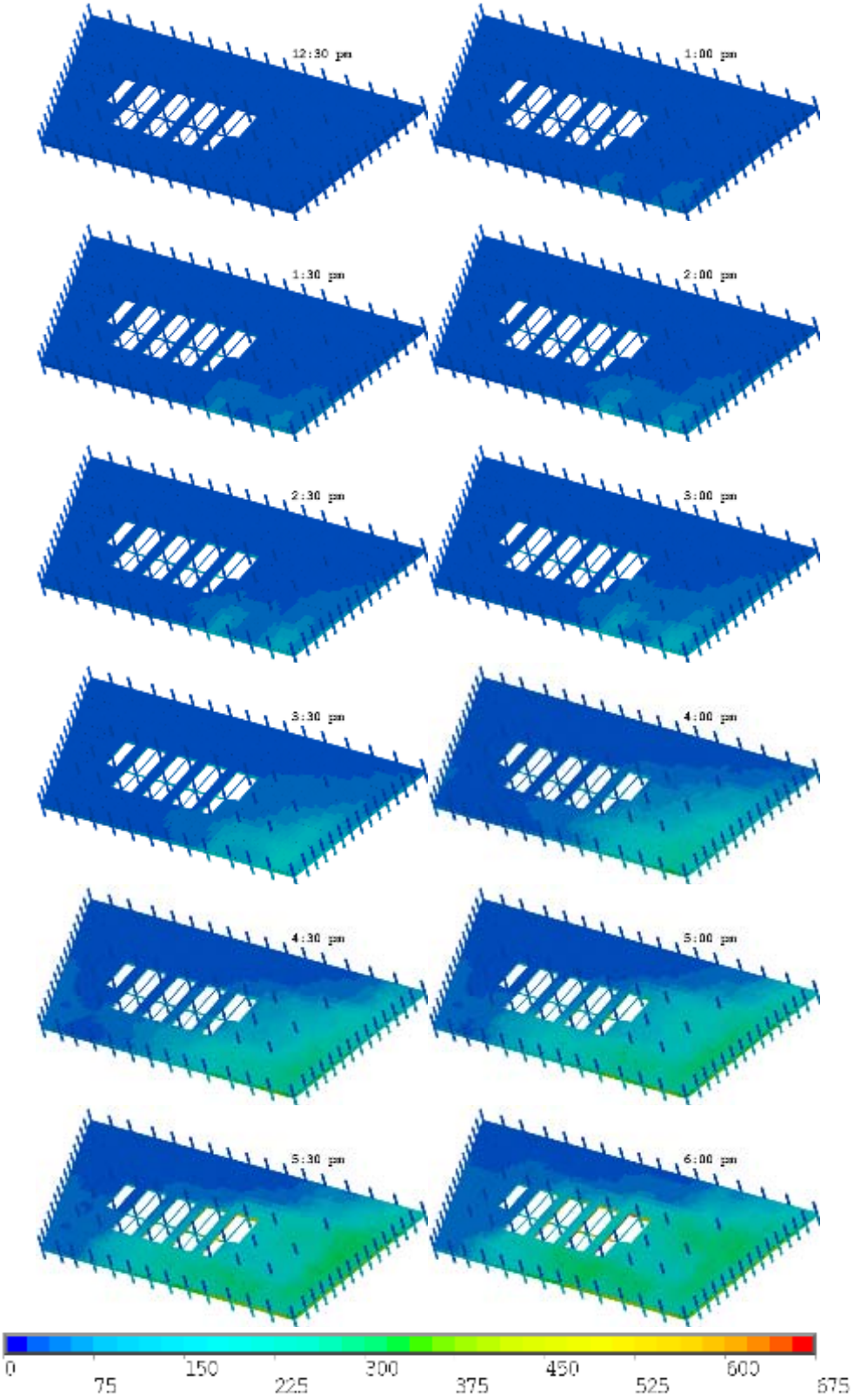

Figure 10–39. Computed temperature distribution (ºC) in the top layer of the concrete slab of floor 14 at 12 different instants in time (Case B).

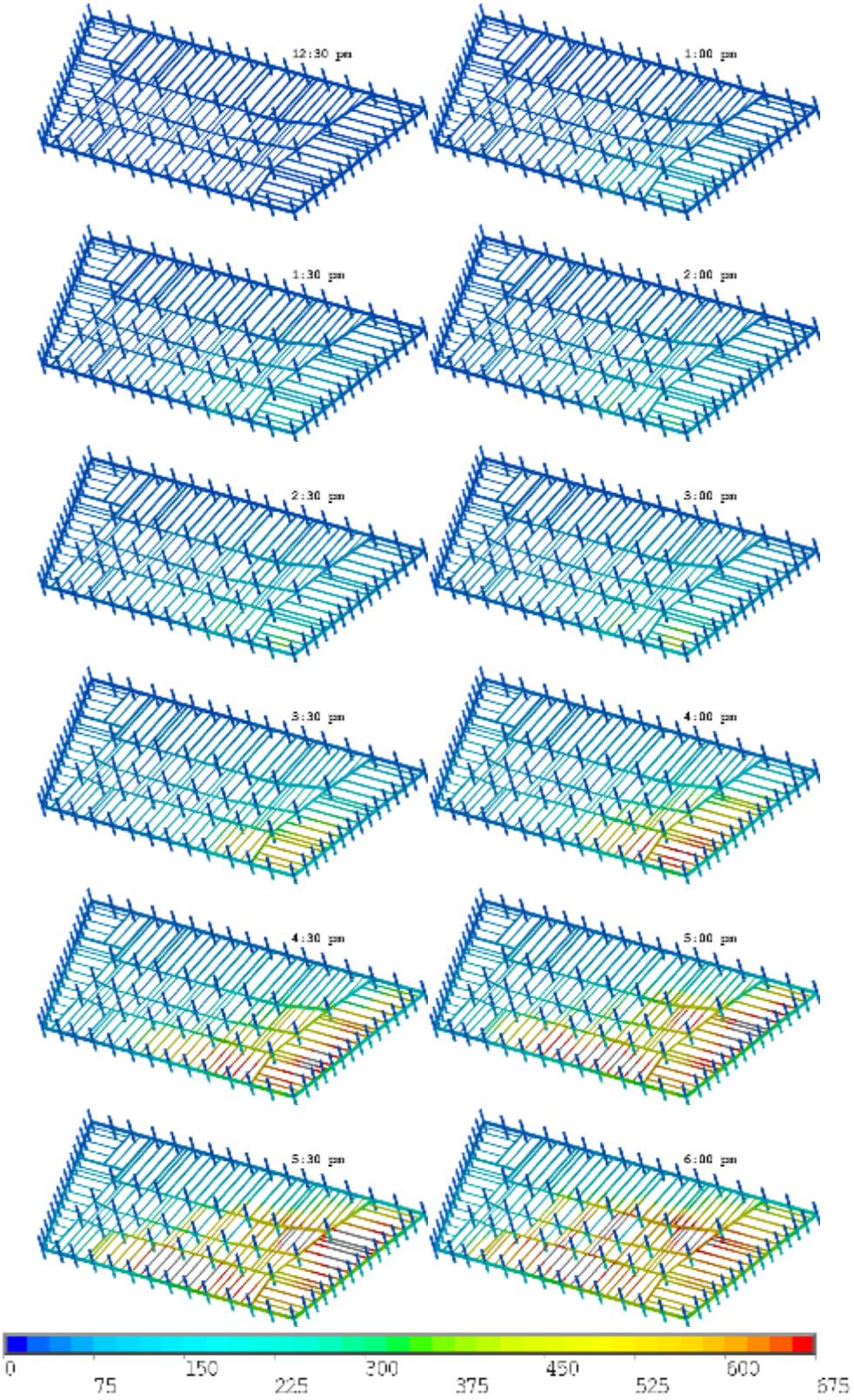

Figure 10–40. Computed temperature distribution (ºC) on the floor beams of floor 14 at 12 different instants in time (Case B, floor slabs removed).

10.3.4 Case C

For Case C, the air temperature increase at each location on Floors 7 through 14 was assumed to be 10 percent lower than that computed from the FDS simulation of Case A, which was within the expected range of reasonable and realistic fire-generated temperatures. Figure 10–41 and Figure 10–42 compare the temperatures of the building at two times for these two cases. Case A is on the left, and Case C is on the right. As expected, Case C resulted in mildly lower temperatures in the steel and concrete, narrower hot zones, and lesser overlap of hot zones between adjacent floors.

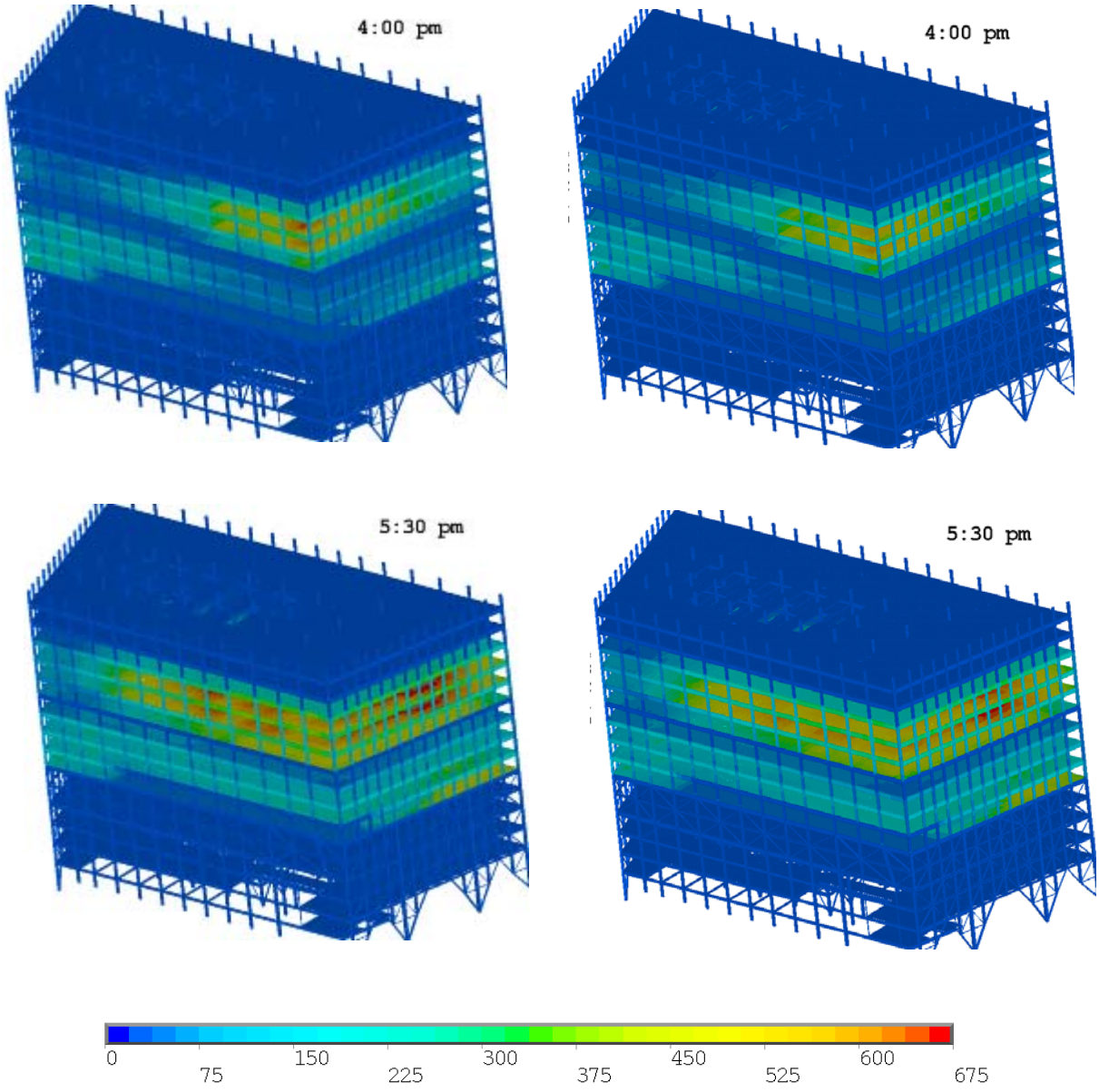

Figure 10–41. View from the southeast of the 16 lower floors of WTC 7, comparing Case A (left) and Case C (right) temperatures at two different times.

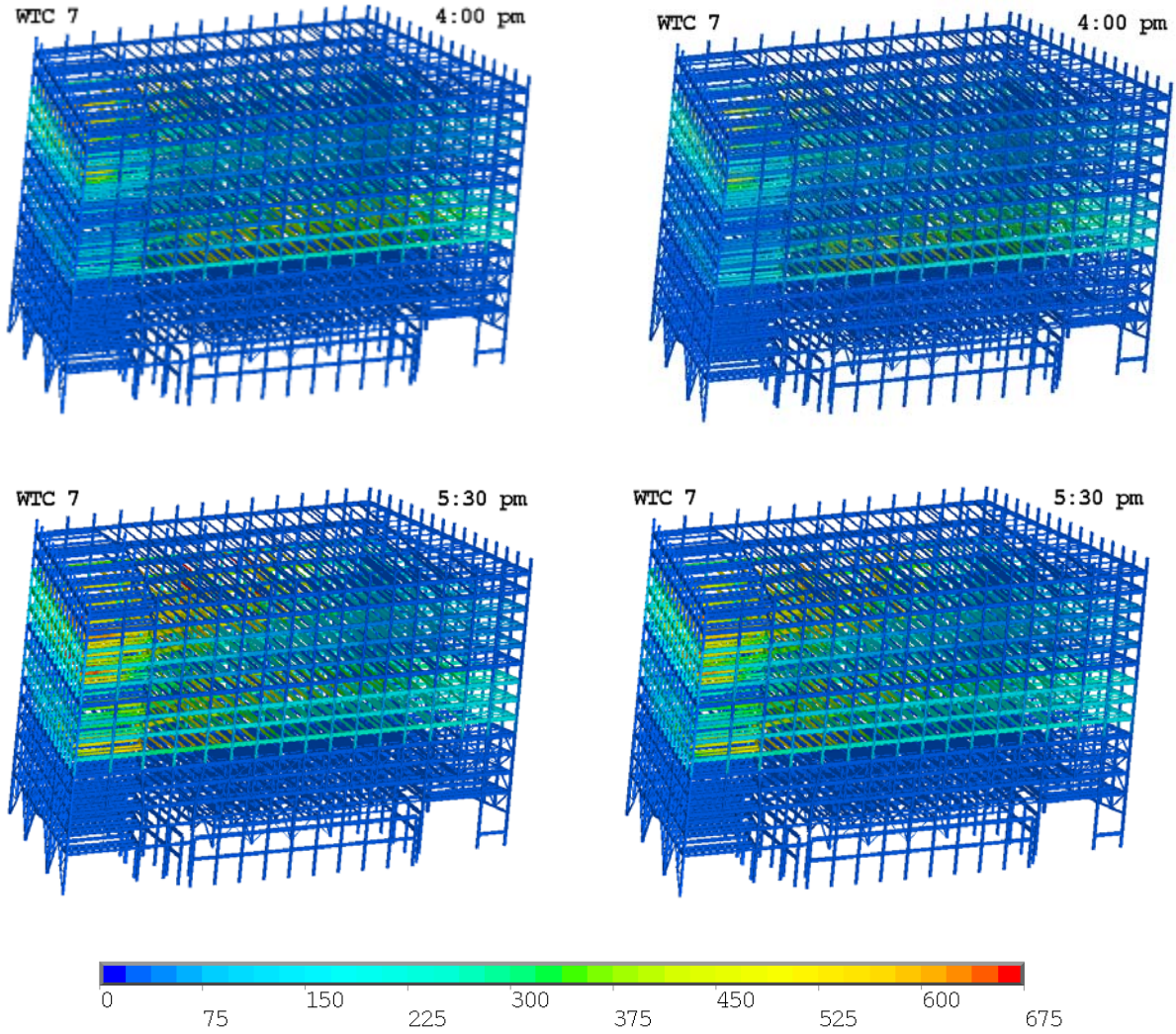

Figure 10–42. View from the northeast of the 16 lower floors of WTC 7, comparing Case A (left) and Case C (right) temperatures at two different times (floor slabs removed).

Figure 10–43 and Figure 10–44 show the full timed Case C sequence from which these examples were drawn. (The Case A sequences were shown in Figure 10–3 and Figure 10–4.) Figure 10–45 through Figure 10–60 show the floor-by-floor heating for Case C.

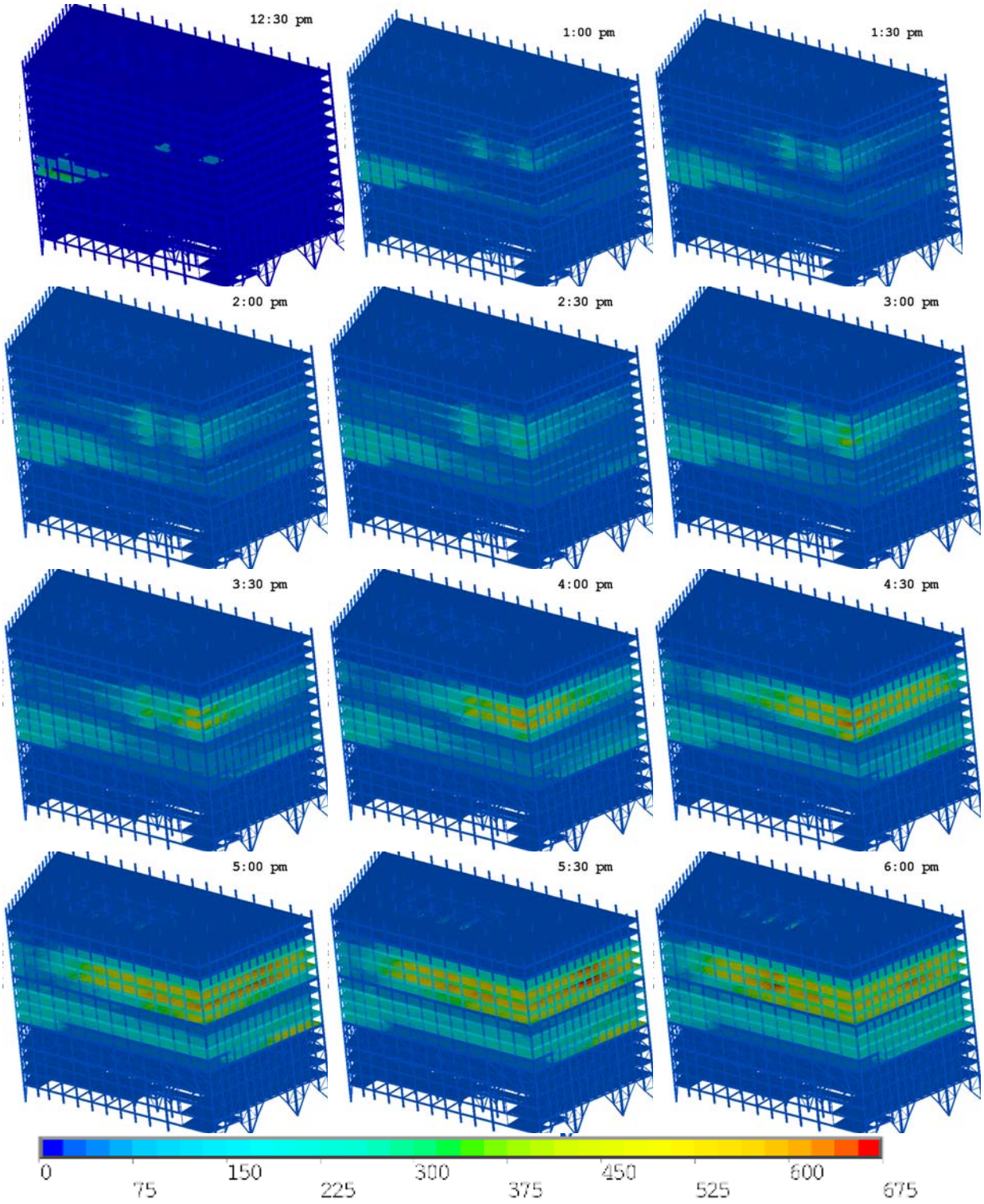

Figure 10–43. View from the southeast of the computed thermal loading of the lower 16 floors of WTC 7 at 12 instants in time (Case C).

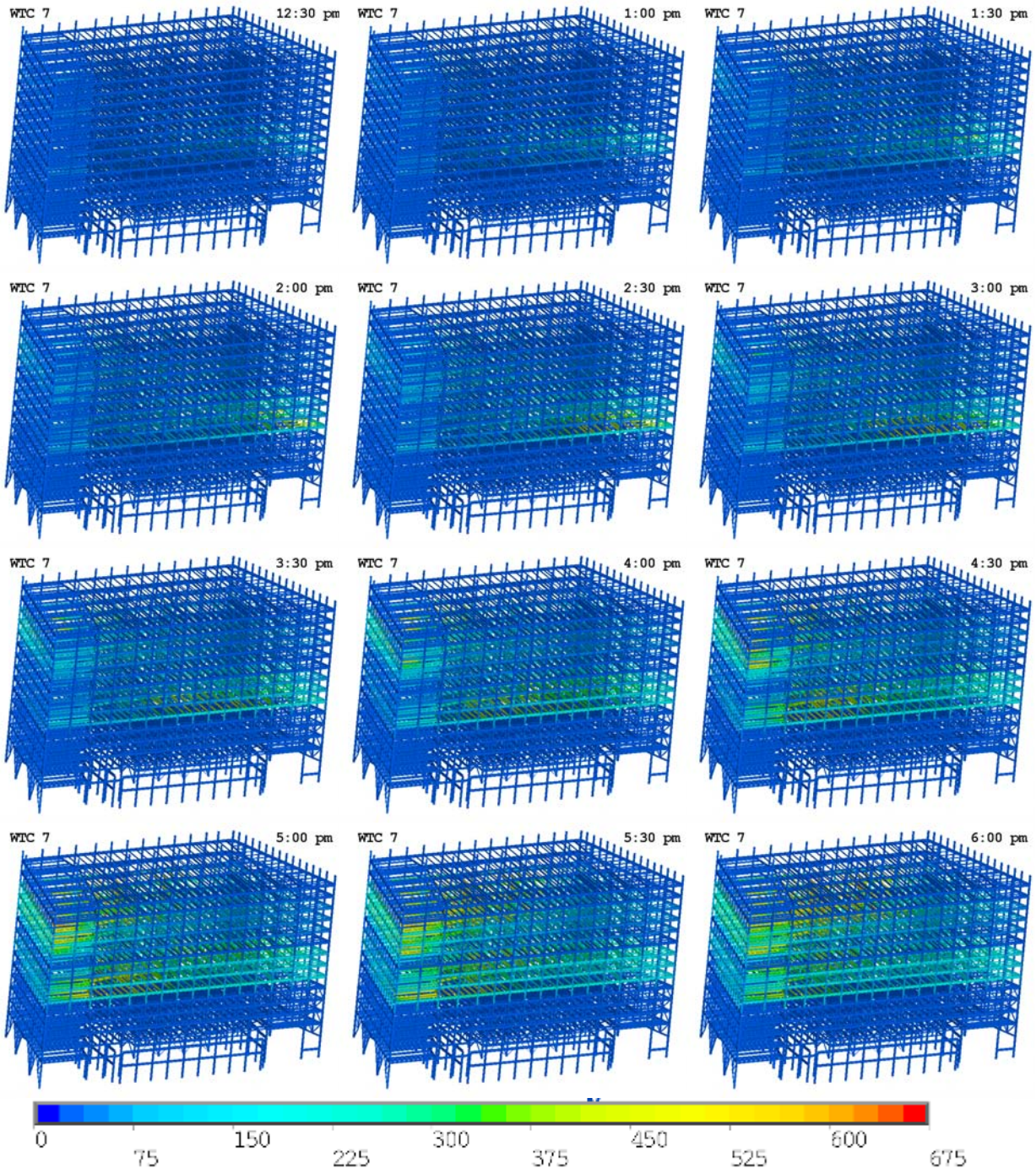

Figure 10–44. View from the northeast of the computed thermal loading of the lower 16 floors of WTC 7 at 12 different instants in time (Case C, floor slabs removed).

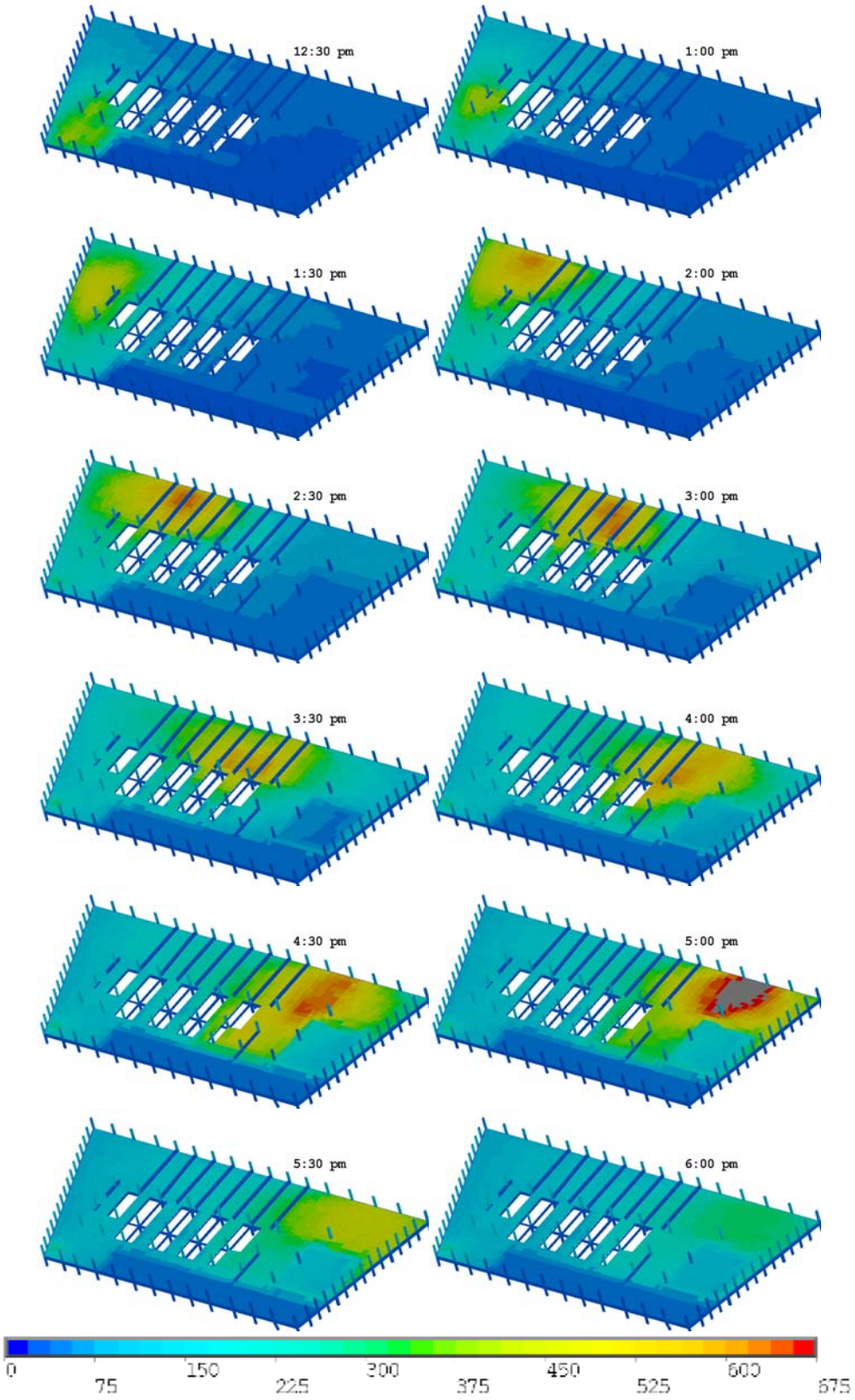

Figure 10–45. Computed temperature distribution (ºC) in the top layer of the concrete slab on floor 7 at 12 instants in time (Case C).

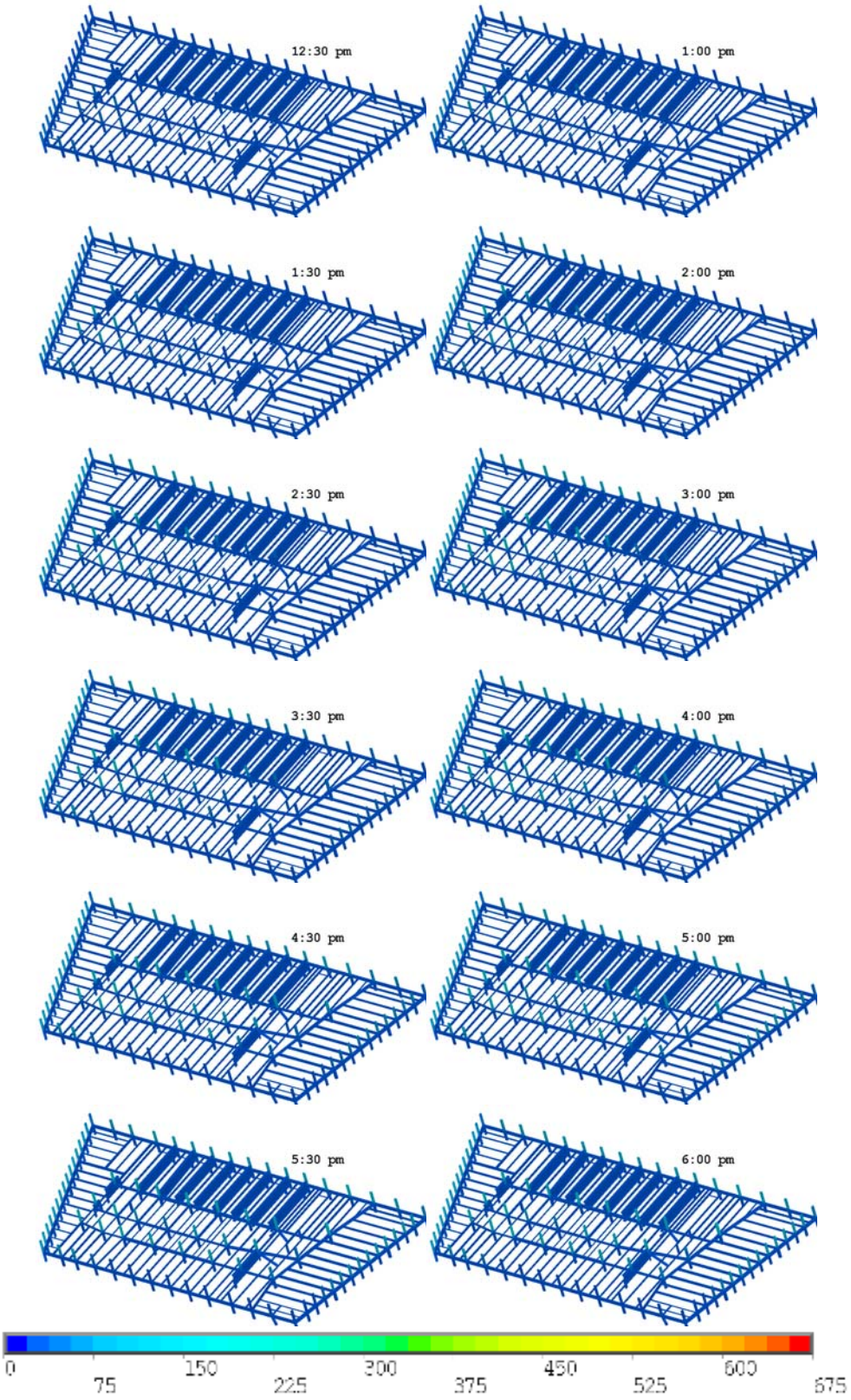

Figure 10–46. Computed temperature distribution (ºC) on the floor beams of floor 7 at 12 different instants in time (Case C, floor slabs removed).

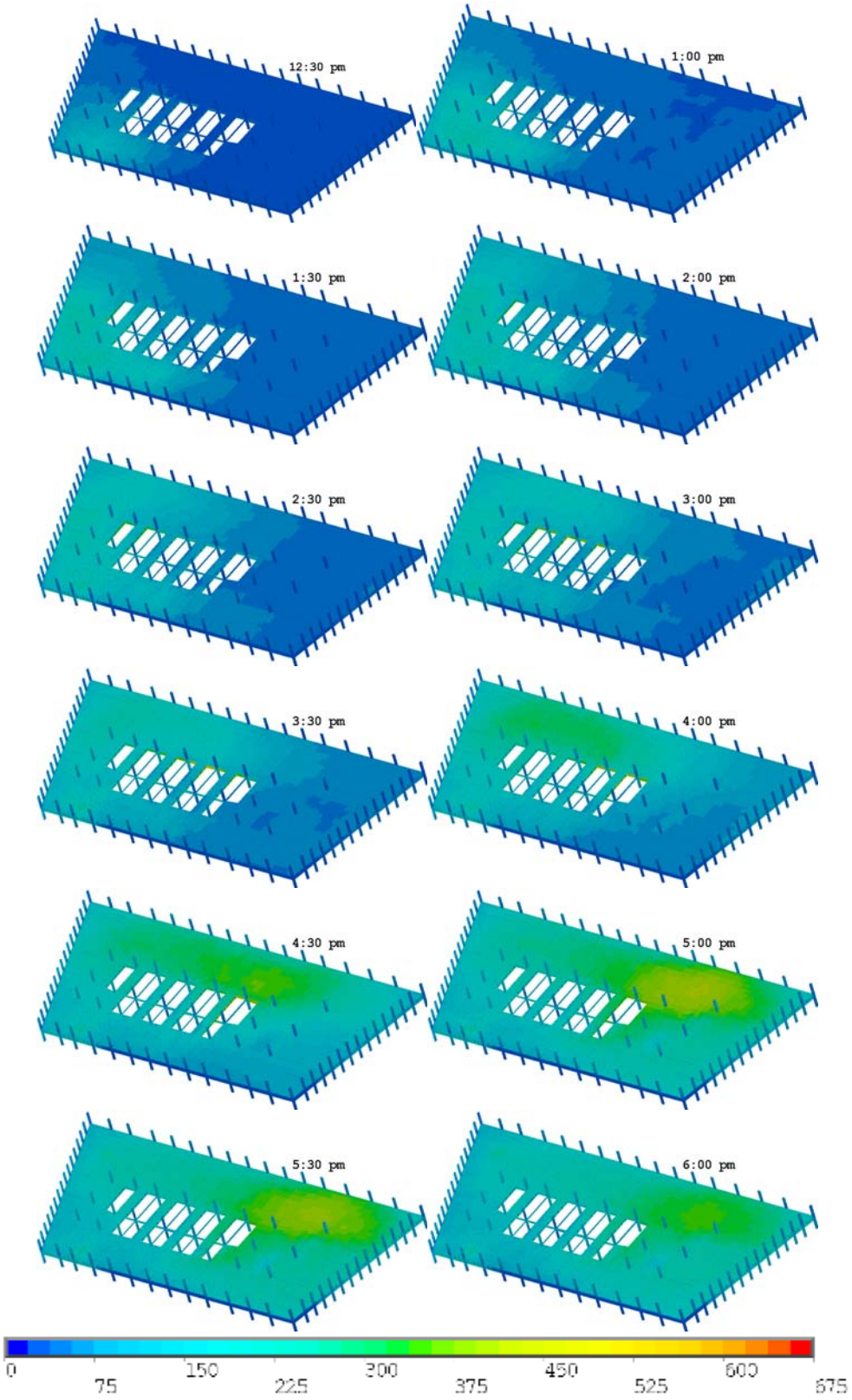

Figure 10–47. Computed temperature distribution (ºC) in the top layer of the concrete slab on floor 8 at 12 instants in time (Case C).

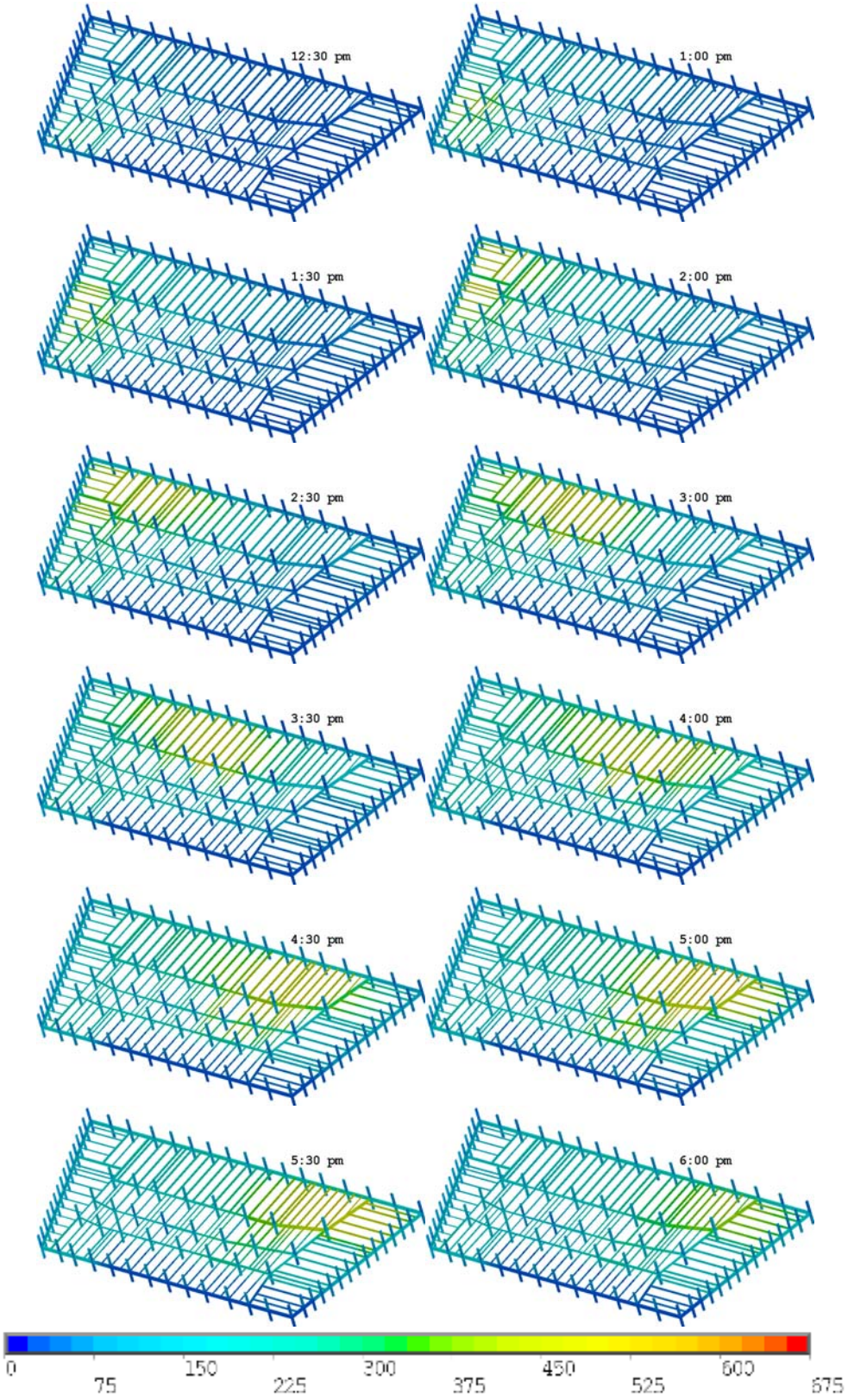

Figure 10–48. Computed temperature distribution (ºC) on the floor beams of floor 8 at 12 different instants in time (Case C, floor slabs removed).

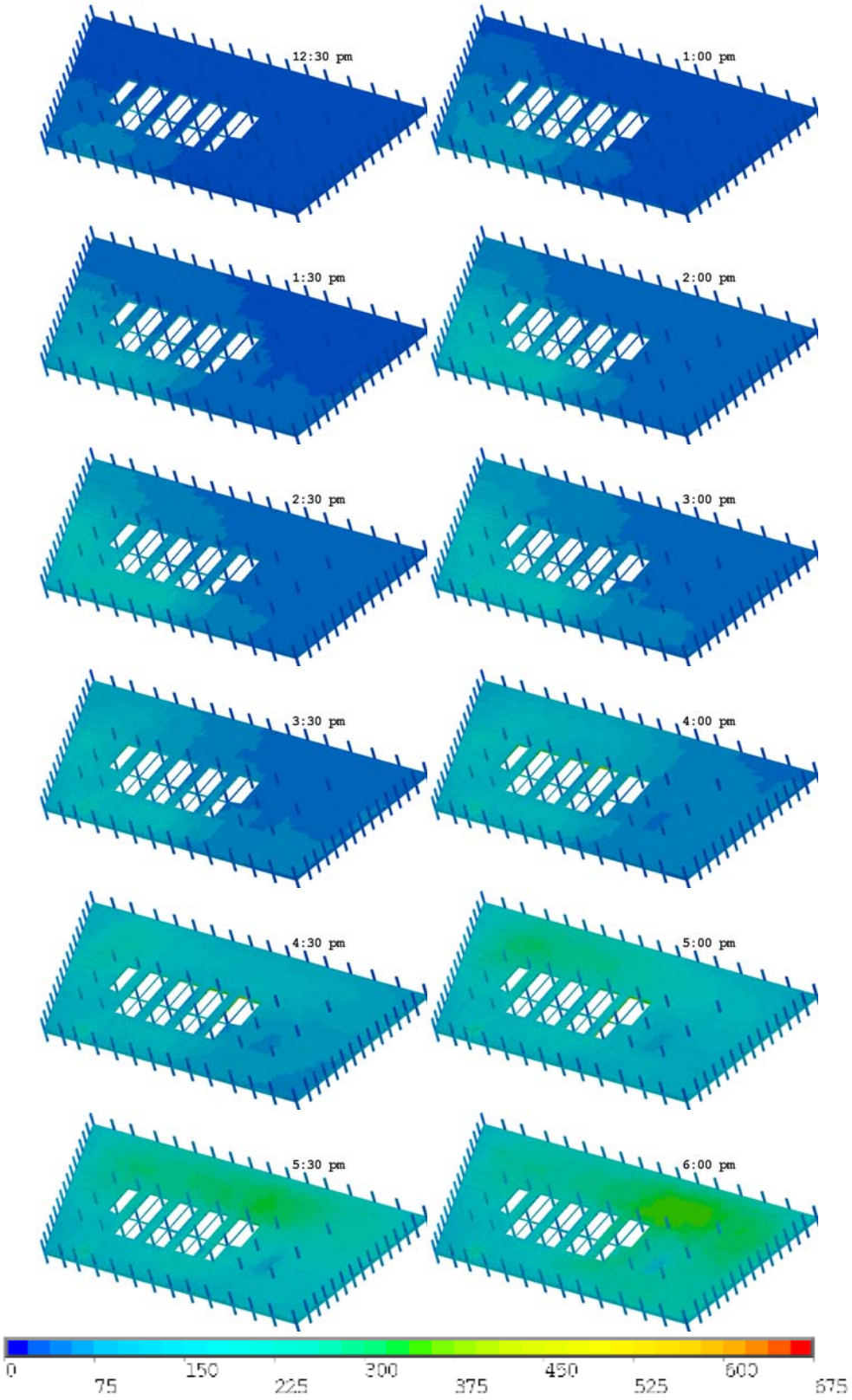

Figure 10–49. Computed temperature distribution (ºC) in the top layer of the concrete slab on floor 9 at 12 instants in time (Case C).

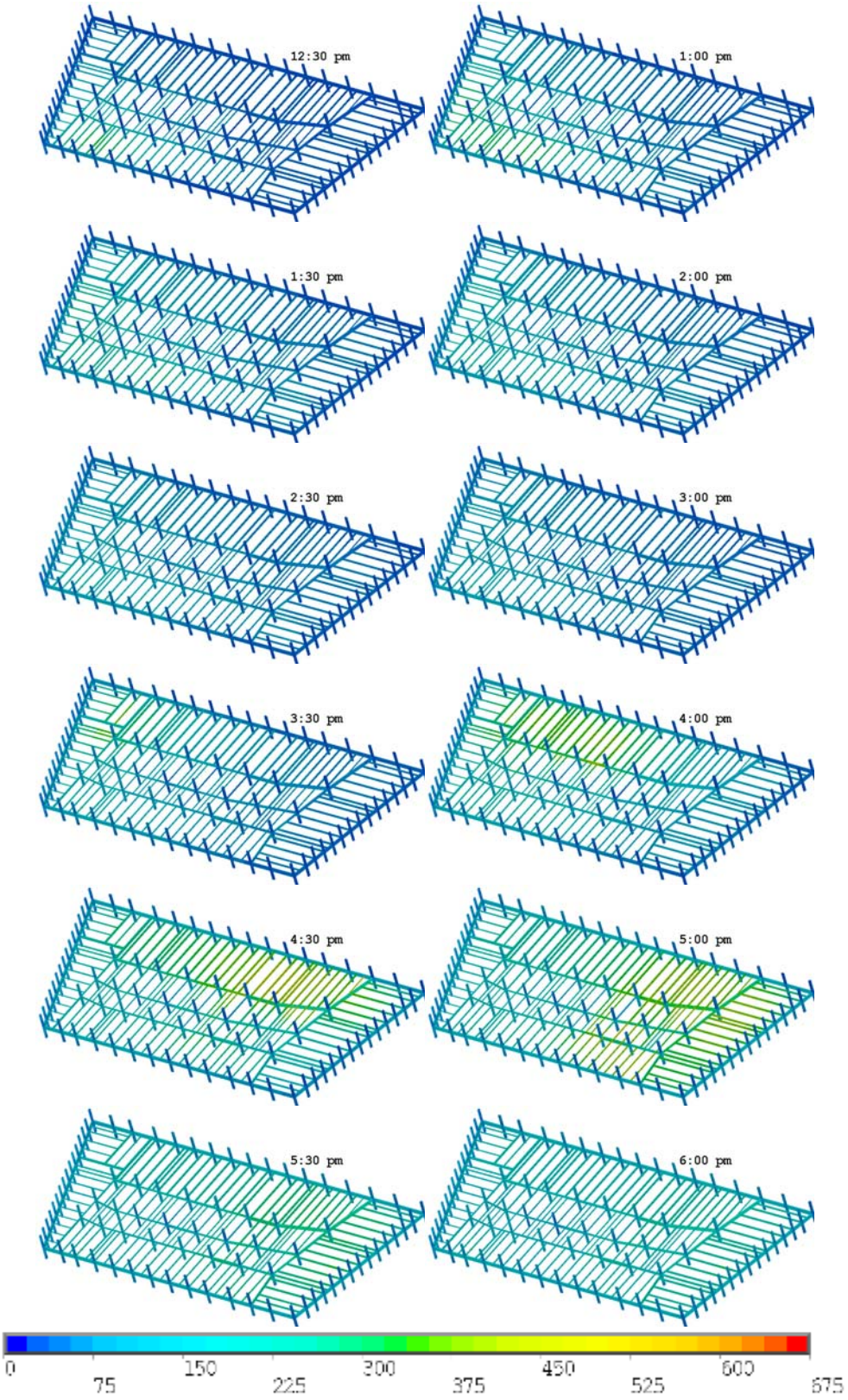

Figure 10–50. Computed temperature distribution (ºC) on the floor beams of floor 9 at 12 different instants in time (Case C, floor slabs removed).

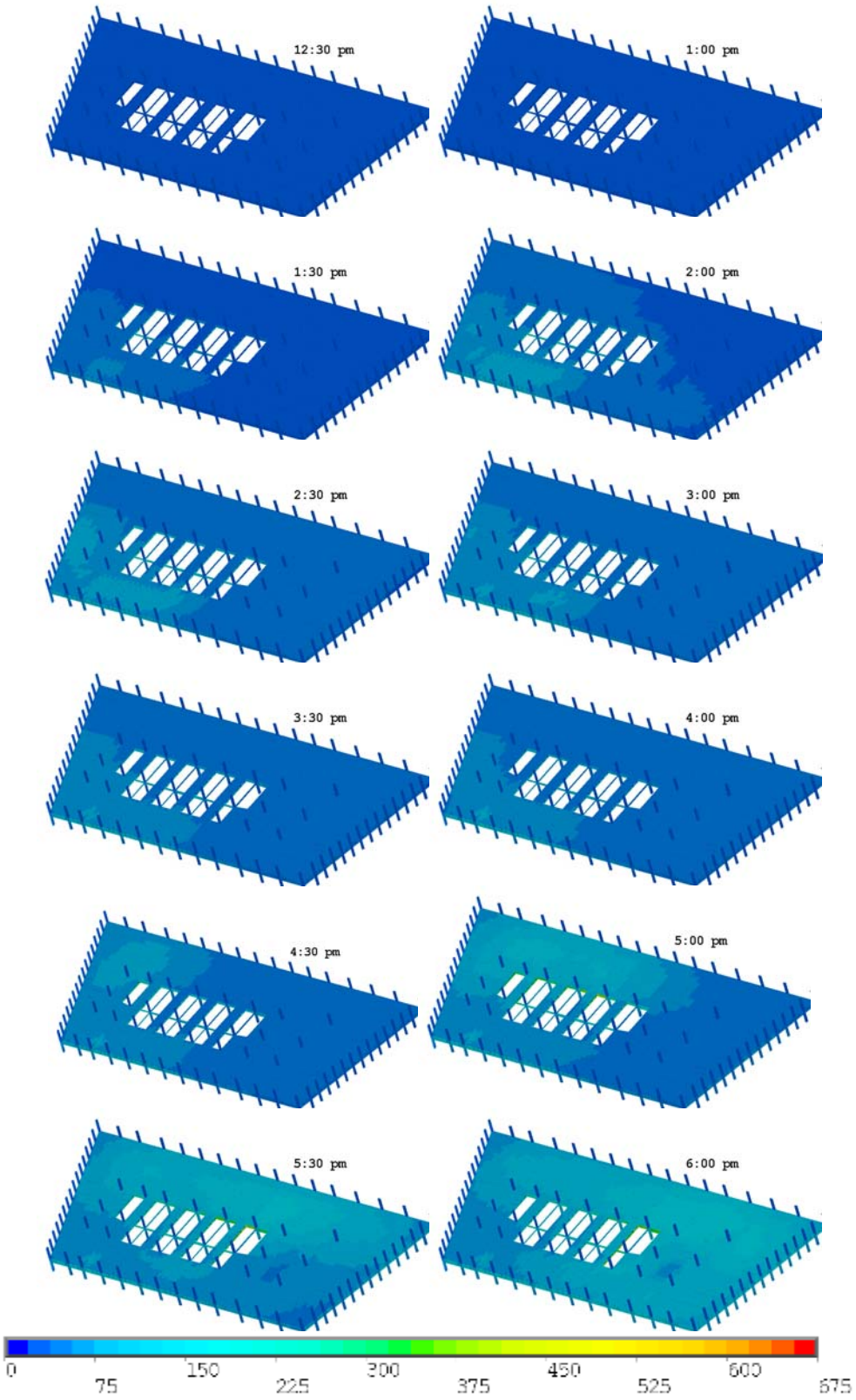

Figure 10–51. Computed temperature distribution (ºC) in the top layer of the concrete slab on floor 10 at 12 instants in time (Case C).

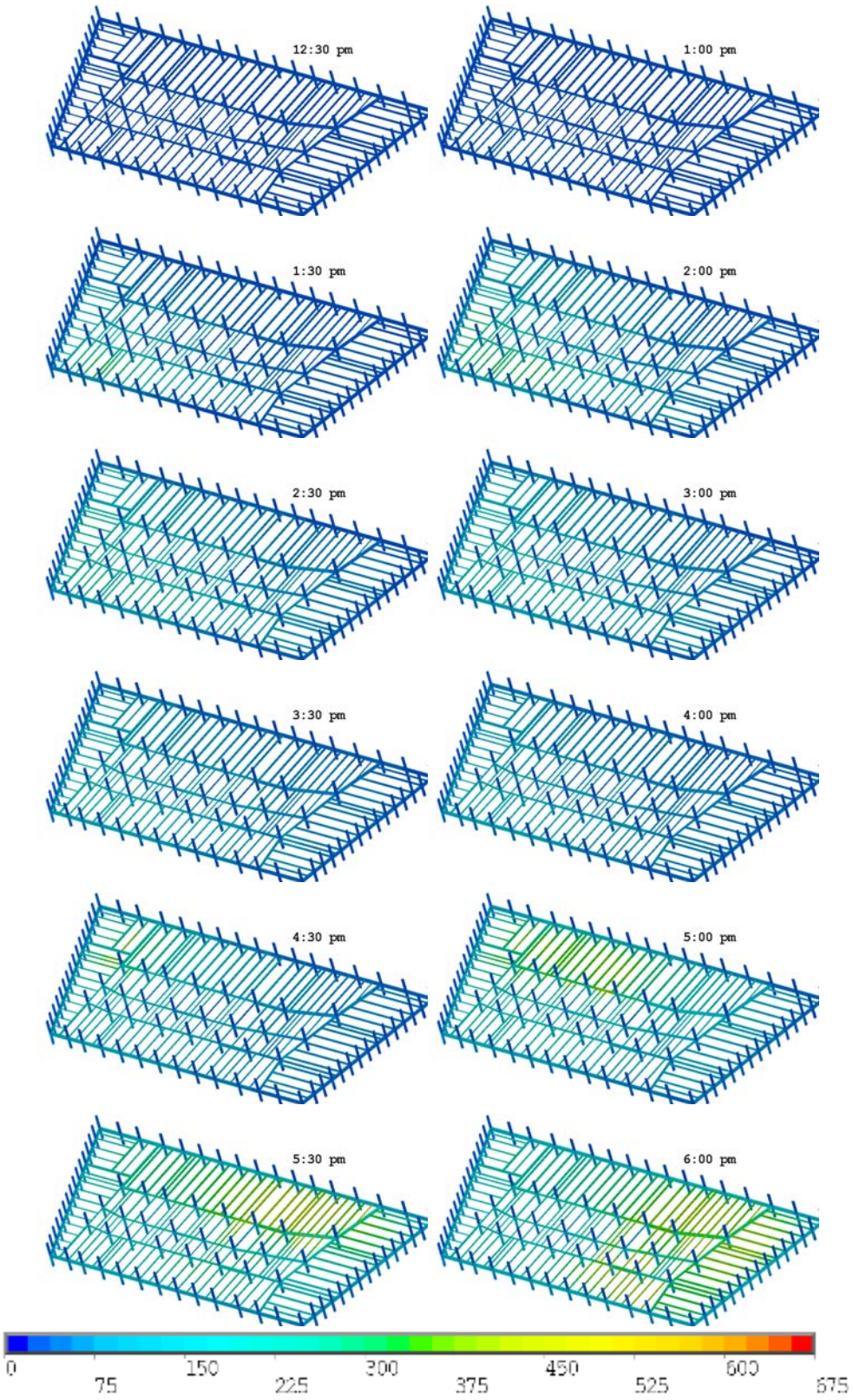

Figure 10–52. Computed temperature distribution (ºC) on the floor beams of floor 10 at 12 different instants in time (Case C, floor slabs removed).

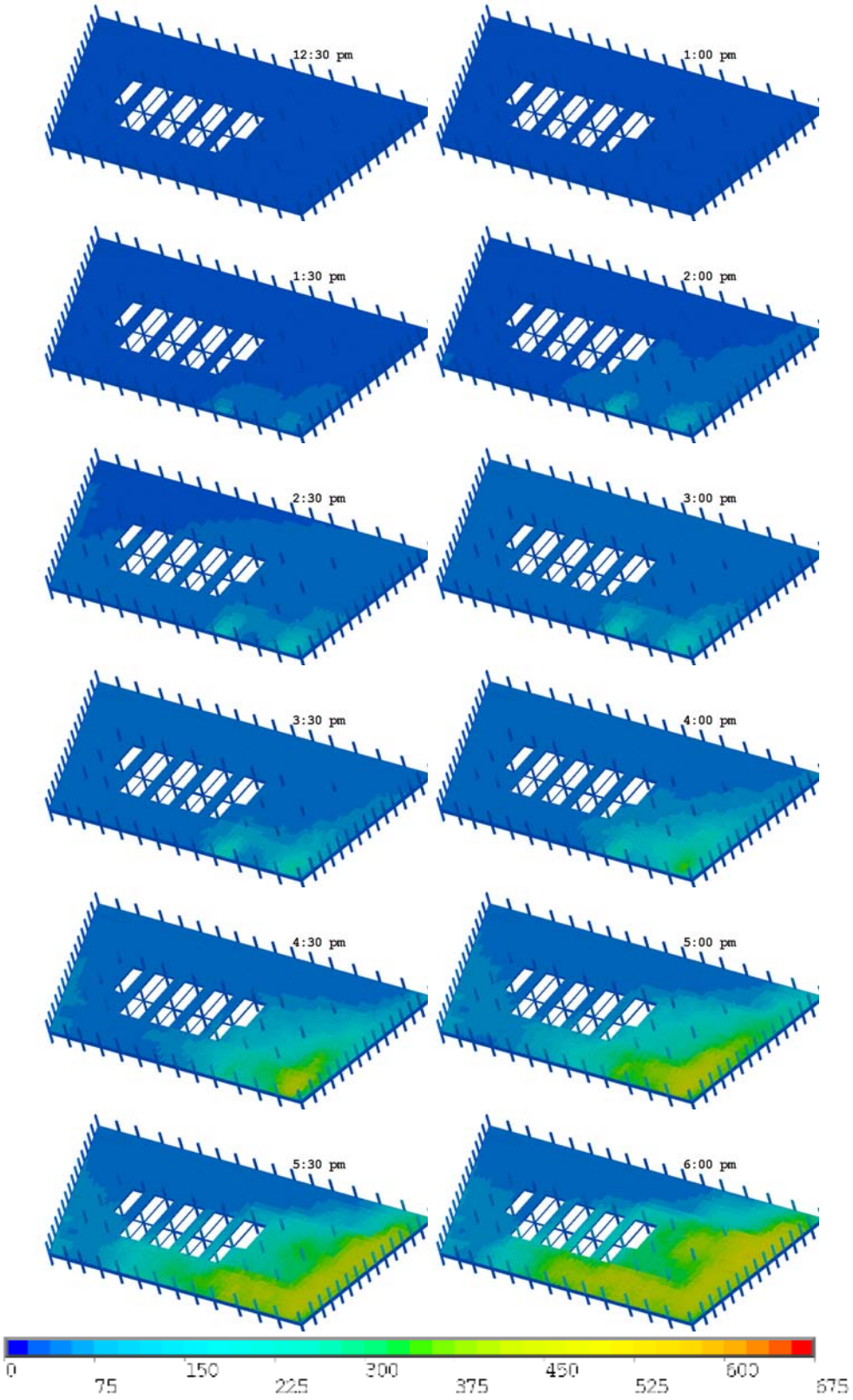

Figure 10–53. Computed temperature distribution (ºC) in the top layer of the concrete slab on floor 11 at 12 instants in time (Case C).

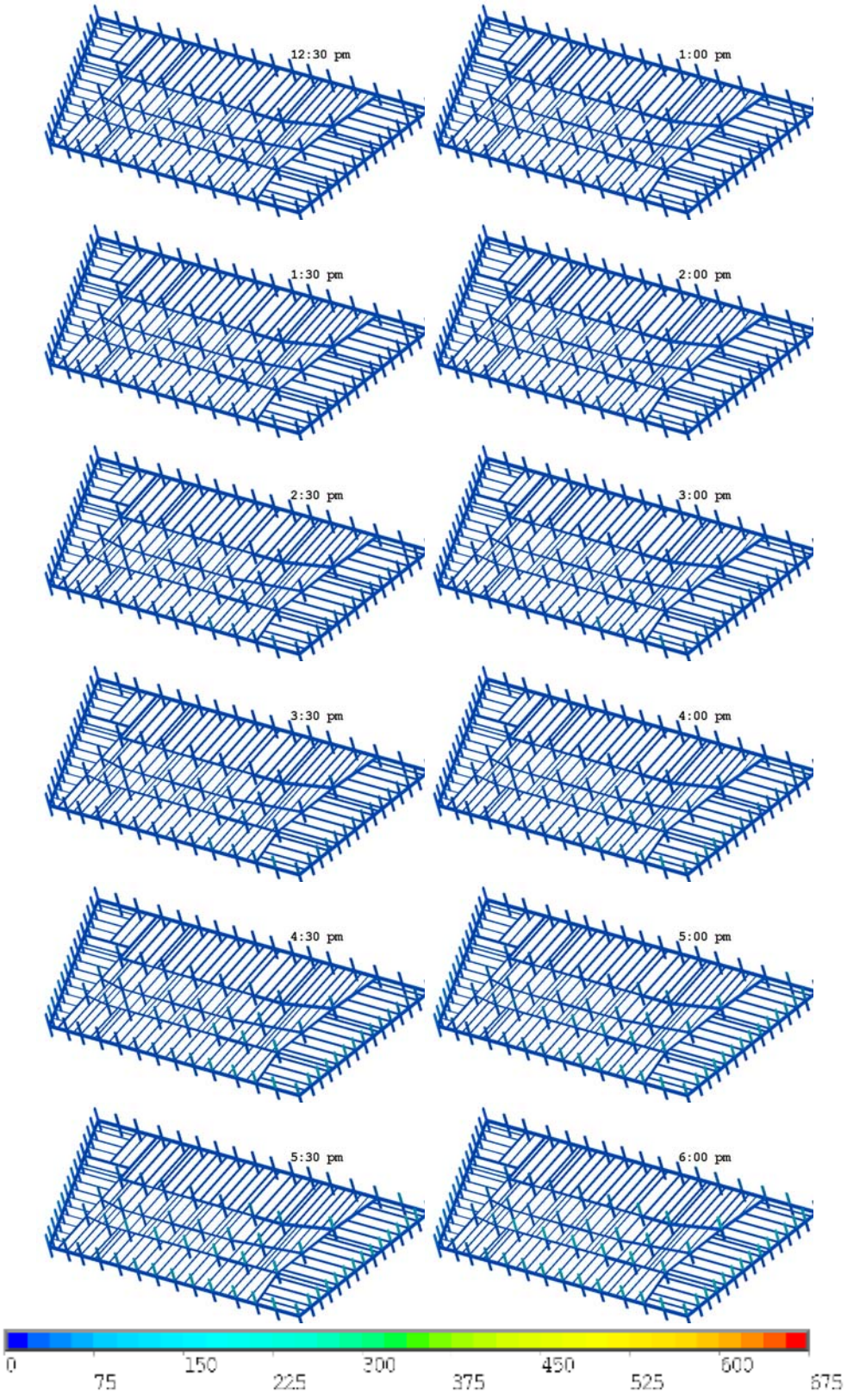

Figure 10–54. Computed temperature distribution (ºC) on the floor beams of floor 11 at 12 different instants in time (Case C, floor slabs removed).

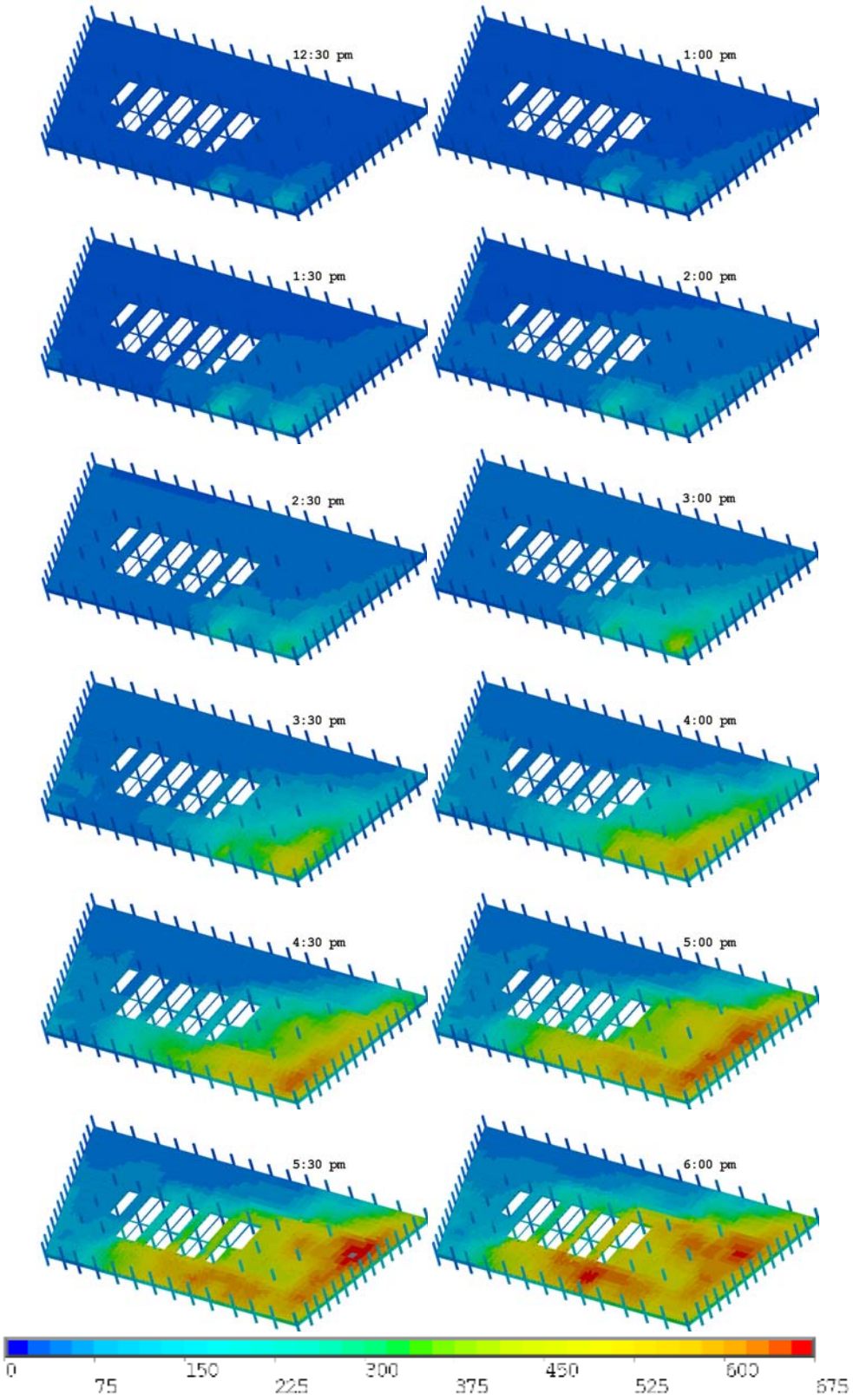

Figure 10–55. Computed temperature distribution (ºC) in the top layer of the concrete slab on floor 12 at 12 instants in time (Case C).

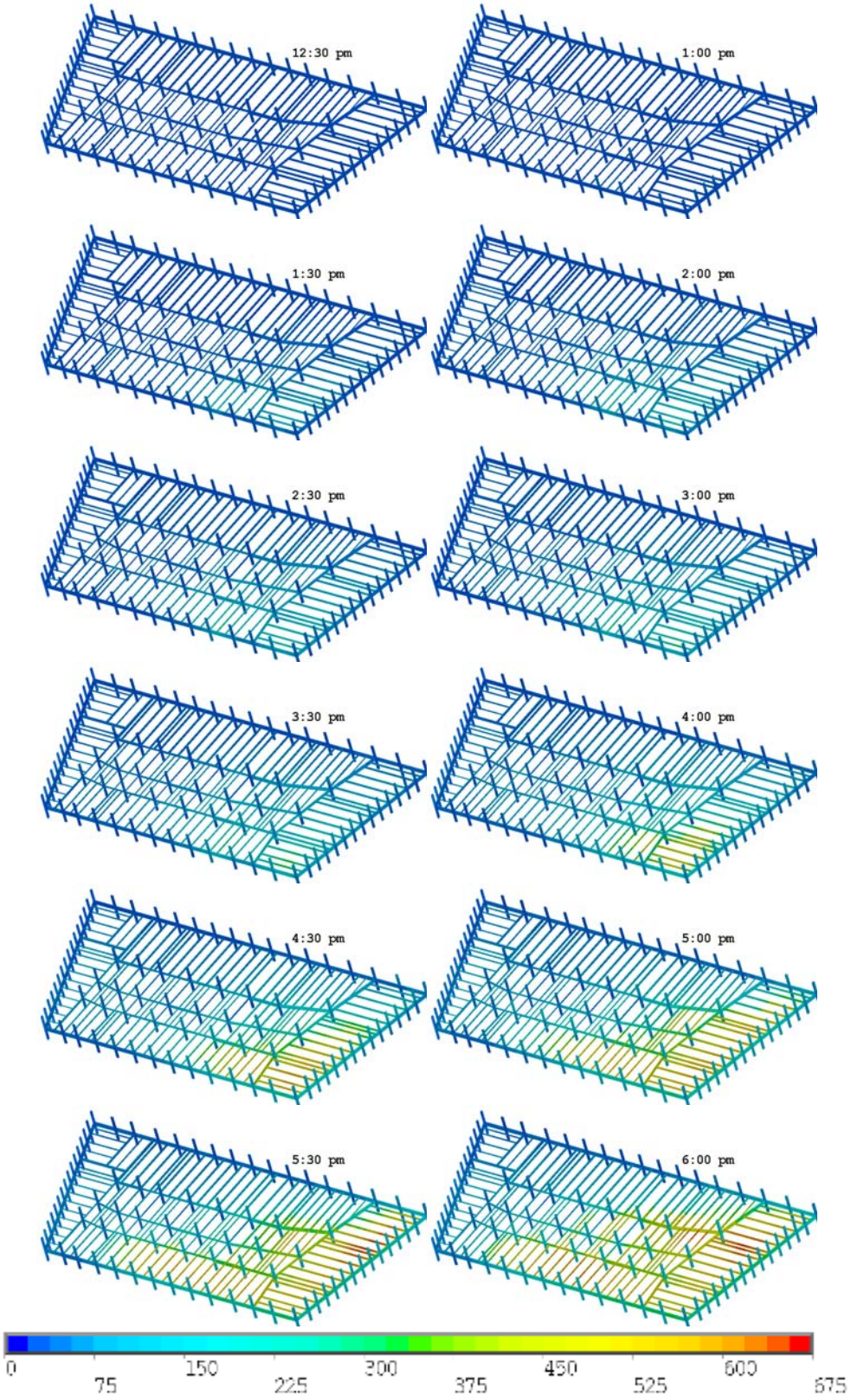

Figure 10–56. Computed temperature distribution (ºC) on the floor beams of floor 12 at 12 different instants in time (Case C, floor slabs removed).

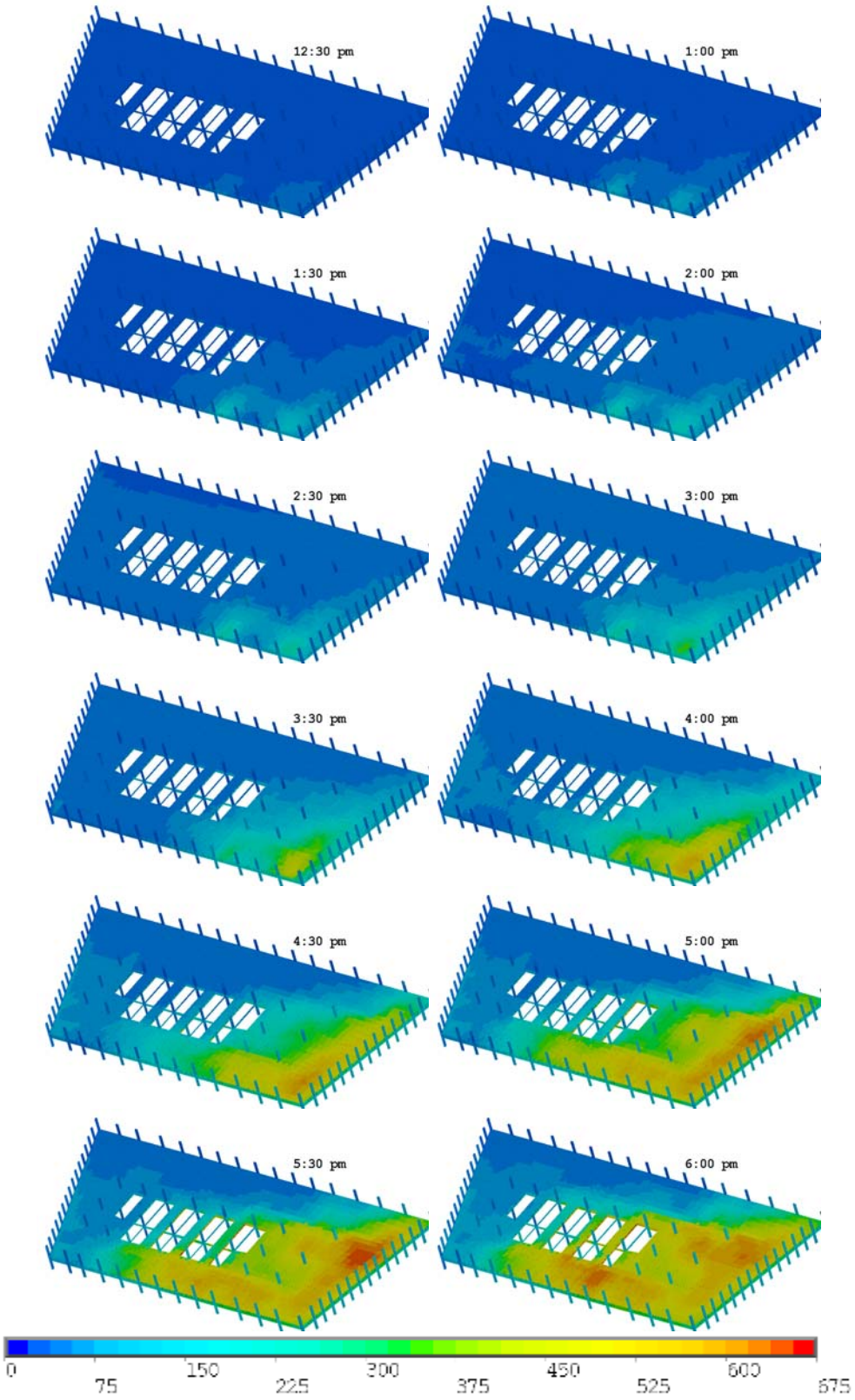

Figure 10–57. Computed temperature distribution (ºC) in the top layer of the concrete slab on floor 13 at 12 instants in time (Case C).

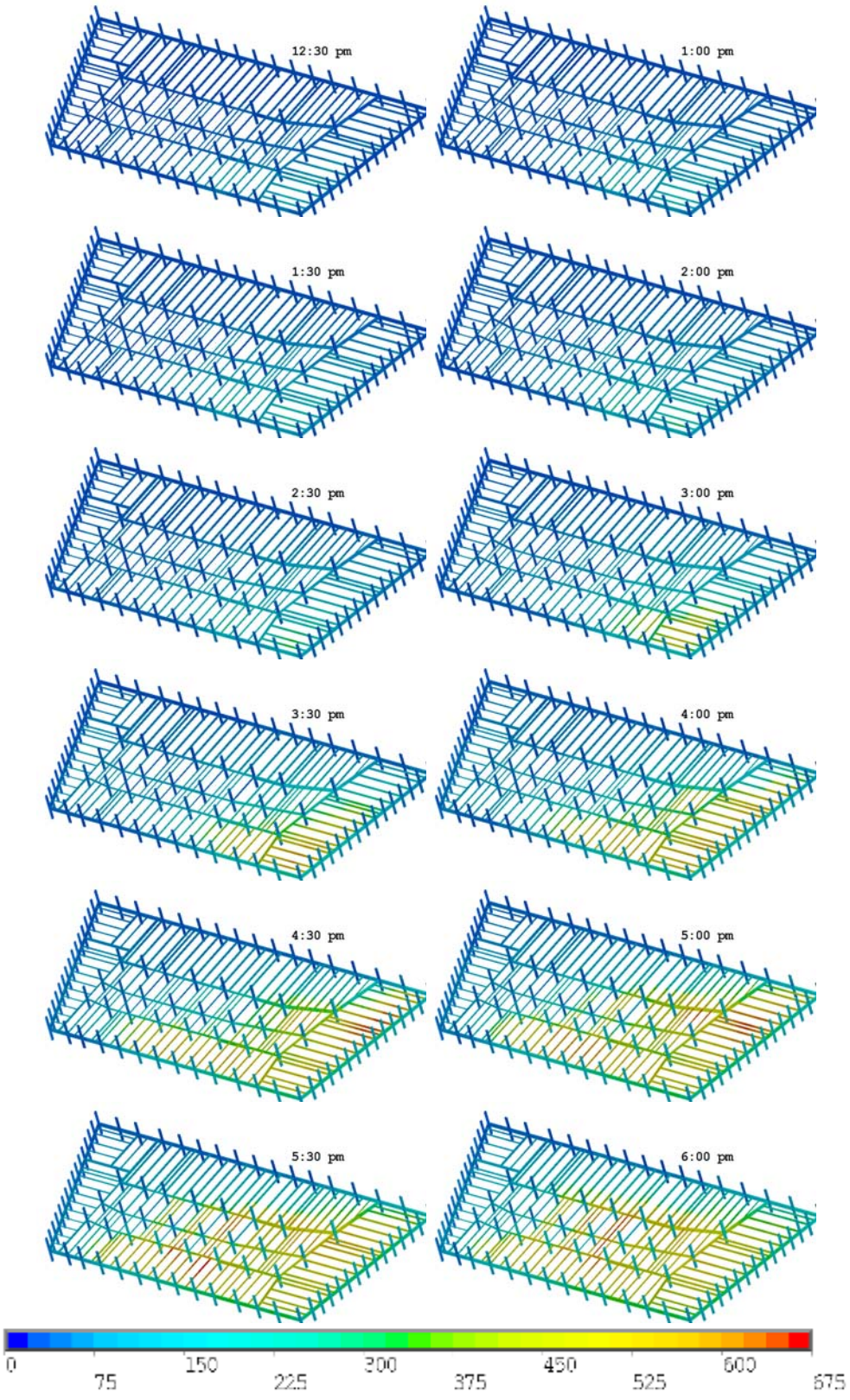

Figure 10–58. Computed temperature distribution (ºC) on the floor beams of floor 13 at 12 different instants in time (Case C, floor slabs removed).

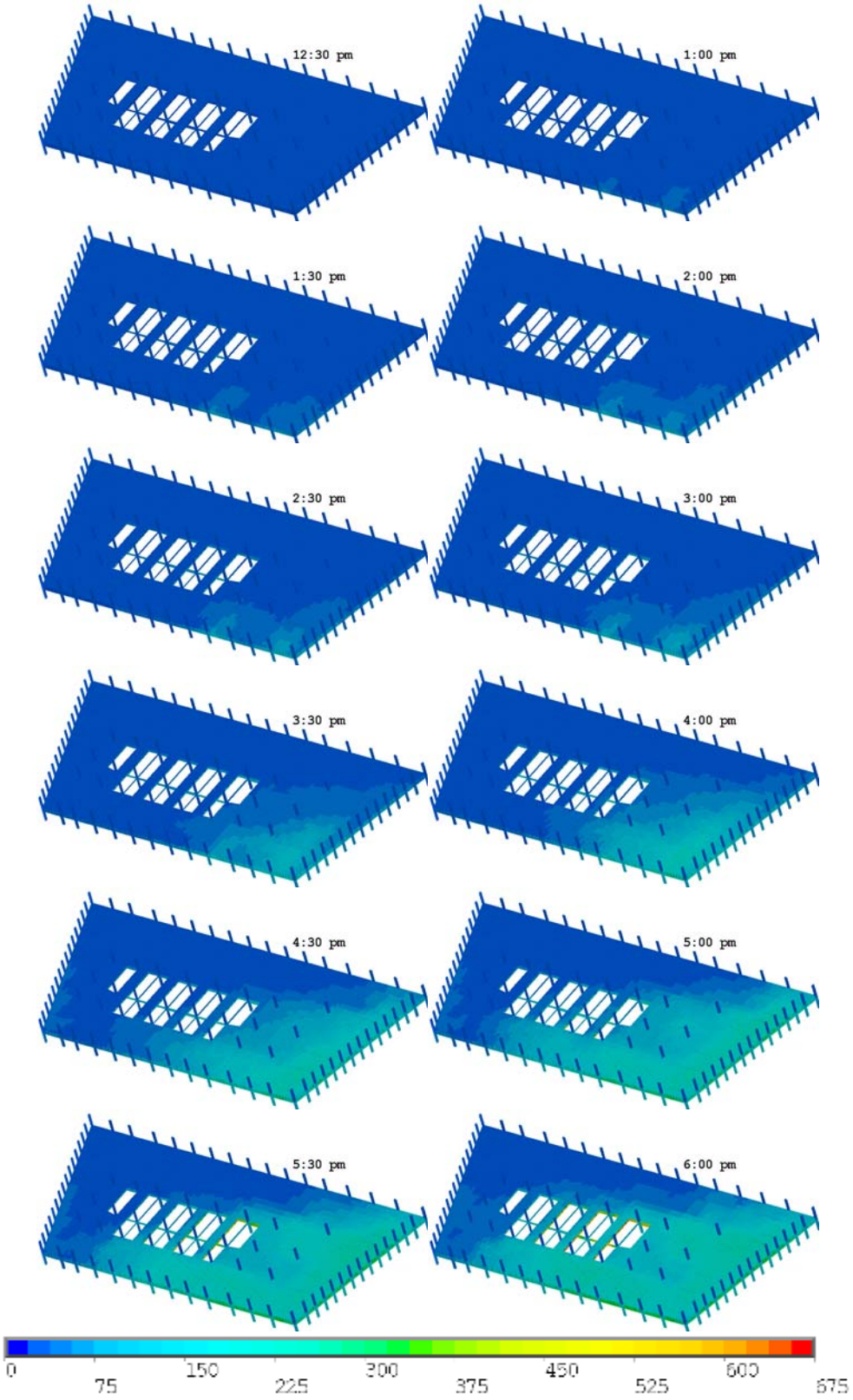

Figure 10–59. Computed temperature distribution (ºC) in the top layer of the concrete slab on floor 14 at 12 instants in time (Case C).

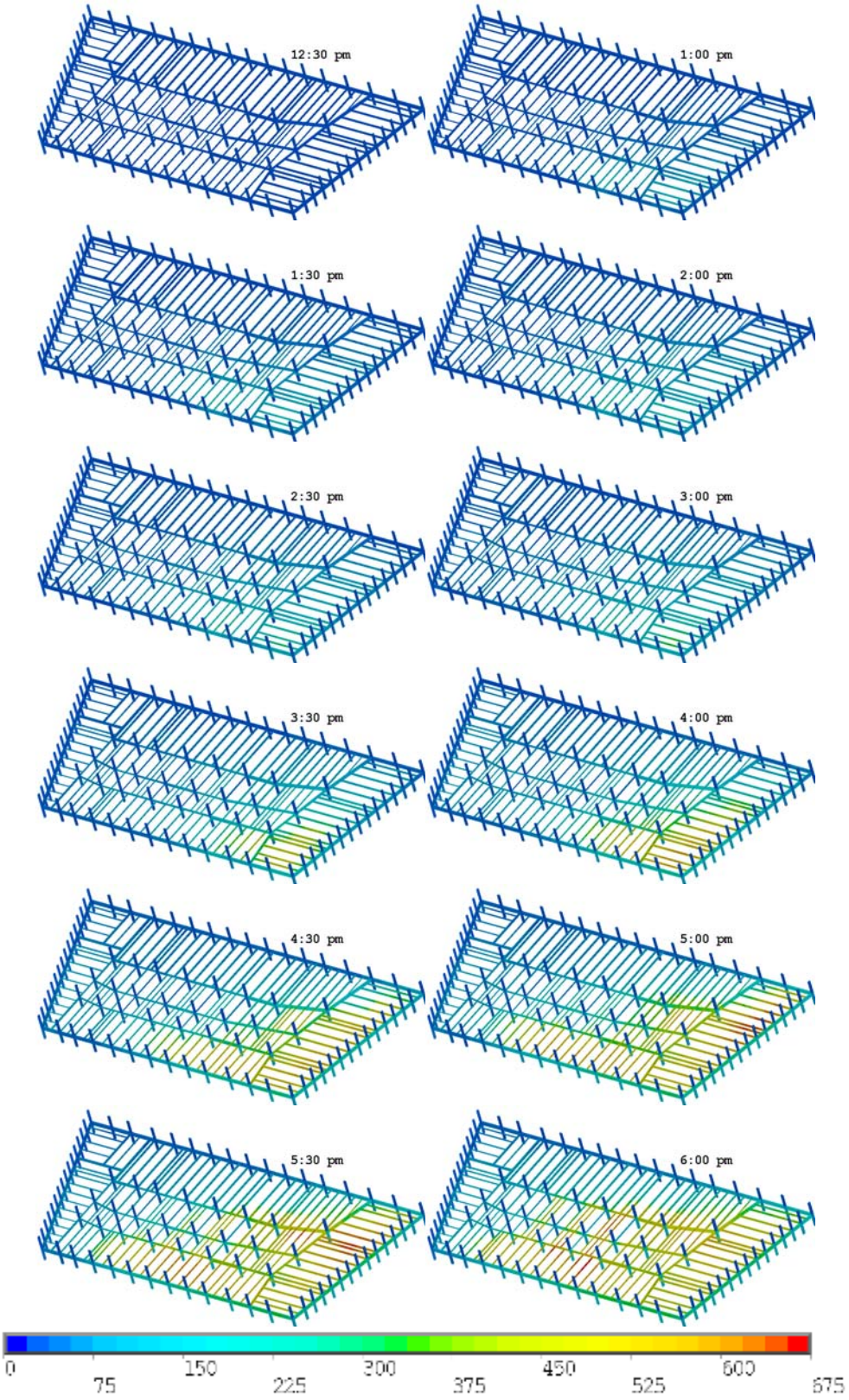

Figure 10–60. Computed temperature distribution (ºC) on the floor beams of floor 14 at 12 different instants in time (Case C, floor slabs removed).

10.4 FINDINGS FROM THE CALCULATED FIRE-INDUCED THERMAL RESPONSE OF WTC 7

Imposing the heat from the simulated WTC 7 fires floor on the building structure led to local temperatures of some structural components that would have significantly diminished the load bearing capacity of those elements. Other structural components, protected by SFRM, remained relatively cool. FSI calculations were performed using the temperatures directly from the FDS simulations (Case A), using temperature rises above ambient that were 10 percent larger than the FDS temperatures (Case B), and temperature rises above ambient that were 10 percent lower than the FDS temperatures (Case C). The temperatures in the latter two Cases were within the expected range of realistic and reasonable fire-generated temperatures.

The following is a list of findings common to the three Cases.

- In none of the Cases did any of the columns, all of which were insulated, reach temperatures sufficiently high for significant loss of strength or stiffness.
    - The temperatures of the large interior Columns 79, 80, and 81 stayed below 200 ºC on all of the floors.
    - Only on floors 12 and 13 did any of the exterior column temperatures exceed 150 ºC. On these floors, the temperatures on the east and south perimeter columns reached 300 ºC.
- The fires on the 7th, 12th, and 13th floors heated portions of the tops of the floor slabs to over 900 ºC. In all cases, significant temperature gradients were observed through the thickness of the concrete slab.
- The temperatures of some sections of the beams supporting the 8th, 12th, 13th, and 14th floor slabs exceeded 600 ºC, except for the 8th floor beams in Case C. The temperatures of some sections of the beams supporting the 9th and 10th floors reached 400 ºC.
- The temperatures of the beam-column connectors in these regions would also have reached levels at which they would have experienced significant loss of strength.

For each of the three cases, Table 10–1 indicates, in blue, those regions of the steel structure that reached a temperature at which nominally half the steel strength remains. It also indicates, in blue, the regions where the tops of the floor slabs reached a similar temperature. An arrow connecting two regions indicates a moving hot zone; a comma connecting two regions indicates both were heated simultaneously.

For the Case B computation, the following characteristics were observed.

- The peak temperatures in the tops of the floor slabs increased by about 80 ºC. The peak temperatures in the floor beams increased by about 75 ºC.
- The floor area over which the temperatures of the supporting beams exceeded 600 ºC increased significantly.
- The overlap between adjacent floors of these > 600 ºC zones increased significantly.

- The change in the temperatures of the perimeter and core columns was not significant, as compared to Case A.

For the Case C computation, the following characteristics were observed.

- The peak temperatures in the tops of the floor slabs decreased by about 80 ºC. The peak temperatures in the floor beams decreased by about 60 ºC
- The floor area over which the temperatures of the supporting beams exceeded 600 ºC decreased significantly.
- The overlap between adjacent floors of these > 600 ºC zones decreased significantly.
- The change in the temperature of the perimeter and core columns was not significant, as compared to Case A.

Table 10–1. Regions in WTC 7 in which computed temperatures of structural components exceeded 600 ºC.

Floor →	Case	7	8	9	10	11	12	13	14
Floor Beams	A	None	NE	None	None	None	E→S	E,SE	E,S
	B	None	NE	None	None	None	E→S	E,SE	E,S
	C	None	None	None	None	None	E→S	E,SE	E,S
Floor Slabs	A	NW→NE	None	None	None	E, SE	E,S	E,SE	None
	B	NW→NE	None	None	None	E, SE	E,S	E,SE	None
	C	NW→NE	None	None	None	E, SE	E,S	E,SE	None
Perimeter Columns	A	None	None	None	None	None	None	None	None
	B	None	None	None	None	None	None	None	None
	C	None	None	None	None	None	None	None	None
Interior Columns	A	None	None	None	None	None	None	None	None
	B	None	None	None	None	None	None	None	None
	C	None	None	None	None	None	None	None	None

This page intentionally left blank.

Chapter 11
STRUCTURAL ANALYSIS OF INITIAL FAILURE EVENT

11.1 OVERVIEW

Two global structural models of WTC 7 were developed to simulate the response of the building to debris impact damage from the collapse of WTC 1 and subsequent fire effects and to evaluate the collapse hypothesis.

The first model, developed in ANSYS (2007), was used to determine how and where the building failure began, which is referred to as the initial failure event or collapse initiation event. The model accounted for nonlinear geometric effects, the temperature dependent behavior of the various members and connections in the fire-affected floors, such as thermal expansion, stiffness and strength degradation, the sequential failure of structural framing and connections under fire conditions, and removal of failed elements (with user intervention). The ANSYS model estimated the structural response to elevated temperatures of the lower 16 stories of the building, where the fires grew and spread, until an initial failure event developed from a series of local structural failures in the floor systems. Since the spatial and temporal changes in the temperature of structural members were slow relative to the dynamic characteristics (i.e., natural frequencies) of the building, the structural response to thermal loads was static. Thus, the ANSYS analysis used a non-linear static procedure with an implicit solution algorithm that guaranteed equilibrium at each time step. The ANSYS analyses are presented in this chapter.

The second model, developed in LS-DYNA, analyzed the collapse propagation phase by accounting for the structural response of the full 47 story structure to the initial failure event due to fire (from the 16 story ANSYS model) up to the collapse of WTC 7, and is presented in Chapter 12. This model accounted for the possibility for the development of progressive collapse of the entire building, including buckling instability of columns due to loss of lateral support, dynamic effects associated with failure progression, and debris impact from falling floors. The results of the ANSYS model were input into the LS-DYNA model as initial conditions.

The floor framing geometry, member sizes, and gravity loads for both models were obtained from structural and architectural drawings, as well as erection and fabrication shop drawings of connections for the steel framing (Chapter 2). Mechanical properties of steel and concrete materials, which included room and elevated temperature behaviors, were based on the relevant information developed during the investigation of the WTC towers.

An important feature of the WTC 7 ANSYS model was the user-defined elements developed to model the behavior and failure of floor framing connections at elevated temperatures. The structural floor connections were analyzed for all possible failure modes. The failure modes and their associated capacities were used to develop user-defined connection elements, which are also referred to as break elements. Break elements were used on the east side of Floors 7 to 14, where the fires were dominant prior to collapse. Including break elements at every connection location on these floors would have

greatly increased the model size and affected the rate of solution convergence. Since the failure of WTC 7 clearly initiated on the east side of the structure (Chapters 5 and 8), the break elements were used only in the east side of the model.

Debris impact damage from the collapse of WTC 1 was included in the LS-DYNA model, but not in the ANSYS model. The structural damage that was observed following the collapse of WTC 1 was located between Floors 7 and 17 in the southwest quadrant of the building (Chapter 5). The WTC 7 structure redistributed loads around this damage through the Vierendeel truss action[5] provided by the exterior moment frame. The ANSYS model, which modeled the structure from the ground level to Floor 16, did not include a sufficient number of floors to capture the load redistribution following the debris impact damage. The model did not include the debris damage since this was unnecessary to analyze the initiating event which occurred in the northeast region of the building.

Analysis with the ANSYS model included the effects of gravity and temperature loads. Gravity loads included: the dead load of the structure; superimposed dead loads consisting of the weight of ceilings, mechanical and electrical equipment, thermal insulation, and floor finishes; and service live load, which was taken as 25 percent of the design live load specified in the original design documents. The gravity loads from the floors above Floor 16 were applied to the top of the columns. Wind loads were not considered in the analyses, as the wind speeds on September 11, 2001, were not structurally significant.

Temperature data were input at 30 min intervals for the fires observed on Floors 7 to 9, and 11 to 13. The temperature data were obtained from the FSI analysis (Chapter 10), which was based the FDS analysis of the fires (Chapter 9). Three different thermal cases were developed and were used in the ANSYS analysis. These cases were within the range of realistic and reasonable fires in WTC 7 on September 11, 2001. Case A used the temperature data as obtained from the FDS simulations. Cases B and C increased and decreased, respectively, the Case A gas temperature by 10 percent, which was judged to be within the range of uncertainty for these fires.

11.2 ANSYS MODEL

11.2.1 Model Description

A finite element model, referred to hereafter as the 16 story model, was developed and is illustrated in Figure 11–1. As fires were observed on Floors 7 to 9 and 11 to 13, the floors and columns in these areas were subject to heating and possible thermally induced failures, while floors and columns above Floor 14 and below Floor 7 were not. Floor framing between Floors 8 and 14 and columns between Floors 7 and 14 were explicitly modeled, while Floor 7 and below and Floors 15 and 16 were modeled using superelements. Superelements reduce the degrees of freedom, and hence, computational time, while appropriately representing the stiffness at the top and bottom of the model.

The gravity load was applied in stages to represent the effects of construction sequence. The thermal loading was applied in the form of temperature-time histories. Examination of temperature changes in structural elements with time during the FSI analysis found that the temperature state of steel and concrete

[5] Most trusses have a triangular shape and pinned joints that can transfer forces but not bending moments. A Vierendeel truss has a rectangular shape and fixed joints that can transfer and resist forces and bending moments.

members could be provided at 30 min intervals to the ANSYS model, and linearly interpolated between these intervals, to reasonably model the spatial and temporal temperature changes in the structural system. Therefore, each temperature state of the structural system was defined discretely at 30 min intervals and temperatures were linearly interpolated between the 30 min interval temperature states.

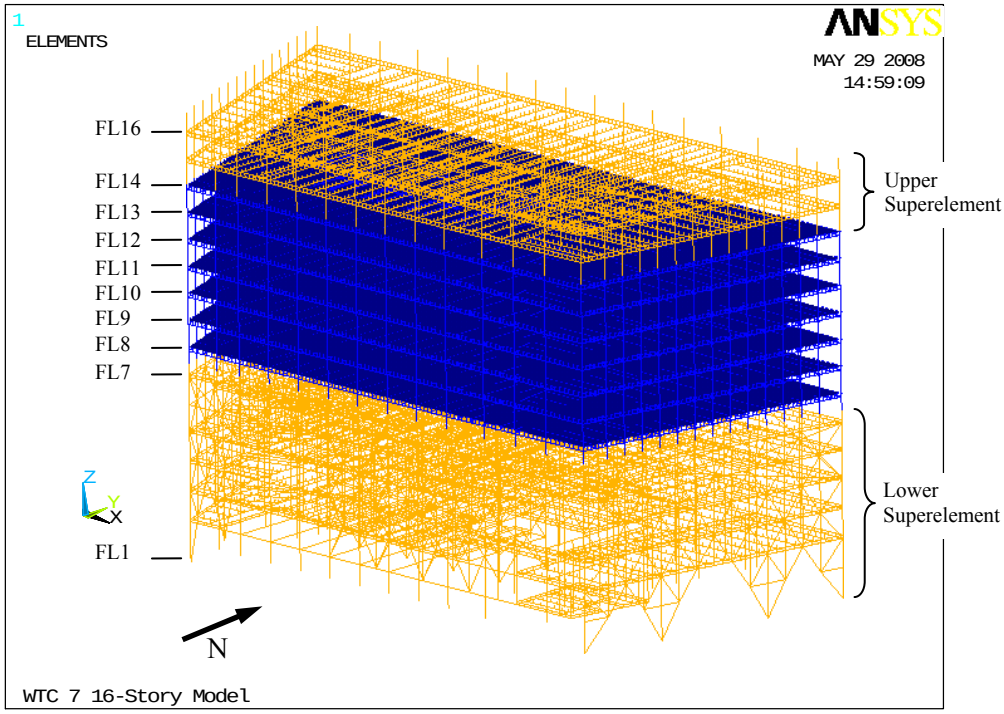

Figure 11–1. 16 story model representing lower 16 floors of the WTC 7 building.

In developing the 16 story model, various subsystems were analyzed to (1) evaluate the performance of connection element models, (2) evaluate the performance of a composite floor beam model with connections under temperature effects, and (3) determine the number of elements needed to capture lateral-torsional buckling of beams and girders and buckling of columns. Results of the subsystem analyses were used in the development of the 16 story model.

Element types used in developing the 16 story model are summarized in Table 11–1. Beams and girders for floor framing and columns were modeled using ANSYS BEAM188 element type with temperature-dependent inelastic material properties. Typically, the columns were meshed with 2 ft long elements, and beams were meshed with 3 ft long elements. Typical mesh size for the floor slab was selected as 3 ft x 3 ft. BEAM188 elements are suitable for analyzing slender to moderately stubby/thick beam structures, and are based on Timoshenko beam theory and include shear deformation effects. The floor slab was modeled using SHELL181 element type with temperature-dependent inelastic material properties.

Rigid beams were typically used in connection models between beams and girders, girders and columns, and shear studs between floor beams and the floor slab to simulate composite action in the floor system. BEAM4 element type was used in modeling rigid beams. The CONTA178 element type was used to model contact and sliding between two nodes in floor beam, girder, floor slab, and connection components. COMBIN37, COMBIN39, USER102, USER103, and USER104 element types were used to

model beam-to-girder and girder-to-column connections. COMBIN37 is a unidirectional element with the capability of turning on and off during an analysis. COMBIN39 is a unidirectional element with nonlinear generalized force-deflection capability. USER103 and USER104 elements were used to model shear connections. USER105 element type was used to model failure of shear studs. Details of how these connections were modeled are discussed in Section 12.2.5.

Due to the nonlinearities in the analysis, as well as sequential local failures, a 30 min analysis could take several weeks to complete. Due to the range of time steps that were required to reach equilibrium (e.g., from 10^{-6} seconds to 10s of seconds), a complete ANSYS analysis for a given thermal case took approximately six months to complete on a 64 bit workstation with a quad-core, 3.0 GHz processor, and 64 GB of Random Access Memory (RAM). The inclusion of user-defined elements prevented parallel processing on a Linux cluster.

Table 11–1. Element types used in 16 story model.

Element Type	Number of Elements	Material Model	Where Used
BEAM188	21,095	Inelastic	Beams, girders, and columns
BEAM4	28,182	Elastic	Beams between floor slab and beams and in modeling connections
SHELL181	34,461	Inelastic	Floor slab
CONTA178	6,342	Inelastic	Contact between floor beams/girders and floor slab
COMBIN37	504	Inelastic	User-defined connections
COMBIN39	812	Inelastic	User-defined connections
USER102 (Break Element)	1,176	Inelastic	User-defined connections
USER103 (Break Element)	2,520	Inelastic	User-defined connections
USER104 (Break Element)	1,512	Inelastic	User-defined connections
USER105 (Break Element)	4,753	Inelastic	User-defined shear stud connections
Total Number of elements = 101,357			
Total number of nodes = 93,413			

11.2.2 Temperature-dependent Material Properties

The mechanical properties of steel are affected significantly by elevated temperatures. The steel for all beams and interior columns was ASTM A572 Grade 50, and the steel for exterior moment frames was ASTM A36. Material specifications for cover plates on the interior columns were based on plate thickness t (in.), where:

$2 < t < 4$ ASTM A588 Grade 50

$4 < t < 6$ ASTM A572 Grade 42

$t > 6$ ASTM A588 Grade 42

The steel used for the connections was a Canadian Algoma steel plate, specified as CSA G40.21-44W with a nominal yield strength of 44 ksi.

The same procedure used for the WTC towers to develop temperature dependent material properties was used for the WTC 7 steel (see Appendix E). For WTC 7, material properties were developed for the Algoma 44W steel plate and temperature-dependent material properties were developed for ASTM A325 and A490 bolts.

No test data existed for the CSA G40.21-44W steel. The true stress-strain behavior was modeled as an average of the A572 and A36 behaviors, but chemically the steel is more like A572 than A36. Therefore, the estimated tensile strength was developed with strain criteria for A572. The yield and tensile strength of bolts degrade more rapidly with increasing temperature than do ordinary structural steels. A separate relationship to describe their yield and tensile behavior, based on limited data available in the literature, was developed. The development of these data is described in Appendix E.

The analysis used the ANSYS multilinear isotropic hardening model (MISO) for temperature dependent material properties for steel and concrete. MISO defines piecewise linear stress-strain curves at specified temperatures. The origin is not included, and the slope of the first segment between the implied (0,0) and the first point, which is the yield strength, must equal the elastic modulus for the specified temperature. The models were expressed as eleven data files at specific temperatures: (20, 400, 450, 500, 550, 600, 650, 700, 750, 800, 850) ºC. Each data set contained eleven stress-strain points. The piecewise linear MISO models for A572 steel and the concrete slab are shown in Figure 11–2 and Figure 11–3, respectively.

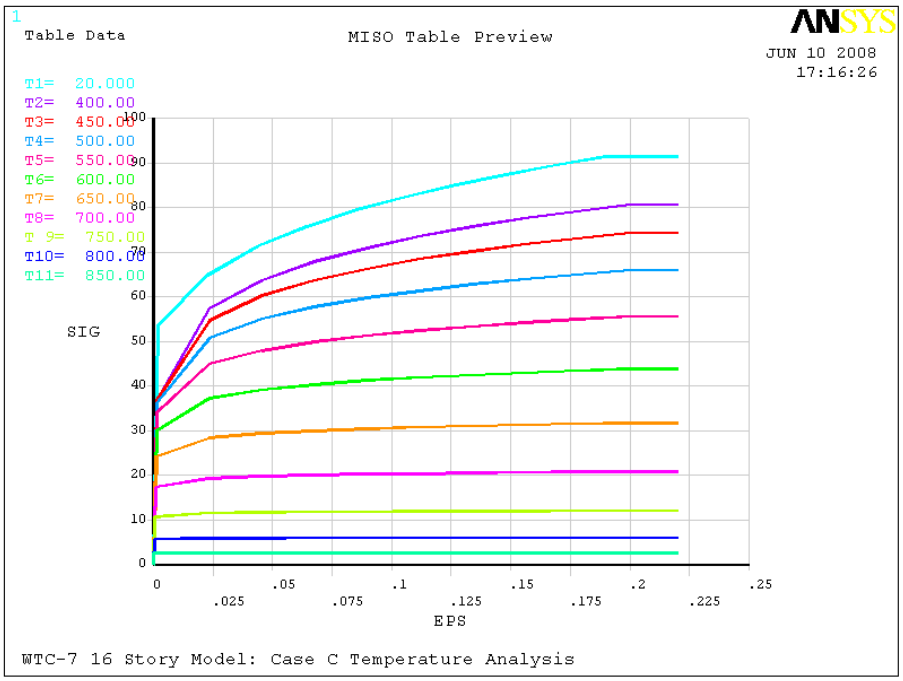

Figure 11–2. ANSYS multilinear isotropic hardening (MISO) model for temperature-dependent behavior of ASTM A572 grade 50 steel.

The concrete slabs had a normal weight concrete with a specified compressive strength of 3,500 psi. Even though concrete behavior is different in compression and tension, ANSYS did not have a material model that could input different compression and tension stress-strain curves. Therefore, concrete was modeled using a compressive stress-strain relationship for both tension and compression (compressive failures occur at approximately 4,000 psi relative to tensile failures at approximately 500 psi). Concrete failure by crushing in compression and cracking in tension were accounted for by checking element strains against limiting strain criteria. Once these strain criteria were met, elements were either softened or removed as described in Section 11.2.9.

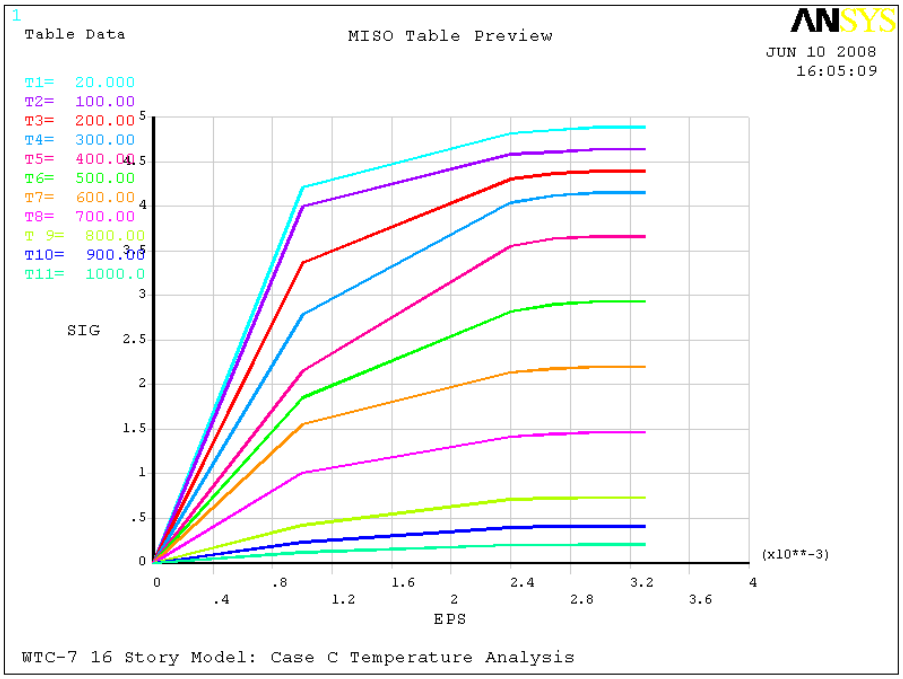

Figure 11–3. ANSYS multilinear isotropic hardening (MISO) model for temperature-dependent behavior of 4000 psi normal weight concrete slab.

11.2.3 Modeling Composite Floor System

In WTC 7, the floor system was designed for composite behavior between the floor beams and the slab (Chapter 2). Composite behavior was achieved through shear studs that were welded to the top flanges of the beams and embedded in the concrete slab. The shear studs transferred shear loads between the slab and beams, so that the floor system acted as a single component in flexure. Floor beams and exterior spandrel beams had shear studs, but the girders that supported the floor beams did not have shear studs.

The composite floor system was modeled as shown in Figure 11–4. The floor slab was modeled at the centerline elevation of the slab, using the SHELL181 element type. Beams and girders of the floor framing were modeled at their section centroid, using the BEAM188 element type. The mesh of the floor slab was aligned with that of beams and girders.

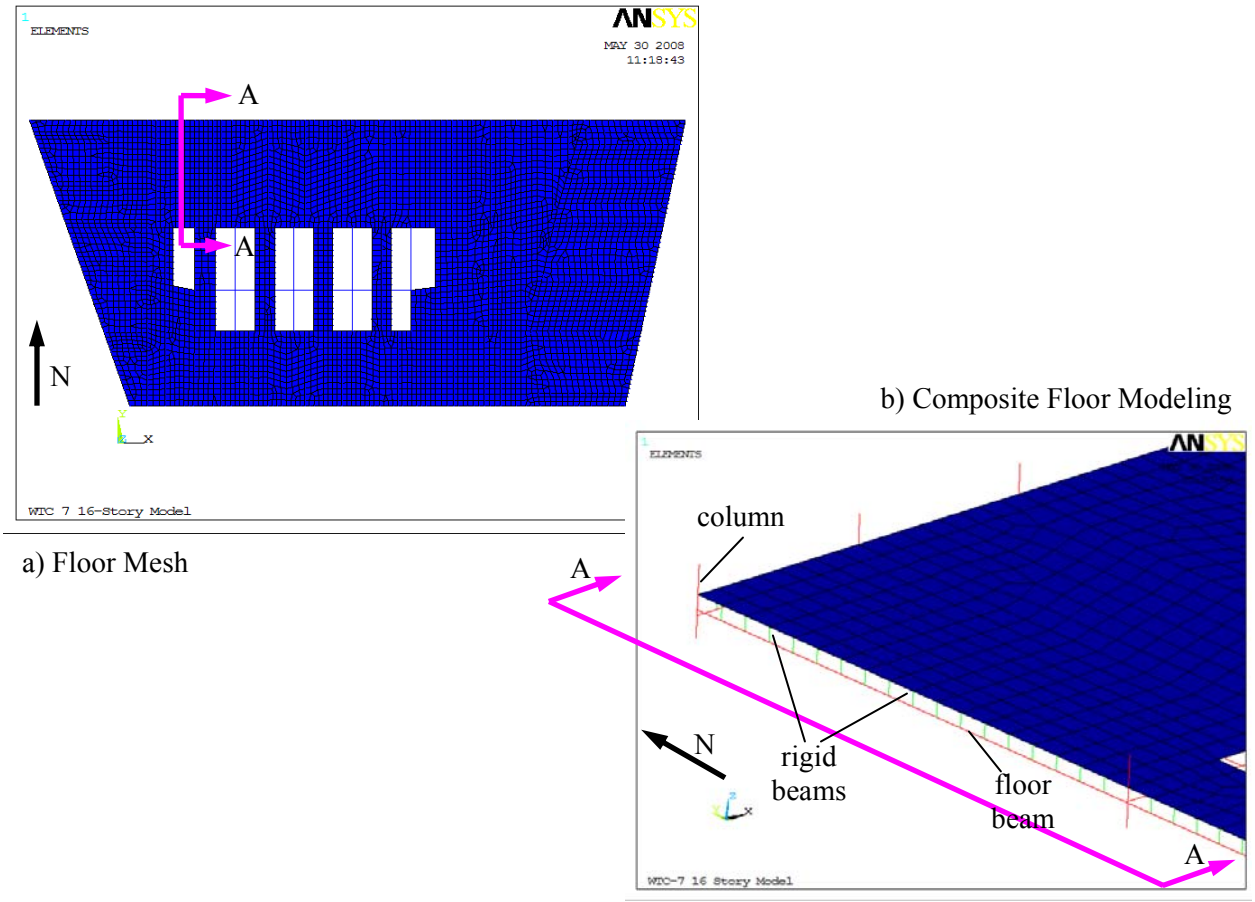

Figure 11–4. Finite element representation of the composite floor system.

Contact elements were used between the slab and girder to allow the slab to transfer gravity loads, but not shear forces to the girder. Contact elements also allowed the girders to sag independently of the floor slab, and prevented slab penetration through the girder in the analysis. To model composite action between floor beams and slabs, break elements were used to represent shear studs. These break elements represented the temperature-dependent shear stud capacity and captured shear failures between the slab and the shear stud. Details of modeling the shear studs using break elements are discussed in Section 11.2.5.

The gravity load on the floor slab was transferred to the floor beams, then to the girders, and finally to the columns. The floor slab did not have structural connections to the girders or columns.

11.2.4 Floor Framing Connection Failure Modes

To determine the capacities of the various types of floor connections (Chapter 2), failure modes were evaluated for each connection type. Failure modes included weld failure, bolt failure (both shear and tension), plate tear-out, and block shear failure. Capacities, also referred to as failure loads or ultimate strength, were based on the AISC LRFD design provisions (AISC 2005). To determine failure loads instead of design loads, load and resistance factors were set to 1.0.

Weld Failure

The ultimate strength of a fillet weld loaded in plane, $R_{n\text{-}weld}$, was given by

$$R_{n\text{-}weld} = F_w A_w \qquad \text{(Eq. J2-4, LRFD)}$$

where

$$F_w = 0.60\, F_{EXX}\,(1.0 + 0.50 \sin^{1.5} \theta) \qquad \text{(Eq. J2-5, LRFD)}$$

and

F_{EXX} = electrode classification number, ksi

θ = angle of loading measured from the weld longitudinal axis, degrees

A_w = effective area of the weld, in.^{2}

The area of a fillet weld was taken as the throat × length, or

$$A_w = L_w \times (\sqrt{2}/2)\,(D/16)$$

where

L_w = length of weld, in.

D = size of fillet weld (leg) in 16ths of an inch.

Weld electrodes were specified as E70xx, for which F_{EXX}= 70 ksi. Therefore, the nominal weld strength was given by

$$R_{n\text{-}weld} = 1.86\,(1+ 0.50 \sin^{1.5} \theta)\, L_w \times D$$

When a weld group is loaded eccentrically, as occurs in the header connections under a vertical shear force, there is a combined effect of the shear force and the moment resulting from the eccentric application of the shear force to the weld group[6]. To account for this combined effect, the "instantaneous center of rotation" method, found in AISC Manual (AISC 2005), was used to determine the weld group ultimate capacity.

Bolt Shear Failure

Bolt shear failure occurs when two surfaces, such as a connector plate and a beam web, are displaced relative to each other and sever the bolt across its cross section. The ultimate shear strength of a single high strength bolt, $R_{n\text{-}bolt\ shear}$, was given by

[6] A weld group is a set of several welds in a single connection. The welds typically are oriented perpendicular to each other and may have different lengths. For instance, to weld a connector plate to a beam web, a weld group consisting of a weld along the end and both sides of the plate may be used.

$R_{n\text{-}bolt\ shear} = A_b \times F_{nv}$ (Eq. J3-1, LRFD)

where

A_b = area of the bolt shank, in.^{2}

F_{nv} = nominal bolt shear stress, ksi.

For determination of bolt shear capacity, the threads were assumed to be excluded from the shear plane. This is a conservative assumption since the bolt section with threads has a reduced cross-sectional area. In bearing-type connections, the nominal shear stress of ASTM A325 bolts is 60 ksi (AISC 2005, Table J3.2). Kulak (2002) states that the values in Table J3.2 were decreased by 20 percent to account for the uneven load distribution that occurs in splice connections, where a line of bolts are parallel to the applied load. However, in shear connections, the loads are distributed evenly among all bolts under both vertical and horizontal loading. Thus, the nominal shear stress was adjusted (divided by 0.8) to give

$F_{nv\text{-}A325} = 60 / 0.8 = 75$ ksi

For a 7/8 in. A325 bolt, the bolt shear capacity was

$R_{n\text{-}bolt\ shear} = 0.601\ \text{in}^2 \times 75\ \text{ksi} = 45\ \text{kip}$

Similarly, the ultimate shear strength of ASTM A490 bolts is 75 ksi (AISC 2005, Table J3.2), so following the same procedure gave

$F_{nv\text{-}A490} = 75 / 0.8 = 93.75$ ksi.

In determining the shear strength of a bolt group, it was possible that the last bolt in a line would tear out before its shear strength was developed. Thus, tear-out failure, as described below, had to be accounted for in determining the shear strength of a bolt group.

Bolt Tension Failure

The ultimate tensile strength of a single high strength bolt, $R_{n\text{-}bolt\ tension}$, where the tensile force is applied along the length of the bolt, was given by

$R_{n\text{-}bolt\ tension} = A_b \times F_{nt}$ (Eq. J3-1, LRFD)

where

A_b = area of the bolt shank, in.^{2}

F_{nt} = nominal bolt tensile strength, ksi.

For ASTM A325 bolts, $F_{nt\text{-}325}$ is 90 ksi and for ASTM A490 bolts, $F_{nt\text{-}490}$ is 113 ksi (from AISC 2005, Table J3.2).

Tear-out Failure

Tear-out failure for a single bolt occurs under tensile loads along two shear planes in the connector plate, as indicated in Figure 11–5. The ultimate tear-out strength, $R_{u\text{-}tearout}$, was given by

$$R_{u\text{-}tearout} = 1.5\, L_c\, t\, F_u \quad \text{(J3-6c, LRFD)}$$

where L_c is the clear distance between the edge of the hole and the edge of the plate, t is the plate thickness, and F_u is the ultimate tensile stress. Ultimate strengths for tear-out failure were calculated for both the beam web and the connection plate.

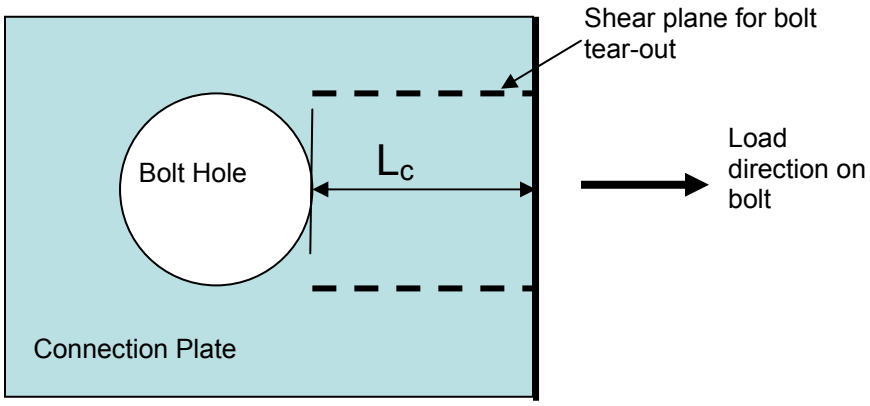

Figure 11–5. Tear-out mode of failure.

Block Shear Failure

Block shear is a rupture or tearing phenomenon, where the ultimate strength is computed as the sum of the shear strength and tensile rupture strength along a failure path. Block shear under a vertical load is a possible failure mechanism in single shear plate (fin) connections in both the coped beam and shear plate as shown in Figure 11–6. Figure 11–7 shows possible shear failure paths when a double angle connection is subjected to horizontal loading. Cases 1, 2 and 3 are for failure in the connection angles and Case 4 corresponds to failure in the beam web. Note that in Figure 11–6 and Figure 11–7, the element or member that fails in block shear is white, and the failed block is cross-hatched.

All possible failure paths in the connected elements (beam web, angles or plates) were checked and the block shear failure strength of the connection was determined from the lowest value obtained. The nominal block shear strength along a shear failure path and a perpendicular tension failure path was given by

$$R_{u\text{-}block\ shear} = 0.6\, F_u\, A_{nv} + U_{bs}\, F_u\, A_{nt} \leq 0.6\, F_y\, A_{gv} + U_{bs}\, F_u\, A_{nt} \quad \text{(J4-5, LRFD)}$$

where,

A_{gv} = gross area subject to shear, in^2

A_{nt} = net area subject to tension, in^2

A_{nv} = net area subject to shear, in^2

and, for uniform tension stress (assumed here), $U_{bs} = 1$. Note that the gross area subjected to shear was used for the yield limit state and the net area subjected to shear (i.e., the gross area less the area of the bolt holes) was used for the rupture limit state. Both the yield and rupture limit states had to be computed and the smaller (minimum) value used. Thus, Equation J4-5 was rewritten as:

$$R_{u\text{-}block\ shear} = F_u A_{nt} + \min(0.6 F_y A_{gv}, 0.6 F_u A_{nv})$$

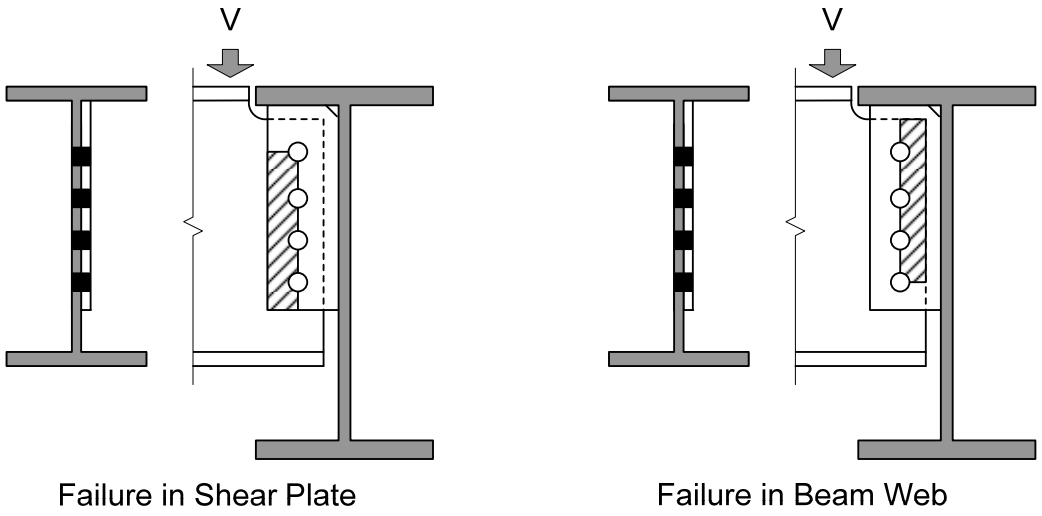

Figure 11–6. Block shear failure planes for vertical shear forces.

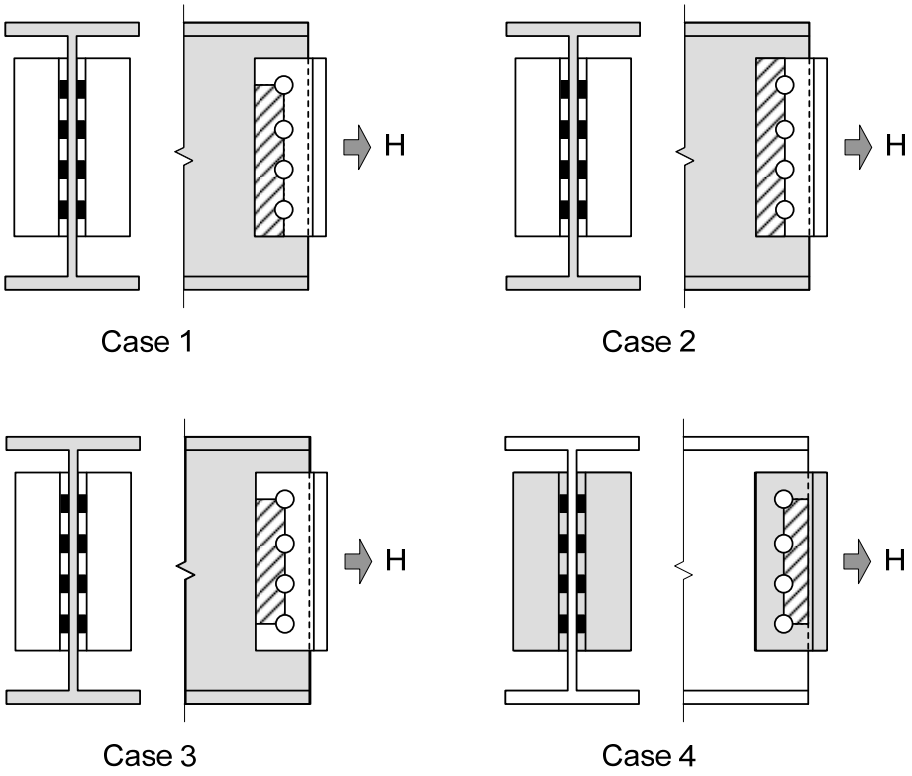

Figure 11–7. Block shear failure planes for horizontal tension force.

Shear Stud Failure

Shear stud failure in a composite floor system occurs when the concrete slab is either crushed or cracks around the shear stud, or the shear stud separates from the floor beam. Nearly all shear stud failures are due to failure of the concrete slab, so that failure mode was modeled in ANSYS. Shear stud failure in a composite floor system depends on a number of variables, including the depth and rib geometry of the metal deck, slab thickness, concrete properties, location of the studs relative to the beam axis, and the stud strength.

Metal decks typically have stiffeners in the center of the rib section that rests on the steel beam flange, as shown in Figure 11–8. The stiffener requires that the shear stud be placed off center from the center of the rib, which affects the strength of the shear connection perpendicular to the span of the metal deck. This is because the amount of concrete between the steel deck and the stud depends on the direction of the load relative to the amount of concrete that the stud can bear on when transferring the shear load between the slab and the floor beam. The direction of load transfer is termed "strong" or "weak", to refer to the relative load capacity associated with each direction, as shown in Figure 11–8.

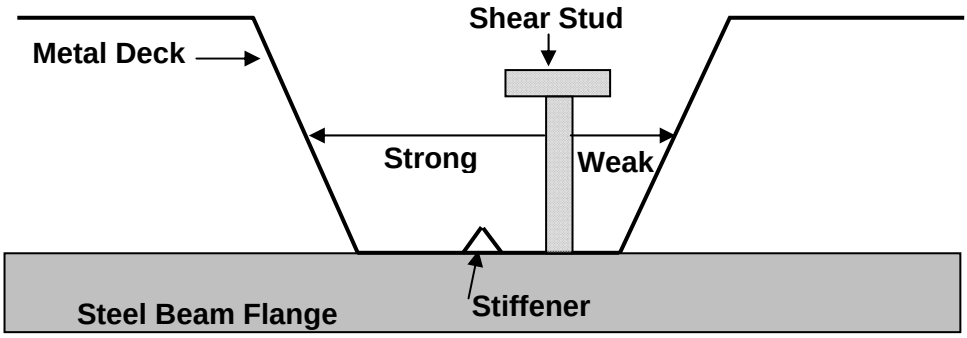

Figure 11–8. Schematic of shear stud placement relative to the metal deck.

Two sources were found for predicting shear stud strength in a composite floor system with a metal deck. For shear studs in a 3 in. metal deck, where the applied load is perpendicular to the metal deck ribs, the shear stud strength, Q_{sc}, is given by (Rambo-Rodenberry, 2002)

$$Q_{sc} = R_p R_n R_d A_s F_u = 19.5 \text{ kip}$$

where

R_p = 0.68 for e ≥ 2.2 in. (e is the distance from center of stud to mid-height of deck web on the loaded side) for strong position studs

R_n = 1.0 for one stud per rib or staggered position studs

R_d = 1.0 for all strong position studs

A_s = 0.44 in.^{2} for 0.75 in. shear stud cross sectional area

F_u = 65 ksi (this ultimate strength value has been shown to accurately predict published experimental results for shear stud failure in a composite floor system)

Values given by AISC (2005) using Table 3-21 for metal deck ribs that are perpendicular to the floor beam are given as

Qn = 21.5 kip Strong studs per rib

and

Qn = 17.2 kip Weak studs per rib

The average of the strong and weak directions give a shear stud strength of

Qn = 19.4 kip Average of strong and weak

The shear stud capacity was taken as Q_{sc} = 19.5 kip. This value was used for forces that were both perpendicular and parallel to the metal deck ribs.

Failure Loads of Shear Connections

The shear connections in WTC 7 were designed to support dead and design live gravity loads, but they were not designed for horizontal loads from the floor beams due to thermal expansion or other fire effects. The shear connections on the typical tenant floors were evaluated for horizontal and vertical failure loads for room temperature material properties, using the failure modes previously described in this section. The seated connections with a top clip (STC) and seated connection with a tip plate (STP) were evaluated for horizontal loads only, as the vertical capacity of the welded seat plates for these connections (i.e., at Columns 79 and 81) was much greater than the applied vertical loads, even for full design loads. The SWC connections were evaluated for horizontal and vertical failure loads, but the web clip and the seat capacities were evaluated separately.

The ratio of vertical failure load (no load or resistance factors) to the design load for the fin, header, and knife shear connections was determined for the typical tenant floor construction, as shown in Table 11–2, Table 11–3, and Table 11–4. The average vertical failure load-to-design load ratio was approximately 3.2 for the core floor beams and girders and 4.4 for the tenant floor beams and girders; the values ranged from a minimum of 1.9 to a maximum of 7.2. A vertical failure load to design load ratio of approximately 2.0 to 4.0 is within the typical range expected for these types of connections.

Failure loads for forces applied in the horizontal direction depended on the direction of load. For instance, if a knife connection was subject to a compressive axial load, the failure mode would be bolt shear, but if it were subject to a tensile load, the failure mode would be fracture of the weld at the column face. Since the shear connections were not designed for a horizontal load, no comparison of horizontal load capacity to design load could be made.

Table 11–2. Ratio of vertical capacity to design shear load of shear connections for floor beams and girders on a typical tenant floor.

Tenant Floor Beams and Girders	Connection Type	Failure Load (kip)	Failure Mode	Design Shear Load (kip)	Failure Load/ Design Shear Load
Floors 8 to 20, 24 to 45					
South Tenant Floor					
W24x62	H4	217	Block Shear-plate	69	3.1
W24x62	K4	190	Block Shear-web	69	2.7
W16x77	F4	166	Block Shear-plate	73.4	2.3
W16x26	F4	123	Block Shear-web	23	5.3
W16x31	F4	135	Block Shear-web	28	4.8
W18x40	F5	185	Block Shear-web	41	4.5
East Tenant Floor					
W21x44	F6	229	Block Shear-plate	40	5.7
W24x55	F6	229	Block Shear-plate	46	4.9
North Tenant Floor					
W12x26	F3	91	Block Shear-web	15	6.0
W12x26	H2	100	Weld	15	6.7
W21x44	F5	200	Block Shear-plate	41	4.9
W24x55	F6	229	Block Shear-plate	48	4.7
W24x55	F7	309	Block Shear-web	48	6.4
W30x116	H5	267	Block Shear-plate	109	2.5
W16x31	F4	135	Block Shear-web	26	5.1
W24x76	H4	223	Block Shear-plate	73	3.0
West Tenant Floor					
W16x26	F4	123	Block Shear-web	25	4.9
W16X31	F4	135	Block Shear-web	28	4.9
W14x22	H2	118	Block Shear-plate	36	3.3
W30X99	H5	267	Block Shear-plate	100	2.7
W18x35	F5	176	Block Shear-web	52	3.4
W12X19	H2	118	Block Shear-plate	23	5.0
				Average	4.4
				Minimum	2.3
				Maximum	6.7

Table 11–3. Ratio of vertical capacity to design shear load of shear connections for core floor beams on a typical tenant floor.

Core Floor Beams	Connection Type	Failure Load (kip)	Failure Mode	Design Shear Load (kip)	Failure Load/ Design Shear Load
Floors 8 to 20, 24 to 45					
South Floor					
W12X14	F3	79	Block Shear-web	16	5.1
W12X19	K3	81	Block Shear-web	22	3.6
W16x26	K3	87	Block Shear-web	40	2.2
W16x31	K3	95	Block Shear-web	50	1.9
W18x35	H3	168	Block Shear-plate	60	2.8
North Floor					
W16x31	F4	135	Block Shear-web	36	3.8
W18x40	K4	140	Block Shear-web	50	2.8
W18x35	F5	176	Block Shear-web	42	4.2
W12X35	K3	104	Block Shear-web	33	3.1
W14x26	K3	68	Block Shear-web	26	2.6
W16x40	K3	106	Block Shear-web	47	2.2
W21x50	H4	217	Block Shear-plate	69	3.1
W21x44	H4	217	Block Shear-plate	60	3.6
				Average	3.2
				Minimum	1.9
				Maximum	5.1

Table 11–4. Ratio of vertical capacity to design shear load of shear connections for core floor girders on a typical tenant floor.

Core Girders	Connection Type	Failure Load (kip)	Failure Mode	Design Shear Load (kip)	Failure Load/ Design Shear Load
Floors 8 to 20, 24 to 45					
South Floor					
W16X31	K3	95	Block Shear-web	19	4.9
W24x62	K4	190	Block Shear-plate	79	2.4
North Floor					
W21x44	K4	155	Block Shear-plate	48	3.2
W27x94	K5	264	Block Shear-plate	118	2.2
South Girders					
W21x50	H4	217	Block Shear-plate	65	3.3
W18x40	H3	168	Block Shear-plate	56	3.0
W21X68	H4	217	Block Shear-plate	72	3.0

Core Girders	Connection Type	Failure Load (kip)	Failure Mode	Design Shear Load (kip)	Failure Load/ Design Shear Load
W24x62	H4	217	Block Shear-plate	75	2.9
40 in girder 'S'	H8	415	Block Shear-plate	75	5.5
W27x84	H5	267	Block Shear-plate	113	2.3
Middle Girders					
W21x44	H4	217	Block Shear-plate	56	3.8
W18x40	H4	217	Block Shear-plate	56	3.9
W21x57	H5	253	Weld	63	4.0
MG-141 (14)	H4	217	Block Shear-plate	30	7.2
W27x84	H5	267	Block Shear-plate	122	2.2
W27x94	H5	267	Block Shear-plate	108	2.5
North Girders					
W24x55	H4	217	Block Shear-plate	80	2.7
W21x50	H4	217	Block Shear-plate	77	2.8
W24x76	H4	217	Block Shear-plate	100	2.2
W36x135	K8	436	Weld	168	2.6
				Average	3.3
				Minimum	2.2
				Maximum	7.2

11.2.5 Modeling Connections

As illustrated in Chapter 8, the simple floor framing connections and shear studs are critical to the behavior of a structure subject to the effects of fire. The modeling of connections to include the failure modes described in Section 11.2.4 is covered in this section.

User-defined connection models, referred to as break elements, were developed for each connection type. These connection models used the elements described in Section 11.2.4 to capture the various temperature-dependent failure modes. Failure in connections was determined by checking the exceeding of either a limiting force or a deformation limit (for example, "walking off" the seat). The inclusion of contact elements in the connection models allowed for slip and construction clearances (gaps) to be taken into account. The connection models included temperature-dependent properties and allowed for a different response in horizontal tension and compression.

The temperature of connection and shear stud components (e.g. bolts, plates, angles, and welds) in break elements were taken as the average of the temperature between two steel components (e.g., a girder and a column) for connection components and between the slab and the beam at shear stud locations. Connection and shear stud capacity at elevated temperature were modeled using room temperature capacity and the tensile strength reduction factor for steel.

Modeling Failure with Break Elements

User-defined finite elements were developed to capture complex modes of failure in connections, including temperature-dependence, with relatively few degrees of freedom. The element is referred to as a "break element" in this report. A user-define break element is a multi-degree of freedom elastic spring element with the capability of turning "off" once its capacity is reached. The stiffness of the element in the "off" mode was reduced to a predefined post-failure stiffness, which was set to a significantly small value, 10^{-6} to 10^{-9} times the initial stiffness. The force and moment capacity of the element were defined as temperature-dependent properties. Different tension and compression force capacity were assigned where appropriate.

Connections with multiple failure modes required use of several break elements connected in series and/or parallel. To model independent failure modes, that is, one failure mode that did not cause other failures, break elements were connected in parallel so that when one break element turned "off", the other break elements remained "on". For example, in a seated connection, failure of the bolts in shear did not lead to vertical failure of the connection. To model dependent failure modes, break elements were connected in series so that when one break element turned off, all elements turned off. For example, bolt shear and tear-out were modeled as two break elements in series, where failure by either bolt shear or tear-out caused a disconnect.

Break elements connected two nodes in the "on" mode and disconnected them in the "off" mode, depending on the relative displacement of the two nodes. The break element was defined as follows:

$$B_m[(i,j,dof_{ij});(k,l,dof_{kl});(K,\Delta_0)] \quad (1)$$

where m is the break element number, i and j are the active nodes, dof_{ij} is the degree of freedom for the active nodes, k and l are the control nodes, dof_{kl} is the degree of freedom for the control nodes, K is the elastic stiffness of the break element, and Δ_0 is the differential displacement limit of the control nodes.

To make the connection capacity temperature-dependent, a beam element with a temperature-dependent coefficient of thermal expansion was added to the break element. Figure 11–9 illustrates the basic mathematical model of the connection using break elements.

A list of break element types developed in ANSYS is summarized in Figure 11–9. To include temperature-dependent capacities, the break elements were formulated with temperature-dependent material properties for steel.

Failure in connections was determined by checking the exceedance of either a limiting force or a deformation limit (for example, "walking off" the seat). The inclusion of contact elements in the connection models allowed for slip and construction clearances (gaps) to be taken into account. The connection models included temperature-dependent properties and allowed for a different response in horizontal tension and compression.

Basic mathematical model:

– Let node *l* and *i* have same displacement.

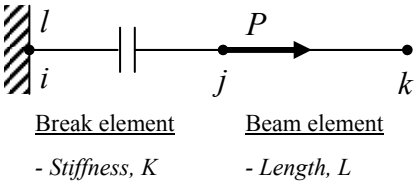

– In this example, control nodes *k* and *l* relative displacement has the form:

$$U_k - U_l = \frac{P}{K} + \alpha L \Delta T$$

– Break element status is by definition

$$U_k - U_l \le \Delta_0, \text{ status : on}$$
$$U_k - U_l > \Delta_0, \text{ status : off}$$

– Define break element to turn off when capacity, P_u, has been reached

$$\Delta_0 = \frac{P_u}{K} + \alpha L \Delta T$$

– Element capacity at room temperature is given as

$$P_{u.rm} = K\Delta_0$$

– Hence for a given P_u and ΔT relationship, the required thermal expansion to turn the break element off can be found by

$$\alpha = \frac{P_{u.rm} - P_u}{KL\Delta T}$$

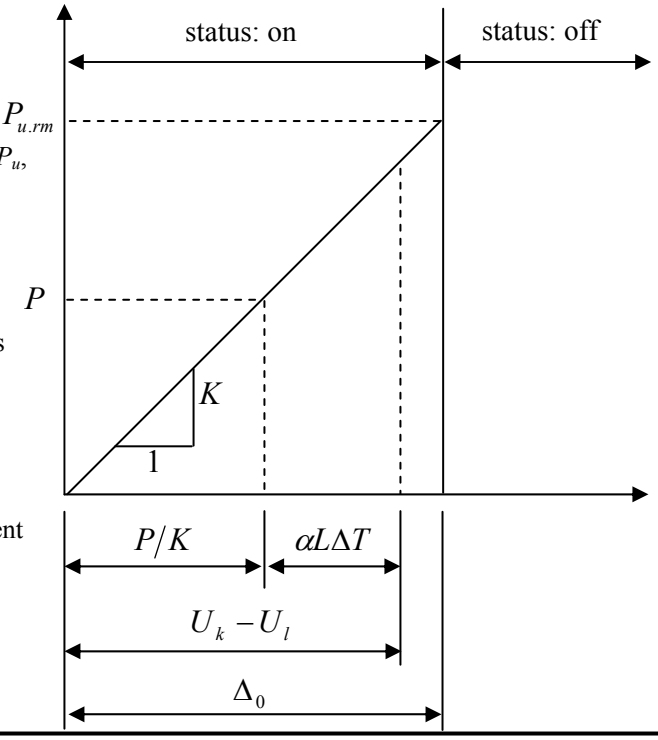

Figure 11–9. Basic mathematical model of connection failure.

Analytical Modeling of Connections Using Break Elements

A list of break element types developed in ANSYS is summarized in Table 11–5. A connection model was developed for each of the following connection types (Chapter 2), using the break elements in Table 11–5 in series or parallel as needed to model the appropriate failure modes:

- Single shear plate
  - Fin (beam-to-girder)
- Double angle shear connections

  - Knife (beam or girder-to-column)
  - Header (beam-to-girder)
- Seated web clip (SWC) connection (beam-to-girder)
  - Seat with web clip
- Seated top plate (STP) connections (beam or girder-to-exterior column)
  - Seat connection to columns on the east face
- Seated top clip (STC) connections (girder-to-interior column)
  - Seat connection to columns on the north and south face
  - Seat connection at Columns 79 and 81

The floor area where failure of floor framing connections and shear studs was modeled with break elements on Floors 8 to 14 is shown in Figure 11–10. This area is east of the north-south line passing through Column 76 and the core area east of Column 73.

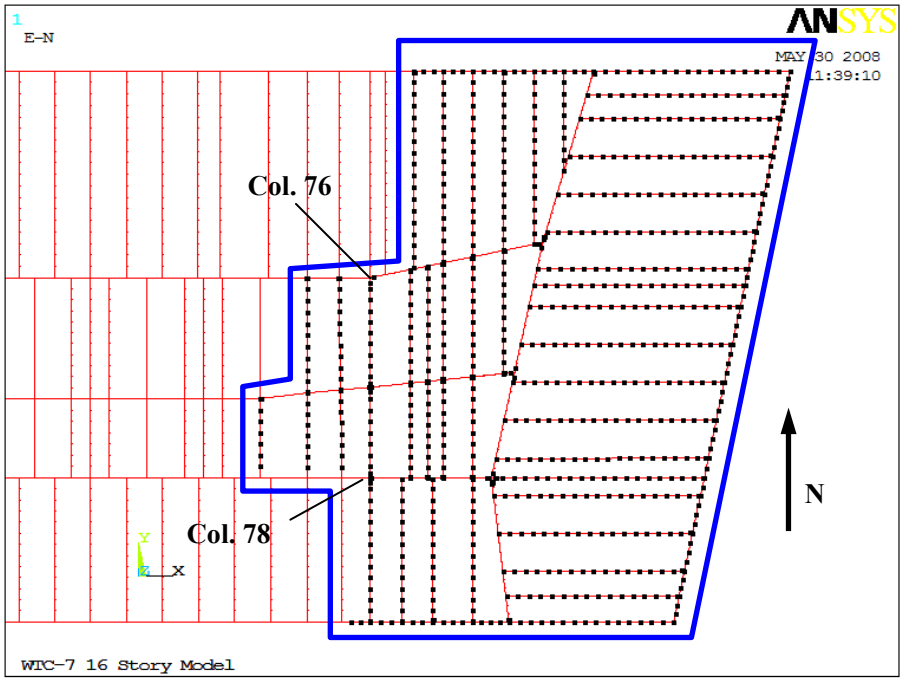

Note: Black colored dots show the location of shear studs and connections modeled with break elements.

Figure 11–10. Area of the floor where connection failures were modeled.

Outside the selected area, structural damage, such as buckling of the steel frame and crushing and cracking of the concrete slab, was modeled over the entire floor, but connection failures were not modeled. The extent of the area modeled with break elements was based on the results of single floor fire simulations, where connection damage west of Columns 73 through 76 were not found to contribute to the an initial failure event on the east side of the structure. The area where break elements were modeled was selected to reduce the model size without biasing the results for simulating the initial failure event.

Table 11–5. Types of break elements defined in ANSYS.

Type	Degree of Freedom	Capacities to be defined	Stiffness to be defined	Description
102	UX UY UZ ROTX ROTY ROTZ	Positive FX Negative FX Positive FY Negative FY Positive FZ Negative FZ MX MY MZ	Initial stiffness for UX Post-failure stiffness for UX Initial stiffness for UY Post-failure stiffness for UY Initial stiffness for UZ Post-failure stiffness for UZ Initial stiffness for ROTX Post-failure stiffness for ROTX Initial stiffness for ROTY Post-failure stiffness for ROTY Initial stiffness for ROTZ Post-failure stiffness for ROTZ	All force and moment components are checked with corresponding capacities.
103 K1 = 0	UX UY UZ	Positive F Negative F	Initial stiffness for UX, UY, and UZ Post-failure stiffness for UX, UY, and UZ	SRSS* of three force components is checked with the capacity. The sign of force is determined by the direction specified by the user.
103 K1 = 1	UX UY UZ	Positive F Negative F	Initial stiffness for UX, UY, and UZ Post-failure stiffness for UX, UY, and UZ	SRSS* of force components FX and FY is checked with the capacity. The sign of force is determined by the direction specified by the user.
104	UX UY UZ	Positive FX Negative FX Positive FY Negative FY Positive FZ Negative FZ	Initial stiffness for UX Post-failure stiffness for UX Initial stiffness for UY Post-failure stiffness for UY Initial stiffness for UZ Post-failure stiffness for UZ	All force components are checked with corresponding capacities.
105 K1 = 0	UX UY UZ ROTX ROTY ROTZ	Positive F Negative F	Initial stiffness for UX, UY, and UZ Post-failure stiffness for UX, UY, and UZ Initial stiffness for ROTX, ROTY, and ROTZ Post-failure stiffness for ROTX, ROTY, and ROTZ	SRSS* of three force components is checked with the capacity. The sign of force is determined by the direction specified by the user.
105 K1 = 1	UX UY UZ ROTX ROTY ROTZ	Positive F Negative F	Initial stiffness for UX, UY, and UZ Post-failure stiffness for UX, UY, and UZ Initial stiffness for ROTX, ROTY, and ROTZ Post-failure stiffness for ROTX, ROTY, and ROTZ	SRSS* of force components FX and FY is checked with the capacity. The sign of force is determined by the direction specified by the user.

*SRSS: square-root-of-sum-of-square

Framing connections outside of the selected area, or on other floors not subjected to fire, were modeled as either fixed or pinned, using typical modeling approaches. Connections were not modeled in the exterior moment frame, as no failures were observed there prior to the onset of global collapse. Connections were also not modeled for interior columns, as the purpose of the ANSYS model was to accumulate local failures up to the point of buckling in a column. When column buckling appeared to be imminent, the analyses were continued in the LS-DYNA 47 story model.

Analytical Model for Fin Connections

The analytical model used for the fin connection is depicted in Figure 11–11. The column is located on the right side in each diagram in Figure 11–11. The figure shown has three bolts, but a fin connection in WTC 7 had up to 6 bolts. The connection model accounts for: (1) shear failure of individual bolts, (2) tear-out failure at each bolt location, (3) vertical block shear failure of the connection plate, (4) horizontal block shear failure of the web or angles, and (5) vertical and horizontal failure of the connection plate-to-column weld.

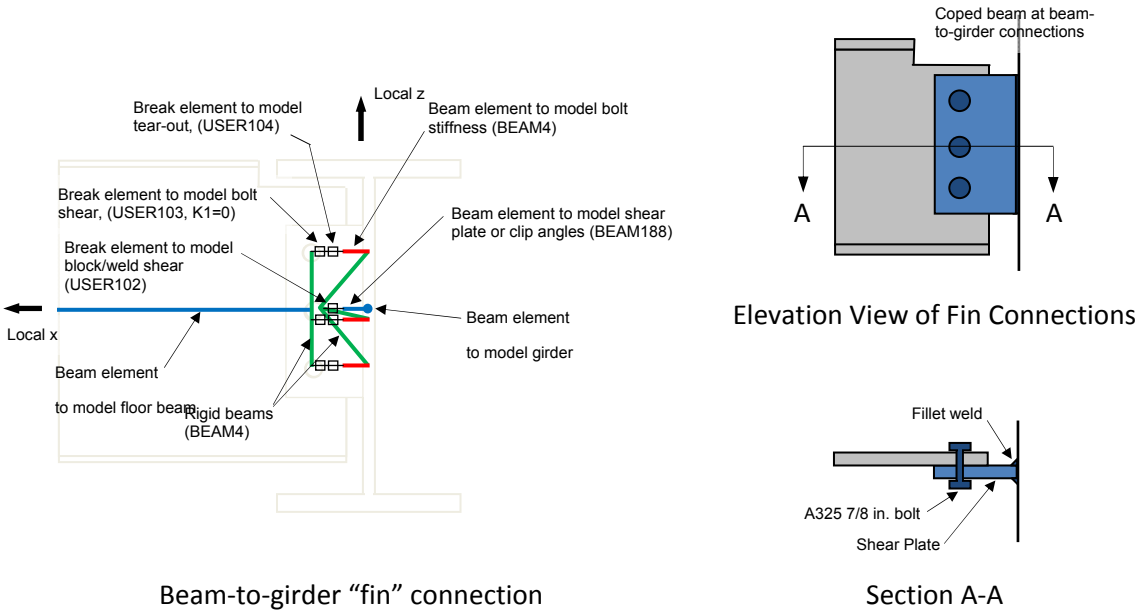

Figure 11–11. Analytical model for a fin connection.

At each bolt location two break elements and one elastic beam were defined. The break elements represented the shear strength of the bolt and the tear-out strength of the connection plate. These break elements were defined at the centerline of each bolt. The bolt shear strength was modeled with break element type USER103 with K1 = 0 (see Table 11–5), i.e., failure occurred when the square-root-of-sum-of-squares (SRSS) of the force components in the x- y- and z-directions in the break element exceeded the temperature-dependent shear strength of the bolt. The tear-out strength of the connection plate was modeled with break element type USER104. The properties of this break element were defined such that the failure occurred only in the positive local x-direction when the force in the positive local x-direction exceeded the temperature-dependent tear-out strength of the connection plate. The elastic beam represented the stiffness of each bolt in shear. The axial stiffness of the beam was set equal to the secant stiffness of the non-linear force-displacement relationship for a bolt in shear at the ultimate strength.

Bending and torsional stiffness of the beam were set equal to a large value to prevent any deformation due to bending and torsion.

Block shear and weld failure of the connection plate were modeled using break element type USER102. This break element was defined at the centroid of the connection plate. Failure in the vertical direction occurred when the force in the z-direction exceeded the temperature-dependent strength of the weld or plate block shear. Failure in the horizontal direction occurred when the force in the positive x-direction exceeded the temperature-dependent strength of the weld.

Analytical Model for Knife Connections

The analytical model used for the knife connection is depicted in Figure 11–12. The figure shown has three bolts, but knife connections in WTC 7 had up to 8 bolts. The connection model accounts for: (1) shear failure of individual bolts, (2) tear-out failure at each bolt location, (3) vertical block shear failure of the double angles, (4) horizontal block shear failure of the web or angles, and 5) vertical and horizontal failure of the angle-to-column filet welds.

The analytical model for the knife connection was the same as that for the fin connection. The only differences were that the two outstanding legs of the angles replaced the shear plate, and the fillet welds at the toes of the angles replaced the double-sided fillet at the shear plate.

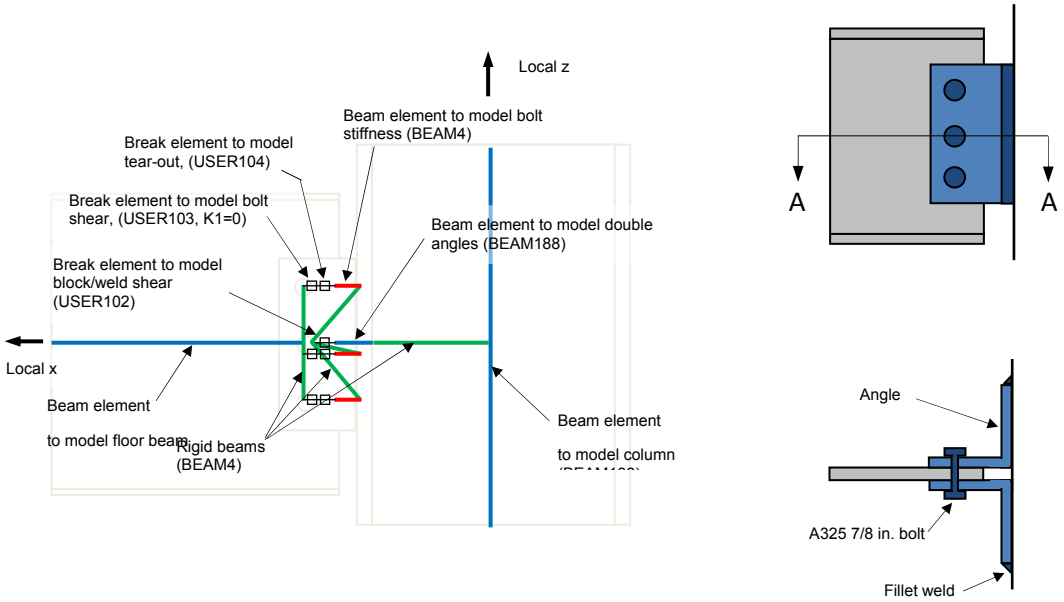

Beam or Girder-to-Column Knife Connection Section A-A

Figure 11–12. Analytical model for a knife connection.

Analytical Model for Header Connections

The analytical model for the header connections is depicted in Figure 11–13. The figure shown has six bolts (three per row), but a header connection had up to 10 bolts (five per row). The connection model accounts for: (1) shear failure of individual bolts, (2) tension failure of individual bolts, and (3) vertical and horizontal failure of the fillet weld connecting the angles to the beam web.

For each connection a local coordinate system was defined as shown in Figure 11–13. At each bolt location one break element, one elastic beam element, and one node-to-node contact element were defined. The break element represented the shear and tension strength of the bolt. The break element was defined at each bolt location in the connection. The bolt shear and tension strength was modeled with break element type USER102, i.e., failure occurred when the force in the z-direction exceeded the temperature-dependent shear capacity of the bolt, and also failed if the force in the x-direction exceeded the temperature-dependent tensile capacity of the bolt. The properties of this break element were defined such that the failure did not occur in the negative x-direction. The elastic beam represented the stiffness of each bolt. The node-to-node contact element (CONTA178) represented contact interaction between the angles and column flange. Initially, a full contact was assumed between the angles and column flange. In the case of bolt failure, either due to vertical shear or horizontal tension, the contact element became active and allowed separation when beam or girder end pulls away from the column and prevented penetration of the angles into the column when beam or girder end moves toward the column.

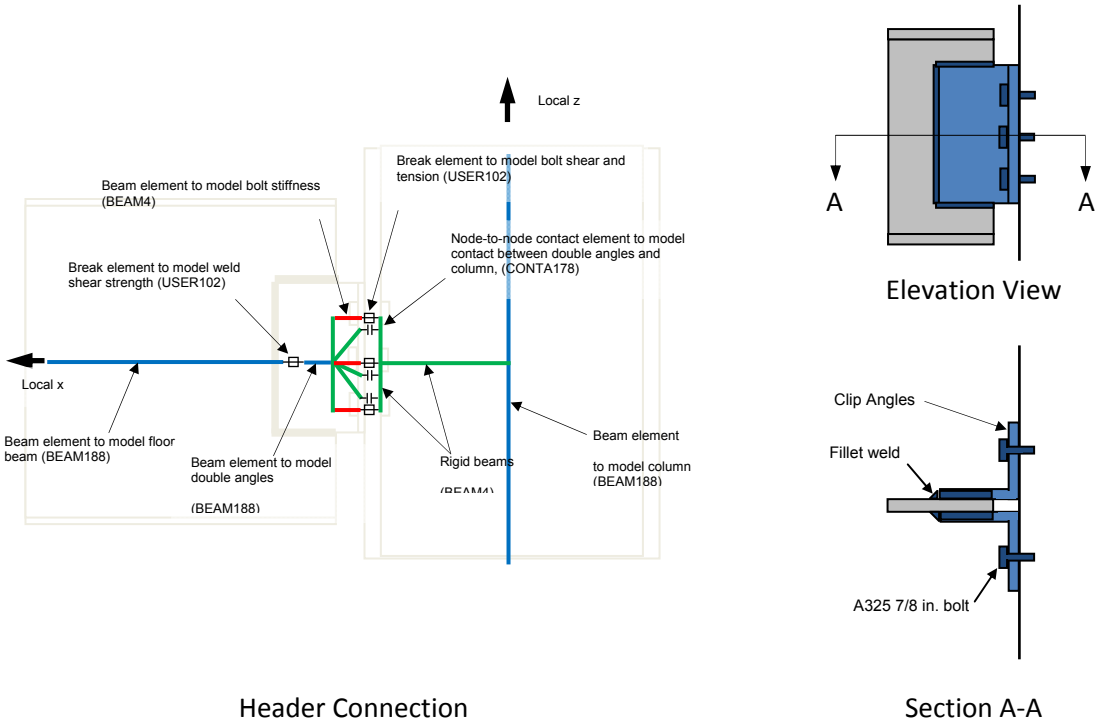

Figure 11–13. Analytical model for header connection.

The vertical and horizontal weld failure of the connection plate was modeled using break element type USER102. This break element was defined at the centroid of the connection plate. Failure in the vertical direction occurred when the force in the z-direction exceeded the temperature-dependent strength of the weld. Failure in the horizontal direction occurred when the force in the positive x-direction exceeded the temperature-dependent strength of the weld.

Analytical Model for SWC Connections

The analytical model used for a seat with a web clip (SWC) connection is depicted in Figure 11–14. The connection model accounted for: (1) shear failure of individual bolts, (2) vertical and horizontal failure of weld connection at web clip angle, (3) vertical and horizontal failure of weld connection at seat angle, and (4) beam walking off the seat.

For each connection a local coordinate system was defined as shown in Figure 11–14. At each bolt location one break element and one elastic beam element were defined. The break element represented the shear strength of the bolt. These break elements were defined at the bolt centerlines. The bolt at the web clip was modeled with break element type USER103 with K1 = 0, i.e., failure occurred when square-root-of-sum-of-squares (SRSS) of the force components in the x- y- and z-directions exceeded the temperature-dependent shear capacity of the bolt. The bolt attaching the beam to the seat was modeled with break element type USER103 with K1 = 1, i.e., failure occurred when square-root-of-sum-of-squares (SRSS) of the horizontal force components in the x- and y-directions exceeded the temperature-dependent shear capacity of the bolt. The elastic beam represented the stiffness of each bolt. Contact interaction between end of beam or girder was modeled using node-to-node contact element (CONTA178) with a defined initial gap.

Vertical and horizontal weld failure of the connections at the web clip and at the seat were modeled using break element type USER102. Failure in the vertical direction occurred when the force in the z-direction exceeded the temperature-dependent strength of the weld. Failure in the horizontal direction occurred when the force in the positive x-direction exceeded the temperature-dependent strength of the weld.

If the bolts that attached the beam to the seat were sheared, the beam could walk off the seat if the beam moved laterally or pulled off the seat if the beam sagged sufficiently. The shear strength of the bolts controlled the horizontal capacity of the connection. The shearing of the bolts did not cause the beam to lose vertical support, but was the prerequisite for the beam end walking off the seat. The travel distance for a beam to walk off a seat was 2.5 in. A control element (COMBIN37), a unidirectional linear spring element with the capability of turning on and off during an analysis, was used to model walk-off. The element was a part of the structure that connected two active nodes in the on mode and disconnected them in the off mode, depending on the relative displacement of two control nodes.

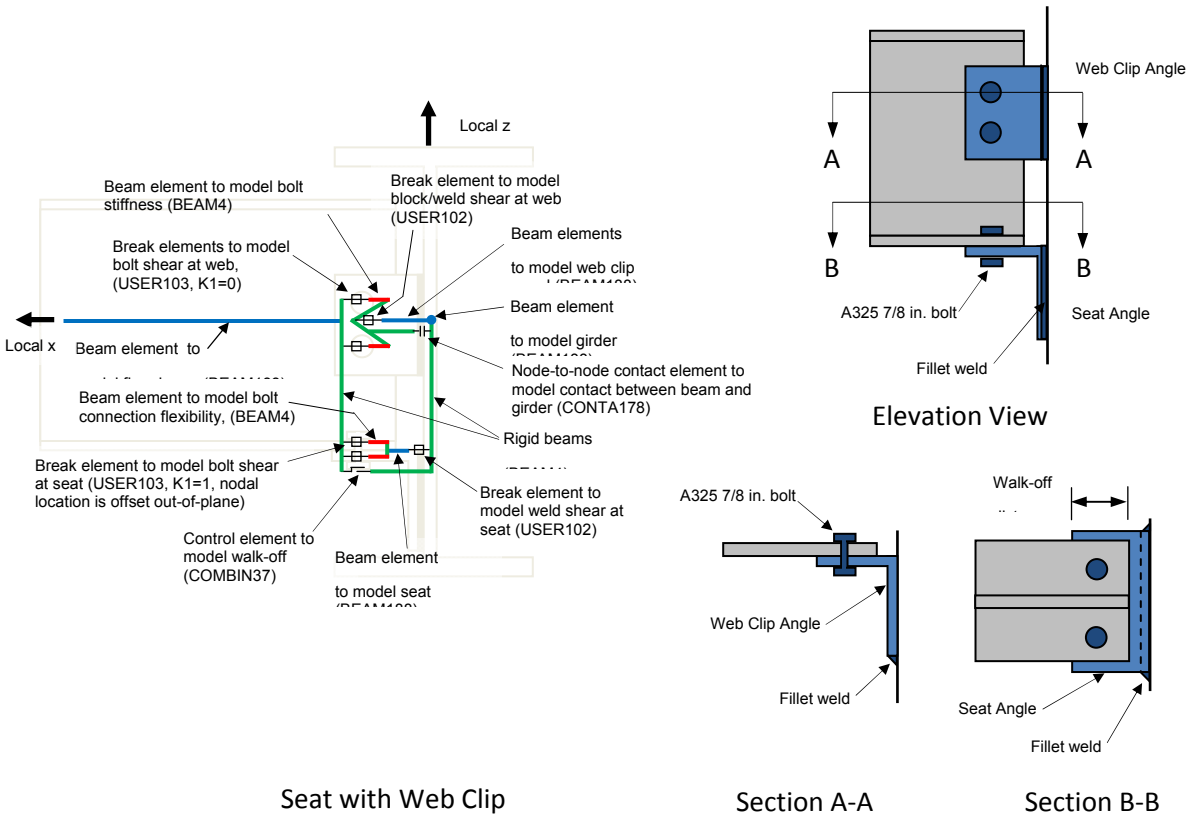

Figure 11–14. Analytical model for SWC connection.

Analytical Model for Seated Connection at North, South, and East Face Columns; and Columns 26 and 44

The analytical model used for seated connections at the north and south face columns is depicted in Figure 11–15. The same model was used for seated connections at Columns 26 and 44 and east face columns, but with the beam framing into the column at a different angle and with bolts at a different location. The analytical model included: (1) shear failure of individual bolts, and (2) beam walk off of the seat. The failure of the connection was governed by bolt shear followed by walk-off before loss in vertical support.

For each connection a local coordinate system was defined as shown in Figure 11–15. At each bolt location one break element, one elastic beam, and one non-linear spring were defined. The break element represented the shear strength of the bolt. The break element was defined at the bolt location in the connection. The bolt shear strength was modeled with break element type USER103 with K1 = 1, i.e., failure occurred when square-root-of-sum-of-square (SRSS) of the horizontal force components in the x- and y-directions exceeded the temperature-dependent shear capacity of the bolt. The elastic beam element represented the flexibility of bolt connection in shear. The non-linear spring was used to capture slip in the connection before bolt bears against the hole. Slotted bolt holes were used at the top flange clip angle, while standard bolt holes were used at the bottom seat angle.

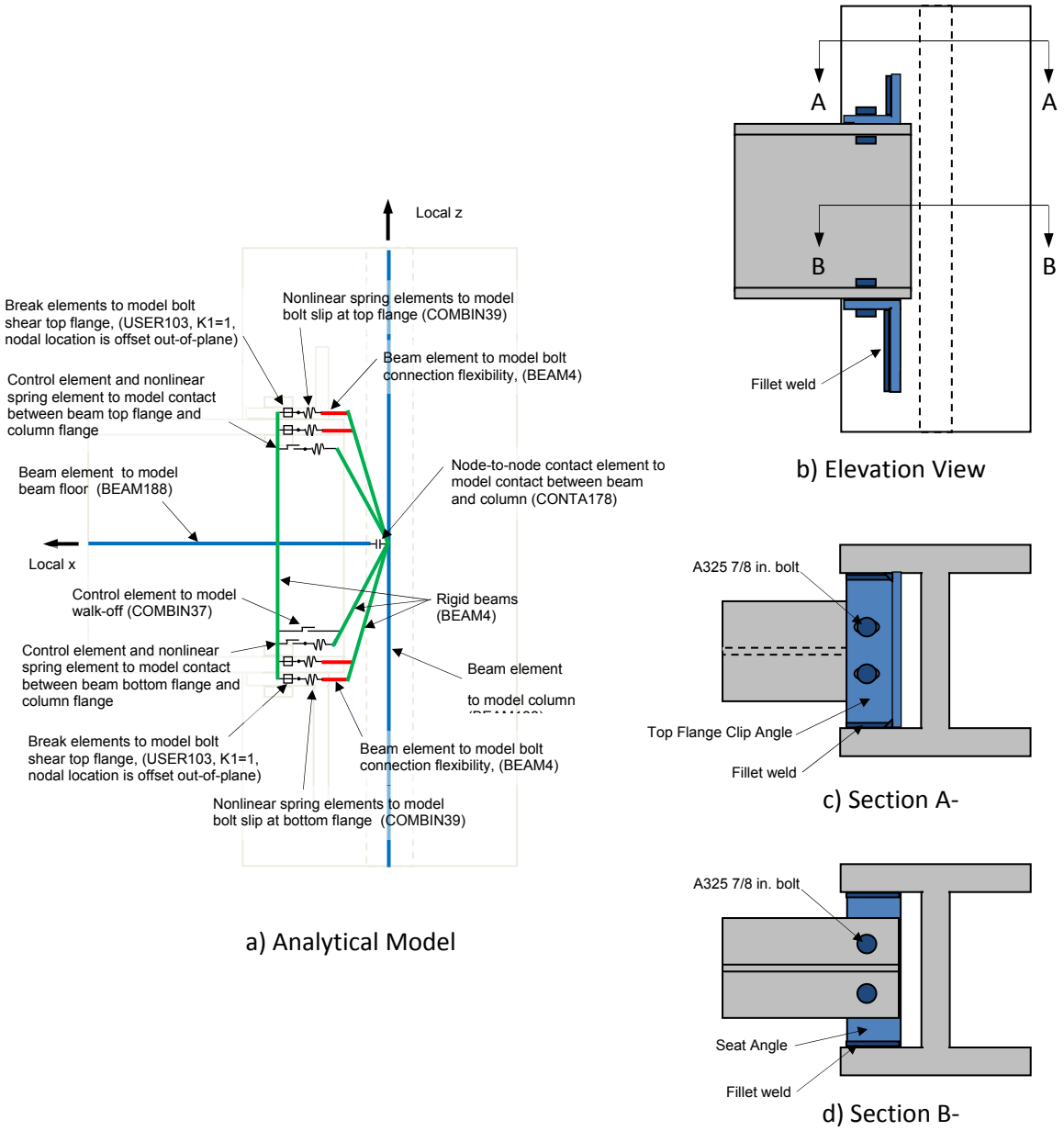

Figure 11–15. Analytical model for seated connection at north and south face columns.

Contact interaction between the end of the beam and the girder was modeled using node-to-node contact element with an initial gap to represent clearance. When the connection was subjected to a large horizontal tension force, failure was by bolt shear off followed by the beam walking off the seat. The shear strength of the bolts controlled the beam horizontal tension capacity. The bolt shear by itself does not cause the beam to lose its vertical support, but it is the prerequisite for the beam end walking off the seat. The travel distance for a beam to walk off a seat was 4.5 in. A control element was used to model walk-off.

When the connection was subjected to a large horizontal force perpendicular to beam axis or a large twisting moment at the beam end, failure was by bolt shear followed by the beam end being restrained from lateral motion or twisting by the column flanges. One nonlinear spring element and one control

element were used at the beam top and bottom flanges to model beam flange and column flange contact interaction. The control elements were needed to remove the restraint after beam walk-off.

Analytical Model for Seated Connection at Columns 79 and 81

The analytical model for the seated connection at Column 79 is depicted in Figure 11–16. The same model was used for Column 81, but with the beam connected to the column at a different angle. The analytical model includes: (1) shear failure of individual bolts, (2) beam walking off the seat, and (3) horizontal weld failure of the top flange clip angle. The failure of the connection was governed by bolt shear followed by walk-off before loss in vertical support.

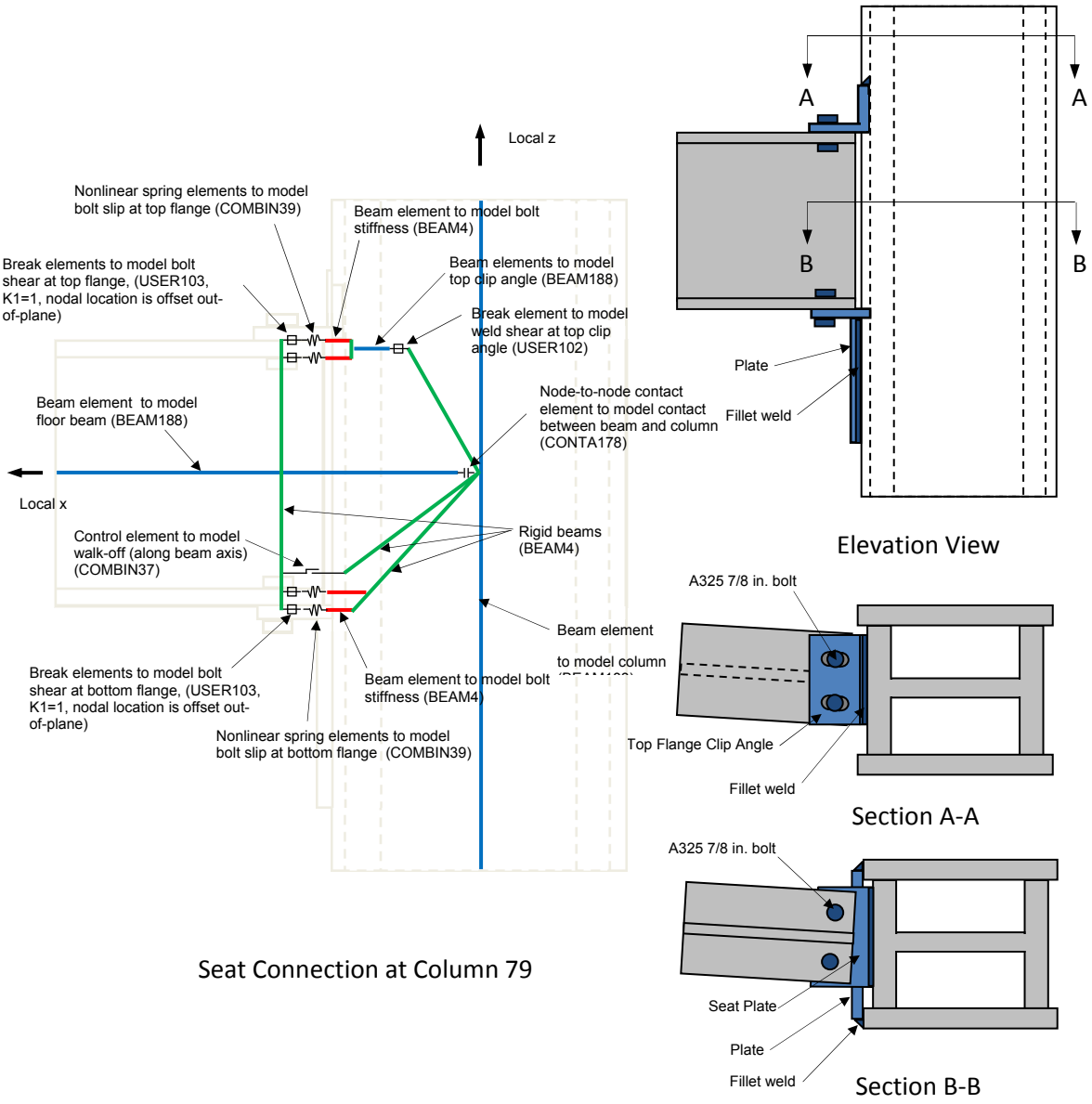

Figure 11–16. Analytical model for bearing connection at Column 79.

For each connection, a local coordinate system was defined as shown in Figure 11–16. At each bolt location, one break element, one elastic beam, and one non-linear spring were defined. The break element represented the shear strength of the bolt. The break element was defined at the bolt centerline. The bolt shear strength was modeled with break element type USER103 with K1 = 1, i.e., failure occurred when square-root-of-sum-of-squares (SRSS) of the horizontal force components in the x- and y-directions exceeded the temperature-dependent shear capacity of the bolt. The elastic beam represented the stiffness of the bolt connection. The non-linear spring was used to capture slip in the connection before a bolt bears against the hole. Slotted bolt holes were used at the top flange clip angle, while standard bolt holes were used at the bottom seat plate.

Contact interaction between the end of the beam and the girder was modeled using a node-to-node contact element with an initial gap. When the connection was subjected to a large horizontal tension, a walk off failure occurred when the bolts sheared at the seat connection, the bolts sheared or the weld failed at the top clip angle, and the beam walked off the seat. The failure of the bolts and weld was a prerequisite for the beam end walking off the seat. The travel distance for walk off was 6.25 in. along the axis of the beam and 5.5 in. lateral to the beam. A control element was used to model axial walk-off. Lateral walk-off was monitored during the analysis.

Analytical Model for Shear Studs

The analytical model for shear stud connections is depicted in Figure 11–17. Each shear stud was represented by one break element and one node-to-node contact element. Break element type USER105 with K1 = 1 (Figure 11–9) was used, wherein failure occurred when the square-root-of-sum-of-squares (SRSS) of the force components in the x- and y-directions (i.e., in the plane of the floor slab) exceeded the temperature-dependent shear capacity of the stud. After shear failure of the shear stud connection, node-to-node contact elements insured gravity load transfer from the slab to the floor beam, allowed the beam to sag independently of the floor slab, and prevented slab penetration into the beam.

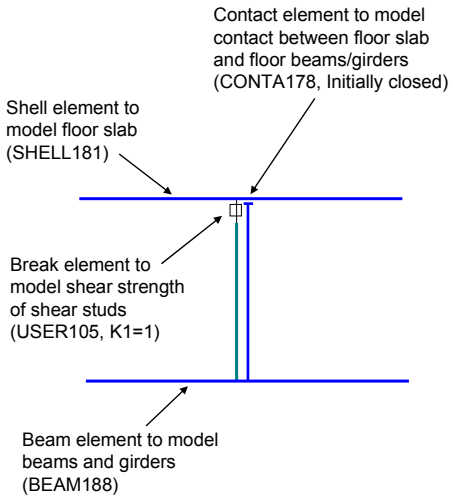

Figure 11–17. Analytical model for shear studs.

11.2.6 Substructuring

To further improve the computational efficiency of the 16 story model, the lower 7 floors and Floors 15 and 16 were replaced with "superelements." "Superelement" is the term used for sub-structuring and results from condensing an elastic portion of a structure and representing it with a stiffness matrix to reduce the size of the main model. This modification was based on the condition that these floors remained elastic, as there was no fire on these floors.

11.2.7 Boundary Conditions and Loads

Displacement Boundary Conditions

The column nodes at the base of the 16 story model were fully fixed to model the rigidity of the grillage and foundation (Chapter 2). The top of the columns at Floor 16 were fixed in the global x- and y-directions so that lateral displacements were prevented and were free in the global z-direction so that they could move vertically in response to gravity loads and thermal expansion.

Structural Loads

The 16 story model was analyzed for the effects of gravity and temperature loads. Gravity loads were based on the WTC 7 design loads, shown in Figure 11–18, and included:

- the dead load (self-weight) of the structural steel and concrete floor slabs;
- superimposed dead load consisting of the estimated weights of ceilings, mechanical and electrical equipment, thermal insulation, and floor finishes; and
- service live load, taken as 25 percent of the design live load.

The gravity loads from the portion of the building above Floor 16 were applied as concentrated forces to each column at Floor 16. Wind loads on September 11, 2001, were assumed to be negligible and were not considered.

LOADING SCHEDULE

LOAD (PSF) / AREA	CONCRETE SLAB	FILL, FINISH, ROOFING	CEILING, DUCTWORK	PARTITIONS	FLOORING	BEAMS, ENCASEMENT, FIREPROOFING	TOTAL DEAD LOAD	LIVE LOAD	TOTAL LOAD
MAIN ROOF, BULKHEAD ROOF	50	10	8			7	75	30	105
8TH-20TH FL. 24TH-46TH FL.	50		5	12		8	75	50	125
21ST-23RD FL.	50		5	12	15	8	90	75	165
7TH FLOOR NORTH SIDE	80		5	12		93	190	50	240
7TH FLOOR SOUTH SIDE	80	38	8	12		27	165	50	215
6TH FLOOR OFFICE SPACE	56		5	12		7	80	50	130
6TH FLOOR SWITCHBOARD ROOM	62	38				55	155	100	255
5TH FLOOR OFFICE SPACE	150	38	5			17	210	50	260
5TH FLOOR MECHANICAL SPACE	150	38	5			17	210	150	360
4TH FLOOR	56	75	5			10	146	100	246
3RD FLOOR NEW CONSTRUCTION	56	75	5			10	146	100	246
3RD FLOOR OVER EXISTING SUBSTATION							240	100	340
2ND FLOOR NEW CONSTRUCTION	56	60	5			10	131	150	281
2ND FLOOR EXISTING SUBSTATION							240	150	390
1ST FLOOR LOBBY	175	90				50	315	100	415
1ST FLOOR EXISTING SUBSTATION							300	225	525

Source: Reproduced with permission of The Port Authority of New York and New Jersey. Figure 5-4 in NIST NCSTAR 1-1

Figure 11–18. Design load criteria for WTC 7.

Thermal Loads

Three thermal cases (A, B, and C) were developed in the thermal analyses (Chapter 10) that were within the range of realistic and reasonable fires in WTC 7 on September 11, 2001. Case A was based on the temperature data obtained from the FDS simulations (Chapter 10). Cases B and C increased and decreased, relatively, the gas temperatures from Case A by 10 percent. Based on engineering judgment, a 10 percent variation from Case A gas temperatures was deemed to appropriately reflect the uncertainty in the extent and intensity of the fires. The thermal data were input at each 30 min time step as temperatures at the nodes of the structural elements.

Each beam and column was assigned a single temperature (i.e., no thermal gradients across the section). Component studies had shown that columns were not heated sufficiently to warrant inclusion of a gradient, and that steel beams in the typical floors heated at a nearly uniform rate, with the exception of

the top flange which was adjacent to the floor slab. However, since the top flange was located near the neutral axis of a composite floor section, it did not contribute much to the overall response. When composite action was lost, separation from the slab increased the rate of heating to the top flange.

The concrete slab had temperatures applied to the element nodes at four locations through the slab thickness and did include temperature gradients through the slab.

The temperature at beam-to-girder or girder-to-column connections was taken as the average of the temperatures of the beam and column nodes where the connection was located. Similarly, temperature of a shear stud was computed as the average of the temperatures at the beam and slab nodes at the ends of the shear stud. This was based on detailed thermal analyses, such as the analysis of Column 79 shown in Figure 11–19, which demonstrated that (1) the web and bottom flange of the girders heated at a nearly uniform rate at a given point along the girders (except where girders were connected at their ends) and (2) the connection temperatures were approximately midway between the temperature of the end beam node and the column node.

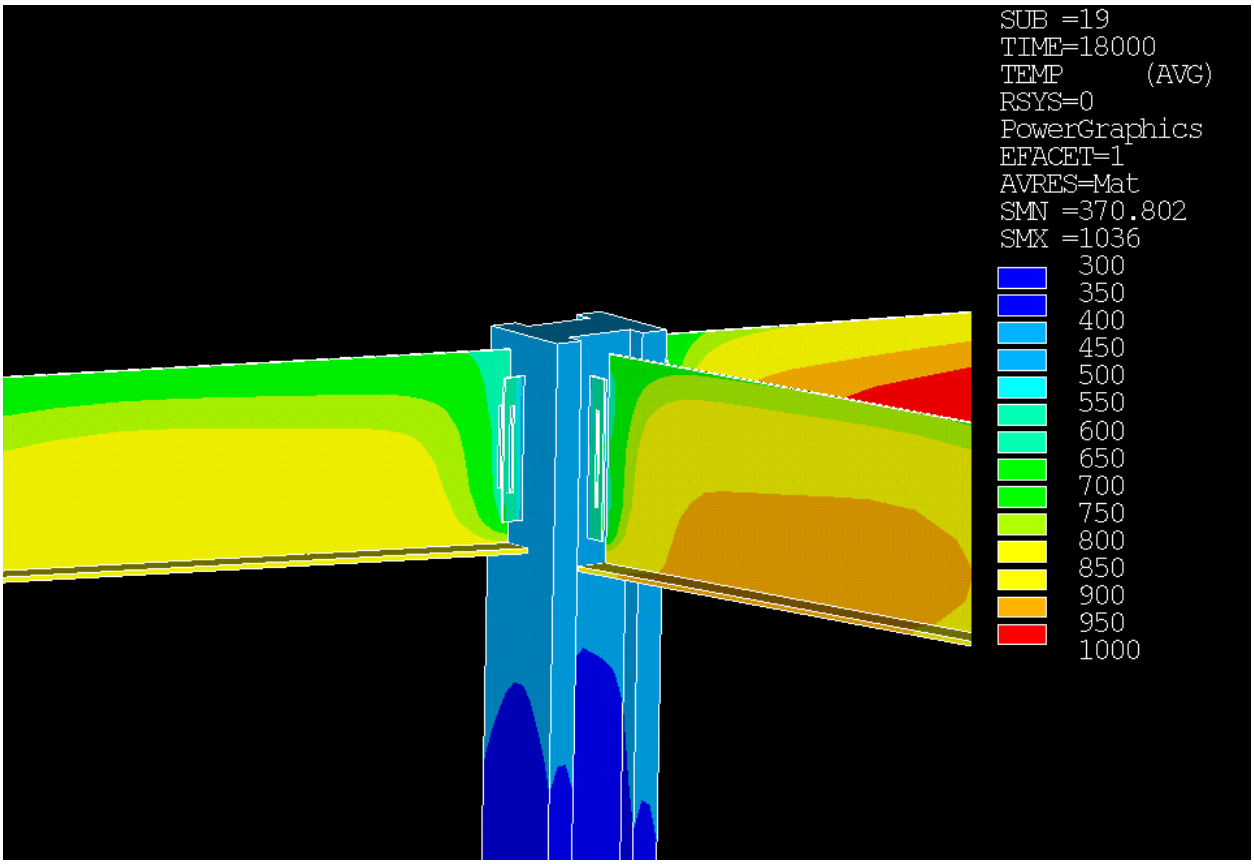

Figure 11–19. Detailed thermal analysis showing the gradient between girders, Column 79, and their connections.

11.2.8 Load Application Sequence

Gravity Load Sequence

The gravity loads were applied in steps to simulate the effects of construction sequence. During construction, the floor framing deflects under the weight of poured concrete, but the fresh concrete does not participate in supporting its self-weight. After the concrete has hardened and gained strength, the slab acts compositely with the steel beams (through the shear studs) to support the superimposed dead and live loads. In the first step of the gravity load analysis, the self weights of the floor framing and the fresh concrete were applied, as well as the self weight of the floors above Floor 16 (applied as concentrated forces to Floor 16 columns). At this stage, the stiffness of the slab was negligible and the beams were assumed to have a pinned connection at their ends. In the second step, the stiffness of the slab was activated (the floor became fully composite with the supporting frame) and the superimposed dead and service live loads were applied.

Temperature Load Sequence

Thermal loading was applied in the form of temperature-time histories. Each temperature-time history was defined discretely at 30 min intervals. Temperatures were linearly interpolated for times between consecutive intervals.

11.2.9 Criterion to Determine Component Failures

A procedure was developed for addressing buckled and/or failed components so that any member that did not structurally contribute to the response of the building was removed from the analysis to improve computational efficiency and avoid convergence problems. This procedure was used to modify the model at the end of each 30 min interval, or as necessary when the analysis halted due to non-convergence.

The removal of framing and slab elements from the model was performed in ANSYS by reducing the stiffness and mass of the selected elements to a very small fraction of the original values. These elements remained part of the stiffness matrix and solution process, but they did not contribute to the structural response of the model. When elements were removed, any temperature, distributed load, or concentrated forces that were assigned to these elements were automatically set to zero.

Criteria to Determine Lateral-Torsional Buckling of Beams and Girders

When lateral support of the top (compression) flange was lost, floor beams and girders could laterally displace and buckle in a lateral-torsional mode. In the ANSYS analysis, buckling of flexural members led to convergence difficulties. To improve analysis progress, buckled members were removed from the analysis. The criterion used for removal of buckled beams or girders was based on the destabilizing effect of gravity loads on laterally displace beams or girders. It was assumed that any beam or girder that twisted to the extent that its top flange moved half of its flange width laterally was unable to support its gravity loads and was removed from the analysis. The rotation corresponding to this condition is shown in Figure 11–20 and is expressed as follows:

$$\theta_{critical} = \tan^{-1}\left(b_f / d\right) \quad (2)$$

where, b_f = flange width

d = depth of beam/girder

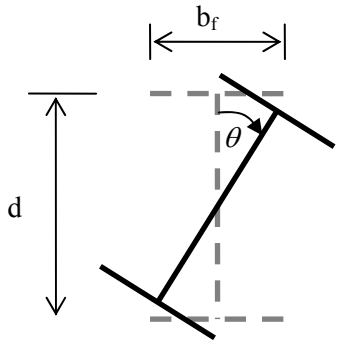

Figure 11–20. Critical Twist Angle in Beams/Girders.

Criteria to Remove Locally Unstable Members Due to Loss of Vertical Support

Under elevated temperatures, a beam could lose vertical support at one end through connection failure (including walk-off). Walk-off failure of beams and girders was defined to occur when (1) the end of the beam or girder moved along the axis of the beam until it was no longer supported by the bearing seat, or (2) the beam or girder was pushed laterally until its web was no longer supported by the bearing seat. Gravity shear loads in a beam were transferred to the bearing seat primarily in the proximity of the web on the bottom flange. Therefore, when the web was no longer supported by the bearing seat, the beam was assumed to have lost support, as the flexural stiffness of the bottom flange was assumed to be insufficient for transferring the gravity loads. Under such conditions, the beam would fall to the floor below under its self weight. When this occurred in the ANSYS analysis, the beam was removed. When a girder failed in this manner, the floor beams that it supported were removed at the same time.

Criteria to Determine Cracking and Crushing of Floor Slab

Temperature effects and failure of supporting beams and girders caused slab elements to undergo large tensile or compressive strains. The ANSYS material model used for slabs was based on an isotropic plasticity formulation without strength degradation at high strains and, hence, it could not represent cracking under tensile strains or crushing under compressive strains. To address this issue, slab elements that reached the tensile or compressive failure strains were softened or removed. Any slab element with a principal tensile strain equal to or greater than 0.0015 at mid-depth of the section was assumed to be fully cracked in tension[7]. Similarly, any slab element with a principal in-plane compressive strain equal to or less than -0.004 was considered fully crushed in compression.

[7] Concrete starts to microcrack at a tensile strain of approximately 1.4×10^{-4}. Beyond this strain level, the microcracking will grow and coalesce, and the concrete will soften with increasing strain. At a strain level of about 1.5×10^{-3}, the concrete can no longer support any tensile force.

When these strain levels were reached in the slab, that portion of the slab was softened. Softening of slab elements refers to replacing the material property of concrete with a reduced elastic modulus. The reduced elastic modulus was equivalent to the in-plane stiffness that would be provided by the welded-wire-mesh in the slab at high temperatures ($T \geq 700$ °C). Softening of a section of the slab, and not removing it from the analysis, allowed the service live loads that were applied to the slab elements to be transferred to the remaining beams, girders, or spandrel beams without affecting the stiffness of the remaining floor system. However, as the analysis progressed, some floors had a large area where the floor beams and girders had been removed and the softened floor slab caused rotation in the exterior spandrel beams, as the sagging slab applied a torque to the top of the spandrel beam and transferred floor loads to the spandrel beams (which was never intended in the original floor design). This behavior created numerical difficulties in the analysis, which were not representative of the structural response, since it was unlikely that the slab would remain in place when a number of floor beams or a girder had failed. When this situation occurred in the analysis, the slab elements were removed from the analysis.

11.3 ANALYSIS RESULTS

The three different thermal response cases (Cases A, B, and C) were used as input to the ANSYS analysis. It became apparent as the ANSYS analyses progressed that the connection, beam, and girder failures were essentially at the same locations and with similar failure mechanisms, but shifted in time between the three cases. Case B failures occurred at the earliest time, followed by Case A, and then Case C. The results of the Case B and C analyses are presented to show the similarity in failure types and locations and the time lag between Case B and Case C, since Case A results fall between these two Cases.

The analysis of the structural response of WTC 7 to the effects of elevated temperatures produced a large volume of output data. Results for Floors 2 to 7 and Floors 15 and 16 are not presented as they were subject only to gravity loads and were not subjected to thermal loads. The analysis results for Floors 8 to 14 were first examined graphically for a selected response, such as vertical displacement or strains. Areas of interest were then examined in more detail by listing the results of interest.

Heating of structural components resulted in several possible structural responses, depending on the temperature of the components, amount of thermal expansion, end restraint, and degradation of stiffness and strength. Structural parameters that were monitored and evaluated to determine the structural thermal response included:

- Vertical displacements of the floor framing and the slab
- Axial stresses in floor beams and columns
- In-plane strains of the floor slab
- Degree of damage in connections
- Lateral displacement and rotation of floor beams and girders

Damage to the floor framing depended primarily on the heating from fires on the floor below, whereas the slab was affected by fires on the top of the slab as well as from fire on the floor below. The vertical displacements generally increased as the structural temperatures increased.

Axial stresses in the floor beams increased as the beam temperatures increased, but the column axial stresses remained relatively constant during the response. Interior columns were not thermally restrained and were free to expand. Exterior columns had some thermal restraint, due to the moment framing, but the temperatures remained low. The axial column stresses remained essentially constant because (1) their temperatures remained below 300 °C and (2) the failure of girders in a floor did not noticeably decrease the shear load transferred to the column. The change in column load following a girder failure at any given floor was small compared to the total column loads from the tenant floors above. Additionally, the only path for redistribution of gravity loads in WTC 7 between columns was through the floor framing. Any load redistribution would have occurred until the beam or girder connections failed at the column.

A damage index was computed for the horizontal and vertical direction (shear and axial load) for each connection. Connection failures of fin, knife, and header connections resulted in loss of support for both horizontal and vertical directions, whereas, loss of horizontal and vertical support in the seated connections (SWC, STC, and STP) occurred separately. For example, if all the bolts in a fin connection were sheared, the connection would be fully damaged (failed) in both the horizontal and vertical directions. However, if all the bolts of a seated connection were sheared, the connection would be fully damaged in the horizontal direction, but not in the vertical direction as the beam or girder would still be resting on the seat. Failure in the vertical direction would occur when either the member supported by the connection walked off the seat or the weld at the bearing seat failed.

The damage state of connections, floor beams, and girders was summarized in graphics for each floor in Sections 11.3.2 and 11.3.3. Connection damage is shown separately for the horizontal and vertical directions. For example, in Figure 11–23 (first graphic in Section 11.3.2), tan dots represent connections without any damage and black dots represent connections with full damage for a given direction. The other colors indicate the degree of damage to the connection at a given time in the analysis. For example, a blue dot, with the degree of damage labeled as "0.5 to 0.74," represented a 6-bolt fin connection with 4 failed bolts, which gives a damage index of 0.66. Connection damage was typically gradual, with bolts and/or welds failing sequentially over time. In addition to showing connection damage, these graphics also present the floor beams and girders that buckled (pink lines) or failed an end connection (red line). Prior to end connection failures, many, if not all, of the shear stud connections had failed in the floor beams due to thermal expansion effects. Any beam that was connected to a girder that lost vertical support also lost vertical support at the girder, and is indicated with a red line.

Graphics are presented in Sections 11.3.1, 11.3.2, and 11.3.3 to describe key observations for the building response to gravity loads (Figure 11–21 and Figure 11–22), Case B temperatures at 3.5 h (Figure 11–23 through Figure 11–30) and 4.0 h (Figure 11–31 through Figure 11–38), and Case C temperatures at 4.0 h (Figure 11–39 to Figure 11–46). The Case B temperatures at 4.0 h resulted in significant damage to the floors subjected to fires. The difference between the damage at 3.5 h and 4.0 h presents the increase in damage in the last half hour. The Case C temperatures at 4.0 h show how the structural response was similar to the Case B response, but with a time lag.

Section 11.4 has a general discussion of results for Case B at 3.5 h and 4.0 h and for Case C at 4.0 h.

11.3.1 Analysis of Building Response to Gravity Loads

The structural response to gravity loads was the same for all tenant floors. Figure 11–21 shows the vertical displacements in the floor framing and slab, the axial stresses in the floor framing and columns, and the in-plane strains of the floor slab for Floor 8.

Displacements. The typical vertical floor displacement on the tenant floors was about 3.5 in. as shown in Figure 11–21a. The maximum vertical deflection of 4.5 in. occurred at the northwest corner. The floor beams were cambered in the design drawings (1.75 in. to 2.5 in. at the east tenant floor, 1.75 in. to 2.75 in. at the north tenant floor, 1.0 to 1.25 at the west tenant floor, and 1.0 in. at the south tenant floor). The camber could not be modeled in ANSYS. Thus, the vertical floor displacements would have been about one to two inches, if the camber was subtracted from the computed displacements.

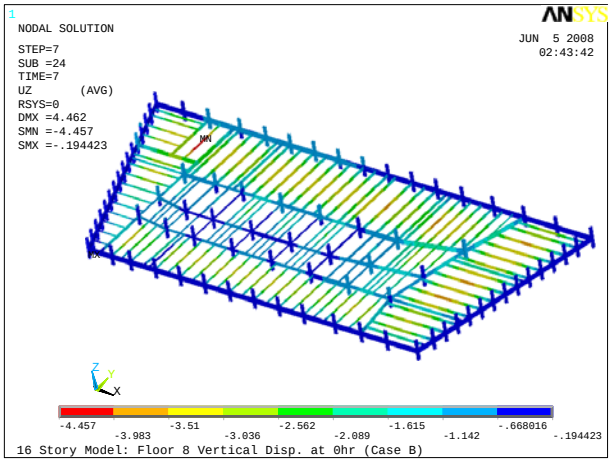

a) Vertical displacements in floor framing.

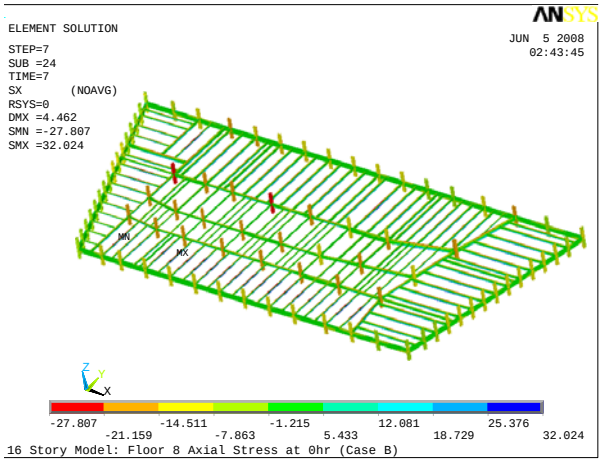

b) Axial stress in floor framing.

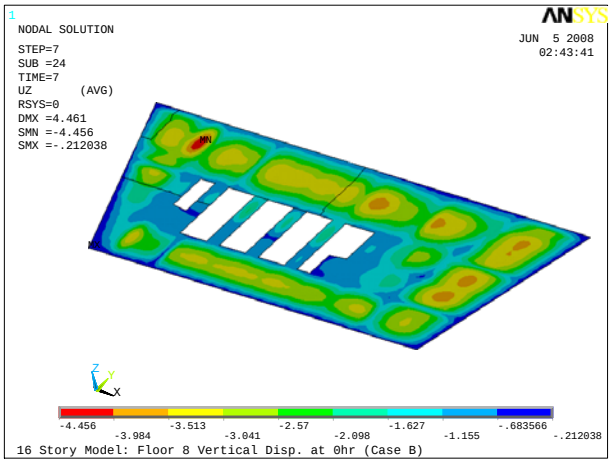

c) Vertical displacements in floor slab.

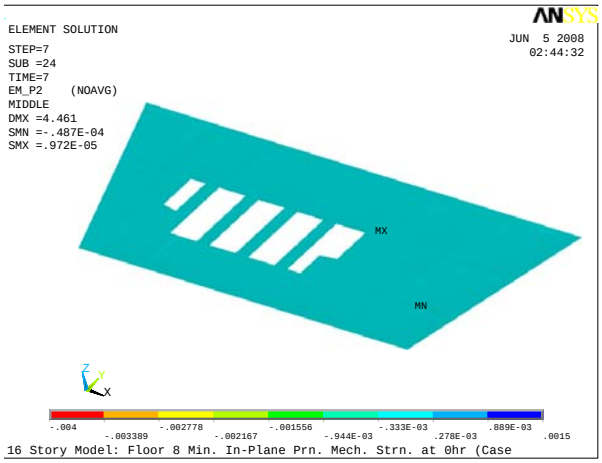

d) Minimum in-plane principal strains in floor slab.

Grey color indicates areas with ε < -0.004 and purple color indicates areas with ε> 0.0015.

Figure 11–21. Structural response of Floor 8 to gravity loads.

Axial stresses from axial forces in the floor beams and in-plane slab strains were small, as expected for gravity load conditions. The stress in the floor beams due to axial loads was less than 1 ksi (floor beams had a nominal yield strength of 50 ksi). The in-plane slab strains were less than -5×10^{-5} (concrete failure strain in compression was -4×10^{-3} and failure strain in tension was 1.5×10^{-3}).

Axial column stresses (Figure 11–21b) ranged from 15 to 28 ksi in the interior columns and in exterior Columns 44 and 55 on the north face. The axial column stress in the other exterior columns ranged from 8 to 15 ksi.

Column Loads. The column loads at Floor 8 are presented for comparison to the column loads at 3.5 h and 4.0 h of heating, which are presented at the end of Sections 11.3.2 and 11.3.3. Axial forces in the columns at Floor 8 are shown in Figure 11–22. The maximum column force of 7,525 kip was at Column 79. The axial force ranged from 2,000 kip to 5,000 kip in the rest of the interior columns and 1,000 kip to 3,000 kip in the exterior columns. The sum of all column forces was 176,500 kip, with the interior and exterior columns carrying these loads in about equal parts. Based on the design drawings, the sum of all column loads for a loading condition of dead loads and service live loads was 174,100 kip.

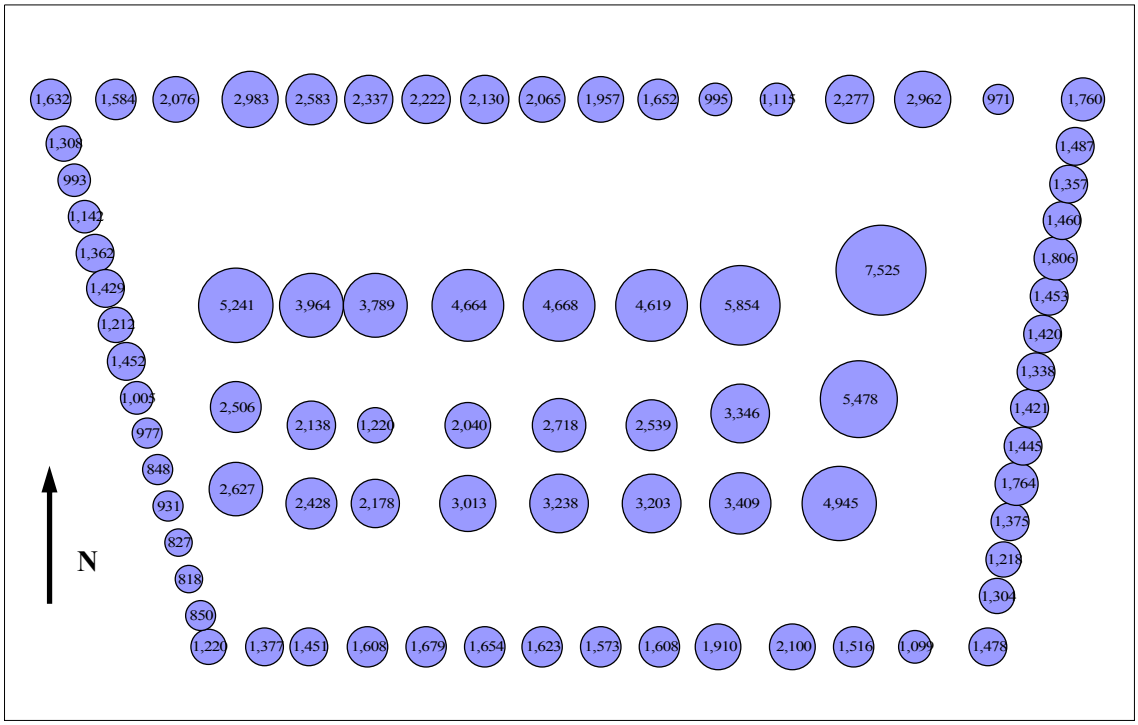

Summation of Column forces:

North face: 33,300 kip East face: 18,850 kip

South face: 21,900 kip West face: 15,150 kip

Interior: 87,350 kip Total: 176,550 kip

Compression is positive

Figure 11–22. Column forces (kip) above Floor 8 for gravity loads.

11.3.2 Analysis of Building Response for Case B Temperatures

The fires on Floors 11, 12, and 13 generated significantly more heat than the fire on Floors 7, 8, and 9. This was in large part due to the higher fuel load and the window breakage on Floors 11, 12, and 13 (see Section 10.4). The difference in the heating of structural elements subject to fire is reflected in the location and extent of fire-induced damage to the floor systems described below. (As a reminder, a fire on a given floor, such as Floor 12, will primarily heat the top of the slab on Floor 12 and the floor framing and bottom of the slab on Floor 13).

The building response is examined at 3.5 h and 4.0 h of heating. At 3.5 h, the floor systems had fire-induced damage and some failures of connections, beams, and girders. After 4.0 h of heating, there was substantially more damage and failures in the WTC 7 structural system, particularly in the northeast region surrounding Column 79. The structural condition at these two times illustrates how the structure developed sufficient fire-induced damage to reach the collapse initiation event.

Building Response at 3.5 h

Figure 11–23 to Figure 11–29 show the damage to the connections, beams and girders of Floors 8 to 14, respectively.

After 3.5 h of heating, there were failures of floor beams, girders, and floor slab sections on Floors 8, 12, 13, and 14 due to the fires. The fires on Floors 7, 8, and 9 had primarily heated the north tenant floor area from west to east. The fires on Floors 11, 12, and 13 had heated the south tenant floor area and the southern region of the east tenant floor area. Figure 10-27 to Figure 10-40 in Section 10.3.3 show the temperatures of structural members on these floors[8].

Floors 8, 13, and 14 had the most damage in response to the fires at this time, with the largest vertical deflections, greatest axial stresses in beams and girders, crushed slab areas, and areas with failed beams and girders. Floor 12 also had thermally induced damage, but to a lesser degree than Floors 8, 13, and 14. Results for Floors 8, 12, 13, and 14 are discussed here.

Floor 8. Elevated temperatures in the north floor framing on Floor 8 ranged from about 150 °C at the east end to 500 °C at the west end. The downward (vertical) floor deflections had increased to 19 in. in the north floor beams on the west side. Axial compression due to beam axial forces had increased to between 20 ksi and 30 ksi in many of the core and north floor beams, from less than 1ksi due to gravity loads alone. The increase in axial compression in the floor beams is the result of restrained thermal expansion in the floor system. The slab in the northwest region had reached the crushing strain limit under the compressive strains, and was softened as explained earlier.

Fin connections failed for the north floor beams on Floor 8 that were attached to the girder between Columns 76 to 79 (see Figure 2-4 for column locations), due to thermal expansion in the beams, by shearing the bolts at the girder. Figure 11–23 shows connection and floor framing damage that occurred.

[8] The thermal analysis in Chapter 10 determined the temperature of structural members when subjected to the gas temperatures from the FDS analysis, but it did not account for thermally-induced damage; the temperatures from Chapter 10 were input to the ANSYS model to determine the structural response, which is presented in this Chapter.

The northeast beam-to-girder fin connections had a 0.75 to 0.99 damage level between Columns 44 and 79 and a 0.25 to 0.49 damage level at the east exterior columns. The header connections failed at Columns 74 and 78, due to thermal expansion of the girder. The beams that were supported by these girders are also indicated as failed, since they would fall with the girder.

Floors 9 to 11. Floors 9 to 11 had downward displacements ranging from 9 in. to 15 in. The largest downward displacements tended to be adjacent to failed floor beams, as the remaining beams were loaded by the slab.

Floors 12, 13, and 14. Elevated temperatures in the southeast region on Floors 12, 13, and 14 of the floor framing ranged from 150 °C to 350 °C for Floor 12, 500 °C to 700 °C in Floor 13, and 300 °C to 500 °C in Floor 14. However, the thermal analysis did not account for failed floor framing as the structure was heated over time. Figure 11–27, Figure 11–28, and Figure 11–29, based on the ANSYS analysis of the structural response to heating, show that floor beams had failed in areas where the steel temperatures were greater than 400 °C to 500 °C. The following beam and girder failures occurred:

- Floor 12 had six floor beam failures, by Columns 78, 80, and 81, due to buckling of the floor beam near Column 80 or connection failures (Figure 11–27). The beam on the east side of Column 81 had a weld failure in the header connection to the exterior spandrel beam. The remaining removed beams either buckled or lost vertical support when all connection bolts were sheared.

- Floor 13 had failure of all tenant floor beams near Columns 78, 80, and 81 (Figure 11–28) and Floor 14 framing had failure of all tenant floor beams near Columns 78 and 81 (Figure 11–29). The floor beams either buckled (i.e., the east floor beam that framed into Column 80) or had connection failures (i.e., all the bolts were sheared) at the girder or spandrel beam, which were induced by thermal expansion of the beams.

- At Floors 13 and 14, the girder between exterior Column 26 and interior Column 81 buckled and walked off the bearing seat due to the combined effects of (1) gravity loads, (2) lateral westward displacement due to the thermal expansion in the east floor beams prior to their failures, and (3) thermal expansion in the girder.

Axial beam stresses due to axial beam forces had increased in the south and east floor beams on Floors 12 to 14, reflecting restrained thermal expansion. The southeast floor slab was softened, as the compressive strain criteria was exceeded on Floors 12 and 13, due to the local thermal expansion that developed from the fires on those floors. Floor 14 did not have a fire, so its slab was not softened.

Figure 11–27, Figure 11–28, and Figure 11–29 show the connection and floor framing damage that occurred in Floor 12, 13, and 14, primarily due to the effects of thermal expansion. The east beam-to-girder fin connections had a 0.75 to 0.99 damage level between the south face (Column 26) and Column 79 at most of the floor beams. This level of connection damage also extended toward the north face (Column 44) on Floor 13; only two connections remained undamaged. The seated connection at Column 79 had horizontal connection damage, with shear failure of all the erection bolts on Floor 13 and two to three bolts on Floors 12 and 14, respectively

Column Loads. Figure 11–30 shows the axial force in columns at Floor 8 at 3.5 h. The axial forces in the columns were reduced by less than 0.04 percent relative to the forces based on the gravity analysis (Figure 11–22), which equaled the weights of the removed beams. The change in axial forces in columns and redistribution of loads among floor columns was negligible.

Summary. The connections between the girders and interior columns were all intact, except for the girder between exterior Column 26 and interior Column 81 on Floors 13 and 14. At the seated connection at Column 79, all the bolts had sheared on Floor 13 and 2 to 3 bolts had sheared on Floors 12 and 14. Approximately one-half to three-quarters of the east floor beams had a connection damage index of 0.75-0.99 on Floors 11, 12, 13, and 14. While the floor systems had experienced fire-induced damage to connections, beams, and girders after 3.5 h of heating, primarily due to the effects of thermal expansion, the WTC 7 structural system had damage on the north floor and east side of the core on Floor 8 and the south and east area of Floors 12, 13, and 14.

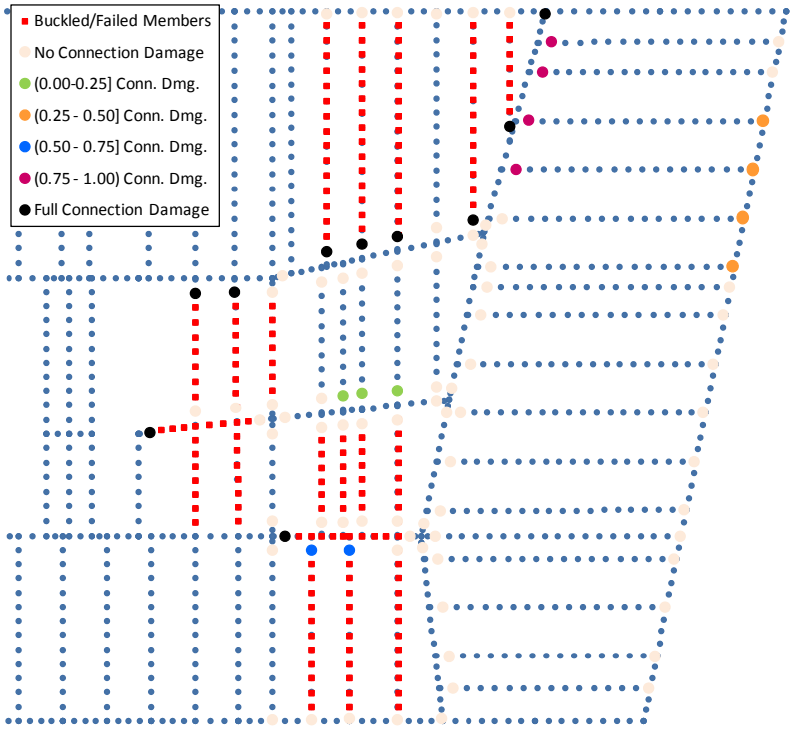

a) Damage state of connections in the horizontal direction

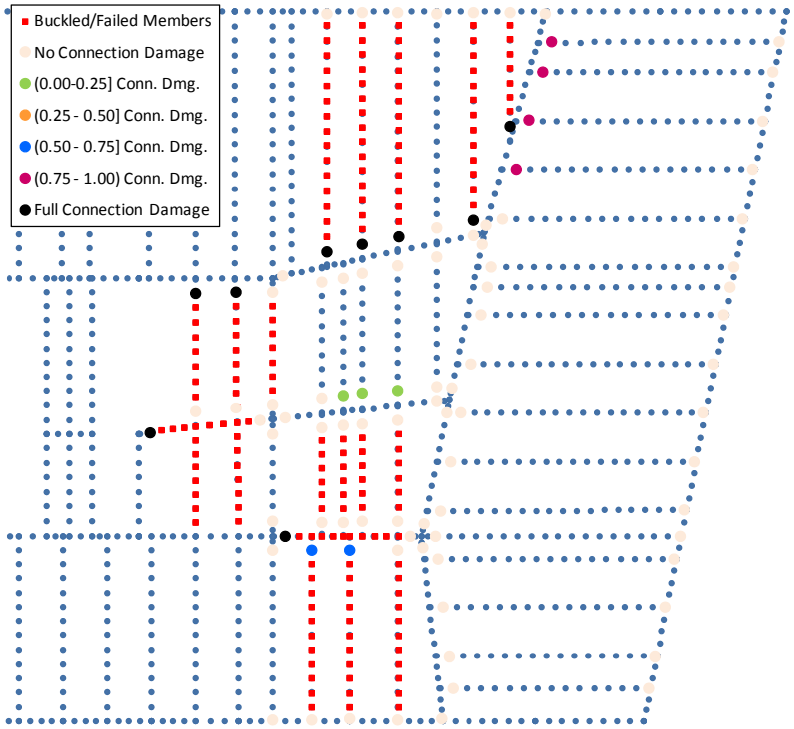

b) Damage state of connections in the vertical direction

Figure 11–23. Damage state of connections, beams, and girders in Floor 8 at 3.5 h for Case B temperatures.

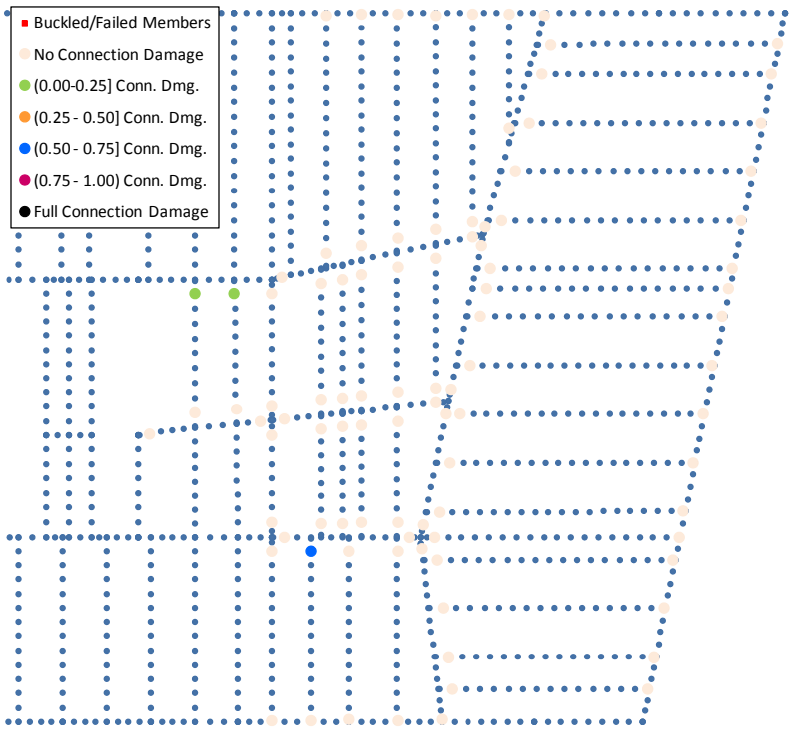

a) Damage state of connections in the horizontal direction

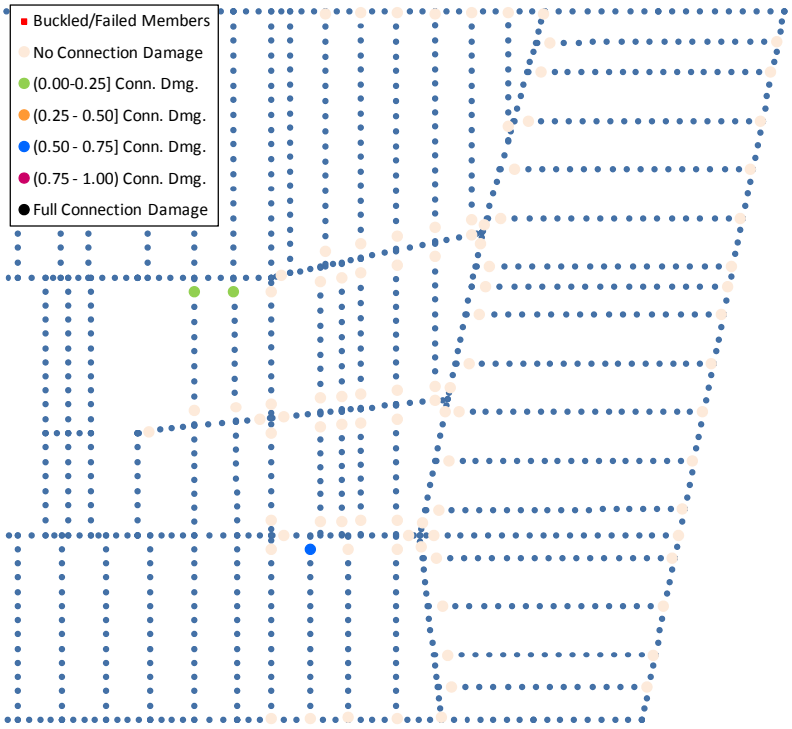

b) Damage state of connections in the vertical direction

Figure 11–24. Damage state of connections, beams, and girders in Floor 9 at 3.5 h for Case B temperatures.

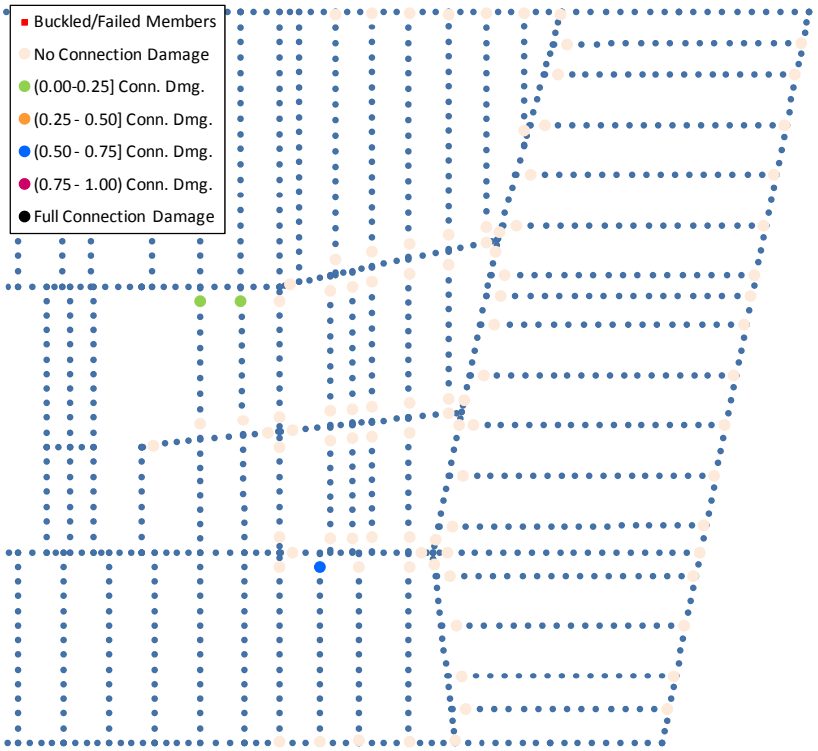

a) Damage state of connections in the horizontal direction

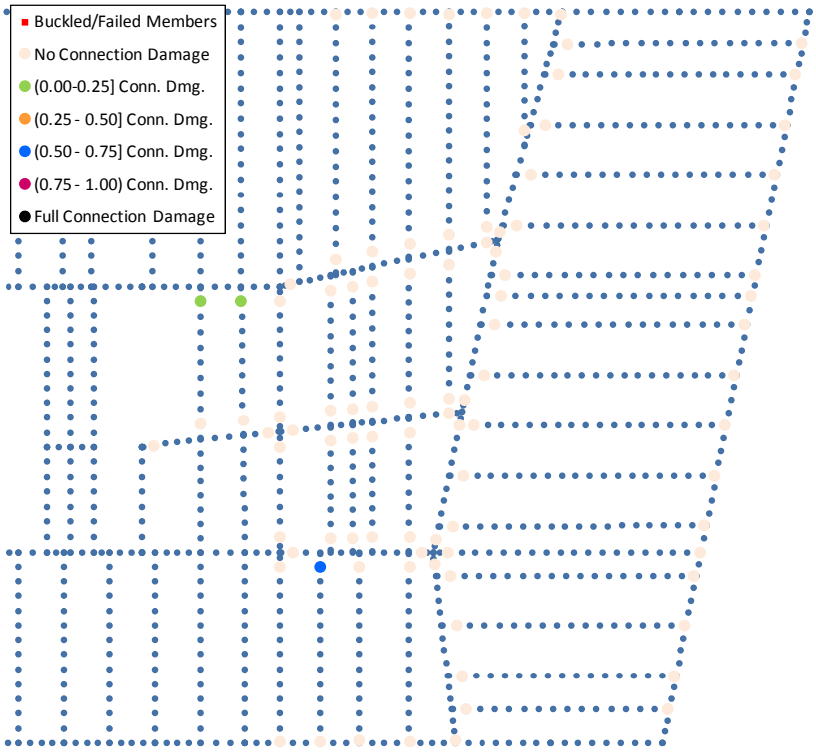

b) Damage state of connections in the vertical direction

Figure 11–25. Damage state of connections, beams, and girders in Floor 10 at 3.5 h for Case B. temperatures.

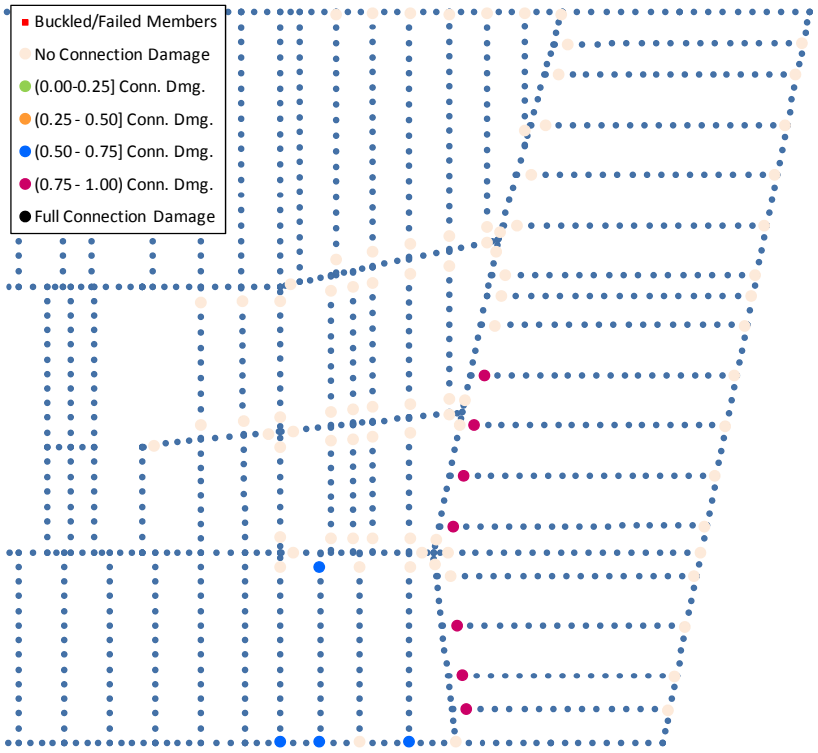

a) Damage state of connections in the horizontal direction

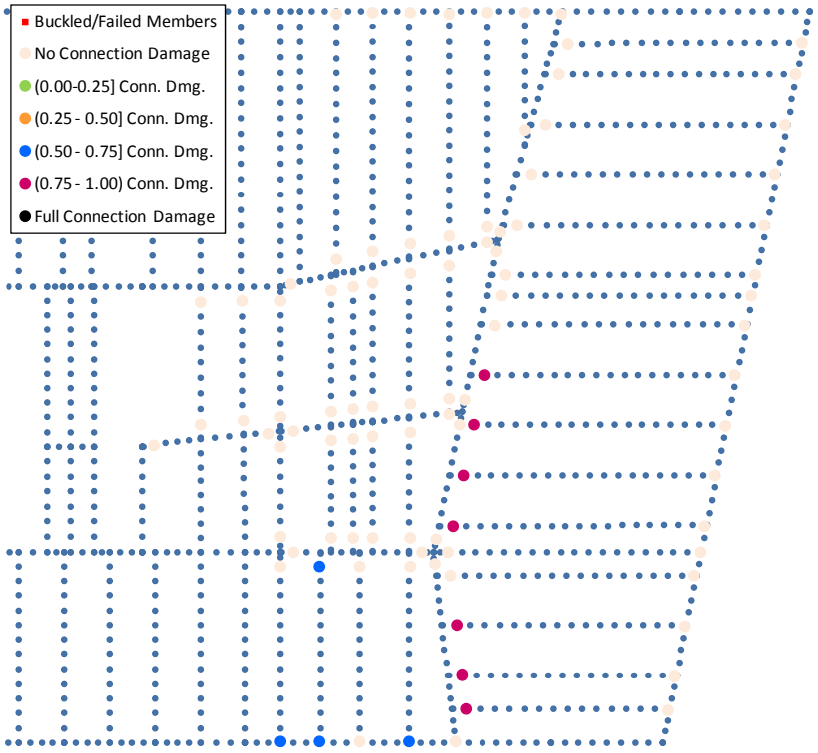

b) Damage state of connections in the vertical direction

Figure 11–26. Damage state of connections, beams, and girders in Floor 11 at 3.5 h for Case B temperatures.

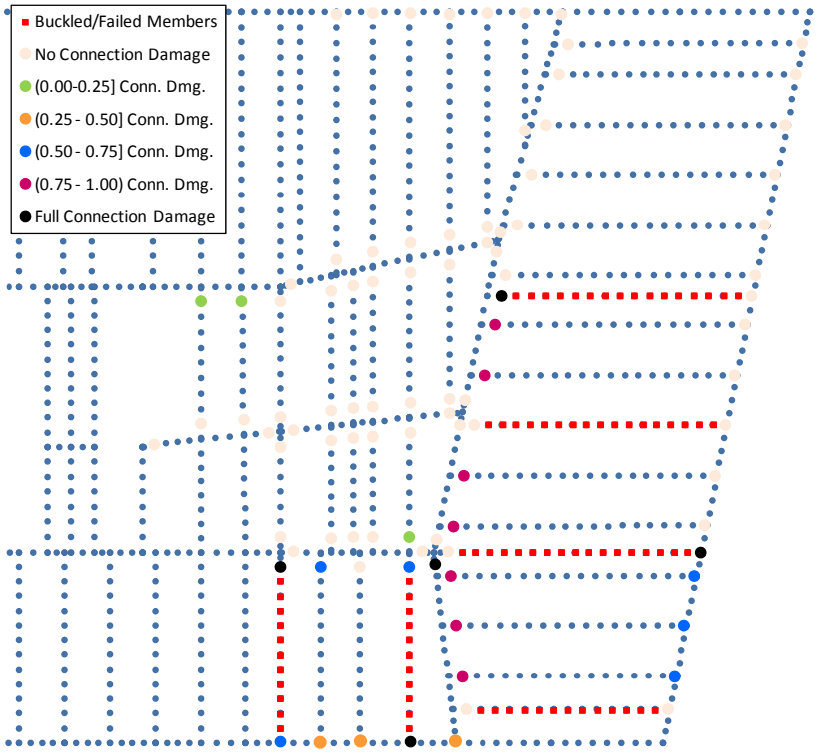

a) Damage state of connections in the horizontal direction

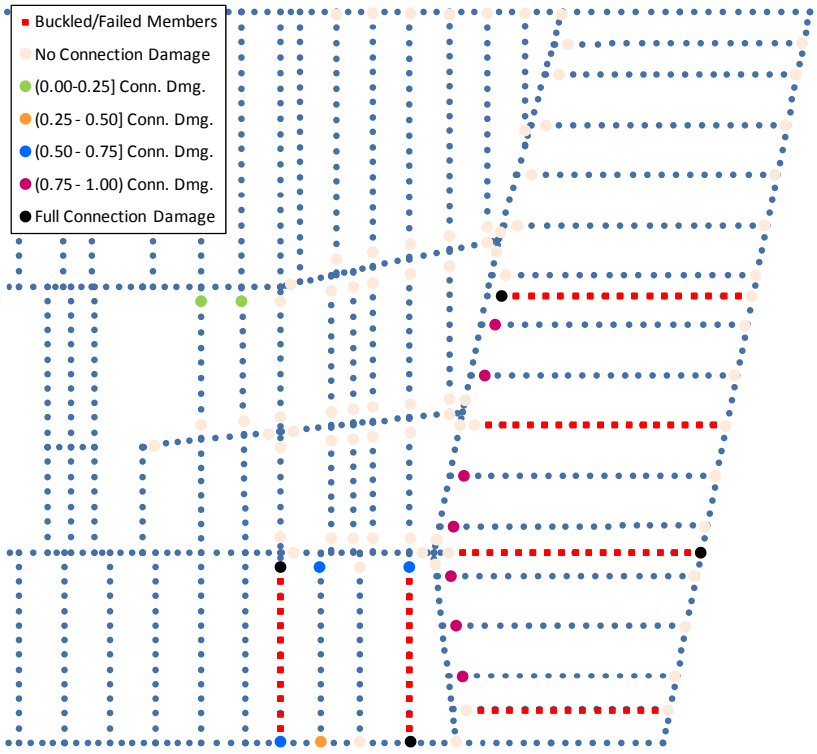

b) Damage state of connections in the vertical direction

Figure 11–27. Damage state of connections, beams, and girders in Floor 12 at 3.5 h for Case B temperatures.

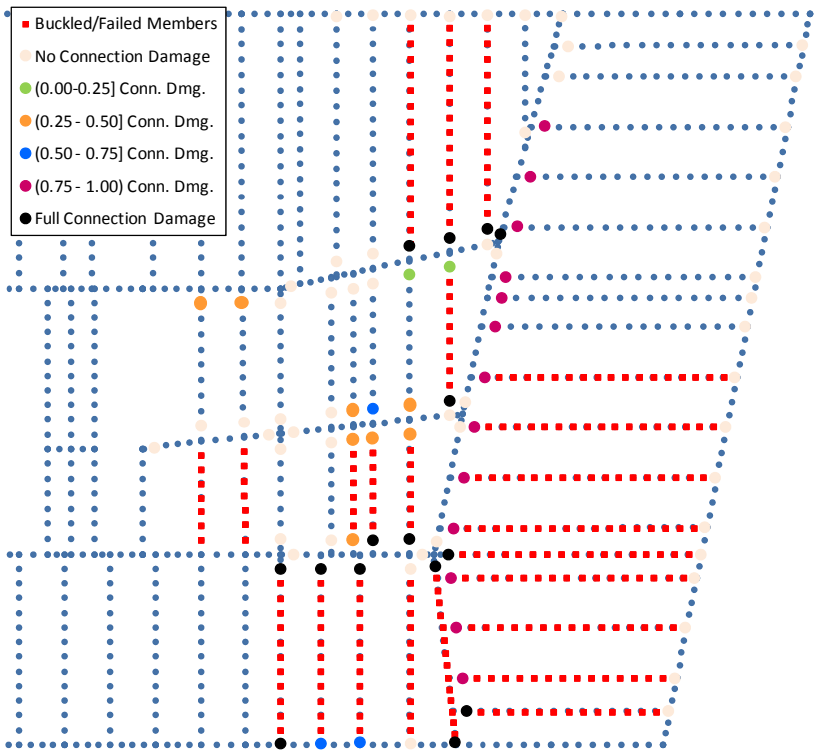

a) Damage state of connections in the horizontal direction

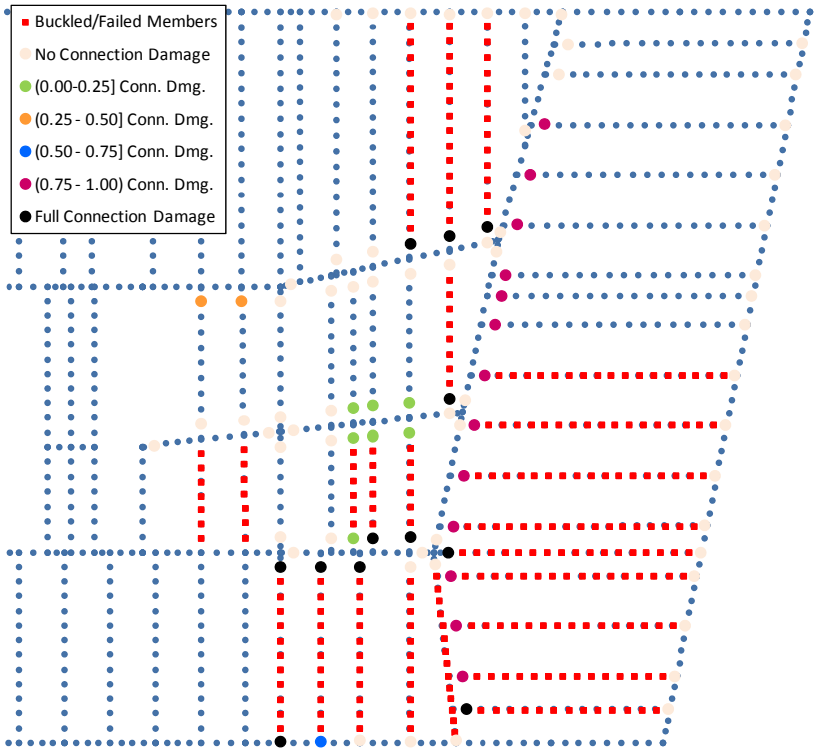

b) Damage state of connections in the vertical direction

Figure 11–28. Damage state of connections, beams, and girders in Floor 13 at 3.5 h for Case B temperatures.

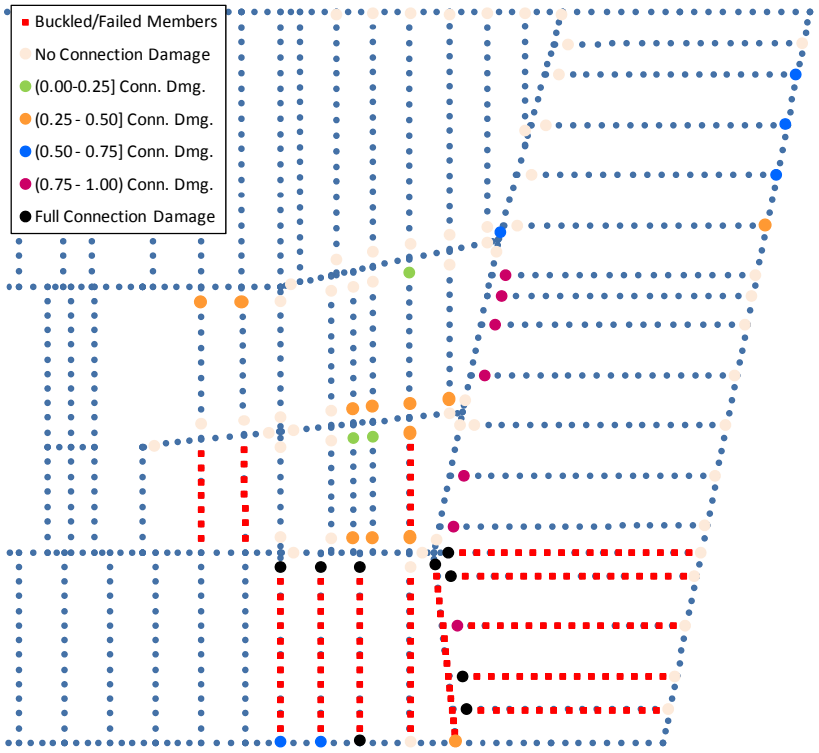

a) Damage state of connections in the horizontal direction

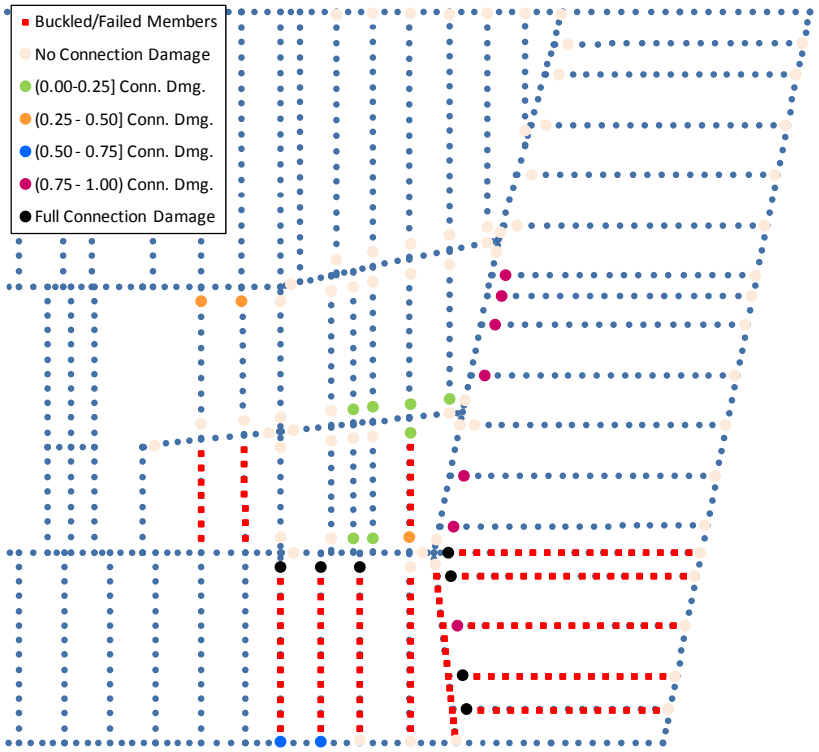

b) Damage state of connections in the vertical direction

Figure 11–29. Damage state of connections, beams, and girders in Floor 14 at 3.5 h for Case B temperatures.

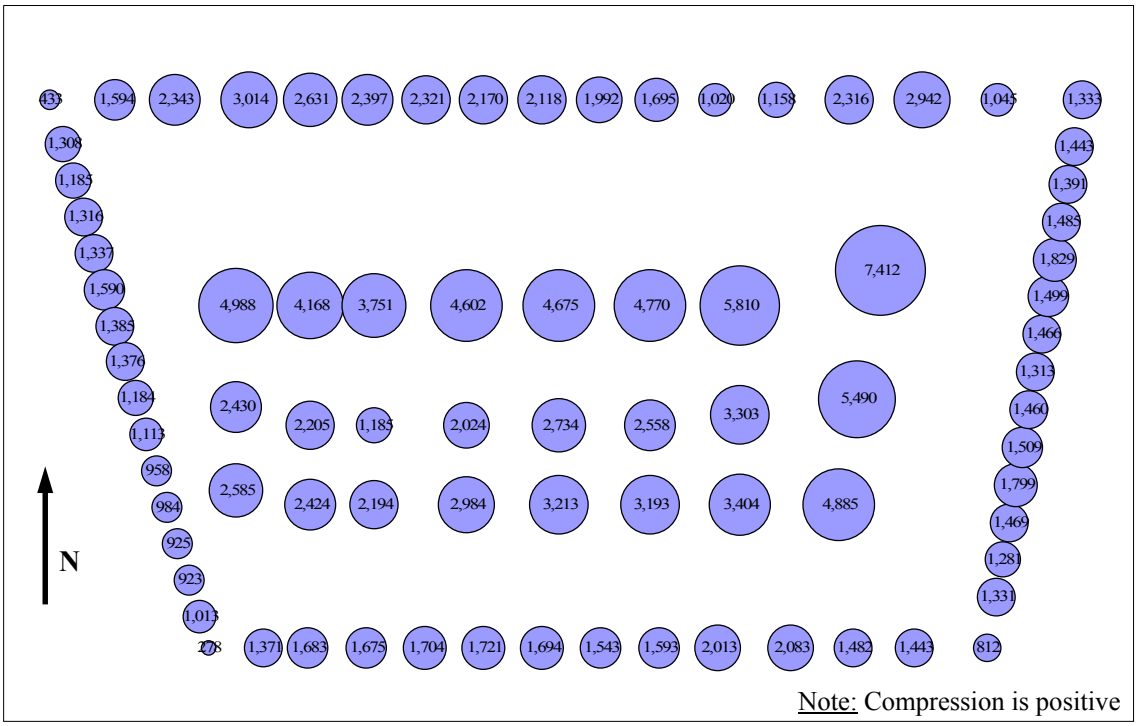

Summation of Column forces:

North:	32,500 kip	East:	19,300 kip
South:	21,100 kip	West:	16,600 kip
Core:	87,000 kip	Total:	176,500 kip

Figure 11–30. Column forces (in kip) above Floor 8 at 3.5 h for Case B temperatures.

Building Response at 4.0 h

After 4.0 h of heating, there were considerably more failures of floor beams, girders, and floor slab sections at Floors 8, 10, 11, 12, 13, and 14 due to the fires. Fire-induced damage on Floor 9 was limited to the failure of three floor beams and several connections. Figure 11–31 through Figure 11–37 show the failures in the connections, beams, and girders. Figure 10-27 to Figure 10-40 in Section 10.3.3 show the temperatures of structural members on these floors.

Floors 8, 12, 13, and 14 had the most damage, with the largest vertical deflections, axial stresses in beams and girders, areas of crushed slab, and areas of failed beams and girders. Floors 10 and 11 had girder and beam failures at the east end of the north face adjacent to Column 79. Additional damage that occurred between 3.5 h and 4.0 h is described below.

Floor 8. Elevated temperatures in the north floor framing on Floor 8 ranged from about 550 °C at the east end to 300 °C at the west end. Axial stresses were compressive and remained at 20 ksi to 30 ksi in many of the core and north floor beams, but had increased to 52 ksi in some locations in the core near the failed floor framing. Figure 11–2 shows that the yield strength for the A572 Grade 50 steel used for the beams was 54 ksi at room temperature. As the temperature in these beams was less than 400 °C, the beam strength and stiffness was not reduced.

As before, beams and girders failed by loss of vertical support at connections or by buckling of beams or girders. The girder between Columns 70 to 73 and Columns 73 to 76 buckled, as shown in Figure 11–31. The floor beams that were supported by the girder between Columns 78 and 81 and Columns 71 and 74 also failed when the girder lost vertical support at an end connection, due to the effects of thermal expansion. Seven fin connections in the east tenant floor between Columns 44 and 80 had a 0.75 to 0.99 damage level.

Floors 10, 11, and 12. On Floors 10, 11, and 12 (Figure 11–33, Figure 11–34, and Figure 11–35), the girder between Columns 76 and 79 failed due to a tensile weld failure in the knife connection on the west side of Column 79. Temperatures in this region were less than 100 °C on these floors. The tensile force in the connection was due to an eastward lateral displacement of Column 79, which was primarily caused by thermal expansion of the girder between Column 76 and Column 79 at Floor 13.

There was connection damage and beam buckling around the southeast corner of Floor 11, but there were no fires on Floor 10 to heat the steel framing from below. The fires on Floor 11 caused heating and thermal expansion of the Floor 11 slab in this area. The concrete slab thermally expanded until it exceeded the compressive strain criteria, so that the floor system no longer acted as a composite system. As a result, the floor beams began to act independently, and connection damage and beam buckling occurred.

Floors 12, 13, and 14. Elevated temperatures in the southeast and east floor framing on Floors 12, 13, and 14 ranged from 150 °C to 550 °C for Floor 12, 300 °C to 700 °C in Floor 13, and 150 °C to 700 °C in Floor 14. However, the thermal analysis did not account for failed floor framing as the structure was heated over time. Figure 11–35, Figure 11–36, and Figure 11–37 show that the floor beams had failed by connection failures or buckling of beams or girders in areas where the steel temperatures were greater than 400 °C to 500 °C. The following beam and girder failures occurred:

- On Floors 12 and 14, most of the floor beams on the south and east floor areas near Columns 78, 81, and 80 (Figure 11–35 and Figure 11–37) had failed. The floor beams had either buckled or lost vertical support when all the fin connection bolts were sheared off due to thermal expansion. Both Floors 12 and 14 had a 0.75 to 0.99 damage level in several east floor beam connections near Column 79.

- On Floor 12, the girder between Column 26 and Column 81 had failed due to buckling, followed by walk-off of the bearing seat, at Column 81.

- On Floor 13 (Figure 11–36), all the north-south girders to Columns 79, 80, and 81 had failed, due to either buckling or girder walk-off of the bearing seat at Columns 79 and 81.

- On Floor 14, all four of the erection bolts in the seated connection at Column 79 on Floor 14 had failed due to the effects of thermal expansion.

- On Floor 14, the header connection for the girder west of Column 80 had failed at the weld to the girder web.

The compressive strains in the southeast area of the slab for Floor 12 gradually increased to exceed the crushing criterion ($\varepsilon < -0.004$) and covered the full east side and half of the south side of the tenant floor

area. The compressive strains in the southeast and east slab areas for Floor 13 exceeded the crushing criterion, and the damage to the slab extended westward on the south face. As a result, slab elements were removed from the model. Due to the large area of failed floor beams, the slab was unsupported over a large area and was not able to carry its loads. A portion of the slab was removed, and the mechanical strains were set to zero. The slab area in which compressive strains in the floor exceeded the crushing strain limit expanded towards the west at the south side of the tenant floor.

Column Loads. Figure 11–38 shows the axial force in columns at Floor 8 at 4.0 h. The axial forces in columns were reduced by less than 0.50 percent relative to the gravity load analysis. This reduction is due to the weights of the removed beams. At the end of 4.0 h, the change in axial forces in columns and redistribution of loads among columns was still negligible, as expected.

Summary. After 4.0 h of heating, Columns 79, 80, and 81 had lost lateral support in the north-south direction at Floor 13, due to failure of the girders between the columns. The girders between Columns 80 and 81 had buckled and the girders between Columns 79 and 44 and Columns 26 and 81 had walked off the bearing seat at Column 79 and 81, respectively. In addition, all of the bolts had sheared at Column 79 on Floor 14, and two to three bolts had sheared on Floor 12. Approximately one-half to three-quarters of the east floor beams had a connection damage index of 0.75-0.99 on Floors 11, 12, and 14 and all of the east floor beams had failed on Floor 13. After 4.0 h of heating, there was substantially more damage and failures in the WTC 7 structural system than after 3.5 h of heating. Columns 79, 80, and 81 had lost lateral support at one or more floors.

The impact of a floor section falling on the floor below was not analyzed in the 16 story ANSYS model, but was simulated in the 47 story LS-DYNA model (Chapter 12).

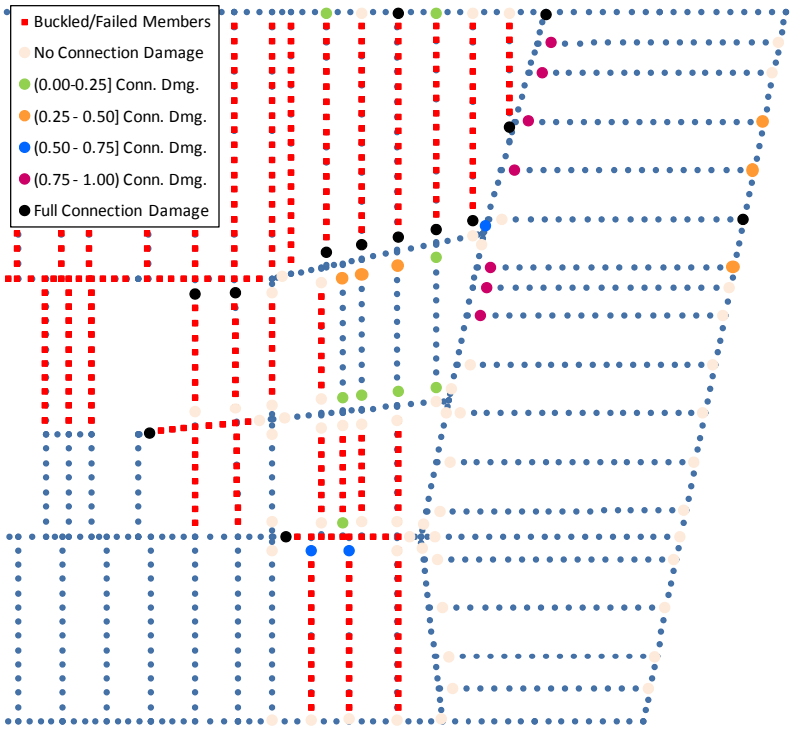

a) Damage state of connections in the horizontal direction

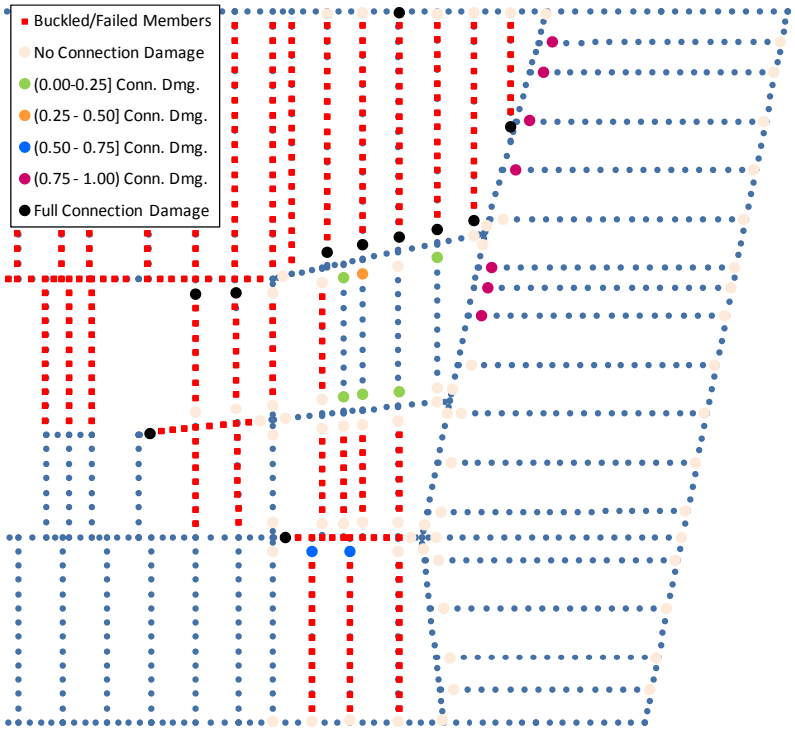

b) Damage state of connections in the vertical direction

Figure 11–31. Damage state of connections, beams, and girders in Floor 8 at 4.0 h for Case B temperatures.

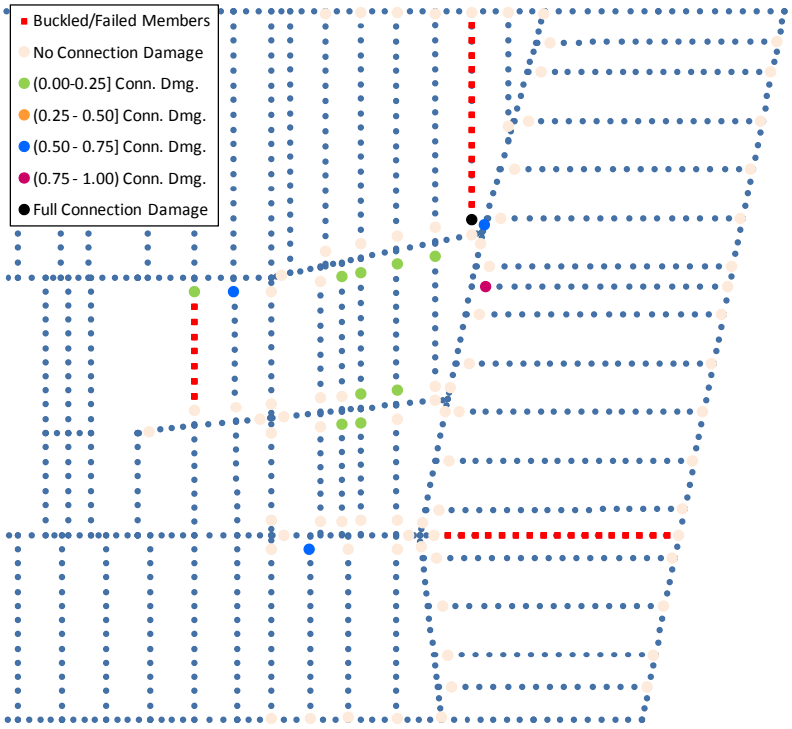

a) Damage state of connections in the horizontal direction

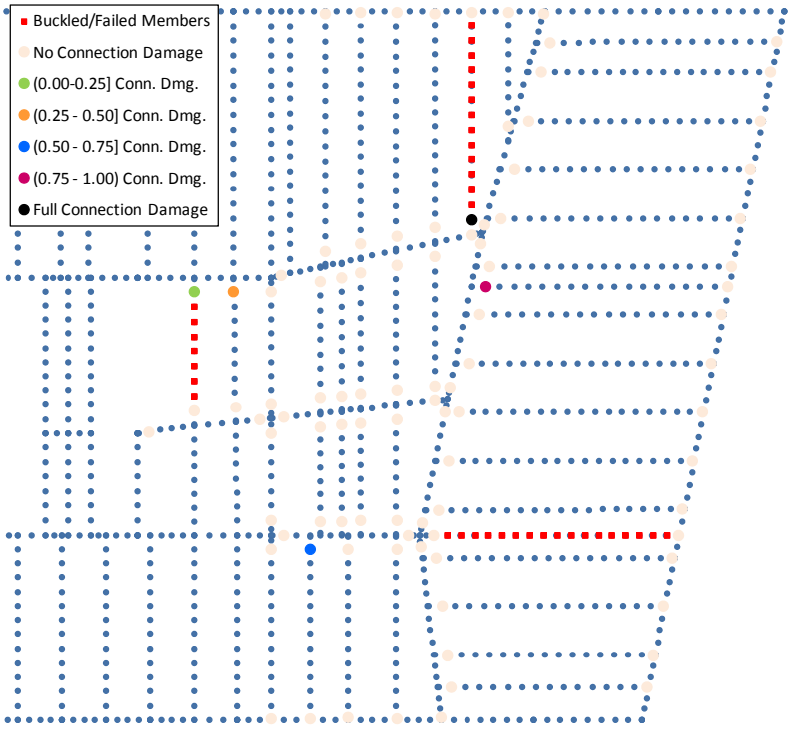

b) Damage state of connections in the vertical direction

Figure 11–32. Damage state of connections, beams, and girders in Floor 9 at 4.0 h for Case B temperatures.

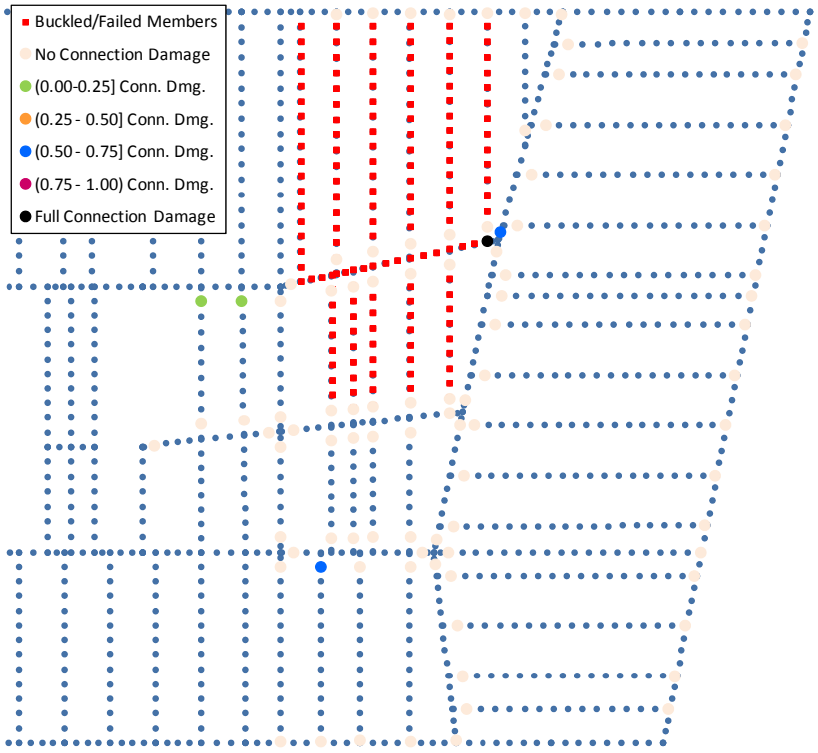

a) Damage state of connections in the horizontal direction

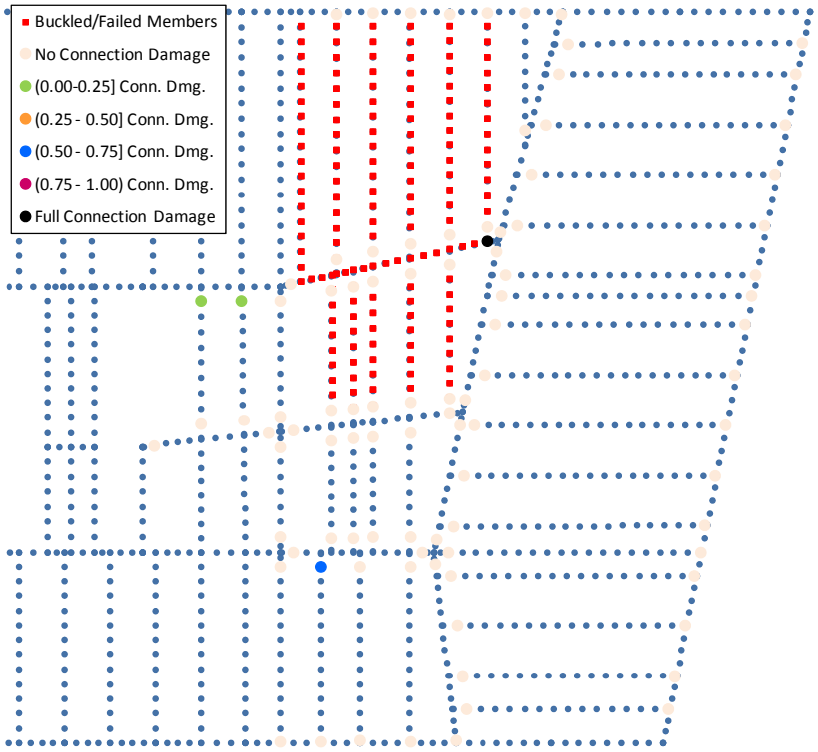

b) Damage state of connections in the vertical direction

Figure 11–33. Damage state of connections, beams, and girders in Floor 10 at 4.0 h for Case B temperatures.

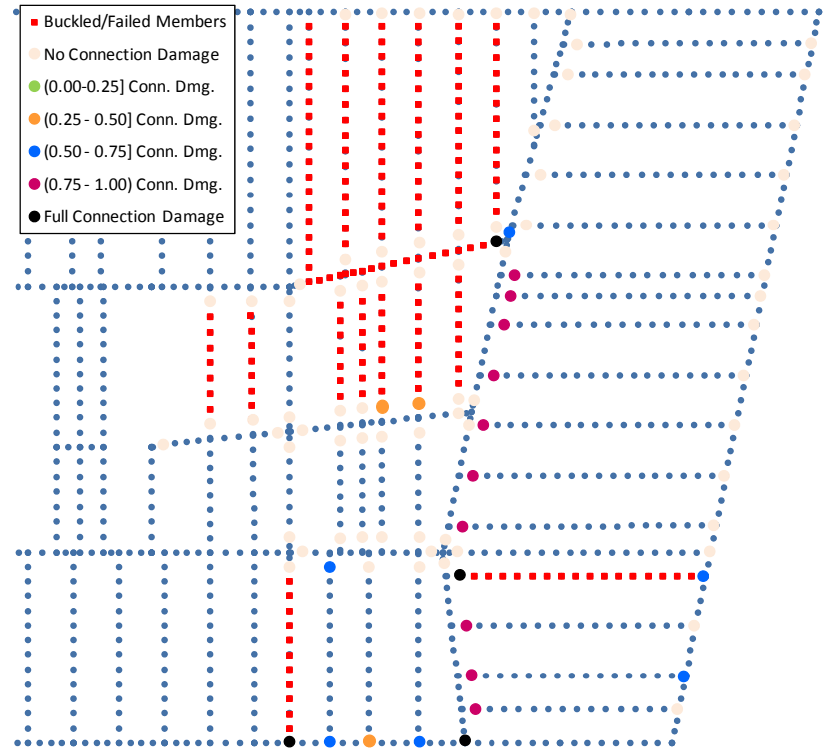

a) Damage state of connections in the horizontal direction

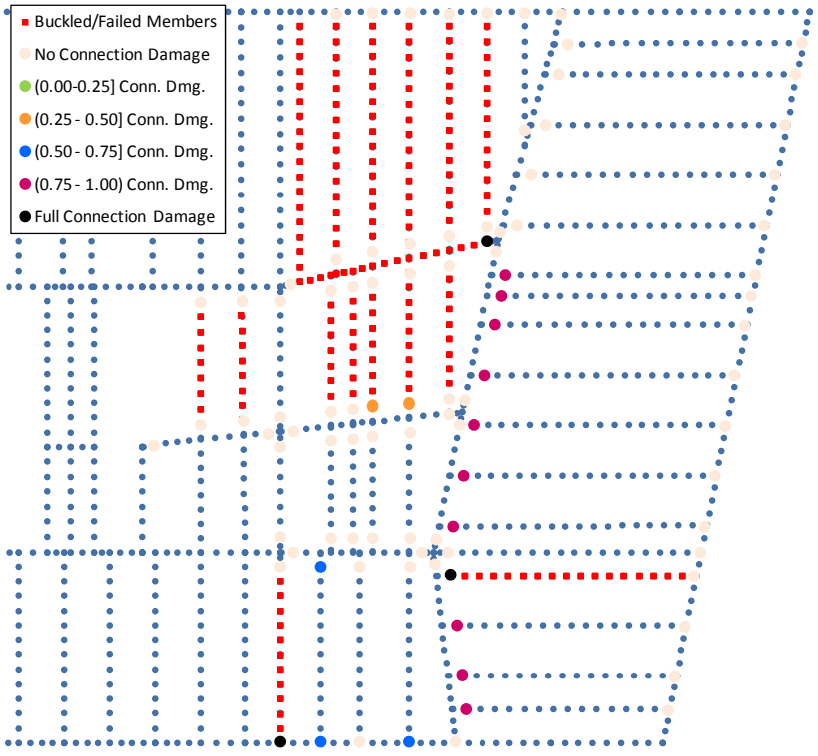

b) Damage state of connections in the vertical direction

Figure 11–34. Damage state of connections, beams, and girders in Floor 11 at 4.0 h for Case B temperatures.

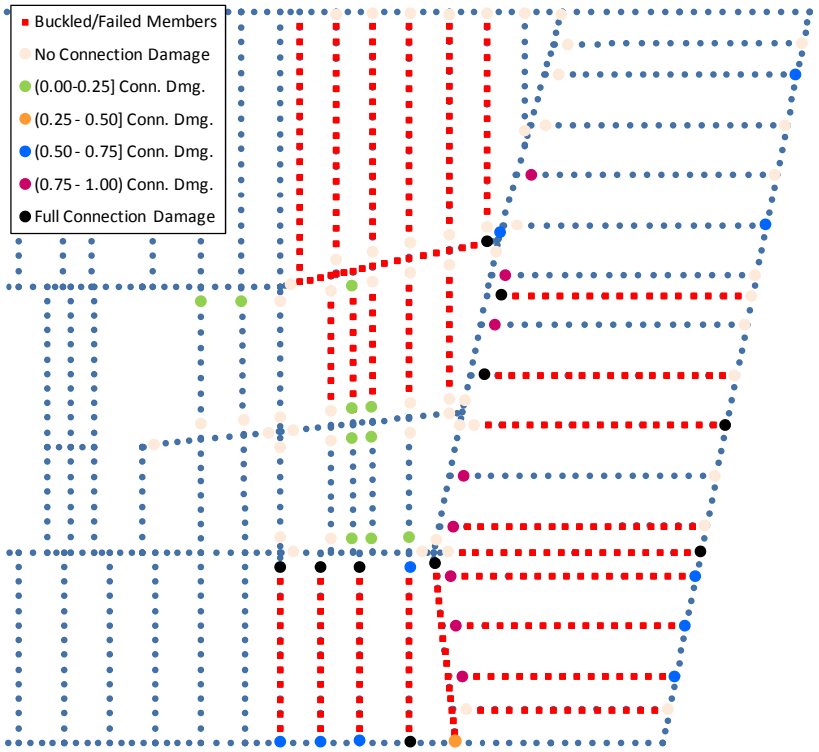

a) Damage state of connection in the horizontal direction

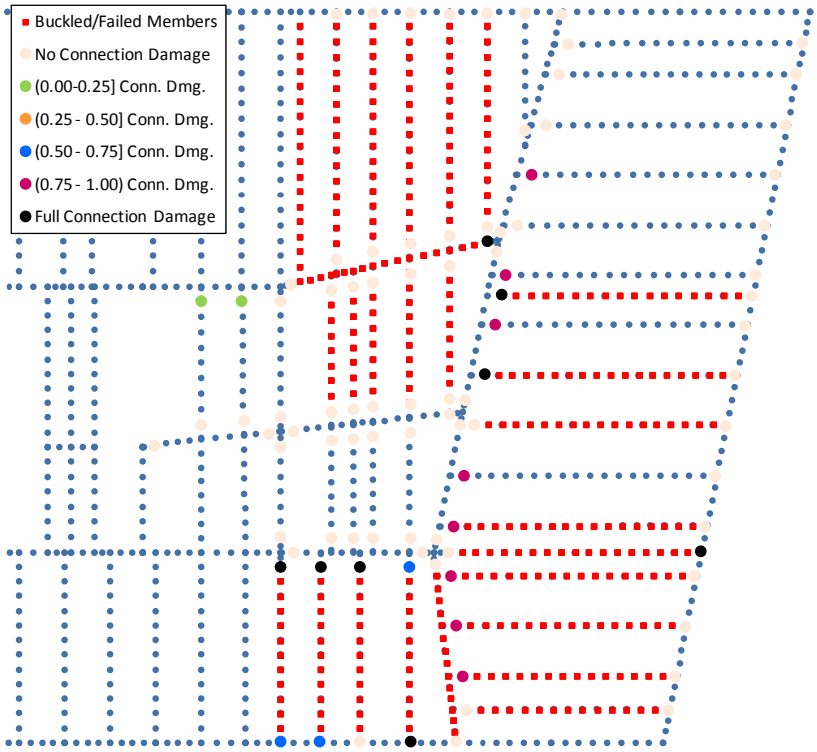

b) Damage state of connection in the vertical direction

Figure 11–35. Damage state of connections, beams, and girders in Floor 12 at 4.0 h for Case B temperatures.

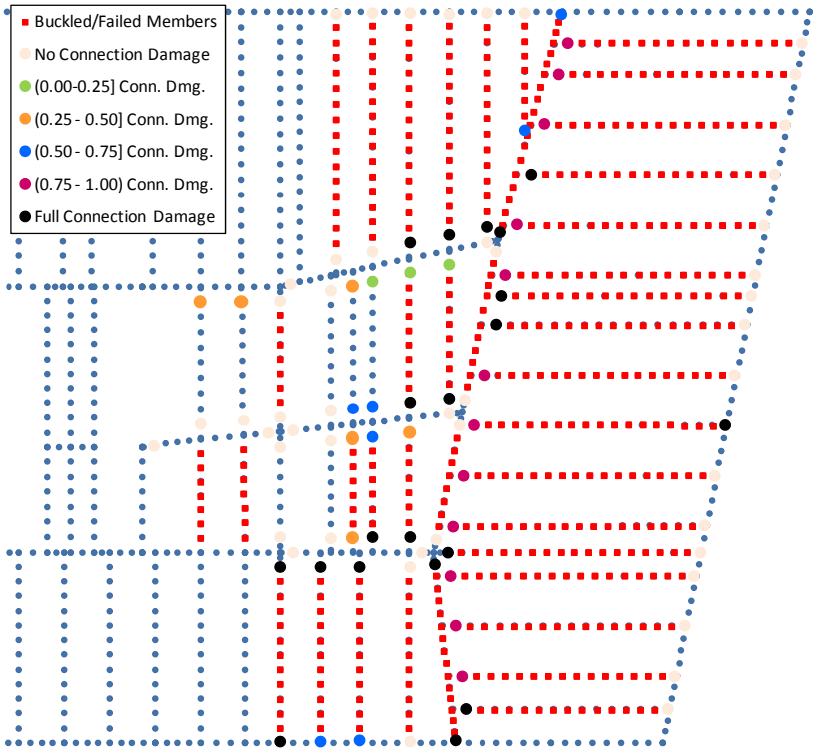

a) Damage state of connection in the horizontal direction

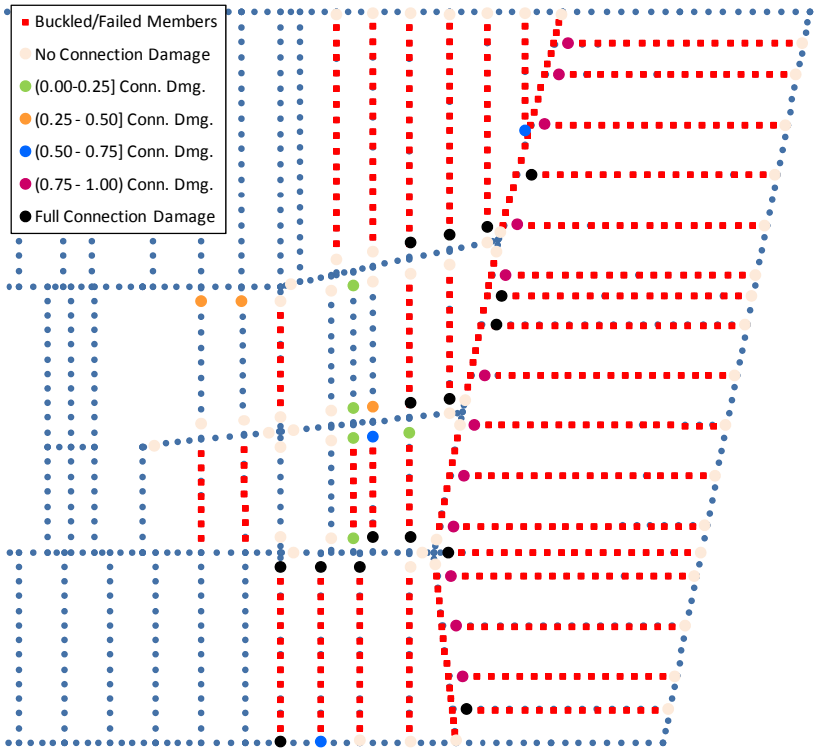

b) Damage state of connection in the vertical direction

Figure 11–36. Damage state of connections, beams, and girders in Floor 13 at 4.0 h for Case B temperatures.

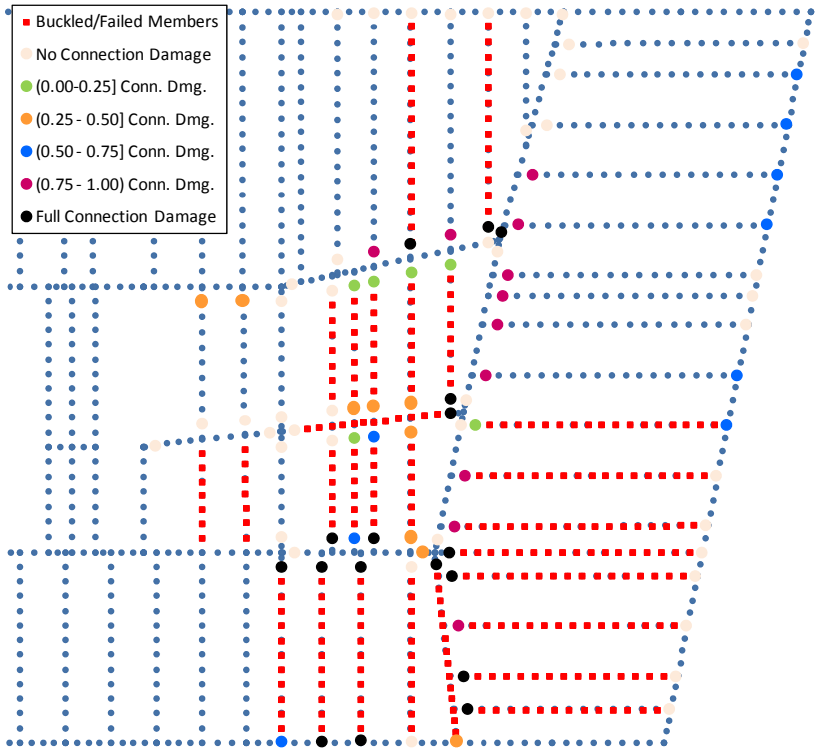

a) Damage state of connection in the horizontal direction

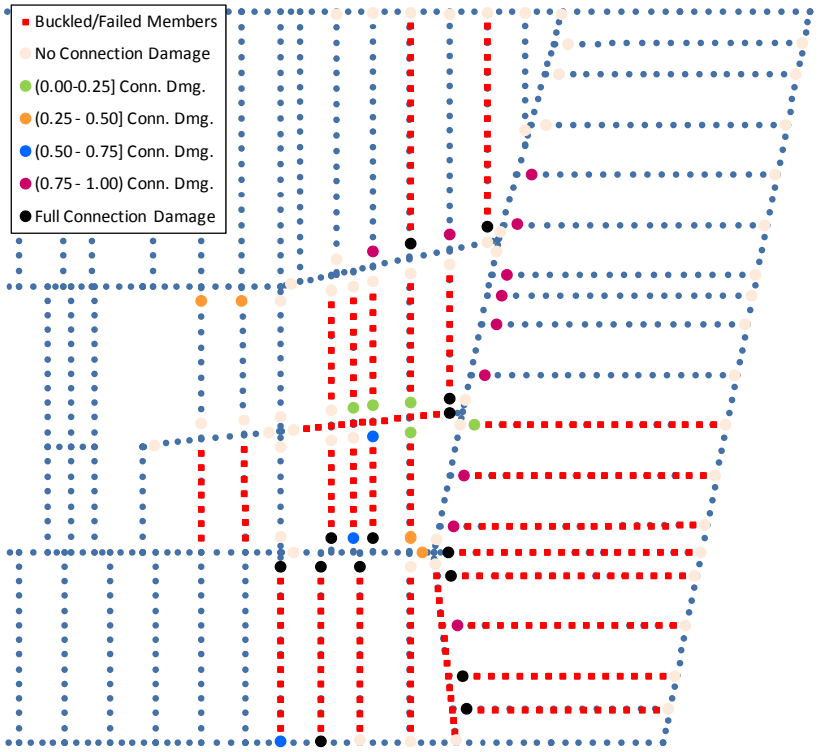

b) Damage state of connection in the vertical direction

Figure 11–37. Damage state of connections, beams, and girders in Floor 14 at 4.0 h for Case B temperatures.

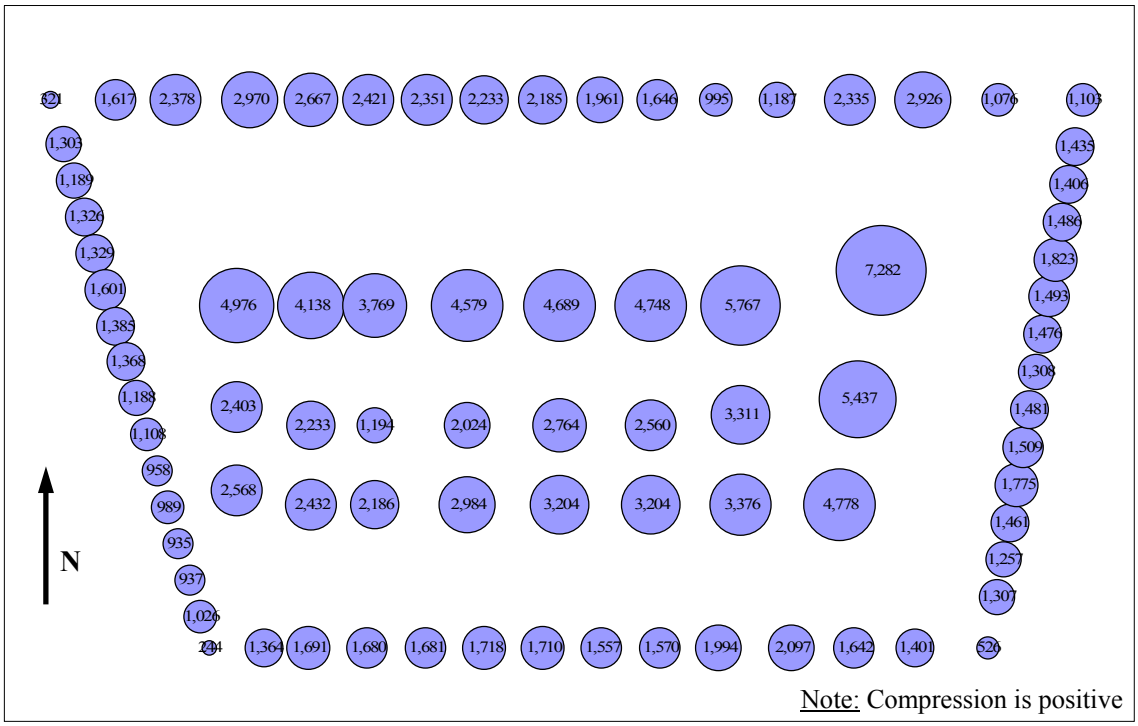

Summation of Column forces:

North:	32,400 kip	East:	19,200 kip
South:	20,850 kip	West:	16,650 kip
Core:	86,600 kip	Total:	175,700 kip

Figure 11–38. Column forces (in kip) above Floor 8 at t = 4.0 h for Case B temperatures.

11.3.3 Analysis of Building Response for Case C Temperatures

The structural response of WTC 7 to Case C temperatures at 4.0 h produced essentially the same damage and failures as the Case B temperatures in the previous section, with a time lag of approximately 10 to 30 min.

Building Response at 4.0 h

The structural damage from Case C temperatures at 4.0 h relative to Case B temperatures at 3.5 h and 4.0 h is summarized in Table 11–6. The thermally-induced damage for Case C temperatures at 4.0 h is shown in Figure 11–39 to Figure 11–46. Figure 10-47 to Figure 10-60 in Section 10.3.4 show the temperatures of the structural framing on these floors.

Elevated temperatures in Floors 12, 13, and 14 in the southeast and east region of the floor framing ranged from 300 °C to 550 °C for Floor 12, 300 °C to 700 °C in Floor 13, and 300 °C to 700 °C in Floor 14. As before, Figure 11–43, Figure 11–44, and Figure 11–45 show that the floor beams had already failed in areas where the steel temperatures were greater than 400 °C to 500 °C. The following beam and girder failures occurred:

Floor 8. Figure 11–39 shows connection and floor framing damage that occurred. Fin connections failed for the north floor beams on Floor 8 that were attached to the girder between Columns 76 to 79 (see Figure 2-4 for column locations), due to thermal expansion in the beams, by shearing the bolts at the girder. The northeast beam-to-girder fin connections had a 0.75 to 0.99 damage level between Columns 44 and 79. The header connections failed at Columns 74 and 78, due to thermal expansion of the girder. The beams that were supported by these girders are also indicated as failed, since they would fall with the girder.

Floors 9 and 10. On Floor 9, SWC connections in the core area between Columns 73 to 79 had damage levels of 0.0 to 0.24 and 0.50 to 0.74, depending on the number of bolts that had sheared (Figure 11–40). Floor 10 had no damage from fire (Figure 11–41).

Floor 11. On Floor 11, (Figure 11–42), the girder between Columns 76 and 79 failed due to a tensile weld failure in the knife connection on the west side of Column 79. Temperatures in this region were less than 100 °C on these floors. The tensile force in the connection was due to an eastward lateral displacement of Column 79, which was primarily caused by thermal expansion of the girder between Column 76 and Column 79 at Floor 13.

Floors 12, 13, and 14. On Floors 12 and 14, most of the floor beams on the south and east floor areas near Columns 78, 81, and 80 had failed. The floor beams either buckled or lost vertical support when all the fin connection bolts were sheared off due to thermal expansion. Both floors had a 0.75–0.99 damage level in floor beam fin connections extending past Column 79 in the east floor beams (Figure 11–43 and Figure 11–45). The girder between Columns 26 and 81 buckled on Floors 12 and 14 and the girder between Columns 80 and 81 buckled on Floor 14. All four of the erection bolts in the seated connection at Column 79 on Floor 14 had failed.

On Floor 13, the north-south girders between Columns 26 and 81 and Columns 80 and 81 had buckled. The girder between Columns 79 and 80 had walked off of the bearing seat at Column 79 due to the effects of thermal expansion.

Summary. After 4.0 h of heating, Column 81 had lost lateral support in the north-south direction at Floor 13, due to failure of the girders framing into Column 81. The girders between Columns 26 and 81 and Columns 80 and 81 had buckled and the girder between Columns 79 and 44 had walked off the seated connection at Column 79. In addition, all 4 bolts had failed at the seated connection at Column 79 on Floor 14. Approximately one-half to three-quarters of the east floor beams had a connection damage level of 0.75 to 1.0 on Floors 11, 12, and 14; all of the east floor beams, except for one, had failed on Floor 13.

Comparison of Case C 4 h to Case B 4h

Similar to the Case B results, the Case C results at 4.0 h had the most failures of floor beams, girders, and floor slab sections at Floors 8, 11, 12, 13, and 14. Floor 9 had partial damage to several beam connections in the northeast area of the core, and Floor 10 had no damage.

Table 11–6. Structural response of WTC 7 to Case B and Case C temperatures.

Floor	Case C Response	Case B Response	Comment
Floor 8			
Floor framing (beams, girders, and connections)	Nearly the same as Case B 3.5 h		
Concrete slab	Area of compression failure is less than Case B 3.5 h		Case C fire (gas temperatures) was less severe than Case B
Floor 9			
Floor framing	Between Case B 3.5 h and 4.0 h		Frame deflections Case B -8 in. to -12 in. Case C -10 in.
Concrete slab	None	None	
Floor 10			
Floor framing	None	3 connections damaged at 3.5 h Girder failed at Col 76-79 at Case B 4.0 h	Frame deflections Case B -6 in. Case C -6 in.
Concrete slab	None	None	
Floor 11			
Floor framing	Nearly the same as Case B 4.0 h		
Concrete slab	Between Case B 3.5 h and 4.0 h		
Floor 12			
Floor framing	Between Case B 3.5 h and 4.0 h Girder not failed at Col 76-79 at Case C 4.0 h	Girder failed at Col 76-79 at Case B 4.0 h	
Concrete slab	Nearly the same as Case B 4.0 h		
Floor 13			
Floor framing	Nearly the same as Case B 4.0 h		
Concrete slab	Nearly the same as Case B 4.0 h		
Floor 14			
Floor framing	Nearly the same as Case B 4.0 h Girder failed at Col 80-81 at 4.0 h		
Concrete slab	None	None	

The same type of failures in the connections, beams, and girders occurred on each floor, with the extent of damage falling somewhere between the damage that occurred between 3.5 h and 4.0 h for Case B temperatures. The exceptions, which are minor, are noted below.

- **Case C 4 h.** The girder between Columns 76 and 79 failed due to tensile weld failure of the knife connection at Column 79 on Floor 11 (Figure 11–34).
  Case B 4 h. After 4 h of heating, the girder between Columns 76 to 79 had failed due to tensile forces on Floors 10, 11, and 12 (Figure 11–33, Figure 11–34, and Figure 11–35).

- **Case C 4 h.** The girder between Columns 80 and 81 on Floor 14 failed (Figure 11–45).
  Case B 4 h. This girder had not yet failed (Figure 11–37).

Table 11–6 lists the floor number and its components (floor framing and concrete slab). The second column indicates how the Case C 4.0 h results compare to the Case B results at either 3.5 h or 4.0 h. The third column lists damage from the Case B response that did not occur in the Case C response at 4.0 h. The fourth column provides comments to explain the basis for noted differences.

Table 11–6 shows that the damage for Case C temperatures at 4.0 h on Floors 8, 9, and 10 more closely matches the damage for Case B at 3.5 h, and that the damage for Case C on Floors 11, 12, 13, and 14 more closely matches the damage for Case B at 4.0 h. The fires on Floors 11, 12, and 13 generated significantly more heat than the fire on Floors 7, 8, and 9. Even though the temperatures were reduced in Case C relative to Case B, there was still a substantial amount of heating taking place on Floors 11, 12, 13, and 14.

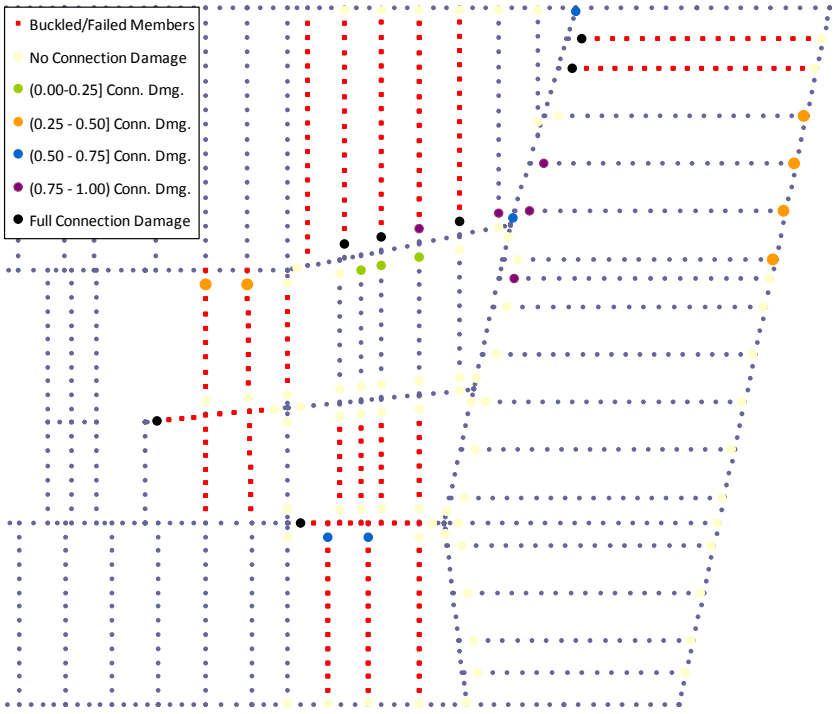

a) Damage state of connections in the horizontal direction

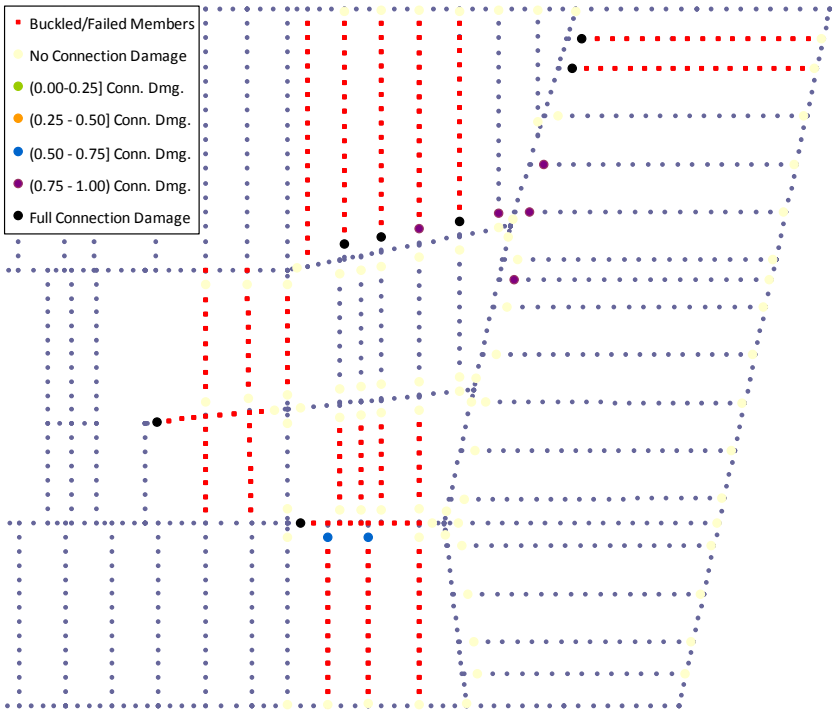

b) Damage state of connections in the vertical direction

Figure 11–39. Damage state of connections, beams, and girders in Floor 8 at 4.0 h for Case C temperatures.

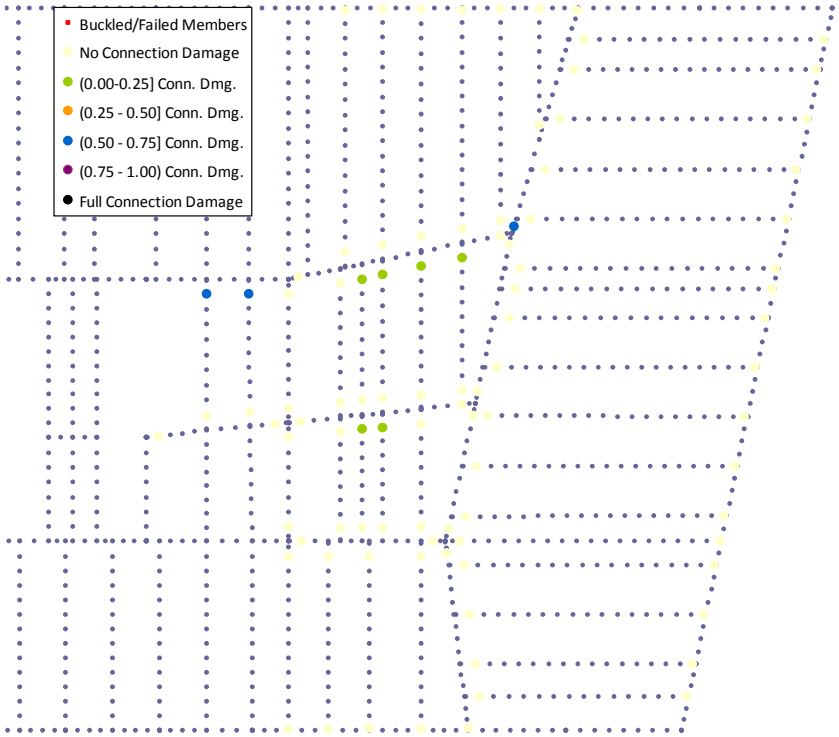

a) Damage state of connections in the horizontal direction

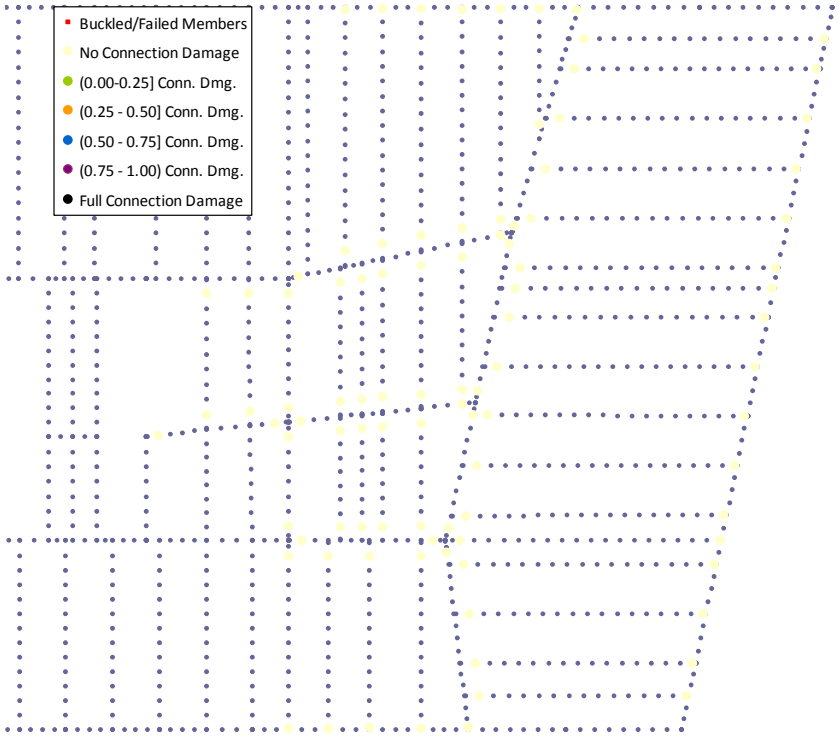

b) Damage state of connections in the vertical direction

Figure 11–40. Damage state of connections, beams, and girders in Floor 9 at 4.0 h for Case C temperatures.

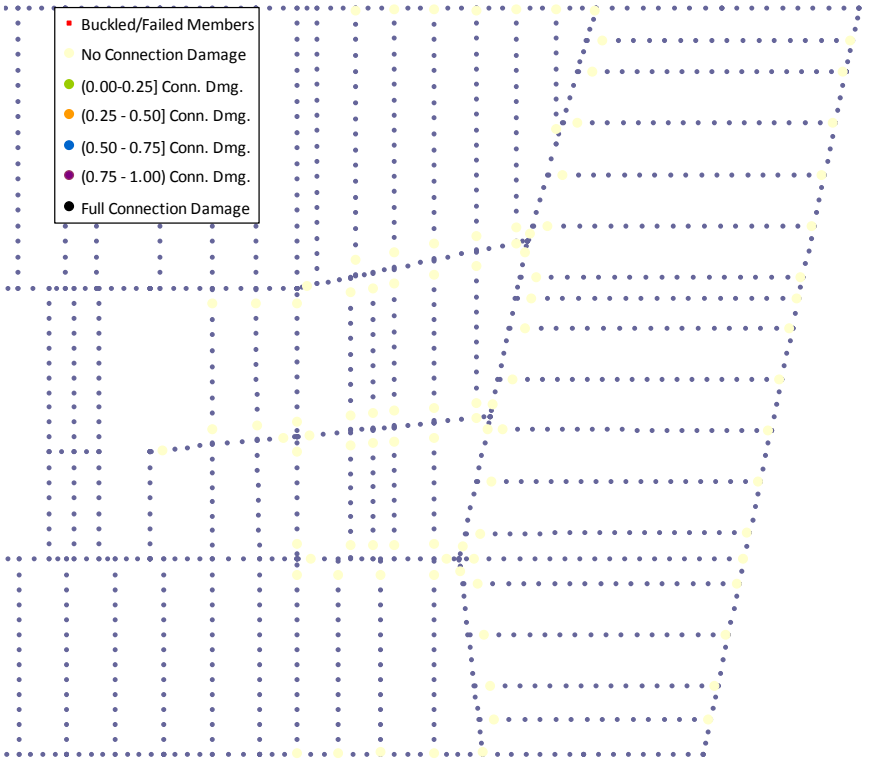

a) Damage state of connections in the horizontal direction

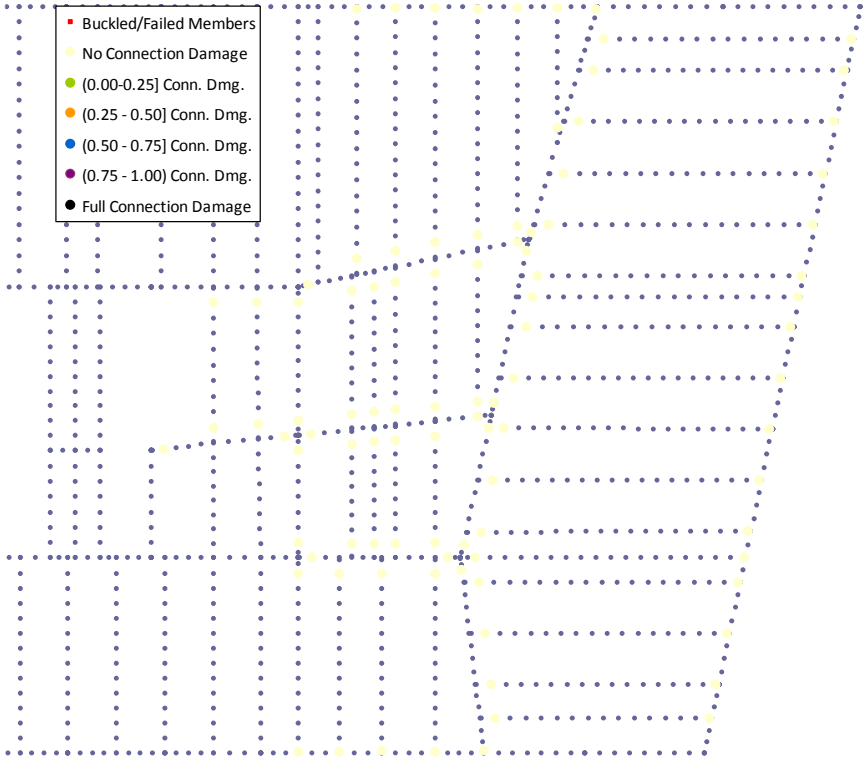

b) Damage state of connections in the vertical direction

Figure 11–41. Damage state of connections, beams, and girders in Floor 10 at 4.0 h for Case C temperatures.

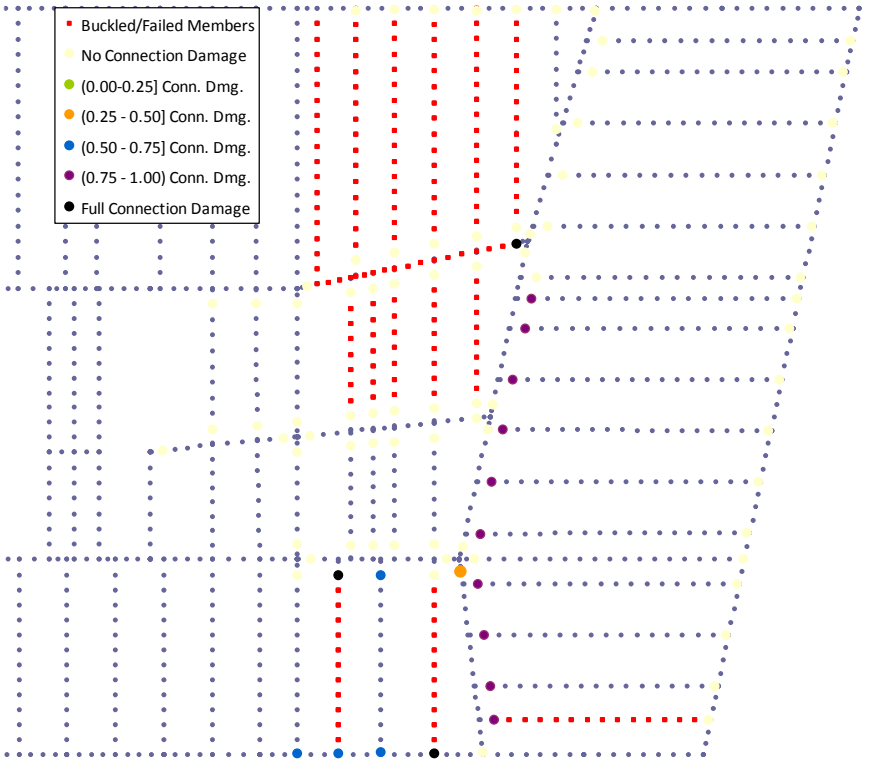

a) Damage state of connections in the horizontal direction

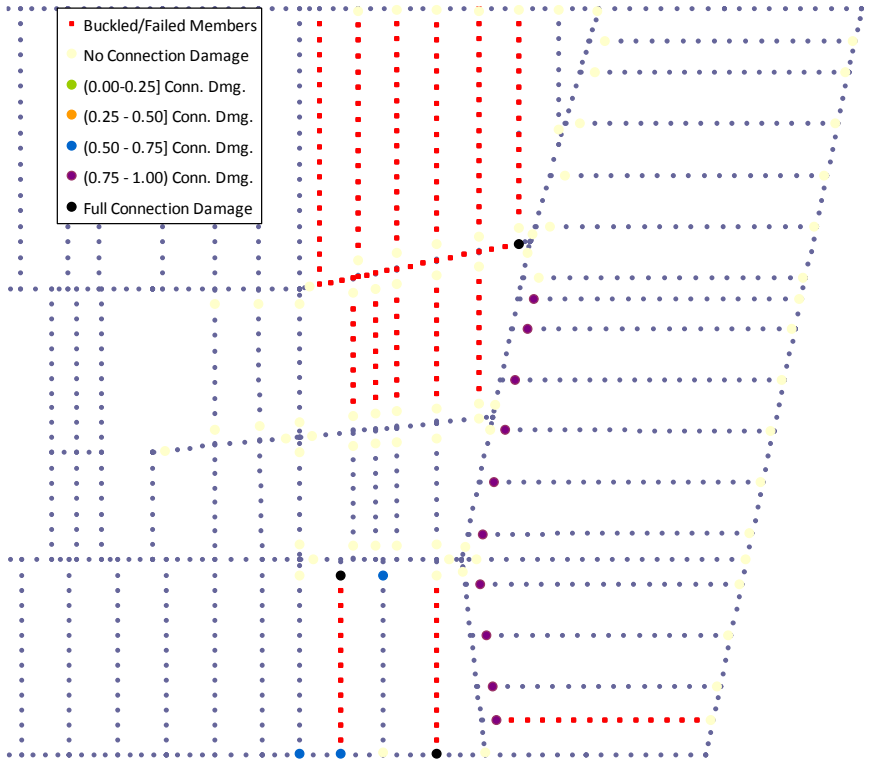

b) Damage state of connections in the vertical direction

Figure 11–42. Damage state of connections, beams, and girders in Floor 11 at 4.0 h for Case C temperatures.

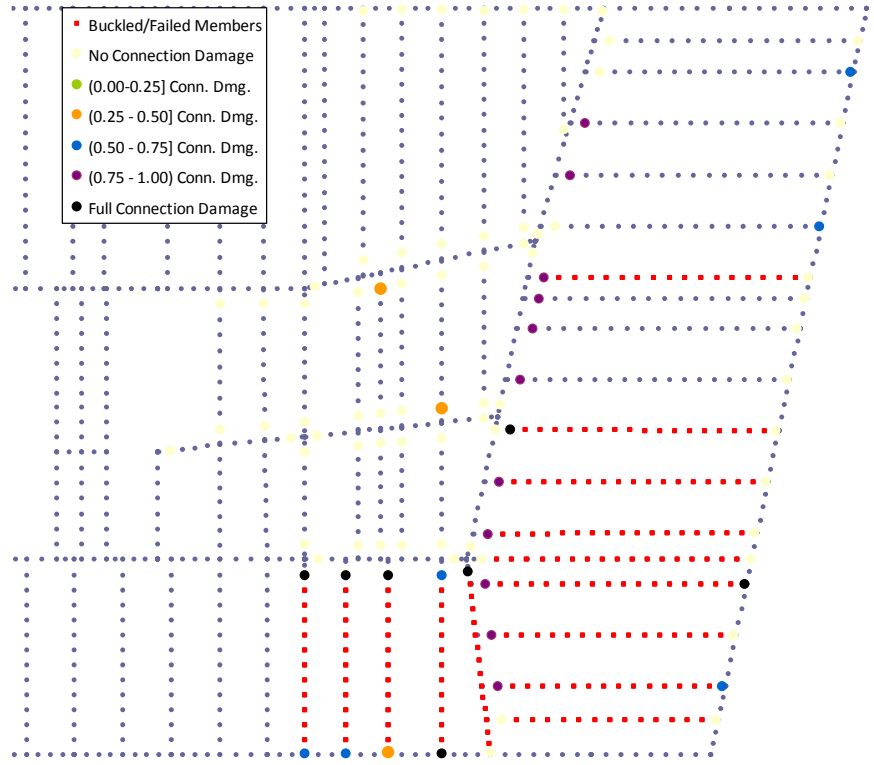

a) Damage state of connection in the horizontal direction

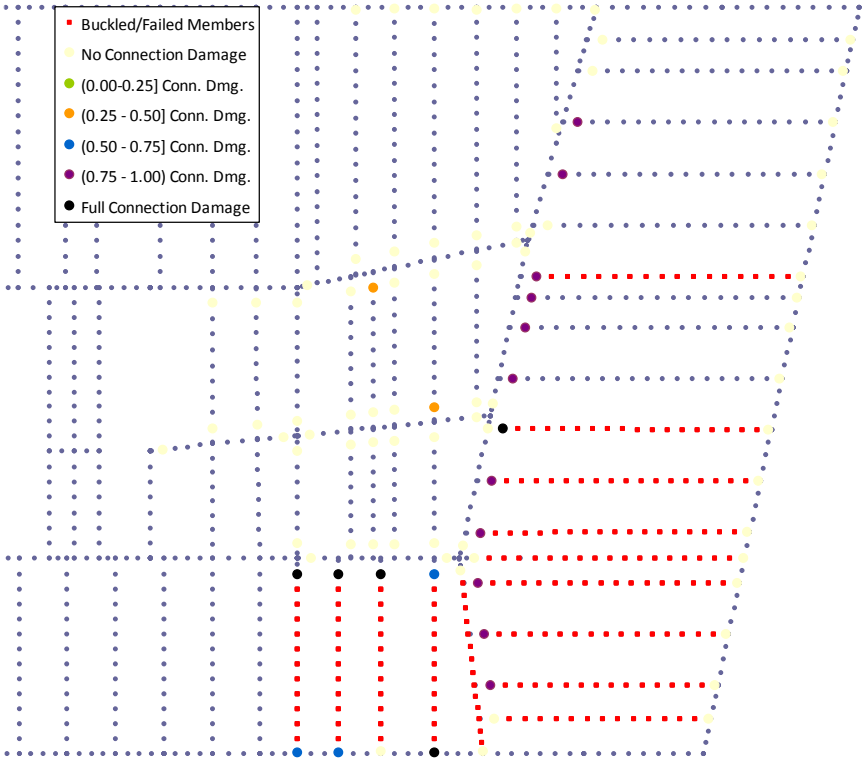

b) Damage state of connection in the vertical direction

Figure 11–43. Damage state of connections, beams, and girders in Floor 12 at 4.0 h for Case C temperatures.

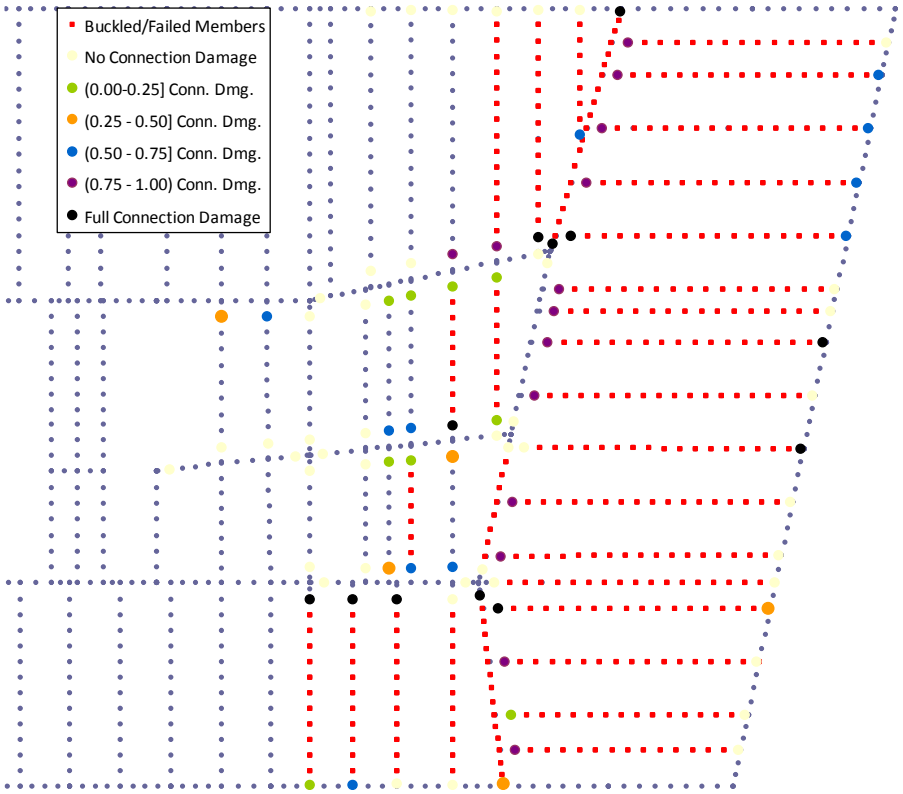

a) Damage state of connection in the horizontal direction

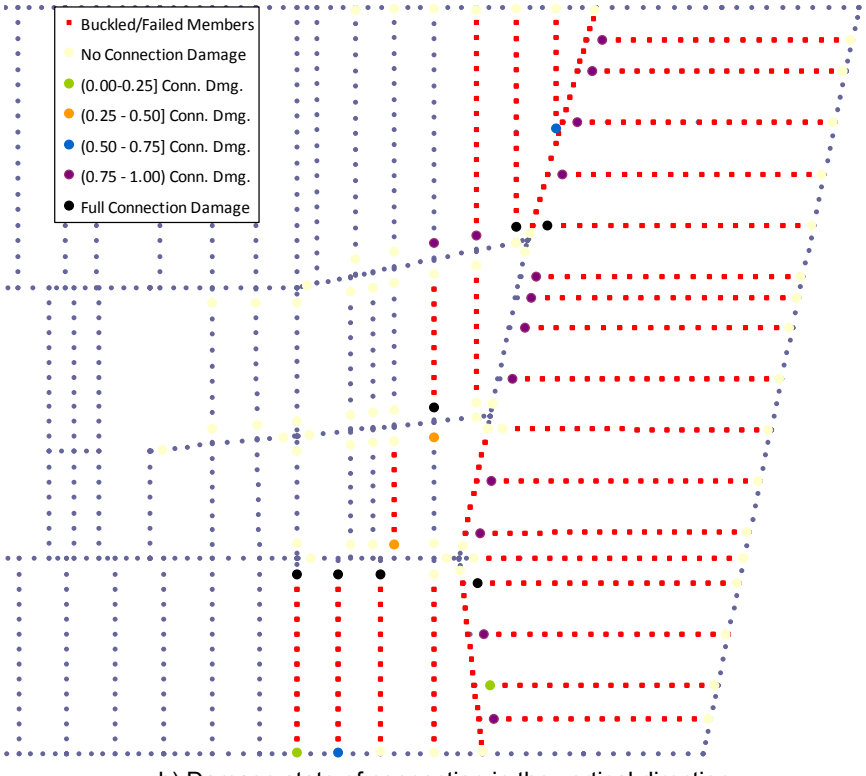

b) Damage state of connection in the vertical direction

Figure 11–44. Damage state of connections, beams, and girders in Floor 13 at 4.0 h for Case C temperatures.

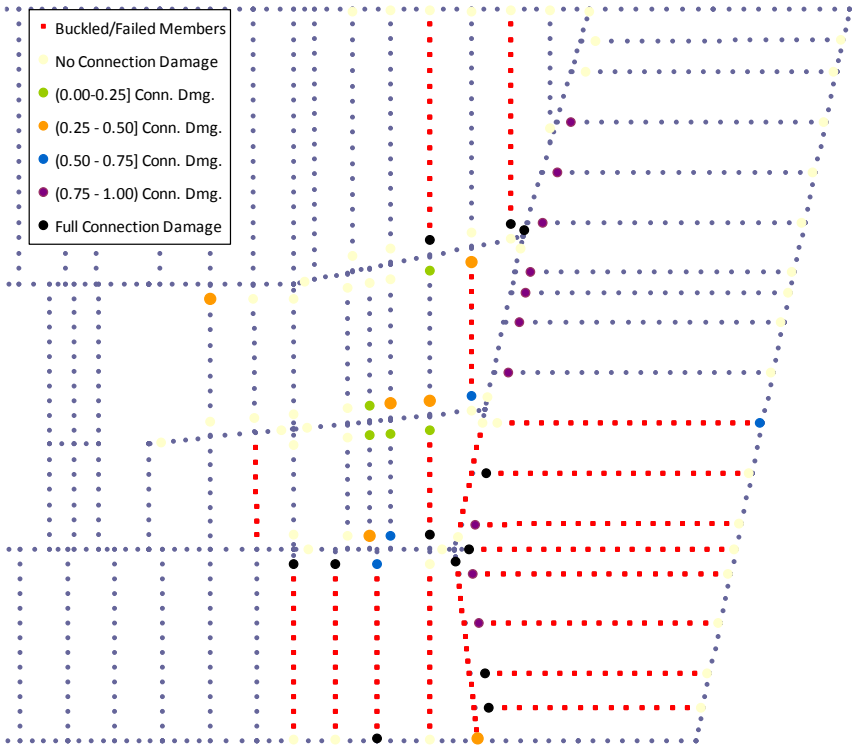

a) Damage state of connection in the horizontal direction

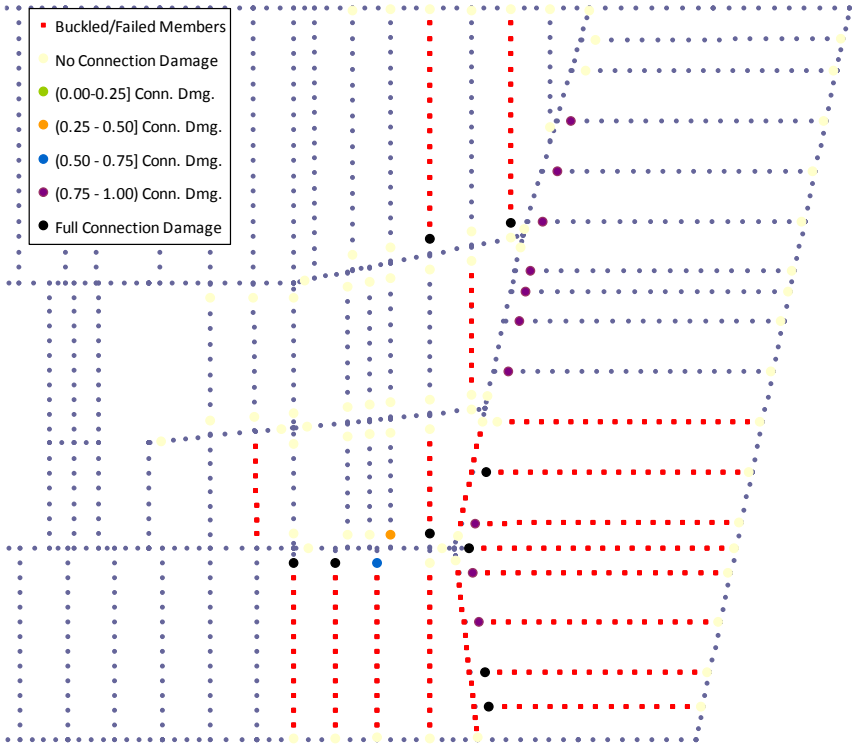

b) Damage state of connection in the vertical direction

Figure 11–45. Damage state of connections, beams, and girders in Floor 14 at 4.0 h for Case C temperatures.

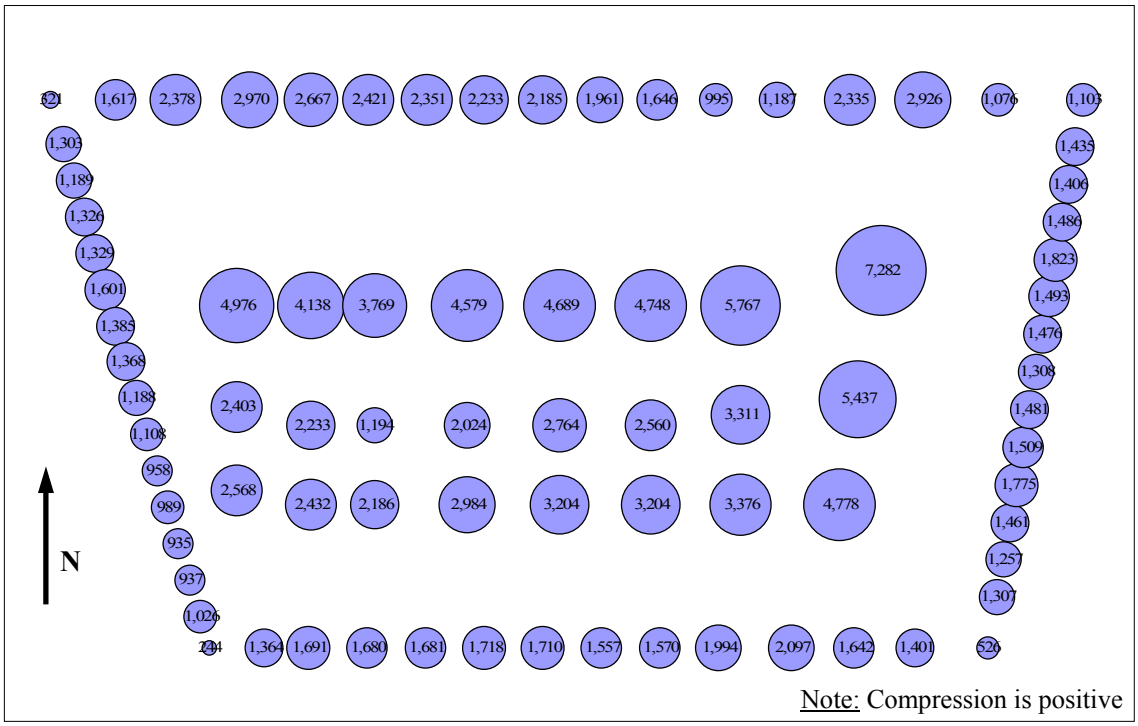

Summation of Column forces:

North:	32,400 kip	East:	19,200 kip
South:	20,850 kip	West:	16,650 kip
Core:	86,600 kip	Total:	175,700 kip

Figure 11–46. Column forces (in kip) above Floor 8 at t = 4.0 h for Case C temperatures.

11.4 DISCUSSION OF RESULTS

The structural response of WTC 7 to Case B temperatures is presented in Section 11.4.1. The structural response of WTC 7 to Case C temperatures is presented in Section 11.4.2.

11.4.1 Discussion of Results for Case B Temperatures

The fires on Floors 11, 12, and 13 generated significantly more heat than the fires on Floors 7, 8, and 9. This was in large part due to the higher fuel load and the larger concurrent burning area on Floors 11, 12, and 13.

After 3.5 h of heating, the fire had damaged the floor beams, girders and floor slab sections on Floors 8, 12, 13, and 14. The girders bracing interior Columns 79, 80, and 81 were still intact, except for the girder between exterior Column 26 and interior Column 81, which had buckled and walked off of the bearing seat on Floors 13 and 14. At the seated connection at Column 79, all the bolts had sheared on Floor 13 and two to three bolts had sheared on Floors 12 and 14. Approximately one-half to three-quarters of the east floor beams had a connection damage level of 0.75-0.99 on Floors 11, 12, 13, and 14.

By 4.0 h of heating, there was substantially more damage in the WTC 7 structural system, particularly the loss of lateral support to Column 79 after the failure of girder connections at Floors 10, 11, 12, and 13. Floor beams, girders and floor slab sections at Floors 8, 10, 11, 12, 13, and 14 were damaged in the vicinity of Column 79, primarily from the effects of thermal expansion within the structural system. All the north-south girders framing into Columns 79, 80, and 81 on Floor 13, and the east tenant floor beams, had been damaged. The girder between Columns 44 and 79 had walked off the bearing seat at Column 79 on Floor 13, and all 4 bolts had failed on Floor 14 and two to three bolts had failed on Floor 12 at this seated connection. The girder between Columns 79 and 80 and Columns 80 and 81 had buckled on Floor 13. The girder between Columns 81 and 26 had buckled and walked off the bearing seat on Floor 12. Approximately one-half to three-quarters of the east floor beams had a connection damage level of 0.75-0.99 on Floors 11, 12, and 14.

Thermal Effects on Columns

None of the columns reached temperatures over 300 °C and, therefore, did not buckle due to fire-induced thermal weakening (thermal weakening occurs at temperatures greater than about 500 °C). The interior columns were not thermally restrained, so they could not develop increased loads due to thermal expansion. The exterior columns had some restraint to thermal expansion, due to the moment frame construction of the exterior framing. However, the exterior columns tended to have lower temperatures than the interior columns as they were only heated on one side and the heat was dissipated to the outside. Thermal expansion of either interior or exterior columns had little or no effect on the failure mechanisms that occurred in the floor systems.

Thermal Effects on Floor Beams and Girders

Figure 11–47 shows temperatures in the steel framing for Floor 13 at 3.0 h, 3.5 h, and 4.0 h (Chapter 10). The temperature in the steel framing was linearly ramped between the temperatures at 3.0 h and 3.5 h, and at 3.5 h and 4.0 h, as the ANSYS structural analysis progressed. Figure 11–48 and Figure 11–49 show the floor beams and girders that had failed at different points in time as the temperatures were applied. Beams and girders subject to fires were loaded and/or displaced by the combined effects of gravity loads from the floor slab and compressive axial forces that developed due to thermal expansion that was restrained by the structural system. At temperatures below approximately 400 °C (when averaged over the beam length), thermal expansion effects caused two types of failures in the floor beams and girders: the buckling of beams and girders and the failure of end connections (discussed in the next section). At temperatures greater than 400 °C, the strength and stiffness of the steel floor beams, girders, and their connections began to degrade, depending on the component temperatures reached.

Figure 11–48 shows the east floor beam failures (due to buckling and connection failures) that occurred between 3.25 h and 3.5 h on Floor 13. Comparison of Figure 11–47 and Figure 11–48 showed that floor beams had failed prior to the beam temperatures reaching 400 °C.

Buckling in the floor beams was due to the combined effects of (1) loss of lateral restraint, (2) increasing axial loads due to thermal expansion effects, and (3) gravity loads from the floor slab. Floor beams lost lateral restraint when the majority of their shear stud connections failed, either by differential thermal expansion between the steel beams and the concrete slab, or by local concrete failure due to fires on the floor slab.

Primarily for the east tenant floor, when a floor beam thermally expanded, the beam displaced the girder at the interior end of the floor beam but did not displace the exterior frame at the other end of the floor beam. The exterior frame underwent minimal lateral displacement when floor beams thermally expanded, since the exterior framing with moment connections was much stiffer than the interior girders. In comparison, the girders were simply supported, laterally restrained by the floor beams only as they did not have shear stud connections to the slab, and loaded laterally by the floor beams in their weak axis (Section 8.7.4). Many failures of the east floor beams on Floors 12, 13, and 14 were buckling failures, as shown in Figure 11–28 and Figure 11–36.

The girder between Columns 26 and 81 buckled and walked off the bearing seat between 3.25 h and 3.5 h. In a similar fashion, the girders between Columns 79 and 80 and Columns 80 and 81 buckled and the girder between Columns 44 and 79 buckled and walked off the bearing seat between 3.7 h and 4.0 h. Girder buckling was due to the combined effects of (1) gravity loads from the floor beams, (2) lateral westward displacement due to the thermal expansion in the east floor beams, and (3) increasing axial loads due to thermal expansion in the girder.

Thermal Effects on Connections for Floor Beams and Girders

Thermal expansion of beams and girders also caused connection failures. Restrained thermal expansion of steel beams and girder within the structural system resulted in (1) bolt shear due to increased axial forces, (2) walk-off of seated connections after bolts had sheared, and (3) failure of connection welds to beam webs under shear forces.

Shear failure of all the bolts in fin and knife connections, or failure of the weld to the beam or girder web in header connections, resulted in a loss of horizontal and vertical support to the beam or girder. In seated connections (SWC, STP, and STC), the shear failure of bolts at the bearing seat and top clip or plate, caused loss of horizontal support but not vertical support. As the east floor beams and the girder continued to thermally expanded, the four bolts at the seated connection were sheared, resulting in a loss of horizontal support at the connection. Loss of vertical support occurred when the beam or girder "walked off" the bearing seat or when the bearing seat weld failed. Walk-off occurred when beams that framed into the girders from one side thermally expanded and the resulting compressive forces in the beams pushed laterally on the girder from one side, sheared the girder bolts, and then continued to laterally push the girder until it walked off the bearing seat.

A girder was considered to have lost vertical support when its web was no longer supported by the bearing seat. The bearing seat at Column 79 was 11 in. wide. Thus, when the girder end at Column 79 had been pushed laterally at least 5.5 in., it was no longer supported by the bearing seat. Additional factors that contributed to this failure were the absence of shear studs on the girders that would have provided lateral restraint and the one-sided framing of the northeast corner floor beams that allowed the floor beams to push laterally on the girder due to thermal expansion.

On Floors 10, 11, and 12, tensile failure of knife connections occurred in the girder between Columns 76 and 79. The temperature of the girders between Columns 76 and 79 on Floor 13 was sufficient to displace Column 76 to the west and Column 79 displaced to the east. The forced displacements at Floors 10, 11, and 12 created a tensile load in the girder knife connections to the columns, and failed the connection fillet weld at the column surface, which was loaded normal to the weld axis.

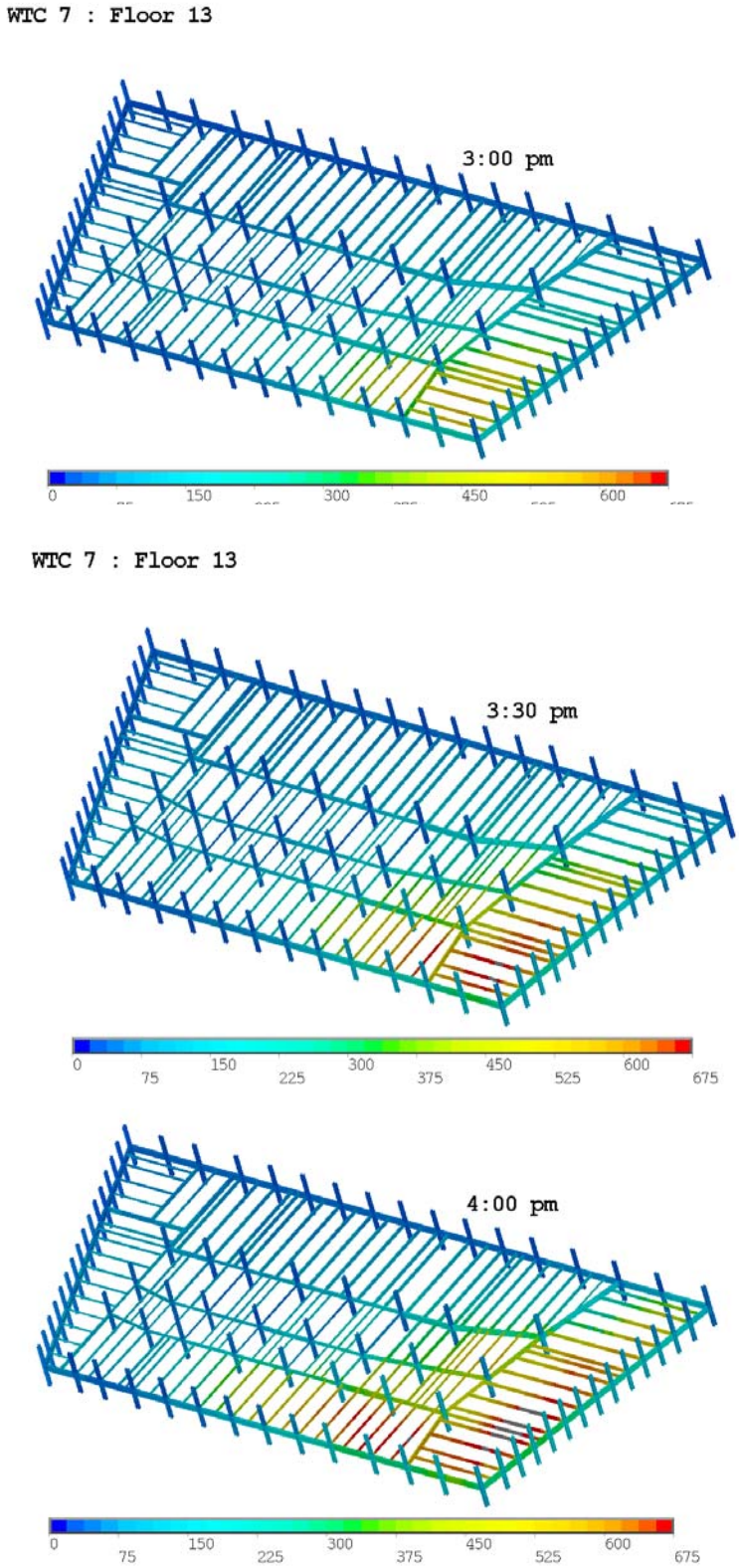

Figure 11–47. Floor 13 Case B temperatures at 3.0 h, 3.5 h, and 4.0 h.

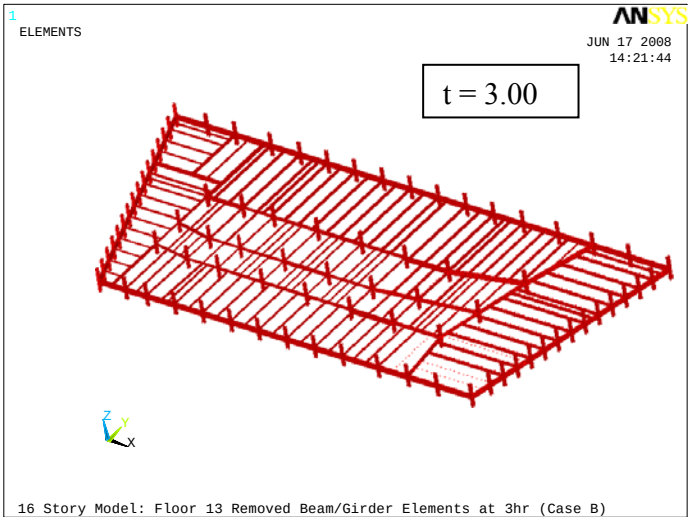

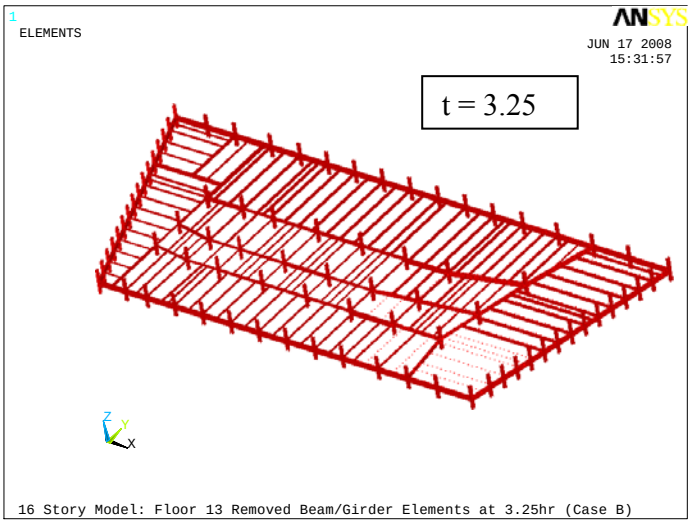

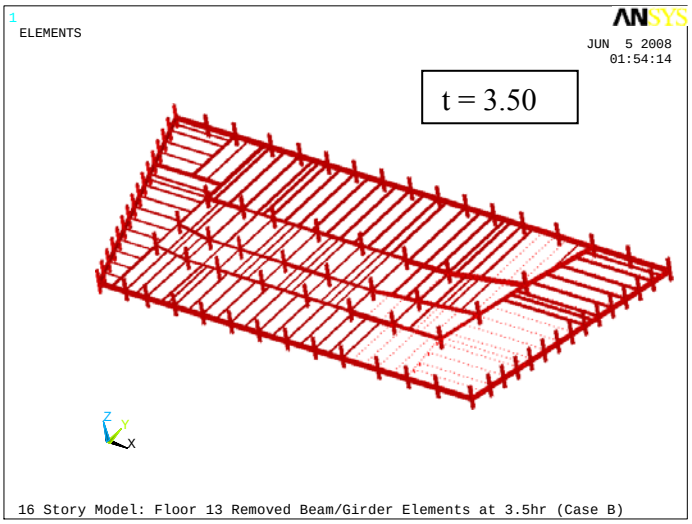

Beams and girders that buckled or had end connection damage are indicated with dotted lines.

Figure 11–48. Floor 13 Case B temperatures at 3.0 h to 3.5 h.

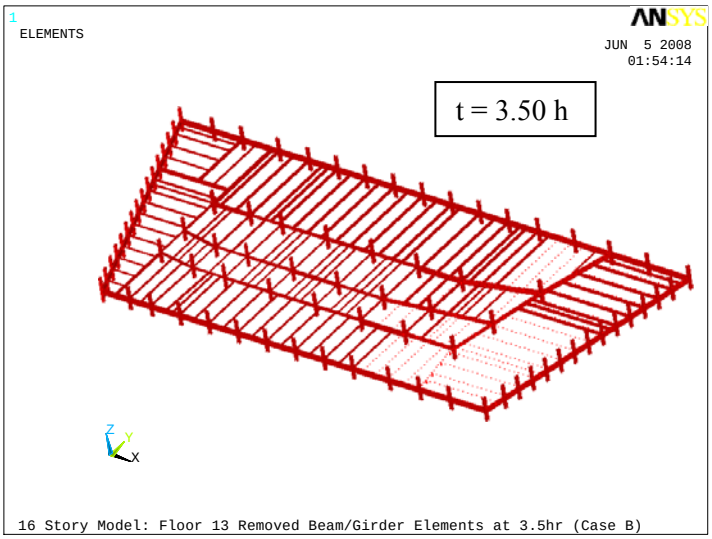

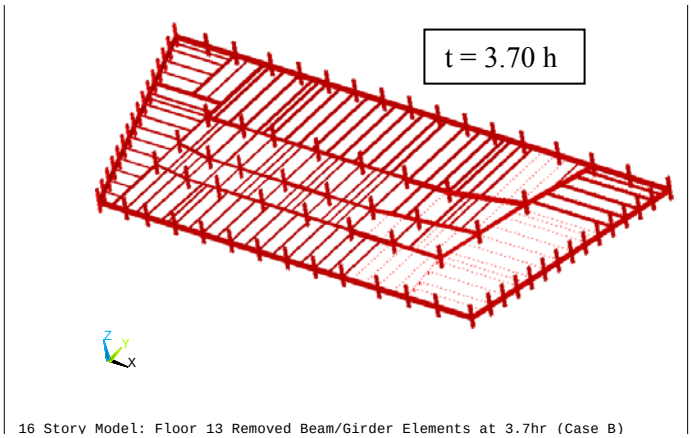

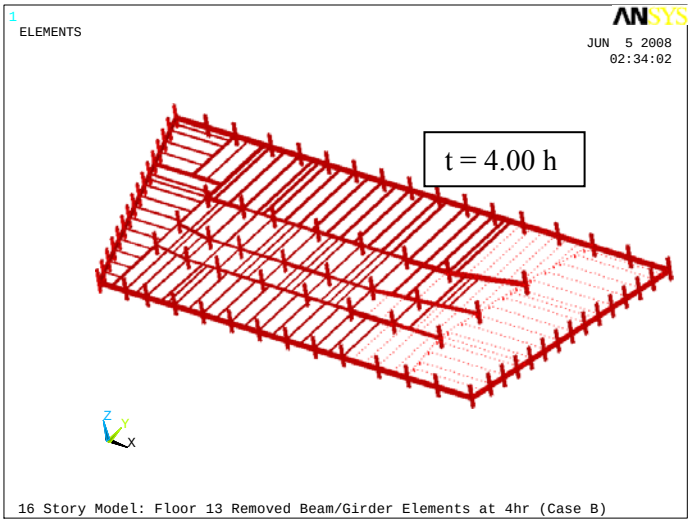

Beams and girders that buckled or had end connection damage are indicated with dotted lines.

Figure 11–49. Floor 13 Case B temperatures at 3.5h to 4.0 h.

Thermal Effects on Concrete Floors

Thermal expansion of concrete floors was restrained by the unheated slab sections, the interior and exterior columns, and shear studs at the floor beams and exterior spandrel beams. Restraint of thermal expansion led to compressive failure of the concrete slab through crushing, which softened the slab in tenant floor areas, and also led to loss of composite action with the floor beams. This failure mechanism usually occurred at slab surface locations where fires were burning, and slab temperatures were much higher in a localized area.

Slab tensile failures were related to the response of floor beams and girders to thermal effects. When beams and girders failed at their connections, affected slab section cracked under tensile stresses where reverse curvature in the slab occurred over adjacent intact girders.

Floor Failures Leading to an Initial Failure Event

After 4.0 h of heating, the floor framing and slabs at Floors 8 to 14 were weakened by fires, and Columns 79, 80, and 81 had lost lateral support at several floors due to the failure of connections, floor beams, and girders. The fire-induced failures of the floor framing resulted in increased unsupported column lengths for Columns 79, 80, and 81, as shown in Figure 11–50, where floor beams or girders that failed (by either buckling or end connection failure) are red and intact members are blue.

In the east-west direction, Columns 79 and 80 were laterally supported by one member that was directly connected to the columns at each floor, while Column 81 had two members providing lateral bracing, as shown in Figure 11–50. The east floor beams that were connected to the north-south girders by Columns 79 and 80 could only provide lateral bracing as long as the girders were intact. The floor beams with fin connections provided indirect lateral bracing to Columns 79 and 80, as the beams framed into the girders at locations close to the columns. In the north-south direction, Columns 79, 80, and 81 were laterally supported by two girders that were directly connected to the columns. Neglecting the lateral support provided by the east floor beams at Columns 79 and 80, the unsupported lengths for these columns at 4.0 h can be described as follows: Column 79 was laterally unsupported at three floors in the east-west direction and one floor in the north-south direction, Column 80 was laterally unsupported at one floor in the east-west and north-south directions, and Column 81 was laterally unsupported at one floor in the north-south direction. (Even though there were three failed girders on the south side, there was one failed girder on the north side, so lateral support was still provided at the floors above and below the failed girder.)

As noted previously, the ANSYS analysis used a non-linear static procedure with an implicit solution algorithm that solved for equilibrium at each time step, but did not account for the dynamic effects of falling debris from framing failures in the floor systems. Based on preliminary analyses in LS-DYNA, which included the effects of dynamics caused by debris impact from failed floor sections and engineering judgment, the level of failures, damage, and thermal weakening in ANSYS at 4.0 h was identified as likely to result in an initiating event in an LS-DYNA analysis. The procedures used for transferring the ANSYS data to LS-DYNA are discussed in Section 11.5.

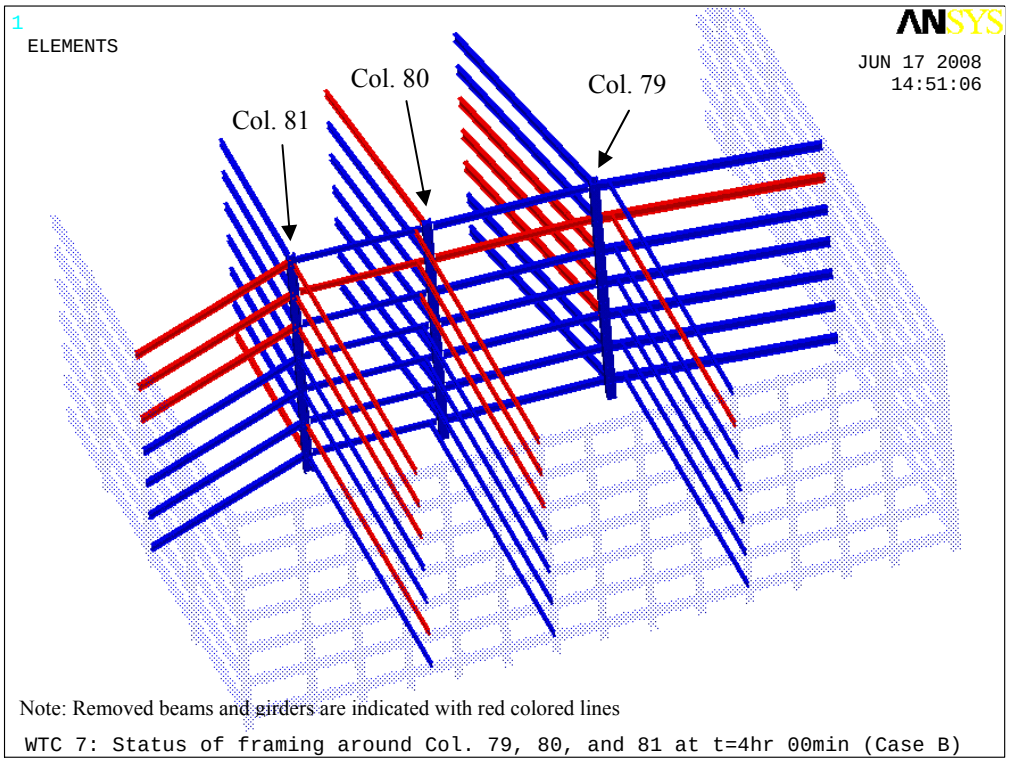

Figure 11–50. Beam and girder failures around Columns 79, 80, and 81 at 4.0 h for Case B temperatures.

Effects of SFRM Thickness

A SFRM thickness of 0.5 in. was specified for the floor beams in the composite floor system and independent testing found that the floor beams had an average applied thickness of 0.53 in. To evaluate the effect of reduced passive fire protection for the floor beams, the effect of increasing the SFRM thickness on the floor beams by 25 percent to 0.625 in. (5/8 in.) and by 50 percent to 0.75 in. (¾ in.) was examined with the ANSYS analyses described below.

Figure 11–51 and Figure 11–52 show the temperature versus time for a typical floor beam in the north and east tenant floor areas for two different fire exposures, a uniform 1100 °C gas temperature and the ASTM E 119 temperature curve, respectively, and four different SFRM thicknesse:

- 0.4375 (7/16) in.
- 0.53 in. (average applied SFRM thickness)
- 0.625 (5/8) in.
- 0.75 (3/4) in.

The uniform 1100 °C gas temperature and the ASTM E 119 temperature curve were selected as bounding conditions for the floor beam when subjected to the fires in WTC 7 (i.e., typical floor fires). Thus, the

actual rate of heating of the W24x55 floor beam in a composite floor would be expected to fall between the times shown in the figures.

When the steel beam reached 600 °C under the uniform 1100 °C gas temperature, the additional protection provided by increasing the SFRM thickness to 0.625 in. (5/8 in.) or 0.75 in. (¾ in.) was approximately 10 min to 20 min, as shown in Figure 11–51.

When the steel beam reached 600 °C under the ASTM E 119 temperature curve, the additional protection provided by increasing the SFRM thickness to 0.625 in. (5/8 in.) or 0.75 in. (¾ in.) was approximately 8 min to 15 min, as shown in Figure 11–52.

Thus, an increase in the SFRM thickness on the floor beams would have delayed heating of the floor beams by 10 min to 20 min, which was unlikely to have prevented the heating of the floor system and initiation of collapse.

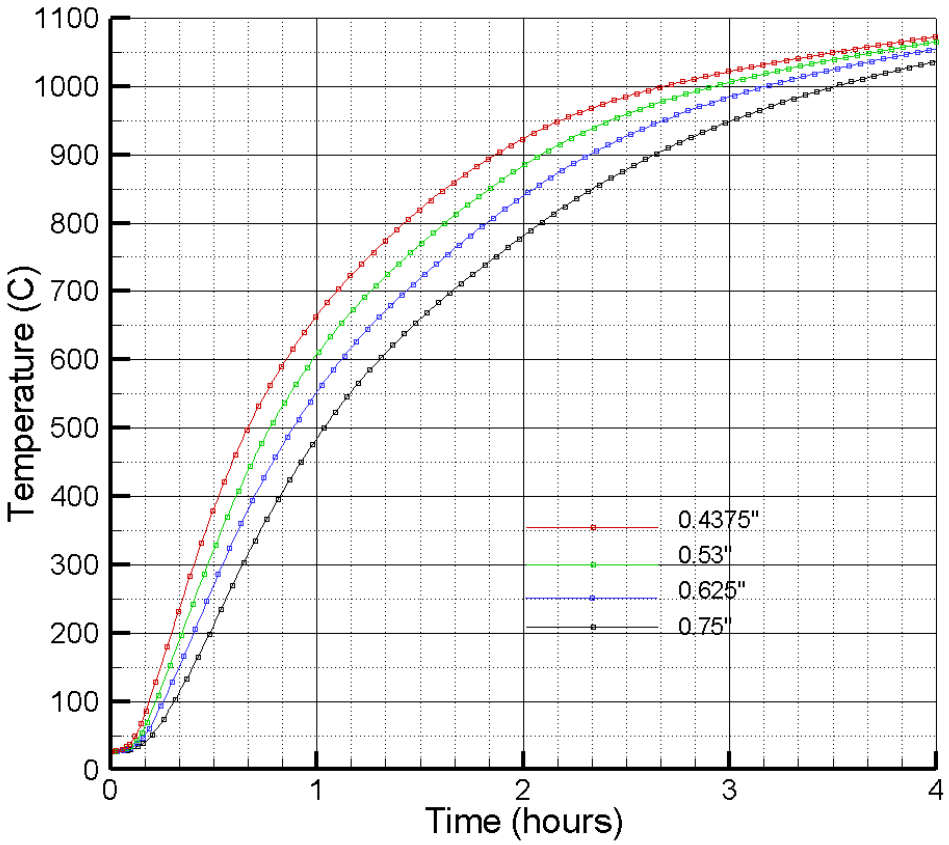

Figure 11–51. Heating of a typical floor beam (W24 x 55) subject to a uniform 1100 °C gas temperature for different SFRM thicknesses.

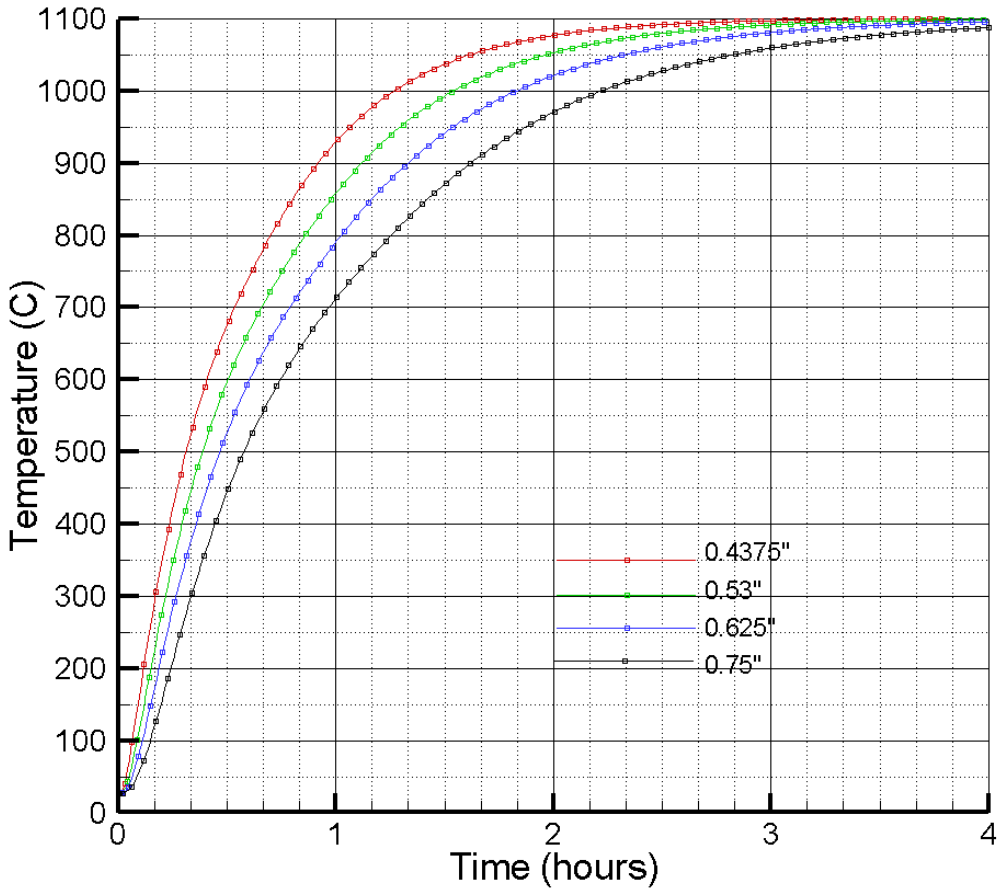

Figure 11–52. Heating of a typical floor beam (W24 x 55) subject to an ASTEM E 119 temperature profile for different SFRM thicknesses.

11.4.2 Discussion of Results for Case C Temperatures

As the Case B and Case C analyses progressed, essentially the same sequence of damage and failures occurred, but they were shifted in time (i.e., Case C failures occurred at a later time than Case B failures) as a consequence of the difference between the Case B and Case C temperatures. However, even though the temperatures were reduced in Case C relative to Case B, there was still a substantial amount of heating taking place on Floors 11, 12, 13, and 14.

The same type of failures in the connections, beams and girders occurred on each floor in Case C, with the timing (and hence, extent) of damage falling somewhere between the damage that occurred between 3.5 h and 4.0 h for Case B. Similar to the Case B results, the Case C results at 4.0 h had considerably more damage in the beams, girders, and floor slab sections at Floors 8, 11, 12, 13, and 14.

The time lag in damage was not uniform over Floors 8 to 14. The damage in Floors 8, 9, and 10 was closer to the Case B damage at 3.5 h, but the damage for Case C on Floors 11, 12, 13, and 14 was closer to the Case B damage at 4.0 h.

The comparison of Case B and Case C results at 4 h (Section 11.3.3) showed that the Case C structural response would be nearly identical to the Case B structural response at a time between 4.0 h and 4.5 h. Thus, the temperature differences between Case B and C were not sufficient to produce different failure patterns, and both cases provided the same damage (i.e. location and degree) to the floors with a time lag between the two solutions.

As a result, there was only one solution to input to the global analysis of the collapse. The fire-induced damage produced by Case B temperatures at 4.0 h was carried forward as the initial condition for the LS-DYNA analysis (Chapter 12).

11.5 TRANSFER OF ANSYS RESULTS TO THE LS-DYNA ANALYSIS

The description of the fire-induced floor damage was input to the LS-DYNA model to determine if the predicted floor failures would lead to an initiating collapse event, followed by a failure progression to global collapse. The transferred data included temperatures in structural elements and failures of floor beams, girders, and connections.

When the ANSYS analysis had reached a point where buckling instability of columns appeared imminent, the accumulated damage due to thermally-induced failures of floor framing was summarized as input for the LS-DYNA model. This evaluation was based on preliminary LS-DYNA analyses, which included the effects of dynamics caused by debris impact from failed floor sections, and engineering judgment. The transferred data also included the temperature of structural components at that time and buckled beams and girders.

The damage state of the connections was indicated by a numerical value ranging between 0.0 for no damage and 1.0 for full damage (i.e., there was no remaining strength). The damage state of each connection type was defined as shown in Table 11–7:

Table 11–7. Connection damage level estimate for data transfer to the LS-DYNA model.

Support Direction	Damage Level (0: no damage, 1: full damage)	Conditions
Fin and Knife Connections		
Horizontal Damage	(# of Failed Bolts)/(Total # of Bolts)	
Vertical Damage	(# of Failed Bolts)/(Total # of Bolts)	
Header Connections		
Horizontal Damage	1.0	if there was weld failure
	(# of Failed Bolts)/(Total # of Bolts)	if there was no weld failure
Vertical Damage	1.0	if there was weld failure
	(# of Failed Bolts)/(Total # of Bolts)	if there was no weld failure
SWC Connections (SWC connections always have 2 welds and 4 bolts)		
Horizontal Damage	max{(# of Failed Bolts)/(4), (# of Weld Failures)/(2)}	
Vertical Damage	(# of Weld Failures)/(2)	

Support Direction	Damage Level (0: no damage, 1: full damage)	Conditions
STC and STP Connections		
Horizontal Damage	1.0	if there was walk off
	(# of Failed Bolts)/(Total # of Bolts)	if there was no walk off
Vertical Damage	1.0	if there was walk off
	0	if there was no walk off

11.6 SUMMARY OF FINDINGS

A finite element model of the WTC 7 building was developed in ANSYS to evaluate its structural response to the fire environment and to determine the sequence of events that led to an initial failure event or collapse initiation event. The ANSYS model consisted of the lower 16 stories of the building. The ANSYS model included nonlinear effects, such as: nonlinear temperature-dependent material properties including thermal expansion, plasticity and creep; nonlinear geometry; and user-defined elements that captured the details of temperature dependent connection failures. The following findings are based on the ANSYS finite-element analysis of the structural response of WTC 7 to the fires observed between Floors 7 through 14:

- The failures in the floor systems were caused by the following structural responses to elevated temperatures:
    - At temperatures less than approximately 400 °C, restrained thermal expansion of beams and girders caused axial compressive forces to develop in the beams and girders, which led to the following connection failures:
        - bolt shear failure in fin, knife, and seated connections,
        - girder walk-off of seated connections after all the bolts had sheared at Columns 79 and 81, and
        - failure of header connection welds.
    - The failure of the girder-to-column seated connection at Columns 79 and 81 occurred in two stages: (1) horizontal loss of support occurred when the bolts at the seated connection were sheared, primarily due to thermal expansion of the floor beams in the east floor system, and (2) further thermal expansion of the floor beams pushed the girder off the bearing seat.
    - Many floor beams on Floors 12, 13, and 14 in the east floor region had buckled prior to beam temperatures reaching 400 °C (averaged over the beam length). Floor beams buckled under the combined effects of
        - loss of lateral restraint due to failure of the majority of shear studs,

  - increasing axial loads due to thermal expansion that was restrained by the exterior and interior structural frame, and
  - gravity loads from the floor slab.
- The girders that framed into interior columns on Floor 12, 13, and 14 failed by either
  - buckling due to the combined effects of gravity loads from the floor beams, lateral displacement due to the thermal expansion in the floor beams, and increasing axial loads due to thermal expansion in the girder, or
  - loss of vertical support due to girder walk off the bearing seat, or due to thermally-induced failure of a connection.
- Loss of lateral support to Columns 79, 80, and 81 resulted from the failures of the girders to the north, west, and south, and the floor beams to the east, where
  - girders between Columns 79 and 80 and Columns 80 and 81 buckled on Floor 13, due to the combined effects of thermal expansion and the lateral displacement caused by the thermal expansion in the east floor beams,
  - girders west of Column 79 failed due to tensile weld failures in the knife connections on Floors 10, 11, and 12 from restrained thermal expansion on other floors,
  - girder west of Column 80 failed due to weld failures in the header connections on Floor 14,
  - girders between Columns 44 and 79 and Column 26 and 81 failed due to girder walk off of the bearing seat.
  - The buckling failure of the east floor beams and exterior columns was caused by restrained thermal expansion and failure of the shear studs along the beam length, which primarily resulted from the thermally-induced crushing failure of the slab.
- Restrained thermal expansion of slabs, particularly in locations where fires were directly heating the slab, resulted in a compressive failure of the concrete slab (crushing) and reduced slab stiffness.

- The simple shear connections used in the typical floor framing were not able to resist the axial compressive forces that developed in the floor framing due to thermal expansion effects that were restrained by the structural system.
- The failure of the girder-to-column seated connection at Columns 79 and 81 was primarily caused by thermal expansion of the long span floor beams in the east tenant floor.
- Additional factors that contributed to the girder failures were the absence of shear studs that would have provided lateral restraint and the one-sided framing of the east floor beams, which pushed laterally on the girders.

- Columns 79, 80, and 81 were not weakened by temperatures; temperatures rarely exceeded 300 °C in the columns in WTC 7.

- An increase in the SFRM thickness on the floor beams, from 0.53 in. to 0.625 in. or 0.75 in., would have delayed heating of the floor beams by 10 min to 20 min, which was unlikely to have prevented the thermal response of the floor system and initiation of collapse.

- The temperature differences between Case B and C were not sufficient to produce different failure patterns, and both cases resulted in similar damage (i.e., location and degree) to the floors with a time lag between the two solutions.

11.7 REFERENCES

AISC (2005), American Institute of Steel Construction Inc., Manual of Steel Construction, Thirteenth Edition, Chicago, IL.

ANSYS (2007), ANSYS Mechanical Release 11.0, ANSYS Inc., Southpointe, 275 Technology Drive, Canonsburg, PA 15317

M. D. Rambo-Roddenberry (2002), Behavior and Strength of Welded Stud Shear Connectors, Dissertation submitted to the faculty of the Virginia Polytechnic Institute and State University, April 8, 2002.

Chapter 12
WTC GLOBAL COLLAPSE ANALYSIS

12.1 OVERVIEW

This chapter presents the description and analysis results of the global model, which was developed to determine the collapse sequence of the World Trade Center (WTC) 7 building and to test the leading collapse hypothesis presented in Chapter 8. This model analyzed the response of the full 47 story structure to initial failure events due to fire to determine the events that led to the global collapse of WTC 7. The results of the fire-induced damage from the 16 story ANSYS analysis (Chapter 11) were used as an input into the global model in LS-DYNA to analyze the collapse propagation.

The nonlinear dynamic collapse analyses were performed using LS-DYNA, which was capable of explicitly modeling sequential failures, falling debris, and debris impact on other structural components. LS-DYNA was well suited for this type of analysis, since it can model the dynamic failure processes, including nonlinear material properties, nonlinear geometry, material failures, contact between collapsing structural components, and element erosion based on a defined failure criterion. In addition, LS-DYNA has capabilities to include thermal softening of materials and thermal expansion.

The global LS-DYNA model had the following input data:

- Extent of initial damage to the building due to debris impact from the collapse of WTC 1 (Chapter 5).
- Photographic and videographic records with time stamps that documented the observed collapse sequence (Chapter 5).
- Mechanical properties of steel (Appendix E and NIST NCSTAR 1-3D) and concrete (NCSTAR NIST 1-6A) used in the construction of WTC 7.
- Temperature-dependent mechanical properties of steel (Appendix E and NIST NCSTAR 1-3D).
- Temperatures for structural components and connections, at the time when the ANSYS analysis data was transferred to the LS-DYNA analysis (Chapter 10).
- Fire-induced damage to floor beams, girders, and their connections from the 16 story ANSYS analysis (Chapter 11).

The floor framing geometry, component sizes, connection details, and gravity loads were obtained from structural and architectural drawings, as well as erection and fabrication shop drawings of connections for the steel framing (Chapter 2). The global LS-DYNA model analyzed the effects of gravity and temperature loads. Gravity loads included: the dead load of the structure; superimposed dead loads consisting of the weight of ceilings, mechanical and electrical equipment, thermal insulation, and floor

finishes; and service live load, which was taken as 25 percent of the design live load specified in the original design documents.

Three simulations were performed with the global LS-DYNA model.

- The first was based on NIST's best estimate of both the debris impact damage form WTC 1 and the fire-induced damage as developed using the ANSYS modeling. This occurred at 4 h in the ANSYS computation.
- The second simulation differed only in the input of a lesser degree of fire-induced damage, which occurred at 3.5 h in the ANSYS computation. The purpose of this LS-DYNA simulation was to determine whether a lesser degree of fire-induced damage could lead to the collapse of WTC 7.
- The third simulation was the same as the first, except that no debris impact damage was included. The purpose of this analysis was to determine the contribution of debris impact to the WTC 7 global collapse sequence and whether WTC 7 would have collapsed solely due to the effects of the fires.

Section 12.2 provides a description of the global 47 story model, including material constitutive models, floor framing, truss and column transfers, penthouse structures on the roof, and modeling of floor system connections. Section 12.3 describes the model boundary conditions and loading sequence applied during the execution of the model. Section 12.4 presents the three simulations and their outcomes. Section 12.5 includes comparison of the simulation outcomes with the photographic and videographic observations and compares the calculated time of descent of WTC 7 with an estimate of the hypothetical free fall time.

12.2 GLOBAL LS-DYNA 47 STORY MODEL

12.2.1 Material Constitutive models

The structural materials in the WTC 7 global model were the steels used in the framing of WTC 7 and the concrete floor slabs. Brief descriptions of the constitutive models for the steels and concrete slabs are provided. The reader is referred to Chapter 2 of NIST NCSTAR 1-9A for further details.

Structural Steel Constitutive Models

The primary constitutive model used for modeling the steel in the framing of WTC 7 was the Piecewise Linear Plasticity model (material type 24 in LS-DYNA). This model captured the nonlinear behavior and failure of steel components, with a tabular effective stress versus effective strain curve that used a pre-defined strain to failure to simulate fracture.

The constitutive models for the WTC 7 steels were based on those developed for the WTC tower steels. (Appendix E and NIST NCSTAR 1-3D). The steels used to construct WTC 7 were ASTM A36 (nominal yield strength Fy = 36 ksi), A572 grade 50 (Fy = 50 ksi), and steel plates produced by Algoma (CSA G40.21-44W, Fy = 42 ksi) for the fabrication of all shear connections in the floor framing. The Algoma steel had not been used in the WTC towers, and a stress-strain curve was developed for this steel for the

analysis of WTC 7. The true stress-strain curves for these grades of steel at room temperature are shown in Figure 12–1.

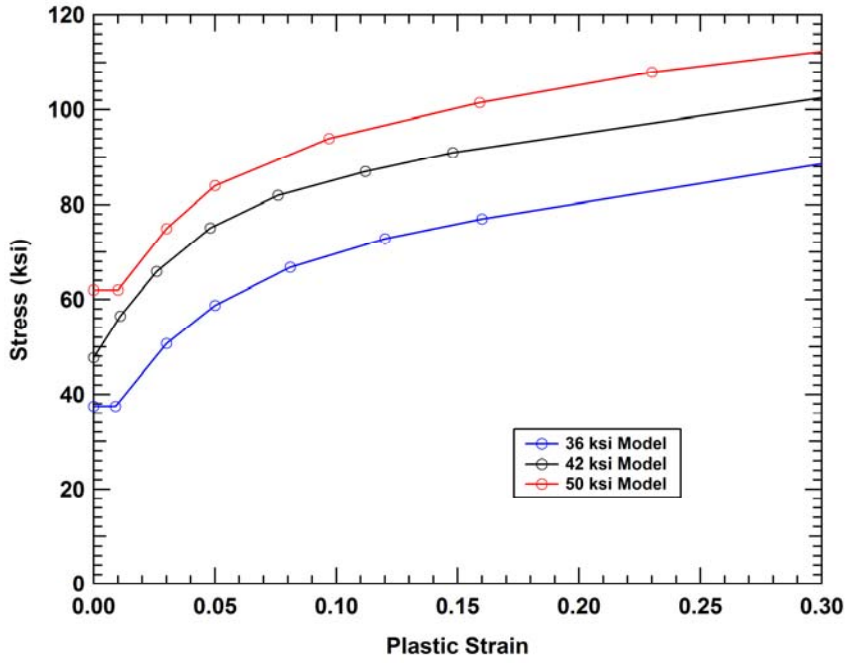

Figure 12–1. Tabular true stress-true strain constitutive model curves for WTC 7 steels.

For the regions of WTC 7 subjected to heating by fires (between Floors 7 and 14), temperature-dependent material models were used for the framing. The material model used for the steel in the fire-affected floors was the Elastic-Viscoplastic Thermal (Type 106) model in LS-DYNA, which included thermal expansion and thermal degradation in material stiffness and strength. This model used the same parameters to define the nonlinear material behavior of steel at room temperature as the Type 24 model, but included additional parameters to define temperature dependence. The yield strength, elastic modulus, Poisson's ratio, and thermal expansion coefficient were all identified as a function of temperature. The temperature-dependent models used the same failure criterion as that applied at room temperature. The temperature-dependent material properties and constitutive model parameters for the steels and bolts used in WTC 7 are presented in Appendix E. Example of the stress-strain curves for the 50 ksi steel at various temperatures is shown in Figure 12–2.

The properties obtained for the Algoma steel were a yield strength of 44 ksi and an ultimate tensile strength of 75 ksi corresponding to a true strain of 16 percent. With this limited information, a bilinear constitutive model was generated that had a yield strength of 44 ksi and a plastic hardening modulus of 194 ksi. The temperature-dependent data were interpolated between those for the A36 and A572 steels.

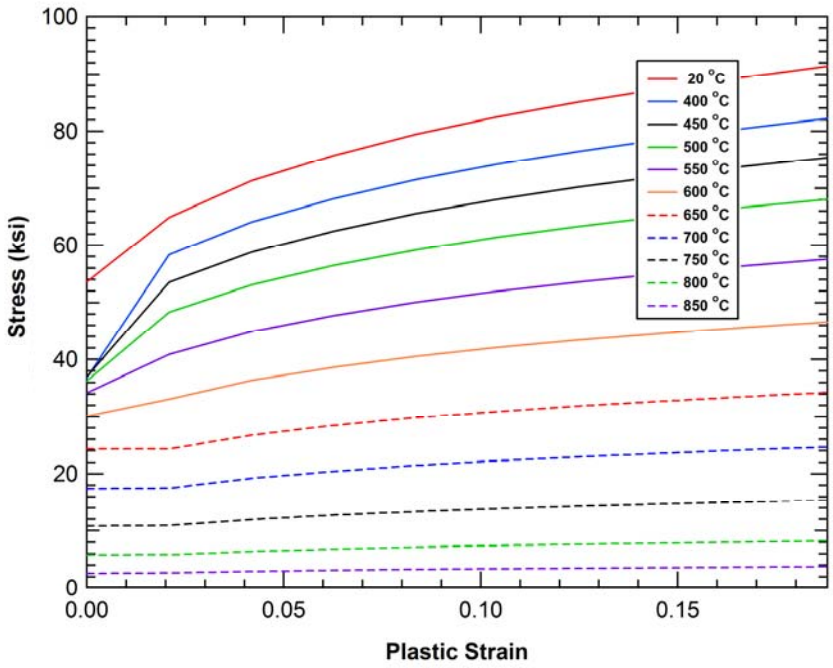

Figure 12–2. Temperature-dependent strength of the ASTM A572 Grade 50 structural steel as a function of temperature.

Floor Slab Constitutive Model

The floor slabs in WTC 7 consisted of a corrugated metal deck with a normal weight concrete slab that had an average thickness of approximately 4 in. The slab had a specified compressive strength of 3500 psi. The analysis used a compressive strength of 4900 psi to account for the effects of aging of concrete (see NIST NCSTAR 1-9A). Welded wire fabric was placed with a 3/4 in. cover to reinforce the slab. Cross sections of the typical floor slab construction details are shown in Figure 12–3 and Figure 12–4.

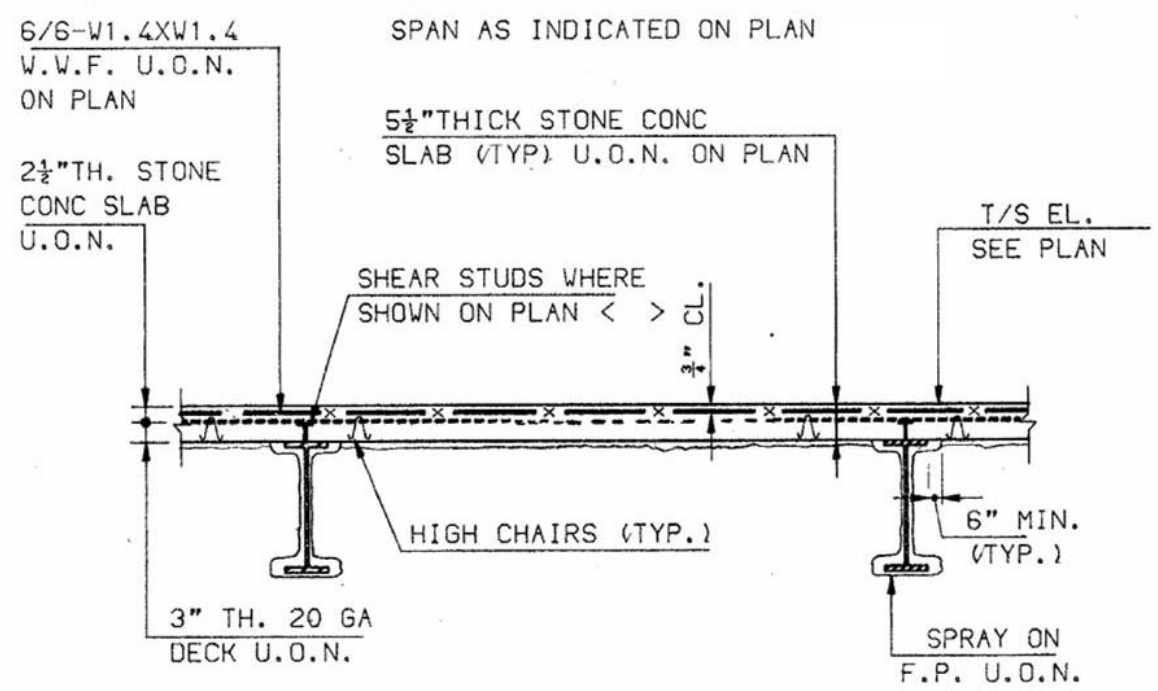

U.O.N. = Unless Otherwise Noted. W.W.F. = Welded Wire Fabric
Based on fabrication shop drawings (Cantor 1985)

Figure 12–3. Typical composite floor construction detail (along strong direction).

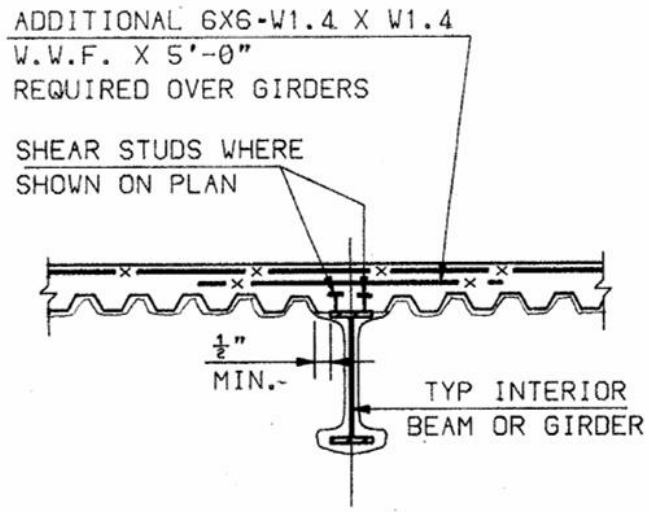

Based on fabrication shop drawings (Cantor 1985)

Figure 12–4. Typical composite floor construction detail (along weak direction).

The primary feature required in modeling the composite slab was the different slab behavior in tension and compression, as concrete cracks in tension at relatively low stresses. By comparison, the strengths of the metal reinforcement are an order of magnitude higher than the concrete compressive strength.

The composite slabs in the WTC 7 global model were represented using shell elements. The constitutive model used in LS-DYNA for the composite floor slab was material type 124 (Mat_Plasticity_Compression_Tension). This material model allowed the specification of separate tabular plastic stress-strain curves in compression and

tension. The separate tension and compression curves for the composite slab were obtained by using the rule of mixtures, which provided average properties of the composite slab based on the volume fraction of the concrete, metal deck, and reinforcement (Chapter 2, NIST NCSTAR 1-9A). The calculated tensile and compressive behaviors for the composite slab are shown in Figure 12–5.

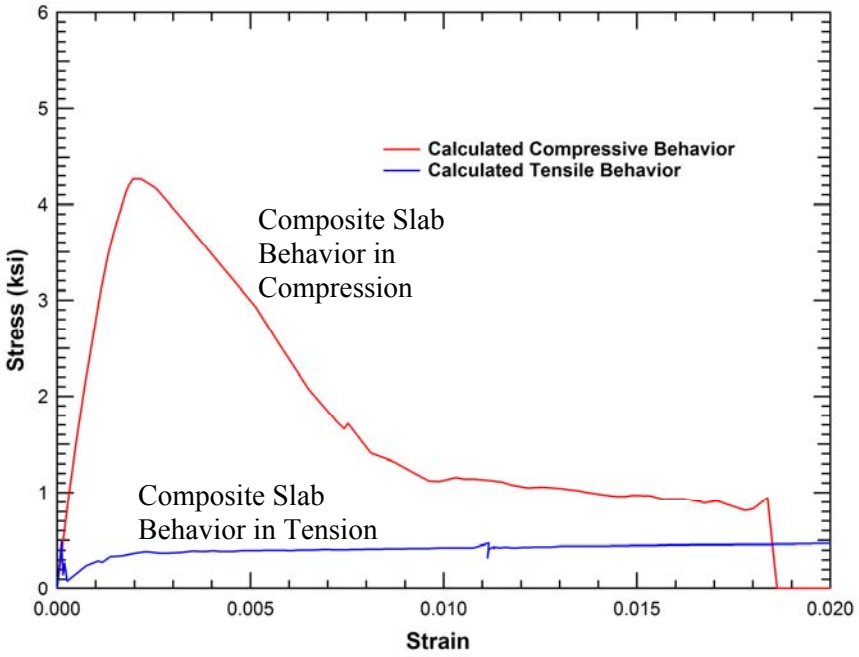

Figure 12–5. Calculated composite slab behaviors in tension and compression.

12.2.2 Global Model Description

This section provides a brief description of the construction of the global 47 story model used to simulate the collapse of WTC 7. Strategies for modeling the various connections in the building are explained in Section 12.2.3. Additional details on the global model development can be found in Chapter 3 of NIST NCSTAR 1-9A.

To model the damage and sequence of failures in WTC 7 following the initial failure event, failure models were used within the framework of the LS-DYNA finite element analyses. For the global collapse analyses of WTC 7, element sizes were a few inches on average to maintain a model size of approximately 3 million elements (see Table 12–1). Even this resolution, the gradients around a fracture could not be accurately resolved, and the damage criteria required adjustment to obtain the appropriate strength and ductility of the structures (see NIST NCSTAR 1-2B). Simulating the global response of WTC 7 required the same level of refinement throughout the model.

The WTC 7 global model was constructed mainly with shell elements, which were used to model the floor beams, girders, slabs, and columns. Typical shell element dimensions were between 6 in. and 12 in. Beam elements were used to model the diagonal bracing elements in the structural frame and the frame of the penthouse structures. Nonlinear discrete (spring) elements were used for the connection components (see Section 12.2.3). Solid (brick) elements were used for some of the foundation structures and for some

rigid masses representing large equipment. A summary of the size of the global model of WTC 7 is presented in Table 12–1. Two views of the global model are shown in Figure 12–6 and Figure 12–7.

All simulations were run on a high speed Linux Beowulf compute cluster. The head node housed two 64 bit AMD Opteron 250 2.4 GHz processors and had 4 GB of RAM and housed 1.5 terabytes of RAID 5 disk storage. Each compute node housed two 64 bit AMD Opteron Dual-core 285 2.6 GHz processors. Six of the compute nodes had 8 GB of RAM and the remaining two nodes had 16 GB RAM.

The global simulation was first initialized under gravity loading over 4.5 s of simulation time. Then damage and temperature initialization states were applied over 4 additional seconds. Collapse propagation in the global model required approximately 16 additional seconds after initialization, for a total of about 25 s of simulated time, which generally took up to 8 weeks using 12 cores across three nodes. The analysis was performed using the double precision version of LS-DYNA for a better computational accuracy.

Table 12–1 Summary of the size of the global 47 story model of WTC 7

	WTC 7 Tower Model
Number of Nodes	3,593,049
Hughes-Liu Beam Elements	3,190
Belytschko-Tsay Shell Elements	3,006,910
Constant Stress Solid Elements	2,461
Nonlinear Discrete Elements	33,364
Total Number of Elements	3,045,925

Figure 12–6 Global model of WTC 7, viewed from the southwest.

Figure 12–7 Global model of WTC 7, viewed from the northeast.

The global model was constructed in accordance with the structural drawings. All floor beams, girders, and columns were included except for a few non-critical, small section beams in the core. Figure 12–8 shows a view of the model of a typical tenant floor (Floors 8 to 20 and 24 to 45).

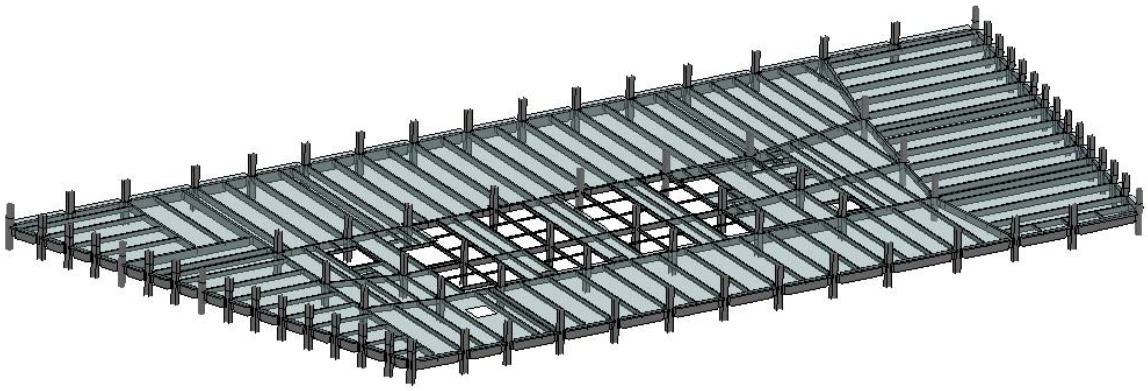

Figure 12–8. Typical tenant floor structural framing and slab model (Floor 8 to 20, 24 to 45)

As described in Chapter 2, the structure of WTC 7 between Floors 5 and 7 included a number of transitions in the column layout due to the presence of the Con Edison substation. As a result, there were a number of load transfer mechanisms in these floors that needed to be considered in the global model. The global model also accounted for variations from the typical floors. For example, Floors 21 to 23 had similar floor layouts to the typical tenant floors, except for several framing members that were slightly larger. Also, Floor 46 had heavier framing to support the cooling towers on the north region of the floor (see Figure 2-13 of Chapter 2), while Floor 47 had a double height space extending from the 46th floor to the underside of the roof for the cooling towers on the north side (see Figure 2-14 of Chapter 2).

Figure 12–9 shows Floor 5, which had a heavily reinforced 15 in. concrete slab and acted as a diaphragm. The slab reinforcement, which were WTs, was approximated in the LS-DYNA model with beam elements. Unlike the actual construction, the beam elements in the model were not embedded in the slab since shear studs were not used between the WTs and the floor slab. The major horizontal truss elements that were part of the diaphragm framing layout were included in the model, as shown in Figure 12–10.

The column models were generated in two-story lengths, as in the actual building construction, and connected with models of the splice plates. The following provides a brief description of some additional structural features of WTC 7 that were included in the global model.

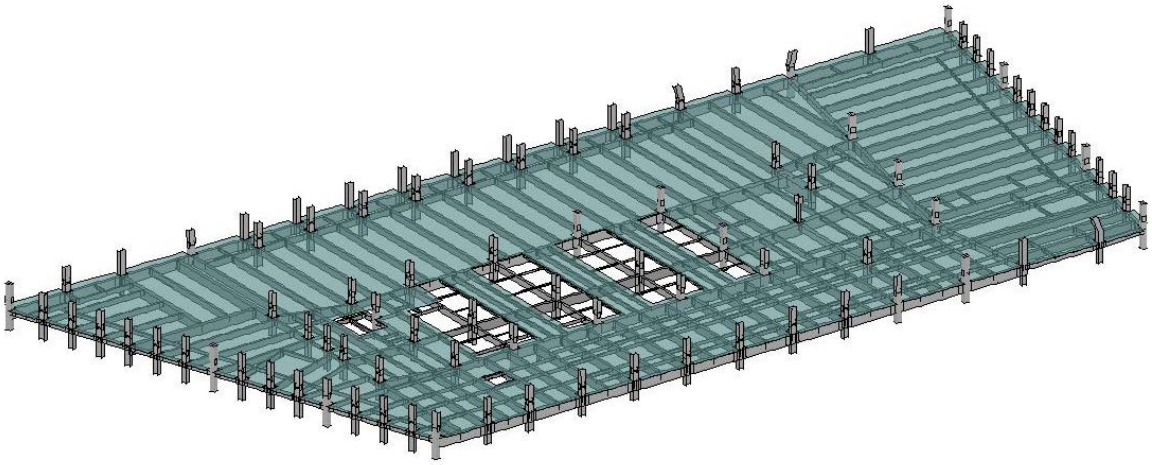

Figure 12–9. 5th floor structural framing and slab model.

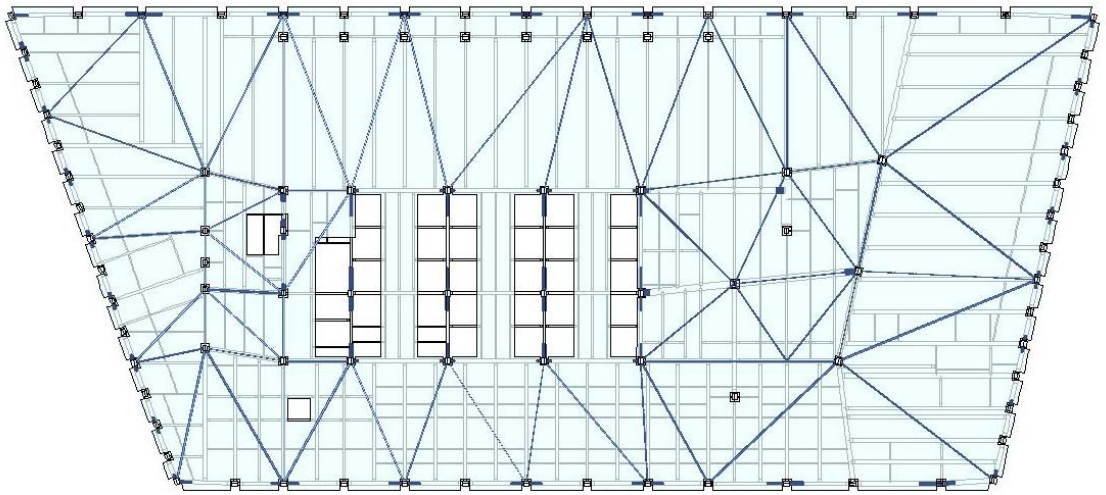

Figure 12–10. Model of the fifth floor diaphragm framing plan.

Truss and Column Transfer Structures

There were a number of truss and column transfer structures between Floors 5 and 7. All of them were included in the LS-DYNA model (NIST NCSTAR 1-9A), but only Truss 1 and Truss 2 are described here due to their contribution to the global collapse mechanism. See Chapter 2 of this report for the description of all of the transfer structures.

Truss 1 is shown in Figure 12–11. The truss supported Column 76 and transferred Column 76 loads to Column 73 to the west and to Columns E3 and E4 to the east. Columns E3 and E4 both started at Floor 7 and carried loads down to the foundation. Moment connections were used to frame the east-west beam at Floor 5 into Column 73 and girder MG-53.[1]

[1] Built-up girders were referred to in the design drawings as MG.

Truss 2 is shown in Figure 12–12. Truss 2 supported Column 77 and transferred Column 77 loads to Columns 74 and 80. Girder MG-23 supported Column 78 and transferred Column 78 loads to Columns 77 and 78A. Column 78A started at Floor 7 and carried loads down to the foundation. Moment connections were used in the Floor 5 girder framing between Columns 74 and 80.

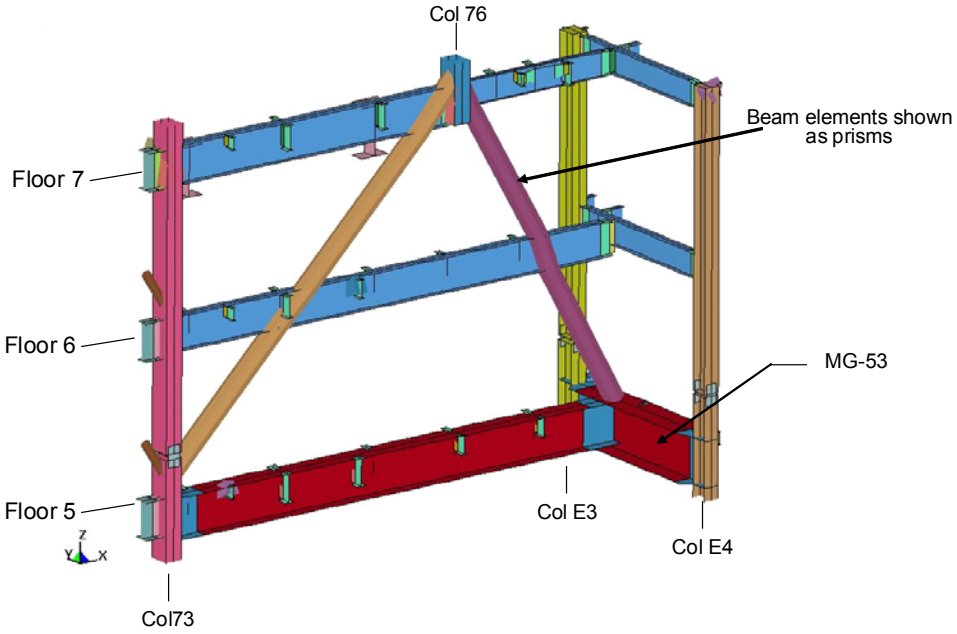

Figure 12–11. Detail of Truss 1 in the WTC 7 global model.

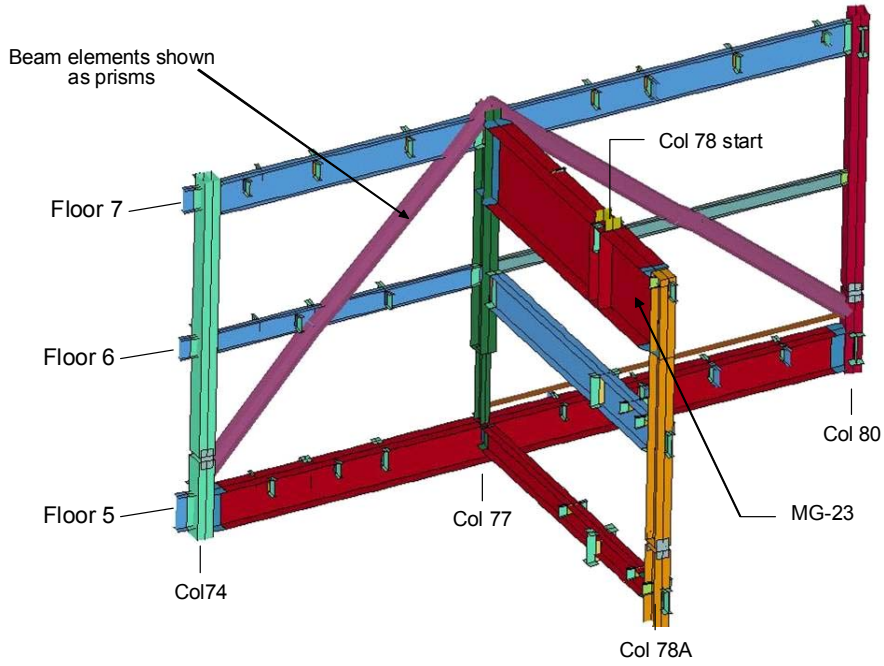

Figure 12–12. Detail of Truss 2 in the WTC 7 global model.

Exterior and Core Wind Bracing

Wind bracing trusses were added to the lower core and exterior walls of WTC 7 and were included in the global model. The belt truss at Floors 22 to 24, which was part of the exterior framing, was also included. Truss members were included as beam elements, and were merged directly into the columns.

The exterior wind bracing at the lower floors in the global model is shown in Figure 12–13. Core wind bracing is shown in Figure 12–14. The belt truss is shown in Figure 12–15.

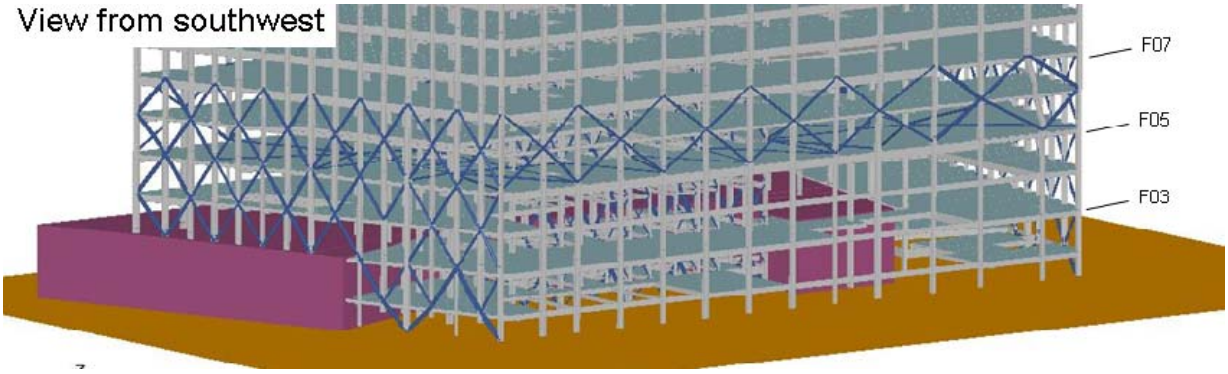

Figure 12–13. Exterior wind bracing in the lower floors of the global model.

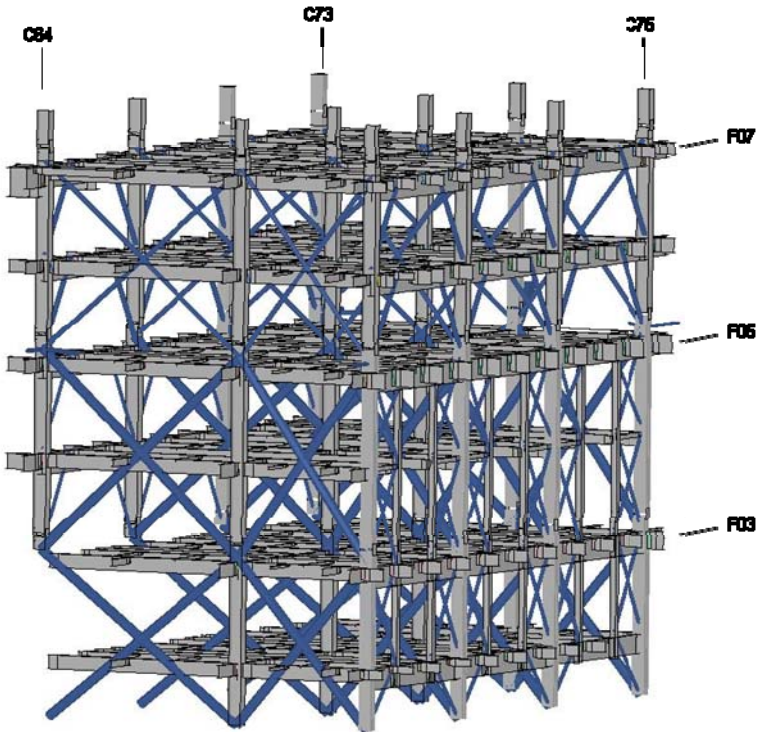

Figure 12–14. Core wind bracing in the lower floors of the global model, viewed from the southwest.

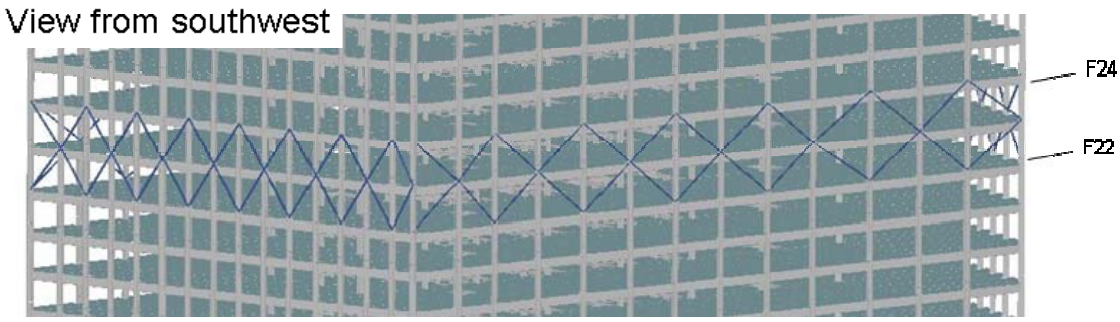

Figure 12–15. Belt truss cross-bracing in the global model.

Penthouses

A simplified model of the penthouse structures was developed using beam elements. The penthouse and the roof model are shown in Figure 12–16. Attachment of the penthouse structure to the global WTC 7 model was achieved by merging the beam ends into supporting columns or other framing in the roof structure. To approximate the weak connections between the east penthouse and the screening wall section of the western penthouse, the two structures were decoupled.

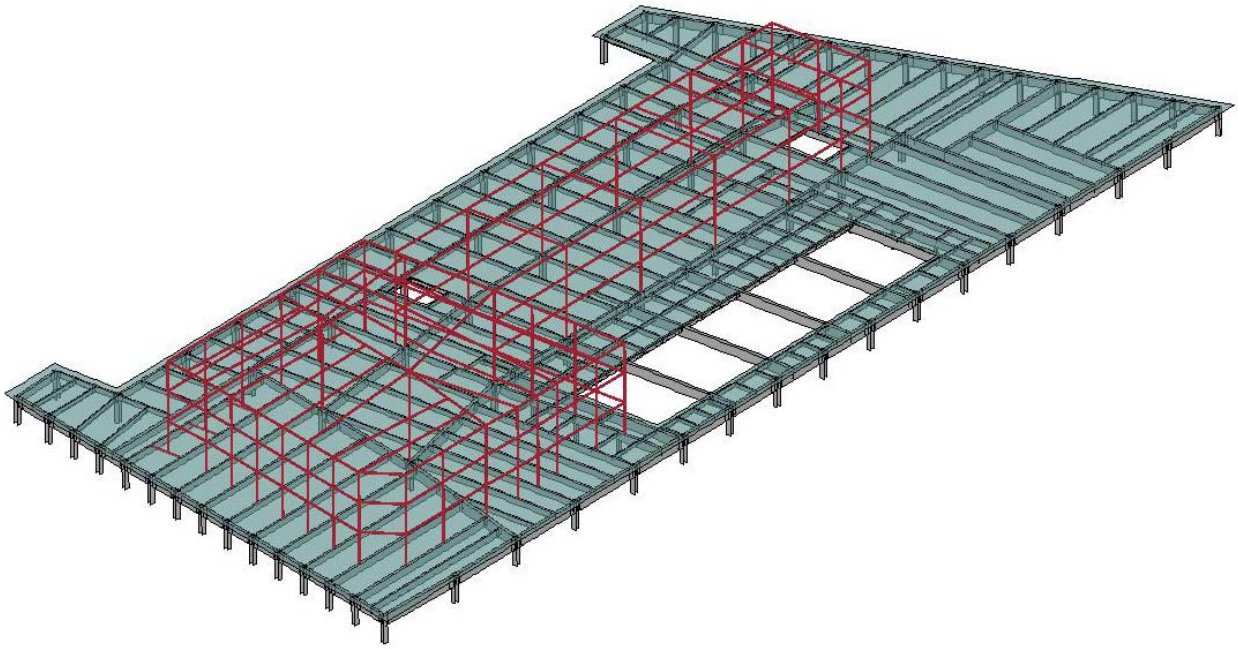

Figure 12–16. Beam element model of the penthouse structure.

12.2.3 Modeling of Connections

A key aspect of modeling the structural response of WTC 7 for collapse progression was the behavior of the floor connections in the building. Similar to the 16 story ANSYS model, a significant portion of the modeling effort was the development of connection models that accurately captured the dominant behaviors and failure modes. The strengths and failure modes of the connections were highly dependent

on the connection details (e.g., whether the connection had welds or bolts) and the loading condition and direction (e.g., connection behavior under shear or axial load).

Given a target element size of 6 in. to 12 in. within the global model, it was not possible to explicitly model connections in fine details. The connections were modeled with a simplified geometry, and connection material models were developed to provide the expected load capacity and ductility. The connection models were based on information extracted from the WTC 7 fabrication shop drawings and structural drawings.

The floor framing connections in WTC 7 (i.e., beam-to-girder and girder-to-column) included a variety of connection types. Simple shear connections were used at all interior floor framing connections. There were six types of shear connections in the floor system: fin (F), header (H), knife (K), seated top plate (STP), seated top clip (STC), and seated web clip (SWC). For the details of these connections, see Section 2.4.3. Fin, header, and knife connections attached interior floor beams to girders and girders to interior columns, except for the seated connections at Columns 79 and 81. Seated connections attached to floor beams and girders to exterior columns and to the north side of Column 79 and the south side of Column 81. Moment connections were used in the exterior frame to attach spandrel beams to exterior columns, and portions of the core framing at Floors 5 and 7, as part of the lateral load resisting system.

The floor framing connections, column splices, and moment connections included in the model are described in the following subsections.

Fin, Knife, and Header Shear Connections

A single model was used to represent three distinct types of shear connections: fin (F), header (H), and knife (K) in the global model. A schematic of each type is shown in Figure 12–17. In the LS-DYNA model, fin connections, also known as shear tab connections, were developed first. Fin connections were grouped by the depth of the beam web, which generally determined the number of bolts in the fin connection.

A series of component calculations were performed to develop fin connection models for the depth-based groupings. The idealized strength and ductility of the connection were obtained from a connection spring element model developed by Sadek el al. (2008). In that study, the connection model used an arrangement of spring elements to model the behavior and failure of the bolted connection. The spring elements accounted for a variety of failure modes including (1) bolt shear, (2) fillet weld failure under transverse load, (3) block shear failure, and (4) tear-out (bearing at bolt holes) of beam web or shear tab. Based on the simplified spring element model of Sadek et al. (2008), a simple LS-DYNA beam-column connection model was developed using shell elements, as shown in Figure 12–18.

The shell element LS-DYNA fin model was calibrated to match the connection behavior obtained from the spring element model in Sadek et al. (2008). In this analysis, the unsupported center column was pushed down vertically, as shown in Figure 12–18, until the connection failed. The appropriate connection strength and ductility in the shell element model were obtained by adjusting the material behavior and failure strain for the connection to match the spring element model. A comparison of vertical load-deflection curves from the shell element model with the spring model for the set of connections considered is shown in Figure 12–19. Good agreement between the results of the spring and shell element fin models was obtained.

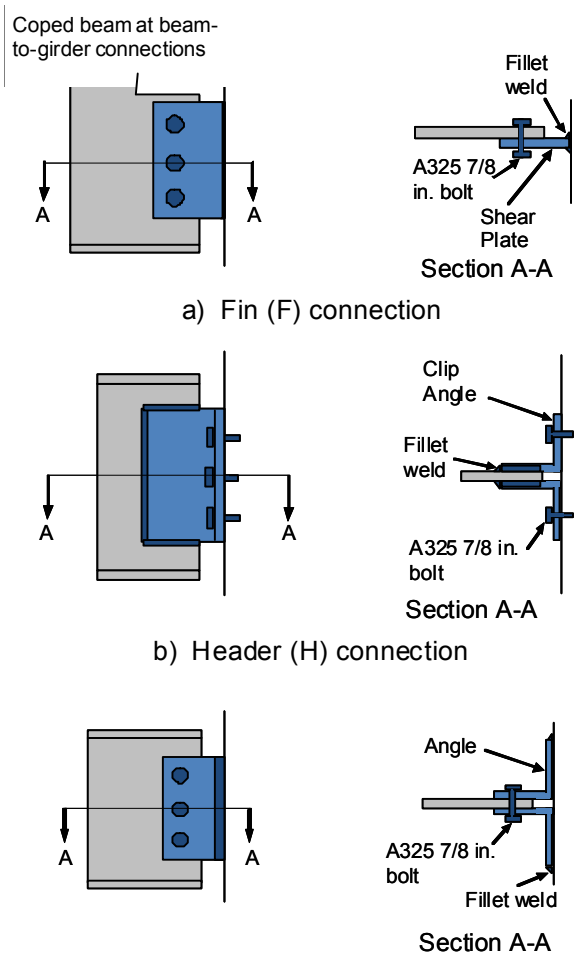

From Figure 12–3

Figure 12–17. Fin, header, and knife shear connection schematics.

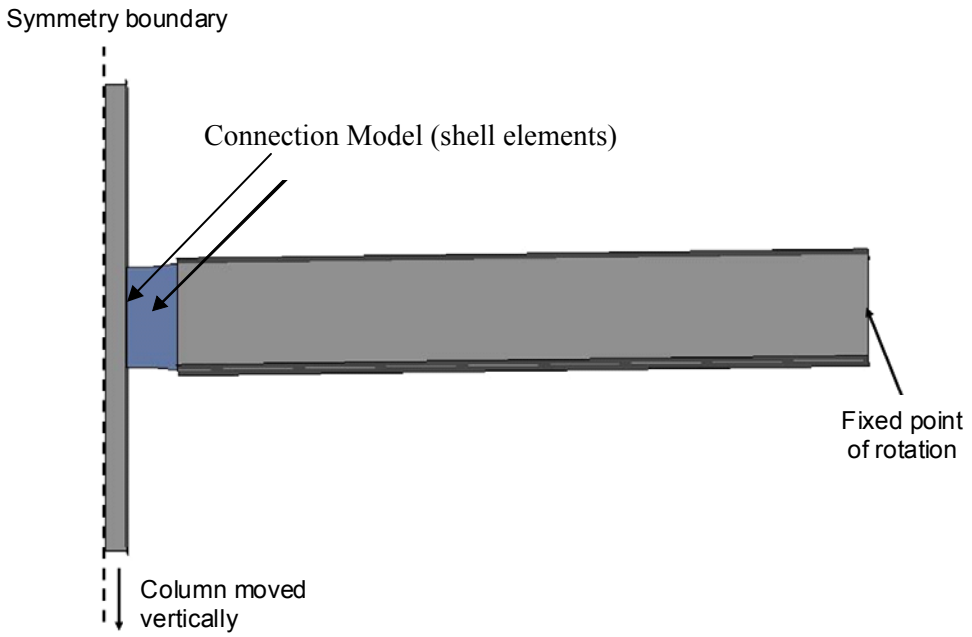

Figure 12–18. Component model used to develop the shear connection model.

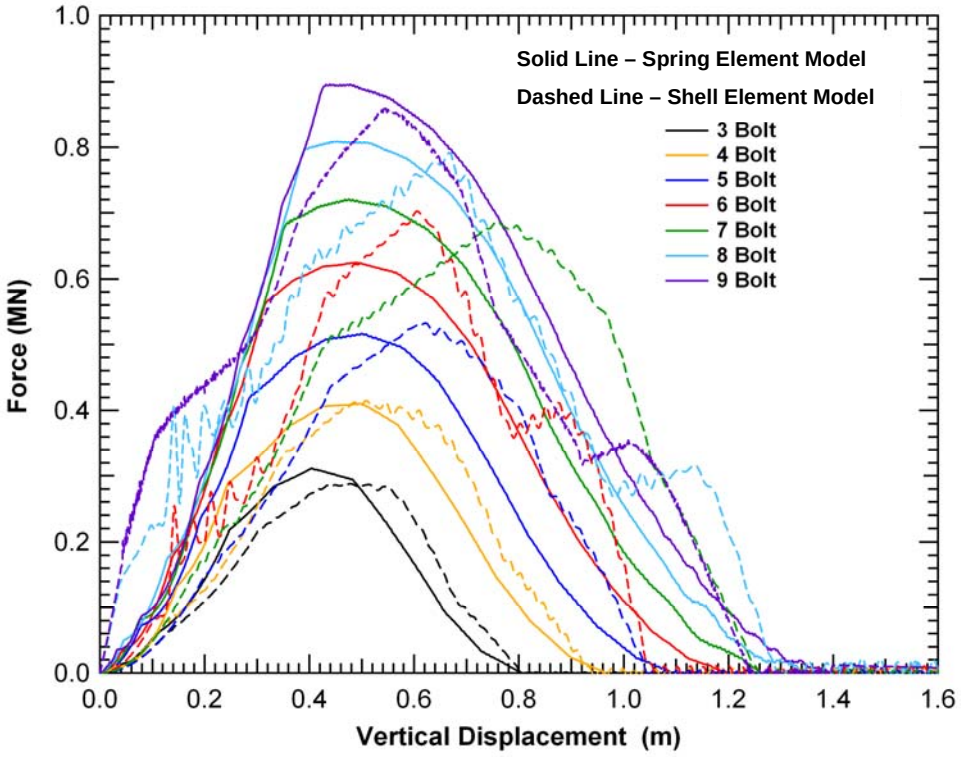

Figure 12–19. Comparison of the spring element and shell element models of the fin connections.

The knife and header connections were developed in a manner similar to that described for the fin connection. A grouping strategy was devised to map the information within the existing framework of the LS-DYNA model based on section depth and critical geometry properties such as weld size and plate thickness. First, the connection information was sorted into groupings by section depth (W12 through W36) then divided into subgroups by connection type (F, H, or K). The groupings revealed that horizontal and vertical failure strengths were dependent on the geometric features of the connections. All horizontal and vertical load capacities within a group were normalized by geometric features (weld or plate thickness, as appropriate) and averaged to formulate a standard, normalized strength for each group. A coefficient of variation of 0.3 was used as a guideline to indicate an appropriately tight grouping of connection strengths. Outliers not conforming to the grouping strategy were handled separately to obtain the correct strength. Shear connection models were generated using the same methodology for approximately 20 unique groups. To obtain the original, non-normalized strength of a given connection in the WTC 7 model, the geometric parameter specific to each connection was input at each location and used as a multiplier for that connection.

The model shown in Figure 12–18 was used to develop the specific connection properties for the connection groupings. During the component analyses, horizontal capacity was calibrated first by pulling on the beam and loading the shell element-based connection in tension. A discrete (spring) element was added to augment the vertical load capacity of each connection to achieve the appropriate vertical strength. The discrete element provided vertical strength while contributing minimally to horizontal capacity, see Figure 12–20.

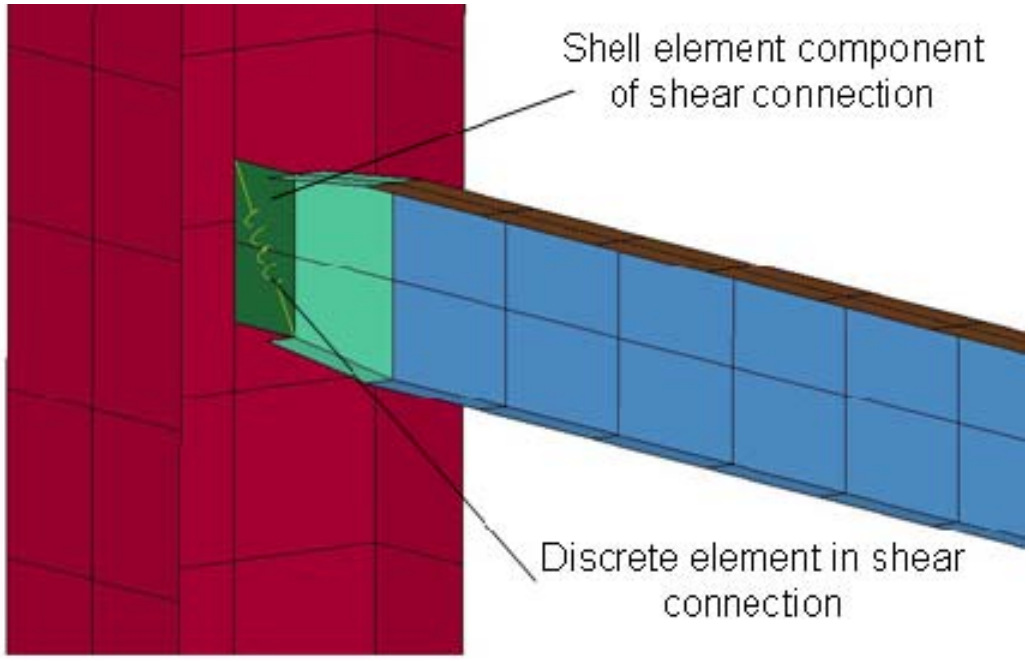

Figure 12–20. Generic LS-DYNA model of a shear connection.

A comparison was performed between the LS-DYNA and ANSYS shear connection models. The ANSYS model used a different approach to modeling the connection failure mechanisms with the use of beam and break elements. The comparison showed good agreement for selected connections, which increased confidence in both of the separately developed modeling approaches.

Seated Top Plate (STP) Connections

STP connections connected interior beams and girders to the exterior columns of WTC 7. A schematic of the connection is shown in Figure 12–21. The connections included plates welded between the column flanges above and below the framing member. During construction, the beam was bolted to the plates with two 7/8 in. A325 bolts per plate. The shear force-deflection behavior of an individual bolt is shown in the figure. The geometry varied slightly in the actual details for north/south and east/west bearing connections. In the model, the same basic geometry was used to approximate both.

The STP connection model developed for LS-DYNA is shown in Figure 12–22. The model included the plates above and below the beam, which provided vertical constraint. The plates were attached to the columns with an edge-to-surface tied interface. Sliding contact was required between the beams and plates. Bolts in the LS-DYNA model were represented with discrete elements. The properties of the discrete elements were tailored to match the bolt resistance in shear (shown in Figure 12–21). Examples showing the STP and shear connections along the building perimeter are shown in Figure 12–23.

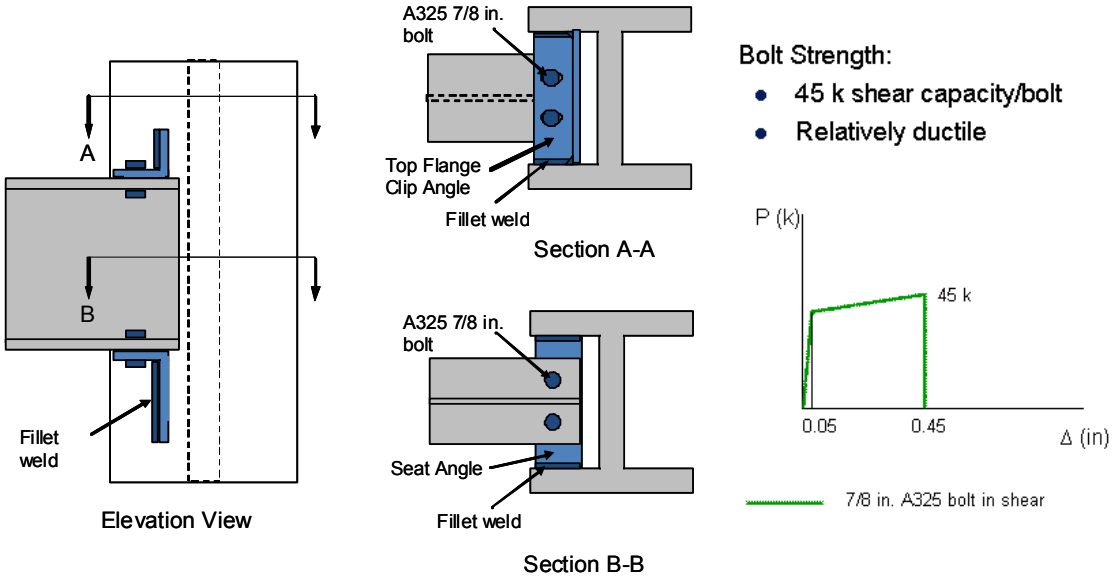

From Figure 12–3

Figure 12–21. Schematic of STP connection at exterior columns.

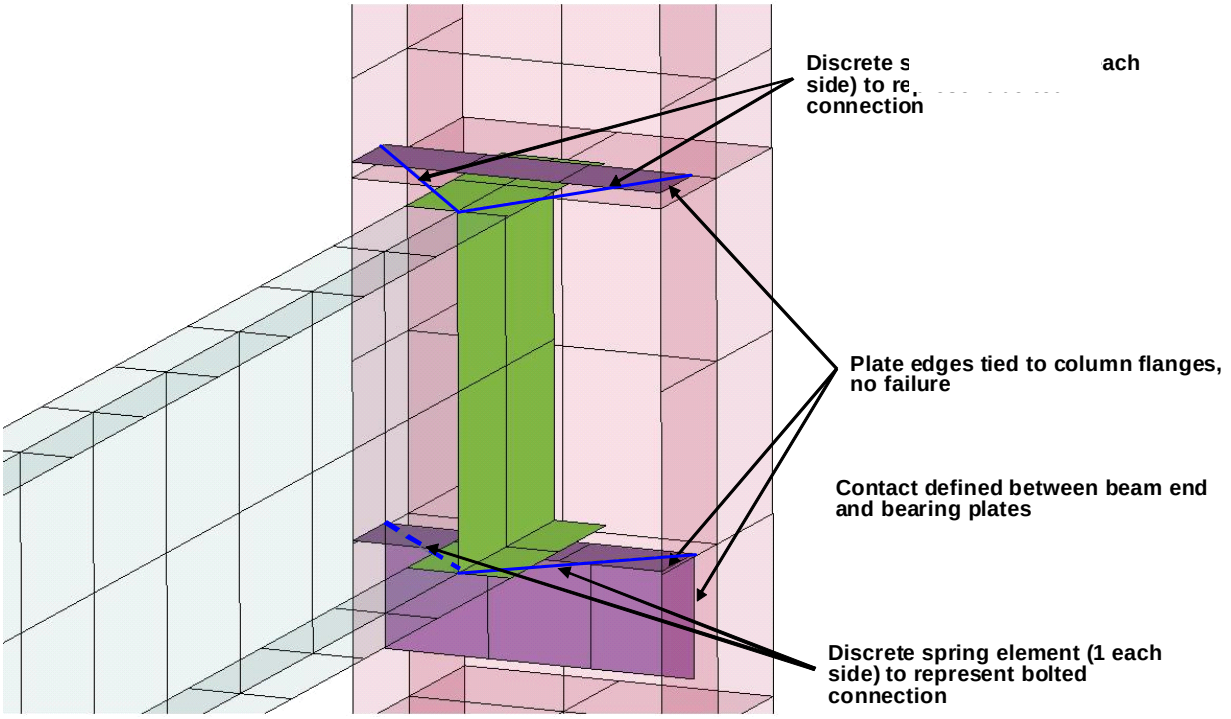

Figure 12–22. STP connection model overview.

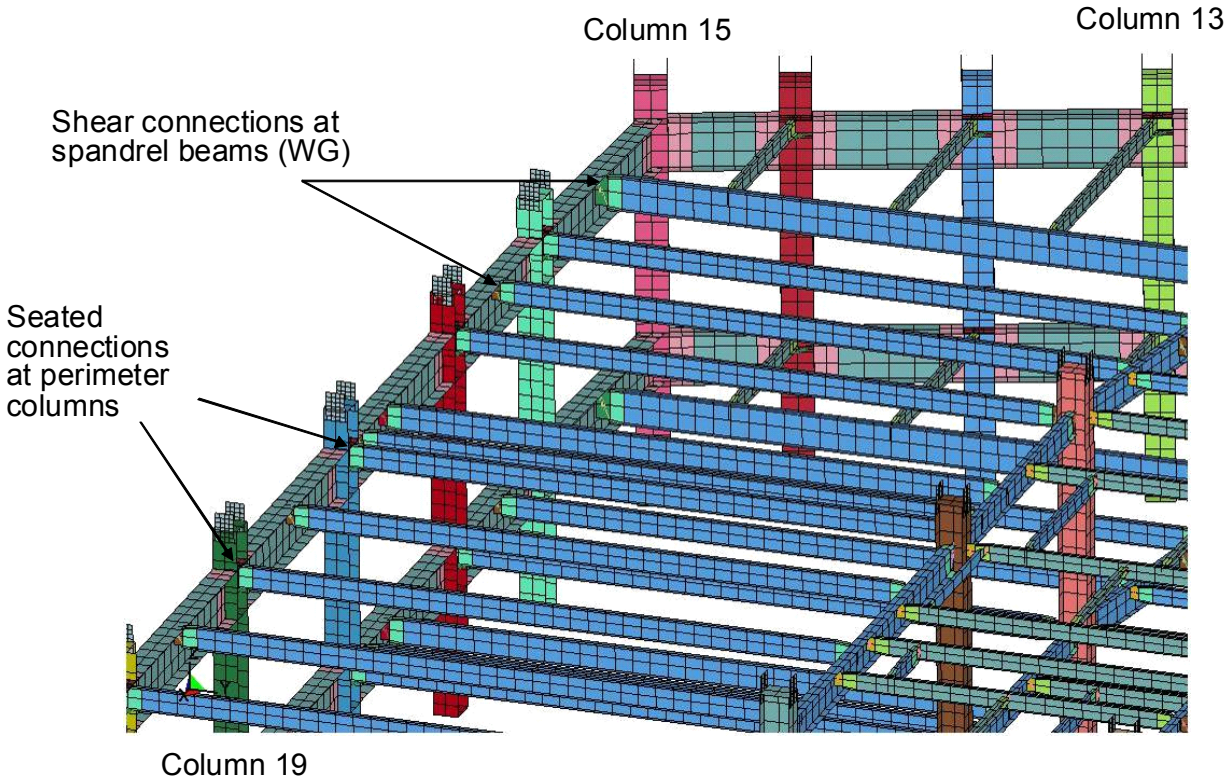

Figure 12–23. STP connection in global model, view of southwest corner above Floor 9.

Seated Top Clip (STC) Connections

According to the shop drawings and photographic evidence of the building construction, the girders that framed into the north side of Column 79 and into the south side of Column 81 were connected with STC connections. A schematic of the Column 79 seated connection is shown in Figure 12–24. The connection had a seat with a stiffener plate under the girder, which constrained vertical motion of the girder, and an angle clip above the girder. Four bolts provided lateral restraint during construction until the floor beams were connected to the girder. The seated connection at Column 81 was the same as that for Column 79, except for the angle of the girder axis relative to the column.

In the model, seat and clip plates, constructed with shell elements, were tied to the column elements and discrete elements representing bolts. The same A325 force-deflection properties for the bolts and the same contact strategy used in the STP connections were used for the STC connection model. Models of the Column 79 and Column 81 seated connections are shown in Figure 12–25 and Figure 12–26, respectively.

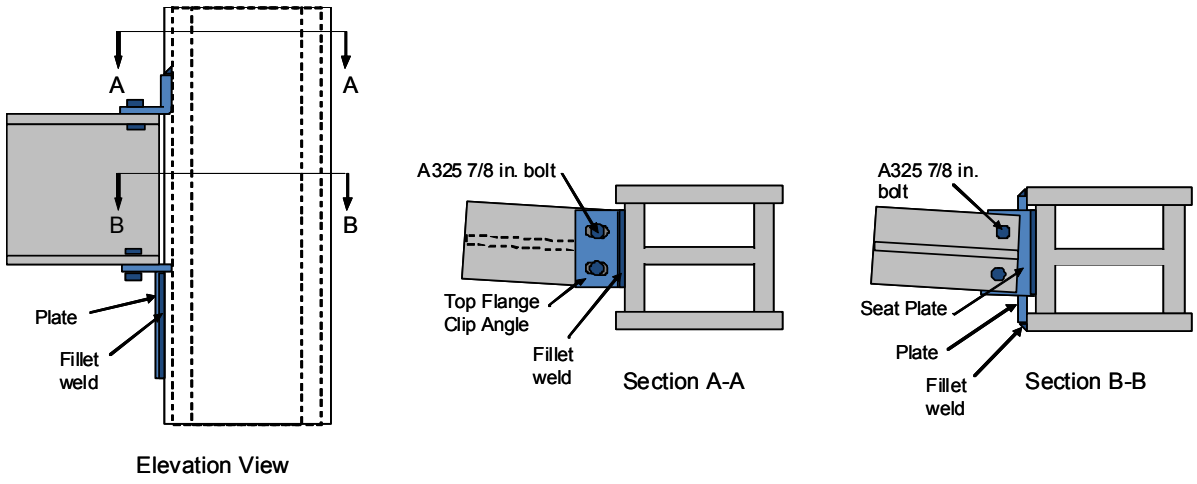

From Figure 12–3

Figure 12–24. Schematic of the STC connection at Column 79.

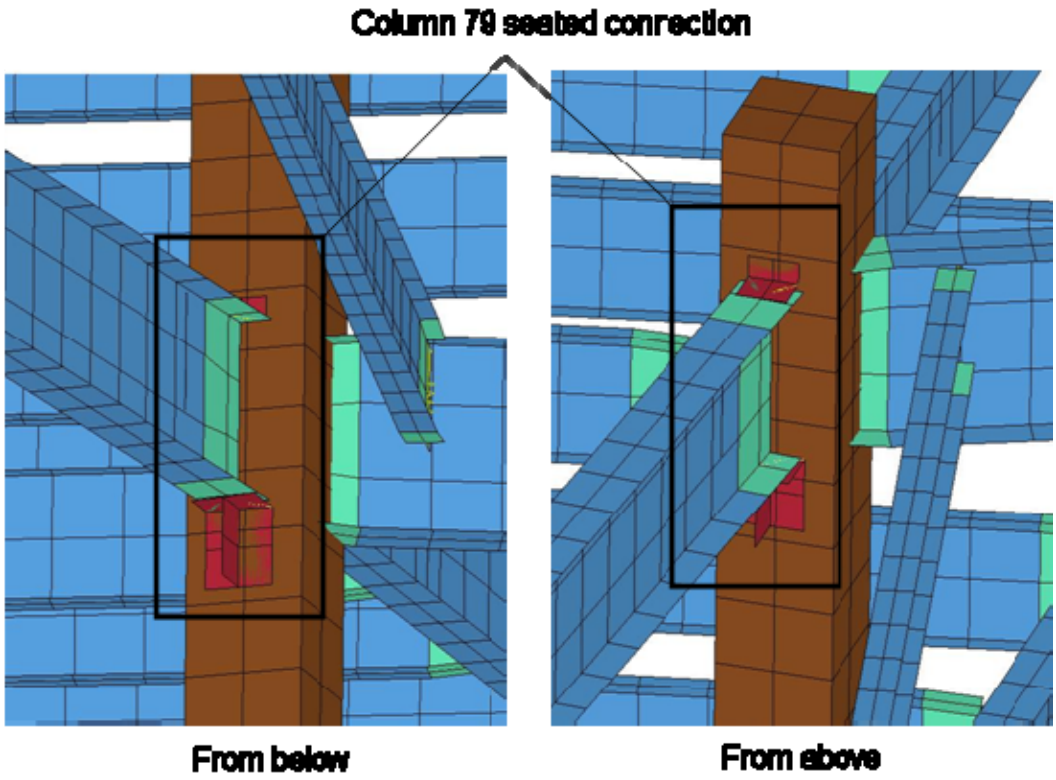

Figure 12–25. Seat connection in global model, Column 79.

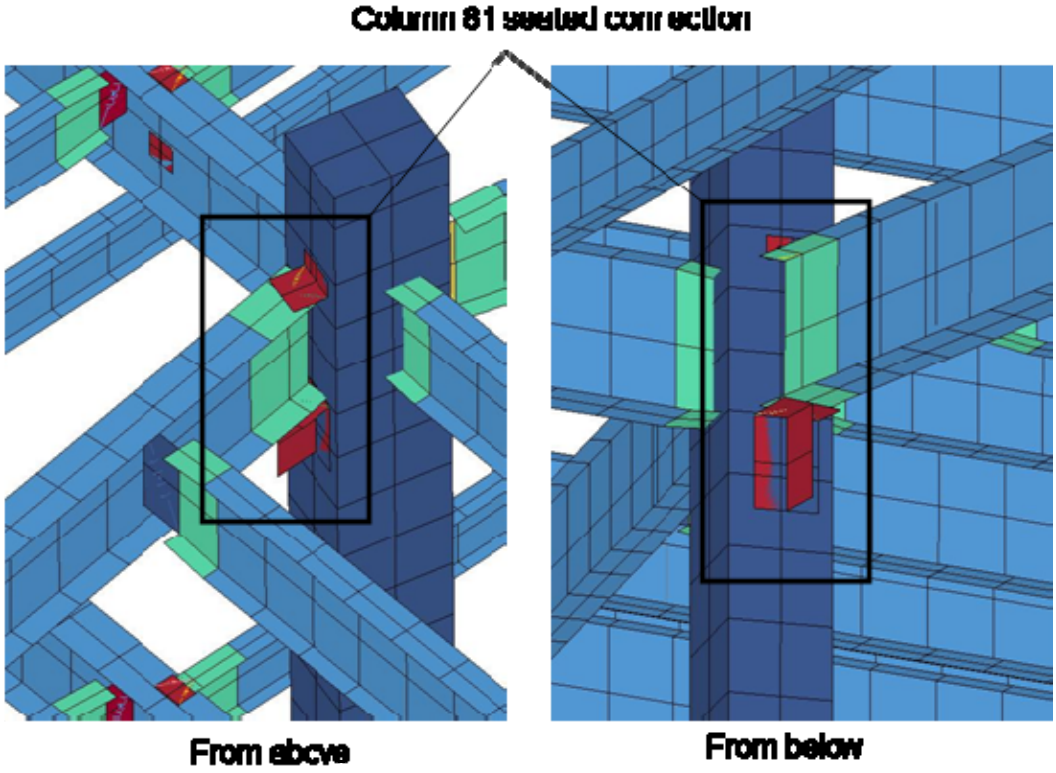

Figure 12–26. Seat connection in global model, Column 81.

Seated Web Clip (SWC) Connections

SWC connections were used to connect some floor beams to girders in the core of WTC 7. This connection had a web clip (angle) instead of a top flange clip, along with an angle seat supporting the beam. As with other seated connections in the building, two 7/8 in. A325 erection bolts were used at the seat plate and web clip. A schematic of the connection is shown in Figure 12–27.

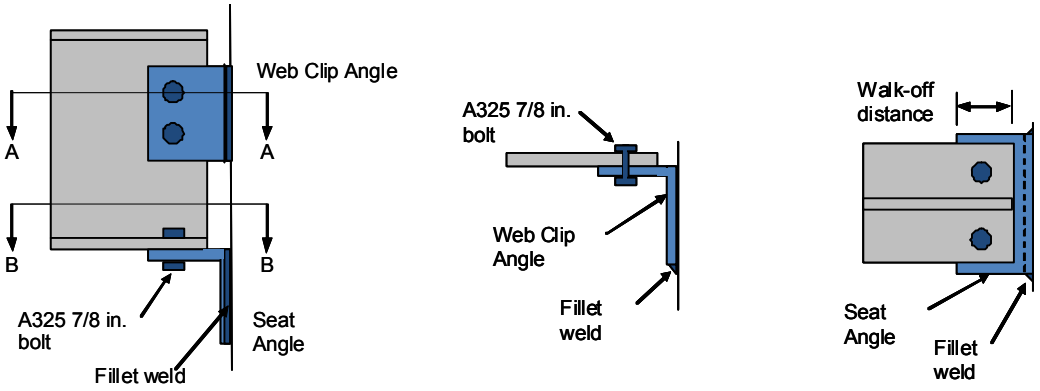

From Figure 12–3

Figure 12–27. SWC connection schematic.

A modified version of the STC connection model was used to represent the SWC connection. In the global model, the web clip was approximated as a flange clip. The same discrete element properties as in other seated connections were used to approximate the bolt's behavior. An example of the SWC implementation in the LS-DYNA model is shown in Figure 12–28.

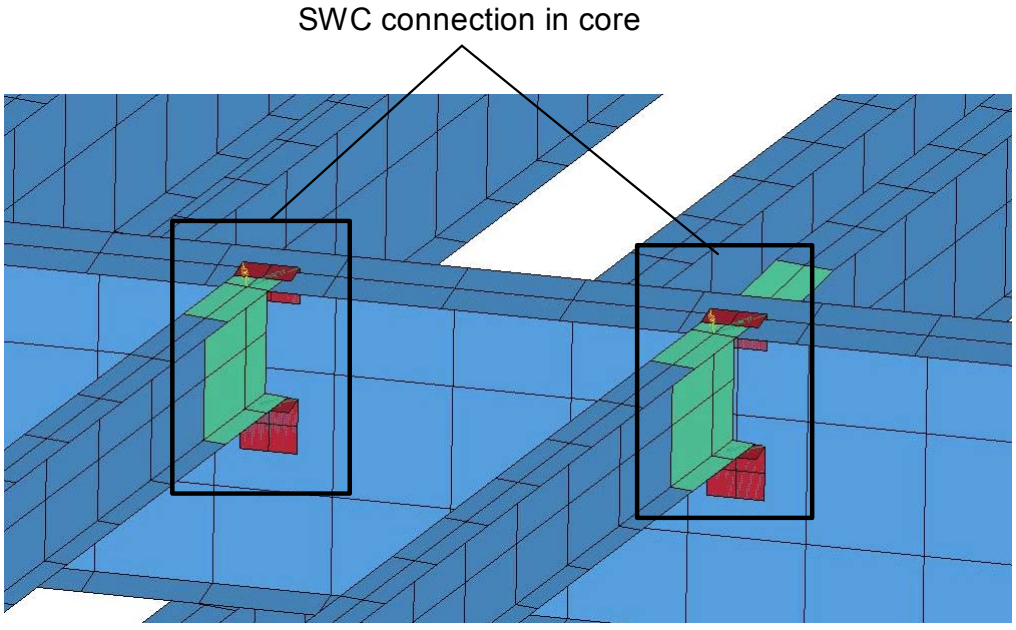

Figure 12–28. SWC connection in LS-DYNA model.

Moment Connections

In the construction of WTC 7, moment connections were used for wind girders (WG, also referred to as spandrel beams) between exterior columns. Moment connections were also used at several core girder locations on Floors 5 and 7.

Figure 12–29 illustrates a moment connection model in the LS-DYNA model. The connection between the girder and column flanges was assumed to have the same material properties as the WG, except the failure strain was lowered by 30 percent to approximate the less ductile weld zone at the connection to the column. For all moment connections, continuity plates were added between the exterior column flanges (at the level of the beam flanges) to resist local crippling of the column.

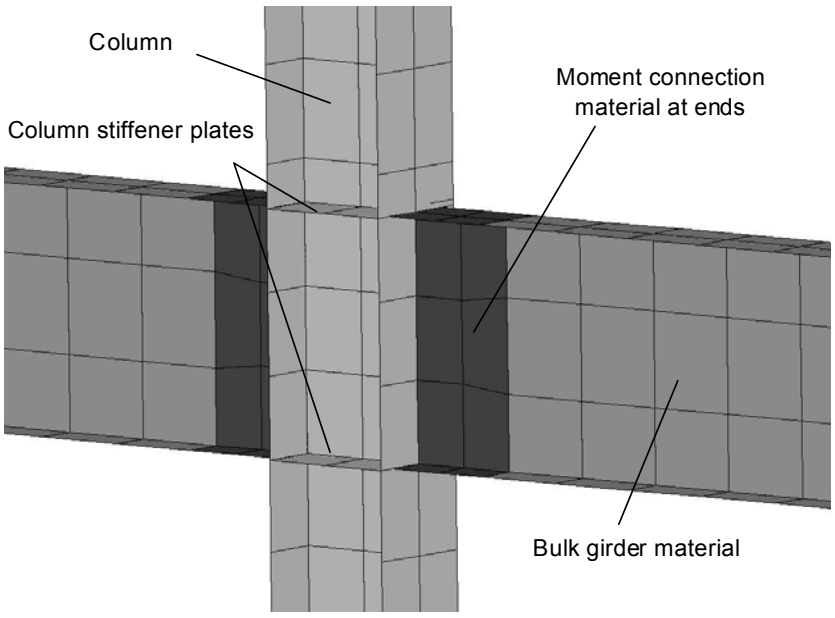

Figure 12–29. Moment connection model for a wind girder.

Column Splices

In the construction of WTC 7, columns were spliced at every other floor. Column splices used bolted and/or welded flange plates. In the global model, all column splices were explicitly represented with shell element models of the splice plates. An example of a column splice in the model is shown in Figure 12–30.

Splice plates were connected to the column flanges with a tied contact interface. Changes in column section dimensions were compensated for by using an offset tied interface between the columns and splice plates. This allowed for gaps between the splice plate and columns when a larger section column below was attached to a smaller section column above. To avoid contact instability common with edge-to-edge contacts, a plate was added to column section ends to produce a more numerically stable surface-to-surface contact condition between column ends. Thickness of the end plate was equivalent to the flange thickness for a given column section. In Figure 12–30, a gap can be seen between column end

plates. This gap was created by a half shell thickness clearance between the two end plates to improve contact stability. The end plates were not expected to alter the structural response, and they were necessary to ensure contact stability in the model.

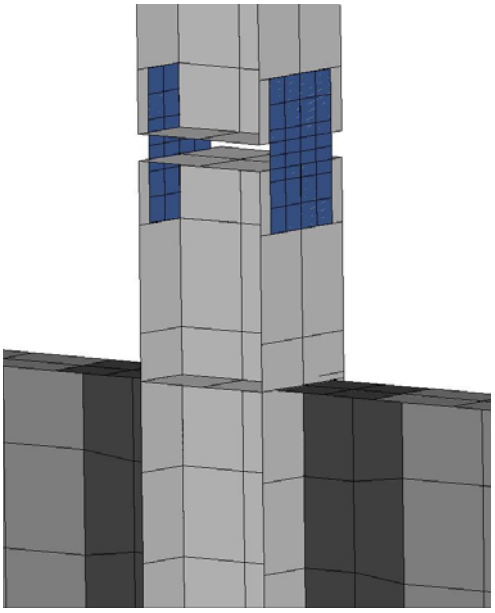

Figure 12–30. Column splice connection in LS-DYNA model.

Shear Stud Connections

The floor slab acted compositely with the floor beams by transferring shear loads through the shear studs. Shear stud connectors were modeled with a tied node (located at the center nodes along top flange of beams) to surface (slab shell element nodes) contact definition. The contact definition approach is illustrated in Figure 12–31. No failure was allowed in the tied contact. Individual connections failed when a node or shell element in the contact list exceeded its material failure criteria. This usually occurred when the composite slab material failed. Once a node or element was freed from the tied contact, it could interact with other contacting materials. The slab-to-beam tied contact was applied only to the interior floor beams and spandrel beams (WGs) where shear studs were located. Interior girders and MG sections did not have shear studs.

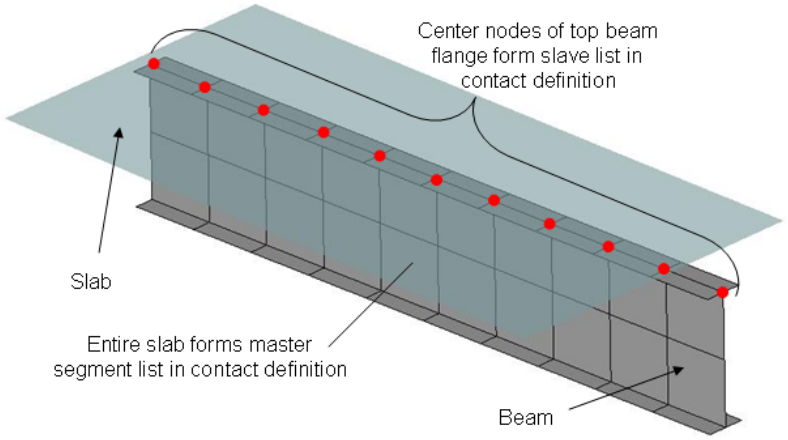

Figure 12–31. Modeling of shear stud connection between beams and slabs.

12.3 BOUNDARY CONDITIONS AND LOADING SEQUENCE

12.3.1 Displacement Boundary Conditions

To approximate the connection of the columns to the foundation, the free column ends below the second floor framing were fully constrained in translation and rotation. The base of the Con Edison substation was fully fixed and the substation model was treated as a rigid (non-deformable) body. The columns originating from the top of the substation were, therefore, fully constrained with a tied contact interface between the base of the columns and the substation. Several lateral members in Floors 2 and 3 framed directly to the substation. The ends of the framing members were connected to the substation with a tied interface to the rigid substation. Connections were modeled at the beam ends and connection failure was allowed, but the connected edge was, in essence, fixed to the rigidly constrained substation.

12.3.2 Model Initialization and Loading Sequence

The global model was initialized as follows to minimize any dynamic effects associated with loading sequence.

- First, gravity was applied slowly to the 47 floor structure over 4.5 s of elapsed simulation time to damp residual vibrations and eliminate dynamic response. The loads were applied smoothly with a sinusoidal load curve.
- Then, the debris impact damage from the collapse of WTC 1 was applied to the structure instantaneously by removing damaged elements from the model that were no longer capable of bearing their loads. The structure was then allowed to damp residual vibrations for 2 s.
- Next, the structural temperatures were applied at the same time as the damage data from the ANSYS simulation. The temperatures were applied smoothly with a sinusoidal curve and allowed to damp residual vibrations for 2 s.
- Last, the fire-induced damage obtained from the 16 story ANSYS analysis, including damage to floor beams, girders, and connections, was applied instantaneously. The heated, damaged structure was then free to react.

Figure 12–32 presents the initialization sequence with the load curve profiles. The individual initialization steps are summarized in the following subsections.

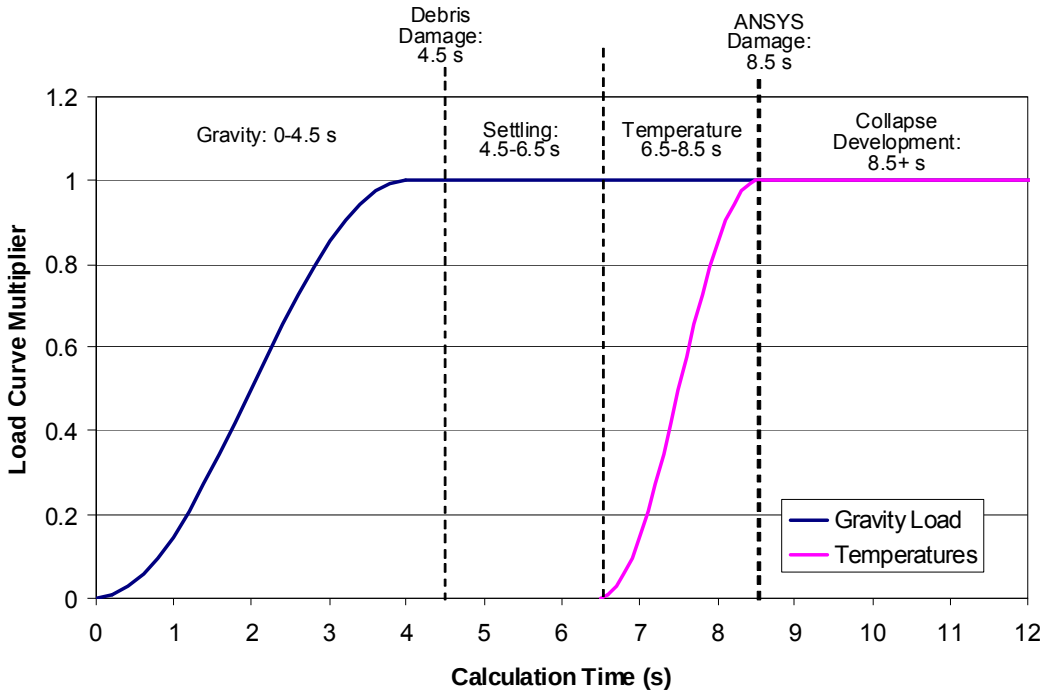

Figure 12–32. Initialization sequence for global model.

Gravity Loads

Similar to the 16 story ANSYS analysis (Chapter 11), gravity loads included: the dead load of the structure; superimposed dead loads consisting of the weight of ceilings, mechanical and electrical equipment, thermal insulation, and floor finishes; and service live load, which was taken as 25 percent of the design live load specified in the original design documents. The dead load of the structure, which was the self-weight of the steel and concrete slabs, was applied throughout the structure. At Floors 7 and 46, discrete loads were added to model the heavy localized weights of mechanical equipment. Live loads were applied by multiplying the modeled material densities with a scale factor to achieve a 25 percent live load. Gravity loads were applied as a smooth sinusoidal load curve over a duration of 4.5 s as shown in Figure 12–32.

Debris impact damage

After gravity initialization, debris impact damage due to the collapse of WTC 1 (Chapter 5) was applied to the global model instantaneously. The damage was applied to the building through the sudden removal of a number of elements from the model. The damage included two zones, as shown in Figure 12–33. Zone 1 was in the lower southwest quadrant of the building and included damage to the exterior columns and floor framing extending to the south core perimeter. In Zone 1, exterior Columns 14A through 20 were severed above Floor 7. Some floor sections in the debris zone that were not removed cantilevered out from the core. Damage to Zone 2 at the upper floors along the central-southern face was less extensive. Column 20 and some floor structure extending to the core perimeter were removed from the calculation above Floor 43. After the damage was instantaneously applied to the model, the calculation was allowed to progress for 2 s prior to temperature application.

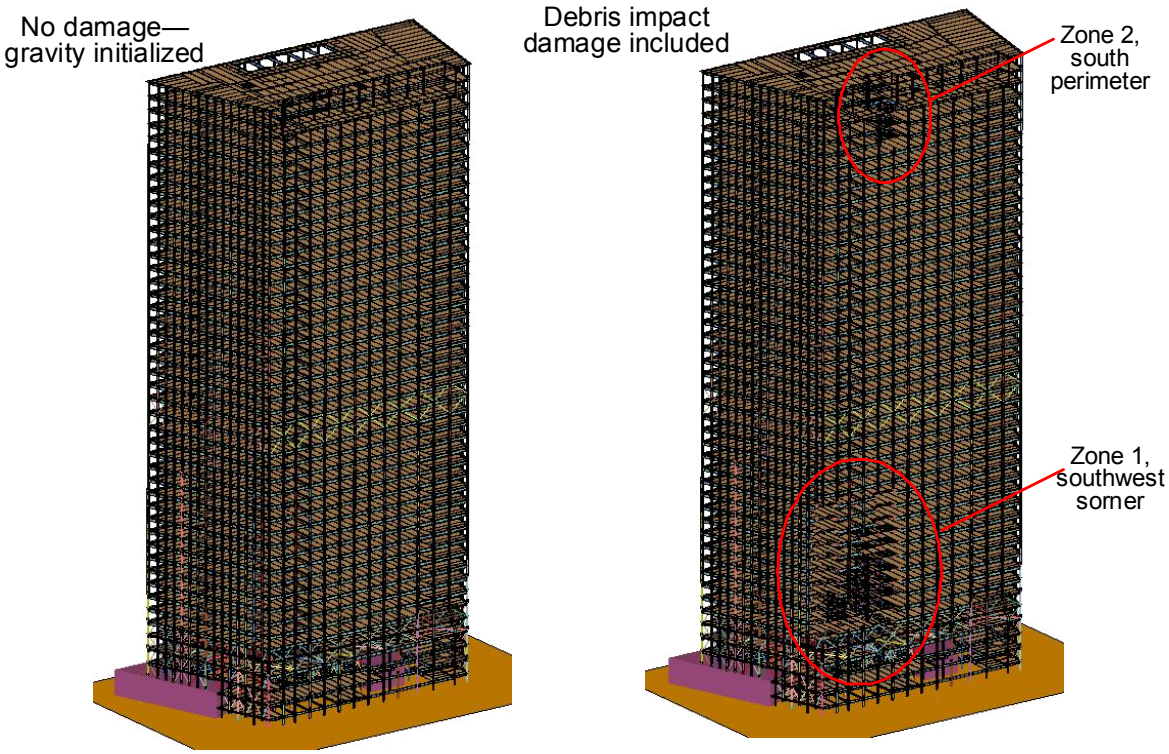

Figure 12–33. Debris impact damage application to the global LS-DYNA model.

Thermal Loading

As shown in Figure 12–32, temperatures were applied to the model smoothly over the duration of 2 s. Temperatures applied to the fire-affected zone in the global model were Case B temperatures at 4.0 hours (Chapter 10). The affected zone was between Floors 7 and 14. The temperatures were applied to the nodes in the model and followed the prescribed time-dependent load curve. The final temperature distribution applied to Floor 7 to 14 in the global model is shown in Figure 12–34.

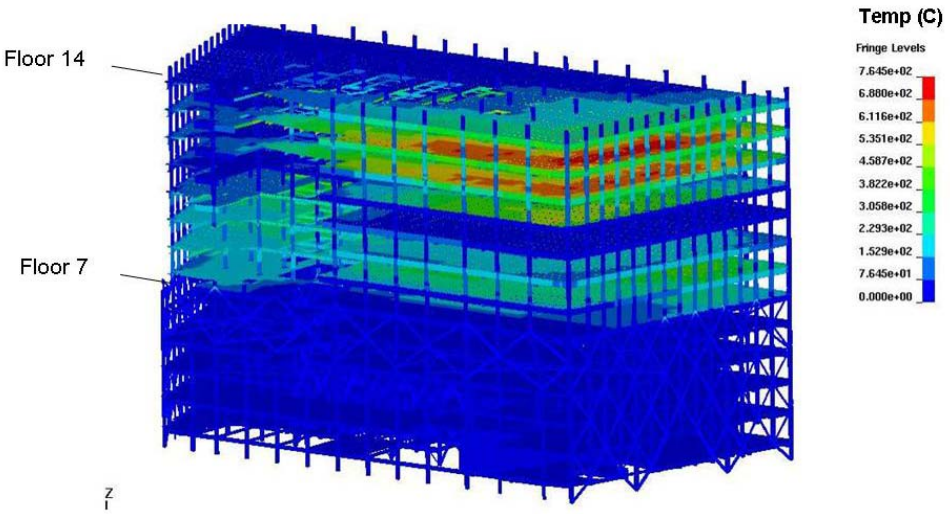

Figure 12–34. Temperature profile in Floors 7 through 14.

Fire-induced Damage

The final step in the initialization process was to apply the fire-induced damage obtained from the 16 story ANSYS model (Chapter 11). The ANSYS model estimated the damage that occurred as the fires grew and spread on Floors 7, 8, and 9 and on Floors 11, 12, and 13. The LS-DYNA model, by comparison, considered only a temperature profile at the time when damage was transferred from the ANSYS model.

The ANSYS model was capable of capturing the progression of accumulated damage over a long period of time, as fires spread through the lower floors. In contrast, the LS-DYNA model was able to predict damage due to the temperatures for a specific point in time and the subsequent dynamic progression of failures leading to global collapse of WTC 7.

The damage estimated from the ANSYS model was, therefore, input to the LS-DYNA model as the final step before analyzing the structural response. The damage was applied immediately after the temperatures had been applied in the LS-DYNA model. The damage was applied as a sudden removal of damaged or failed elements as calculated in the ANSYS analysis. After the application of the fire-induced damage, further damage and failure progression were predicted by allowing the model to progress without further user intervention.

Buckled beam and connection damage due to the fires obtained from the ANSYS analysis were superimposed on the LS-DYNA model. Buckled beams were modeled by removing flange and web elements, such that the beam would lose its axial and flexural strength, but the weight of the beam would remain in the calculation. An example of beams in the LS-DYNA model with the applied damage is shown in Figure 12–35. The figure shows ANSYS buckled beam damage applied to the southeast corner in Floor 14 of the global model. Contours shown are framing temperatures with a range of 0 °C to 736 °C.

The connection damage data from ANSYS was transferred to the LS-DYNA global model using a damage index (Chapter 11). The damage index described the degree of connection damage according to the following groups: 0 to 0.25, 0.25 to 0.5, 0.5 to 0.75, and 0.75 to 1.0, where 0 was no damage and 1.0 was failure. Horizontal support and vertical support were specified separately. Due to the coarseness of the shell element modeling of the fin, knife, and header connections in the LS-DYNA model, approximations of the damage state were made as shown in Figure 12–36.

Damage application to the various seated connections was more straightforward. Discrete elements corresponding to the calculated number of failed bolts were removed for a given connection. Also, specified seat or clip angle damage was applied directly in the global model.

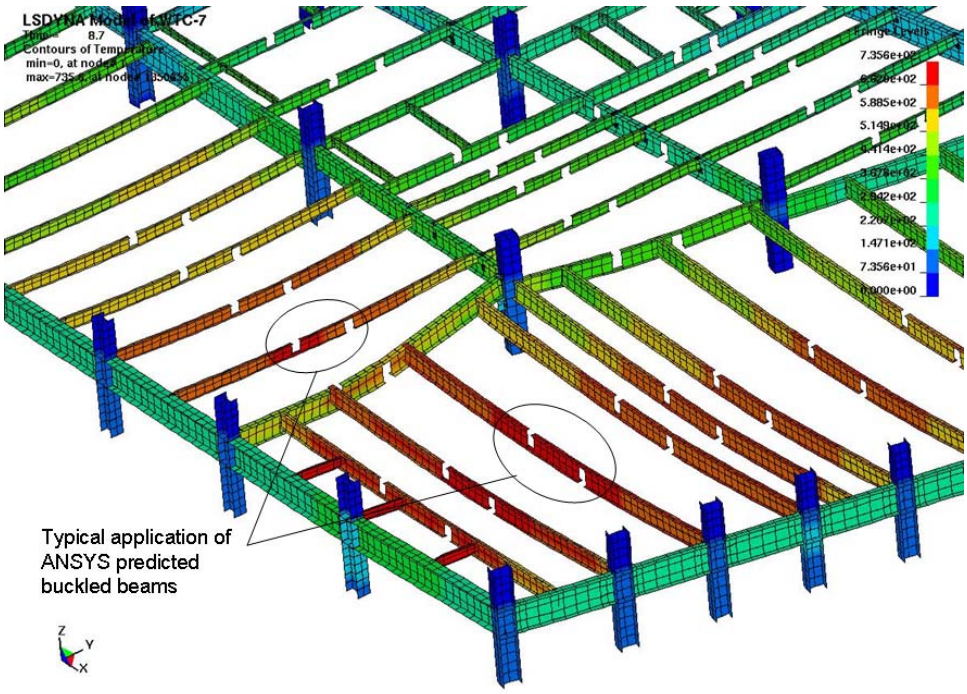

Figure 12–35. Approach used to model buckled beams in LS-DYNA model.

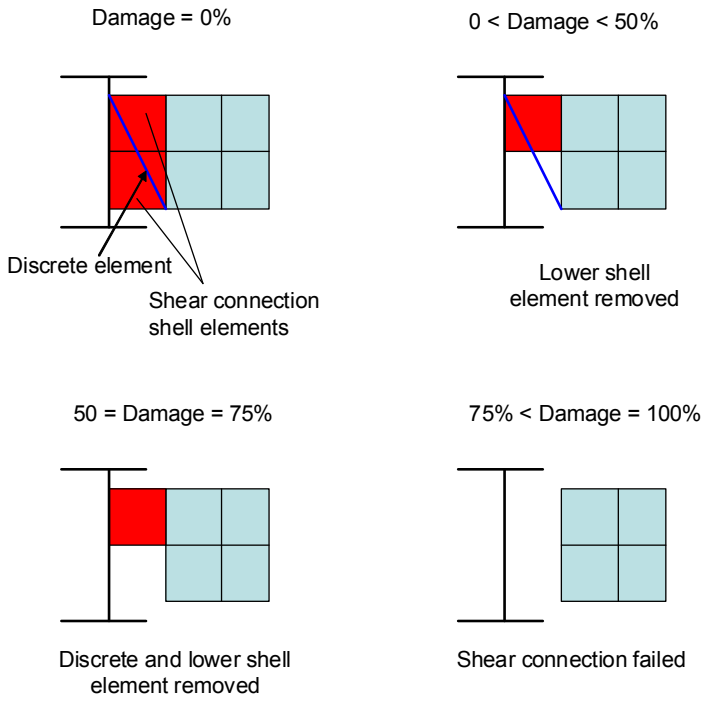

Figure 12–36. Shear connection damage application in LS-DYNA model.

12.4 GLOBAL ANALYSIS RESULTS

This section presents the response of the global model of WTC 7 to gravity loading, debris impact damage, thermal loading, and fire-induced damage from the ANSYS analysis (Chapter 11). The global analyses simulated the response of the full 47 story structure to the initial failure event due to fire and the resulting component and subsystem failures to determine the events that led to the global collapse of WTC 7.

The following analysis results are presented:

Section 12.4.1 describes the building response to gravity loads.

Section 12.4.2 describes the building response to the debris-impact damage from the collapse of WTC 1.

Section 12.4.3 describes the building response to the application of fire-induced temperatures in the structural components.

Section 12.4.4 describes the building response to debris impact damage, temperature effects (Case B, 4.0 h temperatures), and fire-induced damage based on the 16 story ANSYS analysis (Case B, 4.0 h damage).

Section 12.4.5 describes the building response to debris impact damage, temperature effects (Case B, 4.0 h temperatures), and fire-induced damage based on the 16 story ANSYS analysis (Case B, 3.5 h damage).

Section 12.4.6 describes the building response to temperature effects (Case B, 4.0 h temperatures), and fire-induced damage based on the 16 story ANSYS analysis (Case B, 4.0 h damage), but without debris impact damage.

The global analysis with fire-induced damage at 3.5 h was conducted to determine if an earlier fire-induced damage state was sufficient to initiate a global collapse of WTC 7. The global analysis without debris impact damage was conducted to determine the contribution of debris impact damage to the global collapse sequence of WTC 7.

12.4.1 Building Response to Gravity Loads

Figure 12–37 shows the vertical displacements calculated at the end of the application of the gravity loads. The figure shows that the largest floor displacements were estimated at the northeast quadrant of the building. A check on the accuracy of the applied loads was performed. The expected load due to dead, superimposed dead, and service live loads above Floor 8 based on the design drawings (after adjusting for service live loads instead of design live loads) was about 174,100 kip. The initialized model showed a total load of 172,900 kip, for a difference of about 0.7 percent. Figure 12–38 presents the total load above Floor 8 in the model during gravity initialization. The load increased smoothly as expected and without dynamic effects, indicating the gravity initialization duration of 4.5 s to full load was adequate.

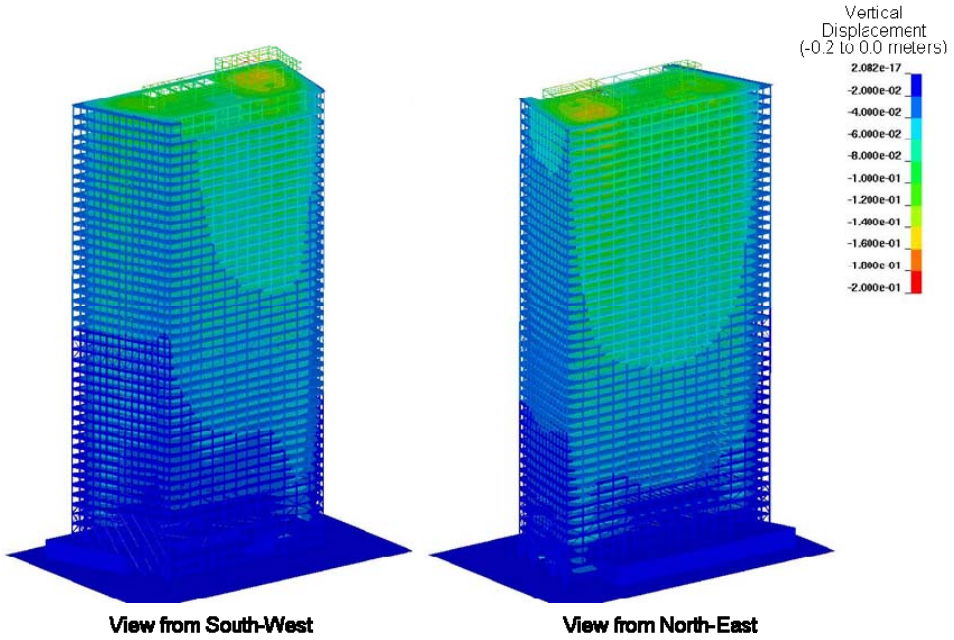

Figure 12–37. Calculated global vertical displacements after gravity initialization.

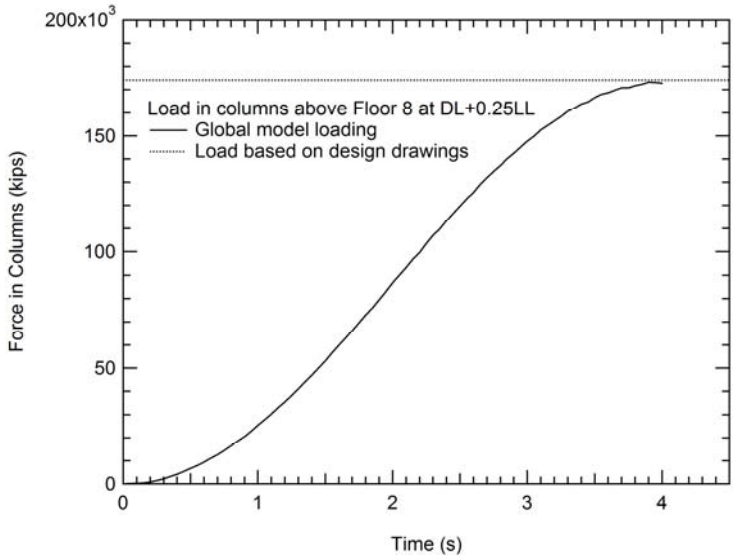

Figure 12–38. Total load history above Floor 8 during gravity initialization.

12.4.2 Building Response to Debris-Impact Damage

Subsequent to the application of the gravity loads, damage due to debris impact from the collapse of WTC 1 was applied to the global 47 story model. Figure 12–39 presents the vertical displacements due to debris impact damage application. The figure shows a downward displacement of up to 8 in. (about 1/900 of the total building height) on the south face toward Zone 1 damage due to column removal. The analysis shows that the building remained stable and that columns and floors above the damaged zone were able to redistribute the loads through Vierendeel truss action.

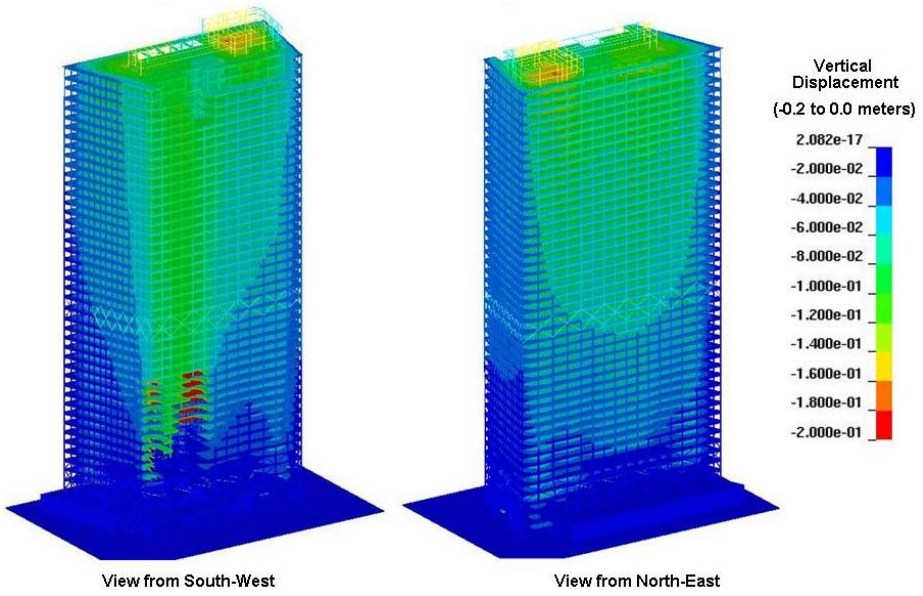

Figure 12–39. Calculated vertical displacements after impact damage.

12.4.3 Building Response to Temperatures

Figure 12–40 shows the subsequent change in vertical displacement after Case B, 4.0 hour temperatures were applied. Detail views illustrating the vertical displacements of the lower floors, up to Floor 14, are shown in Figure 12–41 (a) after debris impact damage application and Figure 12–41(b) after full temperature application. This figure indicates that the heated floors displaced vertically due to damaged floor framing and connections, primarily due to thermal expansion effects (Chapter 11). The analysis also indicates that the combination of the impact damage and thermal loading produced significantly higher stress states throughout the lower floors of the building.

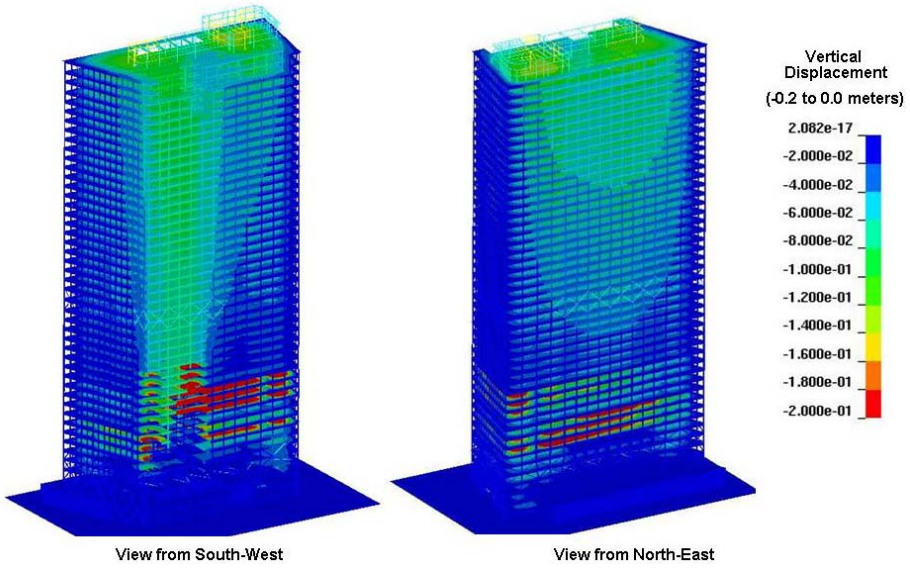

Figure 12–40. Calculated vertical displacements after temperature initialization.

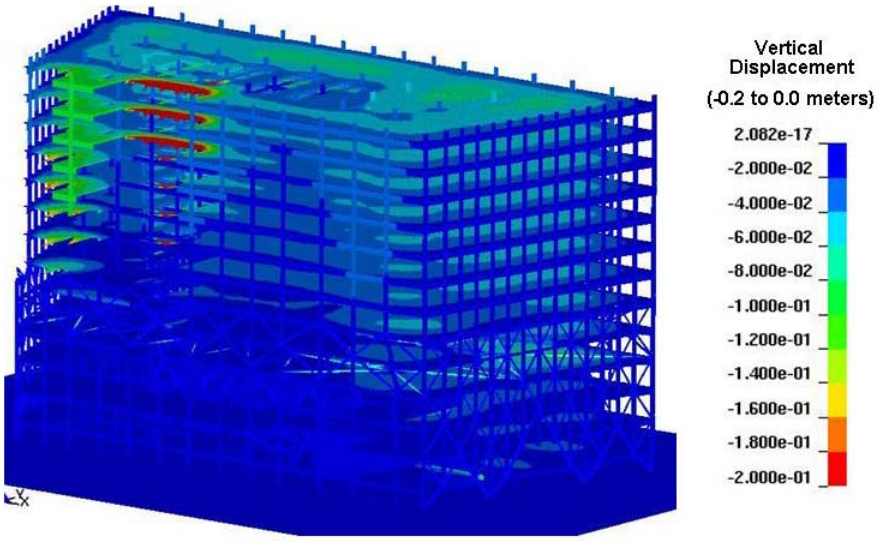

(a) After debris impact damage initialization

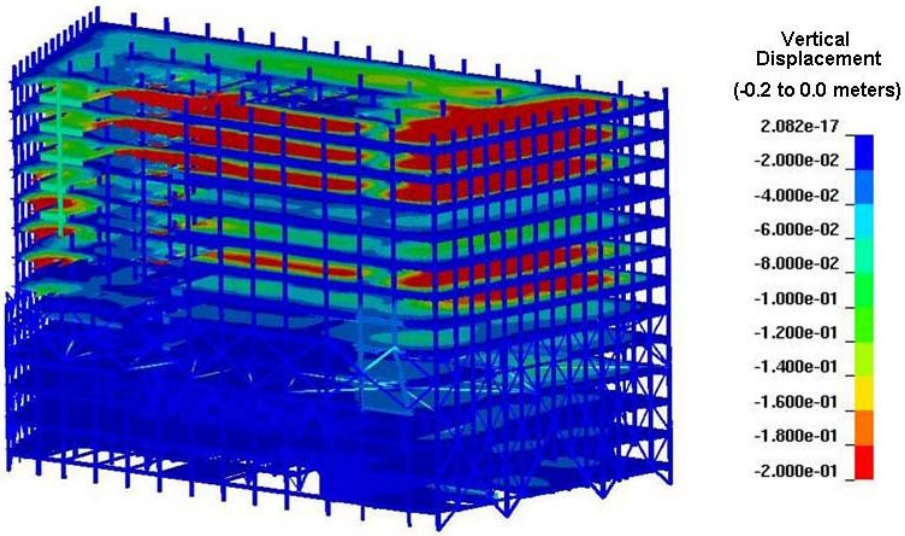

(b) After temperature initialization

Figure 12–41. Detailed comparison of vertical displacements after damage and temperature initializations.

12.4.4 Global Analysis Results with Best Estimate Debris Impact Damage

Following the application of gravity loading, debris impact damage, thermal loading, and fire-induced damage to floor framing and connections, the global analysis of the WTC 7 collapse progressed to calculate the response of the building. The analysis showed that the global collapse of WTC 7 occurred under the applied loading and damage conditions.

Two timing reference frames are used when discussing global model results: a calculation reference frame and a collapse reference frame. The LS-DYNA calculation reference frame is described in Section 12.3.2. The collapse reference frame is based on observation times from photo and video records (Chapter 5). The collapse reference time of 0.0 s starts when a kink was observed in the roofline of the east penthouse,

as viewed from the north. In the global analysis results, the kink in the roofline of the east penthouse occurred at 16.0 s in the calculation reference time. In the following graphics, if both times are quoted, the syntax used is "collapse reference frame (calculation reference frame)."

A series of snapshots of the interior columns and floor systems up to Floor 18 taken from the southwest (see Figure 12–42, Figure 12–48, Figure 12–49, and Figure 12–52 to Figure 12–55) illustrates the progression of failures in the floors and columns of WTC 7. Exterior columns and some of the tenant floor structure spanning between the core and the exterior have been removed from the views to illustrate the damage to the interior of the building. In each figure, contours of resultant lateral displacements are shown. For comparison between snapshots, a constant range of 0 in. to 6 in. was used. Since a resultant lateral displacement is presented, negative and positive values can not be distinguished, and only absolute values are displayed. Any value greater than 6 in. remains red in the figure.

The following sequence of events was observed in the analysis, after the application of the loads and damage, which led to the global collapse of WTC 7. For each step, an overview highlighting the major events is presented first, followed by a discussion detailing these events. For further details on the global analysis results, see Chapter 4 of NIST NCSTAR 1-9A.

Initial Local Failure for Collapse Initiation

The global collapse analysis showed the following sequence of events that resulted in the buckling of critical Column 79 (initial failure event):

- The collapse of Floor 13 onto the floors below, some of which were already weakened by fires, triggered a cascade of floor failures in the northeast region.
- The floor failures progressed down to Floor 5, where debris accumulated, and spread across the east floor area, due to the effects of impact loads from falling debris on thermally weakened floor areas.
- Critical Column 79 became laterally unsupported between Floors 5 and 14 in the east-west and south directions as a result of the progression of floor system failures. There was still some lateral support in the north direction at Floors 8 to 12 and Floor 14, as the erection bolts in the seated connections had all failed at these girder ends, but the girders had not walked off the bearing seat.
- The increase in unsupported length led to the buckling failure of Column 79, which was the collapse initiation event for WTC 7.

The floor framing structure was thermally weakened at Floors 8 to 14, with the most substantial damage occurring in the east region of Floors 12, 13, and 14. Even though each floor had been weakened over hours of exposure to separate and independent fires, it was not until there was substantial damage to the long span floors in the northeast region of Floor 13 that the initial failure event, i.e., buckling of Column 79, was triggered.

After the fire-induced ANSYS damage was applied, floor sections surrounding Columns 79 to 81 on Floors 13 and 14 collapsed to the floors below, as shown in Figure 12–42. The LS-DYNA analysis

calculated the dynamic response of the structure to the floor failures and resulting debris impact loads on the surrounding structure. The thermally weakened floors below the initial collapse event could not withstand the impact from the collapsing floors, and resulted in sequential floor collapses. The floor systems progressively failed down to Floor 5, where the debris accumulated, as shown in Figure 12–42.

Figure 12–43 is a cutaway view that illustrates the structural condition surrounding Column 79 as it buckled to the east. The plot in Figure 12–43 shows that Column 79 buckled 1.3 s before the kink was observed in the East Penthouse roof framing (which occurred at 0 (16.0) s in the analysis). Figure 12–43 includes resultant lateral displacements and column axial stress histories for Columns 79 to 81. The rapid lateral displacement indicates column buckling. Likewise, the column stresses indicated a rapid loss of stress at the time, signifying column buckling. Column 79 was laterally unsupported in the east-west and south directions between Floors 5 and 14. There was still some lateral support in the north direction at Floors 8 to 12 and Floor 14, as the erection bolts in the seated connections had all failed at these girder ends, but the girders had not walked off the bearing seat. Thus, the north girder connection possibly prevented lateral displacement in the north direction, but provided no resistance to lateral displacements in the east, west, or south direction. At Floor 14, the girder to the west of Column 79 (between Column 79 and 76) was still attached and provided lateral restraint from the west. Figure 12–44 illustrates the girder-to-column connection status at the time of buckling of Column 79.

A separate global analysis of the structure with the same gravity loading, debris impact damage, and thermal loading, but with fire-induced damage from ANSYS at 3.5 h (instead of 4.0 h) showed that Column 79 did not buckle at this earlier damage state (Section 12.4.5). The damage state at 3.5 h primarily included failure to beams and connections at the south and southeast regions of the affected floors. This global analysis, therefore, indicated that thermally-induced damage in the southeast floor region was not sufficient to cause an initial failure event.

The buckling failure of Column 79 was the initial failure event that led to the global collapse of WTC 7, as will be shown in the subsequent sections.

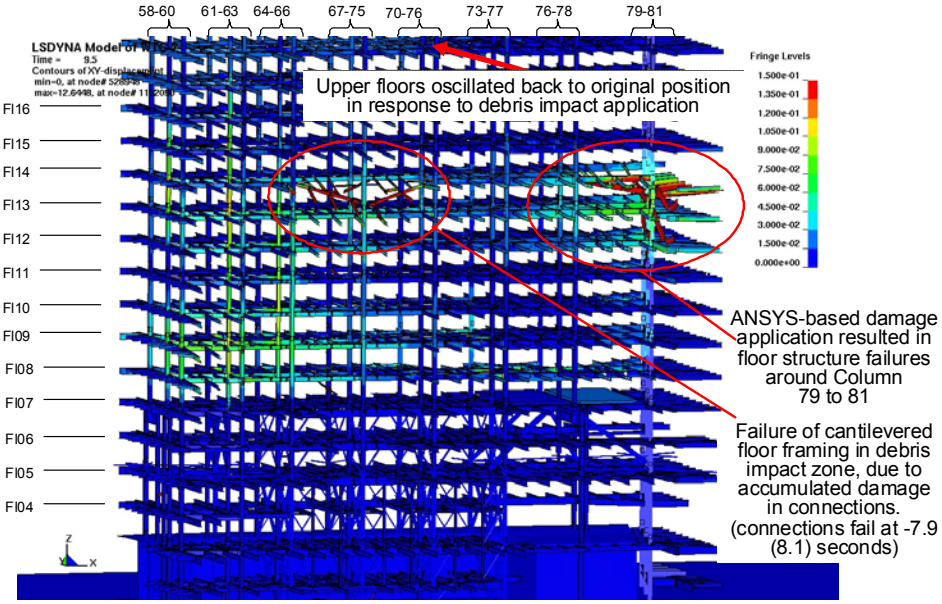

Figure 12–42. The collapse of Floors 13 and 14 in the northeast region [Time: -6.5 (9.5) s]

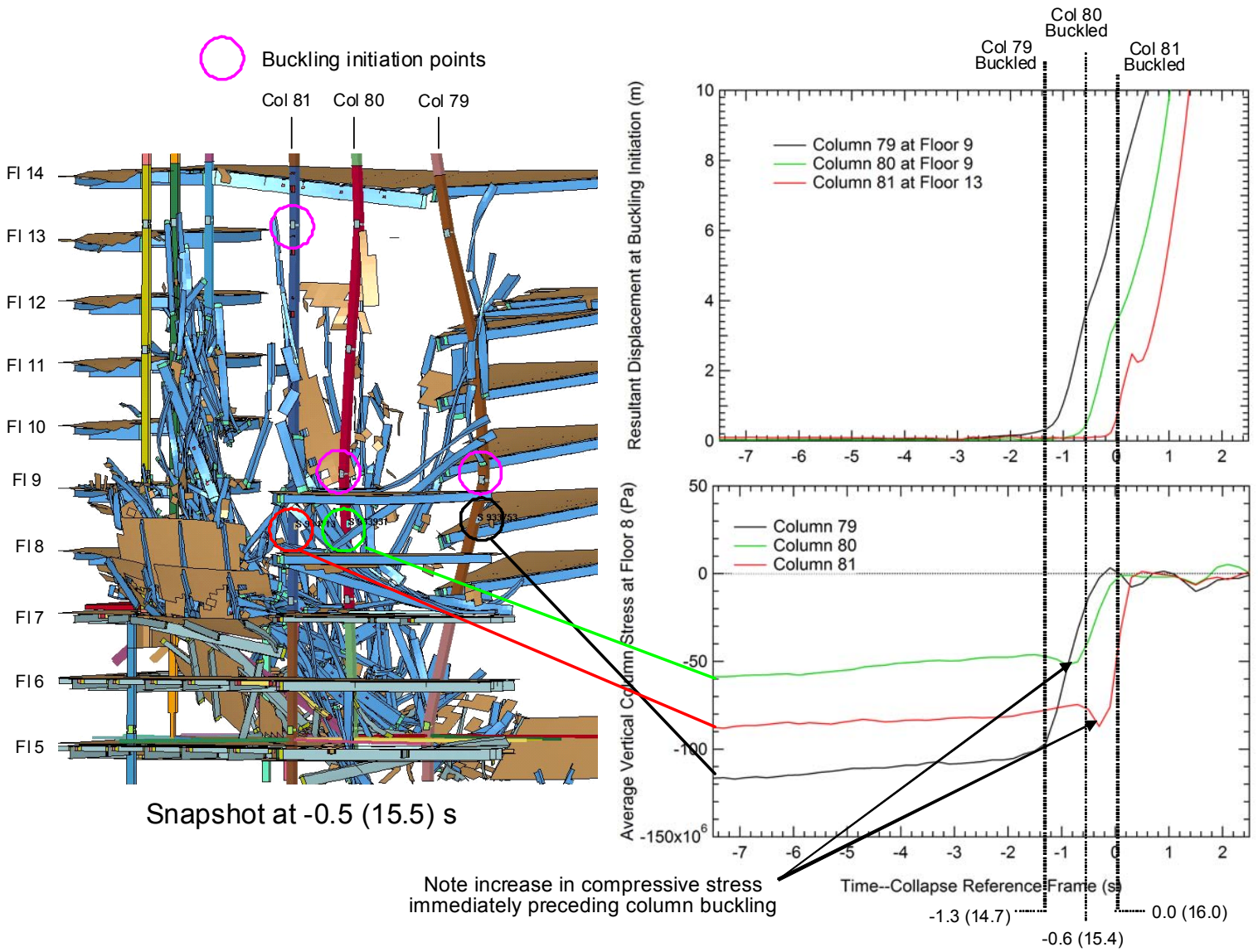

Figure 12–43. Column 79 to 81 stress and displacements.

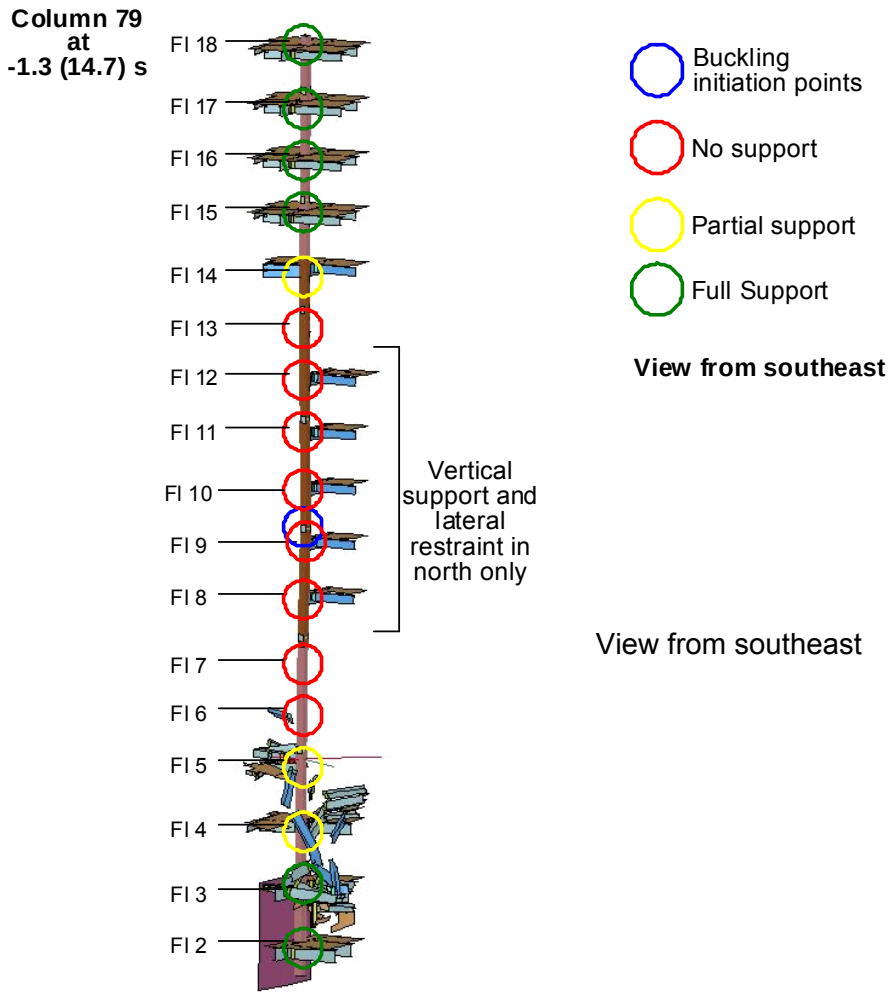

Figure 12–44. Column 79 lateral support status at time of buckling initiation.

Vertical Progression of Failure

The global collapse analysis showed that the buckling of Column 79 (the collapse initiation event) initiated vertical progression of failure of the floor systems on the east side all the way up to the top of the building. Buckling of Column 79 led to a cascading failure of adjacent interior Columns 80 and 81 on the east side of the building:

- Once Column 79 buckled, the column section above Floor 14 began to descend downward. Column 79 began moving downward at the roof level approximately 0.2 s after Column 79 buckled and 0.6 s before Column 80 buckled.

- As Column 79 moved downward, the floor framing adjacent to Column 79 was pulled downward, which led to the observed kink in the East Penthouse roof framing on the north side.

- As Column 79 moved downward, the floor framing connections to interior (Column 80 and Column 76) and exterior columns (Column 44) failed under increasing tensile in-plane floor forces, resulting in a vertical progression of failure of the floor systems around Column 79.

- Column 80 became laterally unsupported in both directions between Floors 5 to 15, as a result of the progressive floor system failures. Column 80 buckled about 0.8 s after Column 79 buckled.

- Column 81 became laterally unsupported in both directions between Floors 7 to 15, as a result of the progressive floor system failures. Column 81 buckled about 1.3 s after Column 79 buckled.

- As Columns 79, 80, and 81 each buckled, their column sections above Floor 14 began to descend downward and pulled the floor structures downward with them, thereby creating a vertical progression of floor collapses that spread across the entire east region of WTC 7.

- The East Penthouse, which was supported by Columns 79, 80, and 81, fell downward.

Figure 12–45 shows that after Column 79 buckled, it started moving downward at the roof level 0.2 s later. This led to a kink in the East Penthouse roof framing, as shown in Figure 12–46, that was visible in videos taken from the north 1.1 s later.

The cascading failures of these floor segments surrounding Column 79 on Floors 6 to 14 led to increased unsupported length in Column 80. Column 80 became laterally unsupported, as shown in Figure 12–47. Column 80 buckled about 0.8 s after Column 79 buckled, as shown in Figure 12–43.

In a similar fashion, Column 81 became laterally unsupported in both directions between Floors 7 to 15, as a result of the progressive floor system failures that occurred as both Columns 79 and 80 buckled (Figure 12–47). Column 81 buckled about 1.3 s after Column 79 buckled, as shown in Figure 12–43. In addition to axial compressive loads that could cause buckling, the columns were in a dynamic environment where lateral loads from falling debris and failure of girder connections occurred. These lateral perturbations aided the onset of column buckling. Note that Columns 80 and 81 buckled after the vertical progression of floor failures around Column 79.

As Columns 79, 80, and 81 each buckled in turn, their column sections above Floor 14 began to descend downward and pulled the floor structures downward with them, thereby creating a vertical progression of floor collapses across the entire east region of WTC 7. The East Penthouse, which was supported by Columns 79, 80, and 81, fell downward.

Figure 12–48 shows a view of the interior of WTC 7 from the southwest from the ground up to Floor 18. The figure shows the vertical progression of floor and column failures on the east side of the building, following the buckling of Columns 79, 80, and 81.

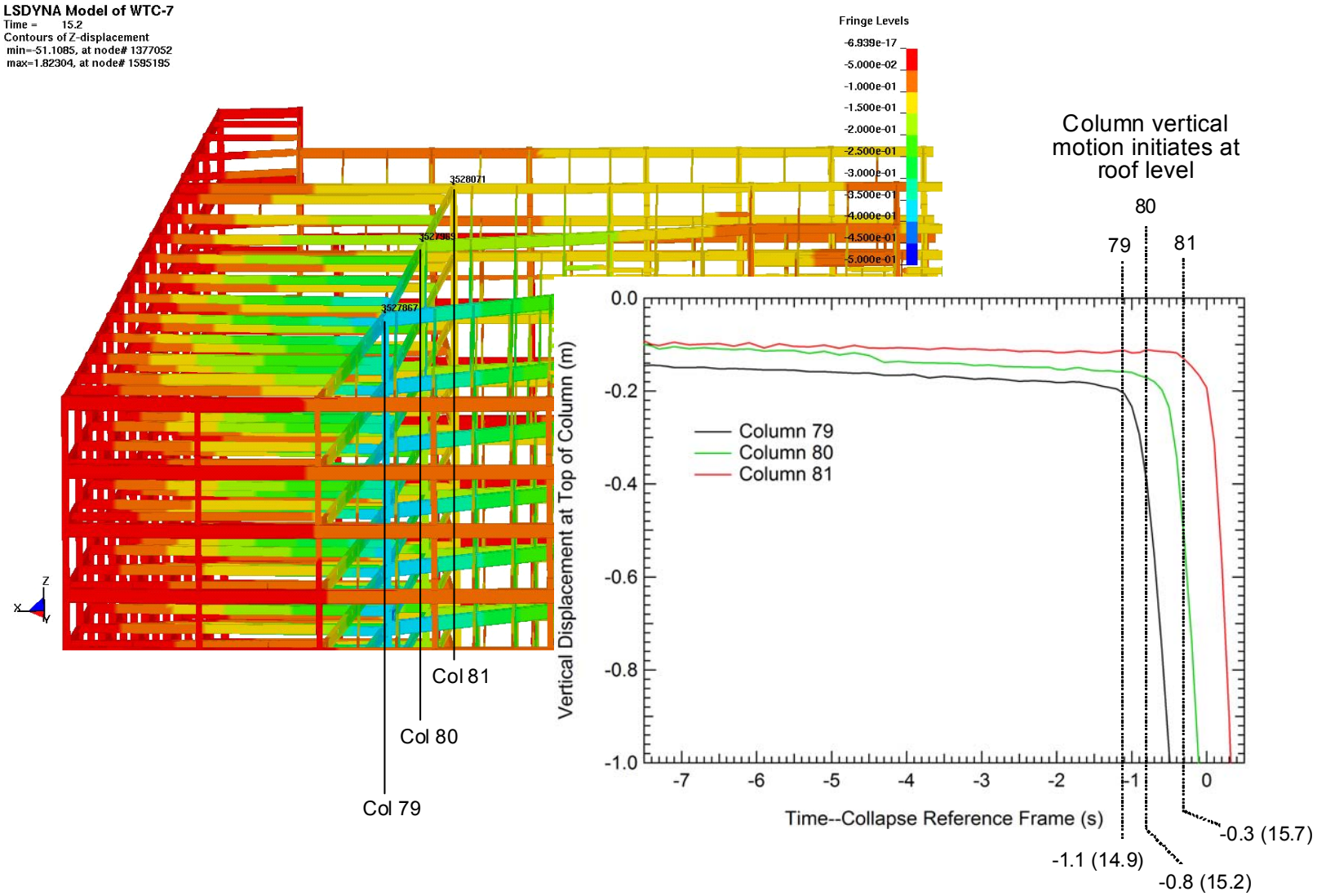

Figure 12–45. Column 79-81 vertical displacement with contours from -0.5 m to 0 m.

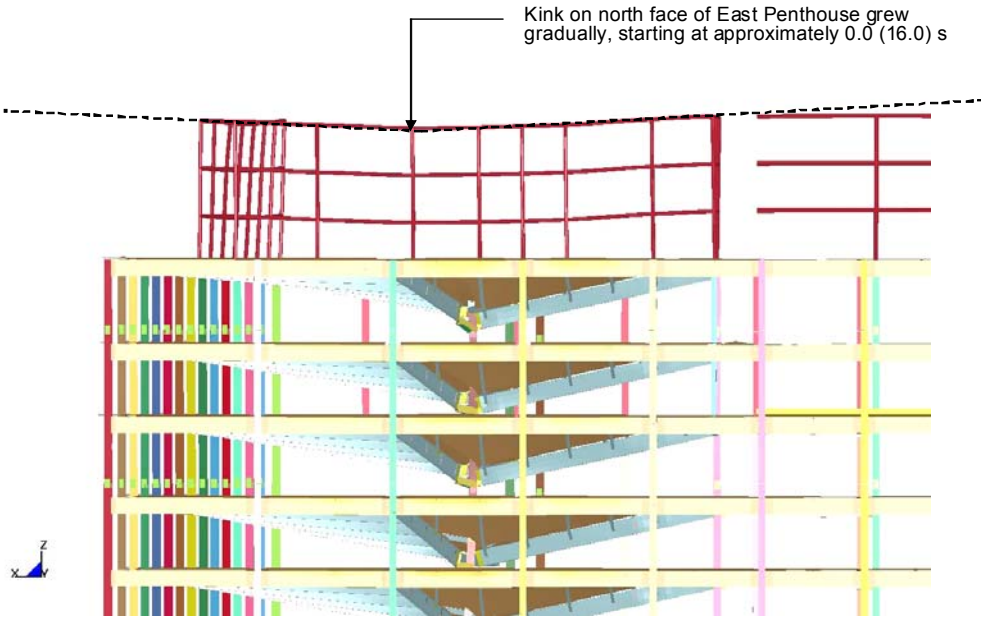

Figure 12–46. Kink on East Penthouse as it moves downward [Time 0.2 (16.2) s]. View from north.

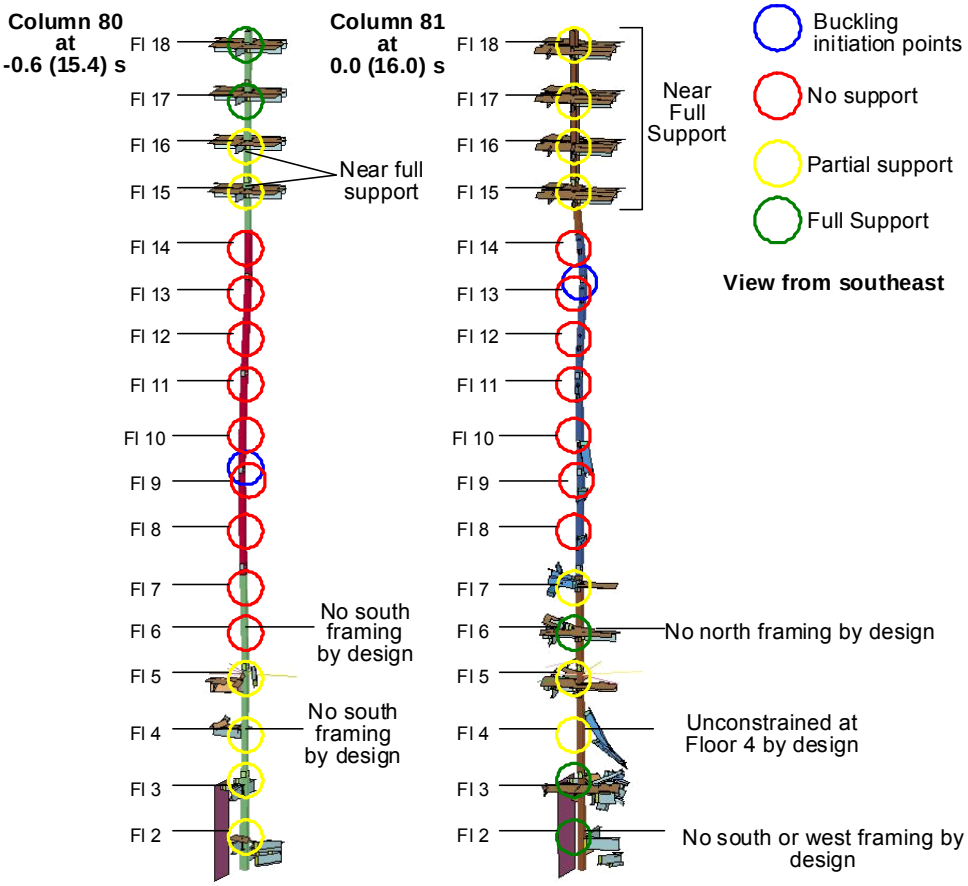

Figure 12–47. Columns 80 and 81 lateral support status at time of buckling initiation.

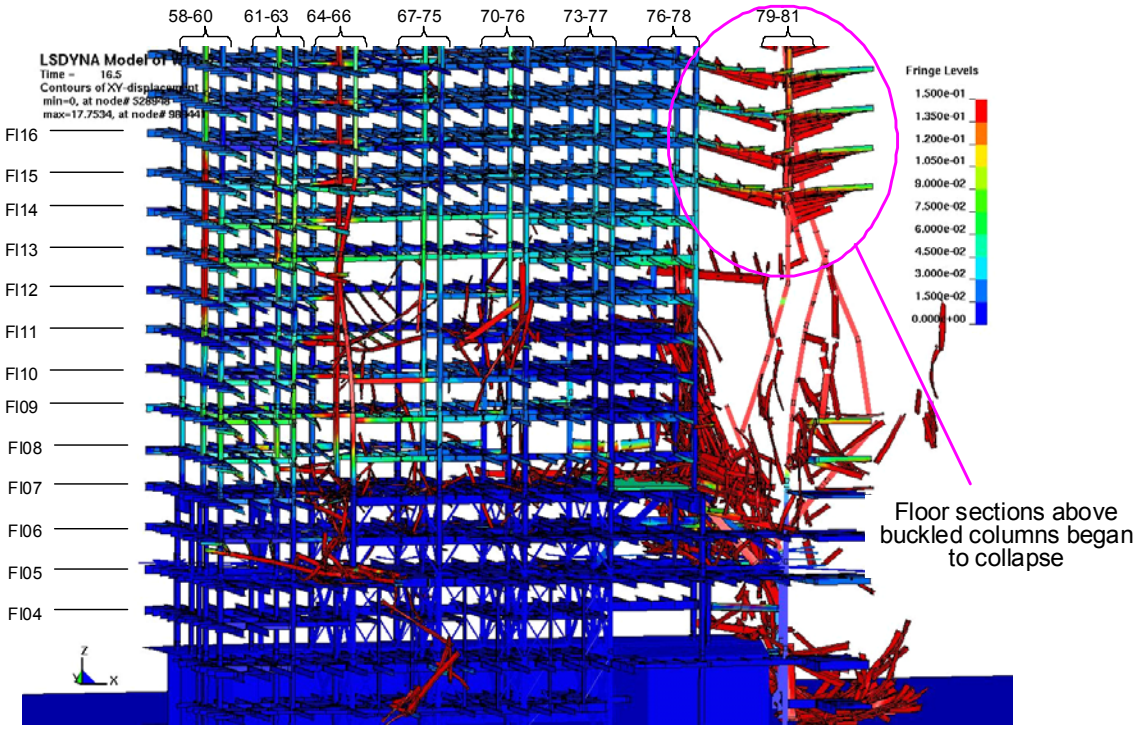

Figure 12–48. Vertical progression of failures on the east side of the building [Time: 0.5 (16.5) s].

Horizontal Progression of Failure

Following the collapse initiation event and vertical collapse progression, the failures progressed westward through the following mechanisms:

- Interior column buckling failures continued to propagate across the core in the lower floors from east to west, due to (1) loss of lateral support from floor system failures, (2) impact of falling debris from adjacent floors and columns, and (3) load redistributed from other buckled columns.

- During the vertical progression, the falling floors pulled on adjacent columns until the floor connections failed on the east side of Columns 76, 77, and 78.

- Truss 2 collapsed due to accumulated weight and impact loads from falling debris. The collapse of Truss 2 precipitated the buckling of Columns 77 and 78, which together with Column 76 had already lost lateral support.

- The occurrence of this westward progression indicates that the failure of Truss 2 was not essential to the failure of Columns 77 and 78, as they would have buckled in a similar fashion to the other columns.

During the vertical failure progression, the falling floors pulled on adjacent columns until the floor connections failed on the east side of Columns 76, 77, and 78, resulting in a loss of lateral support on the east side, as shown in Figure 12–49. Additionally, debris from floor systems and columns fell from the

upper floors, and impacted adjacent intact columns and floors, including Truss 1 and Truss 2. The accumulation of debris and debris impacts eventually caused Truss 2 to fail, as shown in Figure 12–50 and Figure 12–51.

Figure 12–50 shows the failure of the Truss 2 east diagonal between Columns 77 and 80. Most of the fallen debris is removed from view for clarity. Truss 2 supported Column 77 and girder MG-23, which was connected to Columns 77 and 78A and supported Column 78 (see Figure 12–12). Truss 1, which can be seen behind Truss 2, had similar construction with diagonal members, and supported Column 76 (see Figure 12–11). Unlike Truss 2, Truss 1 did not collapse in the analysis.

Figure 12–51 illustrates the structure after the diagonal member of Truss 2 failed and plots the axial force in the diagonal member. The plot shows two large debris impacts that caused sudden changes in axial force.

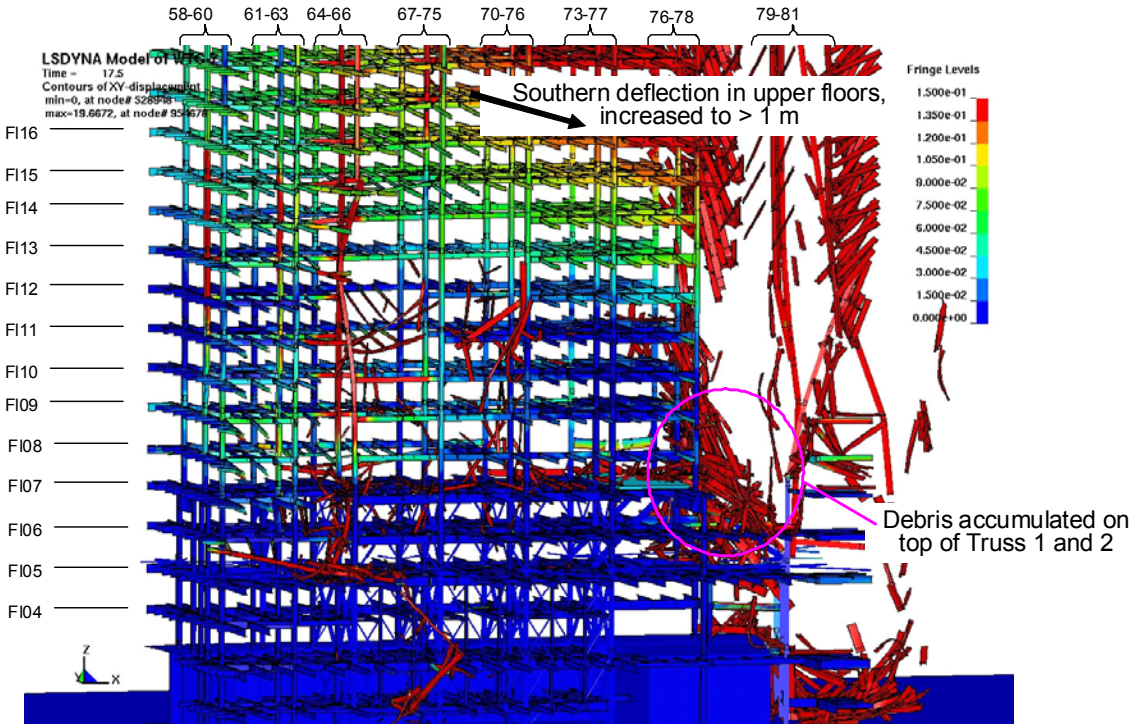

Figure 12–49. Debris from the vertical progression falling onto the lower floors, Trusses 1 and 2, and Columns 76, 77, and 78 [Time: 1.5 (17.5) s].

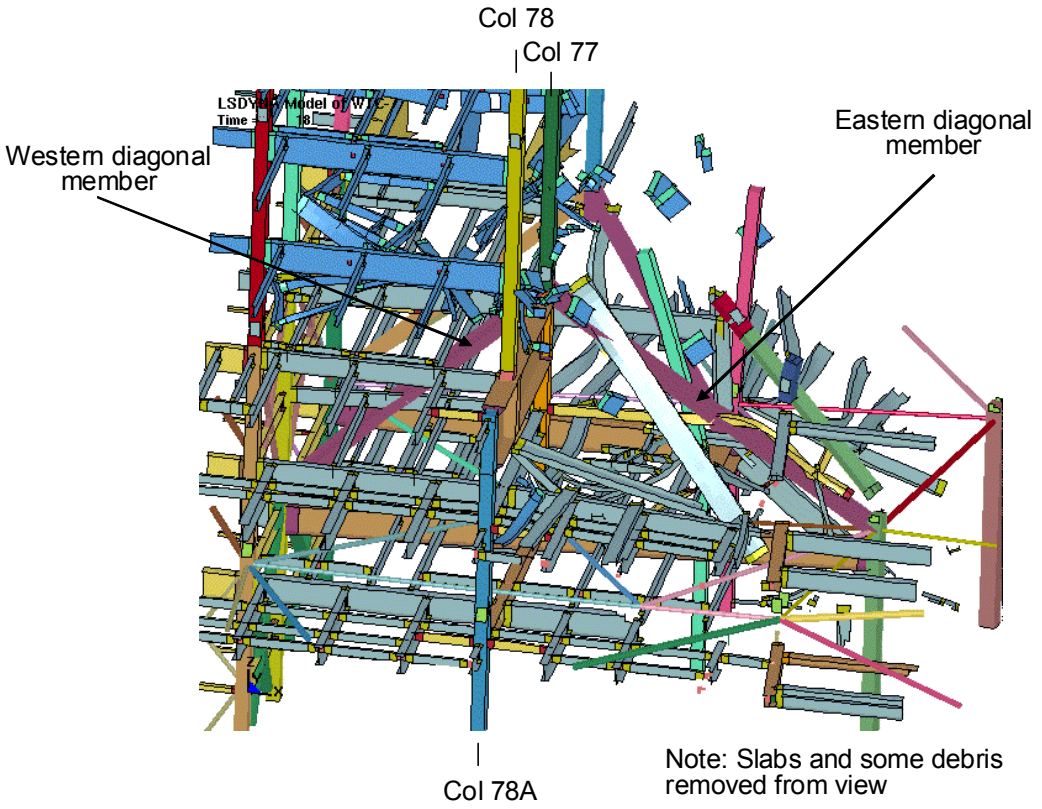

Figure 12–50. Failure of Truss 2 east diagonal. View from southeast and above.

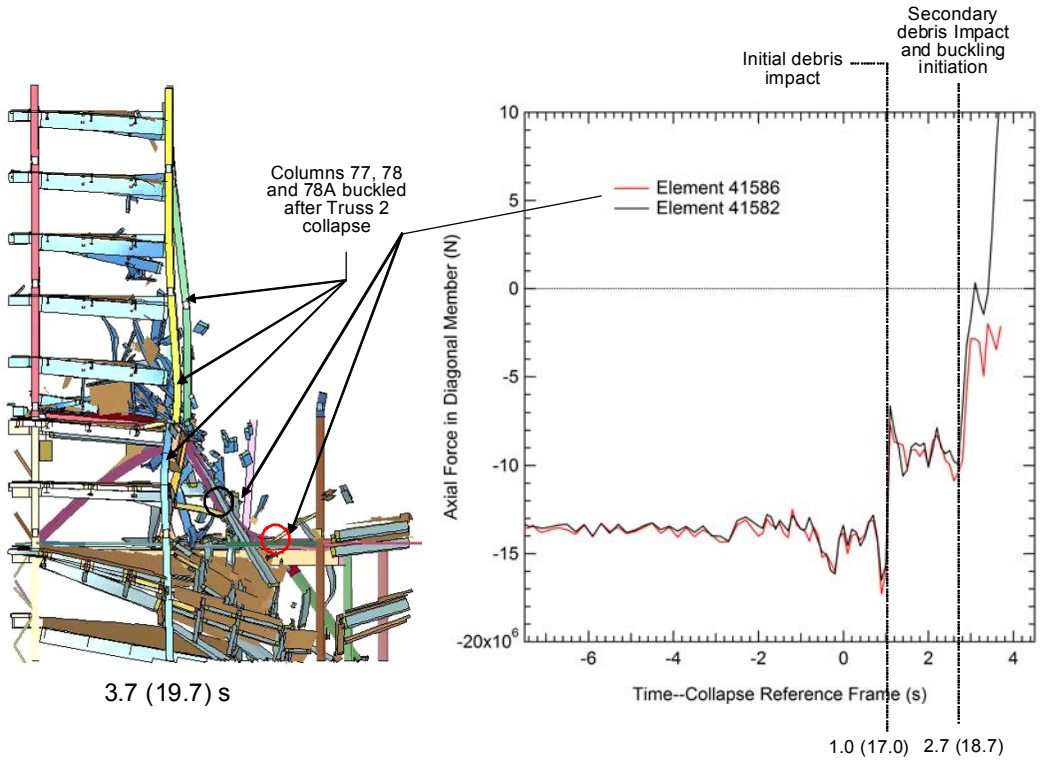

Figure 12–51. Truss 2 collapse. View from south (most of debris removed from view).

The failure of Truss 2 precipitated the buckling of Columns 77 and 78, as shown in Figure 12–52. The loss of the Truss 2 diagonal resulted in a loss of support for Column 77. When the Truss 2 diagonal member failed, support for the girder MG-23 at Column 77 was also lost, which subsequently led to loss of support for Columns 78.

Column 76 failed in the next second, as indicated in Figure 12–53, due to loss of lateral support as the floor connections failed, the impact of falling debris, and load redistribution from adjacent columns.

Columns 73 to 75 buckled in the next second, as shown in Figure 12–54, as the process continued where there were sequential failures of each north-south row of interior columns, due to loss of lateral support as floor connections failed, impact of falling debris, and load redistribution from adjacent failing columns.

Column buckling and floor failures continued to propagate from east to west across the core in the lower floors, until all the interior columns buckled between Floors 9 and 14. This occurred 6.5 s after the kink was observed in the East Penthouse, and 6.7 s after Column 79 buckled, as indicated by Figure 12–55.

Figure 12–56 shows that west interior Columns 59, 62, 65, and 66, which were damaged after the debris impact by WTC 1 and by thermally-induced damage from the fires, did not buckle until 4.7 s after the kink was observed in the East Penthouse, or 6 s after Column 79 buckled. The west interior columns did not buckle until these columns were affected by the horizontal progression of failures due to loss of lateral support as floor connections failed, impact of falling debris, and the load redistribution from adjacent failing columns.

The occurrence of this westward progression also indicates that the failure of Truss 2 was not essential to the failure of Columns 77 and 78, as they would have buckled similar to the other interior columns.

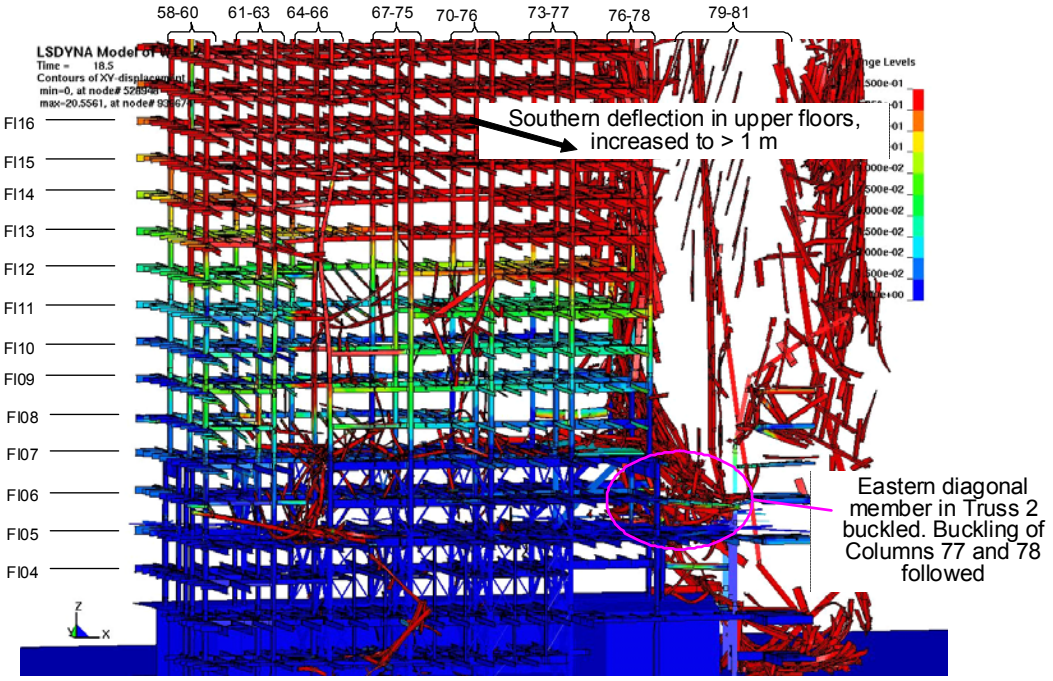

Figure 12–52. Failure of Columns 77 and 78 due to failure of Truss 2 from debris impact [Time: 2.5 (18.5) s].

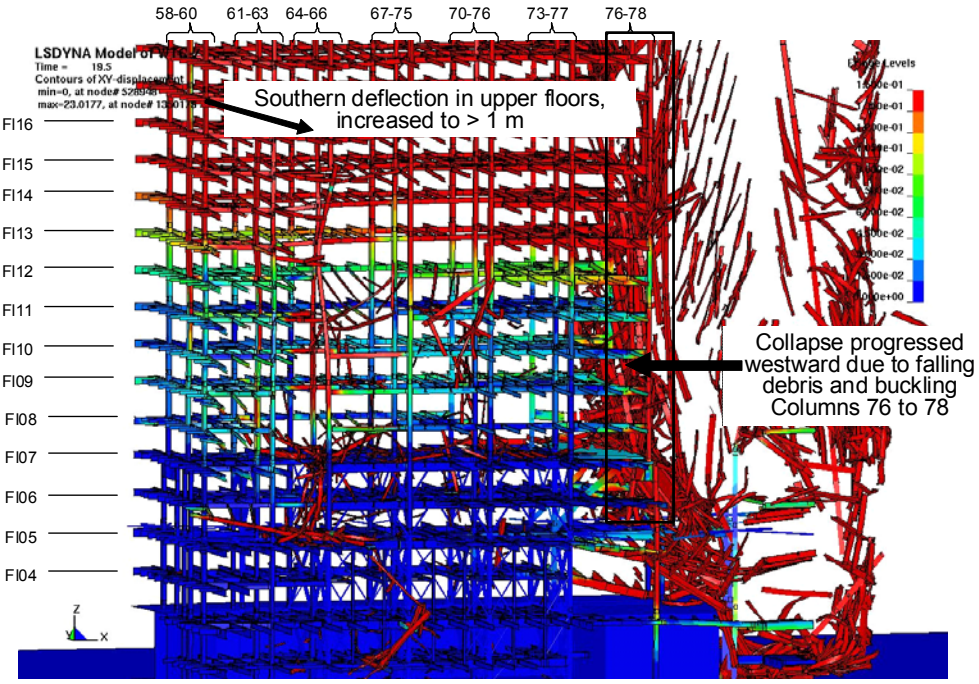

Figure 12–53. Buckling of Column 76 from the load transfer and debris impact from the buckling of Columns 79 and 77 [Time: 3.5 (19.5) s].

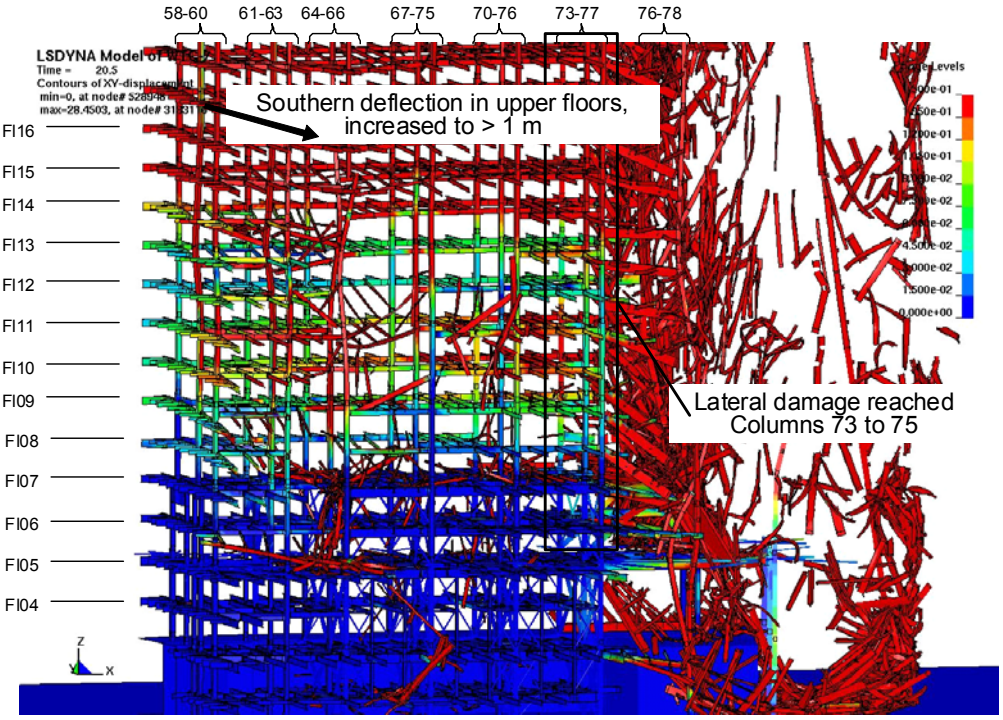

Figure 12–54. Failure of Columns 73 to 75 from the load redistribution and debris impact [Time: 4.5 (20.5) s].

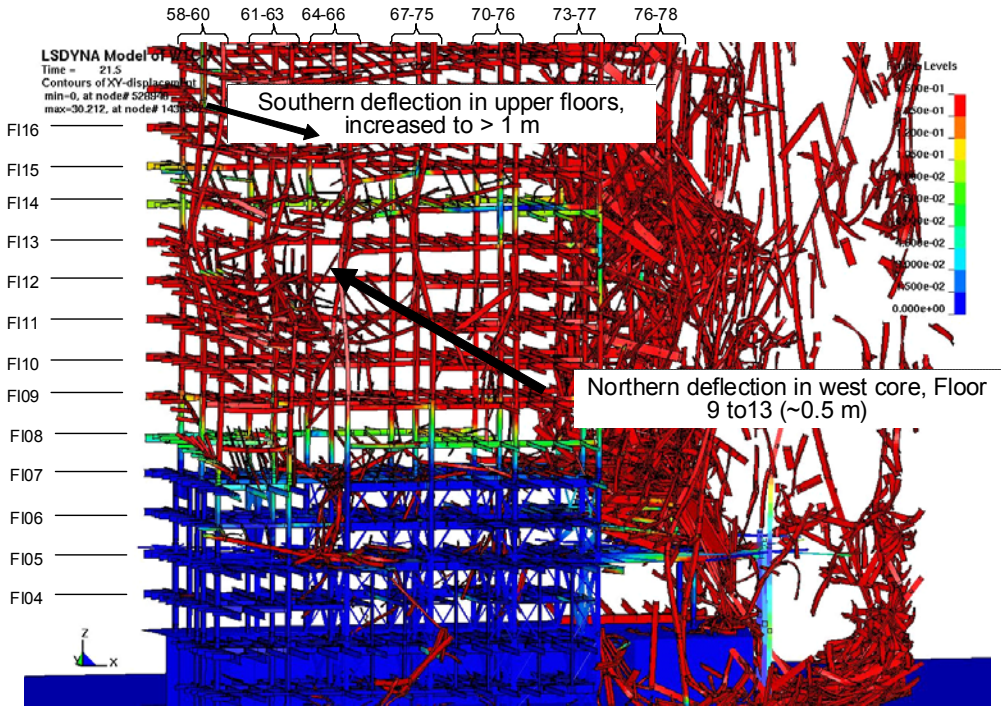

Figure 12–55. Buckling of all interior columns [Time: 6.5 (22.5) s].

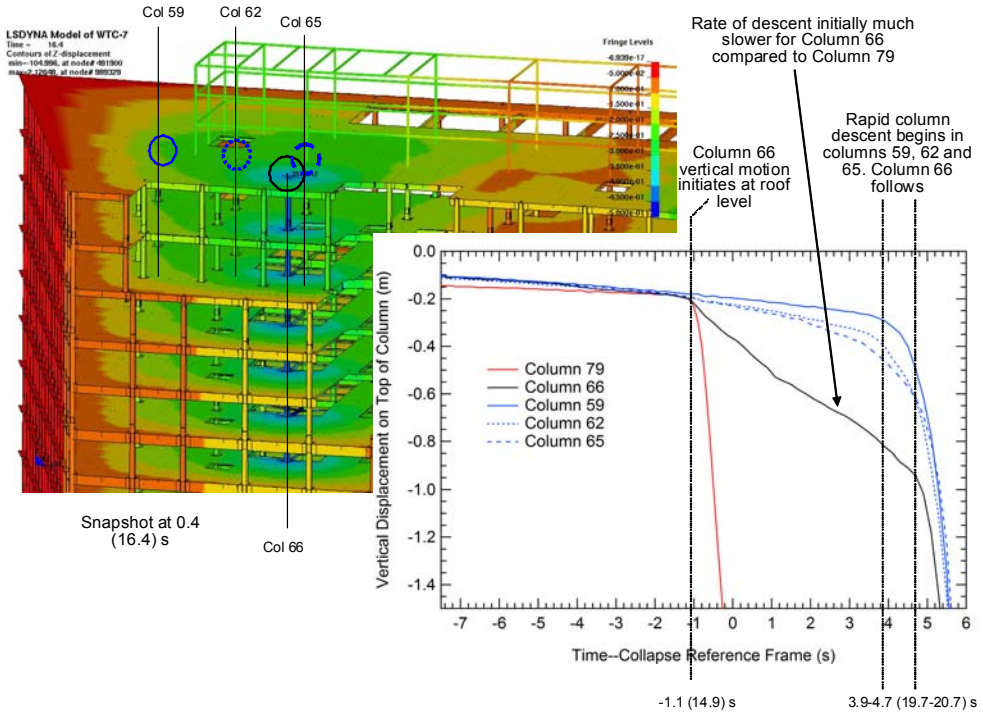

Figure 12–56. Western core column vertical displacements (contours: -0.5 to 0 m).

To better understand the progression of interior column failures, Figure 12–57 illustrates how column loads changed with time in the global collapse analysis. Column loads were grouped as shown. Figure

12–57 shows the general westward progression of interior column failures. Corresponding loads for the column groups 1 to 5 during the horizontal progression of buckling are shown in Figure 12–58. Column group 1 (Columns 79, 80, and 81) failed at -0.5 s before the kink was observed in the East Penthouse, and column groups 1 to 5 had failed by 6.3 s. Column loads for column groups 6 to 8 are shown in Figure 12–59. Column group 7 failed at 4.3 s and column groups 6 to 8 had failed by 6.3 s. At this time, all the interior columns had buckled.

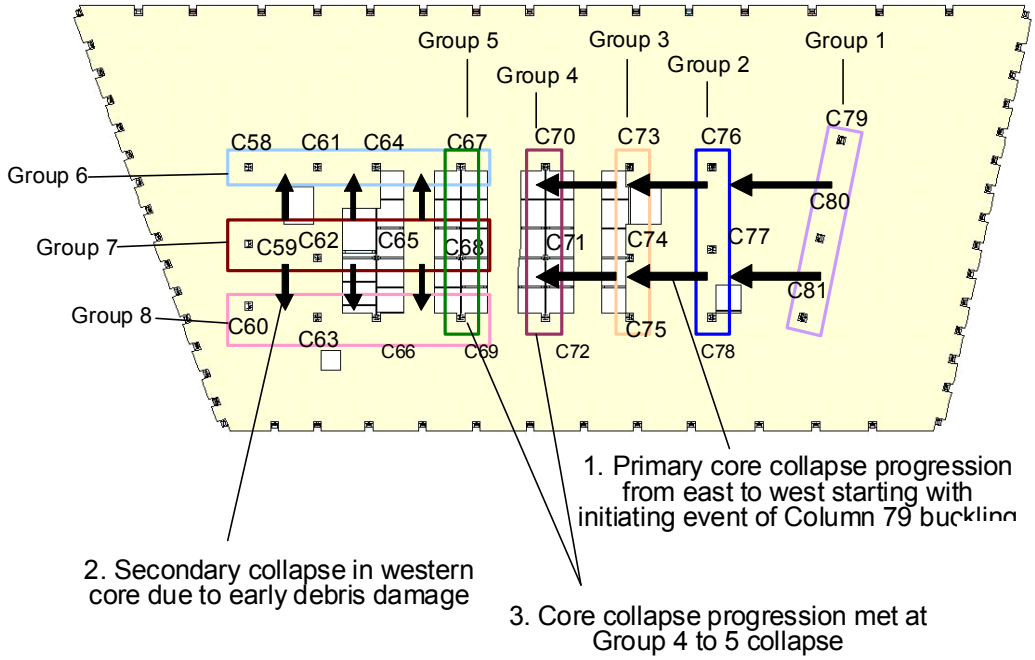

Figure 12–57. Horizontal progression of column buckling and interior column groupings.

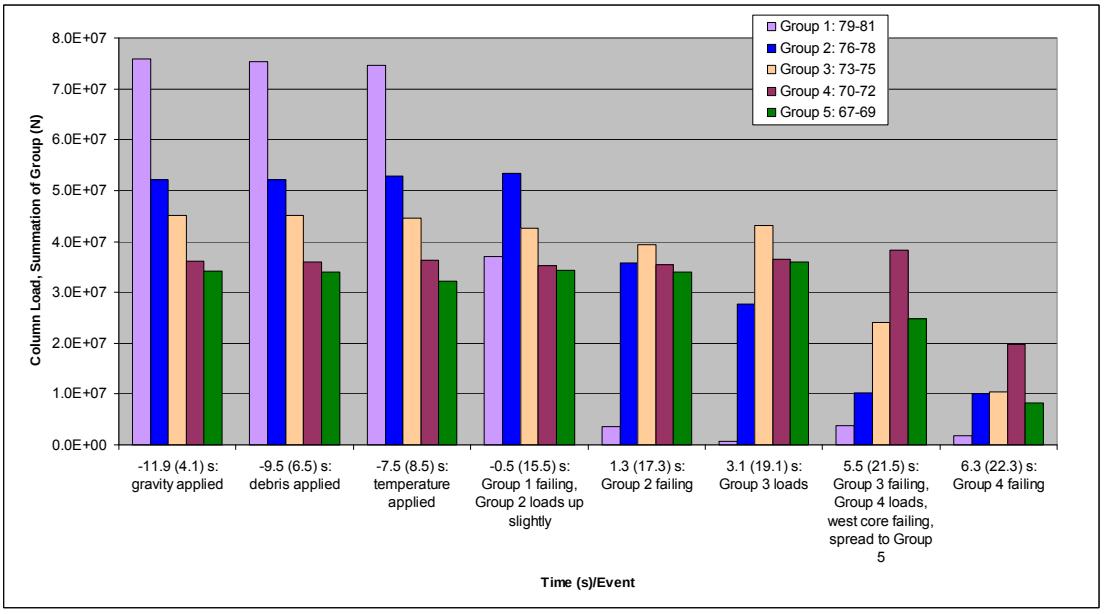

Figure 12–58. Interior column loads illustrating east to west collapse progression.

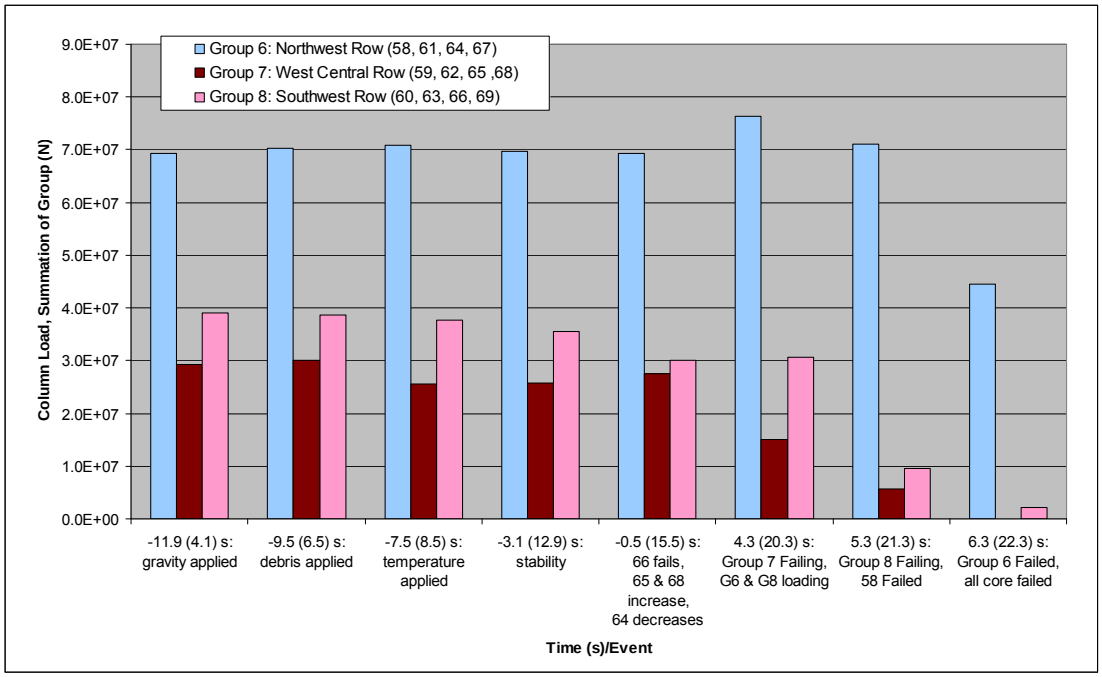

Figure 12–59. West interior column loads illustrating progression of failure.

Global Collapse

After the horizontal progression of column buckling in the core of WTC 7, the exterior columns buckled at the lower floors, completing the global collapse sequence as follows:

- As the interior columns failed, the exterior columns (on the west face) buckled inward at the lower floors as a result of floor pull-in forces due to the downward movement of the building core. The floor connections to the columns had not yet failed in this region because there were no fires observed on the west side on Floors 10 through 14 at any time during the day, and the floors were able to pull the exterior columns inward because the connections were still intact.

- Exterior column buckling began at the southwest corner Column 14, adjacent to the debris impact zone, between Floors 10 and 12. The exterior columns adjacent to the (seven) columns severed in the southwest region due to the collapse of WTC 1 were the first to buckle because additional load was distributed to them as a result of the damage.

- The south and west exterior columns buckled first, followed by the north and east face columns.

- All exterior columns buckled between approximately Floors 7 and 14.

- Once column support was lost in the lower floors, the remaining exterior structure above began to fall vertically as a single unit.

The buckling of the interior columns in the global collapse analysis was followed by the buckling of the exterior columns.

Figure 12–60 shows a schematic view of Floor 8 that highlights the exterior columns that were used to track the column load history for each face. Also noted on the figure is the debris impact zone from the collapse of WTC 1, which shows the southwest columns that were severed. Loads were extracted just above Floor 8 for three columns per face and were averaged to generate the loads shown in Figure 12–61.

Figure 12–61 shows that column loads increased as gravity loads were applied (compressive loads are negative). As indicated at 4.5 s (LS-DYNA calculation time), there was an increase in compressive loads on the west and south faces of the building after debris impact damage was applied. As Columns 79, 80, and 81 buckled and the floor systems failed on the east side of the building (at 15 s to 16 s), column loads reduced in the north and east faces. The west face column loads were dominated by the loads in Column 14, which was adjacent to the severed columns in the southwest corner. At 21.5 s, exterior column buckling began at Column 14, between Floors 10 and 12. The exterior columns adjacent to the (seven) columns severed in the southwest region due to the collapse of WTC 1 were the first to buckle due to the increased loads in these columns following the debris impact damage. The south and west face columns buckled first, followed by the north and east face columns.

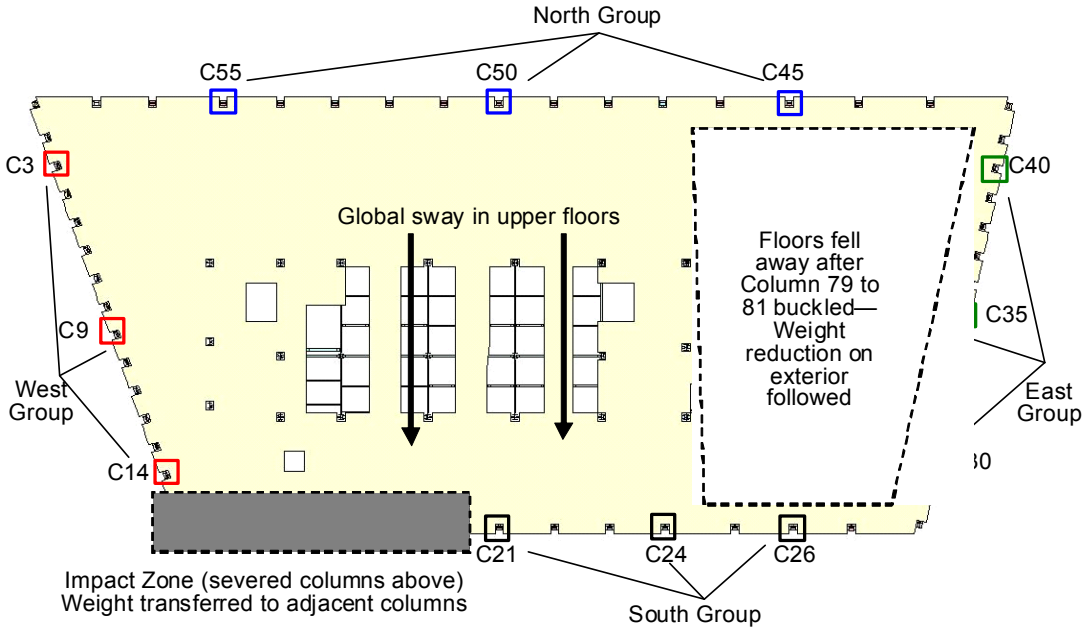

Figure 12–60. Exterior columns used in load groupings.

The floor connections to the west face columns had not failed above Floor 9 because no fires were observed on the west side of Floors 10 through 14. The intact floor framing pulled the exterior columns inward as the interior columns fell downward during the horizontal progression of failure stage and the floors pulled on the exterior columns. As the interior columns buckled across the building, the exterior columns were left laterally unsupported normal to the east, south, and north faces. Exterior column buckling spread from column to column, as loads were redistributed, until all the exterior columns had buckled between Floors 7 and 14 within approximately 2 s.

When all the exterior columns had buckled, the entire building above the buckled-column region moved downward as a single unit, resulting in the global collapse of WTC 7. Detailed views of the lower exterior column buckling are shown in Figure 12–62.

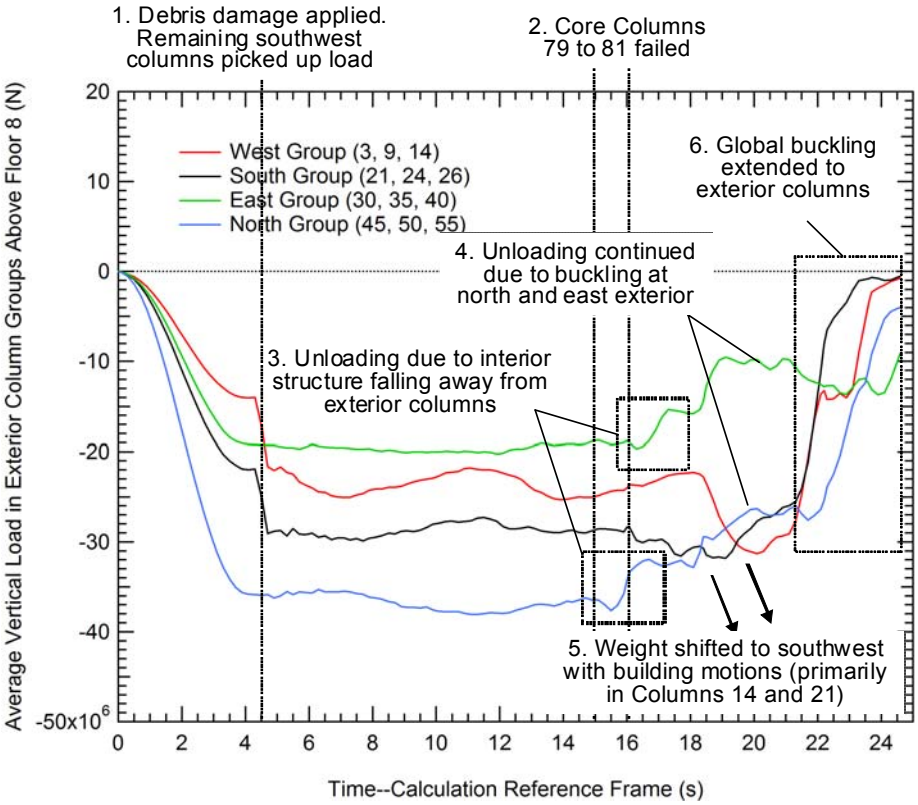

Figure 12–61. Average exterior column loads by group.

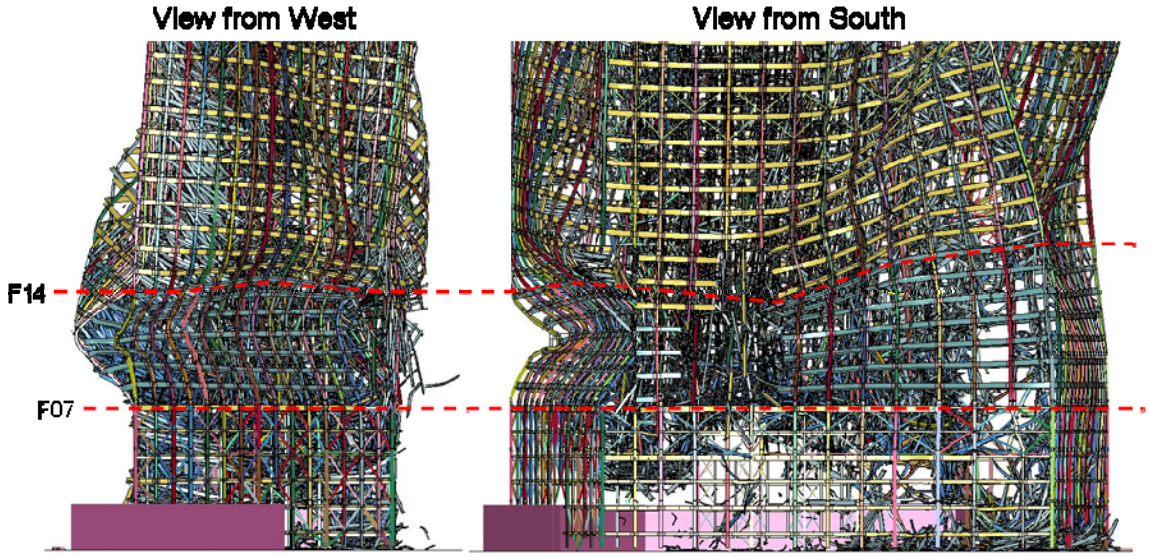

Figure 12–62. Exterior column buckling at lower floors (slabs removed from view).

12.4.5 Global Analysis Results with Earlier Fire Induced Damage

A global analysis similar to the analysis in Section 12.4.4 was conducted with the same loading sequence and parameters, except that the fire-induced damage from the 16 story ANSYS analysis (Chapter 11) was input at 3.5 h, instead of 4.0 h, to determine if an earlier fire-induced damage state was sufficient to initiate a global collapse of WTC 7.

The structural damage at 3.5 h in the ANSYS analysis had floor failures in the southeast corner at Floors 8, 13, and 14 and connection damage at Floor 12. After applying the 3.5 h ANSYS damage at 8.5 s, a few girders connected to Columns 79, 80 and 81 in Floors 12 to 14 fell to floors below, as shown in Figure 12–63. However, the damage was not sufficient to fail other floor structures below Floor 12 or to propagate a vertical collapse. Vertical displacement contours in Figure 12–63 show some significant vertical displacements, but the structure was stable at the end of the analysis. Comparison to Figure 12–43 from the 4.0 h ANSYS damage case (Section 12.4.4) shows that, for the 3.5 h damage case, the overall damage was significantly less severe in the floors surrounding Columns 70 to 81.

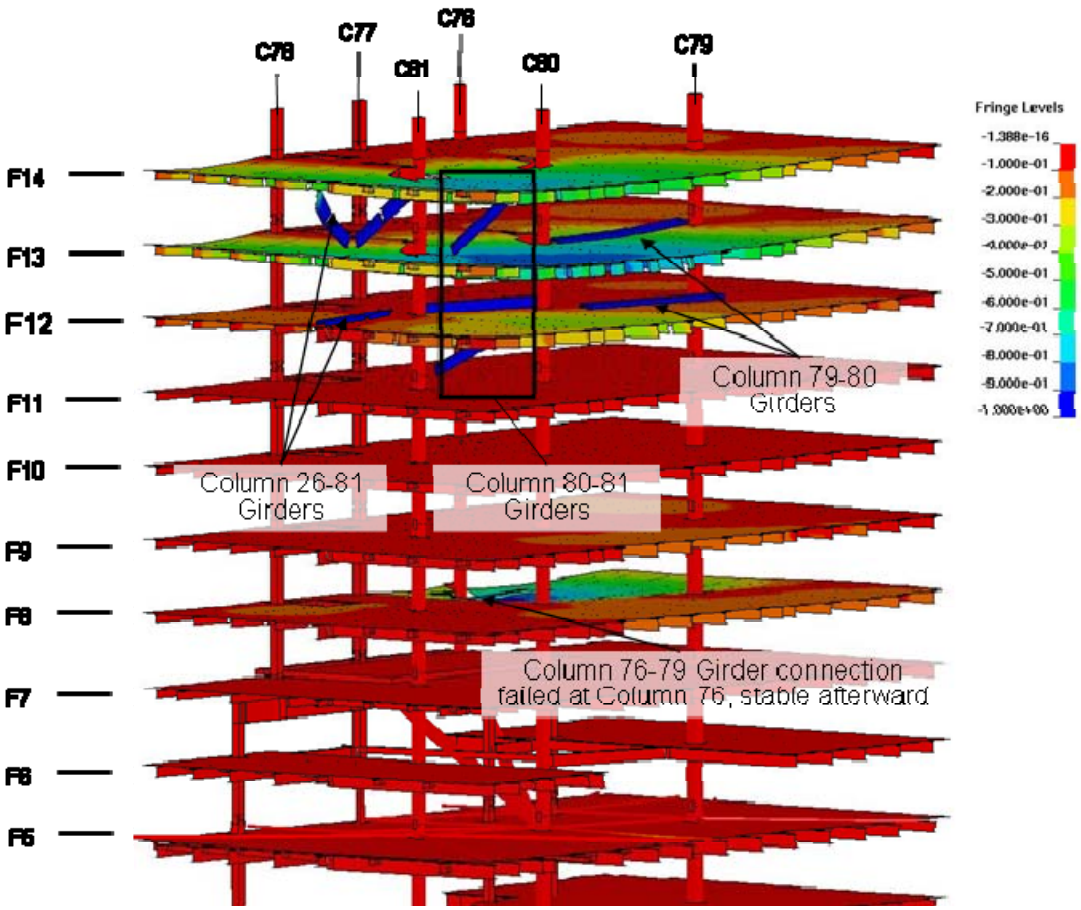

Figure 12–63. Floor framing damage around Columns 76 to 81 after stability has been reached -3.24 s (12.76 s). Contours of vertical displacement shown -39 to 0 in. (-1 to 0 m).

Figure 12–64 illustrates the structural failures across the lower floors after the application of the 3.5 hr debris damage. Similar to the 4.0 h ANSYS analysis with debris damage (Figure 12–42), there was damage to connections at several west core column over 11 stories, which occurred during the WTC 1

debris impact damage application. However, the structure remained stable due to the lack of an initiating event (i.e., buckling of an interior column). The response of WTC 7 to the fire-induced damage at 3.5 h was not sufficient to cause an initiating event that would lead to global collapse.

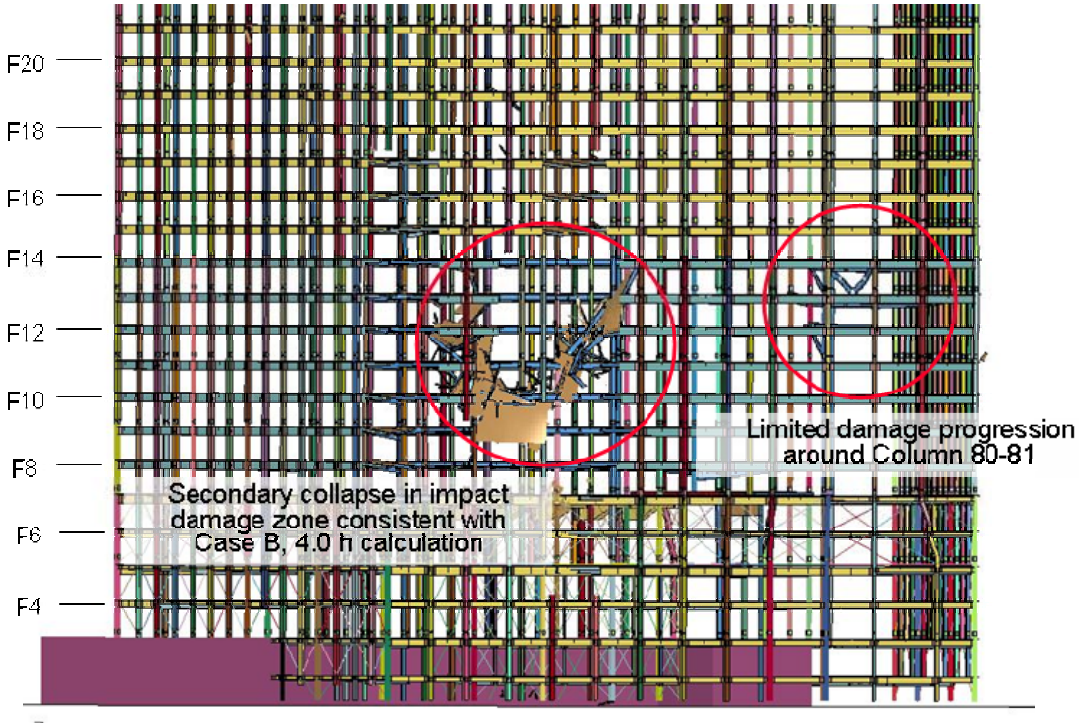

Figure 12–64. Lower floor damage in stable structure at -3.8 s (12.2 s). View from southwest.

12.4.6 Global Analysis Results without Debris Impact Damage

This global analysis was similar to the analysis in Section 12.4.4, except that the debris impact damage due to the collapse of WTC 1 was not included. The purpose of the analysis was to determine the contribution of debris impact damage to the global collapse sequence of WTC 7 and whether WTC 7 would have collapsed solely due to the effects of the fires.

As with the analysis in Section 12.4.4, the collapse reference frame is timed from the observed start of the downward motion of the East Penthouse. The timing reported in this section is shorter because the debris impact damage was not applied during initialization of the global analysis, thereby eliminating 2.0 s from the initialization process. The removal of the debris impact step shifted the East Penthouse kink time to 13.3 s in this analysis, compared to 16.0 s in the Section 12.4.4 calculation.

The initial failure event, vertical progression of failure, and early stages of the horizontal progression of failure occurred in the same order and at essentially the same times as those described for the global analysis in Section 12.4.4. This is illustrated in Figure 12–65 and Figure 12–66 which show the sequence of failure progression from 1.0 s after the application of fire-induced damage at -5.8 s (7.5 s) to 4.2 s after the kink in the East Penthouse was observed, or 3.2 s (17.5 s).

Figure 12–65 shows the structural response from just after application of the fire-induced damage to 1.3 s prior to the kink formation in the East Penthouse. The left and center images show the failures that started in Floors 13 and 14, and the cascade of floor failures that occurred subsequently, due to their thermally weakened condition. The right image shows the loss of lateral support around Column 79 and the start of Column 79 buckling. Similar response was shown in Figure 12–42 for the global analysis with impact damage. Note that in this stage of the analysis, relative to the analysis with debris impact damage, there was no early development of western core column buckling that was caused by the application of debris impact damage.

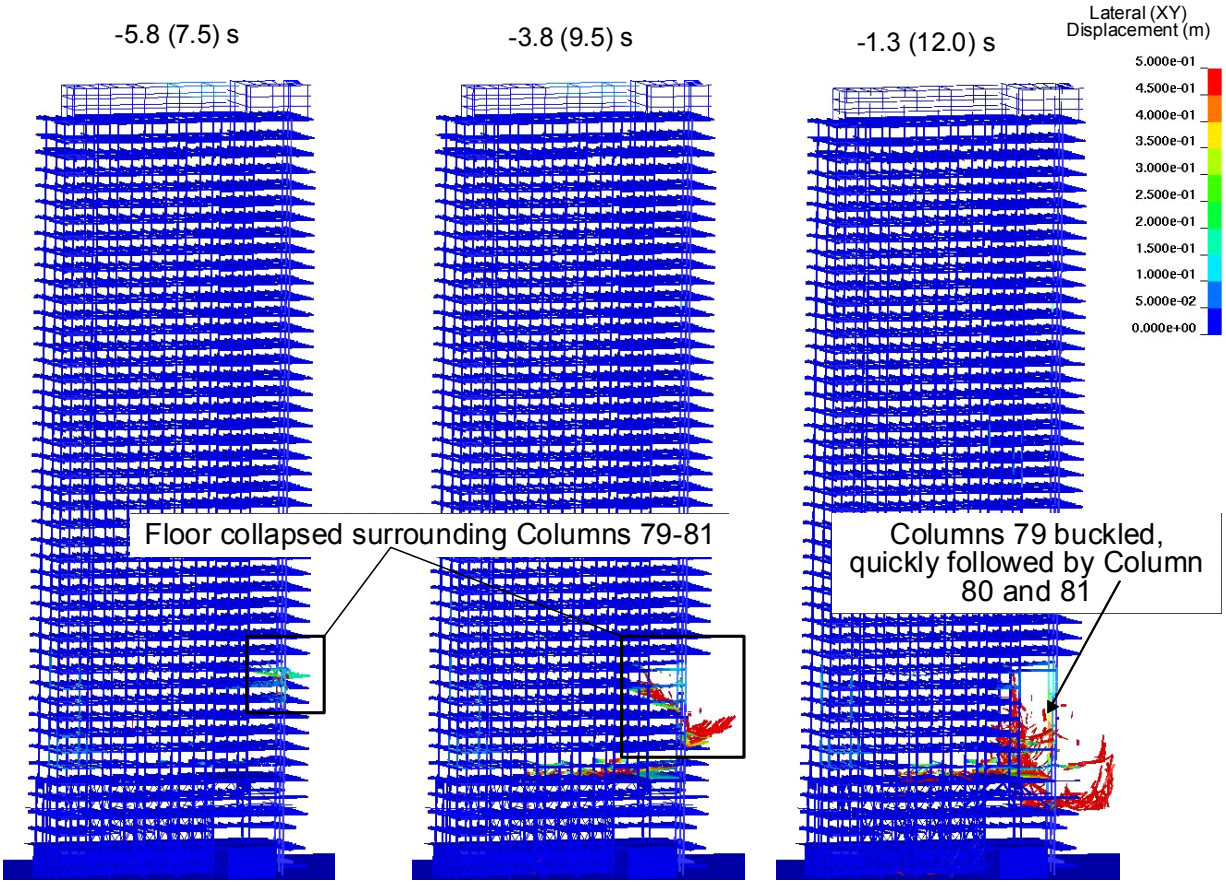

Figure 12–65. Core collapse sequence viewed from the south. Time: -5.8 s to -1.3 s (7.5 s to 12.0 s). Contours of resultant lateral displacement 0 in. to -20 in. (0 m to -0.5 m).

Figure 12–66 shows the structural response from 0.7 s (14.0 s), shortly after the East Penthouse kink was observed, to 3.2 s (17.5 s), when Columns 76 to 78 buckled as the horizontal progression of failure began. The left image shows the vertical progression of failure. The center image shows the loss of lateral support to Columns 76 to 78, as well as the failure of Truss 2, due to the effects of debris accumulation and impact during the vertical progression of failure. The right image shows the buckling of Columns 76 to 78. Similar responses were shown in Figure 11–49, Figure 12–49, and Figure 12–53 for the global analysis with impact damage.

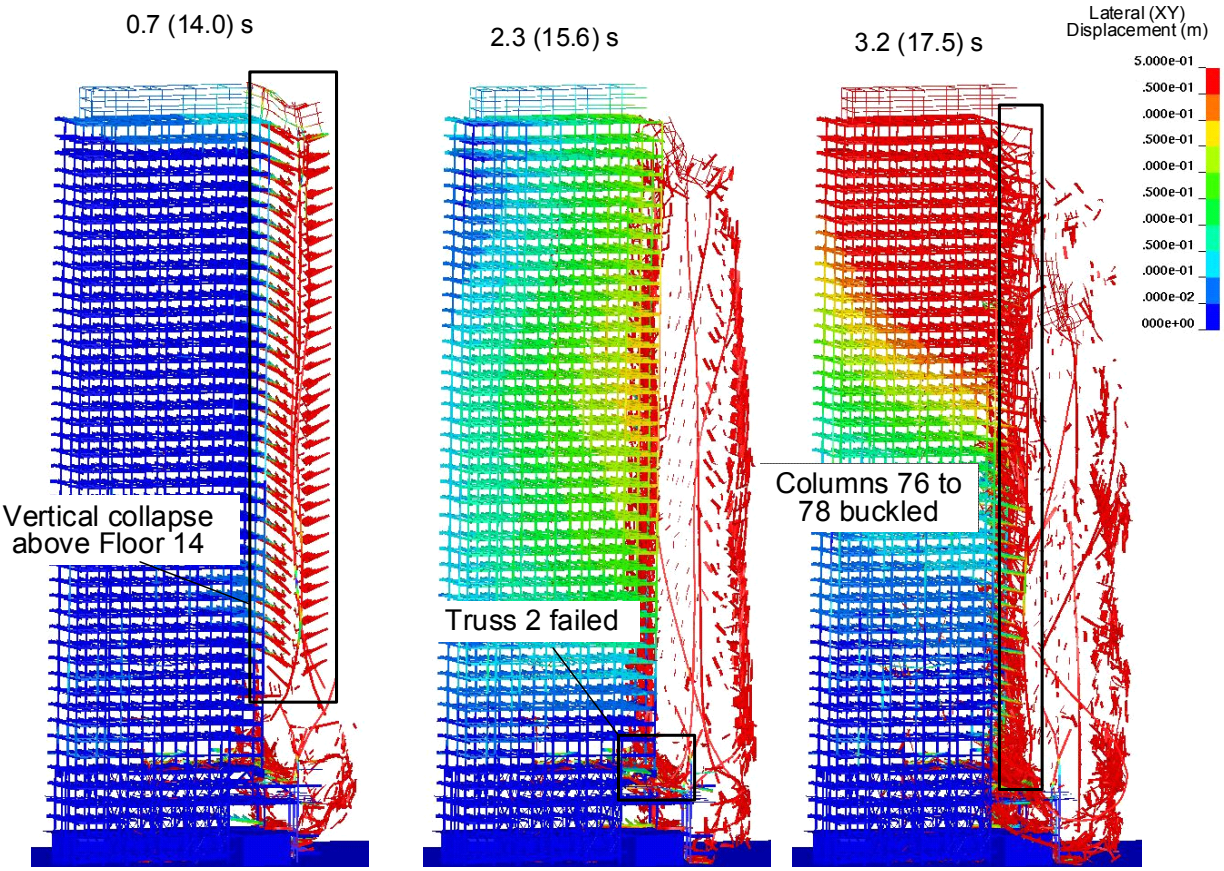

Figure 12–66. Core collapse sequence viewed from south. Time: 0.7 s to 3.2 s (14.0 s to 17.5 s). Contours of resultant lateral displacement 0 in. to -20 in. (0 m to -0.5 m).

The progression of horizontal failure in the analysis without debris impact damage was due to loss of lateral support as floors failed, the effect of debris impact from adjacent failing floors and columns, and load redistribution. The right image in Figure 12–67 shows that the screening wall fell downward prior to the West Penthouse (view is from the southwest), which is consistent with the observed sequence of events. In the analysis without impact damage, the horizontal progression continued to move westward after Columns 70 to 72 buckled. In the analysis with impact damage (Section 12.4.4), the horizontal progression moved westward until Columns 70 to 72 buckled, after which the damaged west core columns also buckled.

As the horizontal progression moved from east to west, some differences began to occur relative to the analysis with impact damage, as shown in Figure 12–67 and Figure 12–68. Some floors failed at mid-height of the building around Columns 73 to 75, leading to the buckling of some interior columns at this location, rather than at lower floors. Between 6.2 (19.5) s and 13.5 (26.8) s, the damage progressed westward and downward across the core as floor structures failed and fell onto the floors below. The horizontal progression in the analysis without debris impact damage moved from east to west over a longer duration. This was due to the lack of western core damage that was caused by debris impact damage in the earlier calculation.

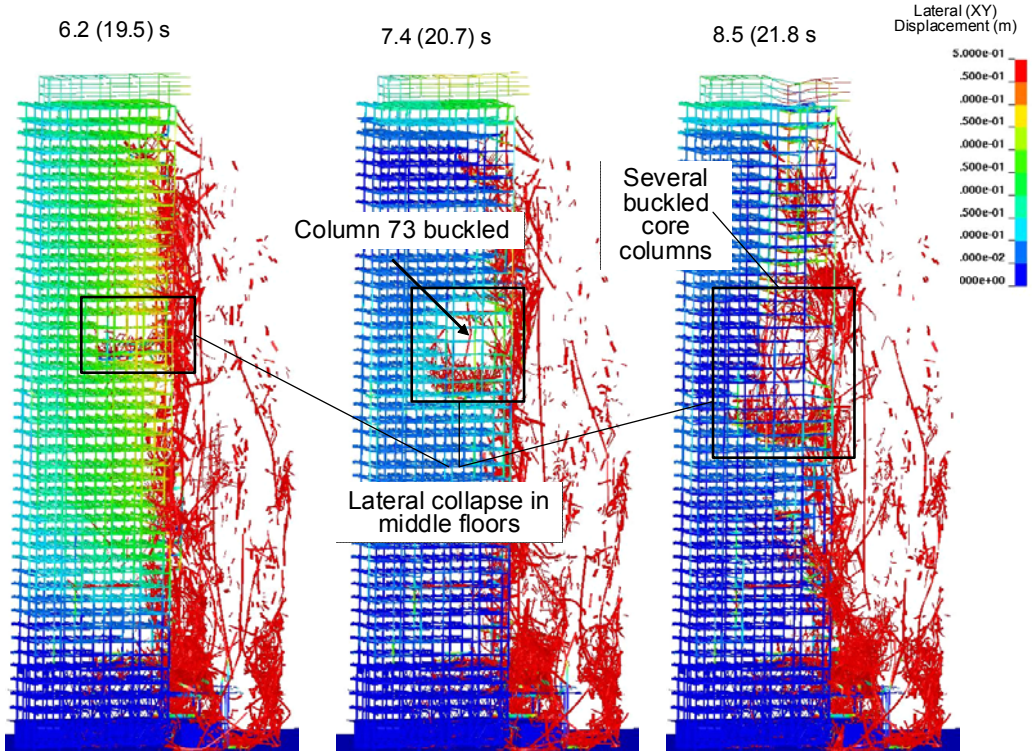

Figure 12–67. Core collapse sequence. Time: 5.5 to 7.8 s (21.5 to 23.8 s). Contours of resultant lateral displacement 0 to -20 in. (0 to -0.5 m).

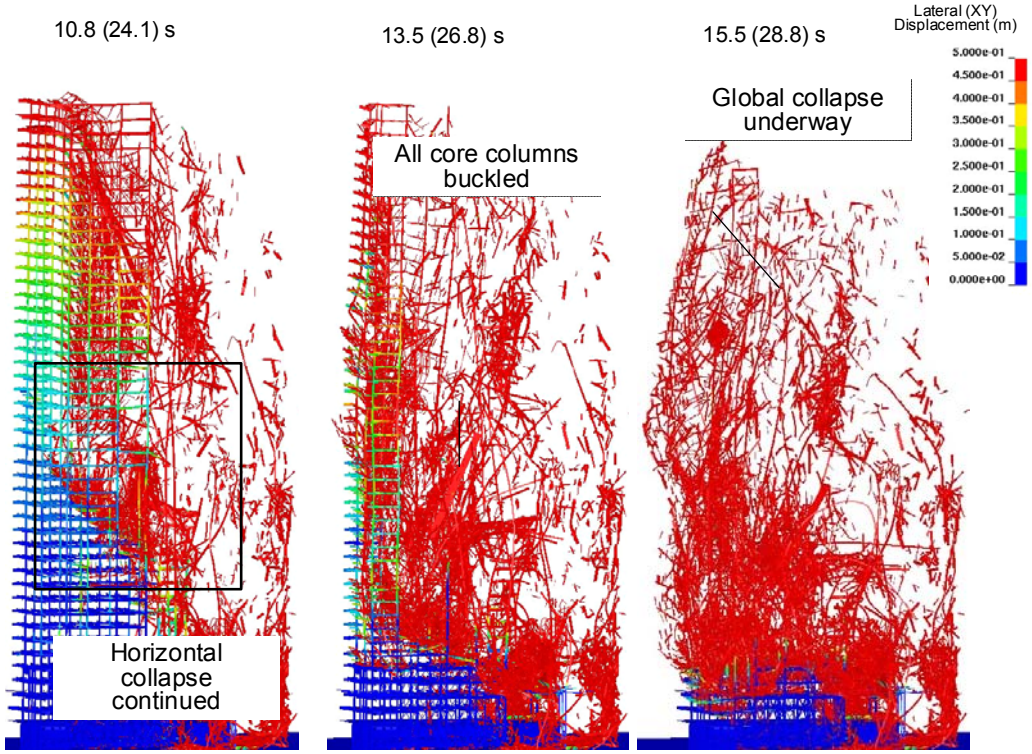

Figure 12–68 Core collapse sequence viewed from the south. Time: 10.8 to 15.5 s (24.1 to 28.8 s). Contours of resultant lateral displacement 0 in. to -20 in. (0 m to -0.5 m).

By 13.5 (26.8) s, all the interior columns had buckled and, at 15.5 (28.8) s, the global collapse (i.e., buckling of exterior columns) was underway, as shown in Figure 12–69. The exterior columns buckled near mid-height of the building, approximately between Floors 17 and 29.

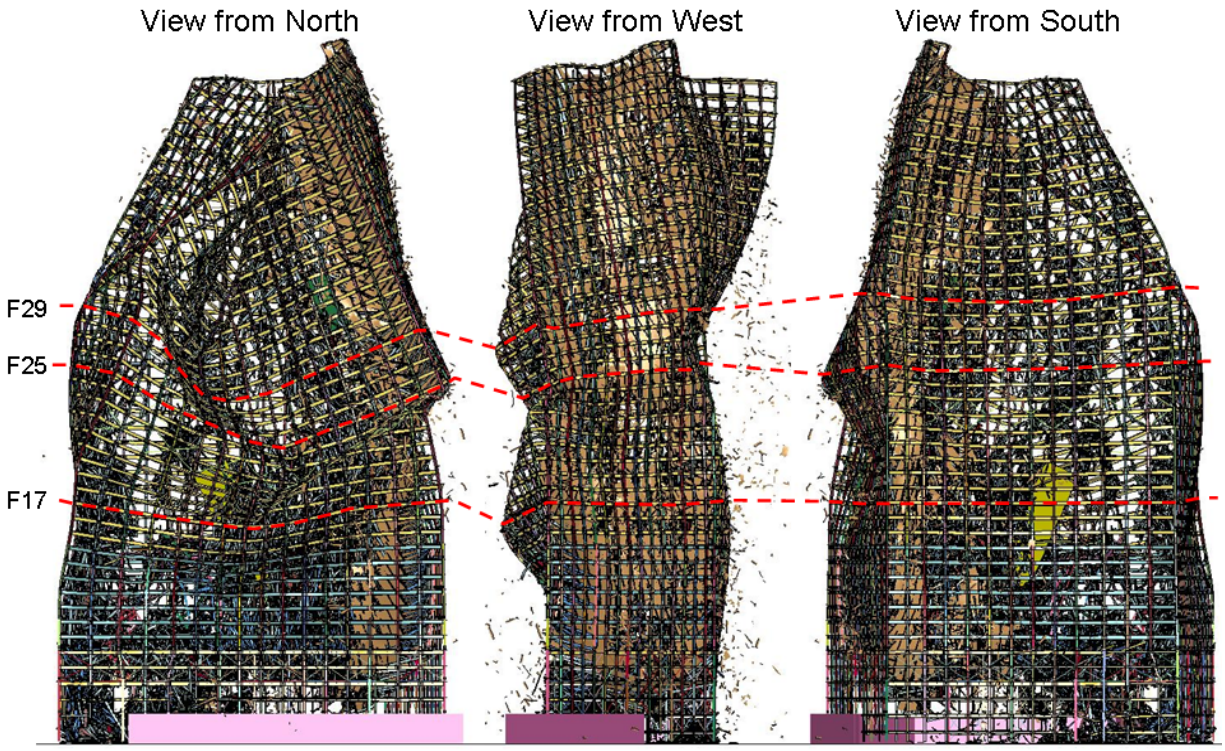

Figure 12–69 Exterior buckling after global collapse initiation.

12.5 COMPARISON OF SIMULATIONS WITH OBSERVABLES

12.5.1 Aspects prior to the Global Collapse

Table 12–2 lists the major observed collapse events with corresponding times (collapse reference time frame) from the observable events and from the two global analyses with and without debris impact damage for Case B temperatures at 4.0 h. As shown in the table, the calculated time for the buckling of Columns 79, 80, and 81, the calculated and observed times for the start of the East Penthouse downward movement due to the vertical collapse progression, and the calculated and observed times for the descent of the East penthouse below the roofline were quite similar, independent of the debris impact damage.

The cascading failure of floors surrounding Column 79 and the buckling of Column 79 could not be ascertained from any videographic evidence. However, analysis of the east-west vibration of the building prior to collapse (Chapter 5 and Appendix C) revealed horizontal motion (± 2 in.) 6 s before the East Penthouse began to move downward. The horizontal building motion started at nearly the same time as the cascading floor failures started in the LS-DYNA analysis (-6.5 s), which preceded the buckling failure of Column 79. The LS-DYNA analyses indicated that Column 79 buckled approximately 1.3 s prior to the downward motion of the East Penthouse.

Table 12–2 Comparison of major collapse events: observable versus analysis timeline.

Observation Time (s)	Analysis Time (s) with Debris Impact Damage	Analysis Time (s) without Debris Impact Damage	Event
≈ -6 s [a]	-6.6 s	-6.6 s	Start of cascading failure of floors surrounding Column 79
N/A [b]	-1.3	-1.4	Buckling of Column 79, quickly followed by buckling of Columns 80 and 81
0	≡ 0	≡ 0	Start of descent of East Penthouse
2.0	2.4-2.7	2.3-2.6	Descent of East Penthouse below roofline
N/A	3.5-6.1	3.2-13.5	Buckling of columns across core, starting with Column 76
6.9	6.2-6.3	7.2-7.7	Initial downward motion of the north face roofline at the eastern section of building
8.5	7.3-7.7	8.7-9.2	Descent of the east end of the screenwall below the roofline
9.3	6.9, 7.3	10.6, 10.9	Descent of the West Penthouse below the roofline (First value: observed from the northwest and below, second value: observed from the north at roofline)

a: From Appendix C; also see Chapter 8.
b: Not available

The horizontal progression of buckling core columns was interior to the building and could not have been observed from the street. The process occurred over a longer duration of 10.3 s (13.5 s minus 3.2 s) for the analysis without debris impact damage than for the duration of 2.6 s (6.1 s minus 3.5 s) for the analysis with impact damage. In the analysis without debris impact damage, the lack of core framing damage on the west side resulted in a sequence of interior column failures from east to west that occurred at a more uniform rate. In the analysis with debris impact damage, the core framing damage on the west side resulted in a more rapid failure of the west interior columns in the last stages of the horizontal progression.

The initial downward movement of the north face from the northeast corner to the east side of the screen wall was observed at 6.9 s after the initial downward motion of the East Penthouse. The LS-DYNA analyses with and without impact damage appear to have straddled that value.

12.5.2 Aspects following the Collapse Initiation

Once simulation of the global collapse of WTC 7 was underway, there was a great increase in the uncertainty in the progression of the collapse sequence, due to the random nature of the interaction, break up, disintegration, and falling of the debris. The uncertainties deriving from these random processes increasingly influenced the deterministic physics-based collapse process, and the details of the progression of the horizontal failure and final global collapse were increasingly less precise.

Thus, while the two predictions of the time of descent of the West Penthouse also straddled the observed time, the mechanisms of building decay were quite different. In the analysis without debris impact damage, the exterior columns buckled near mid-height of the building, approximately between Floors 17 and 29. In the analysis with debris impact damage, the exterior columns buckled between Floors 7 to 14,

due to the influence of the exterior damage near the southwest corner. In both analyses, the eastern exterior wall deflected inward at the roof level as the structure became unsupported after the vertical collapse event. The western wall also deflected inward in the analysis without debris impact damage, as it was pulled inward as the last line of core columns failed.

There was another observable feature that occurred after the global collapse was underway and thus could not be captured accurately in the simulation. After the exterior facade began to fall downward at 6.9 s, the north face developed a line or "kink" near the end of the core at Column 76. As shown in Figure 5-205, the northeast corner began to displace to the north at about 8.8 s, and the kink was visible at 9.3 s. The kink and rotation of the northeast façade occurred 2 s to 3 s after the exterior façade had begun to move downward, as a result of the global collapse.

Given the complexity of the modeled behavior, the global collapse analyses matched the observed behavior reasonably well. The global collapse analysis confirmed the leading collapse hypothesis, which was based on the available evidence.

12.5.3 Collapse Time

NIST was interested in estimating how closely the time for WTC 7 took to fall compared with the descent time if the building were falling freely under the force of gravity.

Assuming that the descent speed was approximately constant, the two quantities needed for the determinations were (1) a length that some feature of the building descended and (2) the time it took to fall that distance. The chosen feature was the top of the parapet wall on the roofline of the north face. The length was the difference between the position of the roofline prior to the collapse and the last position the roofline could be observed before it was obstructed by a building in the foreground.

The elevation of the top of the parapet wall was +925 ft 4 in.[1] The lowest point on the north face of WTC 7 visible on the Camera 3 video (Section 5.7.1) prior to any downward movement was the top of the windows on Floor 29, which had an approximate elevation of +683 ft 6 in. Thus, the distance that the roofline moved downward before it disappeared from view was 242 ft. The relative time at which the roofline began to descend was 20.60 s, and the relative time when the roofline dropped from view behind the buildings was 25.97 s. The time the roofline took to fall 18 stories was 5.4 s, with an uncertainty of no more than 0.1 s.

The theoretical time for free fall (i.e., neglecting air friction), was computed from,

$$t = \sqrt{\frac{2h}{g}} \tag{3}$$

where t is the descent time (s), h is the distance fallen (ft), and g is the gravitational acceleration constant, 32.2 ft/s^2 (9.81 m/s^2). Upon substitution of h = 242 ft. in the above equation, the estimated free fall time for the top of the north face to fall 18 stories was approximately 3.9 s. The uncertainty in this value was also less than 0.1 s.

[1] From plan documents, with the finished first floor lobby elevation being +309 ft 1 in.

Thus, the actual time for the upper 18 stories to collapse, based on video evidence, was approximately 40 percent longer than the computed free fall time and was consistent with physical principles.

The actual collapse time of the upper 18 floors of the north face of WTC 7 (the floors clearly visible in the video evidence) was 40 percent greater than the computed free fall time. This was consistent with physical principles.

12.6 SUMMARY OF FINDINGS

A global finite element model of WTC 7 was developed in LS-DYNA to reconstruct the structural response of WTC 7 to a fire-induced initial failure and to determine the sequence and timing of the events that led to the global collapse of the building. Three simulations were performed with this model.

- The first was based on NIST's best estimate of both the debris impact damage form WTC 1 and the fire-induced damage as developed using the ANSYS modeling. This occurred at 4 h in the ANSYS computation.

- The second simulation differed only in the input of a lesser degree of fire-induced damage, which occurred at 3.5 h in the ANSYS computation. The purpose of this LS-DYNA simulation was to determine whether a lesser degree of fire-induced damage could lead to the collapse of WTC 7.

- The third simulation was the same as the first, except that no debris impact damage was included. The purpose of this analysis was to determine the contribution of debris impact to the WTC 7 global collapse sequence and whether WTC 7 would have collapsed solely due to the effects of the fires.

The following are the principal findings from these simulations.

- The best estimate simulation led to global collapse of WTC 7 and provided a reasonable sequence and timing of the events leading to the initiation of global collapse. As expected, there were some deviations from the observable evidence at computation times after the global collapse was underway.

- The simulation with identical debris impact damage, but reduced fire damage, did not lead to a collapse-initiating event or to collapse itself. This result indicated that the debris impact damage, by itself, was not sufficient to initiate global collapse. It also indicated that the long duration of the multiple floor fires was the primary cause of the eventual collapse.

- The simulation with the same fire-induced damage as the "best estimate" simulation, but with no debris impact damage, identified the same initiating event and timing of that event as did the best estimate simulation. This simulation also led to global collapse of the building, further indicating that the debris impact damage was not a principal contributor to the occurrence of collapse. However, the mechanics of the collapse differed from the best estimate simulation.

The simulations supported the leading collapse hypothesis and provided the following additional insights into the sequence of events leading to the global collapse of WTC 7. Except as noted, these findings were derived from the best estimate simulation.

Initial Local Failure for Collapse Initiation

- The collapse of Floor 13 onto the floors below, some of which were already weakened by fires, triggered a cascade of floor failures in the northeast region.
- The floor failures progressed down to Floor 5, where debris accumulated, and spread across the east floor area, due to the effects of impact loads from falling debris on thermally weakened floor areas.
- Critical Column 79 became laterally unsupported between Floors 5 and 14 in the east-west and south directions as a result of the progression of floor system failures. There was still some lateral support in the north direction at Floors 8 to 12 and Floor 14, as the erection bolts in the seated connections had all failed at these girder ends, but the girders had not walked off the bearing seat.
- The increase in unsupported length led to the buckling failure of Column 79, which was the collapse initiation event for WTC 7.

Vertical Progression of Failure

- Once Column 79 buckled, the column section above Floor 14 began to descend downward. Column 79 began moving downward at the roof level approximately 0.2 s after Column 79 buckled and 0.6 s before Column 80 buckled.
- As Column 79 moved downward, the floor framing adjacent to Column 79 was pulled downward, which led to the observed kink in the East Penthouse roof framing on the north side.
- As Column 79 moved downward, the floor framing connections to interior (Column 80 and Column 76) and exterior columns (Column 44) failed under increasing tensile in-plane floor forces, resulting in a vertical progression of failure of the floor systems around Column 79.
- Column 80 became laterally unsupported in both directions between Floors 5 and 15, as a result of the progressive floor system failures. Column 80 buckled about 0.8 s after Column 79 buckled.
- Column 81 became laterally unsupported in both directions between Floors 7 and 15, as a result of the progressive floor system failures. Column 81 buckled about 1.3 s after Column 79 buckled.
- As Columns 79, 80, and 81 each buckled, their column sections above Floor 14 began to descend downward and pulled the floor structures downward with them, thereby creating a vertical progression of floor collapses that spread across the entire east region of WTC 7.

- The East Penthouse, which was supported by Columns 79, 80, and 81, fell downward.

Horizontal Progression of Failure

- Interior column buckling failures continued to propagate across the core in the lower floors from east to west, due to (1) loss of lateral support from floor system failures, (2) impact of falling debris from adjacent floors and columns, and (3) load redistributed from other buckled columns.

- During the vertical progression, the falling floors pulled on adjacent columns until the floor connections failed on the east side of Columns 76, 77, and 78.

- Truss 2 collapsed due to accumulated weight and impact loads from falling debris. The collapse of Truss 2 precipitated the buckling of Columns 77 and 78, which together with Column 76 had already lost lateral support.

- The occurrence of this westward progression indicates that the failure of Truss 2 was not essential to the failure of Columns 77 and 78, as they would have buckled in a similar fashion to the other columns.

- The horizontal progression of failure was sensitive to the extent of the estimated initial structural damage in WTC 7 due to debris impact from the collapse of WTC 1.

    - For the debris impact damage scenario, some of the interior columns on the west began buckling as the horizontal progression of interior column failures approached the middle of the core. For example, the middle line of interior columns directly behind the initially severed exterior columns buckled before the two north-south lines of columns immediately to their east. The middle line of interior columns lost lateral support in the north-south direction over 11 floors in response to the structural damage that was imposed.

    - For the no debris impact damage scenario, the horizontal progression of column failures occurred in order from east to west after collapse initiation (i.e., buckling of Column 79) and the vertical progression of failures on the east side. This scenario matched the observations where the screenwall on the roof fell downward before the west penthouse. This suggests that the damage scenario that was imposed in the best estimate analysis was slightly more severe than actually occurred.

Global Collapse

- The exterior column failures were sensitive to the extent of the estimated initial structural damage in WTC 7 due to debris impact from the collapse of WTC 1.

    - For the debris impact damage scenario, the exterior column buckling began at the southwest corner Column 14, adjacent to the WTC 1 debris impact zone, between Floors 10 and 12. The exterior columns adjacent to the (seven) columns severed in the southwest region due to the collapse of WTC 1 were the first to buckle because additional

load was distributed to them as a result of the damage. The analysis with debris impact damage closely simulated the observed failure of the exterior façade, where the façade moved downward as a single unit.

- For the no debris impact damage scenario, the exterior columns buckled near mid-height of the building, approximately between Floors 17 and 29. If the exterior columns had buckled at mid-height, it would have been visible in the videographic records. The analysis without debris impact damage did not closely simulate the observed failure of the exterior façade.

- The observed behavior of the exterior columns during the global collapse was more closely simulated by the analysis with debris impact damage.

- As the interior columns buckled at the lower floors and the corresponding upper column sections began to move downward, the exterior columns buckled inward at the lower floors as a result of floor pull-in forces caused by the downward movement of the building core. The floor connections to the columns had not yet failed in this region, as there were no fires observed on the west side of Floors 10 through 14 at any time during the day, so the floors were intact and able to pull the exterior columns inward.

- The south and west exterior columns buckled first, followed by the north and east face columns.

- All exterior columns buckled between approximately Floors 7 and 14.

- Once column support was lost in the lower floors, the remaining exterior structure above began to fall vertically as a single unit.

12.7 REFERENCES

Irwin G. Cantor P.C., Structural Engineers (1985). Structural Design Drawings, 7 World Trade Center (provided to NIST by Silverstein).

"LS-DYNA Keyword User's Manual," Livermore Software Technology Corporation, Version 971, May, 2007.

Sadek, F., El-Tawil, S., Lew, H.S., (2008), "Robustness of Composite Floor Systems with Shear Connections: Modeling, Simulation, and Evaluation," *J. Struct. Eng.,* ASCE, in press.

This page left blank intentionally.

Chapter 13
THE PROBABLE COLLAPSE SEQUENCE

13.1 SUMMARY PROBABLE COLLAPSE SEQUENCE

1. **Collapse of the WTC Towers.** The collapse of WTC 2 did not cause any structural damage or start any fires in WTC 7. The collapse of WTC 1 damaged seven exterior columns on the lower floors of the south and west faces and initiated fires at five separate locations between Floors 7 and 30.

2. **Growth and Spread of Fires**. Fires on the lower floors (Floors 7 to 9 and 11 to 13) grew and spread since they were not extinguished either by the automatic sprinkler system or by FDNY because water was not available. By 3:00 p.m. to 4:00 p.m., these fires were generally concentrated on the east and north sides of the northeast region. The local fires on the upper floors (Floors 19, 22, 29, and 30) were not observed after approximately 1 p.m.

3. **Initial Local Failure for Collapse Initiation.** Fire-induced thermal expansion of the floor system surrounding Column 79 led to collapse of Floor 13 that triggered a cascade of floor failures. This, in turn, led to loss of lateral support to Column 79 over nine stories, resulting in the buckling failure of Column 79.

4. **Vertical Progression of Failure.** The buckling of Column 79 (the collapse initiation event) triggered a vertical progression of floor system failures to the east penthouse and subsequent cascading failure of the adjacent interior columns on the east side of the building (i.e., Columns 80 and 81). The vertical progression of floor system failures spread to include the entire east region all the way to the top of the building.

5. **Horizontal Progression of Failure.** The interior columns buckled in succession from east to west in the lower floors due to loss of lateral support from floor system failures, forces exerted by falling debris, and load redistributed from other buckled columns.

6. **Global Collapse.** The exterior columns buckled at the lower floors (between Floors 7 and 14) due to load redistribution to the exterior columns from the downward movement of the building core. The entire building above the buckled-column region then moved downward in a single unit, as observed, completing the global collapse sequence.

7. **Other Possible Hypotheses.**

   - Fuel oil fires did not contribute to the collapse of WTC 7.

   - Hypothetical blast events did not contribute to the collapse of WTC 7. NIST concluded that blast events could not have occurred and found no evidence of any blast events.

   - The Con Edison substation played no role in the fires that caused the collapse of WTC 7.

13.2 DETAILED PROBABLE COLLAPSE SEQUENCE

8. **Collapse of WTC 2.** The collapse of WTC 2 did not cause any structural damage to WTC 7, nor did it ignite a fire in WTC 7. Damage caused by WTC 2 was limited to window breakage in the four-story lobby area on the south face of WTC 7.

9. **Collapse of WTC 1.** The collapse of WTC 1 caused (1) structural damage that severed seven (out of 58) exterior columns on the lower floors of WTC 7; (2) initiation of fires at 10 floors between Floors 7 and 30; (3) extensive window breakage on the south face of WTC 7; and (4) loss of city water that supplied the automatic sprinkler system on the lower zone of WTC 7.

    - The severed columns were located between Floors 7 and 17 on the south face (5 columns) and the west face (2 columns) near the corner. The analysis considered two scenarios: (1) a region of structural damage consistent with the seven severed columns extending over all 12 damaged floors and inward to the core where columns, girders, beams, and floors were removed; and (2) no structural damage. In the first scenario, the damage extended from the south face all the way to the core over the lower seven floors (only at areas where the columns were observed to be damaged), extended half way from the south face to the core over the middle three floors, and was limited to just the exterior structural framing members over the upper three floors.

    - Observations indicate that the fires were located in five distinct groups of floors (7/8/9, 11/12/13, 19, 22, and 29/30). These fires were first observed between 11 a.m. and 12:30 p.m. (WTC 1 collapsed at 10:28:22 a.m.). They were typically observed as single floor fires. Fires observed later on floors adjacent to the single floor fires were observed to lag by one half to one hour.

    - Observations support a single point of ignition on any given floor in WTC 7. In most instances, the fire on any given floor likely initiated near the damaged southwest region, though collapse initiation did not occur until nearly seven hours later in the northeast region. Unlike the WTC towers, there was no dispersion of jet fuel in WTC 7 causing simultaneous fire initiation over extensive areas of a single floor or over multiple adjacent floors.

    - There was no evidence to suggest that the sprayed fire resistive material (SFRM) was damaged, except in the immediate vicinity of the debris impact on WTC 7 from the collapse of WTC 1. This is consistent with observations NIST made in the Deutsche Bank building that suffered similar debris damage from the collapse of WTC 2.

10. **Growth and Spread of Fires.** The fires that caused the collapse of WTC 7 were located on the lower floors where there was no gravity-fed tank to supply the automatic sprinkler system. Fires on Floors 11, 12, and 13 were more severe due to higher combustible loads (6.4 psf) than those on Floors 7, 8, and 9 (4 psf). By 3:00 p.m. to 4:00 p.m. (about two hours before the collapse of WTC 7), the fires were generally concentrated on the east and north sides around the northeast region.

    - The automatic sprinkler system on the lower floors of WTC 7 (below Floor 21) required direct water supply from the street level mains. The city water mains were unavailable to

supply the lower zone following the collapse of WTC 1. Also, FDNY decided not to fight the fires due to the lack of water and safety considerations.

- The fires on Floors 7, 8, and 9 spread in a clockwise direction (southwest to north to east) while the fires on Floors 11, 12, and 13 spread in a counterclockwise direction (southwest to east to north).

- Fires on the upper floors (Floor 19 and higher) were not observed after approximately 1 p.m. It is possible that some of these fires could have been extinguished by the gravity-fed sprinkler system that supplied Floors 21 and higher.

11. **Initial Local Failure for Collapse Initiation.** The simple shear connection between Column 79 and the girder that spanned the distance to the north face (to Column 44) failed on Floor 13. The connection failed due to shearing of erection bolts, caused by lateral thermal expansion of floor beams supporting the northeast floor system and, to a lesser extent, by the thermal expansion of the girder connecting Columns 79 and 44. Further thermal expansion of the floor beams pushed the girder off its seat, which led to the failure of the floor system surrounding Column 79 on Floor 13. The collapse of Floor 13 onto the floors below—some of which were already weakened by fires—triggered a cascade of floor failures in the northeast region. This, in turn, led to loss of lateral support to Column 79 in the east-west direction over nine stories (between Floors 5 and 14). The increase in unsupported length led to the buckling failure of Column 79, which was the collapse initiation event.

    - The failure of the girder-to-column connections was caused primarily by the thermal expansion of the large span-length northeast floor beams. Additional factors that contributed to the failure were the absence of girder shear studs that would have provided lateral restraint and the one-sided lateral support to the girder provided by the northeast corner floor beams.

    - In addition to the failure of the connection to Column 79 for the girder spanning to Column 44 on Floor 13, which had the most severe fire condition, the same connection on Floors 8 to 12 were partially damaged due to the failure of some or all of the four bolts. Complete failure of the connection required girder walk-off in addition to the failure of all four bolts.

    - The temperatures in the columns in WTC 7 did not exceed 300 °C and, therefore, the columns did not buckle due to direct fire-induced thermal expansion or weakening. The interior columns were not thermally restrained and, therefore, did not develop increased loads due to thermal expansion which could have led to buckling.

12. **Vertical Progression of Failure.** The buckling of Column 79 (the collapse initiation event) triggered a vertical progression of floor system failures to the east penthouse and subsequent cascading failure of the adjacent interior columns on the east side of the building (i.e., columns 80 and 81). The vertical progression of floor system failures spread to include the entire east region all the way to the top of the building since all three columns in this region had buckled.

    - The buckling of Column 79 at the lower floors led to downward movement of the upper section of Column 79. The adjacent floor framing was pulled downward, leading to the observed kink in the east penthouse roof framing.

- A line of window breakage was observed over multiple floors (Floors 37 to 44) between exterior Columns 43 and 45, centered around Column 44, which was connected directly to Column 79 with a girder at each floor.

- Under increasing tensile in-plane floor forces, the floor framing connections to Column 79, adjacent columns (i.e., 80, 76), and the exterior columns all failed. The cascading failures of the lower floors (Floors 6 to 14, both inclusive) surrounding Column 79 led to increased unsupported length in, falling debris impact on, and loads being re-distributed to adjacent columns. This led to buckling of Column 80 and, through a similar process, buckling of Column 81, resulting in a vertical progression of failure of the floor systems across the entire east side of WTC 7.

13. **Horizontal Progression of Failure.** The interior columns buckled in succession from east to west in the lower floors due to loss of lateral support from floor system failures, forces exerted by falling debris impact, and load redistributed to them from other buckled columns.

    - The first north-south line of core columns (i.e., Columns 76 to 78) buckled since they had lost lateral support, were impacted by falling debris, and had loads redistributed to them from adjacent buckled columns.

    - Truss 2, which collapsed due to accumulated weight and impact loads from falling debris, precipitated the buckling of Columns 77 and 78 a few moments earlier than Column 76. The failure of Truss 2 caused the failure of the transfer girder linking Columns 77 and 78A which supported Column 78.

    - The horizontal progression of failure was sensitive to the extent of the estimated initial structural damage in WTC 7 due to the collapse of WTC 1.

        - For the debris impact damage scenario, some of the interior columns on the west began buckling as the horizontal progression of interior column failures approached the middle of the core. For example, the middle line of interior columns directly behind the initially severed exterior columns buckled before the two north-south lines of columns immediately to their east. The middle line of interior columns lost lateral support in the north-south direction over 11 floors in response to the structural damage that was imposed. The results of this scenario were consistent with observations except that the screening wall on the roof fell downward before the west penthouse.

        - For the no debris impact damage scenario, the horizontal progression of column failures occurred in order from east to west after collapse initiation (i.e., buckling of Column 79) and the vertical progression of failures on the east side. This scenario matched the observations where the screening wall on the roof fell downward before the west penthouse.

14. **Global Collapse.** The exterior columns buckled at the lower floors (between Floors 7 and 14) due to load redistribution to the exterior columns from the downward movement of the building core. The entire building above the buckled-column region then moved downward in a single unit, as observed, completing the global collapse sequence.

- A line of window breakage was observed over multiple floors (Floors 33 to 39) initially in line with exterior Column 55, then spreading east toward Column 54. Column 55 was tied back to the west edge of the building core by a girder (similar in size to the girder connecting Column 44 and 79 on the east side) and a floor beam.

- The buckling of the exterior columns initiated on the west face of the building. The floor connections to the columns had not yet failed in this region because there were no fires observed on the west side on Floors 10 through 14 at any time during the day (unlike on the east side) and the floors pulled the exterior columns inward.

    - The exterior columns adjacent to the (seven) columns severed in the southwest region due to the collapse of WTC 1 buckled first because additional load was distributed to them as a result of the damage.

- The overall simulation of the collapsing building with debris impact damage better matched the video observations of the global collapse.

- The building collapsed under the no structural damage scenario with a fire having the same characteristics as was experienced in WTC 7 on September 11, 2001.

- There are greater uncertainties in predicting the precise progression of the collapse sequence as the analysis proceeded due to the random nature of the interaction, break up, disintegration, and falling of the debris. The uncertainties deriving from these random processes increasingly influence the deterministic physics-based collapse process. Thus, the details of the progression of horizontal failure and final global collapse were sensitive to the uncertainties in how the building materials (steel, concrete) and building systems and contents interact, break up, and disintegrate.

13.3 OTHER POSSIBLE HYPOTHESES

15. **Role of Diesel Fuel Fires.** The hypothetical fuel oil fires on the 5th and 6th floors did not contribute to the collapse of WTC 7. The worst-case scenarios associated with fires being fed by the ruptured fuel lines could not be sustained long enough, or could not have generated sufficient heat, to raise the temperature of a critical column (i.e., Column 79) to the point of significant loss of strength or stiffness. Column 79 was critical because observations and analysis indicated clearly that the failure of this column initiated collapse. Additionally, such fires would have produced large amounts of visible smoke that would have emanated from the exhaust louvers; however, no such smoke discharge was observed.

    - The 5th Floor was the only floor with a pressurized fuel line supplying nine of the emergency power generators on that floor. Two 6,000 gallon underground tanks supplied these nine generators, were always kept full for emergencies, and were full on September 11, 2001.

    - Both 6,000 gallon tanks were found to be damaged and empty in the rubble pile several months after the collapse. This raised the possibility that the fuel may have contributed to a fire on Floor 5, a possibility that could not be distinguished from the fuel being consumed or dissipated in the burning rubble fire subsequent to the collapse of WTC 7.

- The gas temperatures from a pool fire on the 5th floor would have exceeded the boiling point of the coolant for the diesel generators in not much more than an hour, leading to engine failure. With all nine generators out of commission, there would have been no power to operate the fuel pumps for more than an hour or two, and the fires would have burned out well before columns in the region of the fire, including Column 79, experienced significant loss of strength.

- The day tanks on Floors 5 (supplying the remaining two emergency generators), 7, 8, and 9 that supplied fuel to the emergency generators on those floors did not contain enough fuel to be a significant contributor to the combustible load on the floors where fires were observed; it is unlikely that the tanks would have been re-supplied because of multiple safeguards in the fuel delivery system. In addition, none of the day tanks was located near the location of critical Column 79.

- FDNY personnel reported that they did not see any indication of burning liquid fuels before the building collapsed.

16. **Role of Hypothetical Blast Events.** Hypothetical blast events did not cause the collapse of WTC 7. NIST concluded that blast events could not have occurred and found no evidence of any blast events.

    - The minimum explosive charge (lower bound) required to fail a critical column (i.e., Column 79) would have produced a pressure wave that would have broken windows on the north and east faces of the building near Column 79. Such a blast event would have resulted in a sound level of 130 to 140 decibels (a sound level consistent with a gunshot blast or a jet plane that is 10 to 20 decibels louder than a rock concert in front of speakers), at a distance of at least half a mile (if unobstructed by surrounding buildings, for example, along Greenwich Street). There were no witness reports of such a loud noise, nor was such a noise heard on audio tracks of videotapes that recorded the WTC 7 collapse.

    - Prior to preparing a column for controlled demolition, walls and/or column enclosures and SFRM would have to be removed and replaced without being detected. Preparing the column includes steps such as cutting sections with torches (which produces noxious and odorous fumes) and careful placement of charges and an initiation device. Controlled demolition usually prepares most, if not all, interior columns in a building with explosive charges, not just one column. It is unlikely that explosive charges would have been applied to just one column or that such activity could have taken place without being detected.

    - Observations for WTC 7 do not match the typical sequence of events for a controlled demolition. Video evidence clearly shows a sequence of failures (initiation, vertical progression, horizontal progression, and global collapse) based on a single point of initiation. This collapse sequence is inconsistent with a typical controlled demolition where charges are placed in multiple locations across the building and detonated in rapid succession.

17. **Role of Con Edison Substation.** The Con Edison substation played no role in the fires that caused the collapse of WTC 7. Electronic communications into and out of the Con Ed substation

show that the substation continued to operate until it was intentionally shut down at 4:33 p.m. Additionally, there was no evidence of a fire in the Con Edison substation.

- Even though utility power to the rest of WTC 7 was lost at 9:59 a.m., auxiliary utility power to the Con Edison substation from transmission switching station feeders allowed internal operations to be maintained. At 4:33 p.m., the utility control center isolated the WTC 7 Con Edison substation by opening the 138 kV circuit breakers feeding the WTC 7 substation.

- Fire detector signals from the Con Edison substation were monitored off-site throughout the day. One fire detector within the Con Edison substation gave an alarm when WTC 1 collapsed, and stayed in alarm mode until the substation was isolated from incoming feeders at 4:33 p.m. However, there were no other indications (e.g., no high temperature alarms from the transformers, no visible smoke emanating from the Con Edison building) that a fire occurred within the substation during that period of time. Likely causes of the fire alarm were the smoke and dust dispersed in the area of the substation from the collapse of WTC 1.

This page left blank intentionally.

Chapter 14
PRINCIPAL FINDINGS

14.1 INTRODUCTION

This chapter presents the findings of the NIST Technical Investigation, organized according to the first three of the four Investigation objectives for Building 7 of the New York World Trade Center (WTC). The fourth objective ("Identify areas in current building and fire codes, standards, and practices that warrant revision") is the subject of Chapter 5 of this report. The findings were derived from the extensive documentation summarized in the preceding chapters and described in detail in the accompanying reports. While NIST was not able to compile a complete documentation of the history of WTC 7, due to the loss of records over time and due to the collapses, the investigators were able to acquire information adequate to arrive at and firmly support the findings and recommendations compiled in this chapter and the next. The chapter begins with summary statements and continues with the listing of the full set of principal findings.

14.2 SUMMARY

Objective 1: Determine why and how WTC 7 collapsed.

- WTC 7 withstood debris impact damage that resulted in seven exterior columns being severed and subsequently withstood conventional fires on several floors for almost seven hours.

- The collapse of WTC 7 represents the first known instance of the total collapse of a tall building primarily due to fires. The collapse could not have been prevented without controlling the fires before most of the combustible building contents were consumed.

- WTC 7 collapsed due to uncontrolled fires with characteristics similar to previous fires in tall buildings. The fires in WTC 7 were similar to those that have occurred previously in several tall buildings (One New York Plaza, 1970, First Interstate Bank, 1988, and One Meridian Plaza, 1991) where the automatic sprinklers did not function or were not present. However, because of differences between their structural designs and that of WTC 7, these three buildings did not collapse. Fires for the range of combustible contents in WTC 7 (4.0 lb/ft^2 on Floors 7 to 9 and 6.4 lb/ft^2 on Floors 11 to 13) persisted in any given location for approximately 20 minutes to 30 minutes. Had a water supply for the automatic sprinkler system been available and had the sprinkler system operated as designed, it is likely that fires in WTC 7 would have been controlled and the collapse prevented.

- The probable collapse sequence that caused the global collapse of WTC 7 was initiated by the buckling of Column 79, which was unsupported over nine stories, after local fire-induced damage led to a cascade of floor failures. The buckling of Column 79 led to a vertical progression of floor failures up to the east penthouse and to the buckling of Columns 80 and

81. An east-to-west horizontal progression of interior column buckling followed, due to loss of lateral support to adjacent columns, forces exerted by falling debris, and load redistribution from other buckled columns. The exterior columns then buckled as the failed building core moved downward, redistributing its loads to the exterior columns. Global collapse occurred as the entire building above the buckled region moved downward as a single unit.

- The collapse of WTC 7 was a progressive collapse. The American Society of Civil Engineers defines progressive collapse—also known as disproportionate collapse—as the spread of local damage, from an initiating event, from element to element, eventually resulting in the collapse of an entire structure or a disproportionately large part of it (ASCE 7-05). Despite extensive thermal weakening of connections and buckled floor beams, fire-induced damage in the floor framing surrounding Column 79 over nine stories was the determining factor causing the buckling of Column 79 and, thereby, initiating progressive collapse. This is the first known instance where fire-induced local damage (i.e., buckling failure of Column 79; one of 82 columns in WTC 7) led to the collapse of an entire tall building.

- The transfer elements (trusses, girders, and cantilever overhangs) did not play a significant role in the collapse of WTC 7. Neither did the Con Edison substation play a significant role in the collapse of WTC 7.

- Prior to the collapse, there had been no damage to the SFRM that was applied to the steel columns, girders, and beams, except in the vicinity of the structural damage from the collapse of WTC 1, which was near the west side of the south face of the building.

- Even without the initial structural damage caused by debris impact from the collapse of WTC 1, WTC 7 would have collapsed from fires having the same characteristics as those experienced on September 11, 2001.

- Early fires in the southwest region of the building did not play a role in the collapse of WTC 7. The fires in this region were not severe enough to heat the structure significantly; and, unlike the northeast region, where collapse initiated, there were no columns supporting long span floors in the southwest region.

- The collapse time of the upper 18 stories of the north face of WTC 7 (the floors clearly visible in the video evidence) was 40 percent greater than the computed free fall time. This is consistent with physical principles.

- Diesel fuel fires did not play a role in the collapse of WTC 7. The worst-case scenarios associated with fires being fed by the ruptured fuel lines (a) could not have been sustained long enough, or could not have generated sufficient heat, to raise the temperature of a critical column (i.e., Column 79) to the point of significant loss of strength or stiffness, or (b) would have produced large amounts of visible smoke that would have emanated from the exhaust louvers. No such smoke discharge was observed.

- Hypothetical blast events did not play a role in the collapse of WTC 7. Based on visual and audio evidence and the use of specialized computer modeling, NIST concluded that blast events did not occur, and found no evidence whose explanation required invocation of a blast

event. Blast from the smallest charge capable of failing a critical column (i.e., Column 79) would have resulted in a sound level of 130 dB to 140 dB at a distance of at least half a mile if unobstructed by surrounding buildings (such as along Greenwich Street or West Broadway). This sound level is consistent with standing next to a jet plane engine and more than 10 times louder than being in front of the speakers at a rock concert. There were no witness reports of such a loud noise, nor was such a noise heard on the audio tracks of video recordings of the WTC 7 collapse.

Objective 2: Determine why the injuries and fatalities were so high or low depending on location, including all technical aspects of fire protection, occupant behavior, evacuation, and emergency response.

- There were no serious injuries or fatalities because the estimated 4,000 occupants of WTC 7 reacted to the airplane impacts on the two WTC towers and began evacuating before there was significant damage to WTC 7. Evacuation of the building took just over an hour.

- The occupants were able to use both the elevators and the stairs, which were as yet not damaged, obstructed, or smoke-filled.

- Building management personnel held the occupants in the building lobby until they identified an exit path that was safe from the debris falling from WTC 1 across the street.

- The decision not to continue evaluating and fighting the fires was made hours before the building collapsed, so no emergency responders were in or near the building when the collapse occurred.

Objective 3: Determine what procedures and practices were used in the design, construction, operation, and maintenance of WTC 7.

- The design of WTC 7 was generally consistent with the NYCBC.

- Consistent with the NYCBC, there was no redundancy in the source of water supply for the sprinkler system in the lower 20 floors of WTC 7. Since there was no gravity-fed overhead tank supplying these floors, the sprinkler system could not function when the only source of water, which was from the street mains, was not available.

- Current practice for the fire resistance design of structures, based on the use of ASTM E 119 standard test method, is deficient since the method was not designed to include key fire effects that are critical to structural safety. Specifically, current practice does not capture: (a) important thermally-induced interactions between structural subsystems, elements, and connections—especially restraint conditions; (b) system-level interactions—especially those due to thermal expansion—since columns, girders, and floor subassemblies are tested separately; (c) the performance of connections under both gravity and thermal effects; and (d) scale effects in buildings with long span floor systems.

- Current practice also does not require design professionals to possess the qualifications necessary to ensure adequate passive fire resistance of the structural system. In current

practice, architects typically rely on catalogued ASTM E 119 test data to specify the required passive fire protection that is needed for the structure to comply with the building code. They are not required to explicitly evaluate the fire performance of the structure as a system (such as analyzing the effect of the thermal expansion or sagging of floor beams on girders, connections, and/or columns). Structural engineers are not required to consider fire as a load condition in structural design. Fire protection engineers may or may not be called upon to assist the architect in specifying the required passive fire protection. Thus, none of these professionals has been assigned the responsibility to ensure the adequate fire performance of the structural system.

- There is a critical gap in knowledge about how structures perform in real fires, particularly considering: the effects of the fire on the entire structural system; the interactions between the subsystems, elements, and connections; and scaling of fire test results to full-scale structures (especially for structures with long span floor systems).

14.3 THE MECHANISMS OF BUILDING COLLAPSE

14.3.1 Debris Impact Damage from the Collapse of WTC 1

- WTC 7 was damaged by debris from the collapse of WTC 1, which occurred at 10:28:22 a.m. However, WTC 7 collapsed at 5:20:52 p.m., nearly seven hours later.

- The structural damage to WTC 7 was primarily located at the southwest corner and adjacent areas of the west and south faces, on Floors 5 through 17. Severed columns were located between Floors 7 and 17 on the south face (six columns) and the west face (one column) near the southwest corner. Cladding damage extended over much of the south face, and ranged from broken windows to removal of granite panels and windows.

14.3.2 Reconstruction of the Fires

- There were fewer photographs and videos of the WTC 7 fires than there were of the fires in the WTC towers. This resulted in intermittent coverage of the building exterior from about 11:00 a.m. until just after the collapse at 5:20:52 p.m. Nonetheless, the visual evidence was sufficient to guide the reconstruction of the growth patterns of the fires.

- Fires were observed on multiple floors of WTC 7 following the collapse of WTC 1. The fires were likely to have started at locations facing WTC 1, caused by flaming debris, induced electrical failures, etc.

    - Early fires were seen on the southwest corner of Floors 19, 22, 29, and 30 shortly after noon. These were short-lived. Firefighters reported seeing fires on the south and west faces of WTC 7 as soon as visibility allowed (estimated to be 11:00 a.m. to 12:00 p.m.).

    - Sustained fires occurred on Floors 7, 8, 9, 11, 12, and 13. The fires on these six floors were fed by combustibles (e.g., desks, chairs, papers, carpet) that were ordinary for commercial occupancies.

- Unlike the situation in the WTC towers, there was no widespread spraying of jet fuel to ignite numerous workstations simultaneously. Rather, in the earlier hours of the fires, the flames would have spread from one workstation to another, which is a much slower process.

- On each floor, ignition was likely of a single workstation component or office furnishing item; growth over the full cluster of workstations or office took several minutes.

  - On Floors 7 through 9 (open landscaping), the initial fire spread was likely by flame contact with an adjacent workstation and then radiative ignition of a workstation cluster across an aisle. By the time this second cluster was fully involved, the prior cluster would have burned out. Eventually the upper gas layer over enough of the huge open space would likely be hot enough for radiatively enhanced ignition of multiple workstations, i.e., non-linear growth.

  - On Floors 11 through 13 (enclosed offices), the fire would likely have grown within an office, reaching flashover in several minutes. After about 15 minutes, the ceiling tile system would likely fail and the hot gases would create a local hot upper layer. Thermal radiation from this layer would have ignited adjacent offices. Offices across a corridor would likely have ignited more slowly.

- The collapse of WTC 7 was not caused by diesel fuel fires or by fire-induced failure of the transfer trusses on Floors 5 and 6.

  - Simulation of hypothetical, worst-case fire scenarios on these floors showed that pool fires, associated with ruptured diesel fuel lines, (a) would have raised the temperatures near the generators to the point where they all would have failed, cutting off the electrical power to the fuel pumps, (b) could not be sustained long enough, or generated too little heat, to raise the temperatures of the steel and concrete structure to the point of significant loss of strength or stiffness, and/or (c) would have exhausted smoke from the exhaust louvers, which was not observed.

  - A diesel fuel spray fire on Floor 5 would have been less damaging than a pool fire. To be a spray, the fuel escape rate would have been too small to heat Column 79, even if it hit it directly.

  - The day tanks on Floors 7, 8, and 9 contained diesel fuel equivalent to only a few percent of the office combustibles on those floors. Safeguards in the fuel delivery system would have prevented the tanks being re-supplied. The supply tanks for the day tanks on Floors 8 and 9 were found to be nearly full several months after the collapse of WTC 7. The heat from a day tank fire on Floor 7 would not have reached the transfer trusses or Column 79.

  - The absence of diesel fuel fires on Floor 5 was consistent with the information from interviews that sometime after 1:00 p.m., OEM and FDNY staff climbed the east stairway of WTC 7 and did not see much damage on Floors 4, 5, or 6 from their viewing location. They made no mention of fire, heat or smoke.

  - The transfer trusses and a girder were isolated from the diesel fuel lines and the generators by masonry walls. No mechanism for indirect heating of Transfer Trusses 1 or 2 was found.

- There was no evidence that the fires spread from floor to floor, except, perhaps, just prior to the collapse of the building.

- The fires on Floors 7 through 9 generally spread clockwise from the southwest corner of the floor. The fires on Floors 11 through 13 generally spread counterclockwise. All the fires were burning in the northeast region at around mid-afternoon.

- Simulations of the fires using the Fire Dynamics Simulator (FDS) generated air temperatures comparable to those in large-room fire tests of office workstations. Compared to the actual fires, the simulated fires followed the same general paths. The simulations of the Floor 12 fires (and thus the derivative Floor 11 and 13 fires) may have overestimated the duration of the fires and the fraction of the burning near the north face windows, relative to the fraction of burning in the interior of the tenant space.

- Doubling the estimated combustible fuel load on the open-landscaped Floor 8 from 20 kg/m^2 (4 lb/ft^2) to 40 kg/m^2 (8 lb/ft^2) led to a predicted fire spread rate that was slower than actually observed. Decreasing the combustible fuel load on the highly partitioned Floor 12 from 32 kg/m^2 (6.4 lb/ft^2) to the estimated load on Floor 8 had no significant effect on the fire spread rate. This indicated that the overestimation of burning duration was less likely due to overestimation of the fuel load and more likely due to excess burning (of combustible vapors from fire-heated office furnishings) near the windows relative to the burning in the building interior.

14.3.3 Fire-induced Thermal Effects

- Calculated fire-elevated temperatures in the interior columns, including Columns 79, 80, and 81, stayed below 200 ºC on all of the floors. The exterior column temperatures were below 150 ºC, except on Floors 12 and 13, where the east and south exterior columns reached 300 ºC. At these temperatures, structural steel experiences relatively little loss of strength or stiffness. Thus, WTC 7 did not collapse due to fire-induced weakening of critical columns.

- The simulated fires on Floors 7, 12, and 13 heated portions of the tops of the floor slabs to over 900 ºC. The temperatures of some sections of the beams supporting Floors 8, 12, 13, and 14 exceeded 600 ºC. The temperatures of some sections of the floor beams at Floors 9 and 10 reached 400 ºC.

- Raising the fire-generated air temperatures by 10 percent, which was within the range of reasonable and realistic fires, raised the peak temperatures in the floor beams and slabs by about 70 ºC. Additionally, the areas over which the temperatures of the floor beams exceeded 600 ºC increased. Comparable changes in the opposite direction resulted from lowering the fire-generated air temperatures (Case A).

14.3.4 Structural Response and Collapse

Initiating Event

- The buckling failure of Column 79 between Floor 5 and Floor 14 was the initiating event that led to the global collapse of WTC 7. This resulted from thermal expansion and failures of connections, beams, and girders in the adjacent floor systems.

- The connection, beam, and girder failures in the floor systems, and the resulting structural responses, occurred at temperature below approximately 400 °C, well below the temperatures at which structural steel loses significant strength and stiffness.

- Thermal expansion was particularly significant in causing the connection, beam, and girder failures, since the floor beams had long spans on the north and east sides (approximately 15 m, 50 ft).

    - Heating of the long beams resulted in proportionately large thermal elongation relative to the other components of the floor system, in effect, compressing the beams along their length. This led to distortion of the beams and breaking of the connections of the beams to the floor slabs. Furthermore, the simple shear connections used in the typical floor framing were not able to resist these axial compressive forces that developed as the floor framing was heated.

    - At Column 79, heating and expansion of the floor beams in the northeast corner caused the loss of connection between the column and the key girder. Additional factors that contributed to the failure of the critical north-south girder were (1) the absence of shear studs that would have provided lateral restraint and (2) the one-sided framing of the east floor beams that allowed the beams to push laterally on the girders, due to thermal expansion of the beams.

    - The fires thermally weakened Floors 8 to 14. As Floor 13 fell onto the floor below, a cascade of floor failures continued until the damage reached the massive Floor 5 slab, leaving Column 79 without lateral support for nine floors. The long unsupported length of Column 79 led to its buckling failure.

- Hypothetical blast events did not play a role in the collapse of WTC 7. NIST concluded that blast events could not have occurred, and found no evidence whose explanation required invocation of a blast event. Blast from the smallest charge capable of failing a critical column (i.e., Column 79) would have resulted in a sound level of 130 dB to 140 dB at a distance of at least half a mile if unobstructed by surrounding buildings (such as along Greenwich Street and West Broadway). This sound level is comparable to a gunshot blast, standing next to a jet plane engine, and more than 10 times louder than being in front of the speakers at a rock concert. The sound from such a blast in an urban setting would have been reflected and channeled down streets with minimum attenuation. However, the soundtracks from videos being recorded at the time of the collapse did not contain any sound as intense as would have accompanied such a blast

Vertical Progression of Collapse

- Once Column 79 buckled, there was a vertical progression of floor system failures up to the east penthouse, followed by the buckling of Columns 80 and 81.
    - The buckling of Column 79 at the lower floors led to downward movement of the upper section of Column 79. The adjacent floor framing was pulled downward, leading to the observed kink in the east penthouse roof framing.
    - As the lower floors surrounding Column 79 fell downward, Column 80 and Column 81 had increased unsupported lengths as well as falling debris impacts and loads being redistributed from adjacent columns. This led to buckling of Columns 80 and 81, and resulted in a vertical progression of failure of the floor systems up to the roof level across the entire east side of WTC 7.
- Columns 79, 80, and 81 were the only interior support for the gravity loads in the eastern region of the building. Once these three columns buckled and their upper sections began to descend, there was insufficient support for the floors, up to the east penthouse.
- None of these columns were significantly weakened by elevated temperatures; temperatures did not exceed 300 °C in the core or perimeter columns in WTC 7.

Horizontal Progression of Collapse

- Columns 76 through 78 were the next line of columns to buckle, due to loss of lateral support, impact by falling debris, and load redistribution from Columns 79 through 81. The failure of Truss 2 was not essential to the failure of Columns 77 and 78, as they would have buckled like the other columns.
- The remaining interior columns buckled in succession from east to west in the lower floors due to loss of lateral support from floor system failures, forces exerted by falling debris impact, and load redistributed to them from other buckled columns.
- The initial westward progression and the overall speed of the collapse was not sensitive to the extent of the estimated structural damage to WTC 7 due to the debris from the collapse of WTC 1. When the global collapse was nearly complete, there was some small sensitivity to the extent of the initial damage in the southwest portion of the building.

Global Collapse

- The exterior columns buckled at the lower floors (between Floors 7 and 14) due to load redistribution to the exterior columns from the building core as the interior columns buckled and the building core moved downward. The entire building above the buckled-column region then moved downward in a single unit, as observed, completing the global collapse sequence.

- Computer simulations of the fires, the thermal heating of the structure, the thermally induced damage to the structure, and the structural collapse can be used to predict a complex degradation and collapse of a building. The overall features and timing of the prediction were consistent with the videographic evidence.

- The uncertainties in predicting the precise progression of the collapse sequence increased as the analysis proceeded due to the random nature of the interaction, break up, disintegration, and falling of the debris. The uncertainties deriving from these random processes increasingly influence the deterministic physics-based collapse process. Thus, the details of the progression of horizontal failure and final global collapse were sensitive to the uncertainties in how the building materials (steel, concrete) and building systems and contents interacted, broke up, and disintegrated.

- These computational models comprise a set of research tools that can take months (eight months in this case) for a complete simulation. Their adaptation for engineering practice would forestall future disasters, while reducing the potential for structural overdesign.

14.4 LIFE SAFETY FACTORS

14.4.1 Evacuation of WTC 7

- By the conventional measure of life safety, the evacuation of WTC 7 was successful, as NIST identified no life-threatening injuries or fatalities among the estimated 4,000 building occupants on September 11, 2001.

- Most of the occupants initiated their own evacuation shortly after WTC 1 was attacked.

- Evacuation of the building took just over an hour to complete, which was about 30 min longer than the estimated minimum time if the elevators and stairs had been used to maximum advantage. Nonetheless, the building was safely evacuated prior to the collapse of WTC 2. Some of the additional evacuation time was due to the considerable crowding in the lobby. Occupants arrived in the lobby from both stairwells, from the elevators, and from other WTC buildings, and were held in the lobby until a safe exterior exit was identified by emergency management officials.

- The calculated stairwell capacity was insufficient to meet the requirements of the NYCBC in effect during the design and construction period, if the building were occupied at the calculated maximum level (≈ 14,000 people). The capacity was sufficient for the normal occupancy of the building (≈ 8,000 workers plus visitors), estimated by NIST, and was more than sufficient for the occupancy on September 11, 2001 (≈ 4,000 people), also estimated by NIST. The stairwell capacity met the requirement of the (subsequent) 2000 edition of the IBC, but not the 2003 edition of NFPA 5000.

- The separation of the stairwell doors met the requirement of the 1968 NYCBC. On some floors, the separation of the stairwell doors was below the remoteness requirements in the (current) 2000 IBC and the 2003 NFPA 5000.

- Evacuation management at every level did not provide timely evacuation instructions to building occupants during the event. NIST was not able to determine whether specific guidance was delivered to the occupants via the public address system.

- In addition to the length of time that WTC 7 withstood the internal fires, some specific people actions likely contributed to the speed and overall success of the evacuation.

  - Evacuation drills had been conducted every six months.

  - The decision to prevent occupants from exiting the stairwells out into the streets where they could be impacted by debris from WTC 1 and WTC 2 likely prevented injuries or deaths.

  - Using the loading dock exit to provide overhead protection, combined with the scaffolding protection along the other side of Washington Street, was an example of spontaneous decision-making on the part of the building management personnel which likely contributed to the positive outcome.

14.4.2 Emergency Response

- Faced with a disaster of an unprecedented nature, the involvement of the emergency management personnel with regard to WTC 7 was limited. Nonetheless, no lives were lost as a result of the collapse of WTC 7.

- The loss of numerous firefighters, company officers, and chief officers in the collapses of WTC 1 and WTC 2 led to a changing command structure for the rest of the morning, as new command posts were established and several different chief officers took command and relinquished command of operations at the WTC site.

- Due to the focus on rescuing people trapped in the debris field, providing aid to the injured, and the loss of water in the hydrant system, FDNY was not able to consider the possibility of fighting the fires in WTC 7 until approximately 1:00 p.m. At approximately 2:30 p.m., FDNY gave the order to forego firefighting activity and for personnel to withdraw to a safe distance from the building.

- Con Edison shut of all power to the substation under WTC 7 at 4:33 p.m.

14.5 CODES, STANDARDS, AND PRACTICES

14.5.1 General

- WTC 7 was designed and constructed as a “Tenant alteration project” of The Port Authority. Its design and construction followed the requirements of the 1984 edition of the Tenant Construction Review Manual.

- Although the PANYNJ was not subject to the NYCBC, the 1968 NYCBC, including amendments to January 1, 1985, appears to have been used for the design and construction provisions of WTC 7, based on citations in the construction documents.

- The type of building classification used to design and construct the building was not clear from the available documents. Based on the height, area, primary occupancy classification, and installation of a fire sprinkler and standpipe system, the minimum construction type (permitted by NYCBC) was type 1-C (2 h protected) classification. However, some documentation, including some building drawings and specifications for bidders on the contract for applying SFRM to the structural steel, indicate a type 1-B (3 h protected) classification.

14.5.2 Building Design and Structural Safety

- NIST found no evidence to suggest that WTC 7 was not designed in a manner generally consistent with applicable building codes and standards.

- WTC 7 was adequately designed for vertical loads due to gravity and lateral loads due to wind.

  - The vertical (gravity) load resisting system comprised the core and exterior columns, which received gravity loads from the floor framing. Of particular note were the three core columns on the east side of the building (Columns 79, 80, and 81), which supported large span floor areas with approximately 15 m (50 ft) spans on at least one side.

  - Above Floor 7, the lateral load resisting system comprised the exterior moment frame with a perimeter belt truss at Floors 22 through 24. There were also a perimeter belt truss between Floors 5 and 7, diaphragms at Floors 5 and 7 that transferred lateral wind loads to the core columns, and bracing in the core below Floor 7 that transferred lateral loads to the foundation. However, this system was not able to provide a secondary load path for gravity loads.

  - Above Floor 7, there was no bracing, or other load redistribution mechanism, to transfer gravity loads between interior columns. The floor framing, which was the only load path between columns, could not redistribute loads between columns because the shear connections from the interior floor beams to columns were only designed for transferring vertical shear loads.

  - Transfer girders, trusses, and cantilever overlays were used to transfer column loads above Floor 7 to a different column layout below Floor 5.

- The structural design did not explicitly evaluate fire effects, which was typical for engineering practice at that time and continues to remain so today. Many of the shear connections in WTC 7 were not capable of resisting lateral loads resulting from thermal expansion effects in the steel floor framing when the floor beams were heated.

14.5.3 SFRM Requirements and Application

- It is likely that the Monokote MK-5 SFRM, applied to the steel framing and metal decks, was undamaged by the impact of the debris from the collapse of WTC 1, except in the area where direct structural damage to WTC 7 occurred.

- NIST simulations showed that, for the heaviest columns in WTC 7, when properly insulated, it would have taken an exposure of about 7 h at post-flashover upper layer gas temperatures to raise the steel temperature to 600 ºC, the point at which the steel strength would have been reduced by half. A similar calculation indicated it would have taken about 4 h to reach this temperature for an insulated lighter column. These times are both far longer than the time over which post-flashover gas temperatures were sustained in the computed WTC 7 fires. For comparison, this steel temperature would have been reached in under one-half hour if the insulation were not applied.

- It is unlikely that the collapse of WTC 7 would have been prevented had the insulation thickness on the floor beams been increased by 50 percent (from ½ in. to ¾ in.). NIST calculations indicated that the time to reach the steel temperature of 649 °C (1200 °F) would have increased by about 10 min to 20 min.

- The ASTM E119 test does not capture critical behavior of structural systems, e.g., the effect of thermal expansion or sagging of floor beams on girders, connections, and/or columns. The thermal expansion of the WTC 7 floor beams that initiated the probable collapse sequence occurred at temperatures below approximately 400 °C. Thus, to the extent that thermal expansion, rather than loss of structural strength, precipitates an unsafe condition, thermal expansion effects need to be evaluated. The current fire resistance rating system, which does not include thermal expansion effects, is not conservative.

14.5.4 Fire Safety and Fire Protection Systems

- WTC 7 had the following active fire protection systems: fire alarms, smoke and heat detectors, manual pull stations, smoke control systems, and automatic sprinklers. Each was designed, constructed, and apparently maintained consistent with applicable building codes and standards.

- The standpipe and automatic sprinkler systems were divided into three zones. As prescribed by the NYCBC, each zone had a primary and secondary water supply.

    - The primary water supply for the high zone (Floors 40 through 47) and mid-level zone (Floors 21 through 39) was from two water storage tanks on the 46th floor. The secondary supply was pumped from the city water main.

    - The primary water supply for the low zone, floors 1 through 20, was a direct connection to the city water mains. The secondary supply was from an automatic fire pump, which was connected to the city water main as well.

- Since the city water main had been compromised as a result of the collapses of the two towers, there was no water supply to control the fires on the 7th through 13th floors. By contrast, the early fires on the 22nd, 29th, and 30th floors may have been controlled by the sprinkler system on the upper floors, whose primary water supply was from the storage tanks on the 46th floor.

- The architectural drawings indicated that there were fire-rated walls between tenant spaces on the same floor and between tenant spaces and the building core. Spaces housing mechanical equipment, power transformers, emergency power generators, and other such equipment were enclosed in fire-rated partitions. While the partitions between offices, conferences rooms, etc. were not required to be fire-rated, there was evidence from both the visual evidence and the fire simulations that some of these partitions did retard the spread of the fires.

- There was no evidence of floor-to-floor fire spread until perhaps just before the WTC 7 collapse. Thus, the fire-rated floors were successful as fire penetration barriers.

14.6 FUTURE FACTORS THAT COULD HAVE MITIGATED STRUCTURAL COLLAPSE

In the course of the Investigation, NIST and its contractors were aware that there were existing, emerging, or even anticipated capabilities that could have prevented the collapse of WTC 7, had they been in place on September 11, 2001. NIST has not conducted studies to evaluate the degree to which building performance could have been improved on September 11, 2001, had the capabilities been available. These include:

- More robust connections and framing systems to better resist the effects of thermal expansion on the structural system.

- Structural systems expressly designed to prevent progressive collapse. The current model building codes do not require that buildings be designed to resist progressive collapse.

- Better thermal insulation (i.e., reduced conductivity and/or increased thickness) to limit heating of structural steel and to minimize both thermal expansion and weakening effects. Currently, insulation is used to protect steel strength, but it could also be used to maintain a lower temperature in the steel framing to limit thermal expansion.

- Automatic fire sprinkler systems with independent and reliable sources for the primary and secondary water supply.

- Improved compartmentation in tenant areas to limit the spread of fires.

- Thermally resistant window assemblies which limit breakage, reduce air supply, and retard fire growth.

14.7 HUMAN PERFORMANCE FACTORS

There were factors that contributed to the outcome of no loss of life at WTC 7.

- Reduced number of people in WTC 7 at the times of airplane impact on the towers.
- Shortness of delay in starting to evacuate.
- Evacuation assistance provided by emergency responders to evacuees.
- Participation of the building occupants in recent fire drills.
- Decision not to continue reconnaissance of the building and not to fight the fires within.

There were also factors that did not play a life safety role in WTC 7 on September 11, 2001, but could have been important had the fires been more widespread, the building damage more severe, or the building occupancy at full capacity.

- Accuracy and reliability of communications among emergency responders and building occupants.
- Efficiency of management of large-scale emergency incidents.

Appendix A
THE CON EDISON SUBSTATION IN WORLD TRADE CENTER 7

A.1 INTRODUCTION

A unique feature of WTC 7 was that the 47 story high-rise building was constructed above a Consolidated Edison Company of New York (Con Edison) substation (SS)[11] that supplied power to the entire WTC complex, as well as lower Manhattan. As a result, details about the construction and operation of the Con Edison substation were required in order to have a more complete understanding of the behavior of WTC 7 on September 11, 2001.

Based on numerous records, many furnished by Con Edison, this appendix:

- documents the general operation of the Con Edison power grid that served the WTC site on September 11, 2001;
- chronicles the events that took place on the electric power system supplying the WTC complex following the aircraft impacts on WTC 1 and WTC 2 to determine whether the power system behaved normally and predictably, and to establish the availability of power for rescue and fire fighting purposes in the immediate aftermath of the attack; and
- documents the distribution of power to WTC 7 between the time that WTC 2 collapsed and the time that WTC 7 began to collapse.

This appendix does not address the subsequent restoration activities to re-establish power to the area.

This effort provided insight into the availability of electrical power to pump water for the automatic sprinkler systems, the possible links between the fires that were observed in WTC 7 and the power distribution system, and whether any dramatic events may have initiated at the substation that could have contributed to the building's structural collapse.

[11] Technically, a substation consists of a set of transformers used to supply power to a specific area. As such, the Con Edison substation in WTC 7 was actually comprised of two substations. When referred to individually in this report, these substations are identified as "Substation #1" (SS #1), which consisted of transformers 1 through 5, and "Substation #2" (SS #2), which consisted of transformers 6 through 9. When the entire Con Edison complex within WTC 7 is referenced, it is identified as the "substation" or the "Con Edison substation."

Table A–1. Times for major events on September 11, 2001.(Chapter 5)

Event	Time (± 3 s)
First Plane Strike – WTC 1	8:46:30 a.m.
Second Plane Strike - WTC 2	9:02:59 a.m.
Collapse of WTC 2	9:58:59 a.m.
Collapse of WTC 1	10:28:22 a.m.
Collapse of WTC 7	5:20:52 p.m.

A.2 PHYSICAL LAYOUT OF THE CON EDISON WTC 7 SUBSTATION

Figure A-1 provides an overall plan view of the WTC building complex that relates the buildings cited in the text to the geographical layout. The Con Edison substation (indicated in red in Figure A-1) was located on Barclay Street, and comprised the first two levels along the north side of WTC 7. The 47 story building was considered a "tenant alteration" by The Port Authority of New York and New Jersey (PANYNJ) (WTC 7 Project Specifications 1984) to the original building housing the substation. Figure A-2 is a photograph of WTC 7 that shows the roof over the north portion of the substation and the Barclay Street facade, taken some time before September 11, 2001.

Construction of the two story building housing the substation, originally known as the Keystone Building, was begun in 1967. The nine transformer vaults that housed the 138/13.8 kV units were situated along the northern and western edges of the building, covering an area of about 85 m by 43 m (278 ft by 140 ft) on the 1st floor level. There was manhole access to the splicing chambers for both the incoming 138 kV and outgoing 13.8 kV cables (Emery Roth & Sons 1987). The extensive line-up of 13.8 kV switchgear was situated in two rows to the south of the transformer vaults (Emery Roth & Sons 1987). Access within the substation was provided by stairwells on the west side, in the center, and on the east side of the building. None of these stairs extended into the 47 story building above. Roll-up doors secured the two driveways on Barclay Street and Washington Street (PANYNJ 1987).

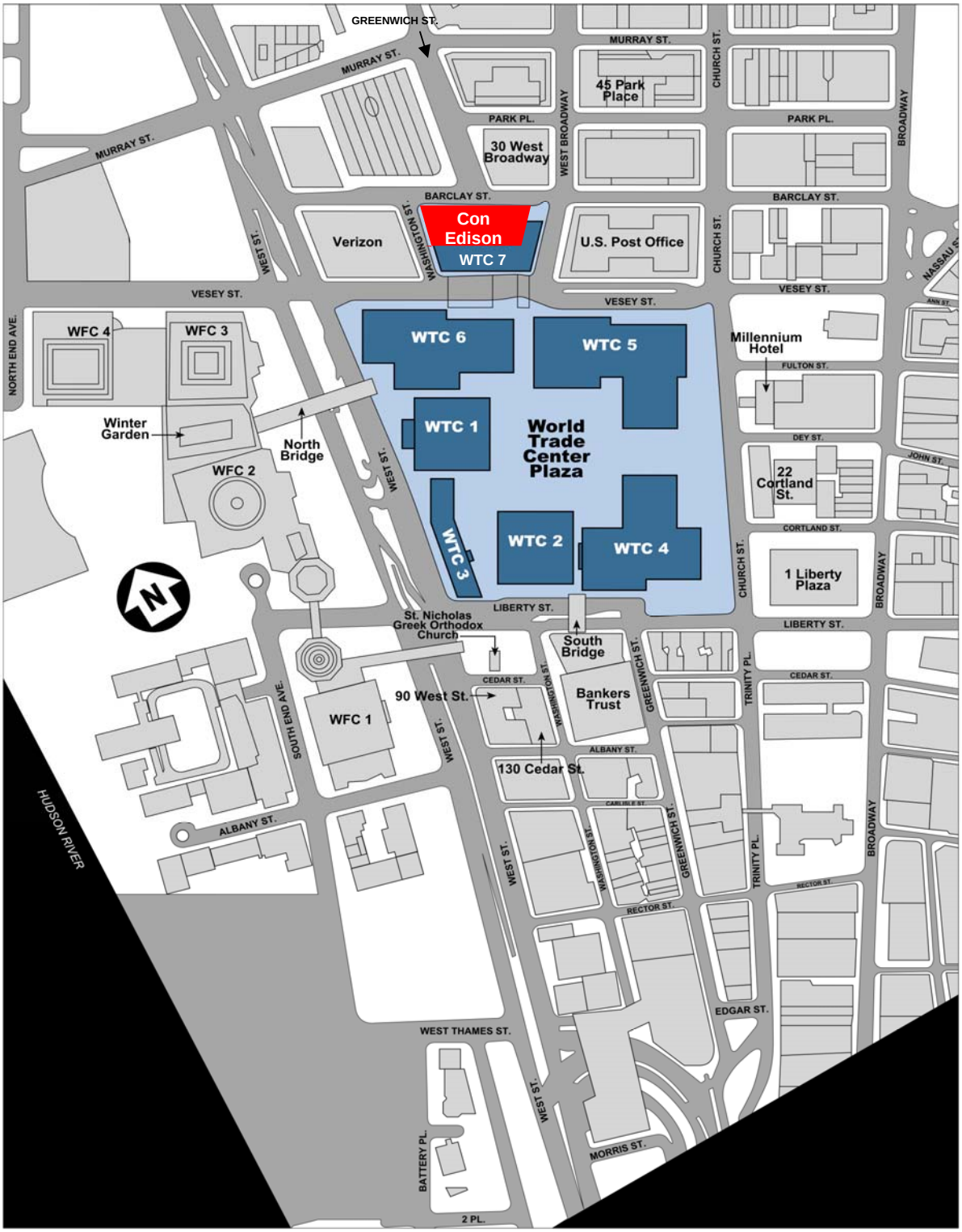

Source: NIST

Figure A-1. WTC site indicating the Con Edison substation location within WTC 7.

Source: Con Edison; reproduced with permission

Figure A-2. Aerial view from the north side of WTC 7 showing the Con Edison substation along Barclay Street. (Photo taken prior to September 11, 2001.)

A.3 OVERVIEW OF THE ELECTRIC POWER NETWORKS SUPPLYING LOWER MANHATTAN

A.3.1 Background on Power Distribution Systems

To understand what happened at the Con Edison substation on September 11, 2001, this section provides a brief description of power distribution systems in general, and, in Table A-2, defines some commonly used technical terms. The remainder of Section A.3 describes the networks supplying the WTC site. The sources material to Section A.3 are the Con Edison references in Section A.8.

Electric power is often generated in locations remote from the major centers of demand. There are a variety of good reasons for this (e.g., the provision of cheap hydro generation in eastern Canada). The transmission of bulk electric power from the locations where it is produced to load centers where it is consumed is accomplished using high voltages (115 kV to 765 kV in North America) in order to reduce the electrical losses that would be a consequence of low voltage transmission. However, safety and space requirements demand that it is ultimately utilized at much lower voltage levels (e.g., 110 V in the residential situation). As a consequence, a transition is needed from the high-voltage (HV) bulk transmission network to the consumer's premises (industrial and residential). This is usually accomplished in a number of stepped voltage reductions through a network which is usually radial. This

means that any break in the network will result in the loss of power at all points "downstream" of the break.

Table A-2. Glossary of Technical Terms Associated with Electrical Power Networks.

Term	Definition
3-phase	a system of electrical power generation and distribution which uses three conductors carrying alternating current which is phase separated by 120°
busbar	high current-carrying conductors (usually in substations) used to connect power system equipment in parallel
capacitor bank	an assembly of capacitors located at strategic points in the network to provide reactive compensation in order to regulate the voltage levels
circuit	see "feeder"
circuit breaker	a switch designed to be able to interrupt on command the high currents encountered during power system fault conditions
disconnect switch	a circuit switch used for isolating sections of a network, but without the ability to interrupt fault current in the same way as a circuit breaker
feeder	a set of conductors used to distribute power from a substation -- A feeder may comprise either underground cables or overhead lines. A circuit is a term sometimes used synonymously with feeder.
generator	a rotating electromechanical device capable of transforming the mechanical power from a prime mover into synchronous 3-phase electrical power
network	an assembly of feeders and substations for the transmission and distribution of electric power
protective relaying	a generic term given to the equipment used to determine, from measurements of voltage and current, whether abnormal conditions exist, and issue trip commands to circuit breakers according to a predetermined protocol
radial structure	a network topography in which electrical power is distributed outwards through radiating feeders from a single source
ring structure	a network topography in which electrical power may be derived from more than one routing
SCADA	acronym for Supervisory Control and Data Acquisition
SOCCSX	Consolidated Edison Company acronym for their Control Center
substation	the location of an assembly of transformers, circuit breakers and control equipment at nodal points in a power system
switchboard	an assembly of switches, fuses and metering equipment used to distribute power at low voltages (<600 V)
switchgear	a generic term for a piece of power system switching equipment (This would include various forms of circuit breaker, fuses, isolators, etc.)
T-connection	the solid junction of two feeders without the facility to isolate either feeder
tap changer	a device associated with a transformer which allows its turns-ratio to be adjusted (sometimes automatically on load) for the purpose of regulating voltage
transformer	an electromagnetic device designed to change the voltage level of a power system network
Y-connection	a system of interconnection of the 3-phase windings in a generator or transformer
Δ-connection	a system of interconnection of the 3-phase windings in a generator or transformer

The radial network from a bulk supply point usually has a "tree" structure so that power is delivered through the tree "trunk" to a plurality of "branches." The places from which the branches radiate are usually termed substations and are the locations in which most of the power system equipment is concentrated. Substations, which vary enormously in size and complexity, are where the voltage step-down is accomplished by means of transformers which supply power to the branches at progressively lower voltages. The connections joining the substations are usually termed feeders, which, in general, could be either overhead lines or underground cables. (In highly urban areas, these are more likely to be cable feeders.) For reasons of optimization, power is both generated and transmitted on a 3-phase basis, which implies that each feeder (or circuit) actually requires three phase conductors. In the case of cables, these may be three separate cables or, sometimes at the lower voltages, the three conductors are combined into a single multi-core cable.

The network is usually segregated, and each end of the feeders is provided with switches (usually located with the transformers at the substations) to permit the isolation of the major elements of such a system. This isolation, which can be accomplished by switch operation, facilitates two important functions: (1) it permits parts of the system to be isolated for maintenance, and (2) it permits the system to be segregated to isolate feeders, or other equipment, which develop faults.

In systems handling large amounts of power it is necessary that faulted sections be isolated quickly to limit the dissipation of large amounts of energy and concomitant damage. To facilitate this, the switches referred to above (called circuit breakers) are capable of fast and automatic operation at power levels which calculations show are the worst case conditions for their location. (Since each feeder is normally 3-phase, the circuit breakers actually have three switches – one for each phase.) The detection of an abnormal condition is accomplished by equipment called protective relays.

Protective relaying is a fundamental underpinning of power system design. Automatic protection systems must be applied to power networks at all levels both to provide safety from electrocution and fire hazards and to safeguard apparatus. Automatic protection systems can vary from fuses applied to low voltage distribution systems to sophisticated and fast-acting systems applied to extra high voltage bulk power networks. The selection and design of protective relaying systems usually involve compromise to achieve both sensitivity and discrimination. The latter is needed to insure that the minimum extent of the network is disconnected to clear a fault, so that disruption of supply to consumers is minimized.

These relays sample both currents and voltages on the network and interpret the findings to diagnose conditions (such as an unacceptably high current) which require operation of the circuit breakers to isolate a section of the network. In order to overcome the inherent unreliability of a radial arrangement, it is common practice to provide dual- or multiple-circuit lines connecting the same points in the system. In that way the loss and automatic isolation of one feeder does not necessarily interrupt the supply since the feeders in parallel may be able to carry the prevailing load.

In the same way that reliability is improved by providing parallel feeders, substations are often provided a bank of transformers. The transformers in a bank are connected in parallel by a series of conductors usually termed busbars. By this means, a transformer may be taken out of service through the operation of circuit breakers on either side (automatically because of a fault in the unit, or manually for maintenance), and the load carried by the remaining units. Equipment in large substations is often provided with other diagnostic sensors to provide an indication of abnormal conditions. The measurement of oil temperature in a transformer would be a simple example.

Conditions in the substation and the status of circuit breakers are often transmitted by a telemetry system to a remote control center responsible for system operation. Manual operation of circuit breakers may also be possible by remote control. Such systems of monitoring and control are often referred to as SCADA (Supervisory Control and Data Acquisition) systems.

A.3.2 Supply of the WTC Complex from the Con Edison System

In common with typical U.S. practice, the power system at the WTC complex was distributed radially from a bulk supply point, and was progressively stepped down in voltage through the system. There was no ring structure which would have permitted power to be fed from more than one direction. The Con Edison substation housed transformers to change the voltage level, circuit breakers to permit system segregation, and numerous other items of support, control, communications, and metering equipment. The substations were connected with underground cables that permitted the flow of power to the consumer. (Con Edison 1969; Con Edison 2005d; Con Edison 2005h; Con Edison 2005j; Con Edison 2005k)

Circuit breakers were located at both ends of the high voltage feeders so as to permit the isolation of parts of the network. These had three important functions:

- Faulted sections of the system could be isolated thus preventing a fault from shutting down the complete network.
- Some limited network reconfiguration could be made under abnormal circumstances.
- Sections of the HV system could be isolated for maintenance.

In the context of the WTC Investigation, the first function was of paramount importance. In the event of a fault on the system, the abnormal condition was detected through the monitoring of voltages and currents at the substation. Various forms of protective relaying were employed to detect the location of the fault and trip the appropriate circuit breaker(s) so as to quickly isolate (automatically and without intervention from the system operator) the minimum extent of the network needed to remove the faulted section (Con Edison 2005d). Because this was a radial system, all supply was lost downstream of the operated breaker.

Figure A-3 is a highly simplified diagram of the power supply arrangements which were in place on September 11, 2001, in the vicinity of the WTC complex. Bulk power was fed into the area at a nominal voltage of 138 kV through five 3-phase feeders that were supplied from a transmission switching station that was operated by Con Edison. These circuits fed the two WTC substations physically located at the base of WTC 7, as well as a third substation at the Seaport location. A "T" connection fed the Seaport substation, as shown in Figure A-3. These substations served to reduce the voltage to a nominal 13.8 kV by means of a series of transformers rated at 65.3 MVA (Megavolt Ampere). The five transformers (one of which was normally not in use) located in SS#1 supplied both the WTC complex and also the Cortland network in Lower Manhattan. The four transformers in SS#2 were supplied at 138 kV from feeds through SS#1 and similarly supplied the Battery Park and Park Place networks through 13.8 kV cables. (Con Edison 2005d; Con Edison 2005g; Con Edison 2005h; Con Edison 2005j; Con Edison 2005k)

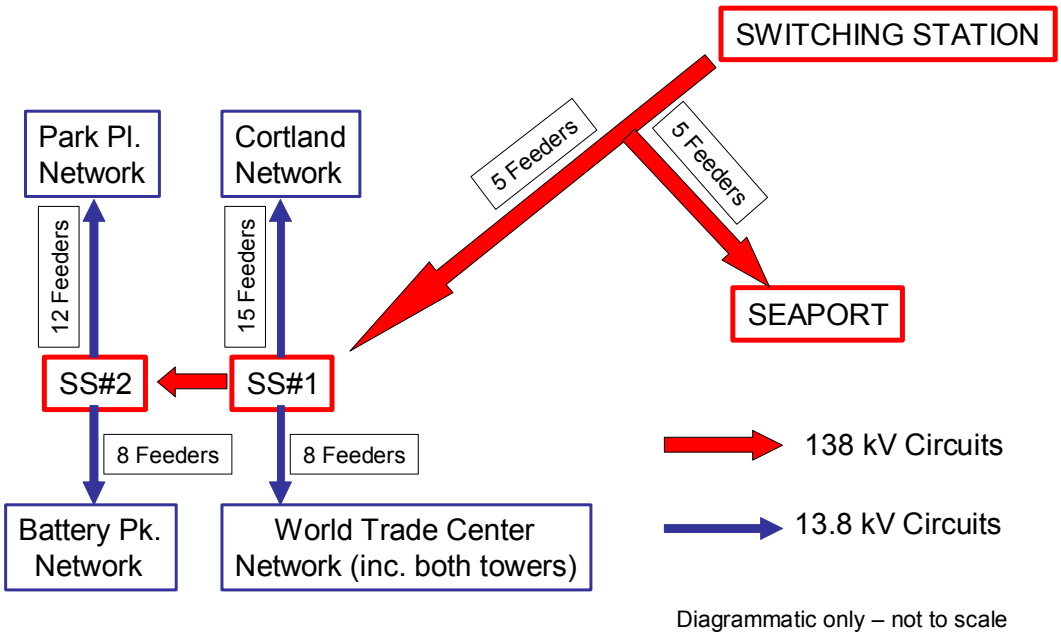

Figure A-3. Simplified diagram of the World Trade Center power supply

The primary electrical supply to the WTC towers was entirely dependent on the feeds from SS#1 in the WTC 7 building. Substation #1, in turn, was supplied at higher voltage from the 138 kV substation at the transmission switching station. The use of multiple feeders for both the 13.8 kV and 138 kV circuits provided considerable redundancy to safeguard against equipment failures. Similarly, the substation arrangement provided a parallel configuration which permitted the sharing of these circuits under abnormal conditions to allow for contingencies (Con Edison 2005h). Prior to the attacks on September 11, 2001, all these circuits were operational, and the load was light. As a result, normal conditions prevailed (Con Edison 2005b; Con Edison 2005i).

A.3.3 Substation Operations and Building Supply

Substation Staffing

The Con Edison substation in WTC 7 was staffed on the daytime shift, Monday through Friday, by a single senior substation operator, who was on duty during the events on September 11, 2001. In addition, two mechanics from the Con Edison Substation Operations Transformer Group were assigned to perform scheduled work at the substation and were on site or arrived shortly after the first aircraft struck WTC 1. After the event began, two senior substation operators and an assistant substation operator were dispatched to and arrived at the substation to assist the senior substation operator (Con Edison 2005b; Con Edison 2005c). Subsequently, four additional substation operations personnel (the area manager, a senior planning analyst, and two field planners) arrived at the substation. The substation was evacuated sometime between 10:20 a.m. and 10:25 a.m. (Con Edison 2005c), just before the collapse of WTC 1, the tower closer to WTC 7. Remote operation of the switchgear was possible for these substations, and telemetry was available to permit monitoring of many of the important parameters and functions from Con Edison's remote Energy Control Center (ECC). From logs of this supervisory system, switching and other operations, including the WTC emergency systems, were chronicled.

Electrical Equipment Utilized in the Con Edison Substation

All nine transformers were rated at 65 MVA (with full cooling) on a 3-phase basis (Rubenstein Engineering PC 1989). They were insulated with conventional oil/cellulose materials, unlike the step-down transformers in WTC 1 and WTC 2, which were filled with silicone fluid to reduce the flammability hazard. The oil impregnant was a naphthalenic-based mineral oil with an autoignition temperature of about 250 °C, in conformance with IEC 60296 (IEC 2003). The units were not identical to each other and were manufactured by more than one supplier. There were small differences in the cooling protocols and in the means for dealing with oil expansion. However, these differences were not considered important in the context of the Investigation. These transformers were rated on a multiple basis (with and without forced air/oil circulation), cooled with radiators and fans, and equipped with load tap changers for making voltage adjustments. All the transformers were Δ-Y connected, with the low voltage Y-connected secondary grounded through a reactor. Facilities were provided for on-site and remote monitoring of the usual critical parameters/functions, including oil temperature, tap change operation, oil level, and nitrogen blanket pressure.

The circuit breakers controlling the incoming (138 kV) and outgoing (13.8 kV) feeders were also not identical to each other (Rubenstein Engineering PC 1989). In SS#1, air-magnetic circuit breakers were the predominant technology. The 13.8 kV breakers were continuously rated at 1200 A, with an interrupting capacity of 1000 MVA. On the other hand, in SS#2, vacuum interrupters were employed, having a current rating of 1000 A or 3000 A and an interrupting capacity of 1000 MVA. In both substations, circuit breaker operation was facilitated through a 125 V DC supply. The power was needed for manual and automatic circuit tripping and closing. The supply was provided by means of batteries which permitted relaying and circuit breaker operation in the event that local power was not available. Two independent battery systems were provided with charging facilities from an auxiliary power supply fed from the 38 kV busbars (Rubenstein Engineering PC 1989).

The circuit breakers controlling the cable feeders supplying the WTC were all provided with timed over-current protective relaying with an instantaneous element set for a rapid disconnection for close-in faults (Con Edison 2005d). This protective scheme was designed to detect over-current and ground faults, and would provide automatic operation of the circuit breakers. Both substations were also provided with reactive support. This took the form of three 20 MVAr (Megavolt Ampere reactive) capacitor banks connected at the 13.8 kV busbars in each substation. The capacitor banks were designed to support the voltage in the presence of line drop in the circuits.

Supply of power to WTC 7

The main power from the Con Edison substation for the 47 story WTC 7 building above was routed through four 3-phase feeders (designated 37M02, 37M03, 37M06 and 37M08) rated at 15 kV each, with circuit breakers at both ends. These cables were routed in two concrete-encased conduits within the south side of the building core, adjacent to the elevator banks, from the 1st floor level to the 5th floor (Emery Roth & Sons 1987a). The main distribution center for WTC 7, including switchgear and transformers, was located along the central south perimeter of the 5th floor (Emery Roth & Sons 1987a). The incoming circuits were protected with conventional ground fault and over-current protection, as well as directional and zero-sequence relaying. (This equipment provided automatic circuit breaker operation in the event of faults.) Each feed was then routed separately, via a further set of circuit breakers, to three collection

busbars through 13.8 kV/480V 2.8 MVA Δ-Y transformers (12 transformers in all). Interlocks were provided to insure that manual switching operations were done in the correct sequence (Emery Roth & Sons 1987b). Since each of these collector busbars derived power independently from each of the four incoming Con Edison feeders, a considerable degree of redundancy existed. Unlike those in the Con Edison substation, these transformers were filled with silicone oil and housed in segregated transformer vaults on the south side of the 5th floor (Emery Roth & Sons 1987c) with the associated switchgear cabinets nearby. From the three collection busbars, power was distributed through the building via numerous switchboards and risers rated at 460V and up to 5000 A.

The 5th floor of WTC 7 also housed a generator room with five generators in the southwest corner, six generators along the north wall, and dual battery banks and associated chargers. Two of the 5th floor generators fed an emergency switchboard through automatic transfer switches, which were designed to be "break-before-make" to avoid the possibility of back-feeding power into the Con Edison system. In this way, essential loads could have been supplied even in the event of a complete failure of the utility network.

A.3.4 Description of the Power Supply for the Remaining WTC Complex

Figure A-3 indicates that eight circuits were employed to feed the WTC complex at 13.8 kV. This was done via cables from the Con Edison SS#1. All the cables were routed through splicing chambers on the A-1 level to a primary distribution center (PANYNJ 1998), where the circuits were split and cables routed to feed numerous other substations in the WTC complex, all nominally at 13.8 kV and 3-phase. The distribution to the various satellite step-down substations was as follows:

- four circuits supplied the NE Plaza substation, WTC 5
- six circuits supplied the Customs House building, WTC 6
- four circuits supplied the SE Plaza substation, WTC 4
- eight circuits supplied WTC 1 through numerous substations
- eight circuits supplied WTC 2 through numerous substations
- seven circuits were used to provide refrigeration power
- two circuits supplied the hotel, WTC 3.

In the case of WTC 1 and WTC 2, distribution of electrical power within the buildings was not done entirely at low voltage, due to the size of the load and the height of the structures. This necessitated 13.8 kV cable risers within the building to feed substations located on floors 7, 41, 75 and 108, in addition to three lower level substations (PANYNJ 1988). Two separate substations were located on each of these floors. Each had a 1500 kVA transformer for each incoming feeder, with a disconnect switch on the primary side (PANYNJ 1990). In each tower, the eight high-voltage circuits were divided into two groups of four, and the four circuits routed (together) to the substations on each side of the tower. For example, in WTC 1, four circuits fed the substations on the north side and four on the south side. However, each group of four circuits was routed all the way to the top (i.e., to the substations on the 108th floor) with 3-

way splices made to provide "T-off" connections to the substations at the 7th, 41st and 75th floors. The transformers fed a common 4000A busbar on the secondary side. Power was then distributed to the relevant locations through a low-voltage switchboard.

The supply of large parts of the structure at a higher voltage does imply that a cable failure, due, for example, to the aircraft impacts, would have necessitated the tripping of the 13.8 kV circuit breaker controlling that entire circuit. Even though each substation obtained a supply from multiple feeders, cables routed in close proximity were all vulnerable simultaneously. However, the practice of splitting the eight circuits into two groups of four does mean that, although damage to the cables would cause connected substations on all levels to lose power, the substations at all levels on the other side of the building could continue to operate. This is discussed further in the context of the aircraft impacts.

A.4 TIME LINE OF CON ED SUBSTATION EVENTS

A.4.1 Tripping Events, Substation #1

Table A-3 provides a record of activity on September 11, 2001, for all the feeders into and out of SS #1, together with the associated circuit breaker designations transcribed from the system diagrams (Con Edison 2005h) . The first number of the circuit ID corresponds to the network being served:

37: World Trade Center (all seven buildings, as described above)

15: Cortland Network

38: In-feed from the transmission switching station (at 138 kV)

Table A-3. WTC Substation #1 tripping sequence.

Circuit ID	Breaker ID	Transformer Circuit	Network	Trip ≈ 8:46	Trip ≈ 9:03	Trip ≈ 9:59	Trip ≈ 10:28	Trip ≈ 16:33
37M01	13N	1	WTC			A		
37M02	23N	2	WTC	A				
37M03	13S	1	WTC			A		
37M04	43N	4	WTC		A			
37M05	33N	3	WTC			A		
37M06	43S	4	WTC		A			
37M07	23S	2	WTC	A				
37M08	33S	3	WTC			A		
15M81	21S	2	Cortland			A		
15M82	41S	4	Cortland			A		
15M83	32N	3	Cortland			A		
15M84	21N	2	Cortland			A		
15M85	22S	2	Cortland					M
15M86	42S	4	Cortland					M
15M87	31N	3	Cortland					M
15M88	22N	2	Cortland					M
15M89	11N	1	Cortland			A		
15M90	11S	1	Cortland			A		
15M91	32S	3	Cortland			A		
15M92	42N	4	Cortland			A		
15M93	41N	4	Cortland					M
15M94	31S	3	Cortland					M
15M96	12S	1	Cortland					M
38M11	CI-1	1	TR 5 138 TSS					M
38M12	CI-2	2	Tr 7 138 TSS					M
38M13	CI-3	3	Tr 10 138 TSS					M
38M14	CI-4	4	Tr 8 138 TSS					M
38M15	CI-5	5	Tr 9 138 TSS					M (16:34)
L&P1	12N	1	Aux.Power					M (17:46)

A: Automatic circuit breaker trip by protective relaying M: Manual trip at control center
TSS: Transmission Switching Station operated by Con Edison

Prior to the impact of the first aircraft, all the feeder circuit breakers were closed, and all indications were that the power system was operating normally. The columns on the right of Table A-3 depict the times at which circuit breaker operations took place (either automatically [A] as a result of the operation of the protective relaying, or manually [M] by operations commanded by the control center). This information was transcribed from the station logs (Con Edison, SOCCSX) and a Con Edison incident report (Con Edison 2005i). Events are given in eastern daylight time.

Of primary interest from Table A-3 is that two of the circuits tripped automatically at 8:46 a.m., as a result of collateral damage caused by the aircraft impact into WTC 1, and a further two were lost at 9:03 a.m. in the same way, when WTC 2 was impacted by an aircraft. Note that for each aircraft impact, all the circuits were not damaged initially, presumably as a result of dividing the power and providing two separate routings to the substations on either side of the towers. At 9:59 a.m., the remaining four circuits feeding the entire WTC complex tripped automatically. As a result, power to all seven of the WTC buildings from the utility was lost. This occurred, as designed, by the operation of the installed protective relays without any utility intervention. No evidence indicated that the faults on the cable system or in the WTC distribution substations were caused by anything other than the collapse of WTC 2.

Unlike the rest of the complex, power supply to WTC 7 was not routed through the primary distribution center, since the Con Edison substation was in the same building. Table A-3 suggests that some utility power was available to all of the buildings, including WTC 7, until almost 10 a.m. After that time, although utility power was available at the Con Edison substation, it was not available to consumers in WTC 7. However, since WTC 7 was still intact at that time, the loss of all utility power would have activated the emergency generator automatic transfer switches to provide emergency power. The two WTC 7 900 kW emergency generators were equipped with auto engine starting controls, and some emergency generation was running in WTC 7 before the building's eventual collapse in the afternoon.[12]

Power was still coming into the WTC Con Edison substation after 10 a.m. since the 138 kV circuits from the transmission switching station were still energized (and some of the feeders supplying the Cortland network were still functional) since circuit breakers designated CI-1 through CI-5 were still closed. (See Table A-3.) Auxiliary power at the Con Edison substation was also still available through two 500 kVA transformers (breaker L&P1 was still closed) fed from the 13.8 kV busbars in both SS #1 and SS #2 even though power to the rest of the building was lost at 10 a.m.

At 4:33 p.m., the utility control center made a decision to open all the remaining Cortland circuits and isolate the WTC 7 substations by opening the 138 kV circuit breakers. This decision was made about two hours after FDNY officers decided to completely abandon WTC 7 and the final order was given to evacuate the site around the building (Chapter 6). Opening the Cortland circuits resulted in the loss of auxiliary power at the Con Edison substation, but because the primary power supply had already been lost to the rest of WTC 7 at 10 a.m., this additional action would have had no effect on the rest of WTC 7 (including emergency generation if it had still been available). The Con Edison substation was also equipped with emergency battery back-up which was designed to operate emergency lighting and fire protection systems for a limited period of time in the event that all other power was lost to the substation.

[12] WTC 7 Interviews 1, 2, 3, January, 2004.

A.4.2 Tripping Events, Substation #2

Analogous information for SS #2 is provided in Table A-4, from which it may be seen that some circuits to the Battery Park network and one to Park Place were lost during the morning due to the automatic operation of the protective relaying. At 4:33 p.m., in concert with the actions taken in SS #1, Con Edison decided to isolate the remaining Battery Park and Park Place feeders and to shut down SS #2 by opening the 138 kV breakers CI-6 through CI-9 supplying the transformers in SS #2.

A.4.3 Isolation of the 138 kV Network

As illustrated in Fig. A-3, the five circuits supplying SS #1 and SS #2 from the transmission switching station were also supplying the Seaport substation. At 4:33 p.m., when Con Edison decided to shut down the WTC substations, all of the 138 kV substation breakers were opened at SS #1 and SS #2. However, two of the feeders (38M13 and 38M15) were left energized from the transmission switching station (Con Edison 2005k). This meant that although both substations were effectively shut down, live terminations were present at the supply side of circuit breakers CI-3 and CI-5 (in SS #1) and CI-7 and CI-8 (in SS #2). This was done with the hope of preventing the Seaport substation also from losing all power, which would have led to the loss of power to consumers fed from that substation in the Fulton Network (Con Edison 2005k). This condition existed until the collapse of WTC 7 at 5:21 p.m. when damage to the cable terminations caused faults on both of the remaining live feeders, and protective relaying at the transmission switching station opened the circuits automatically with the consequent loss of power to the Fulton network that was fed through the Seaport substation. The collapse of WTC 7 destroyed the Con Edison substations within the building.

A.4.4 Monitoring of Safety Systems

The Con Edison substations in WTC 7 were provided with a Supervisory Control and Data Acquisition (SCADA) system (Con Edison 2005i) which continuously monitored and logged the vital parameters of the substations. In particular, it documented switching operations and provided flags when key parameters changed or appeared anomalous. These logs were made available to the NIST team by Con Edison. The Investigation staff studied the entries between 8:00 a.m. and 8:40 p.m. on September 11, 2001. A considerable volume of these log entries involved housekeeping matters such as removing and returning apparatus in the scan sequence, but the entries also were the source of the timing of both automatic and manual tripping of the circuit breakers documented in Tables A-3 and A-4. As soon as a circuit breaker was tripped, the system topology changed, and the load currents in the substation changed accordingly. In turn this often caused key voltages to fall momentarily (as a result of the fault) and then rise (as a result of the fault clearance). Such fluctuations caused voltage deviation alarms and the relaying equipment in the substation to signal operation of transformer on-load tap-changing equipment (a device designed to change the ratio of a transformer to restore its terminal voltage to the prescribed level). The SCADA logs are full of such entries, which chronicle the large number of circuit breaker operations resulting from the sequence of events at the WTC that day.

Table A-4. Con Edison WTC Substation #2 tripping sequence.

Circuit ID	Breaker ID	Transformer Circuit	Network	Trip ≈ 8:46	Trip ≈ 9:03	Trip ≈ 9:59	Trip ≈ 10.:28	Trip ≈ 16:33
14M21	61N	6	Batt. Park					M
14M22	61S	6	Batt. Park					M
14M23	81N	8	Batt. Park				A	
14M24	71N	7	Batt. Park				A	
14M25	71S	7	Batt. Park			A		
14M26	91S	9	Batt. Park			A		
14M27	81S	8	Batt. Park			A		
14M28	91N	9	Batt. Park			A		
34M31	62S	6	Park Pl.					M
34M32	72N	7	Park Pl.					M
34M33	82N	8	Park Pl.					M
34M34	92S	9	Park Pl.					M
34M35	62N	6	Park Pl.					M
34M36	72S	7	Park Pl.					M
34M37	82S	8	Park Pl.					M
34M38	92N	9	Park Pl.				A	
34M39	63S	6	Park Pl.					M
34M40	73N	7	Park Pl.					M
34M41	83S	8	Park Pl.					M
34M42	93N	9	Park Pl.					M
38M11	CI-6	6	TR 5 138 TSS					M (16:47)
38M13	CI-8	8	Tr 10 138 TSS					M
38M14	CI-9	9	Tr 8 138 TSS					M
38M15	CI-7	7	Tr 9 138 TSS					M

A: Automatic circuit breaker trip by protective relaying M: Manual trip at control center
TSS: Transmission Switching Station operated by Con Edison

Careful study of the large number of entries indicated that, with a few notable exceptions, the actions were explicable in terms of the events taking place on that date. The exceptions were fire alarms which occurred in WTC 7 Con Edison SS #1. The following fire alarm signals were recorded for SS #1 on September 11:

- 10:00:10 a.m. "Alarm"
- 10:00:18 a.m. "Normal"
- 10:00:23 a.m. "Alarm"
- 10:01:00 a.m. "Normal"
- 10:28:58 a.m. "Alarm"
- 4:34:07 p.m. "Normal"

These communications were obtained from the SCADA data transmitted from the World Trade Center substation to Con Edison's Energy Control Center (ECC). The substation operator's log on which the substation operator recorded incidents, such as fire alarms, was destroyed when WTC 7 collapsed on the substation (Con Edison 2005b).

The substation building fire alarm system was designed to activate when it detected the presence of smoke, at which time a zone indicator light on the substation fire alarm panel would be illuminated and an audible alarm inside the control room would sound. Activation of the substation fire alarm also would transmit an "alarm" indication to the ECC.

The "normal" notation was transmitted to the ECC when the substation operator acknowledged the alarm by manually pressing the alarm-reset button. This would allow a subsequent fire alarm to be recorded at the ECC and not be masked by the prior alarm. If the smoke condition persisted, pressing the reset button silenced the audible alarm at the substation, but the visual indicator on the substation alarm panel remained lit. The alarm could also clear itself at the substation and transmit a "normal" notation to the ECC without operator intervention, if the condition that triggered the alarm subsided.

Personnel present in the substation on September 11, 2001, before the evacuation observed dust in the substation atmosphere in the proximity of ventilation louvers on the west side of the substation facing Washington Street (Con Edison 2005b). Dust, in addition to smoke and other particulate matter, can trigger a smoke alarm. Since both dust and smoke filled the air at street level along Washington Street after the collapse of WTC 2, it was possible for such smoke and dust to have activated a smoke detector within the substation. The rapid sequence of "Alarm" and "Normal" signals between 10:00:10a.m. and 10:01:00 a.m. is consistent with an automatic clearing of the alarm. Prior to the evacuation of the substation between 10:20 a.m. and 10:25 a.m., the Con Edison building was searched for the presence of personnel. The person who conducted the search did not observe any evidence of fire or burning material at that time (Con Edison 2005b).

The 10:28:58 a.m. alarm condition persisted until the remaining transmission switching station circuit breakers were opened at around 4:33 p.m. A huge amount of additional dust and smoke was generated

when WTC 1 collapsed, and would have remained in the air or contaminated the smoke detector during the period the alarm condition persisted.

A.5 PHYSICAL CONDITION OF THE CON EDISON BUILDING FOLLOWING THE COLLAPSE OF WTC 1

Following the evacuation of the substation shortly before the collapse of WTC 1, the Con Edison portion of WTC 7 was secured by Con Edison, and there was no evidence of anyone reentering the substation building up to the time when WTC 7 collapsed. From the photographs and videos examined, the exterior of the substation suffered no significant direct damage due to the collapse of WTC 1. Figure A-4, a photograph taken sometime in the afternoon, shows the northwest corner of WTC 7, along with a considerable amount of debris on Washington Street. Aside from what appear to be superficial scrapes on the two large street level louvers south of the driveway door, this portion of the building looks intact. (Note that the broken panes above the louvers spanned the 3rd and 4th floors of WTC 7 and were not connected to the Con Edison substation.

George Miller/NYCTA

Figure A-4. Northwest corner of the Con Edison substation (building on left), showing light damage from WTC 1 debris. (Photo taken sometime in the afternoon on Sept. 11, 2001.)

Figure A-5 shows another view of the Con Edison portion of WTC 7, shot from a police helicopter between about 1:00 p.m. and 3:00 p.m. Fires can be seen on the 7th and 12th floors of WTC 7. Light debris is visible on the grill work which formed the roof of the north portion of the Con Edison substation; this portion of the Con Edison substation appears to be intact, with no visible evidence of smoke. No photograph, video record, or witness account gathered during the investigation identified smoke or flames originating from the Con Edison portion of WTC 7.

The collapse of WTC 7 buried the Con Edison structure and all the equipment in it. Figure A-6 shows the collapsed building at the beginning of the salvage and clean up operations, viewed looking south from Greenwich Street.

Figure A-5. Aerial view of the middle of the north side of the Con Edison substation, taken sometime between 1 p.m. and 3 p.m. on September 11, 2001.

Source: NYPD Aviation unit photo, 2-50 #21

Figure A-6. Debris pile from collapse of WTC 7 onto the Con Edison substation, viewed looking south from Greenwich Street, date undetermined.

Source: Con Edison, reproduced with permission

The photographs in Figures A-7 through A-9 were taken during the salvage operations. Four of the nine transformers that were part of SS #1 and SS #2 are depicted in these photographs.

The left photograph in Figure A-7 was taken about five weeks after September 11, 2001. It shows the remnants of the Con Edison substation after the removal of much of the debris. The area outlined in a dotted white line is enlarged in the right photograph in Figure A-7A. From its location in the pile, this appears to be transformer #4, but also may be #8 or #9. The interior of this transformer was described as being severely thermally damaged, possibly by fire (G&S Technologies 2005e)[13].

[13] NIST Interview with G&S Technologies, August, 2005.

Source: G&S Technologies, reproduced with permission

Figure A-7. Photographs taken on mid-October, 2001, showing Con Edison transformer #4 (or #8 or #9) uncovered from the debris pile of WTC 7.

A similar assessment of thermal damage was made for transformer #1, shown on the right in Figure A-8. This is in contrast to transformer #6, which is the unit on the left in Figure A-8. The gray paint on transformer #6 is clearly evident, with little indication of rust or excessive heat.

Figure A-8. Photograph taken in mid-October, 2001, showing Con Edison transformers #6 and #1 uncovered from debris pile of WTC 7.

Source: G&S Technologies, reproduced with permission

Transformer #7 (or possibly #5) is barely visible within the white box in Figure A-9. This transformer and the other three depicted in Figures A-7 and A-8 were not salvageable and were discarded (G&S Technologies 2005e)[4].

NIST was unable to determine whether the thermal damage to the transformers occurred due to electrical overheating, due to a fire in the substation after the SCADA logs were terminated around 4:33 p.m., or due to burning within the rubble pile subsequent to the collapse of WTC 7.

Figure A-9. Con Edison transformer #7 (or #5) uncovered from debris pile of WTC 7; photo taken mid-October, 2001.

Source: G&S Technologies, reproduced with permission

A.6 POWER SOURCES FROM OTHER THAN CON-EDISON

A.6.1 Inventory

Backup electrical generation capacity is common for large commercial and government operations, such as some of those that were housed in the WTC complex and elsewhere in lower Manhattan. Under normal conditions, these distributed organizations receive their electricity from Con Edison, but in the event of a utility power outage they use their own generators to carry them through the power interruption. When the local generation capacity exceeds needs, the excess may be used to back up the utility by connecting to the network. Guidelines exist (IEEE 2003) for the protection of distributed generators and the network to which they are connected. Table A-5 provides an inventory of the distributed generation capacity in Lower Manhattan. The table is organized according to the networks depicted in Figure A-3.

Table A-5. Inventory of Distributed Generation in Lower Manhattan. (Con Edison 2005)

Network	No. of Installations	Total Capacity (MVA)	Connected Load (MVA)
Park Place	4	18.1	10.8
WTC	2	34.4	20.7
Cortland	9	28.6	16.0
Bowling Green	14	38.1	22.4

Although it would appear that many megawatts of excess power were available, none of these machines were network connected, and no contracts were in place for Con Edison to buy back excess capacity. If any of these sources had been available on September 11, 2001, destruction of the feeders caused by the collapses of WTC 1 and WTC 2 would have prevented any dispatch of these sources of power to the grid.

Since all power from the primary Con Edison system to the towers was lost by 10 a.m., it was important to examine the availability of other sources for fire fighting and emergency operations. The emergency systems at the WTC had backup power sources if the primary and secondary sources through the eight feeders from Con Edison were disrupted:

- Tertiary power from a feeder from the PATH substation
- Emergency generator plants
- Local battery backup

A.6.2 PATH Tertiary Connection

Documentation (PANYNJ 1968) indicates that a single 3-phase 2 MW feed was available to the WTC complex from the PATH subway system, which was installed after the 1993 bombing incident as a precautionary measure. This is important since this source of power was independent from Con Edison. The power was derived from Public Service Electric and Gas of New Jersey (PSEG), and originated at the PATH substation #3 through an isolator under PATH operational control (PANYNJ 2005a). This 27 kV, 3-core shielded cable ran about 50 m in concrete-encased conduit to a tertiary emergency switchgear room also located at platform level. The feeder supplied emergency power through a 2 MVA, Δ-Y, 27 kV/480 V 3-phase cast coil dry-type transformer (and a further 480V/120V step down to the emergency control panel through an automatic transfer switch). These arrangements had the capability of maintaining some emergency power from PSEG even in the event of the loss of all connection to Con Edison. In this way, fire fighter service freight elevators, stairwell lighting, and some other emergency loads within the WTC towers could have been maintained.

SCADA logs for September 11, 2001, indicate that at 9:02 a.m., the WTC emergency feed breaker closed automatically, activating this tertiary source of power. This occurred at the instant when WTC 2 was impacted and also corresponded to the time that the Con Edison logs indicated that two of the eight WTC 13.8 kV feeds from Con Edison were destroyed. (See Table A-3.) Emergency power would have been available from the PATH substation until about 9:59 a.m. when automatic protection opened the emergency feed breaker and de-energized the tertiary 27 kV feeder (PANYNJ 2005a). The collateral damage resulting from the collapse of WTC 2 at 9:59 a.m. was such that supplies from both Con Edison and from PSEG were compromised simultaneously.

A.6.3 Emergency Generation for Local Use

Perhaps of equal significance were the emergency generators situated in the WTC complex itself. By design, numerous generators would have been available after the utility supply was interrupted until the generators themselves were destroyed by the building collapses. The main emergency power transfer switching provided limited power not only for WTC 1 and WTC 2 but also for WTC 3, WTC 4, WTC 5,

and WTC 6. The emergency power would have provided electricity to operate emergency lighting, fire pumps, and some elevators in WTC 1 and WTC 2.

An emergency power control and distribution system with six additional 1 MW Waukesha continuously rated generating units was installed in WTC 1 and WTC 2, with the power being routed to critical equipment (exchange fans, sewage ejectors, fire pumps, etc.). It is not known if these units were running or started, but they were provided with automatic synchronizing equipment. If undamaged by the initial impact, they could have provided some emergency power until the collapse. There would have been, for example, enough power to run one elevator in each bank plus the fire fighter's service car. All elevator emergency power controls were relocated to a main lobby console when the new fire command station was built after the 1993 bombing of WTC 1. The presence of an automatic transfer switch also indicates that emergency power may not have been available until normal utility power was lost at about 10 a.m.

There was also a limited amount of local battery backup to provide stairwell lighting. This was known to have operated at the police desk in WTC 5 after the collapse of WTC 2 (PANYNJ 2005b).

Emergency power for WTC 7 was not provided from the main emergency center in the WTC complex, but documentation (Chapter 3) indicates that there were numerous generators on several floors of WTC 7, as shown in Table A-6. The base emergency power for the entire building (other than for the Con Edison substations) was supplied by the two 900 kW generators on the 5th floor. These units were equipped with automatic engine start controls and were known to have been operating after 10 a.m. when utility power to the 47 story building was lost.[12] The base emergency power was sufficient to supply electricity to the fire pumps, the fire alarm system, other emergency equipment, and the fuel pumps and peripheral equipment necessary to keep the emergency diesel generators operating. The other nine generators on the fifth floor were dedicated to providing emergency power to the Salomon Brothers spaces. These were also designed for automatic operation in case utility power was lost to the areas leased by Salomon Brothers.

Emergency power for the Mayor's Office of Emergency Management (OEM) was supplied by the three generators on the seventh floor. Single diesel generators on the eighth and ninth floors provided emergency power for the American Express and Secret Service tenants, respectively (Chapter 3). No information was found regarding the possible operation of these units on September 11, 2001.

Table A-6. Emergency generation available in WTC 7. (NIST NCSTAR 1-1J 2005)

Floor Location	Tenant	Number of Generators	Power/Generator
5	base building	2	900 kW
5	Salomon Smith Barney.	9	1750 kW
7	OEM	3	500 kW
8	American Express	1	350 kW
9	Secret Service	1	125 kW
		Total Capacity:	19.5 MW

A.7 SUMMARY

- The Con Edison substation was comprised of two electrically separated substations (SS #1 and SS #2) in the first two stories of the north side of WTC 7. Bulk power was delivered at 138 kV to the substation supplied from a transmission switching station operated by Con Edison, and distributed at 13.8 kV to the entire WTC complex, as well as to the Cortland, Battery Park, and Park Place networks in Lower Manhattan. At the start of the day on September 11, 2001, normal conditions prevailed at the Con Edison substation.

- Eight feeders supplying the WTC complex from SS #1 in WTC 7 were provided with over-current and ground fault protection, which appears to have operated as designed in response to the damage sustained by the aircraft impacts and subsequent building collapses. These automatic operations occurred at 8:46 a.m., 9:03 a.m., and 9:59 a.m., resulting in the loss of all primary power to the WTC towers by 10 a.m. These were correct automatic operations over which the power company had no control. The damage sustained was so massive that the redundancy that would normally have been provided by having eight separate circuits was not effective in increasing reliability. Indeed, given the overriding need to provide safety in high-voltage apparatus, it would have been difficult for any system at this power level to survive the damage sustained.

- Between the time of initial aircraft impact and the collapse of WTC 2, some utility power remained within all of the WTC buildings.

- All power to the WTC complex was cut at 9:59 a.m., either from automatic circuit breakers tripping or from physical damage to the feeder lines caused by the collapse of WTC 2.

- Alternatives to Con Edison power were potentially available at the WTC complex. A significant amount of electricity for use in the event of an emergency was fed through the subway tunnel from New Jersey. There were emergency supply generators in the towers; however, no evidence was found that these units provided power to aid firefighting and rescue after 10 a.m.

- Even though utility power to the rest of WTC 7 was lost at 9:59 a.m., auxiliary utility power to the Con Edison substation itself was still available from the transmission switching station feeders, allowing internal operations to be maintained. There is also evidence that the emergency diesel generators that supplied base power to the rest of WTC 7 did operate after the collapse of WTC 2, but no information was found regarding the operation of these emergency generators following the collapse of WTC 1.

- At 4:33 p.m., the utility control center made a decision to isolate the WTC 7 Con Edison substation by opening the 138 kV circuit breakers feeding the WTC 7 substation. This decision was made by Con Edison management about two hours after the Fire Department of New York (FDNY) officers had the building and immediate surroundings evacuated.

- Con Edison employees observed no fires or significant physical damage to the substation prior to the time when the substation building was evacuated (between 10:20 a.m. and 10:25

a.m.). NIST found no evidence that significant physical damage to the Con Edison portion of WTC 7 occurred due to the collapse of WTC 1 at 10:28 a.m.

- Signals from the Con Edison substation continued to be monitored offsite throughout the day on the supervisory control and data acquisition (SCADA) logs. One fire detector within the Con Edison substation did go into alarm when WTC 1 collapsed, and stayed in the alarm mode until the substation was totally isolated from incoming feeders at 4:33 p.m. However, there were no other indications (e.g., no high temperature alarms from the transformers, no visible smoke emanating from the Con Edison building) that a significant fire occurred within the substations during that period of time. Possible sources of the fire detector alarm were the smoke and dust dispersed in the area of the substations from the collapse of WTC 1.

- Photographs of several Con Edison transformers uncovered during site clean-up showed clear evidence of thermal damage. NIST acquired no material from these transformers and did not determine whether this thermal damage occurred due to electrical overheating, due to a fire in the Con Edison substation, or due to burning within the rubble pile subsequent to the collapse of WTC 7.

- NIST identified no events initiated at the substation that may have contributed to the structural collapse of WTC 7.

A.8 REFERENCES

Con Edison 1969. Drawing #A175040-17, General Arrangement of 138 kV Equipment and 13.8 kV Switchgear Equipment in 1st Flr.

Con Edison 2005a. photo #2 of WTC 7 prior to 9/11/01, received by NIST Oct. 18.

Con Edison 2005b. response to J.K. Nelson July 21 verbal questions to Con Edison.

Con Edison 2005c. response to W. Grosshandler, August 19 Email Questions.

Con Edison 2005d. response to NIST data request. Appendix D: Con Edison Trade Center #1 Substation (prior to 9/11/01) relay types and settings.

Con Edison 2005e. photo #1 of collapsed WTC 7, received by NIST Oct. 18.

Con Edison 2005f. response to NIST data request. Appendix A: Rubenstein Engineering PC., Specification # EI-5451 and EI-5413.

Con Edison 2005g. Power Network Map of Lower Manhattan.

Con Edison 2005h. response to NIST data request. Appendix B: 13.8 kV Substation one-line diagrams # 1-301 and # 2-302.

Con Edison 2005i. response to NIST data request. Appendix F: Alarm List relating to TC1 and TC2 from SOCCSX.

Con Edison 2005j. response to NIST data request. Appendix E: Con Edison District Operations Incident Report.

Con Edison 2005k. response to NIST data request. Appendix G: 138 kV one-line diagram.

Con Edison 2005l. response to NIST data request. Appendix C: Local connected Distributed Generation.

Emery Roth & Sons 1987A. Drawing # E-23, WTC 7, Single-line diagram.

Emery Roth & Sons 1987a. Drawing # E-3, WTC 7 1st Floor Plan - Power.

Emery Roth & Sons 1987c. Drawing # E-11, WTC 7 5th Floor Plan - Power.

G&S Technologies 2005a. #PA160004 taken 10/16/01 4:06 pm.

G&S Technologies 2005A. #PA160005 taken 10/16/01 4:06 pm.

G&S Technologies 2005c. #PA1010013.

G&S Technologies 2005d. #PA1010016.

IEC 2003. IEC 60296 Ed. 3.0 b:2003 Fluids for electrotechnical applications – Unused mineral insulating oils for transformers and switchgear, International Electrotechnical Commission.

PANYNJ 1968. Drawing # E-P-38, PATH substation one-line diagram.

PANYNJ 1988. Drawing # ES-1, 13.8 kV Service and Distribution System Riser Diagram.

PANYNJ 1990. Drawing # E-PR-7, Typical substation.

PANYNJ 1998. Drawing # E-2, 13.8 kV Feeder Riser Diagram.

PANYNJ 2005a. Email to NIST, May 4.

PANYNJ 2005A. Telephone interview, May 7, with Alan Reiss by K. Nelson.

Port of New York Authority Engineering Department 1987. Drawing # 104-1, Electrical Substation Superstructure, Architectural.

Rubenstein Engineering PC 1989. Specification # EI-5451 and EI-5413.

WTC 7 Project Specifications. 1984 (WTCI-187-P).

This page intentionally left blank.

Appendix B
ANALYSIS OF SEPTEMBER 11, 2001 SEISMOGRAM DATA

B.1 INTRODUCTION

During the September 11, 2001, World Trade Center (WTC) disaster, seismic signals generated by aircraft impacts and building collapses at the WTC site were recorded by seismographic stations around the metropolitan New York City area operated by the Lamont-Doherty Earth Observatory of Columbia University (LDEO). This appendix reports the analysis of the seismic records to assist the WTC Investigation in reconstructing the timing and magnitude of ground motion that may have been linked to specific events surrounding the collapse of WTC 7. The focus was on all recorded seismic signals generated between the times of collapse of WTC 1 and WTC 7. The specific objectives were to:

- analyze seismic records of Sept. 11, 2001 recorded at stations around the metropolitan New York City area for identifying seismic signals that may have been due to partial collapses at the WTC site in general, and WTC 7 in particular;
- characterize all observable seismic signals generated by the WTC disaster for the time window between the collapse of WTC 1 and WTC 7; and
- review data and information provided by NIST to identify seismic signals with possible sources at the WTC site.

The seismic records reviewed in this study were acquired as part of the routine earthquake monitoring network in the northeastern United States, and the seismometers were not optimized to capture the seismic signals from the collapse of the WTC towers or of WTC 7. The Investigation Team attempted to extract as much information as possible from these signals, which in some cases were not much greater than the background noise. This report documents the activities performed by LDEO, including the analysis of the seismic records, the characterization of the observable seismic signals, and the association of identifiable seismic signals with possible collapse events using information available at NIST.

B.2 SEISMIC DATA AVAILABLE FOR ANALYSIS

Seismic events generate three dimensional waves that emanate from the source in a way that is dependent upon the strength and depth of the event and the surrounding geological features. A seismogram is a record of the very small motions created by these waves as they pass a sensor, displayed in graphical form as an oscillating curve (nm/s) over a period of time. The energy radiated from the seismic event is related to the square of this ground speed and the duration in time over which the motion occurs. An accurate estimate of the radiated seismic energy requires complex correction terms; and, as a result, it is customary to characterize the size of an earthquake only in terms of the peak amplitude of the ground motion, M_L, or the familiar Richter scale.

The LDEO seismic station located in Palisades, NY, (referred to as PAL) records three components of seismic waves: north-south, east-west, and vertical. This allows determination of the direction of the

incoming waves. Three-component data are also useful for characterizing source properties. For example, an earthquake generates strong shear waves in the transverse component (perpendicular to the direction of wave propagation). In contrast, an explosion source excites strong longitudinal waves (similar to a sound wave) along the direction of propagation. Seismic signals excited by a building collapse are basically due to a vertical force acting on the ground surface; hence, seismic shear waves (*S*) are excited near the surface, and subsequently travel as surface waves. The primary wave (*P*) excitation is maximum on the axis of force (vertically downward) and is relatively weak compared to *S* wave excitation near the source region (up to a few tens of kilometers). Note that seismic *P* waves are longitudinal and propagate similarly to sound waves. *P* waves travel with a speed of about 6 km/s near the Earth's surface and can propagate through a fluid at a slower speed (≈ 1.5 km/s in water at standard conditions), whereas *S* waves propagate only through planar elastic solids (e.g., competent bedrock), with a speed of about 3.5 km/s near the Earth's surface. Fundamental-mode Rayleigh waves (*Rg*) are short-period, seismic shear waves with strongest amplitudes near the free surface of planar elastic solids. A Rayleigh wave is efficiently excited by a shallow seismic source (at depths less than a few km); and, hence, it can be used as an indicator for a shallow seismic source, such as a building collapse.

There were six stations within 100 km of the WTC site, including the station PAL which was the closest (34 km) to Manhattan. Figure B-1 shows their locations. PAL is the quietest site among the stations, and it serves as the reference station for the analysis. PAL is equipped with a three-component, broadband seismometer as well as three-component short-period sensors. Modern broadband seismometers, widely used since the early 1990s, have a natural period between a few tens to a few hundreds of seconds and are designed to record long-period seismic signals from large distant earthquakes, as well as high frequency signals from small local earthquakes (up to about 20 Hz). The different components of three-component broadband seismometers are designated using the following nomenclature: BHZ (vertical-component), BHN (north-south component) and BHE (east-west component). When two horizontal components are rotated to align with the great circle path between the source and receiver, the pure longitudinal-component (denoted as BHR) and the transverse-component (BHT) are obtained. Short-period seismometers usually have a natural period of about 1 s and are designed to record high frequency signals from local and regional earthquakes (usually up to about 100 Hz). Short-period stations are usually equipped with only a vertical-component seismometer, and its component is designated as EHZ. The sensors used in the stations examined in this study are listed in Table B-1. The components of these sensors are indicated on the figures of recorded seismic signals.

Figure B-2 shows the complete digital seismogram recorded at PAL for the time window from 10:00 EDT to 17:30 EDT on Sept. 11, 2001. Each trace is thirty minutes long. Broadband data sampled at 40 Hz and band-pass filtered from 0.8 Hz to 10 Hz are plotted. Seismic signals in this frequency band correspond to ground velocity, and the amplitude of the background noise level (≈ thickness of the traces) is approximately 100 nm/s. The frequency band between 0.8 Hz and 10 Hz captures most of the signals generated at the WTC site as well as main signals from regional earthquakes and quarry blasts. The aircraft impacts generated signals with dominant frequencies in the 1 Hz to 1.5 Hz range, whereas the collapses of the buildings at the WTC site generated frequencies in the band from 0.6 Hz to 10 Hz (see

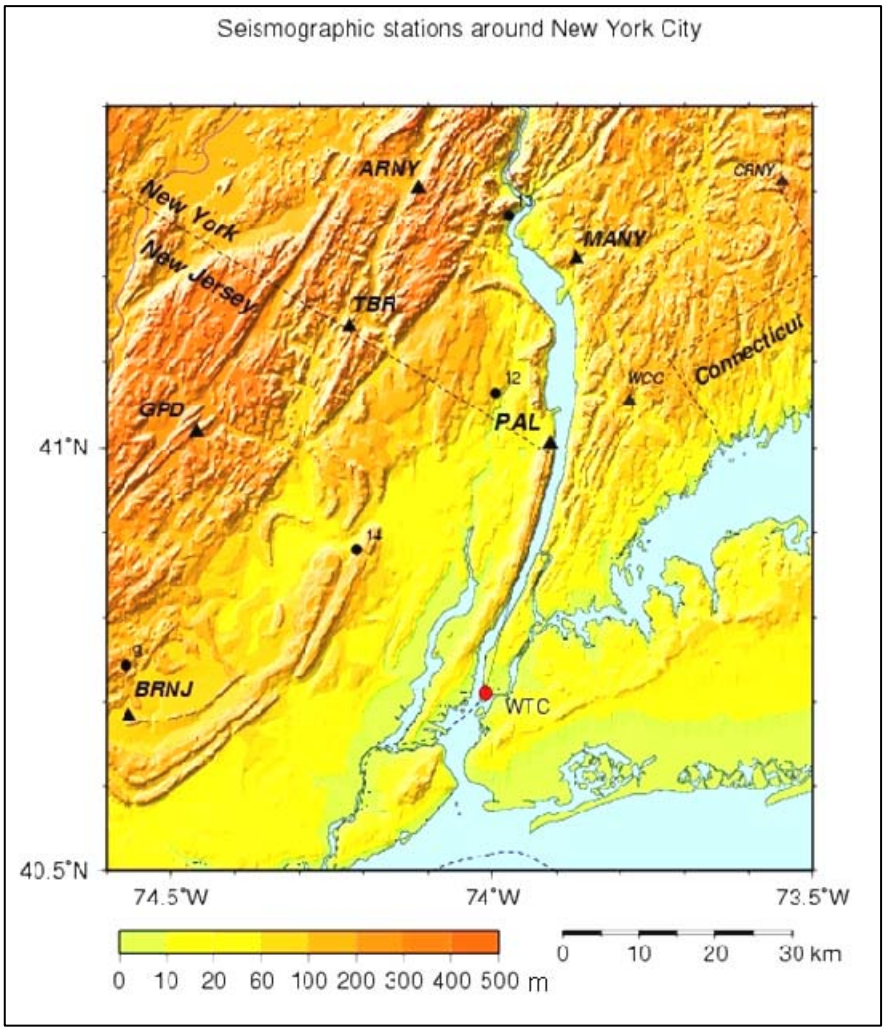

Figure B-1. Seismographic stations (solid triangles) that recorded events at WTC.

Table B-1. List of seismic stations around New York City used in this study.

Station Code	Distance (km)	Azimuth (°)	Sensor type/make	Digitizer/sample rate	Location
PAL	33.8	15.2	BB/STS	24 bit A/D	Palisades
BRNJ	46.7	66.2	BB/CMG	16 bit A/D	Basking Ridge
GPD	50.7	312.2	SP/HS	12 bit A/D	Green Pond
TBR	50.9	339.9	SP/HS	12 bit A/D	Table Rock
MANY	57.9	12.0	SP/HS	12 bit A/D	Mount Airy
ARNY	66.2	352.6	SP/HS	12 bit A/D	Arden House

Notes: Distance = epicentral distance in kilometers from WTC 1 to the station
Azimuth = azimuth of the station from WTC 1 measured clockwise from North.
Sensor type: BB = broad-band seismometer; SP = short-period seismometer
sps = samples/second; A/D = analog-to-digital converter.

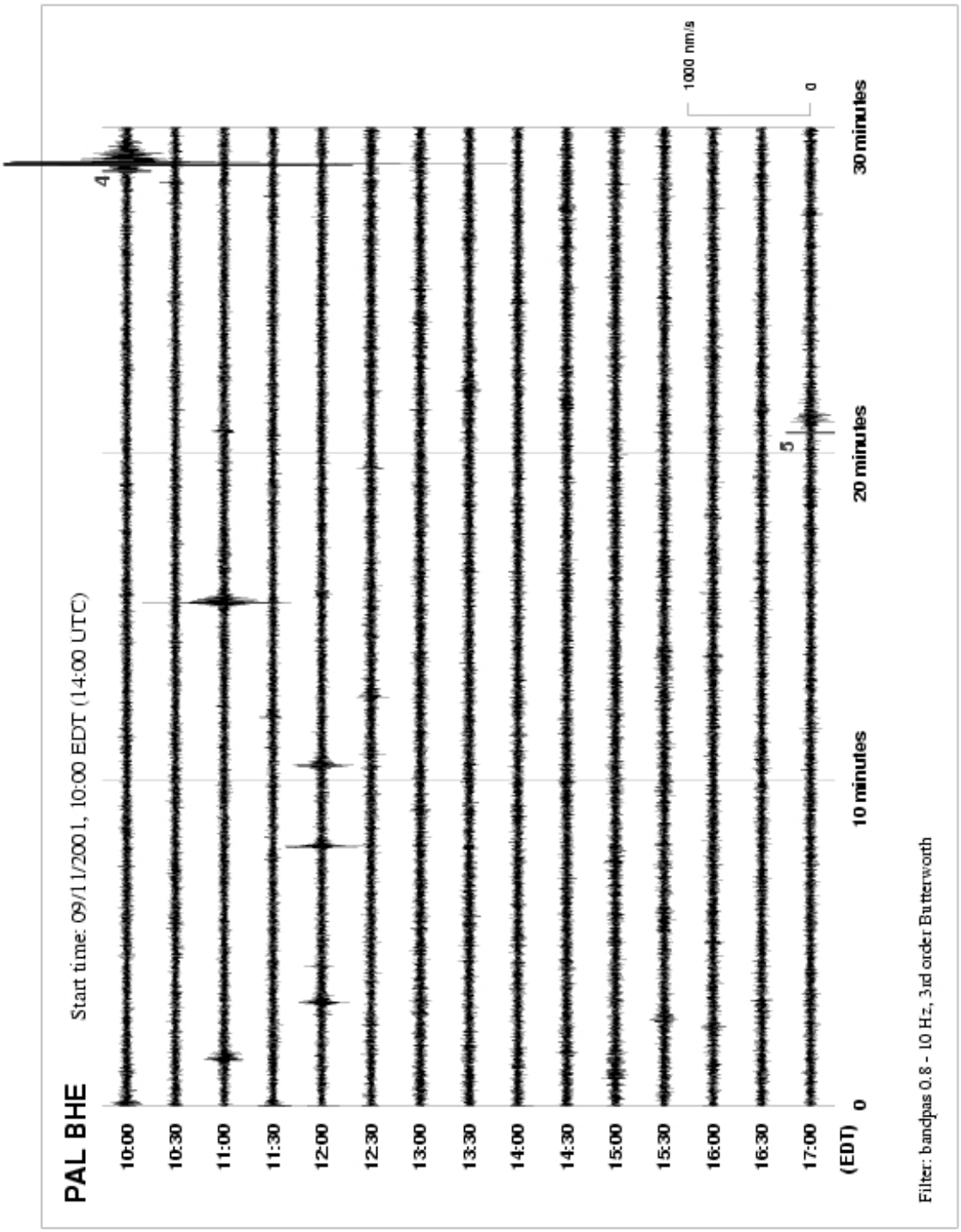

Figure B-2. PAL seismic recordings (nm/s) on EW component, beginning at 10:00 EDT. Sampling rate: 40 Hz; filtered from 0.8 to 10 Hz.

Figure 1, Kim et al. 2001). In this study, the seismic signals in the time window between the collapse of WTC 1 and WTC 7 were analyzed. There are a number of seismic arrivals (signals) identifiable in Figure B-2 among the background noise. Identifying the sources and characterizing these signals were the primary objectives of this study.

B.3 PREVIOUSLY IDENTIFIED SEISMIC EVENTS AT WTC

In September 2001, researchers at LDEO analyzed seismic records from the WTC disaster and reported their findings for five major events at the WTC site (Kim et al., 2001); the event time, equivalent magnitude on the Richter scale, the dominant period of ground vibration, and the duration of the signal are shown in Table B-2 for the major events. The origin times listed in column 3 of Table B-2 are taken from Kim, et al. (2001), and were also used in the FEMA report (McAllister 2002). These times were estimated from PAL records assuming that large amplitude arrivals corresponded to signals that had traveled with a speed of 2 km/s. Hence, 34 km/2 km/s = 17 s and the origin time was estimated as 17 s earlier than the signal arrival time. In the fall of 2003, origin times of the first four events were slightly revised based upon re-examination of the seismic data. There was a seismic arrival about 4 s prior to the surface wave arrival on three-component records from the collapse of WTC 2. The seismic arrival was found on the north–south component record, which is the radial component and is roughly aligned with the longitudinal direction of wave propagation. This seismic arrival was identified as an *S* wave with a speed of about 3.4 km/s propagating through competent bedrock (the Manhattan schist of the Paleozoic age). The travel time of the *S* wave was 10 s (34 km/3.4 km/s), which moved the origin time to 3 s later than the initial determination using 2 km/s Rayleigh waves. The revised estimates for the events associated with WTC 1 and WTC 2 are listed in column 4 of Table B-2.

The origin time for the collapse of WTC 7 (event 5) was also re-examined. In addition to the more accurate wave speed that led to a 3 s adjustment for the events in the towers that also applied to the timing of events originating from WTC 7, a misidentified phase in the earlier paper (Kim et al., 2001) led to the need for an additional 6 s correction to the event time; hence, 9 s was added to the earlier estimate, producing the current value of 17:20:42 EDT for the collapse of WTC 7.

When the current estimates for the time of impact of WTC 1 and WTC 2 by the first and second aircraft, respectively, are compared to the videographic evidence presented in NCSTAR 1-5A and Table 5-3 of Chapter 5 of this report, the agreement is within 2 s, as can be seen by comparing the first two entries of column 4 to the first two entries of column 5 in Table B-2. The times attributed to the collapses of WTC 1 and WTC 2, however, differ between the seismic study and NCSTAR 1-5A by about 10 s (compare entries 3 and 4 of column 4 to entries 3 and 4 of column 5 in Table B-2). The reason for the discrepancy is that NCSTAR 1-5A used the sudden tilting of the upper portion of the towers to signal collapse initiation; a seismic signal, though, is not generated until a substantial portion of the building debris hits the ground. If this time interval is accounted for, the NCSTAR 1-5A times compare well with the seismic origin times.

The current estimate for the collapse of WTC 7 based upon the seismic data is 10 s earlier than the time reported in Table 5-3 of Chapter 5 of this report based upon the video record. (Compare the bottom entries of columns 4 and 5 in Table B-2). Table 5-3 of Chapter 5 used the global collapse of the building as the marker for the event, not the first evidence of downward motion of the east penthouse, which occurred about 7 s earlier. The implication of the relative timing of the seismic signal and the visual

observation is discussed later in this Appendix after the details of the seismic signature have been presented.

Table B-2. Major seismic events previously reported.

Event Source	Event Time (EDT) ID	Kim et al., 2001	LEDO current Estimate[a]	Table 5-1 of Chapter 5 of This Report (± 1 s)[b]	Equivalent earthquake Magnitude (Richter Scale, ± 0.1)	Dominant Period (s)	Sustained Signal Duration (s)
WTC 1 impact	1	8:46:26	08:46:29±2	8:46:30	0.9	0.8	14 ±2
WTC2 impact	2	9:02:54	09:02:57±4	9:02:59	0.7	0.6	6 ±2
WTC 2 collapse	3	9:59:04	09:59:07±2	9:58:59	2.1	0.8	10 ±1
WTC 1 collapse	4	10:28:31	10:28:34±2	10:28:22	2.3	0.9	9 ±1
WTC 7 collapse	5	17:20:33	17:20:42±4	17:20:52[c]	0.6	0.8	17 ±2[d]

a derived from signal arrival and estimated travel times from WTC site to PAL
b based upon events observed in videos and photographs; collapse times were based on collapse initiation, not time of ground impact
c NCSTAR 1-5A timing was based on downward movement of the WTC 7 roofline and not the downward movement of the east penthouse that occurred earlier.
d Total duration of BHE PAL signal in Fig. A-6, including a possible second arrival

B.4 CHARACTERISTICS OF SEISMIC SIGNALS FROM WTC EVENTS

Seismic records from the five major WTC events show no clear *P* or *S* wave arrivals. Short-period seismic surface waves, mainly of the Rayleigh type, are the predominant seismic waves on records at regional distances (few tens to few hundreds of kilometers). Figure B-3 shows the three-component seismic records at stations PAL and BRNJ from the collapse of WTC 1. NS- and EW-component records were rotated to longitudinal-component (BHR) and transverse-component (BHT) orientations to show the effect of wave propagation. The time of 10:28:34 EDT is the estimated origin time (i.e., the estimated travel time has been subtracted from the arrival time) for the PAL BHT signal at the "*Rg*" indicator (note that *Rg* indicates the arrival of a seismic surface wave of the Rayleigh type which propagated at 2.4 km/s). The time scale at the top and bottom of the figure illustrate the relative signal arrival times and durations. Vertical-component seismic records at local stations PAL, BRNJ, TBR, MANY and ARNY from the collapse of WTC 1 are shown in Figure B-4. The epicentral distance and azimuth at each station are given at the end of each trace.

Surface waves on the transverse-component are strongest at PAL, whereas at BRNJ, the transverse-component has the least amplitude. The seismic signals excited by the building collapses are basically due to vertical forces acting on the ground surface, and hence, seismic waves are strongly excited near the surface and subsequently travel as surface waves. In addition, the surface waves recorded at station PAL, located due north from the WTC, are strongest on the EW component record. This is a unique

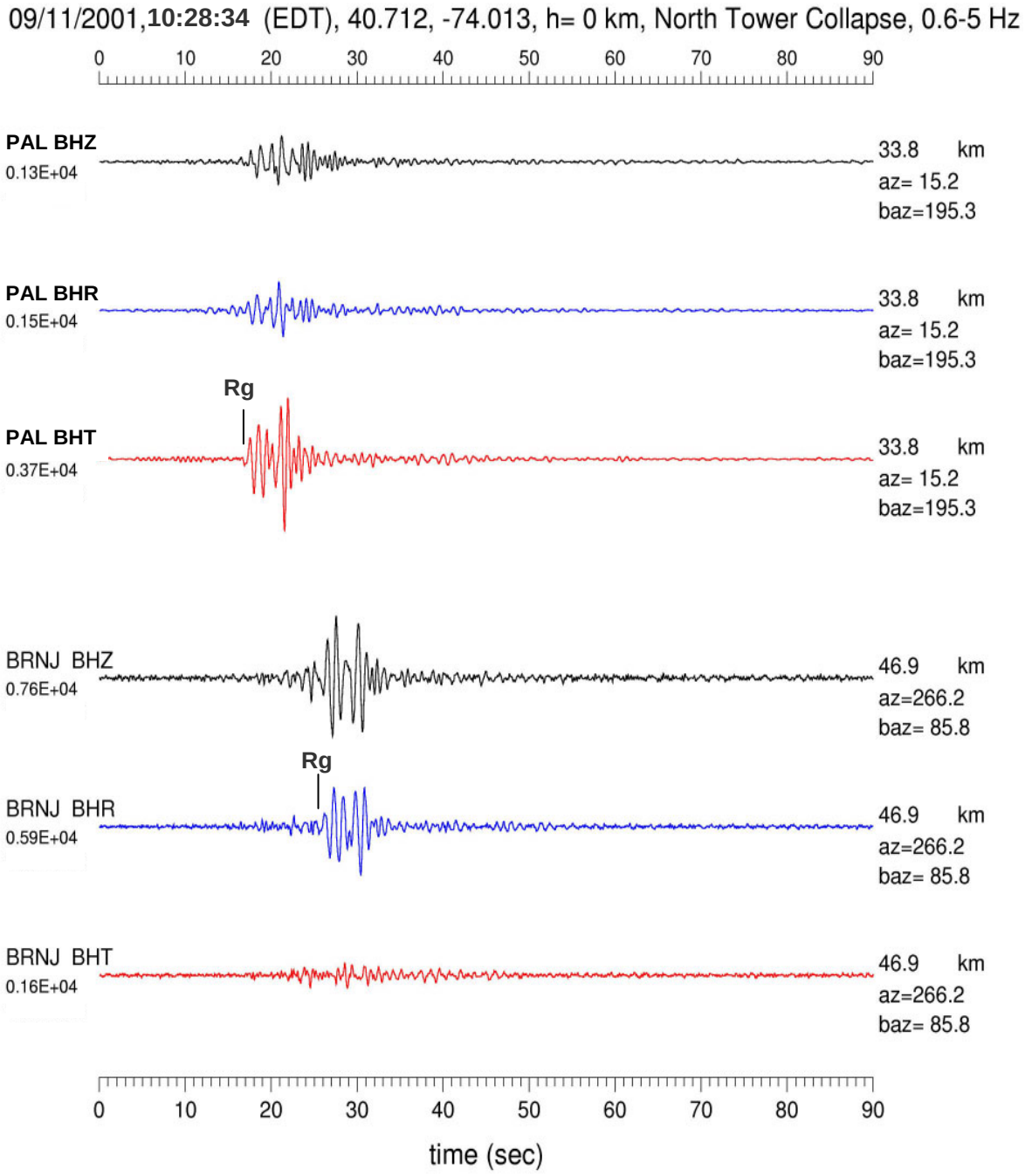

Figure B-3. Three-component seismic records at stations PAL and BRNJ from the collapse of WTC 1.

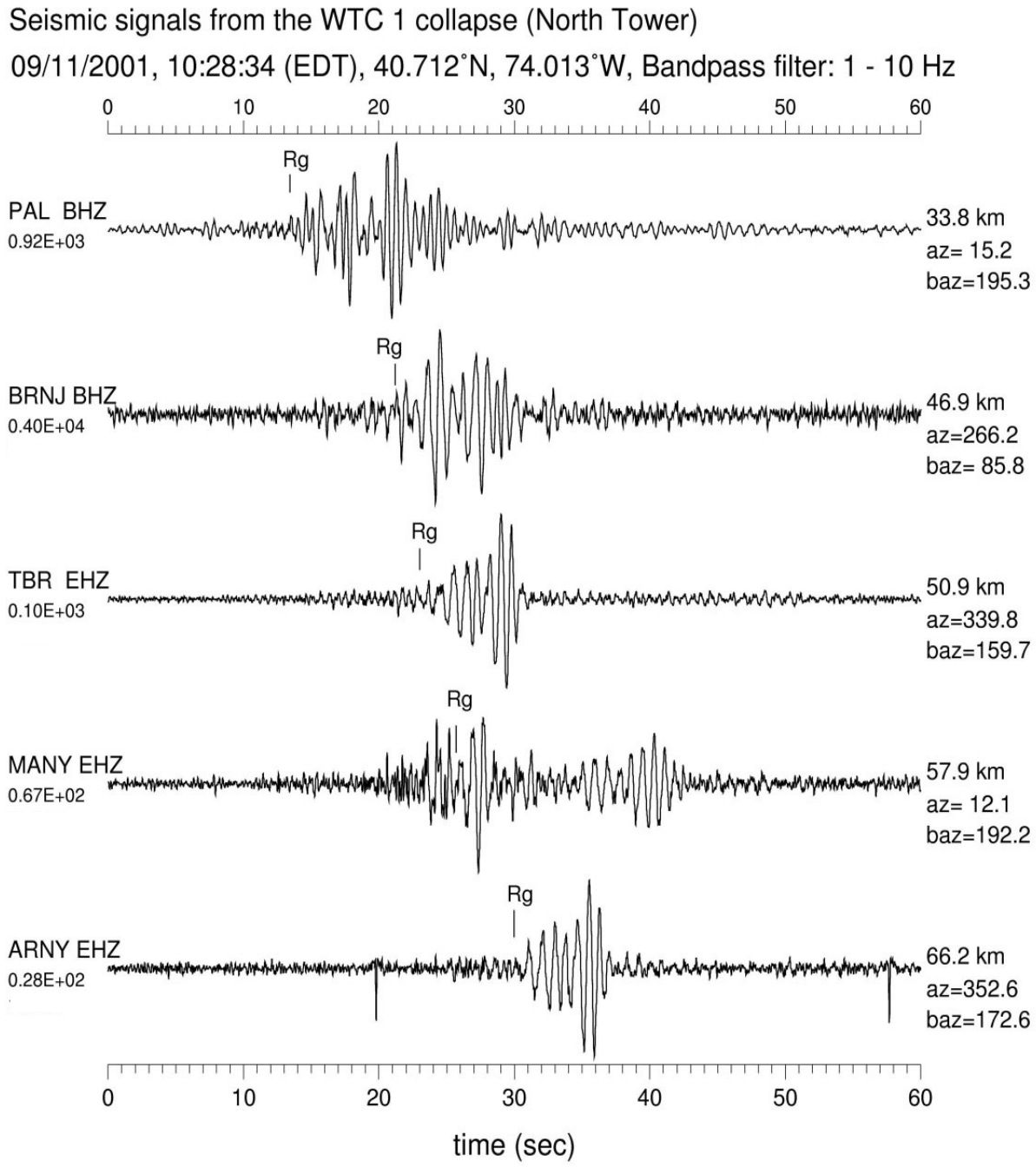

Figure B-4. Vertical-component seismic records at local stations PAL, BRNJ, TBR, MANY and ARNY from collapse of WTC 1.
(Spikes at 20 s and at 58 s on ARNY record are due to electrical noise).

observation because Rayleigh-type seismic surface waves should be strong in the vertical and radial directions, and weak in the transverse direction, as is the case for station BRNJ shown in Figure B-3. This is an interesting propagation effect due to strongly contrasting properties of shallow rock layers along the wave propagation path between the WTC and PAL which is nearly parallel to the Hudson River. Lateral refraction is caused by contrasting shallow rock layers at the boundary between high-velocity crystalline metamorphic rocks of the Manhattan prong and low-velocity Triassic rocks of the Newark basin (Anderson and Dorman 1973). When the wave leaving the source at the WTC site enters the rock underlying the Hudson River, much of its energy can be trapped in a wave guide along the river in the form of a lens or tube and undergo multiple lateral refractions along its passage. Hence, there are several distinct criteria for characterizing seismic waves generated at the WTC site and observed at stations around New York City. These criteria are:

- seismic surface waves generated at the WTC site and observed at PAL have stronger EW-components than vertical- or NS-components (Figure B-3);
- seismic surface waves, mainly of the Rayleigh type, travel at about 2.4 km/s between the WTC site and stations in the region, and the surface waves arrive first at station PAL, followed by BRNJ, GPD, TBR and so on, as listed in Table B-1 (Figure B-4); and
- no clear *P* or *S* wave arrivals are observed due to the vertical force nature of the sources at WTC (Figures B-3 and B-4).

B.5 SEISMIC SIGNALS FROM THE WTC 7 COLLAPSE

East-west and vertical component seismic records from five stations around New York City, filtered to pass signals below 5 Hz, are plotted in Figure B-5 for the time during the collapse of WTC 7. As before, *Rg* indicates the arrival of the seismic surface wave of the Rayleigh type which propagated with a speed of 2.4 km/s. *Pg* and *Sg* indicate *P*- and *S*-wave estimated arrival times from the WTC site using a velocity model for the region (these wave arrivals were not detectable). The Rayleigh waves were quite weak and difficult to discern clearly at most of the stations. Nevertheless, *Rg* waves at PAL, BRNJ, TBR and ARNY were stronger than the background noise in Figure B-5.

Three-component records at PAL associated with the WTC 7 building collapse are shown in Figure B-6 (including frequencies up to 10 Hz). The event origin time, based on the arrival of the Rayleigh type of shear wave *Rg* on the BHE component, was estimated to occur at 17:20:42 EDT with an uncertainty of ±4 s. Notice that the seismic signal strengthens at about 21.5 s, following the initial *Rg* wave arrival at 14.5 s. A *P*-wave from the Fox Islands earthquake (event #17) would have arrived about 11 s after *Rg*, and would have had nearly equal amplitude and duration on both the N-S (middle trace of Figure B-6) and E-W (lower trace) components of the seismic signal. Since the N-S component is small in Figure B-6 (compared to the amplitude of *Rg*), that the signal beginning at 21.5 s is likely due to the sustained period of collapse of WTC 7.

The WTC 7 building collapse was observed to have two distinct phases. First, an internal structural failure occurred which led to the observed east penthouse movement, when it sank below the roofline. Second, the entire building began to collapse about 7 s later, when the roofline and building exterior were observed to start moving downward. The first phase resulted in interior debris falling to the lower floors of WTC 7 on the east side, which transmitted impact loads to the foundation. The debris fell over several

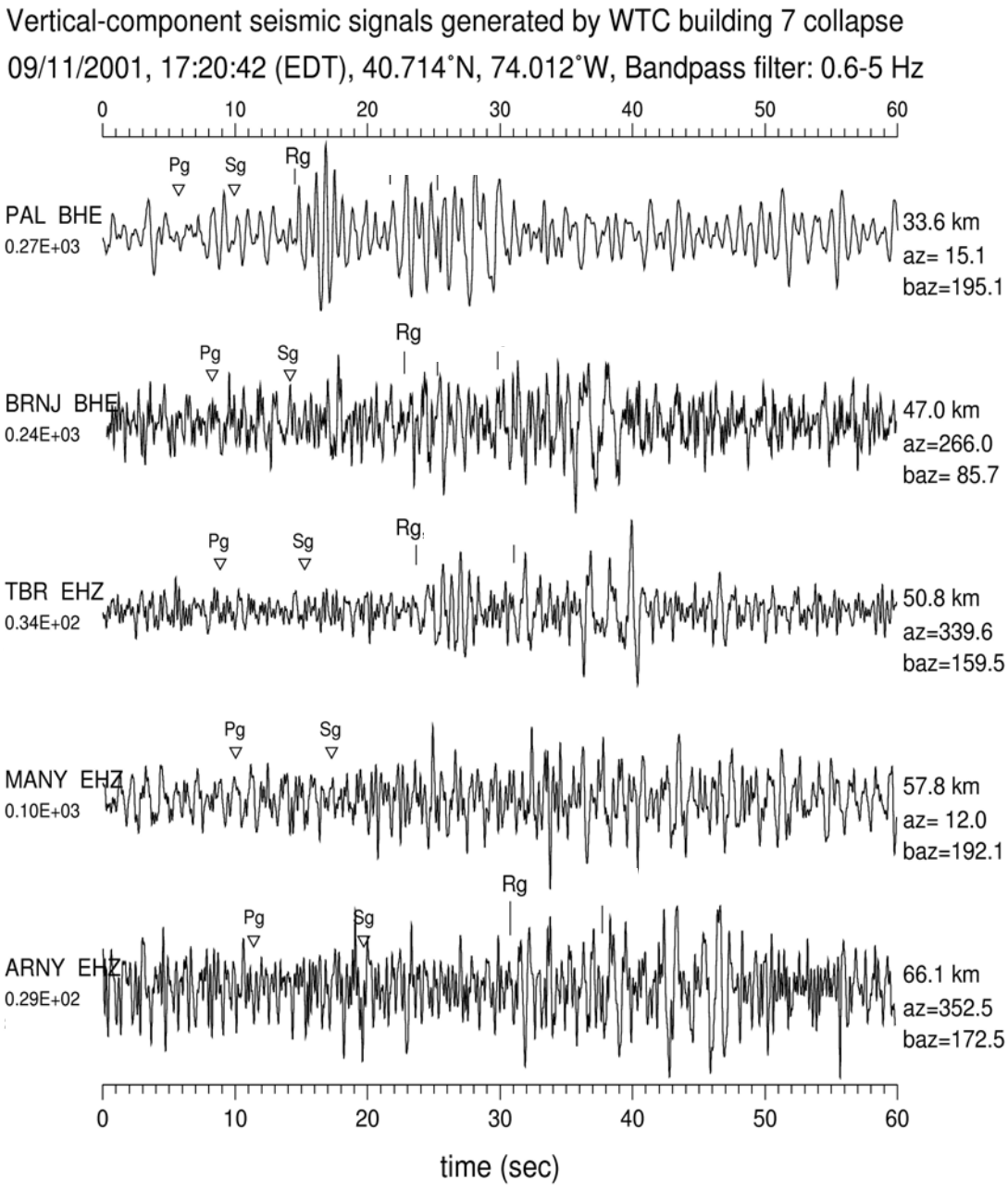

Figure B-5. East-west (BHE) and vertical (EHZ) component seismic records, 0.6 Hz to 5 Hz filtered, at PAL, BRNJ, TBR, MANY and ARNY from collapse of WTC 7.

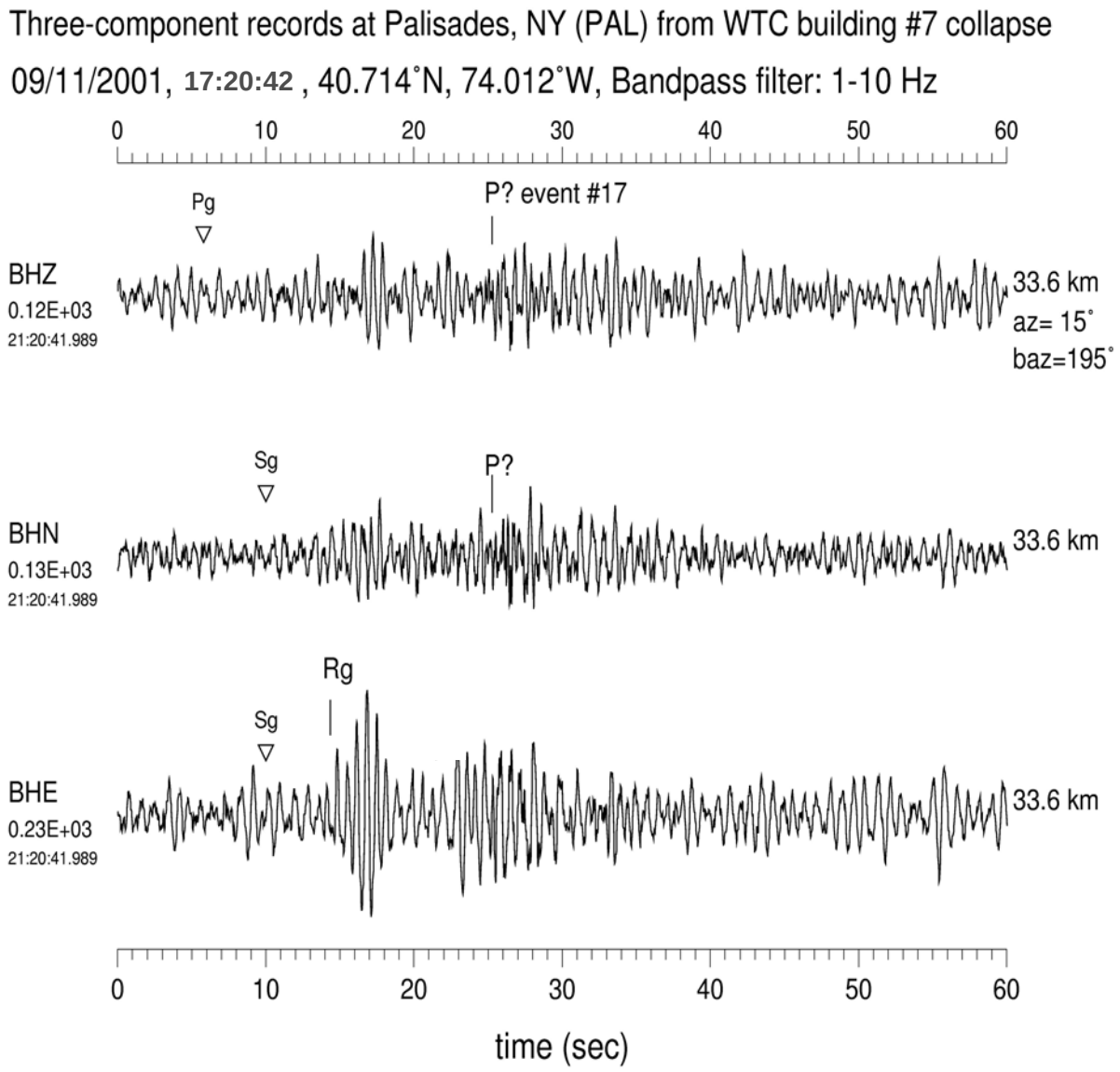

Figure B-6. Three-component seismic records, 1 Hz to 10 Hz filtered, at PAL from collapse of WTC 7.

seconds, but the exact time duration is unknown, as is the timing relative to the observed east penthouse movement. The first phase (likely) triggered other interior structural failures which led to the observed global collapse initiation about 7 s after the east penthouse moved downward. Debris may have fallen prior to the observed movement of the building exterior, but the duration and timing of the falling debris is unknown. The falling debris from the global collapse would also have transmitted impact loads to the foundation.

While this qualitative sequence of events is consistent with what might be construed as two arrivals in the PAL BHE traces shown in Figures B-5 and B-6, caution is required when interpreting signals that are small. For example, the signals in Figures B-3 and B-4 all recorded the same event, the collapse of WTC 1. Even so, signal amplitude and duration vary depending upon the location of signal arrival. The signal variations may be due to differences in the geological features along the signal path as well as local differences in construction. For instance, WTC 1 and WTC 2 were both located inside the foundation bathtub structure and had multi-story basements while WTC 7 was located north of the bathtub structure and had no basement. It is not known how these construction features may have affected signal transmission.

B.6 SCREENING OTHER SEISMIC EVENTS

Using all available seismic data from the six stations around New York City, 17 seismic signals were identified in the time window between the collapses of WTC 1 and WTC 7. These could have been generated by relatively large distant earthquakes (magnitude usually greater than 6), regional earthquakes (distance ranges between few tens to few hundreds of kilometers), and other signals generated by anthropogenic sources such as quarry blasts, chemical explosions, or impacts from heavy falling debris hitting the ground. To determine which seismic signals may have been generated by the WTC buildings, all of these signals were examined to identify their source and location. Table B-3 lists the 17 signals, beginning with ID #6 to distinguish these from the first five strong signals attributed to the events listed in Table B-2. The event origin time, location, and magnitude are provided.

B.6.1 Earthquakes

Two of the events listed in Table B-3 (#6 and #17) were associated with distant earthquakes, as confirmed in the Preliminary Determination of Epicenters bulletin from the National Earthquake Information Center, U.S. Geological Survey. The seismic records show teleseismic *P* wave arrivals from a strong earthquake (ID #6) that occurred in West Irian Jaya (New Guinea), Indonesia. There appears to be a weak teleseismic *P* wave arrival from a second, less intense distant earthquake (event #17 in Table B-3) at around 10 s after the arrival of the Rayleigh wave generated by the collapse of WTC 7. Since the teleseismic *P* waves (epicentral azimuth $\Delta = 61°$) are usually strong only in vertical component records, this signal did not interfere with shear signals from WTC 7.

B.6.2 Local Quarry Blasts

The largest of the remaining signals listed in Table B-3 show relatively clear *P* and *S* arrivals, and were strong enough to be recorded at several stations in the region so that the source location could be identified. Based on the location and characteristics of seismic signals, local quarry blasts in the region were identified. Usually, seismic signals from a local quarry blast show strong short period surface

Table B-3. Minor seismic signals recorded around New York City on Sept. 11, 2001, and examined in this study.

Event ID	Origin Time, EDT (hh:mm:sec)	Latitude (°N)	Longitude (°E)	Depth (km)	Magnitude (M_L)	Comments
6	10:56:51	-0.578	133.13	33	6.5	distant earthquake from Indonesia*
7	11:00:45	40.420	-75.05	0.01	1.1	quarry blast
8	11:14:58	40.620	-74.71	0.01	1.3	quarry blast
9	11:29:41	40.744	-74.57	0.01	0.9	quarry blast
10	11:40:50	43.039	-73.29	0.01	1.4	quarry blast
11	12:02:20	42.472	-73.69	0.01	1.2	quarry blast
12	12:07:52	41.064	-73.99	0.01	0.6	quarry blast
13	12:10:15	41.273	-73.97	0.01	0.6	quarry blast
14	12:42:21	40.879	-74.21	0.01	0.6	quarry blast
15	12:49:14	41.427	-74.14	0.01	0.6	quarry blast
16	16:18:48	41.475	-74.08	0.01	0.2	quarry blast
17	17:10:55	52.461	-169.28	33	5.1	distant earthquake from Fox Islands*
18#	11:20:17	40.71	-74.01	0	< 0.5	only at PAL
19#	12:03:56	40.71	-74.01	0	< 0.5	very weak at PAL
20#	12:40:25	40.71	-74.01	0	< 0.5	very weak at PAL
21#	13:51:32	40.71	-74.01	0	< 0.5	very weak at PAL and GPD
22#	15:32:30	40.71	-74.01	0	< 0.5	very weak at PAL

* Origin time, location, depth and magnitude are from Preliminary Determination of Epicenters determined by NEIC/USGS (National Earthquake Information Center, U.S. Geological Survey).

\# These events could not be located because the signals were detected only on one or two stations, where they were too weak to pick arrival times of *P* or *S* waves. It was necessary to assume that events occurred at the WTC in order to infer a possible origin time.

waves; these blasts involve approximately 100 holes in the bedrock and about 36 000 kg of ammonium nitrate and fuel oil. However, the strength of seismic signals or ground vibration due to these large quarry blasts are much reduced due to the practice of sequential firing of blasting caps with 25 ms delays. The peak amplitudes of the seismic signals from quarry blasts are approximately proportional to the maximum charge size per delay, not the total charges detonated within a quarry blast. Note that each delay consists of shot holes fired within ±8 ms, hence a quarry may have several delays. (Kim et al. 1994). An example of waveform data from a quarry blast (ID #8 in Table B-3) is shown in Figure B-7. (Note that the teleseismic *P* wave also shown in Figure B-7 as event ID #6 is associated with the distant earthquake that occurred earlier.) Ten of the events in Table B-3 (ID #7 through ID #16) were associated with quarry blasts, with magnitudes varying between 0.2 to 1.4. The locations of these events are plotted on the map in Figure B-8.

B.6.3 Unidentified Weak Signals

In addition to the seismic signals already discussed, about a dozen other weak signals were recorded by one or more of the seismic stations in the area. These were screened to identify those that had characteristics of the previously identified signals emanating from the WTC site; namely, signals with the strongest amplitudes in the east-west component at PAL. All but five of the weak signals at PAL were eliminated based on this criterion. Because the signals were very weak and (except for ID # 21) not detectable at stations other than PAL, it could not be positively confirmed that they originated, in fact, from the WTC site. An examination of the video and photographic records by NIST at times corresponding to these weak signals did not reveal any particular events that could have acted as sources for this seismic activity.

B.7 SUMMARY OF SEISMIC DATA

Table B-4 lists, according to the time of occurrence, all 22 seismic signals identified between 8:46 EDT and 17:21 EDT on Sept. 11, 2001, recorded at six stations around the metropolitan New York City area. Figure B-9 is a seismogram of the period starting at 10:00 EDT taken at the PAL station, with event ID numbers included. Events #4 and #5 (in blue) are the collapses of WTC 1 and WTC 7, respectively; events #6 through #17 (in black) have been attributed to distant earthquakes and local quarry blasts; and events #18 through #22 (in red) are undetermined.

The five largest seismic events were due to collisions of the two aircraft into the WTC towers, their subsequent collapses, and the collapse of WTC 7. Consistent event times for the impact of the towers by the aircraft were obtained between the current seismic analysis and the analysis of the photographic evidence in NCSTAR 1-5A.

The times attributed to the collapses of WTC 1 and WTC 2 in Table 5-1, column 3, of Chapter 5 of this report and Table 3-1, column 3, of NCSTAR 1-5A differ from the seismic signal times because the column 3 times refer to the time when the upper portion of each tower above the airplane impact damage was observed to suddenly tilt, while a seismic signal was not generated until a substantial portion of the building debris hit the ground. If this time interval is accounted for, the NCSTAR 1-5A times compare well with the seismic origin times.

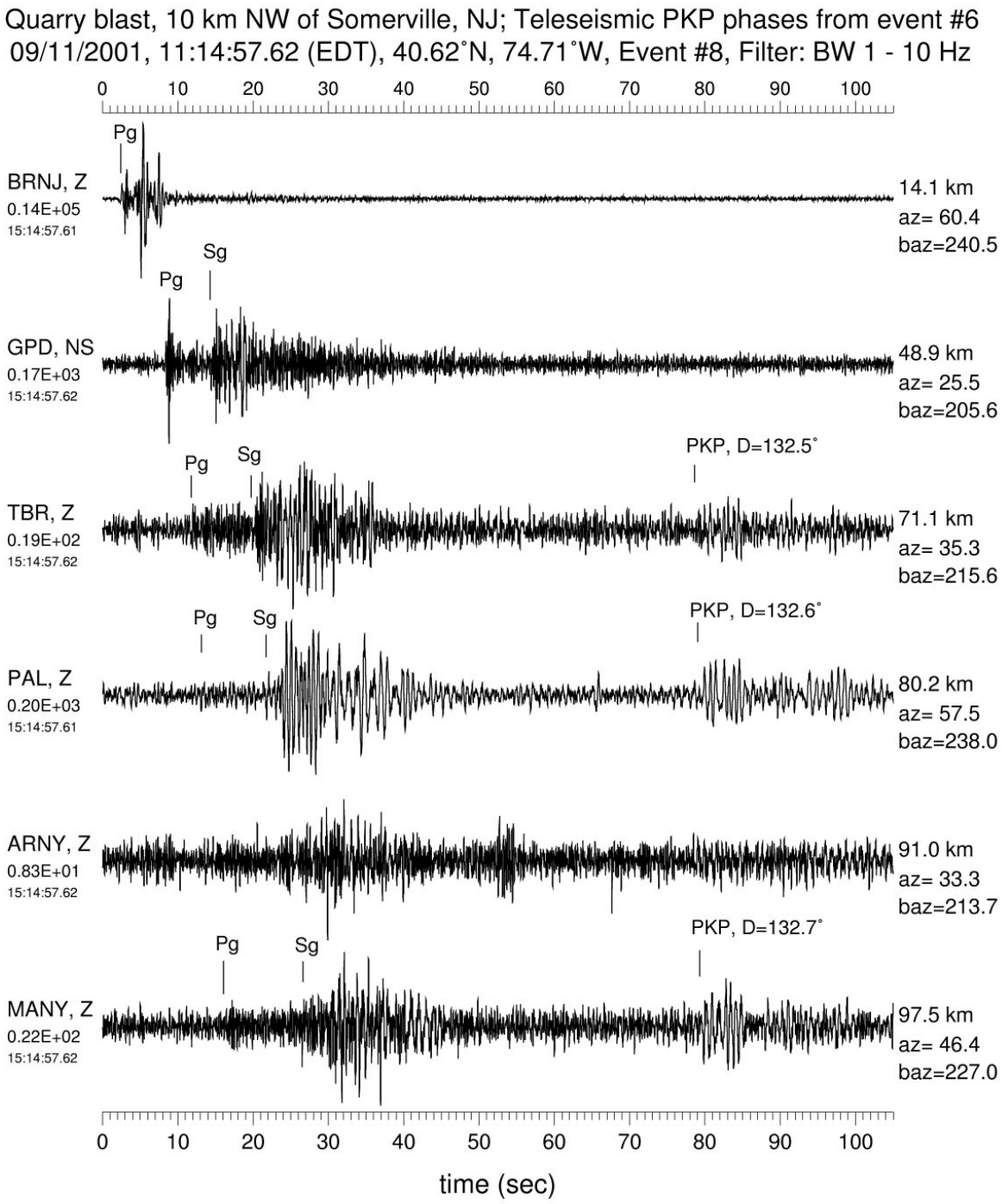

Figure B-7. Vertical component seismic records from quarry blast (ID #8) recorded at seismographic stations around New York City (PKP is ID #6).

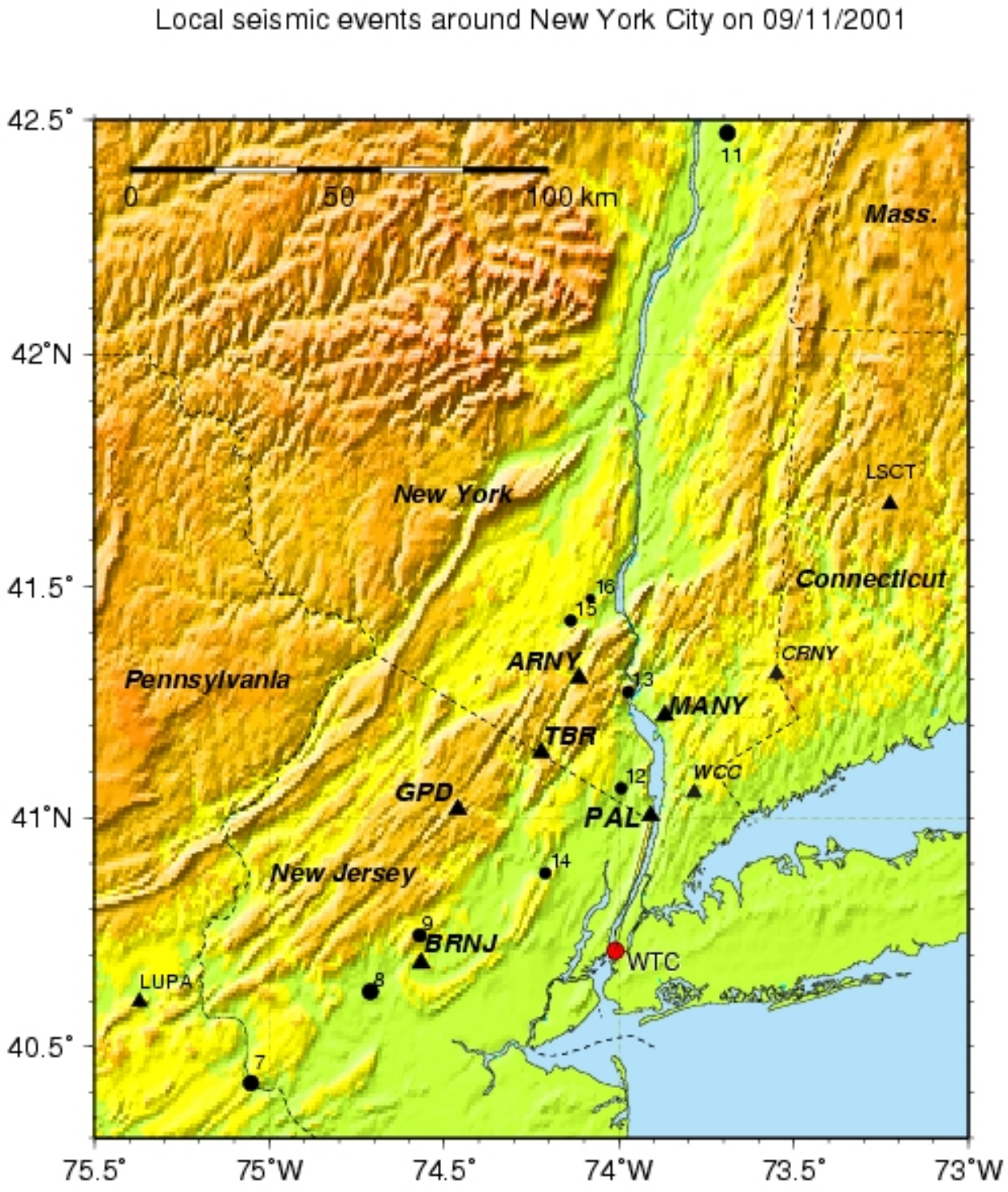

Figure B-8. Epicenters of local quarry blasts on Sept. 11, 2001.
The event ID numbers are given in Table B-3.

As discussed further in Chapter 12, there were two phases in the probable WTC 7 collapse sequence that could have resulted in seismic signals.

- The first comprised the initial local failure and the vertical progression of failure. These began prior to the descent of the east penthouse (as suggested by the increasingly larger magnitudes of vibration of the building as described in Appendix C) and involved a cascade of floor failures within the east side of the building. The interior debris falling onto the lower floors of WTC 7 on the east side transmitted impact loads to the foundation. This impact would have coincided roughly with or slightly preceded the initial descent of the east penthouse, about 7 s prior to the visible initiation of global collapse. This time estimate is within the uncertainty in collapse time determined by NIST from the video record as listed in Table 5-1 (Chapter 5).

- The second seismic phase comprised the global collapse of the building, as seen in the videos (Chapter 5). Here, the entire building above the fire-damaged and buckled floors moved downward as a single unit, transmitting impact loads to the foundation. One would have expected seismic signals from this second phase of collapse to be generated over this entire episode (which lasted approximately 14 s) since debris was continuously impacting the ground either unobserved within the core or externally as seen from the videos of the perimeter walls. However, because the total energy dissipated by the impact was distributed over a long period of time, the strength of the signal at any given time was small and difficult to interpret.

Twelve other signals analyzed in the current study could be associated with specific seismic events, including two natural earthquakes and ten quarry blasts and explosions at construction sites. Five weak signals may have originated from sources at the WTC site based upon the criterion that E-W component signals at PAL are stronger than signals for the N-S or vertical components, but their location and strength could not be confirmed by the other stations. These signals were very small in amplitude (Richter magnitudes below 0.5), and all but one were not recorded at the other stations of the seismic network, putting them close to the level of the "noise" that accompanies daily earthquake monitoring activity at the reference station PAL.

Thus, the collapse of WTC 7 observed in the videographic evidence can be associated with the signals on the seismic record. There were no other seismic signals that could be associated with other specific events at the World Trade Center that were identifiable in the videographic or photographic records gathered by NIST, or with any events reported by witnesses that were interviewed by NIST.

Table B-4. Summary of seismic events recorded 8:46 to 17:21 on Sept. 11, 2001.

Origin Time, EDT (hh:mm:sec)	Event ID	Latitude (°N)	Longitude (°E)	Depth (km)	Magnitude (M_L)	Event Type
8:46:29	1	40.71	-74.01	0	0.9	WTC 1 impact
9:02:57	2	40.71	-74.01	0	0.7	WTC 2 impact
9:59:07	3	40.71	-74.01	0	2.1	WTC 2 collapse
10:28:34	4	40.71	-74.01	0	2.3	WTC 1 collapse
10:56:51	6	-0.578	133.13	33	6.5	distant earthquake from Indonesia
11:00:45	7	40.42	-75.05	0.01	1.1	quarry blast
11:14:58	8	40.62	-74.71	0.01	1.3	quarry blast
11:20:17	18	40.71*	-74.01*	0*	< 0.5	unknown*
11:29:41	9	40.74	-74.57	0.01	0.9	quarry blast
11:40:50	10	43.04	-73.29	0.01	1.4	quarry blast
12:02:20	11	42.47	-73.69	0.01	1.2	quarry blast
12:03:56	19	40.71*	-74.01*	0*	< 0.5	unknown*
12:07:52	12	41.06	-73.99	0.01	0.6	quarry blast
12:10:15	13	41.27	-73.97	0.01	0.6	quarry blast
12:40:25	20	40.71*	-74.01*	0*	< 0.5	unknown*
12:42:21	14	40.88	-74.21	0.01	0.6	quarry blast
12:49:14	15	41.48	-74.14	0.01	0.6	quarry blast
13:51:32	21	40.71*	-74.01*	0*	< 0.5	unknown*
15:32:30	22	40.71*	-74.01*	0*	< 0.5	unknown*
16:18:48	16	41.48	-74.08	0.01	0.2	quarry blast
17:10:55	17	52.46	-169.28	33	5.1	distant earthquake from Fox Islands
17:20:42	5	40.71	-74.01	0	0.6	WTC 7 collapse initiation
17:20:50	5'	40.71	-74.01	0	0.6	WTC 7 perimeter wall collapse

*Although the latitude and longitude are those of the WTC site, the signals were small and, except for ID #21, unconfirmed by a second station; hence the source, location and magnitude of these events could not be accurately determined.

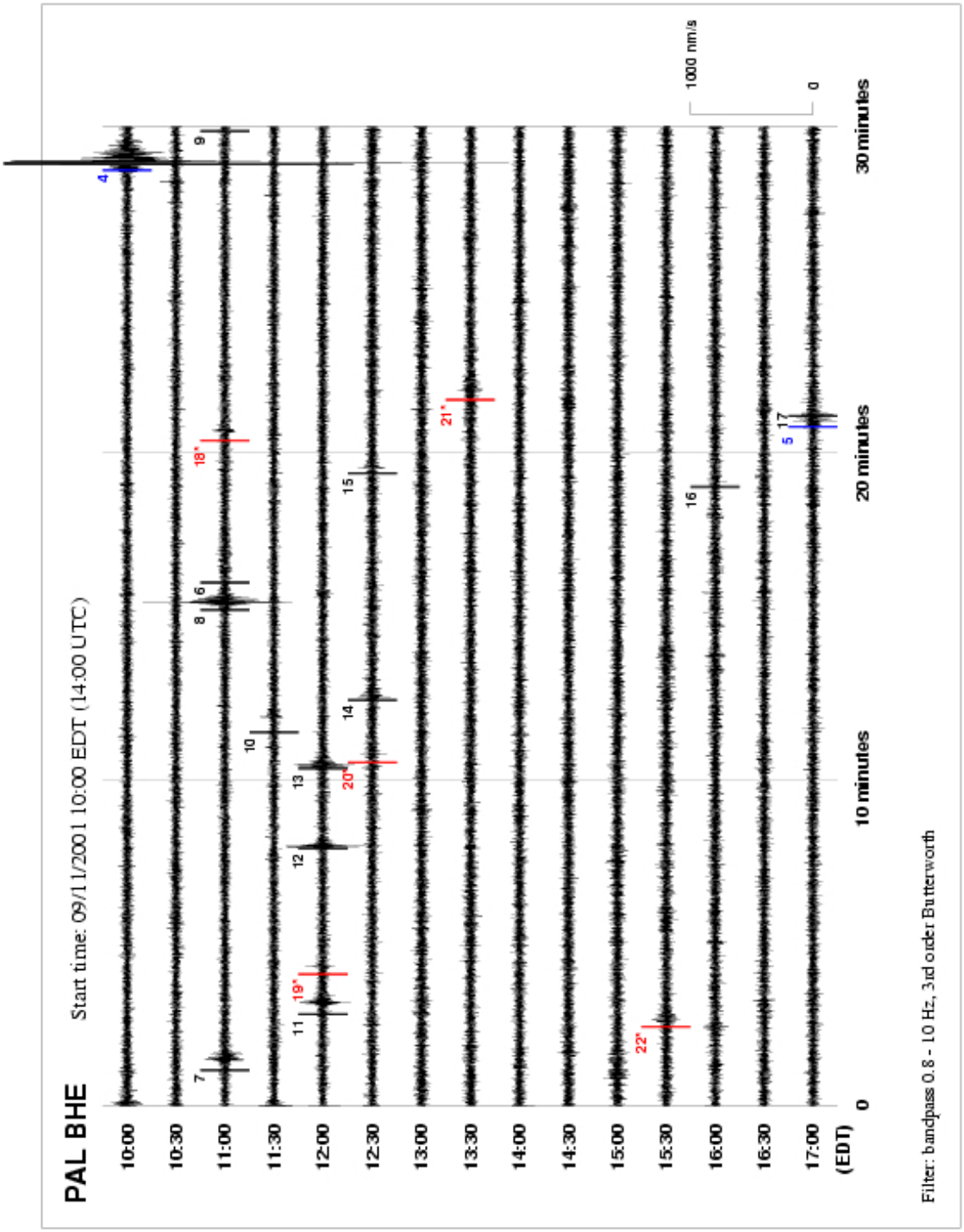

Figure B-9. Events identified on PAL seismogram.
Refer to Table B-4 for location, strength and description of event type.

B.8 REFERENCES

Anderson, J. and J. Dorman, 1973. Local geological effects on short-period Rayleigh waves around New York City, *Bull. Seism. Soc. Am., 63,* 1487-1497.

Kim, W. Y., D. W. Simpson and P. G. Richards, 1994. Characteristics of high-frequency spectra of regional phases from earthquakes and chemical explosions, *Bulletin of the Seismological Society of America, 84*, 1365-1386.

Kim, Won-Young, L.R. Sykes, J.H. Armitage, J.K. Xie, K.H. Jacob, P.G. Richards, M. West, F. Waldhauser, J. Armbruster, L. Seeber, W.X. Du and A. Lerner-Lam, 2001. Seismic waves generated by aircraft impacts and building collapses at World Trade Center, New York City, *EOS*, Transactions of the American Geophysical Union, *82*, 565-571, Nov. 20.

McAllister, T., ed. 2002. World Trade Center Building Performance Study: Data Collection, Preliminary Observations, and Recommendations. *FEMA 403*, Federal Emergency Management Agency. Washington, DC, May.

Appendix C
VIDEO ANALYSIS OF WTC 7 BUILDING VIBRATIONS BEFORE COLLAPSE

C.1 DETERMINATION OF BUILDING VIBRATION DATA

C.1.1 Introduction

A tripod-mounted news camera positioned on the west side of West Street near Harrison Street captured the entire collapse sequence of WTC 7, starting seven minutes before the east penthouse began to fall into the building. The result was the Camera 3 video clip discussed in Chapter 5 (see Figure 5-176 which has been reproduced as Figure C-1). This fixed view from northwest of WTC 7 provided an extended record as events leading to the collapse caused the building to shake. Image analysis of this video clip revealed that WTC 7 started to move prior to its collapse.

Analysis of the vibration pattern of WTC 2 from a video clip in the database of photographs and videos collected by the Investigation Team provided valuable information regarding damage to WTC 2 upon aircraft impact (NIST NCSTAR 1-5A, Appendix K). The Investigation Team felt that a similar analysis of the Camera 3 video clip could reveal the presence of structural disturbances contributing to the collapse sequence of WTC 7, adding information to the visual evidence of the disappearance of the east penthouse and the vertical "kink" or fault line during collapse.

C.1.2 Video Used in Analysis

Figure C-1 shows a single frame taken from the Camera 3 video. The north face of WTC 7 is centered within the frame, with portions concealed by buildings located between WTC 7 and the camera. The top 10 floors of the 47 story building are fully visible, with the top 14 floors visible along the right-hand (northwest) edge.

Figure C-1. A single frame from the Camera 3 news video shot on September 11.

The west edge of WTC 7 (to the right in the frame) was of the most interest in this analysis. This was the northwest corner of the building, which was clear of smoke throughout the recorded period. From the

camera's perspective, the angle of this edge appears close to vertical. This provided excellent amplification of the building motion. The tripod mount kept fluctuations in viewpoint to a minimum, although they were not be negligible. In the previous WTC 2 moiré analysis, frame-to-frame and slow motions of a tripod-mounted camera were found to be a source of error.

The news video was imported into the visual database from a VHS cassette recording of the original broadcast. The importation process saved all video clips in the standard digital video format of DV NTSC. In this process, each analog image from the videotape was converted into a digital image with the standard frame size of 720 pixels wide by 480 pixels high. The pixel width was 0.9 times pixel height, generating the standard video width-to-height ratio of 4:3. The frame rate was 29.97 frames per second.

C.1.3 Moiré Technique for a Single Marker Point

The moiré effect occurs when two closely spaced gratings with a small angle between them are superimposed, generating fringe patterns that attract the eye. An example is shown in Figure C-2. A close look at the moiré pattern in frame (c) shows that the fringes consist of light areas that the human eye links together. These light areas are the points where lines from the two gratings intersect. The smaller the angle between the gratings, the larger will be the distance between the fringes, which is the wavelength of the moiré pattern. Figure C-3 shows the effect of moving one grating sideways relative to the other. If grating #1 were shifted to the right by one-half of the spacing between lines, the intersection points, and thus the moiré fringes, move vertically by half the distance between fringes. The moiré pattern is highly sensitive to the positions and angles of the gratings relative to each other and strongly amplifies any sideways motion of the lines.

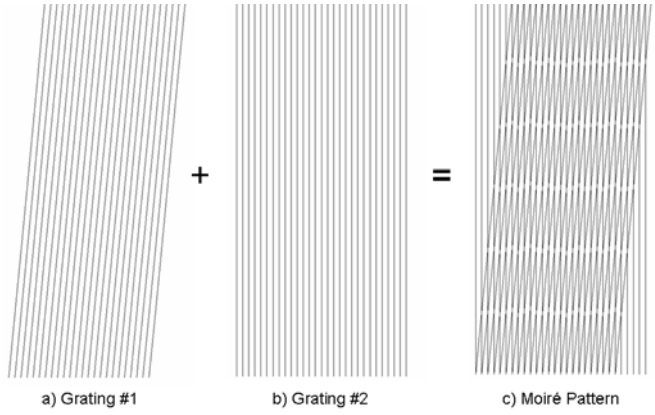

Figure C-2. Demonstration of moiré fringe pattern resulting from two gratings superimposed at a slight angle.

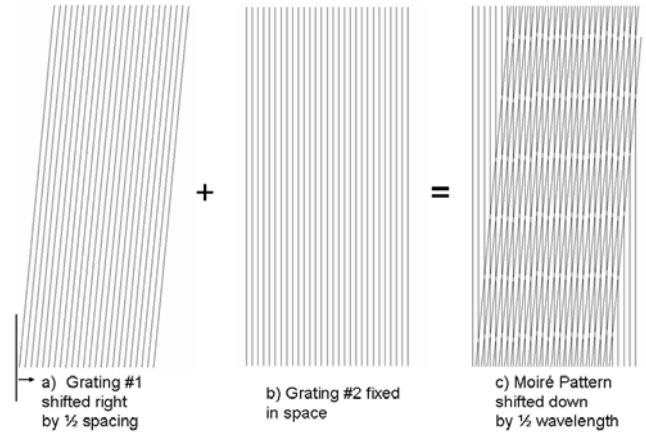

Figure C-3. Effect of a small shift of one grating on the location of the moiré fringe pattern.

A true moiré pattern requires two sets of multiple lines. However, the principle of high sensitivity to motion of the points of intersection works for any lines at small angles to each other, even two single lines. In the video frame shown in Figure C-1, there was a strong, nearly vertical line along the right edge of WTC 7 that defined the northwest corner. The natural set of vertical lines that provided a fixed reference in any digital video was the set of pixel columns. (For a nearly horizontal line, the natural fixed reference would be the pixel rows.)

A close look at the news video was needed to determine how best to use this approach to study the vibrations of WTC 7. Figure C-4 zooms in on the northwest edge of the building in one of the frames. The overlaid grid, marking every tenth pixel, demonstrated that this edge was very close to vertical. In this figure, the pixel rows were numbered from 140 at the top to 380 at the bottom, and the columns were numbered from 300 at the left to 660 at the right. Figure C-5 further enlarges the northwest edge, which was defined by a dark column of pixels (pixel column 518 in this region), surrounded on each side by a lighter column of pixels. However, the location of the darkest pixel shifted with vertical position along the northwest edge. Looking toward the bottom of Figure C-5, pixel column 517 to the left became lighter and pixel column 519 to the right became darker, while looking toward the top, pixel column 517 became darker and pixel column 519 became lighter. As was shown in Figure C-4, this was a result of the slight angle that the northwest edge makes with the vertical in the camera frame.

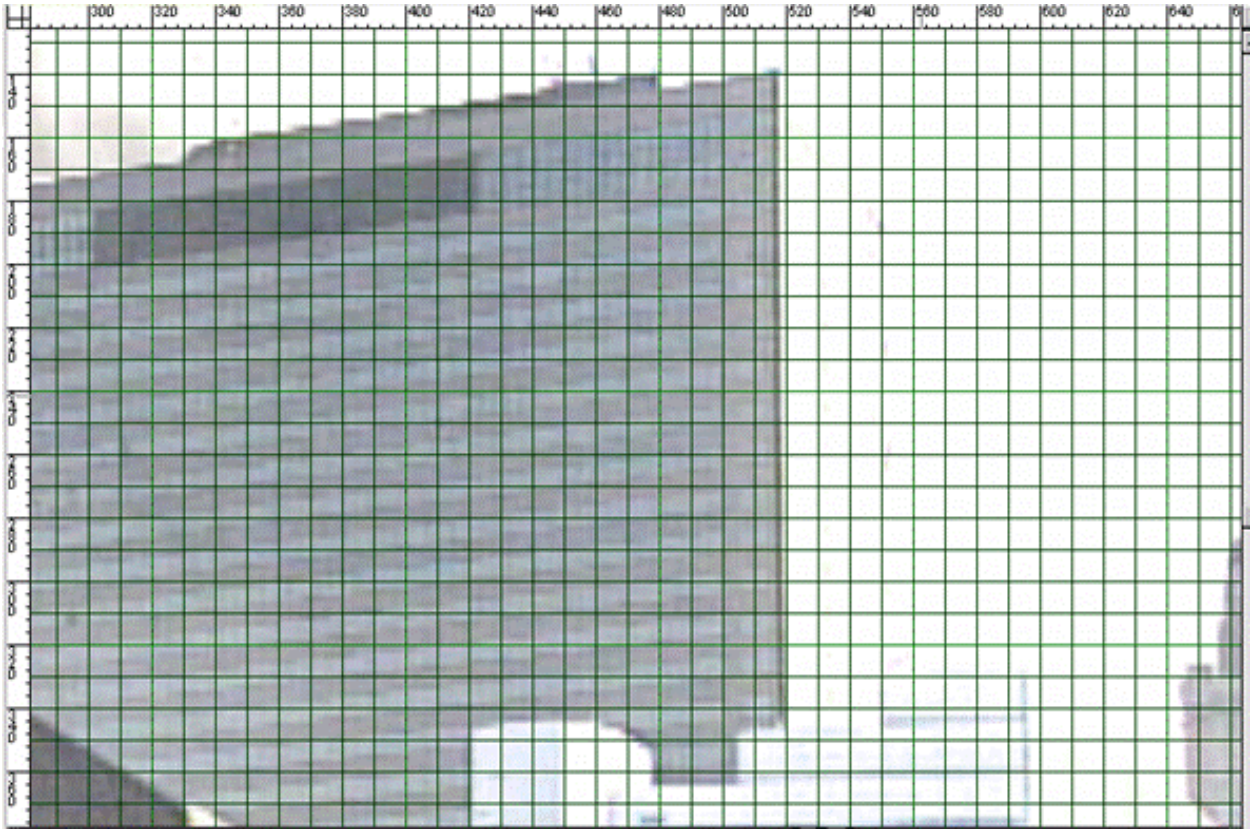

Based on enlargement of Figure C-1. © CBS News Archive

Figure C-4. Pixel grid of the north face of WTC 7, showing that the northwest edge was nearly vertical.

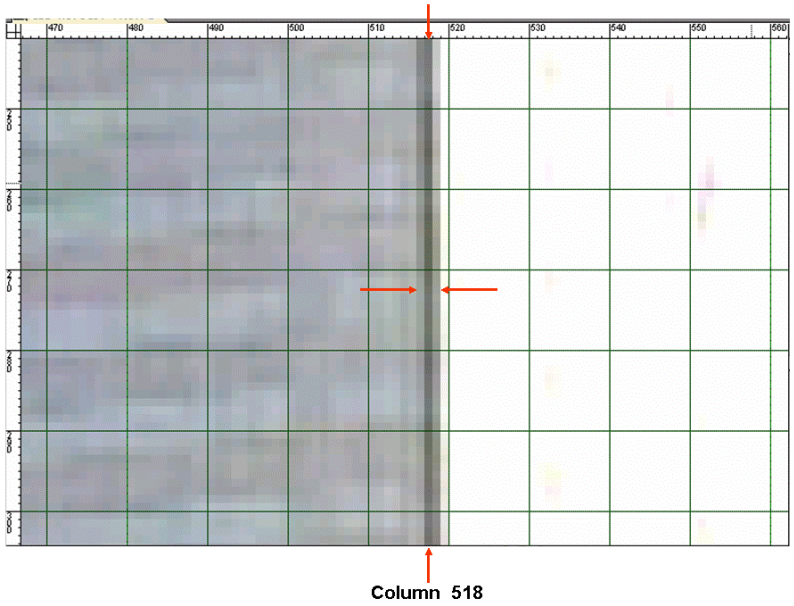

Figure C-5. Enlargement of northwest edge of WTC 7 from Figure C-4.
Center arrows indicate the row at which pixel intensities were judged to be equal to left and right of column 518.

Based on enlargement of Figure C-1. © CBS News Archive

Consider the pixels in the center of Figure C-5 between the two horizontal arrows. At this height, the pixels to either side of the dark pixel in pixel column 518 were of roughly equal intensities. If WTC 7 were to move slightly to the right (westward), pixel column 519 would get darker at this location, and the point at which pixel columns 517 and 519 were of equal intensity would move to a higher location along the northwest edge. For building movement to the left (eastward), the reverse is true, and the marker point of equal intensity would move downward. If the vertical location of the marker point of equal intensity were tracked in time, it should provide information about the motion of WTC 7.

The first estimation of the vertical location of the point at which pixel columns 517 and 519 were of equal intensity as a function of time was completed by eye. The results are shown in Figure C-6 for the final 18 s before initiation of the WTC 7 collapse and the final minute before the collapse initiation.

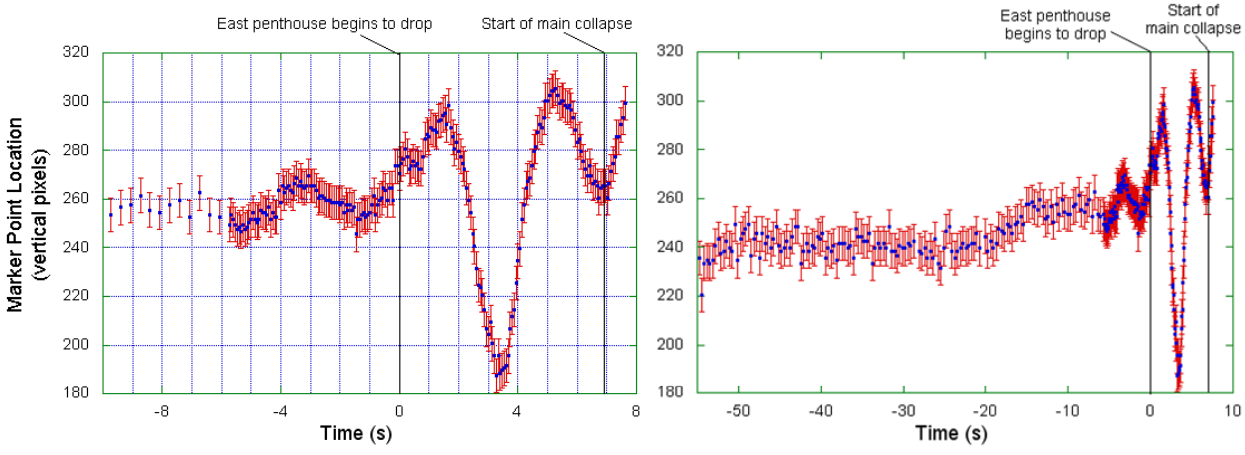

Figure C–6. Marker point data for final 18 s (left) and the final minute (right) prior to the collapse of WTC 7.

Data were collected for every other frame for approximately the final 13.5 s, and for every tenth frame preceding that point. The vertical pixel position of the marker point on the vertical axis was higher for movement downward (indicating northwest corner motion toward the east). The red lines at each data point showed estimated uncertainties of ± 7 pixels. This was a rough estimation, reflecting an inherent risk of error due to the brighter pixels to the right of pixel column 519 and darker pixels to the left of pixel column 517, as well as to the fluctuation of intensity levels along pixel columns 517 and 519. Despite this, the capability of this method to amplify sideways building vibrations was clear. With this near vertical orientation of the northwest edge of WTC 7 relative to the pixel columns, the marker point of equal intensity moved up and down by a total of more than a hundred pixels.

The point at which pixels to either side of the central dark pixel were equal in intensity was not the only point that could have been selected for tracking. A second, easily identifiable marker point was one at which two adjacent pixels had the same intensity, e.g., for pixel columns 518 and 519. However, in order for the selected marker point to be tracked over the course of the video, it had to remain along the northwest edge of WTC 7. Because of the large extent of building motion, the marker point that was chosen was the only one that did not fall off either the top or bottom of the northwest edge during the duration of the video.

As presented in the timeline in Table 5-5 of Chapter 5, the video frame in which the east edge of the east penthouse started to move downward was assigned time t = 0 s. The time at which the initial motion of the main collapse of WTC 7 was detected was found to be t = 6.9 s.

Of particular interest in the initial results from this analysis was the observation that the onset of vibrations preceding the final collapse of WTC 7 occurred several seconds before the east penthouse began to fall, as shown in Figure C-6.

C.1.4 Conversion of Magnitude from Vertical Pixels to Distance

The magnitude of the motion was estimated using the number of vertical pixels that equated to a single horizontal pixel and a conversion factor between horizontal pixels and actual distance.

The vertical motion of the marker point that equated to a single horizontal pixel width was determined by counting the number of vertical pixels between the studied marker point and the next point along the northeast edge of WTC 7 at which pixel values were equal on each side of the central dark column. The marker point used in the analysis was the intersection of intensities along pixel columns 517 and 519; the marker point one horizontal pixel to the left was the intersection of intensities along pixel columns 516 and 518. Where this marker was available and had not dropped off the top of the northeast edge, the difference between these two points one horizontal pixel apart was found to be 100 ± 10 vertical pixels.

The conversion factor between horizontal pixels and distance along the north face of WTC 7 was obtained by determining the width of this face in both horizontal pixels and in feet. Due to the camera location, points on the north face near the northwest edge were closer to the camera than points near the northeast edge. However, this distortion was small, since the width of the north face was much smaller than the distance of WTC 7 from the camera. The perspective view of the camera looking up at WTC 7 also introduced some error into the measurement of the number of pixels for the width, as did the uncertainty of a couple of pixels in the exact location of the edges defining the north face. Given these sources of error, an estimate for this video of the width of the north face of WTC was 301 ± 4 horizontal pixels.

Since the true dimension of the north face was 329 ft, the conversion factor was 1.09 ft ± 0.02 ft per horizontal pixel. Combining this with the equivalence of 100 ± 10 vertical pixels for each horizontal pixel gave the final conversion factor of 1.1 ft ± 0.1 ft (13 in. ± 1 in.) for each 100 pixels of vertical marker motion.

C.1.5 Automation of Moiré Analysis

Because of the inherent risks of error in collecting data from this video by eye, as mentioned in Section C.1.2, an objective determination of the intersection point using the actual intensity values was needed. An automated determination of this point enabled data to be collected over the entire 7.5 min duration of this video from start to WTC 7 collapse, a total of 13,558 frames.

To prepare for analysis, the video clip was exported into a sequence of images, with each image carrying the data for a single frame of the video. Each frame was then converted from the original RGB color into grayscale values. This combined the values from the red, green, and blue channels and simplified the analysis. Possible intensity values for each pixel ranged from 0 for black to 255 for white. This image manipulation was accomplished using Adobe Photoshop software.

Figure C-7 demonstrates the automation procedure for the analysis. The close-up of the northwest edge of WTC 7 in (a) shows the area around the point at which pixel columns 517 and 519 had the same intensity value in this frame of the video. The intensity values for these two columns along the length of the northwest edge, from pixel row 340 near the bottom to 140 at the top, were extracted and plotted in Figure C-7(b). Fluctuations in the values are apparent in this plot. To find the intersection point of the pixel intensity plots for these two pixel columns, the data for each column were first fitted to a smooth curve. A third-order polynomial least-squares fit gave a good compromise between the variance (a measure of the distance of each data point from the curve) and an estimate of the error in determining the intersection point. Figure C-7(c) shows the two curves resulting from this fit and the intersection point for this particular video frame. The analysis procedure was implemented using Mathematica software.

One source of uncertainty in this analysis was the curve-fitting process; another arose from defects in the video images. Many of the frames from this video contained defects, such as the color and black-and-white patterns in the lower center and lower left of Figure C-1. Similar defects occurring along the northwest edge being used for the analysis were responsible for some outlier points in the results.

Figures C-8 and C-9 show the results of performing this analysis on each video frame, over the final 22 s before collapse and over the entire duration of the video, respectively.

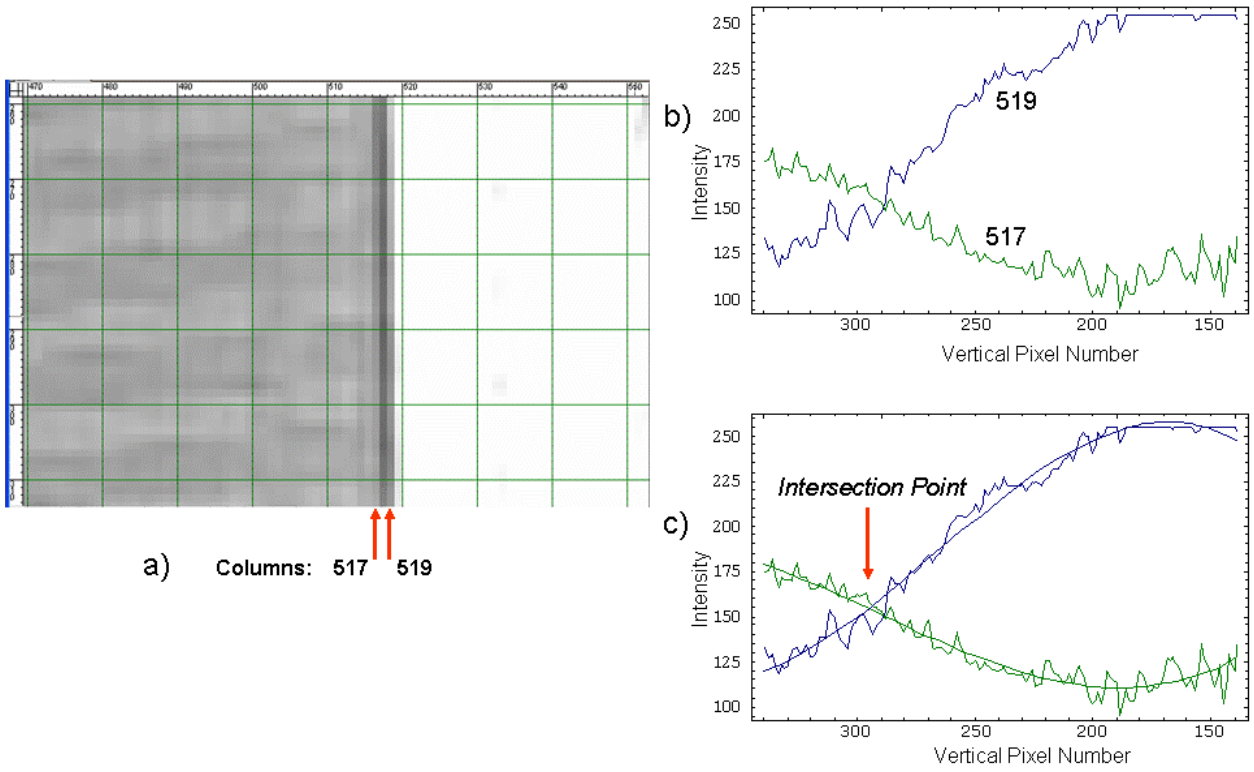

Figure C-7. Automated determination of intersection point. a) close-up of northeast edge of WTC 7 in grayscale, b) plot of pixel intensity vs. vertical pixel number for pixel columns 517 and 519, and c) polynomial fit showing the intersection point.

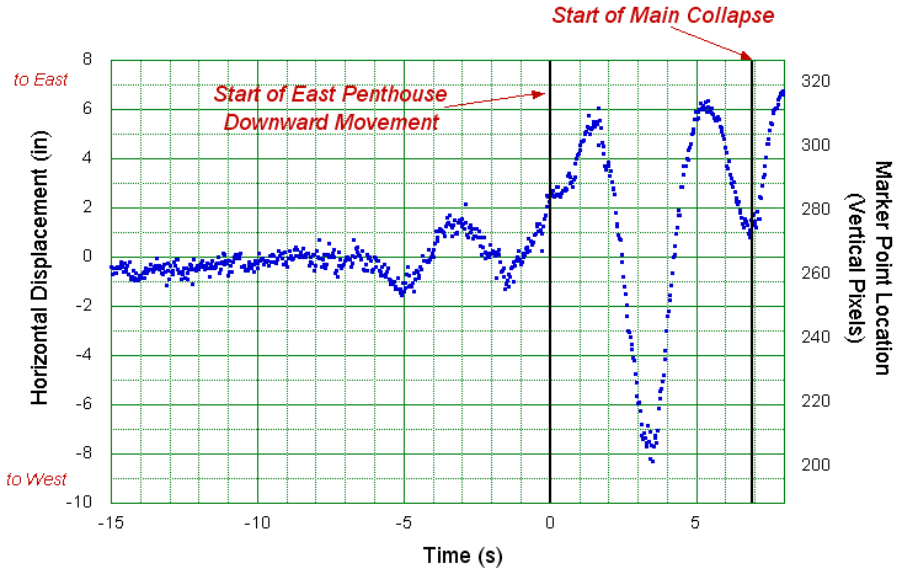

Figure C-8. Horizontal displacement of northwest corner of WTC 7 and marker point location for final 22 s before the start of penthouse downward movement.

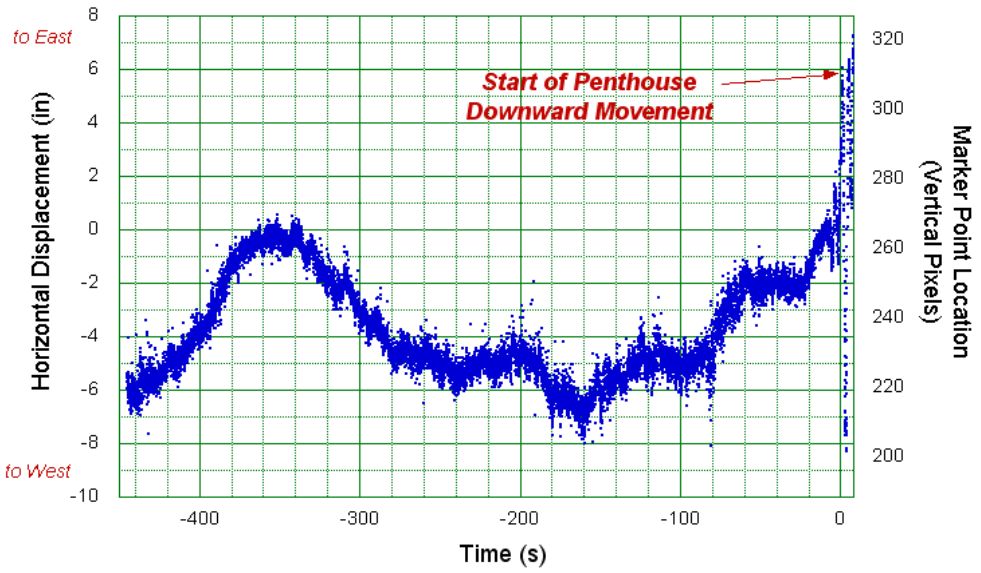

Figure C-9. Horizontal displacement of northwest corner of WTC 7 and marker point location for full 7½ min duration of video before collapse initiation.

Using the conversion factor determined in section C.1.3 allowed labeling of the vertical axis in both marker locations by vertical pixel number and in inches of horizontal displacement. The zero point for displacement was chosen to be vertical pixel number 265, the location of the marker point at the time when final oscillations began. In Figure C-8, some important behavior is apparent. Starting at about 6 s before the penthouse began its downward movement into the building, there was an abrupt change in the slope of the data that marked the beginning of oscillations that continue until collapse. There was also a second abrupt change in the data at about 1.5 s before the penthouse started moving downward.

In Figure C-9, there are major changes in the location of the marker point that occurred over long time intervals of 20 s or greater. These changes were likely due to movement of the camera.

The harmonic motion that began 6 s before the penthouse began to fall had an amplitude of nine vertical pixels, equivalent to sideways motion of 0.1 ft, or slightly over one inch in each direction. The maximum range of motion, which occurred after the penthouse had disappeared, totaled about 107 vertical pixels, or about 14 in. ± 1 in. Section C.2 takes a closer look at these vibrations.

C.2 VIBRATION RESULTS

Of primary interest in this analysis was any information that could shed light on the collapse sequence of WTC 7. The starting point of the final set of building vibrations at 6 s before the east penthouse began to fall indicated that an event had occurred within the building at that time. In addition, a comparison of the oscillatory period with a model of the building's motion indicated the mode that had been excited by the event. Whether the building swayed in a single plane with a translational mode or twisted with a torsional mode, this information provided more insight for the structural engineer trying to piece together the sequence of events.

The frequency content of the data in Figure C-8 was determined using the same method described in NIST NCSTAR 1-5A, Appendix K. The time-dependent displacement of the marker point was assumed to take the form of a damped harmonic oscillator, which is described by the following equation:

$$d = \left[A + B\left(t - t_0\right)\right] + Ce^{-D(t-t_0)} \sin\left[2\pi\left(t - t_0\right)/E + F\right] \quad (1)$$

where

d = displacement, in.

t = time, s

t_0 = time at which the penthouse begins to move downward, s

A = baseline offset, in.

B = linear slope of the baseline, in./s

C = initial amplitude at time t_0, in.

D = decay rate, $(s)^{-1}$

E = oscillatory period, s

F = phase angle, radian

The values to be determined were A, B, C, D, E, and F. The frequency was equal to the reciprocal of the period, E^{-1}. This mathematical model included the period, amplitude, and decay rate of the oscillations, and also included the possibility of a linear change in the zero point of the displacement with time. To accurately fit this model to the data, a good approximation was needed for each of the six variables to be determined. These approximations were then used as starting points for a nonlinear least squares fit of Eq. (1). The calculations were carried out in vertical pixel units and converted to inches. The uncertainty values given in this section do not include the conversion uncertainty.

The video showed that the east penthouse was descending between time t = 0 s and t = 2.0 s. During the time that the east penthouse was falling, the harmonic motion of the building was clearly disturbed, as can be seen in Figure C-8. The displacement of the marker point was on a plateau for the first half second after the penthouse began to fall, and the time from the minimum in the data at about -1.5 s to the maximum at about 1.7 s was about double that for oscillations before t = 0 s or after t = 2.0 s. The mathematical model assumed free harmonic motion and was not appropriate for looking at building motion when a forcing function was being applied. The time periods studied using this model were therefore from t = -6.0 s to t = 0 s and from t = 2.0 s to the start of collapse at t = 6.9 s. The motion from just after the plateau in the data at t = 1.0 s to collapse was also analyzed. All the results are shown in Table C-1.

Table C-1. Modes from nonlinear least squares analysis for WTC 7 data.
Total uncertainties are twice the standard deviation, σ.

Time Range (s)	Period (s)	Amplitude (in.)	Decay Rate (s^{-1})	Phase (radian)	Offset (in.)	Slope (in./s)	2σ (in.)
-6.0 – 0	3.61 ± 0.06	1.3 ± 0.1	-0.05 ± 0.04	0.9 ± 0.1	1.0 ± 0.1	0.22 ± 0.04	0.6
2.0 – 6.9	3.46 ± 0.06	12 ± 1	0.19 ± 0.02	4.7 ± 0.1	-6.6 ± 0.5	1.7 ± 0.1	0.9
2.0 – 6.9 (2^{nd} mode)	1.65 ± 0.02	0.7 ± 0.3	0.1 ± 0.1	3.9 ± 0.4	-0.1 ± 0.1	0.03 ± 0.03	0.5
1.0 – 6.9	3.75 ± 0.04	11 ± 1	0.17 ± 0.02	5.3 ± 0.1	-4.4 ± 0.4	1.2 ± 0.1	1.3
1.0 – 6.9 (2^{nd} mode)	1.85 ± 0.04	2.0 ± 0.4	0.3 ± 0.1	5.3 ± 0.2	0.3 ± 0.1	-0.05 ± 0.04	0.7
0.5 – 6.9	4.04 ± 0.05	9 ± 1	0.10 ± 0.03	5.7 ± 0.1	-2.3 ± 0.4	0.7 ± 0.1	1.8

For the 6 s period from the beginning of oscillatory motion in the data to when the penthouse began to fall, the harmonic motion was found to have a period of 3.61 s, an amplitude of 1.3 in., and an approximately zero decay rate. The total standard deviation from the nonlinear fit to this data (the square root of the estimated variance) was σ = 0.3 in. The total uncertainty, with a confidence level of 95 percent, equaled twice the standard deviation in both positive and negative directions, or ± 0.6 in. Figure C-10(a) shows this mode superimposed on the original data. Subtracting the mode from the data resulted in the residual data shown in Figure C-10(b). The residual appeared random. If an oscillatory pattern had appeared in the residual, it would have suggested that a secondary vibration mode is present. In this case, the first mode found did a good job of matching the data.

The next modal analysis was performed for the time period from t = 2.0 s, at the time when the penthouse was observed to completely disappear from the roof WTC 7, to t = 6.9 s, when the main collapse began. The primary mode has a period of 3.46 s, an amplitude of 12 in., and a decay rate of 0.19 s-1. The total uncertainty was ± 0.9 in. Figure C-11(a) shows a good comparison between the mode and the data. The residual, Figure C-11(b), indicates a secondary mode with a period of 1.65 s, amplitude of 0.7 in., and zero decay rate. This is plotted in Figure C-12(a). The residual, after the combination of these two modes had been subtracted from the original data, is shown in Figure C-12(b). By adding these two modes together, the total uncertainty was reduced to ± 0.5 in., slightly better than the results for the time period before the fall of the penthouse.

To test how long the internal events within WTC 7 during the downward motion of the east penthouse drove the visible motion of the building, modal analyses were performed on wider time ranges of data, from t = 1.0 s to the main collapse at t = 6.9 s and from t = 0.5 s to t = 6.9 s. The total uncertainty for these analyses increased significantly with time range, to ± 1.3 in. for the time range of t = 1.0 s to t = 6.9 s and ± 1.8 in. for the time range of t = 0.5 s to t = 6.9 s. Figure C-13 gives visual evidence of the poorer fit for the former analysis. The discrepancies between the mode and the data were larger than in Figure C-11, and a strongly damped secondary mode was needed to fit the residual in Figure C-13(b). The modal analysis from t = 2.0 s to 6.9 s gave the best quantitative representation of the oscillatory motion of WTC 7 immediately before the final building collapse.

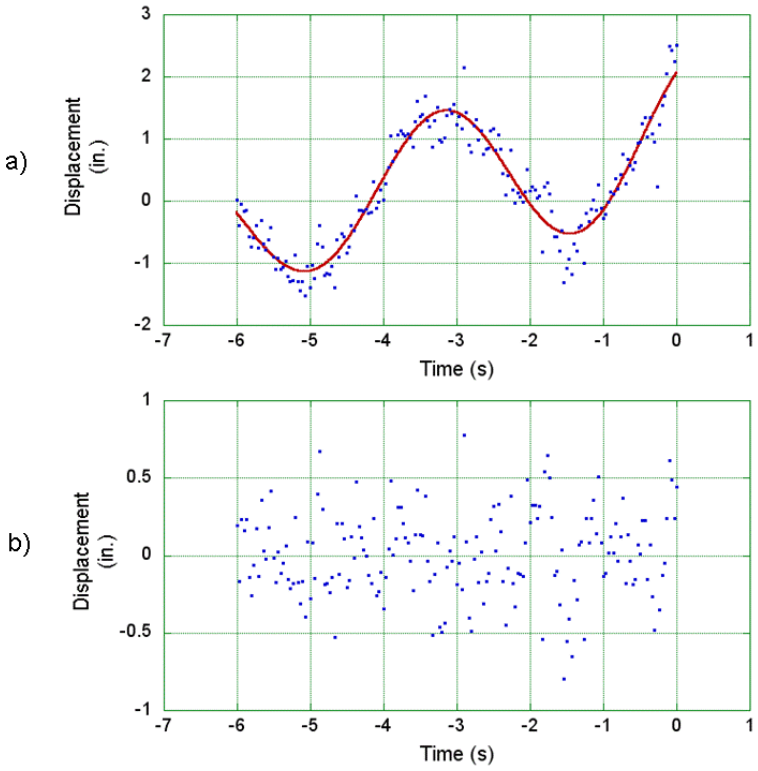

Figure C-10. a) Comparison of oscillation mode with data for 6 s period before the east penthouse began to move downward, b) residual after mode was subtracted from data.

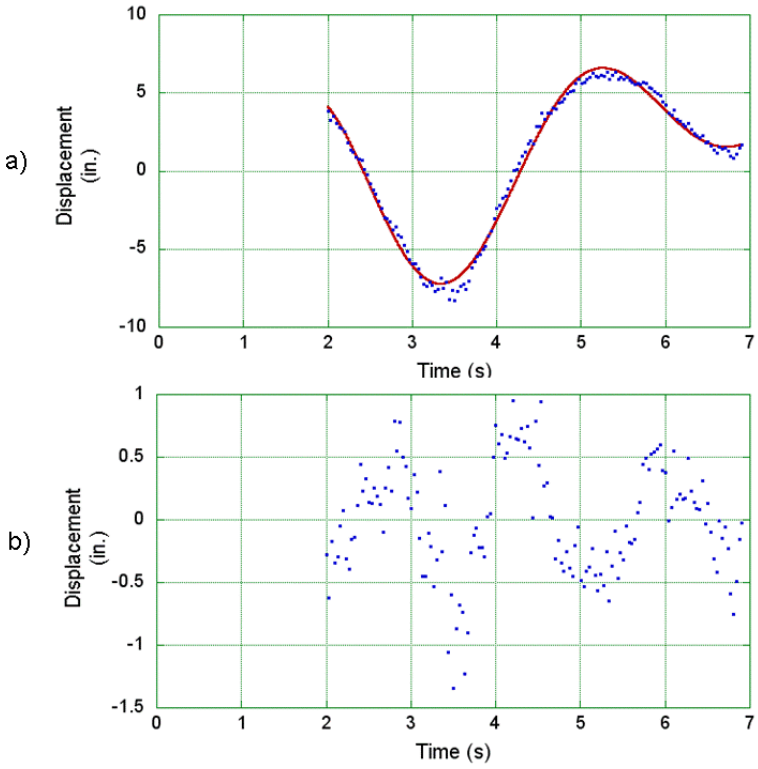

Figure C-11. a) Comparison of mode with data for period from t = 2.0 s to t = 6.9 s, and b) residual.

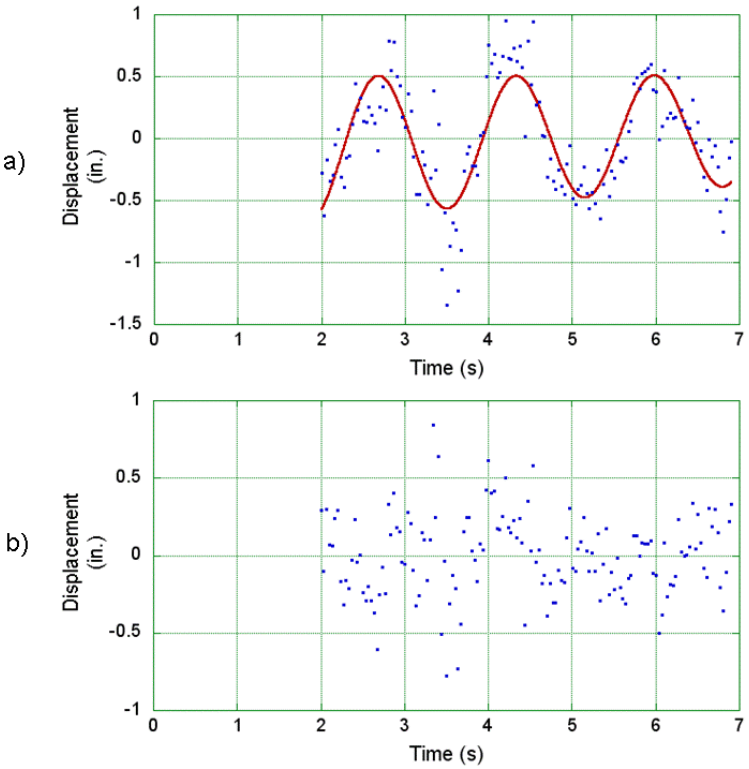

Figure C-12. a) Comparison of secondary mode with residual for period from t = 2.0 s to t = 6.9 s, and b) residual after both modes were subtracted from original data.

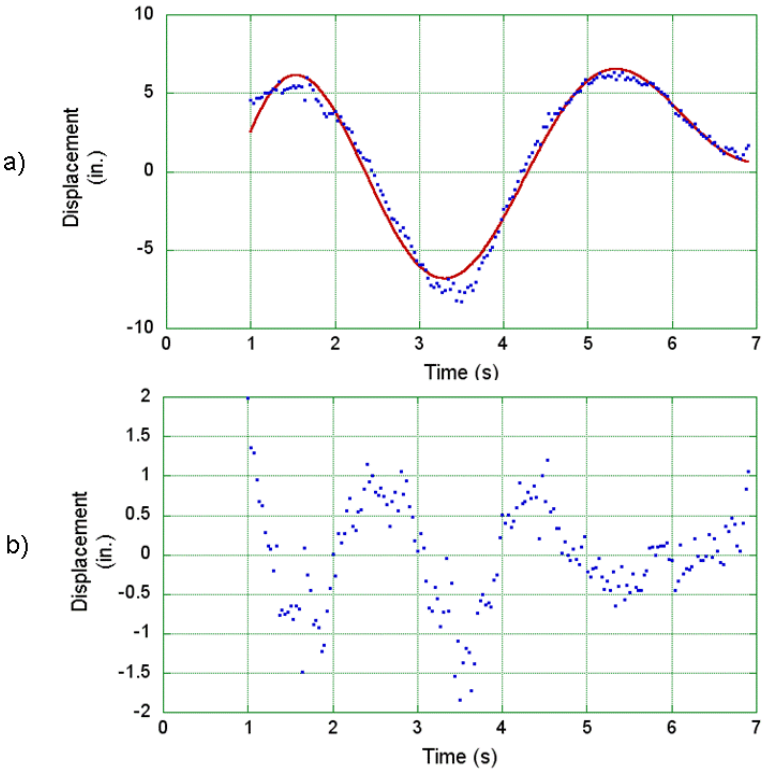

Figure C-13. a) Comparison of mode with data for period from t =1.0 s to t = 6.9 s, and b) residual.

A final comparison of oscillation modes to data is shown in Figure C-14. Before the penthouse began to descend, an undamped mode of period 3.61 s described the building vibrations well. Between the time that the penthouse disappeared and the time that WTC 7 collapsed, a combination of a damped mode of period 3.46 s and an undamped mode of 1.65 s provided a good fit to the data.

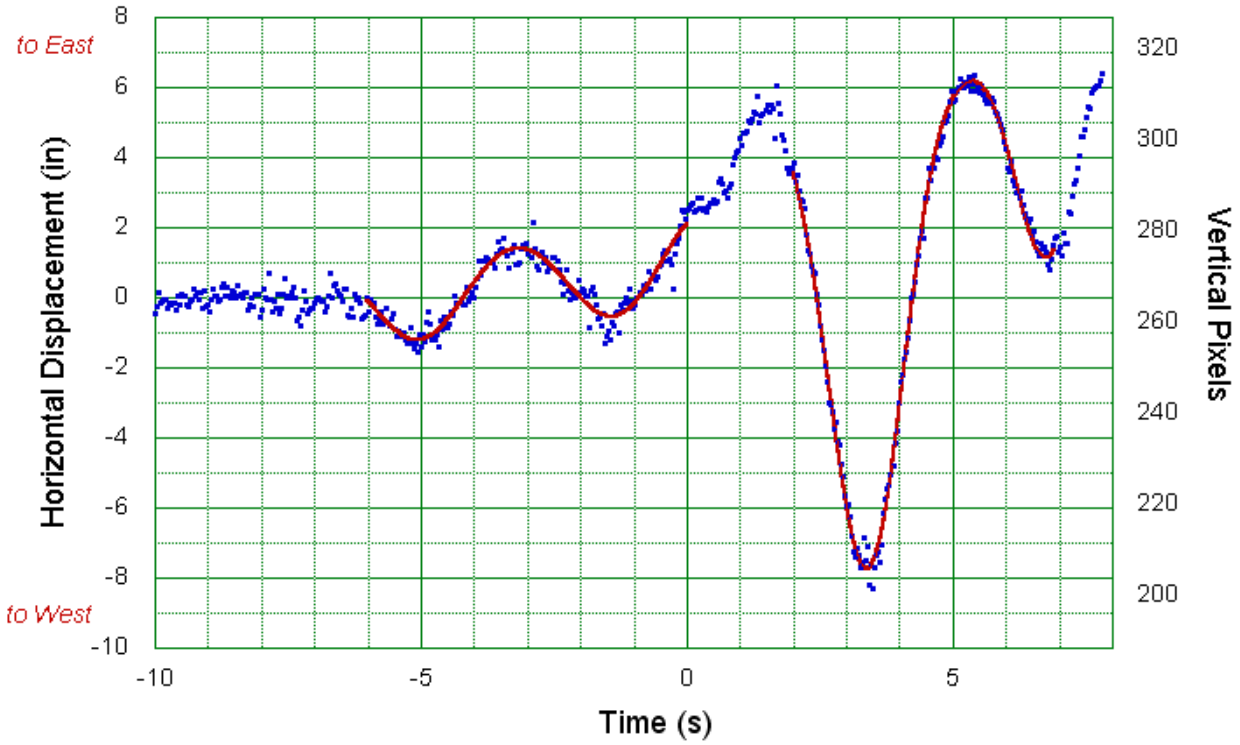

Figure C-14. Comparison of data with modes before and after penthouse fall.

C.3 SUMMARY

The tracking of a point marking the intersection between a near vertical building edge and the pixel columns of a digital video image provided details about the vibrations of WTC 7 just prior to collapse. An undamped vibration mode of period 3.61 s and amplitude slightly over 1 in. was observed during the 6 s before the east penthouse started to fall. A combination of a damped mode of period 3.46 s and an undamped mode of 1.65 s, with a total range of motion of about 14 in., was observed from the time the penthouse had submerged below the roofline to the time of collapse initiation.

This page intentionally left blank.

Appendix D
HYPOTHETICAL BLAST SCENARIOS

D.1 BACKGROUND

As part of assessing alternative hypotheses for initiation of the collapse of WTC 7, a hypothetical blast event was considered. Scenarios of a hypothetical blast event that could have occurred in WTC 7 on September 11, 2001, were assessed, including blast location, size, and timing. Identification and analysis of hypothetical blast scenarios was conducted in three phases, with the results from each phase being used as input to the next phase. The three phases were:

- Phase I: Identify hypothetical blast scenarios to initiate structural collapse.
- Phase II: Assess the blast wave propagation inside the building and the corresponding response of the WTC 7 windows.
- Phase III: Assess the approximate distance from the building that the blast would have been audible in an urban setting.

For Phase I, a controlled demolition expert identified appropriate charge sizes and configurations. In Phase II, based on the specified charge from Phase I, the hydrocode SHAMRC was used to calculate the blast propagation through the building. The pressures at the outer walls of WTC 7 developed by SHAMRC were then used to assess window damage. In Phase III, acoustic analysis of sound propagation outside the building was carried out with a U.S. Air Force low overpressure acoustic wave propagation code called NLAWS.

The following sections describe the work performed in each of the three phases along with results.

D.2 PHASE I: EXPERT RECOMMENDED PREPARATIONS FOR EXPLOSIVELY CONTROLLED DEMOLITION

Phase I identified a single minimum plausible scenario for the explosive demolition of a selected column or truss. This included columns that supported large tributary areas and a critical truss cross-member. The analysis assumed that severance of one of these members could initiate building collapse. For successful demolition of a column, failure was defined as complete severance of the column section, or complete severance of sufficient sections of the flange, web, and cover plates, such that the remaining column section was insufficient to carry the column service loads, or that a lateral deflection of the column section would exceed its section width.

The hypothetical blast scenarios that were addressed fell into two categories:

Those in which there was sufficient time to prepare the structures for an optimum set-up prior to demolition. The objective would have been to use the minimum possible amount of

explosives in the demolition process. Preliminary cutting of structural members could have been performed.

18. Those in which the demolition was to be performed in the shortest possible time. The objective would have been to set up for demolition during approximately a 6 h time frame, i.e., between the time WTC 7 had been evacuated and the time at which collapse occurred.

For each of the scenario categories, the type and quantity of explosive material (e.g., shaped charges, C4 or other non-directional explosive materials) required to fail each of the selected column sections was identified. In addition, any special equipment or supplies, and the time required to prepare the column, were identified. For each scenario, expected secondary effects – fireballs, noise level, extent of window breakage, and dust expulsion – were estimated. Two approaches were considered, in which the column was or was not prepared with preliminary cutting..

Column sections selected for developing hypothetical blast scenarios were:

Column 79 at floor 14 – W14x730 with two 26-in. x 2-in. side cover plates

Column 79 at floor 5 – W14x730 with two 26-in. x 3-in. side cover plates

Column 80 or Column 76 at floor 14 – W14x730 with two 12.5-in. x 4-in. web plates

Truss 2 diagonal – W14x730 with two 8-in. x 3-in. web plates

Column 81 at floor 14 – W14x730 with two 12.5-in. x 1-in. web plates

Column 77 at floor 14 or Column 78a at floor 5 or Truss 1 diagonal – W14x665

For reference, Table D-1 defines section properties for the two considered column types.

Table D-1. Basic wide flange column parameters. (Dimensions in in.)

Section	Web Height	Flange Width	Flange Thickness	Web Thickness
W14X730	22.4	17.9	4.91	3.07
W14X665	21.6	17.7	4.52	2.83

Side plate details are shown in Figure D-1, which illustrates the side plate attachment for the considered columns (Reference WTC 7 Drawing. S-17).

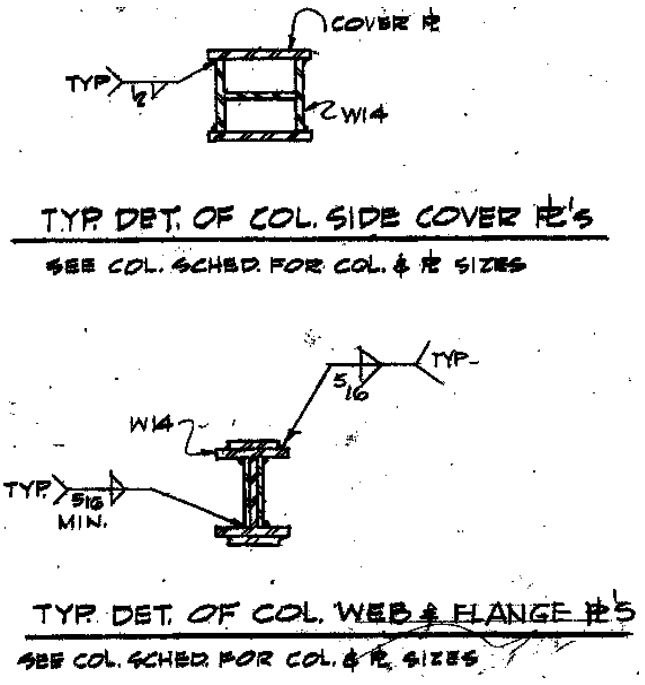

Figure D-1. Column side plate attachment details.

Charges would be placed on either side of the two cover plates and the web and sections would be cut out of the flanges. These would have to be initiated using a detonating cord harness (21 000 feet per second (6 400 m/s) velocity of detonation (VOD)), for simultaneity of initiation.

From all these combinations, a single hypothetical blast scenario was identified for all of the selected column or truss sections. This hypothetical blast scenario included preliminary cutting of the column or truss section, which would have necessitated a smaller mass of explosive than an uncut section. The scenarios considered for the second category (minimum time possible, minimal preparation) were estimated to have required an order of magnitude more explosive and would have been less covert. The lowest mass of explosive needed to sever any of the six column or truss sections was found to be 4 kg (9 lb) of RDX explosives in linear shaped charges. The other scenarios considered would have required more explosive, or were generally considered infeasible to carry out without detection.

The time constraint in the category 2 scenarios was not a determining factor. It would have taken a skilled burner with an oxy-propane torch about 15 minutes to make the cuts necessary to install the required linear charges of RDX. It would have taken another 5 minutes to place the explosive charges, plus the time to set up an initiation device. Note that the time requirements did not consider other preparations required to clear the column for cutting, such as removing walls or other coverings that might have restricted access to bare steel at a column section. Presumably, these activities could have been performed within the available time.

This single hypothetical blast scenario was then applied to Column 79 in the Phase II blast modeling.

D.3 PHASE II: 2-D BLAST MODELING

D.3.1 SHAMRC Blast Modeling Code

SHAMRC [1,2] is a U.S. government-owned hydrocode solver that is used for analysis of explosive detonations, shock propagation and structure loads due to blast and fragments. SHAMRC has a proven record of accurate calculations of airblast structural loading for explosive weights of less than one pound to more than 4 000 tons. SHAMRC has also been used to calculate the formation and propagation of shaped charge jets and their interaction with structures. The code was well suited for the blast propagation analysis performed on WTC 7.

For the blast modeling effort, detailed two-dimensional SHAMRC hydrodynamic calculations were performed. The interior building layout was modeled to determine the transient pressure load inside the building after detonation. A two-dimensional analysis was sufficient to estimate pressures at window locations for a small charge constrained between floors. The pressure histories were then used to determine whether windows would have broken, which would have provided visible evidence of a small charge detonation outside of the building. The window fragility analysis was conducted with a separate computational tool, SFOM, using window geometry, material properties, and construction information as inputs to the model. The output from SFOM was Pressure-Impulse (P-I) failure curve predictions for WTC 7 windows. The SHAMRC-generated pressure histories were compared to the failure curves to predict window failure for each scenario considered.

D.3.2 SHAMRC Blast Model Development

Floor Layout

Three building layout configurations were considered during the blast analysis phase of the project:

- Layout 1: No partitions in the tenant floor area
- Layout 2: Moderate partitions in the tenant floor area
- Layout 3: Significant partitions in the tenant floor area

In preliminary analyses, Layout 1, with an open floor plan in the tenant space, was shown to be less conservative because of a higher level of damage at the building perimeter than Layouts 2 and 3, which both included partitions in the tenant area. Therefore, Layout 1 was not revisited in the final analysis iteration. Analyses were carried out for Layouts 2 and 3 to explore the sensitivity of damage to partition density on the tenant floor space.

Layout 2 was a moderately partitioned floor similar to a Floor 7 layout in WTC 7. Layout 3 was a heavily partitioned floor, similar to a Floor 12 layout. The floor layouts and corresponding 2-D SHAMRC models are shown in Figure D-2 and Figure D-3 for Scenario 2 and Scenario 3, respectively.

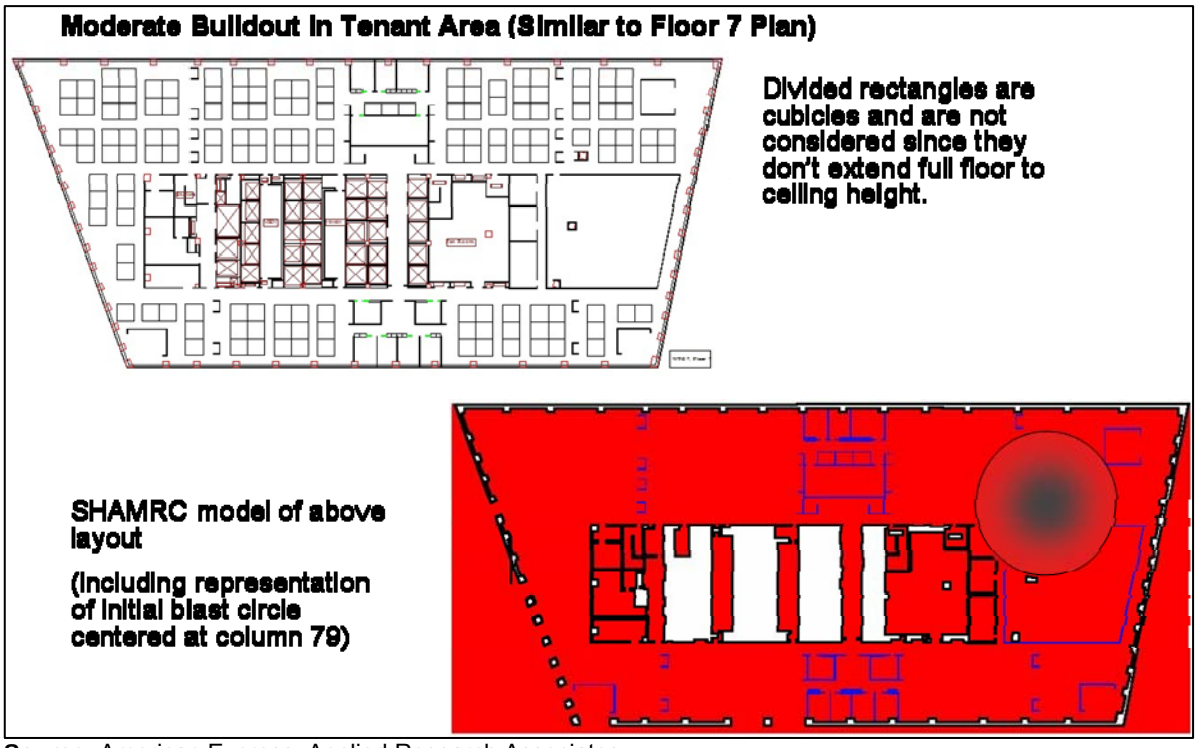

Source: American Express, Applied Research Associates

Figure D-2. Layout 2 floor plan layout and SHAMRC model.

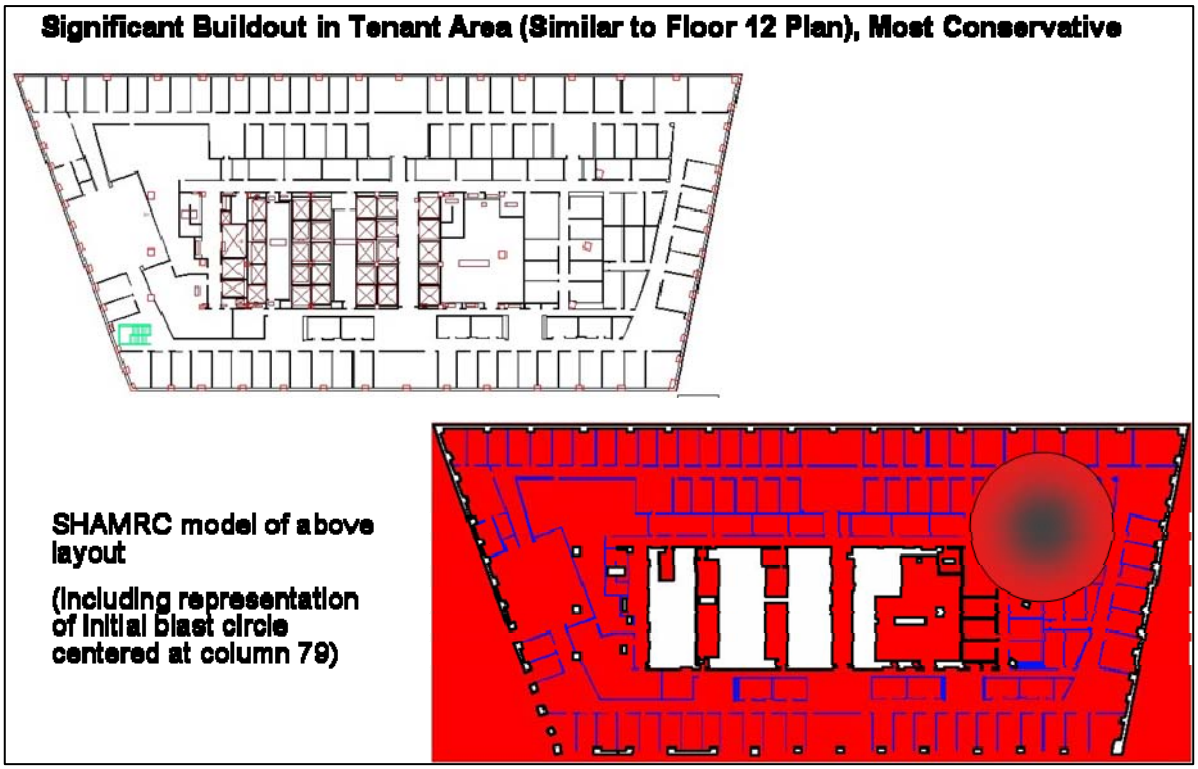

Source: American Express, Applied Research Associates

Figure D-3. Layout 3 floor plan layout and SHAMRC model.

Assumptions

Some assumptions and simplifications were made in setting up and conducting the 2-D SHAMRC models of the WTC 7 floor layouts. Some key considerations for this effort were:

- The core walls and columns were treated as rigid, since the construction was heavy and less damage was expected from blast propagation. The key objective was to estimate blast pressures at window locations for subsequent window fragility and acoustic propagation analysis.

- The Layout 2 and 3 SHAMRC models included openings between columns at locations of window breakage from observations, as indicated in Chapter 5. The window openings were along the south and west perimeters.

- Partition walls in the tenant area that extended from the floor to the drop ceiling were modeled as a dense fluid relative to the surrounding air. This commonly used "heavy air" CFD approach allowed for realistic blast wave reflections and propagation through the walls in the timeframe of the simulation (less than 1 s), before the walls would appreciably deform. Partition wall properties were approximated based on composite wall construction.

- Cubicles were not modeled in this 2-D analysis since they did not extend the full floor height. Cubicles are shown in the Layout 2 Figure D-2 as divided boxes. The Scenario 3 layout did not include any cubicles.

- In the model, a fully developed, axisymmetric initial blast field centered on Column 79 was superposed on a uniform pressure field elsewhere in the model. The partition walls were not considered in this circle, as it was assumed that the blast would breach those walls.

Run Configurations and Procedure

The 2-D SHAMRC calculations were performed for the minimum explosive case identified in Phase I, which was a 9 lb RDX blast centered on Column 79. Calculations were also performed for a lesser charge size of 2 lb to evaluate threshold explosive requirements for window fragility. There were four blast analyses performed in total, consisting of two different charge sizes (2 lb and 9 lb of RDX) and two floor layouts (Scenarios 2 and 3).

For each SHAMRC blast modeling analysis, a 1-D/axisymmetric blast profile was generated for a given charge size and was allowed to fully develop before running the 2-D solution. Next, the circular blast profile developed in the 1-D/axisymmetric analysis was superposed on the 2-D floor layout that had been initialized under atmospheric conditions. Finally, the superposed blast solution was allowed to propagate transiently and interact with the 2-D structure.

Pressure-time data were saved at each station between exterior columns for comparison to predicted window P-I failure criteria. The pressure history was also used as input to the Phase III acoustic propagation analysis. Development of window failure criteria is discussed in the following subsection.

D.3.3 Estimation of WTC 7 Perimeter Window Fragility

A Shard Fly-out Model (SFOM) [3-6] was used to predict window breakage, based on the pressure profiles from the SHAMRC analysis. The SFOM was originally developed for the Defense Threat Reduction Agency (DTRA) to predict window breakage as well as size and shape of shards created by blast loading.

Within SFOM, window breakage can be predicted with a single-degree-of-freedom (SDOF) model, which outputs a pressure-impulse (P-I) failure threshold curve. This can be done for annealed glass and for thermally tempered glass (TTG). For insulated glass units (IGU), composed of two annealed panes, a relationship to monolithic annealed windows with a thickness equal to the sum of the two IGU thicknesses was assumed. The SDOF model assumed a triangular loading function. A stiffness function was defined as the slope of the resistance/displacement curve. Using these loading and stiffness functions and a Newmark integration procedure, displacement and velocity time histories were obtained for input pressure-impulse combinations. A break was defined to occur when a pressure-impulse combination resulted in a window displacement that exceeded the maximum displacement allowable.

In addition to the type of window and blast loading conditions, the SFOM required specification of window dimensions, density, strength and width of the interstitial air gap (assuming an insulated glass unit window configuration). Limited window construction information was available from WTC 7 architectural drawings. Where detailed information was unavailable, industry standards for the unknown specifications were applied. The following section views from the drawings, shown in Figure D-4 to Figure D-7, were used as guidelines of general window construction for the SFOM analysis. In particular, overall window dimensions, general window framing practice, and a 1-inch insulated glass dimension were noted in the drawings.

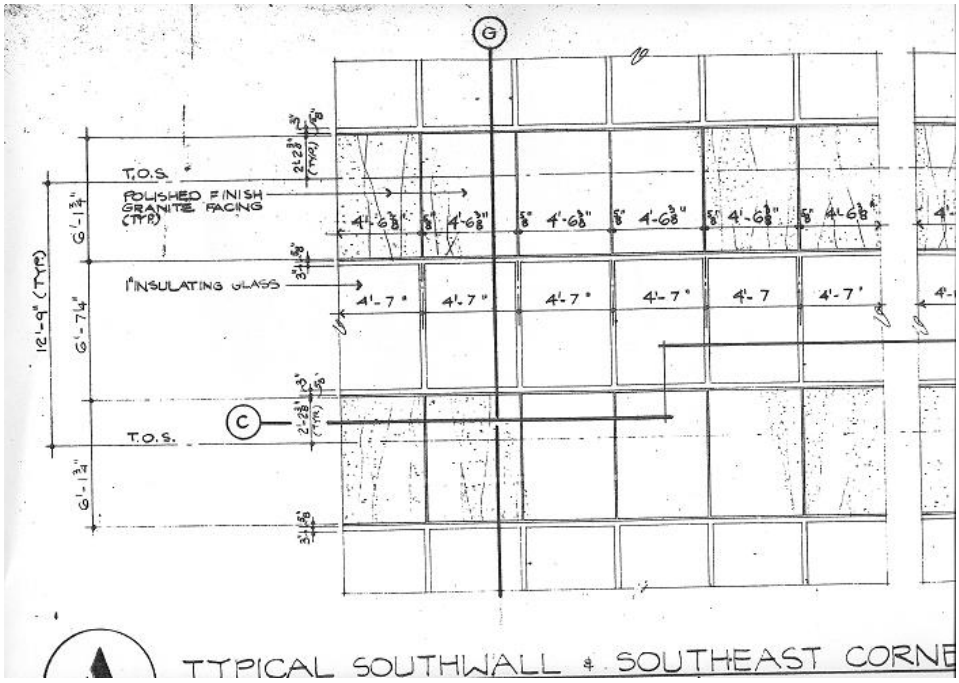

Figure D-4. WTC 7 Architectural Drawing 38, Detail A: Typical Southwall and Southeast Corner Elevation.

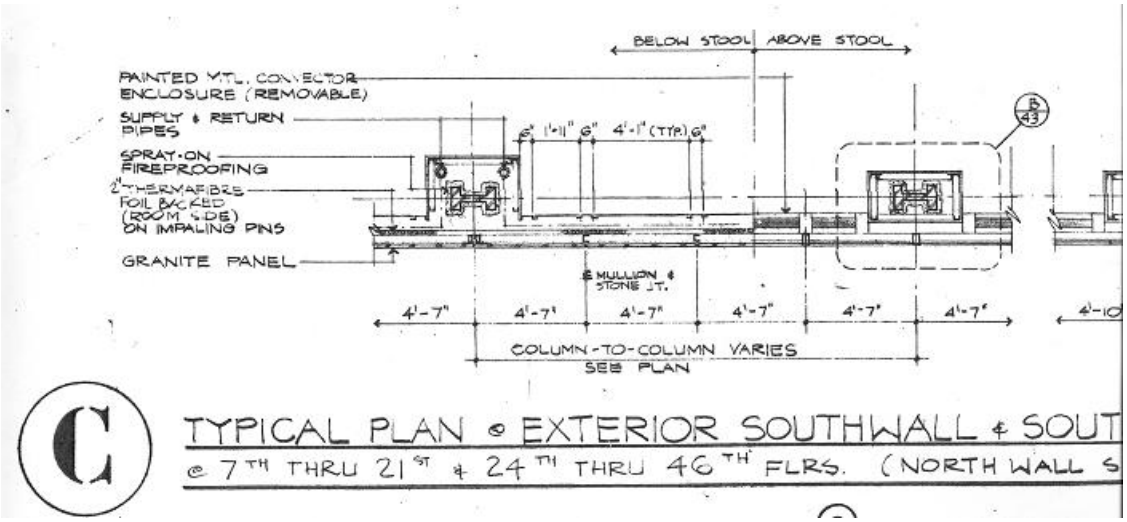

Figure D-5. WTC 7 Architectural Drawing 38, Section C: Typical Plan at Exterior Southwall and Southeast Corner.

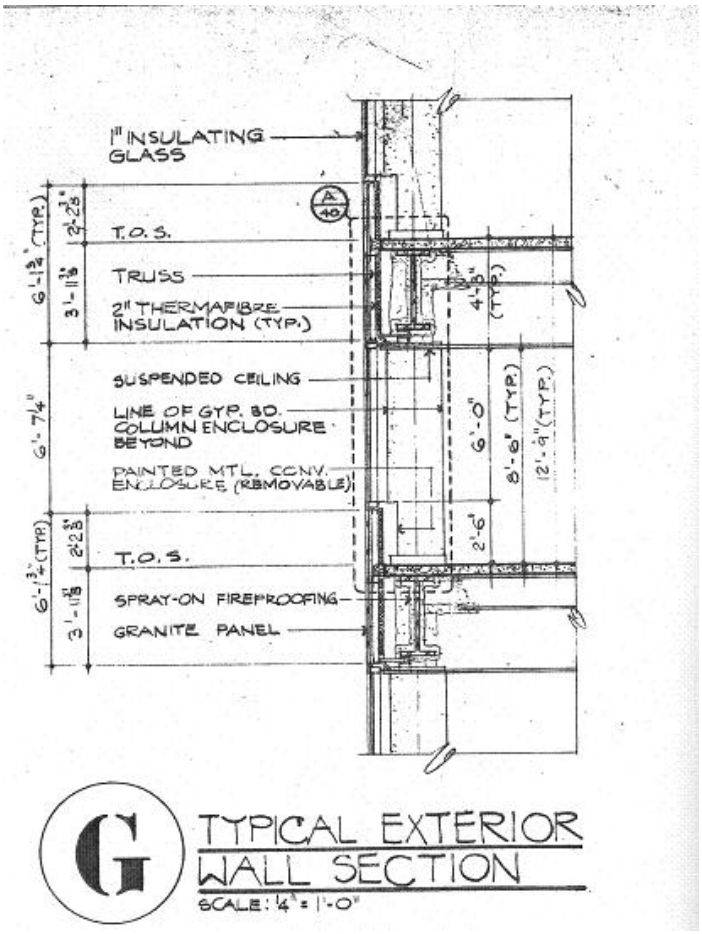

Figure D-6. WTC 7 Architectural Drawing 38, Section G: Typical Exterior Wall Section.

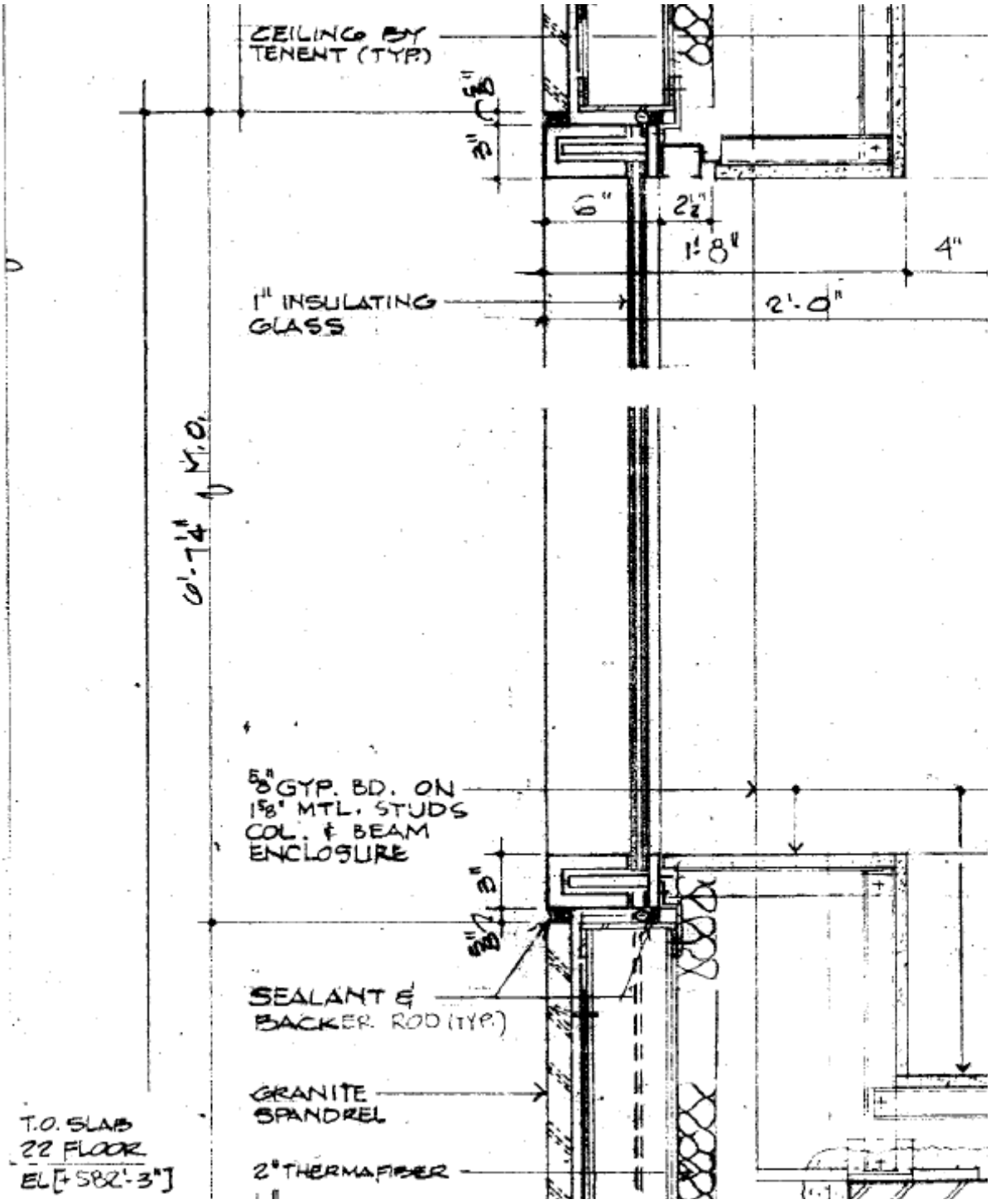

Figure D-7. WTC 7 Architectural Drawing 40, Section A: Typical Exterior Wall at Window.

The SFOM window fragility analysis was conducted using available and assumed window details. The resulting P-I curves for two window sizes are shown in Figure D-8. The P-I curves indicate that a minimum overpressure of 2.5 psi was required for window failure in WTC 7. Slightly different minimum impulses were required for failure for the two window sizes considered in the analysis.

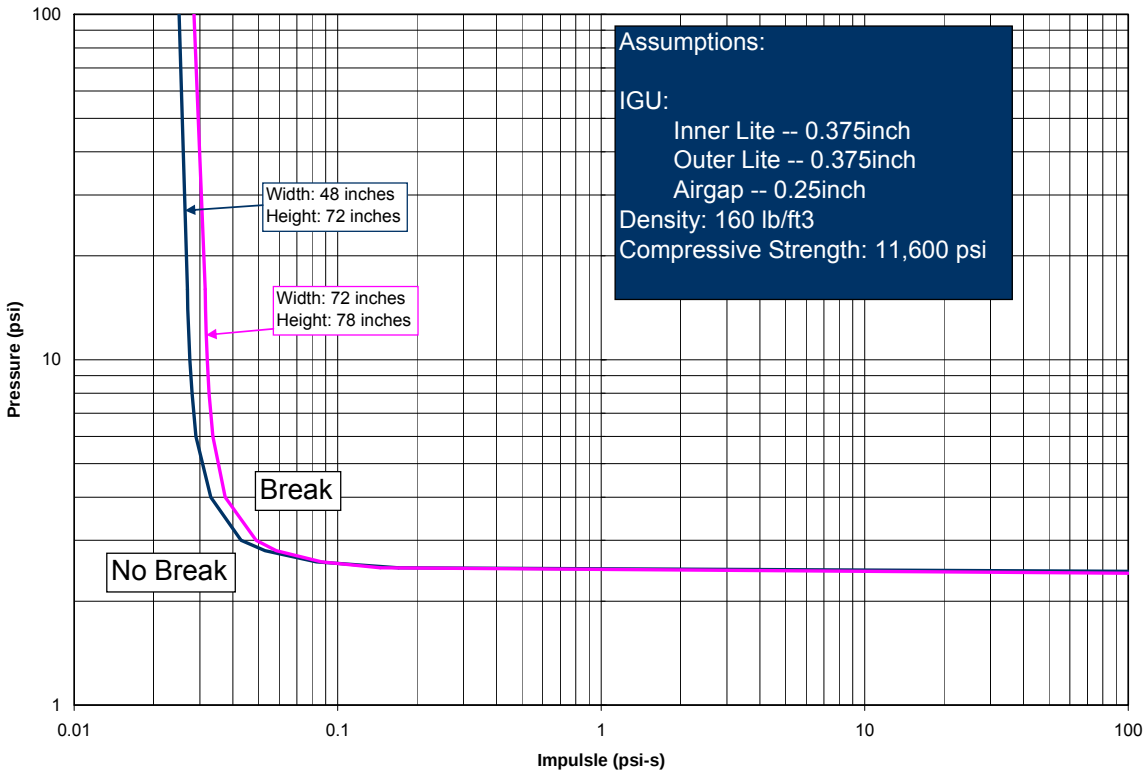

Source: Applied Research Associates, used with permission

Figure D-8. Pressure-impulse requirements for WTC 7 window breakage.

In the next section, the window P-I failure curves were compared to the SHAMRC P-I data as a basis for predicting window failure locations for each blast analysis.

D.3.4 Blast Modeling Results

Key results from the Phase II blast analyses are shown in Figure D-9 through Figure D-14. Figure D-9 and Figure D-10 illustrate the predicted pressure-impulse levels at each window location around the building perimeter for Layouts 2 and 3, respectively. Two blast initiating charge sizes are shown: the minimum recommended 9 lb of RDX explosive from Phase I, and a smaller 2 lb charge to examine the sensitivity of the window breakage to charge size. The P-I values at each window location are overlaid on the predicted break/no-break criteria from the window fragility analysis conducted earlier in Phase II. Failure pressure-impulse curves are commonly used in blast analyses to illustrate system failure sensitivity to transient pressure loads.

Figure D-11 through Figure D-14 show plan views of the 2-D SHAMRC results for predicted window failure locations. Contours of peak overpressure are shown, as well, to illustrate pressure propagation throughout the floor. The maximum contour value, shown as purple, was set at 2.5 psi, which corresponds to the minimum overpressure required to break a window. Any area displayed as purple experienced overpressures at or above the 2.5 psi threshold, but did not necessarily experience the minimum required impulse. Only station numbers shown in blue experienced the necessary combination of pressure and impulse to exceed the failure threshold.

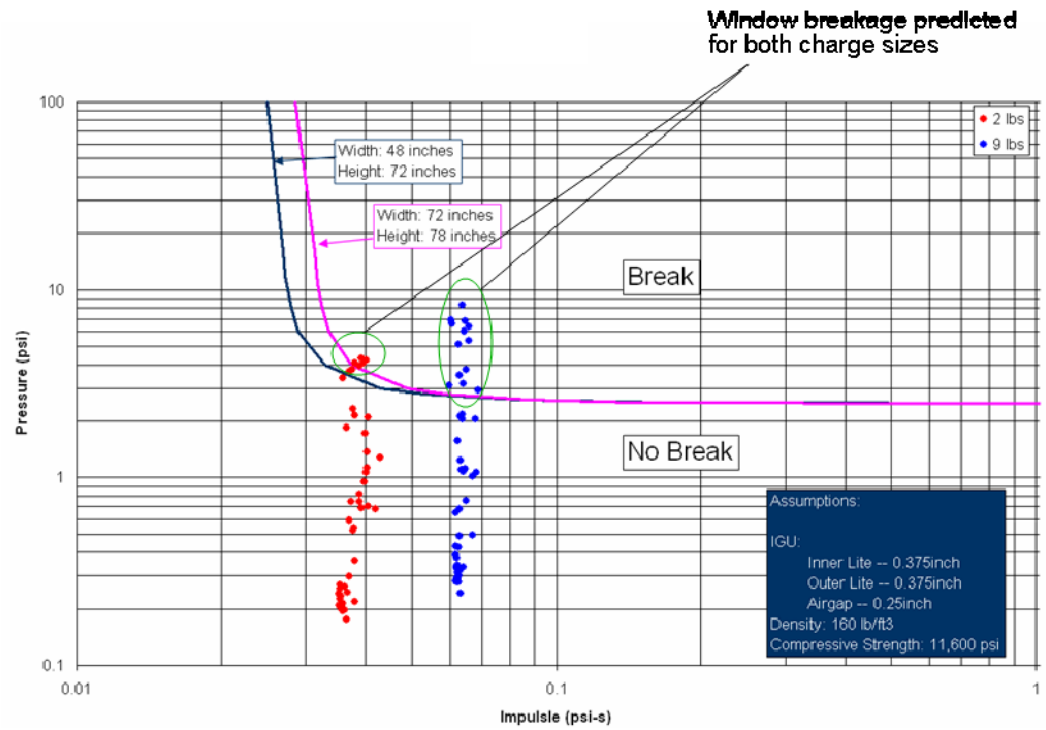

Source: Applied Research Associates, used with permission

Figure D-9. Layout 2 pressure-impulse values at window locations compared to predicted failure profiles.

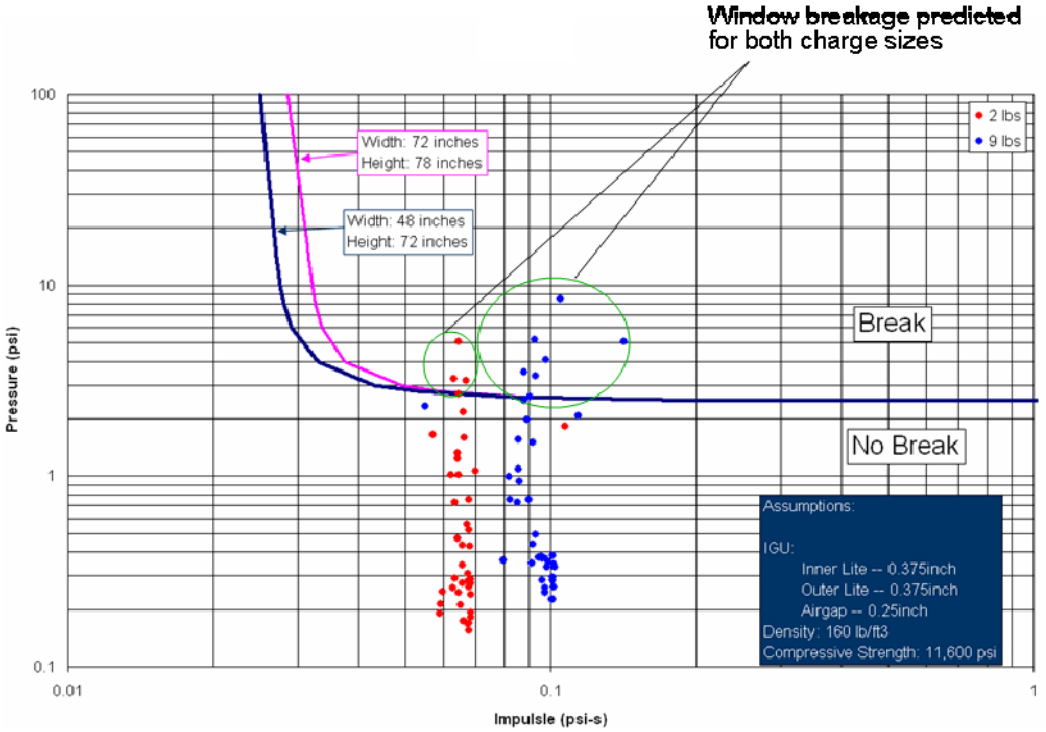

Source: Applied Research Associates, used with permission

Figure D-10. Layout 3 pressure-impulse values at window locations compared to predicted failure profiles.

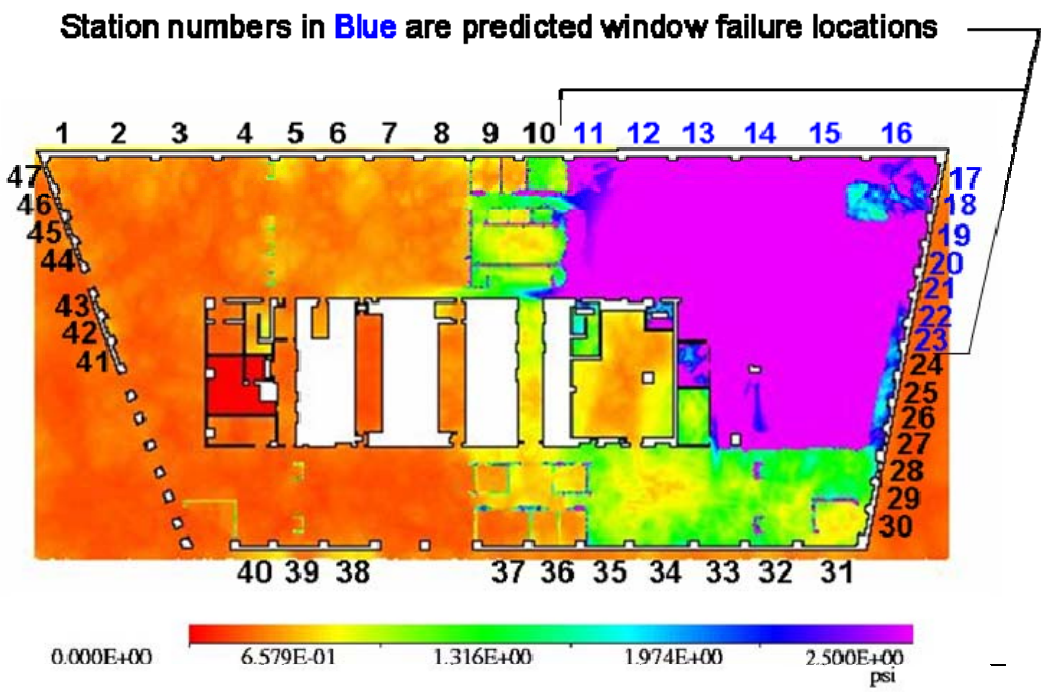

Source: Applied Research Associates, used with permission

Figure D-11. Layout 2 peak overpressure and broken window locations, 9 lb charge.

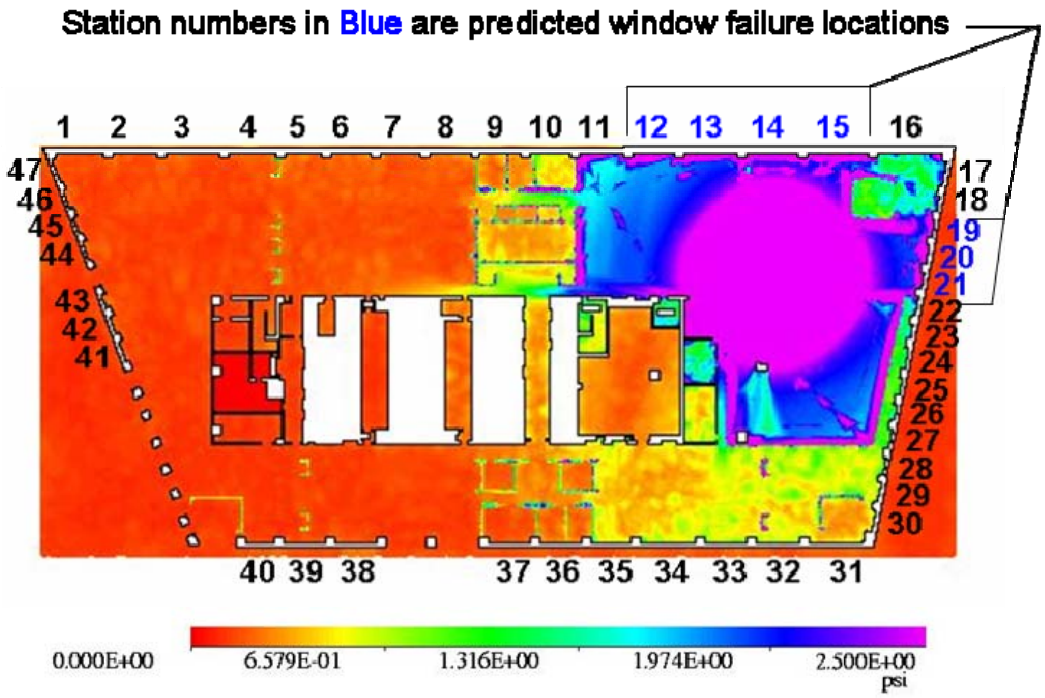

Source: Applied Research Associates, used with permission

Figure D-12. Layout 2 peak overpressure and broken window locations, 2 lb charge.

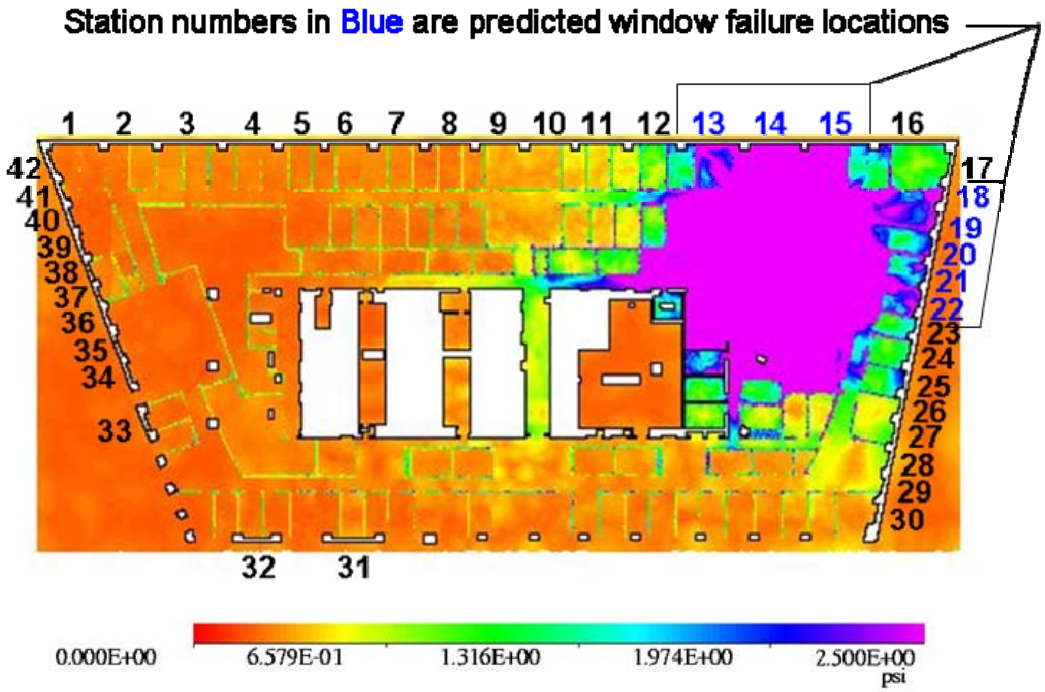

Source: Applied Research Associates, used with permission

Figure D-13. Layout 3 peak overpressure and broken window locations, 9 lb charge.

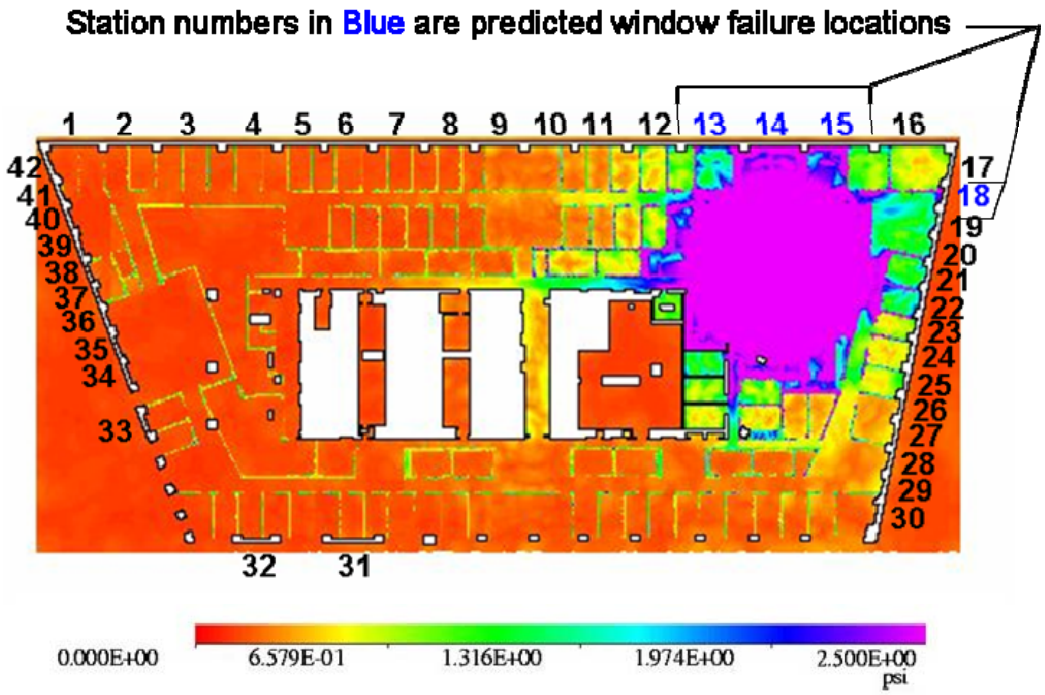

Source: Applied Research Associates, used with permission

Figure D-14. Layout 3 peak overpressure and broken window locations, 2 lb charge.

As expected, the more open Layout 2 resulted in more predicted window failure locations for a given charge size, compared to the more extensively built-out Layout 3. Furthermore, the larger 9 lb explosive charge resulted in more window failures than the corresponding 2 lb charge analyses, predominantly on the east face of the building.

D.4 PHASE III: 1-D ACOUSTIC ANALYSIS

Based on the results from Phase II, representative overpressure waveforms from the predicted broken windows on the north and east faces, as well as from open areas at the southwest corner from WTC 1 debris damage, were used to make sound-distance propagation predictions.

The tool used to make the prediction, NLAWS, is a non-linear acoustic wave propagation solver that was developed about 30 years ago by the U.S. Air Force. The code takes the blast wave parameters of peak overpressure, material velocity and positive duration and constructs a triangular wave. It then uses the radius from the burst at the window to the point where conditions are specified for divergence of the wave. The code then uses spherical divergence to continue propagation of the wave in a constant atmosphere to a distance up to 1 km from the burst.

Figure D-15 shows a typical waveform at a broken window location and its Fourier transformation. Most of the sound lies below 200 Hz. Approximately 40 Hz is the lower limit for human audible perception. In this frequency range, the blast would sound like a low rumble. Figure D-16 illustrates a typical waveform in the vicinity of the open window locations in the southwest corner.

Figure D-17 and Figure D-18 show the results of the acoustic analysis for both floor layouts, in which overpressure and sound pressure level vs. distance from the opening are plotted. Intense audible sound was predicted from all building faces for all four combinations of layout and charge size. If propagation were unobstructed, as would be the case for a person standing on a street with a direct view of any WTC 7 face with open windows, the sound level from all building perimeter openings at 1 km would be approximately 130 to 140 dB. Adjacent buildings and their effect on the sound propagation was not considered in this analysis. The analysis was intended to be a simple estimate of the sound potential emanating from the building due to blast pressures.

To check the validity of the results, the close range values predicted by NLAWS are similar to the limited published data available for sound pressures from small explosives. Specifically, Reference [7] lists 190.6 dB for 2 lb of TNT at a close standoff. Further, 1 lb of TNT is listed as generating 194.1 dB at 6 ft, 186.1 dB at 10 ft and 180.0 dB at 15 ft standoff [8]. These values correlate well with the range of values predicted by the NLAWS model.

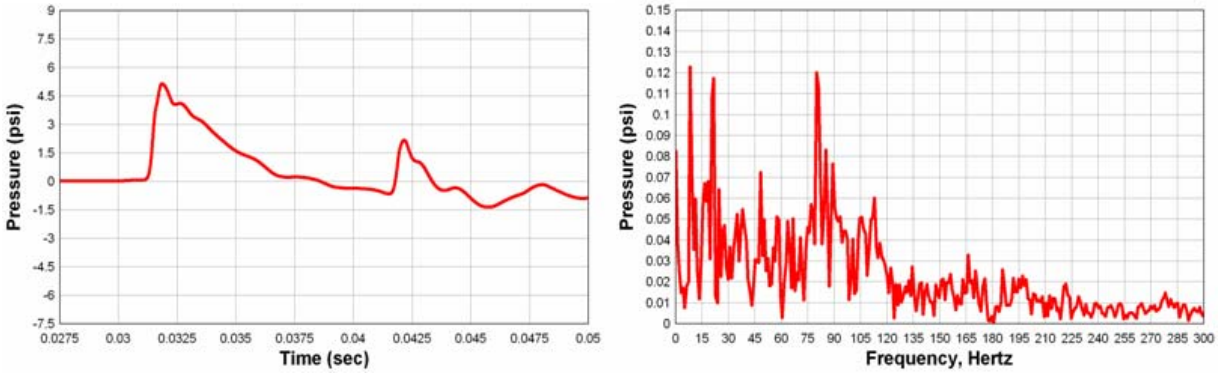

Source: Applied Research Associates, used with permission

Figure D-15. Typical waveform and corresponding Fourier transformation at a broken window location.

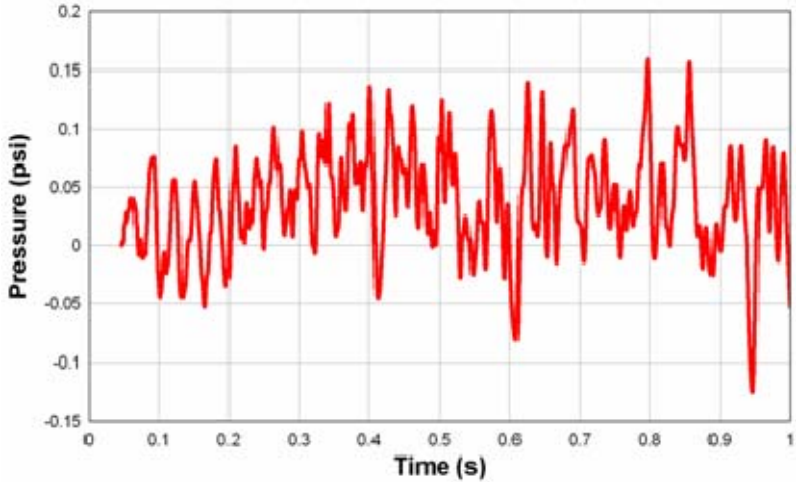

Source: Applied Research Associates, used with permission

Figure D-16. Typical waveform in the southwest corner near the debris damaged windows.

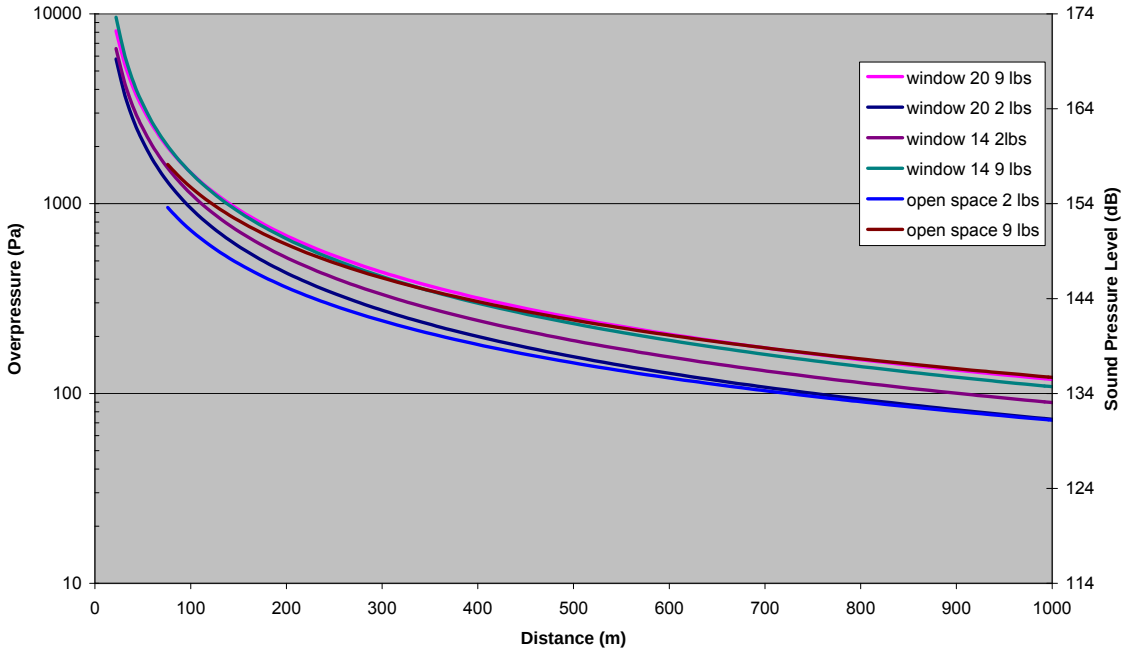

Source: Applied Research Associates, used with permission

Figure D-17. Layout 2 acoustic overpressure-distance predictions.

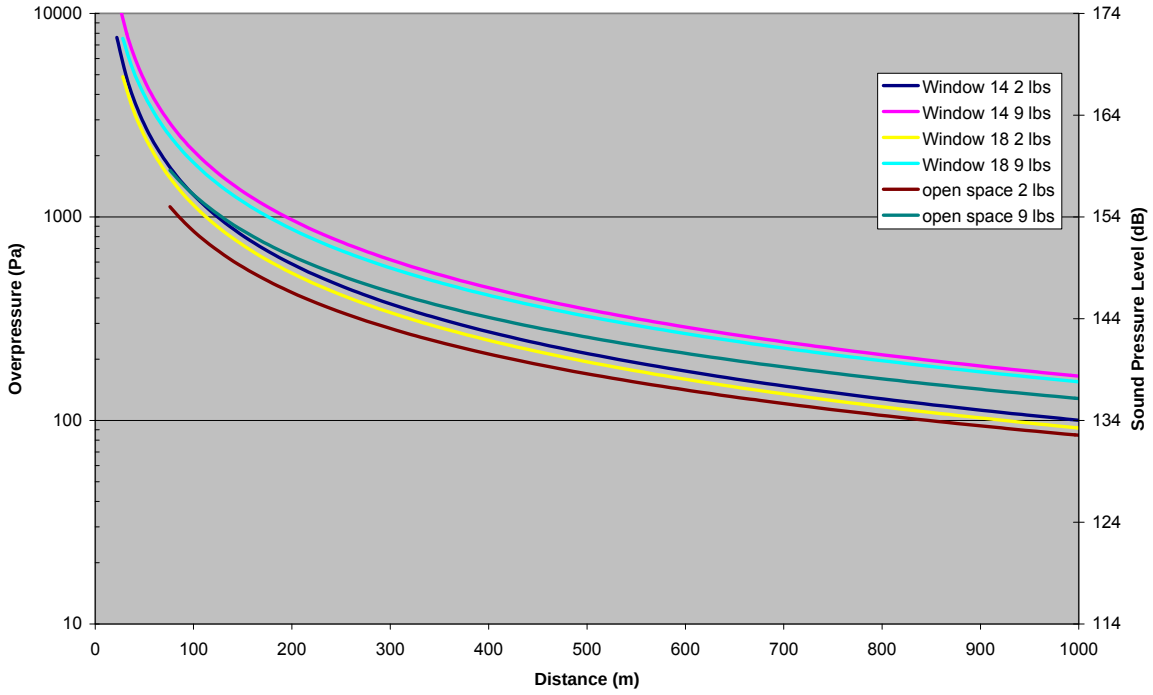

Source: Applied Research Associates, used with permission

Figure D-18. Layout 3 acoustic overpressure-distance predictions.

D.5 SUMMARY

In Phase I, hypothetical blast scenarios to initiate structural collapse were identified. In particular, a plausible scenario with the minimum amount of required explosive was identified and carried forward to the Phase II blast analyses. This scenario proposes a linear shape charge blast consisting of 9 lb of RDX, centered on Column 79. The recommended column preparation for use of this shape charge required a minimum of 15 min to make initial cuts to the column with an oxy-propane torch, plus additional time for charge placement.

In Phase II, 2-D SHAMRC blast propagation calculations were performed for the minimum explosive case identified in Phase I. Calculations were also performed for a lesser charge size (2 lb) in the interest of evaluating threshold explosive requirements. There were 4 blast analyses performed in total, consisting of two different charge sizes (2 lb or 9 lb of RDX) and two floor layouts with differing partition densities in the tenant areas (Layouts 2 and 3). The primary conclusion from Phase II analyses was that windows were expected to fail on the north and east faces for even the most conservative blast loading case considered (the densely-partitioned Layout 3 with a 2 lb charge). Other scenario and charge size combinations resulted in greater predicted damage.

In Phase III, an acoustic analysis was performed to assess the distance from the building that the blast would have been audible. Analyses were performed for both layout scenarios, using the pressure history and window failure location predictions generated during Phase II. For all scenarios and charge sizes, significant audible sound was predicted from all building faces. For locations where sound propagation was unobstructed, the sound level from all building perimeter openings at 1 km would have been approximately 130 dB to140 dB.

D.6 REFERENCES

Crepeau, J., Needham, C. and Hikida, S., SHAMRC second-order hydrodynamic automatic mesh refinement code. 2001. Methodology, 2001. Applied Research Associates, Albuquerque, NM.

Crepeau, J., SHAMRC second-order hydrodynamic automatic mesh refinement code. 1998. User's manual, 1998. Applied Research Associates, Inc., Albuquerque, NM.

Meyer, S.B., Becvar, K.E., Stevens, D.J. and Marchand, K.A., Shard Fly-Out Model, Final Technical Report prepared by Applied Research Associates, Inc. for the Technical Support Working Group, December 2002.

Marchand, Kirk A., 2002. "Analysis of Insulated Glass Units Subjected to Blast Loadings: Model and Data Comparisons," AMSAA Contract DAADM01-97-D-0013, ARA Project Number 0093, Applied Research Associates, San Antonio, Texas, July 19.

Meyer, Sarah B., Becvar, Keith, E., Stevens, David J. and Marchand, Kirk A., 2002a. "Shard Fly-Out Model, User's Guide," TSWG Contract N39998-99-C-0671, ARA Project Number 0515, Applied Research Associates, San Antonio, Texas, November 27.

Meyer, Sarah B., Becvar, Keith, E., Stevens, David J. and Marchand, Kirk A., 2002b. "Shard Fly-Out Model, Technical Documentation," TSWG Contract N39998-99-C-0671, ARA Project Number 0515, Applied Research Associates, San Antonio, Texas, November

Hamby, William, "Ultimate Sound Pressure Level Decibel Table," 2004, http://www.makeitlouder.com/Decibel%20Level%20Chart.txt, 6 Jun 2008.

Kinney, Gilbert and Graham, Kenneth, *Explosive Shocks in Air*, 2nd Edition, Springer, 1985.

Appendix E
PLASTICITY AND CREEP MODELS FOR WTC 7 STEELS

E.1 INTRODUCTION

The finite-element structural analysis of the building required material models for tensile stress-strain and creep behavior of the steels and the strengths of the bolts used. This Appendix documents the methods used to generate those material models.

E.2 METHOD FOR CREATING HIGH-TEMPERATURE STRESS-STRAIN CURVES

At elevated temperature, the deformation characteristics of the steel can be represented in several ways. One is to include a temperature dependence in the ordinary stress-strain behavior. Up to temperatures of about 500 ºC, the stress-strain behavior of structural steel depends only weakly on the deformation rate. At higher temperatures, the strain rate dependence, and hence the time dependence, of the stress-strain behavior becomes more significant. At these elevated temperatures, the behavior is often termed "creep," although the strain rates relevant to fire conditions are often several orders of magnitude larger than those in traditional, long-term creep situations.

The stress-strain behavior represents an upper limit for the strength of the steel at all temperatures. As such, it was developed with data appropriate to a higher strain rate. The creep models captured the time-dependent deformation and should produce all the strain at temperatures above about 500 ºC.

Stress-strain curves and creep models were developed for three steels: ASTM A 36, ASTM A 572, and CSA G40.21-44W. The plastic portions of the stress-strain curves for all three steels were based on the behavior of WTC A 572 specimen HH-F1-1, a $YS = 42$ ksi 12WF92 shape taken from column line 605 between floors 98 and 101 of WTC 1. Data tables in Appendix A of NIST NCSTAR 1-3D described the tensile tests. Other information can be found on page 54 of NIST NCSTAR 1-3D. The first step was to model the room- and elevated-temperature true stress-true strain behavior using a power-law work hardening formalism.

$$\sigma = K\varepsilon^{n} \tag{1}$$

In principle, both K and n depend on temperature, T, and strain rate, $\dot{\varepsilon}$. For the A 572 base steel, the work-hardening exponent, n, does not change monotonically with strain rate (Figure E–1). The dependence on strain rate is small and difficult to model, so it was expedient to ignore the rate dependence and choose an exponential form for the work-hardening exponent:

$$n(T) = n_0 \exp\left(-\left(\frac{T}{n_2} \right)^{n_1} \right) \tag{2}$$

The parameter n_0 sets the room temperature value. The parameter n_2 sets the transition temperature where $n(T)$ begins to drop quickly, and the shape factor parameter n_1 sets the steepness of the transition.

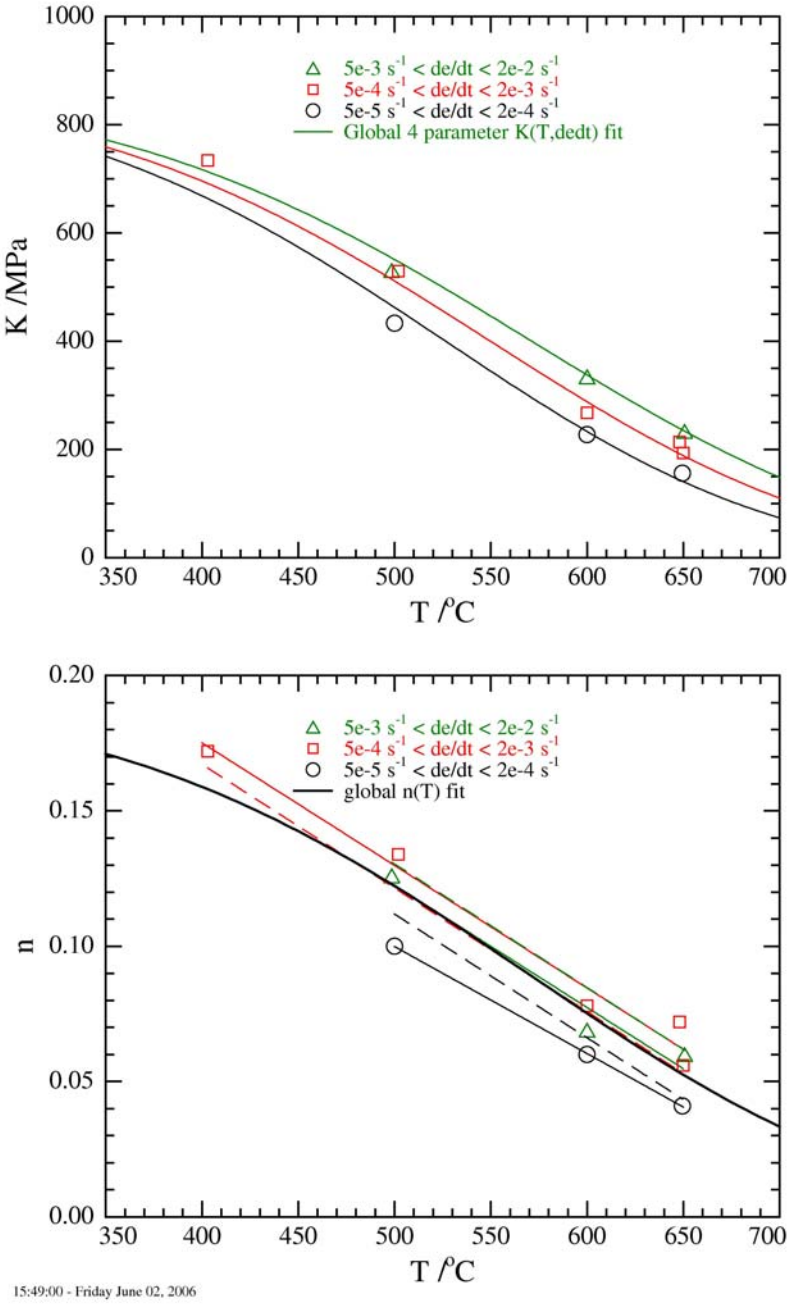

Figure E–1. Behavior of *K(T)* and *n(T)*.

The pre-factor K depends on strain rate in a stronger and more predictable way at elevated temperature.

$$K(T,\dot{\varepsilon}) = k_0 \exp\left(-\left(\frac{T}{k_2 + k_3\dot{\varepsilon}}\right)^{k_1}\right) \tag{3}$$

In this formalism, the parameter k_3 caused the behavior of *K(T)* to depend weakly on strain rate at intermediate temperatures, but not at room temperature.

These equations were purely empirical; the individual parameters were not physically based. Figure E–1 displays the behavior of *K(T)* and *n(T)* for the A 572 steel. summarizes the values of the parameters.

Table E–1. Values of the parameters for *K(T)* and *n(T)*.

Parameter	Value
k_0	+854.0 MPa
k_1	+4.1100
k_2	+660.0 ºC
k_3	+10.27 ºC s
n_0	+0.1890
n_1	+4.0990
n_2	+611.8 °C

For tensile stress-strain behavior, ANSYS requires the first strain point to be at the yield strength, F_y, and that the slope of the stress-strain curve equal the Young's modulus, E, between (0,0) and the first strain point. To use the plastic stress-strain behavior developed for A 572 to describe the behavior of A 36, it was necessary to scale the stress-strain curve in an appropriate manner. The method was to multiply the expression for *K(T)* by a constant that made the true stress at true strain = 0.1 roughly equal to the value of the stress for several WTC A 36 steels at room temperature. That coefficient was k_{A36} = 0.862. The parameter was estimated visually.

No literature data existed for the stress-strain behavior of CSA G40.21-44W plate. Its yield strength, F_y = 44 ksi (300 MPa), is roughly midway between that of A 36, F_y = 36 ksi , and A 572, F_y = 50 ksi. It was therefore reasonable to estimate the coefficient, $k_{G40.21}$, by linearly interpolating between the values for A 572 k_{A572} = 1.0 and k_{A36} = 0.862. The value of the coefficient for CSA G40.21 was $k_{G40.21}$ = 0.941.

The room temperature yield strength behavior of A 36 and A 572 was established using the formalism of the WTC mechanical properties report. (NIST NCSTAR 1-3D, Equation 3-5, Section 3.5.1, page 65)

$$\sigma_{ys} = k_s F_y + k_{\text{dynamic}} + k_{\text{flange}} \tag{4}$$

where the factor k_s = 1.2 is the historical average excess yield strength for rolled shapes.

Because the CSA G40.21-44W is in plate form, the estimate for static yield strength is slightly different (NIST NCSTAR 1-3D, Equation 3-6, Section 3.5.1, page 65):

$$\sigma_{ys} = k_p F_y + k_{\text{dynamic}} \tag{5}$$

where the factor k_p = 1.092 was the historical average excess yield strength for plates.

The additive dynamic to static correction factor is

$$\sigma_{ys} - \sigma_{yd} = -6.895\left(3.2 + 1000\dot{\varepsilon}\right) = k_{\text{dynamic}} \tag{6}$$

where the strain rate is expressed in s^{-1} and the stresses are expressed in MPa.

The strain rate used for the mill test report is assumed to be to be $d\varepsilon/dt = 6\times10^{-4}\ s^{-1}$, which leads to k_{dynamic} = -26.2 MPa. The flange correction factor, k_{flange} = -17.9 MPa represents the correction for the fact

that the specimen for qualification came from the web of the shape, but the flange, which is generally slightly lower strength, represents the bulk of the load carrying area.

Applying those corrections to the specified yield strengths for A 572 (F_y = 50 ksi = 345 MPa), A 36 (F_y =248 MPa), and CSA G40.21-44W (F_y =303 MPa) produced the respective static (zero deformation rate) yield strengths,

$$\sigma_{ys}^{A572} = 369.6\,\text{MPa}$$
$$\sigma_{ys}^{G40.21} = 305.1\text{MPa}$$
$$\sigma_{ys}^{A36} = 253.7\text{MPa}$$

The plastic portion of each stress-strain curve was combined with the elastic portion by first solving for the strain at yield via $\sigma = E\varepsilon_y$ and then solving the plastic stress strain equation for the strain at the yield static yield strength and shifting the strains left until the two strains were equal.

The temperature dependence of the elastic modulus, *E*, was taken from Equation 2-2 of NIST NCSTAR 1-3D:

$$E(T) = e_0 + e_1 T + e_2 T^2 + e_3 T^3 \quad (7)$$

where
e_0= 206.0 GPa
e_1= –0.04326 GPa/ºC
e_2= -3.502×10^{-5} GPa/ºC^2
e_3= -6.592×10^{-8} GPa/ºC^3

Equation 7 was based on modulus measurements made at NIST for the World Trade Center investigation.

The results of this procedure for modeling the stress-strain behavior were reasonable. Figure E–2 compares the model to some actual data. The data for the A 572 are from specimen HH, the base steel for all the steel models. The data for A 36 come from a variety of WTC and literature A 36 steels.

The elevated-temperature stress-strain curves do not follow any pre-ordained "master curve" behavior for yield strength. Instead the yield strength is simply the intersection of the temperature-dependent Young's modulus with the suitably adjusted stress-strain curve evaluated for $\dot{\varepsilon} = 0.01$ 1/s. The intersection point is the first point in the model stress strain curves, and, by design, the slope between (0,0) and the first stress-strain point is equal to Young's modulus at the temperature of interest. Figure E-3 compares the behavior of this "yield strength" for these curves to the master curve behavior generated in the WTC investigation. The small humps in the "yield strength" at temperatures in the range 400 ºC < T < 550 ºC arise from the complex interaction of *K(T)* and *n(T)* , which were evaluated independently of each other. The actual stress-strain behavior, shown in Figures E–4, E–5, and E–6, decreases monotonically with temperature, and the individual stress-strain curves do not cross. All three "yield strength" curves in Figure E–3 lie above the original master curve, as they should because they represent data for larger strain rates. Their trend of generally decreasing strength with increasing temperature is correct.

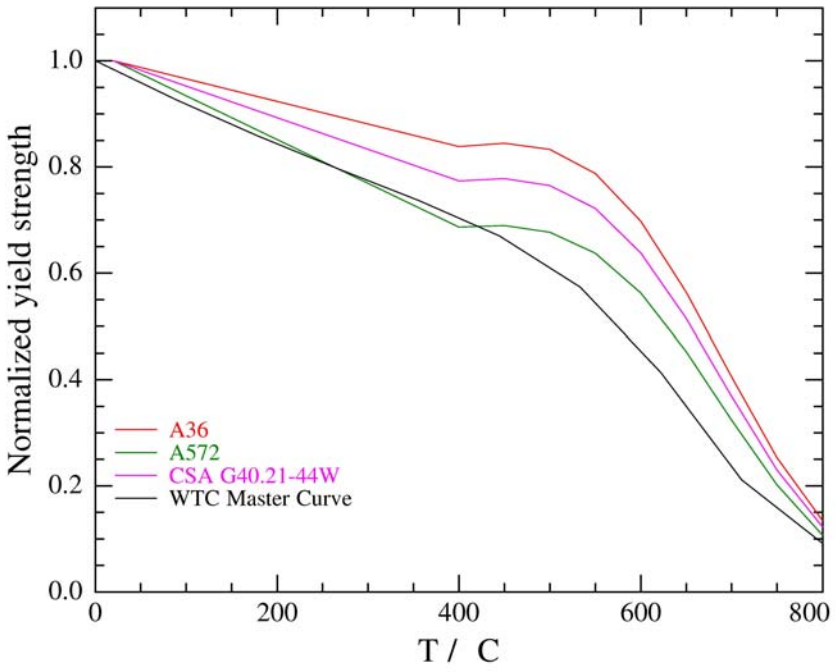

Figure E–2. Base and modeled stress-strain behavior at 20 ºC for A 36 and A 572 steels.

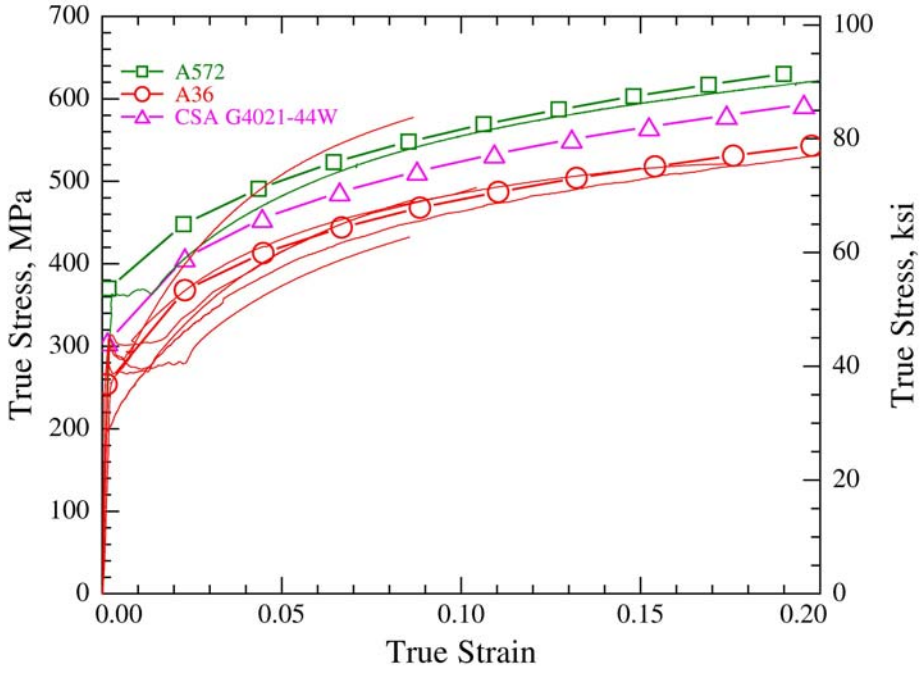

Figure E–3. "Yield strength" evaluated from the high-temperature stress strain curves and the master curve developed for the WTC investigation.

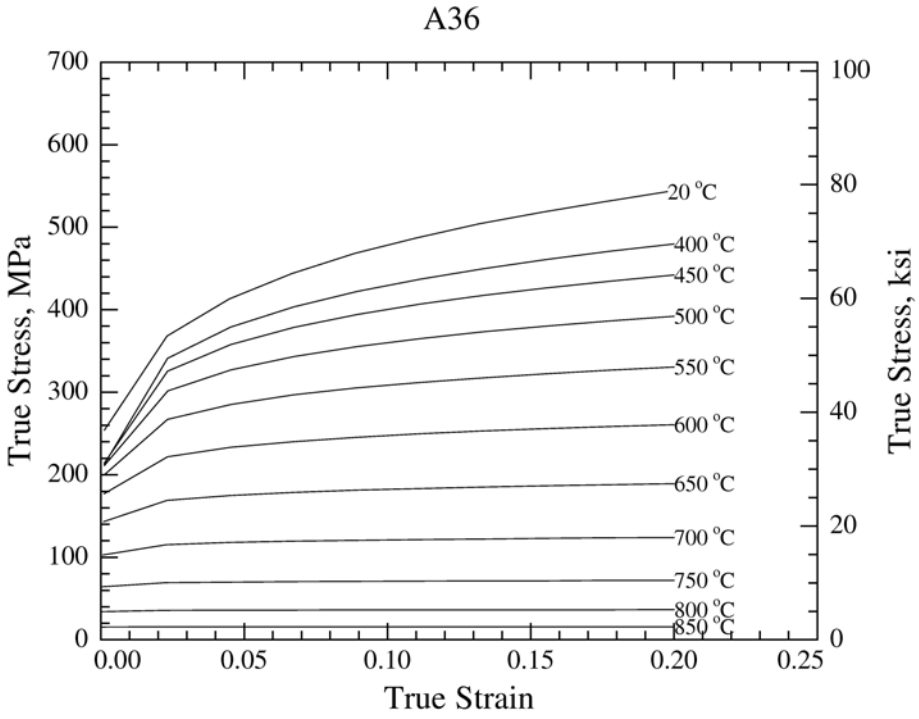

Figure E–4. Elevated-temperature stress-strain curves for $d\varepsilon / dt$ = 10^{-2} s^{-1} for A 36 steel.

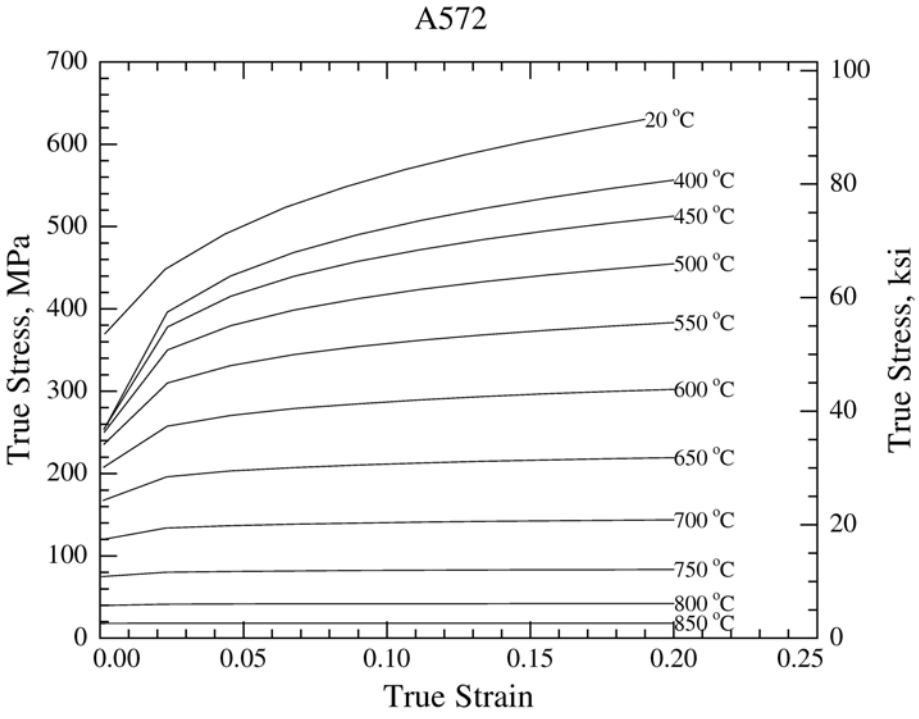

Figure E–5. Elevated temperature stress-strain curves for $d\varepsilon / dt$ = 10^{-2} s^{-1} for A 572 steel.

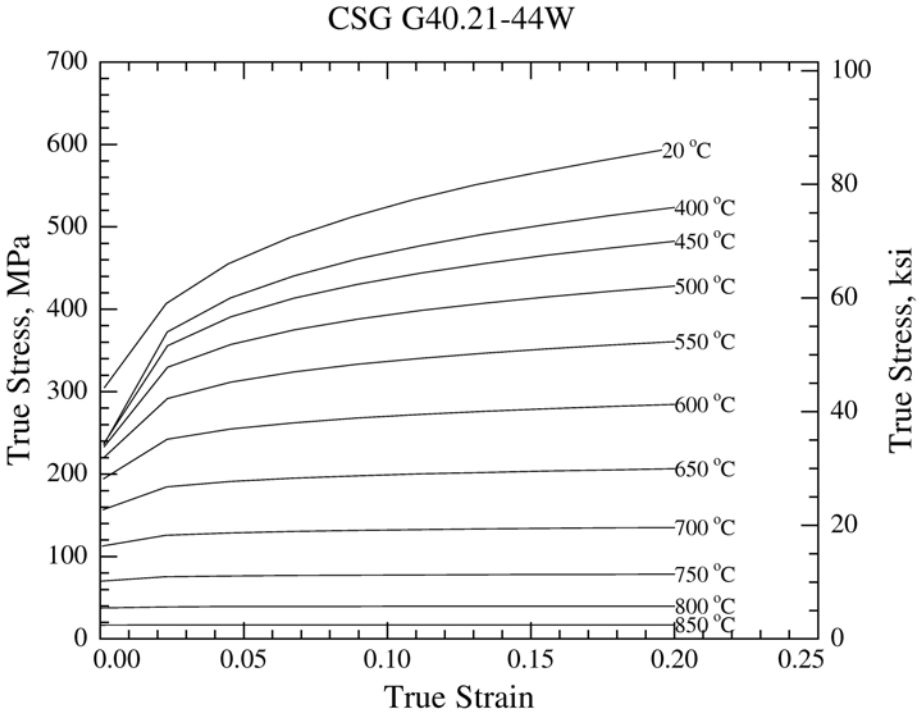

Figure E–6. Elevated-temperature stress-strain curves for $d\varepsilon / dt = 10^{-2}$ s^{-1} for CSA G40.21-44W steel.

E.2.1 Tensile Strength

The stress-strain models were expressed in terms of true stress and true strain. For design and analysis at room temperature, the tensile strength, *TS*, is an essential parameter. Although the true stress-strain behavior does not include a tensile strength, it was important that the tensile strength chosen be consistent with the true stress-strain behavior. The tensile strength of the A 36 steel model used in the WTC investigation for WF shapes was *TS* = 444 MPa, which the test specimen reached at an engineering strain, $e_{TS} = 0.226$. The true stress-strain behavior for A 36 steel in this report was consistent with that value. The tensile strength, *TS*, of A 572 steel used as the model for the plastic behavior of all three steels reached *TS* = 512 MPa at an engineering strain, $e_{TS} = 0.173$. The engineering stress evaluated at this strain from the true-stress-strain curve was slightly larger than the measured value: *TS* = 520 MPa vs. *TS* = 512 MPa (measured). The recommended value was the engineering stress calculated from the true stress-strain curve at $e_{TS} = 0.173$: *TS* = 520 MPa

No experimental data existed for the CSA G40.21-44W steel. The true stress-strain behavior modeled was essentially an average of the A 572 and A 36 behaviors, but chemically the steel is more like A 572 than A 36. Therefore, the estimated tensile strength was evaluated from the CSA G40.21-44W true stress-strain curve, at the true strain of the tensile strength of A 572: $e_{TS} = 0.173$.

Table E–2summarizes the recommended values for all three steels.

Table E–2. Values of the tensile strength, *TS*, of A 36, CSA G40.21-44W, and A 572.

Steel	*TS* (ksi)	*TS* (MPa)	ε_{TS}	e_{TS}
A 36	64.5	444	0.204	0.226
CSA G40.21-44W	70.6	487	0.160	0.173
A 572	74.3	520	0.160	0.173

ε_{TS} true strain at the value of the tensile strength, *TS*.

e_{TS} engineering strain at the value of the tensile strength, *TS*.

E.2.2 ANSYS Stress-strain Models

The analysis used the ANSYS multilinear isotropic hardening model (MISO). This model defines piece-wise-linear stress-strain curves at fixed temperatures. The origin is not included, and the slope of the first segment between the implied (0,0) and the first point, which is the yield strength, must equal the elastic modulus at the appropriate temperature. Each steel model, shown in Tables E–3, E–4, and E–5, consisted of ten stress-strain pairs, plus the implied (0,0) at specific temperatures: (20, 400, 450, 500, 550, 600, 650, 700, 750, 800, 850) ºC. The creep models consist of lines that define the temperature and stress-strain pairs, for example

```
TBTEMP,20
TBPT,,1.2370e-03,36.8
```

The TBTEMP line defines the temperature as 20 ºC. The TBPT line defines the strain-stress pair in which the strain is 1.2370 x 10^{-3} and the stress is 36.8 ksi. Figures E–4, E–5, and E–6show the shapes of the stress-strain curves generated by the ANSYS models of Tables E–3, E–4, and E–5.

E.3 METHOD FOR CREATING HIGH-TEMPERATURE CREEP CURVES

E.3.1 Background

The WTC investigation developed a methodology for estimating the creep properties of untested steels based on creep models of existing steels. We evaluated several different scaling methods. Scaling the applied stress by the ratio of the tensile strength of the reference steel to that of the unknown steel produced the best agreement. We drew this conclusion by predicting, using the fitted creep models of Williams-Leir (1983), the behavior of each of five literature steels from a sixth literature steel, for all possible permutations of those six steels. Although tensile strength scaling produced the best agreement, in many cases the agreement was not very good. Frequently the predicted strain differed from the actual by more than a factor of ten. Differences of this magnitude correspond to temperature offsets of around 35 ºC or stress offsets of 17 MPa. Not surprisingly, the agreement was best when the correction was small, and within a class, e.g., steels specified with *YS* = 36 ksi or *YS* = 50 ksi. Because no steel relevant to the creep modeling was recovered from WTC7, it is impossible to create more accurate models.

Table E–3. ANSYS stress-strain model for A 36 steel.

```
!Generated on  Thu Jun  7 14:32:56 2007
! ANSYS multilinear isotropic hardening (MISO)
model for A36 steel
! Units:
! strain      : true, natural units, dimensionless
! temperature : C
! stress      : ksi
TB,MISO,1,11,10,0
TBTEMP,20
TBPT,,1.2370e-03,36.8
TBPT,,2.3063e-02,53.3
TBPT,,4.4889e-02,60.0
TBPT,,6.6715e-02,64.4
TBPT,,8.8541e-02,67.9
TBPT,,1.1037e-01,70.7
TBPT,,1.3219e-01,73.1
TBPT,,1.5402e-01,75.2
TBPT,,1.7584e-01,77.1
TBPT,,1.9767e-01,78.8
TBTEMP,400
TBPT,,1.1891e-03,30.9
TBPT,,2.3279e-02,49.5
TBPT,,4.5369e-02,55.0
TBPT,,6.7459e-02,58.5
TBPT,,8.9550e-02,61.2
TBPT,,1.1164e-01,63.4
TBPT,,1.3373e-01,65.3
TBPT,,1.5582e-01,66.9
TBPT,,1.7791e-01,68.3
TBPT,,2.0000e-01,69.6
TBTEMP,450
TBPT,,1.2358e-03,31.1
TBPT,,2.3321e-02,47.2
TBPT,,4.5406e-02,51.9
TBPT,,6.7491e-02,54.9
TBPT,,8.9575e-02,57.2
TBPT,,1.1166e-01,59.0
TBPT,,1.3375e-01,60.5
TBPT,,1.5583e-01,61.9
TBPT,,1.7792e-01,63.0
TBPT,,2.0000e-01,64.1
TBTEMP,500
TBPT,,1.2623e-03,30.6
TBPT,,2.3344e-02,43.7
TBPT,,4.5426e-02,47.5
TBPT,,6.7508e-02,49.8
TBPT,,8.9590e-02,51.6
TBPT,,1.1167e-01,53.0
TBPT,,1.3375e-01,54.1
TBPT,,1.5584e-01,55.2
TBPT,,1.7792e-01,56.1
TBPT,,2.0000e-01,56.9
TBTEMP,550
TBPT,,1.2438e-03,29.0
TBPT,,2.3328e-02,38.7
TBPT,,4.5412e-02,41.4
TBPT,,6.7496e-02,43.0
TBPT,,8.9580e-02,44.3
TBPT,,1.1166e-01,45.2
TBPT,,1.3375e-01,46.1
TBPT,,1.5583e-01,46.8
TBPT,,1.7792e-01,47.4
TBPT,,2.0000e-01,47.9
TBTEMP,600
TBPT,,1.1555e-03,25.7
TBPT,,2.3249e-02,32.2
TBPT,,4.5343e-02,33.8
TBPT,,6.7437e-02,34.8
TBPT,,8.9531e-02,35.6
TBPT,,1.1162e-01,36.2
TBPT,,1.3372e-01,36.7
TBPT,,1.5581e-01,37.1
TBPT,,1.7791e-01,37.5
TBPT,,2.0000e-01,37.8
TBTEMP,650
TBPT,,9.8708e-04,20.8
TBPT,,2.3100e-02,24.5
TBPT,,4.5212e-02,25.4
TBPT,,6.7325e-02,25.9
TBPT,,8.9437e-02,26.3
TBPT,,1.1155e-01,26.6
TBPT,,1.3366e-01,26.9
TBPT,,1.5577e-01,27.1
TBPT,,1.7789e-01,27.3
TBPT,,2.0000e-01,27.4
TBTEMP,700
TBPT,,7.5673e-04,14.9
TBPT,,2.2895e-02,16.7
TBPT,,4.5033e-02,17.1
TBPT,,6.7171e-02,17.3
TBPT,,8.9309e-02,17.5
TBPT,,1.1145e-01,17.6
TBPT,,1.3359e-01,17.7
TBPT,,1.5572e-01,17.8
TBPT,,1.7786e-01,17.9
TBPT,,2.0000e-01,18.0
TBTEMP,750
TBPT,,5.0978e-04,9.3
TBPT,,2.2675e-02,10.0
TBPT,,4.4841e-02,10.1
TBPT,,6.7007e-02,10.2
TBPT,,8.9172e-02,10.3
TBPT,,1.1134e-01,10.3
TBPT,,1.3350e-01,10.4
TBPT,,1.5567e-01,10.4
TBPT,,1.7783e-01,10.4
TBPT,,2.0000e-01,10.4
TBTEMP,800
TBPT,,2.9683e-04,5.0
TBPT,,2.2486e-02,5.2
TBPT,,4.4675e-02,5.2
TBPT,,6.6865e-02,5.2
TBPT,,8.9054e-02,5.2
TBPT,,1.1124e-01,5.2
TBPT,,1.3343e-01,5.3
TBPT,,1.5562e-01,5.3
TBPT,,1.7781e-01,5.3
TBPT,,2.0000e-01,5.3
TBTEMP,850
TBPT,,1.4766e-04,2.2
TBPT,,2.2353e-02,2.3
TBPT,,4.4559e-02,2.3
TBPT,,6.6765e-02,2.3
TBPT,,8.8971e-02,2.3
TBPT,,1.1118e-01,2.3
TBPT,,1.3338e-01,2.3
TBPT,,1.5559e-01,2.3
TBPT,,1.7779e-01,2.3
TBPT,,2.0000e-01,2.3
```

Table E–4. ANSYS stress-strain model for A 572 steel.

```
!Generated on  Thu Jun  7 14:32:56 2007
! ANSYS multilinear isotropic hardening (MISO)
model for A36 steel
! Units:
! strain      : true, natural units,
dimensionless
! temperature : C
! stress      : ksi
TB,MISO,1,11,10,0
TBTEMP,20
TBPT,,1.2370e-03,36.8
TBPT,,2.3063e-02,53.3
TBPT,,4.4889e-02,60.0
TBPT,,6.6715e-02,64.4
TBPT,,8.8541e-02,67.9
TBPT,,1.1037e-01,70.7
TBPT,,1.3219e-01,73.1
TBPT,,1.5402e-01,75.2
TBPT,,1.7584e-01,77.1
TBPT,,1.9767e-01,78.8
TBTEMP,400
TBPT,,1.1891e-03,30.9
TBPT,,2.3279e-02,49.5
TBPT,,4.5369e-02,55.0
TBPT,,6.7459e-02,58.5
TBPT,,8.9550e-02,61.2
TBPT,,1.1164e-01,63.4
TBPT,,1.3373e-01,65.3
TBPT,,1.5582e-01,66.9
TBPT,,1.7791e-01,68.3
TBPT,,2.0000e-01,69.6
TBTEMP,450
TBPT,,1.2358e-03,31.1
TBPT,,2.3321e-02,47.2
TBPT,,4.5406e-02,51.9
TBPT,,6.7491e-02,54.9
TBPT,,8.9575e-02,57.2
TBPT,,1.1166e-01,59.0
TBPT,,1.3375e-01,60.5
TBPT,,1.5583e-01,61.9
TBPT,,1.7792e-01,63.0
TBPT,,2.0000e-01,64.1
TBTEMP,500
TBPT,,1.2623e-03,30.6
TBPT,,2.3344e-02,43.7
TBPT,,4.5426e-02,47.5
TBPT,,6.7508e-02,49.8
TBPT,,8.9590e-02,51.6
TBPT,,1.1167e-01,53.0
TBPT,,1.3375e-01,54.1
TBPT,,1.5584e-01,55.2
TBPT,,1.7792e-01,56.1
TBPT,,2.0000e-01,56.9
TBTEMP,550
TBPT,,1.2438e-03,29.0
TBPT,,2.3328e-02,38.7
TBPT,,4.5412e-02,41.4
TBPT,,6.7496e-02,43.0
TBPT,,8.9580e-02,44.3
TBPT,,1.1166e-01,45.2
TBPT,,1.3375e-01,46.1
TBPT,,1.5583e-01,46.8
TBPT,,1.7792e-01,47.4
TBPT,,2.0000e-01,47.9
TBTEMP,600
TBPT,,1.1555e-03,25.7
TBPT,,2.3249e-02,32.2
TBPT,,4.5343e-02,33.8
TBPT,,6.7437e-02,34.8
TBPT,,8.9531e-02,35.6
TBPT,,1.1162e-01,36.2
TBPT,,1.3372e-01,36.7
TBPT,,1.5581e-01,37.1
TBPT,,1.7791e-01,37.5
TBPT,,2.0000e-01,37.8
TBTEMP,650
TBPT,,9.8708e-04,20.8
TBPT,,2.3100e-02,24.5
TBPT,,4.5212e-02,25.4
TBPT,,6.7325e-02,25.9
TBPT,,8.9437e-02,26.3
TBPT,,1.1155e-01,26.6
TBPT,,1.3366e-01,26.9
TBPT,,1.5577e-01,27.1
TBPT,,1.7789e-01,27.3
TBPT,,2.0000e-01,27.4
TBTEMP,700
TBPT,,7.5673e-04,14.9
TBPT,,2.2895e-02,16.7
TBPT,,4.5033e-02,17.1
TBPT,,6.7171e-02,17.3
TBPT,,8.9309e-02,17.5
TBPT,,1.1145e-01,17.6
TBPT,,1.3359e-01,17.7
TBPT,,1.5572e-01,17.8
TBPT,,1.7786e-01,17.9
TBPT,,2.0000e-01,18.0
TBTEMP,750
TBPT,,5.0978e-04,9.3
TBPT,,2.2675e-02,10.0
TBPT,,4.4841e-02,10.1
TBPT,,6.7007e-02,10.2
TBPT,,8.9172e-02,10.3
TBPT,,1.1134e-01,10.3
TBPT,,1.3350e-01,10.4
TBPT,,1.5567e-01,10.4
TBPT,,1.7783e-01,10.4
TBPT,,2.0000e-01,10.4
TBTEMP,800
TBPT,,2.9683e-04,5.0
TBPT,,2.2486e-02,5.2
TBPT,,4.4675e-02,5.2
TBPT,,6.6865e-02,5.2
TBPT,,8.9054e-02,5.2
TBPT,,1.1124e-01,5.2
TBPT,,1.3343e-01,5.3
TBPT,,1.5562e-01,5.3
TBPT,,1.7781e-01,5.3
TBPT,,2.0000e-01,5.3
TBTEMP,850
TBPT,,1.4766e-04,2.2
TBPT,,2.2353e-02,2.3
TBPT,,4.4559e-02,2.3
TBPT,,6.6765e-02,2.3
TBPT,,8.8971e-02,2.3
TBPT,,1.1118e-01,2.3
TBPT,,1.3338e-01,2.3
TBPT,,1.5559e-01,2.3
TBPT,,1.7779e-01,2.3
TBPT,,2.0000e-01,2.3
```

Table E–5. ANSYS stress-strain model for CSA G40.21-44W steel.

```
!Generated on  Thu Jun  7 14:32:56 2007
! ANSYS multilinear isotropic hardening (MISO)
model for CSA G40.21-44W steel
! Units:
! strain      : true, natural units,
dimensionless
! temperature : C
! stress      : ksi
TB,MISO,1,11,10,0
TBTEMP,20
TBPT,,1.4873e-03,44.2
TBPT,,2.3048e-02,59.1
TBPT,,4.4609e-02,65.9
TBPT,,6.6170e-02,70.6
TBPT,,8.7731e-02,74.3
TBPT,,1.0929e-01,77.3
TBPT,,1.3085e-01,79.9
TBPT,,1.5241e-01,82.1
TBPT,,1.7397e-01,84.1
TBPT,,1.9554e-01,86.0
TBTEMP,400
TBPT,,1.3195e-03 34.2
TBPT,,2.3395e-02 54.0
TBPT,,4.5471e-02 60.0
TBPT,,6.7546e-02 63.9
TBPT,,8.9622e-02 66.8
TBPT,,1.1170e-01 69.2
TBPT,,1.3377e-01 71.2
TBPT,,1.5585e-01 73.0
TBPT,,1.7792e-01 74.5
TBPT,,2.0000e-01 75.9
TBTEMP,450
TBPT,,1.3685e-03 34.4
TBPT,,2.3439e-02 51.6
TBPT,,4.5509e-02 56.7
TBPT,,6.7579e-02 60.0
TBPT,,8.9649e-02 62.4
TBPT,,1.1172e-01 64.4
TBPT,,1.3379e-01 66.1
TBPT,,1.5586e-01 67.5
TBPT,,1.7793e-01 68.8
TBPT,,2.0000e-01 70.0
TBTEMP,500
TBPT,,1.3945e-03 33.9
TBPT,,2.3462e-02 47.8
TBPT,,4.5529e-02 51.8
TBPT,,6.7596e-02 54.4
TBPT,,8.9664e-02 56.3
TBPT,,1.1173e-01 57.8
TBPT,,1.3380e-01 59.1
TBPT,,1.5587e-01 60.2
TBPT,,1.7793e-01 61.2
TBPT,,2.0000e-01 62.1
TBTEMP,550
TBPT,,1.3707e-03 31.9
TBPT,,2.3441e-02 42.3
TBPT,,4.5511e-02 45.2
TBPT,,6.7580e-02 47.0
TBPT,,8.9650e-02 48.3
TBPT,,1.1172e-01 49.4
TBPT,,1.3379e-01 50.3
TBPT,,1.5586e-01 51.0
TBPT,,1.7793e-01 51.7
TBPT,,2.0000e-01 52.3
TBTEMP,600
TBPT,,1.2702e-03 28.2
TBPT,,2.3351e-02 35.1
TBPT,,4.5432e-02 36.9
TBPT,,6.7513e-02 38.0
TBPT,,8.9595e-02 38.8
TBPT,,1.1168e-01 39.5
TBPT,,1.3376e-01 40.0
TBPT,,1.5584e-01 40.5
TBPT,,1.7792e-01 40.9
TBPT,,2.0000e-01 41.3
TBTEMP,650
TBPT,,1.0826e-03 22.8
TBPT,,2.3184e-02 26.7
TBPT,,4.5286e-02 27.7
TBPT,,6.7388e-02 28.3
TBPT,,8.9490e-02 28.7
TBPT,,1.1159e-01 29.0
TBPT,,1.3369e-01 29.3
TBPT,,1.5580e-01 29.5
TBPT,,1.7790e-01 29.7
TBPT,,2.0000e-01 29.9
TBTEMP,700
TBPT,,8.2841e-04 16.3
TBPT,,2.2959e-02 18.2
TBPT,,4.5089e-02 18.7
TBPT,,6.7219e-02 18.9
TBPT,,8.9349e-02 19.1
TBPT,,1.1148e-01 19.2
TBPT,,1.3361e-01 19.3
TBPT,,1.5574e-01 19.4
TBPT,,1.7787e-01 19.5
TBPT,,2.0000e-01 19.6
TBTEMP,750
TBPT,,5.5732e-04 10.2
TBPT,,2.2718e-02 10.9
TBPT,,4.4878e-02 11.1
TBPT,,6.7038e-02 11.2
TBPT,,8.9199e-02 11.2
TBPT,,1.1136e-01 11.3
TBPT,,1.3352e-01 11.3
TBPT,,1.5568e-01 11.3
TBPT,,1.7784e-01 11.4
TBPT,,2.0000e-01 11.4
TBTEMP,800
TBPT,,3.2424e-04 5.4
TBPT,,2.2510e-02 5.6
TBPT,,4.4697e-02 5.7
TBPT,,6.6883e-02 5.7
TBPT,,8.9069e-02 5.7
TBPT,,1.1126e-01 5.7
TBPT,,1.3344e-01 5.7
TBPT,,1.5563e-01 5.7
TBPT,,1.7781e-01 5.7
TBPT,,2.0000e-01 5.8
TBTEMP,850
TBPT,,1.6122e-04 2.4
TBPT,,2.2366e-02 2.5
TBPT,,4.4570e-02 2.5
TBPT,,6.6774e-02 2.5
TBPT,,8.8978e-02 2.5
TBPT,,1.1118e-01 2.5
TBPT,,1.3339e-01 2.5
TBPT,,1.5559e-01 2.5
TBPT,,1.7780e-01 2.5
TBPT,,2.0000e-01 2.5
```

Figure E–7 shows that the creep properties of the 36 ksi steels, taken from the models of Williams-Leir (1983) were remarkably similar. Figure E–8 shows that the creep behavior of the higher strength steels, also taken from the models of Williams-Leir (1983) was less consistent.

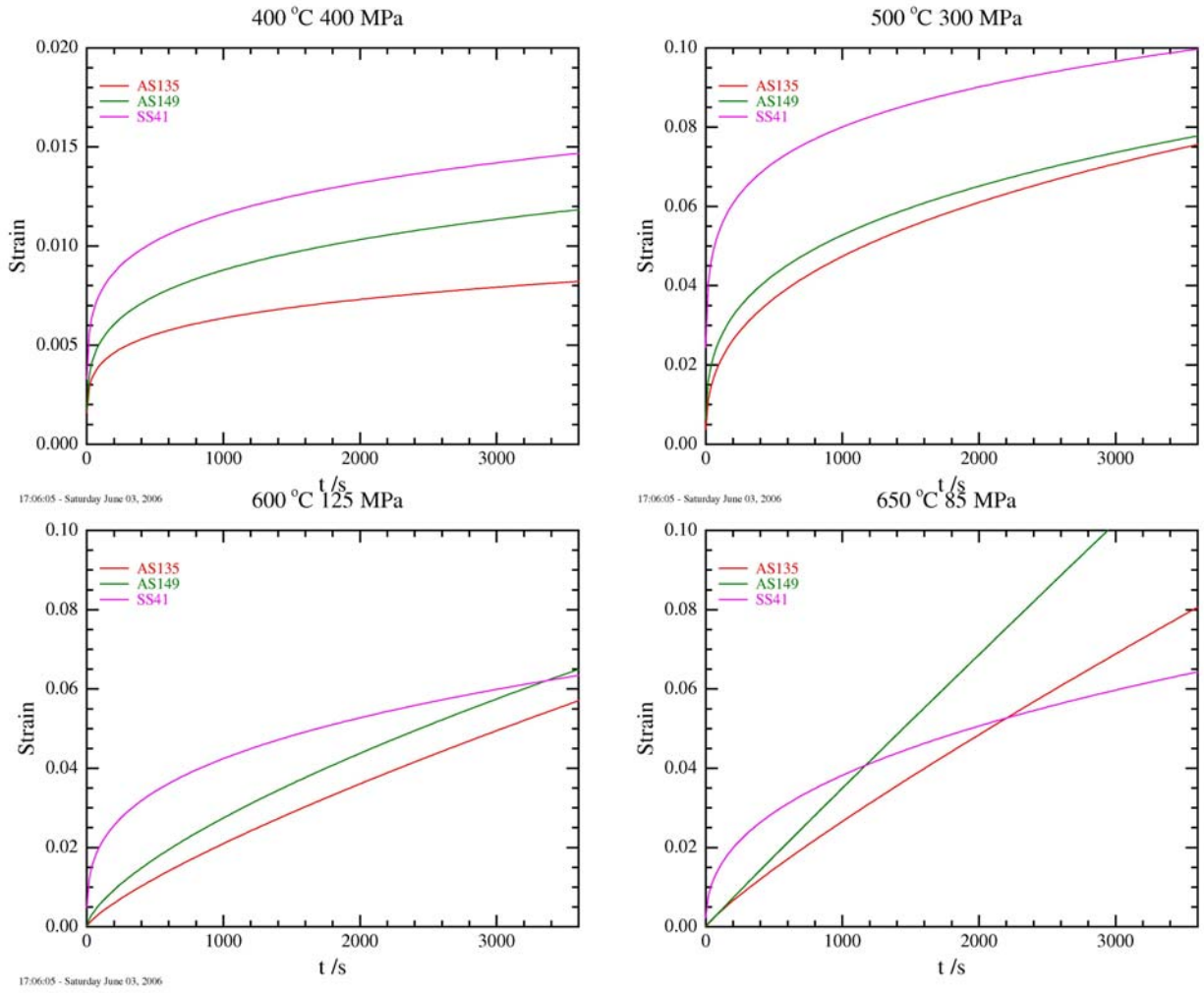

Figure E–7. Creep curves for various 36 ksi steels, from the fits of Williams-Leir, evaluated at convenient temperatures and stresses.

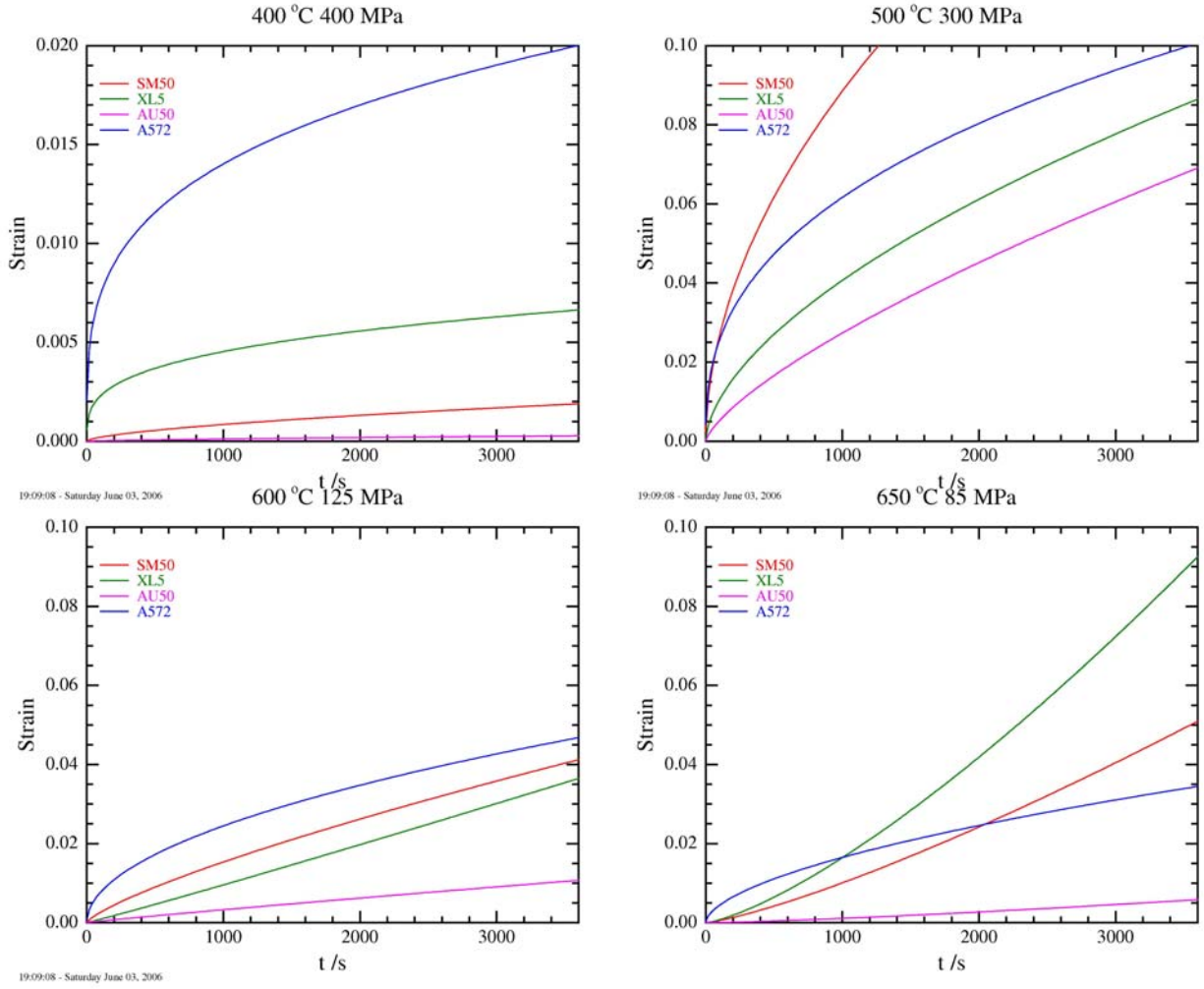

Figure E–8. Creep curves for various high-strength structural steels, evaluated at other convenient temperatures and stresses.

Estimating the A 36 steel creep behavior using the data from the WTC A 572 (specimen HH), scaled using the tensile strength ratio method developed for the WTC investigation, produced unacceptable results. Figure E–9 compares the A 572 creep data, the global model for creep strain of A 572 and the predicted creep strain for AS149 under those conditions, using the Fields (1989) model. Figure E–10 compares the predicted data for AS149, under the same conditions, using the Fields (1989) model, to the predicted creep behavior using the tensile strength scaling model based on the A 572 steel. The agreement for temperatures above 500 ºC was unsatisfactory.

Predicting the behavior of the CSA G40.21 steel plate was even more difficult, because no experimental data existed for comparison. Given the lack of data, it was expedient to assume that the creep properties of CSA G40.21-44W were identical to the A 572. Both steels were specified with $TS \geq 65$ ksi, even though the yield strength of CSA G40.21 is only $YS = 44$ ksi (= 300 MPa). Furthermore, the chemistry specification for CSA G40.21-44W admits both V and Nb, which indicates that its chemistry is more like A 572 than A 36.

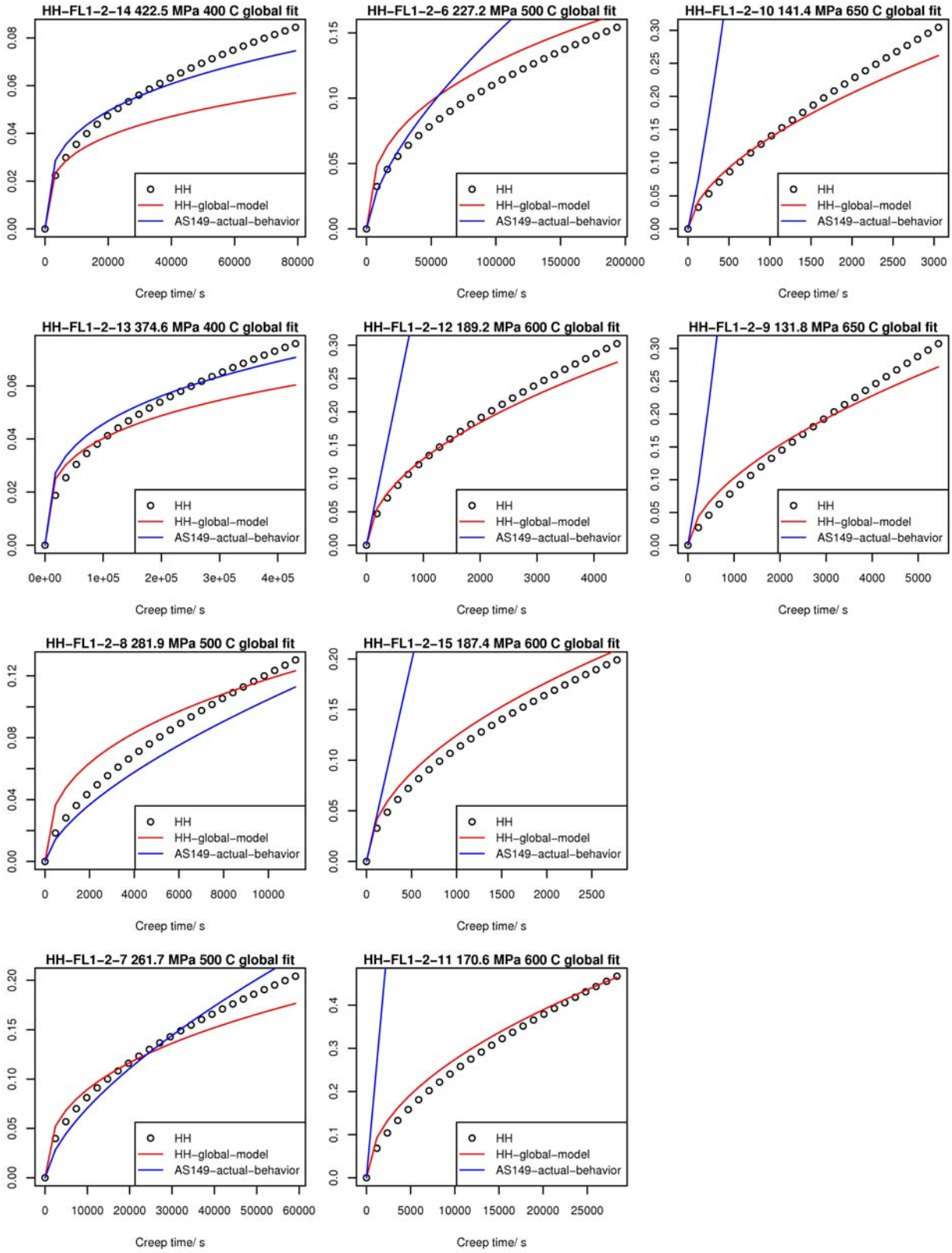

Figure E–9. Comparison of A 572 creep with predictions for AS149 steel.

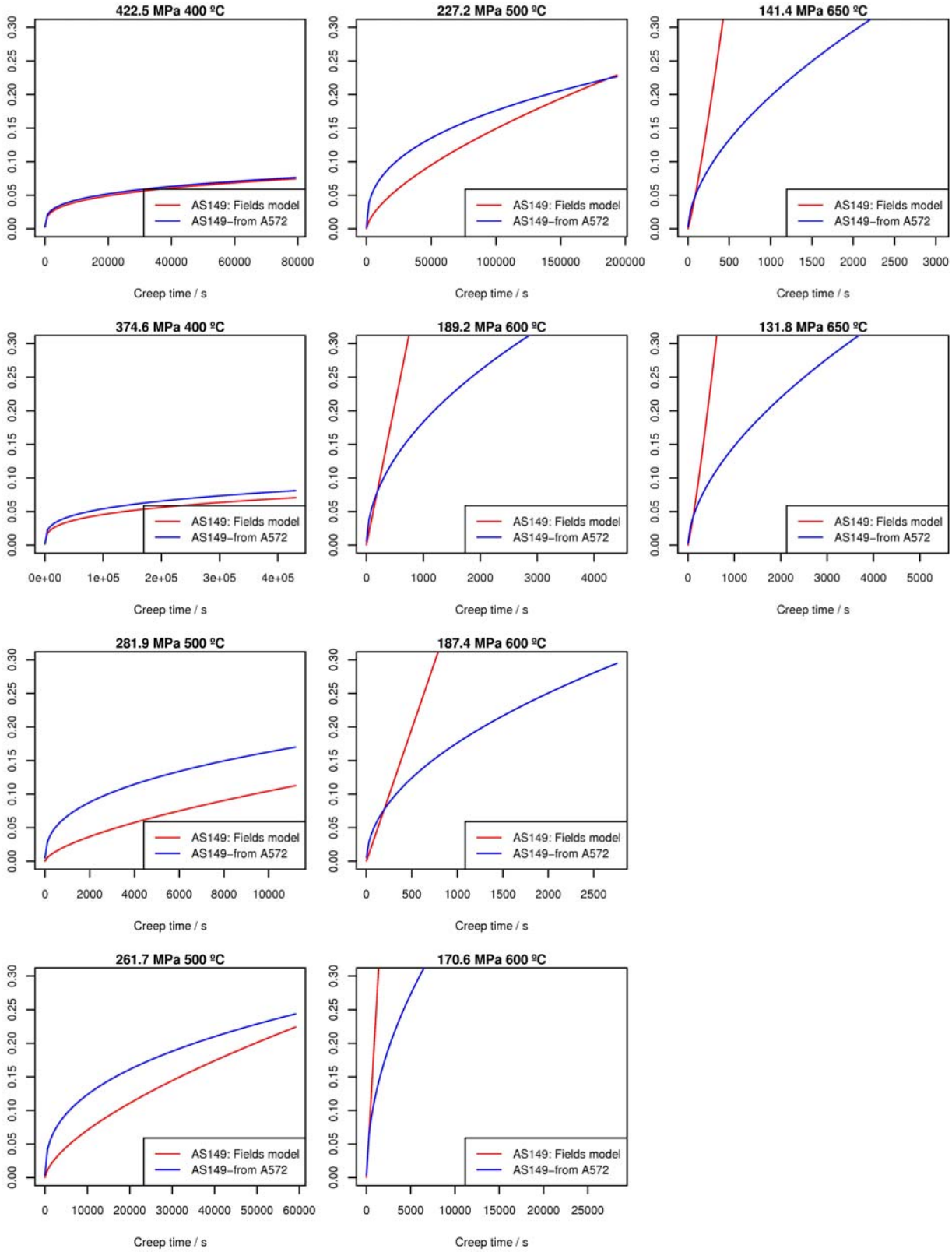

Figure E–10. Comparison of AS149 creep data with predicted data based on A 572 data and tensile strength scaling.

E.3.2 Method

The creep behavior of the *YS*=50 ksi steel was modeled on the behavior of WTC A 572 specimen HH. The creep behavior of A 36 steel was modeled based on the parameters in Fields (1989). That model is based on tests of Australian AS149 steel, which is similar to ASTM A 36. The creep behavior of CSA G40.21-44W was modeled under the assumption that it was identical to *YS* = 50 ksi A 572. The uncertainties in these models were estimated to be up to 40 ºC in temperature and 20 MPa in stress, based on the observation that the predicted behavior could be as much as a factor of ten different from the observed behavior.

E.3.3 ANSYS Creep Models

The ANSYS implicit creep model # 2 (time hardening) used in the analysis modeled the creep rate, $\dot{\varepsilon}_{\text{cr}}$, using independent functions of stress, σ, and time, t:

$$\dot{\varepsilon}_{\text{cr}} = C_1 \sigma^{C_2} t^{C_3} \exp\left(-\frac{C_4}{T}\right) \tag{8}$$

Instead of attempting to model the Arrhenius temperature dependence with a single constant, it was easier to specify the individual C_i at each temperature of interest and set $C_4 = 0$. In that way it was possible to set the creep strain to identically zero below a lower limit temperature.

The Fields (1989) model for creep strain of AS149 as a function of time and stress has the form:

$$\begin{aligned} \varepsilon_{\text{cr}} &= A\sigma^C t^B \\ A(T) &= 10^{-(A_0 + A_1 T)} \\ B(T) &= B_0 + B_1 T \\ C(T) &= C_0 + C_1 T \end{aligned} \tag{9}$$

Expressed in the ANSYS format for creep rate as a function of time, stress, and temperature, the Fields (1989) model is:

$$\begin{aligned} \dot{\varepsilon}_{\text{cr}} &= AB\sigma^C t^{B-1} \\ A(T) &= 10^{-(A_0 + A_1 T)} \\ B(T) &= B_0 + B_1 T \\ C(T) &= C_0 + C_1 T \end{aligned} \tag{10}$$

The ANSYS parameters for creep rate have the form:

$$\begin{aligned} C_1 &= AB = 10^{-(A_0 + A_1 T)}(B_0 + B_1 T) \\ C_2 &= C = C_0 + C_1 T \\ C_3 &= B - 1 = B_0 + B_1 T - 1 \\ C_4 &= 0 \end{aligned} \tag{11}$$

The global model for strain as a function of time, temperature and stress for the WTC A 572 steel takes the same form as the Fields (1989) model, but the individual functions have different forms.

$$\begin{aligned} \varepsilon_{cr} &= A\sigma^{n} t^{B} \\ A(T) &= 10^{-\left(a_0 + a_1 T + a_2 T^2\right)} \\ B(T) &= b_0 + b_1 T^{b_2} \\ n(T) &= n_0 + n_1 T \end{aligned} \tag{12}$$

Tables E–6 and E–7contain the ANSYS creep models used in the analysis.

Table E–6. ANSYS creep model for A 36 steel

```
!ANSYS creep model #2 for A36
!edot = c1*sigma^c2*t^c3
!Fields model: e = A *  sigma^c t^b
!strain = 0.01*Aprime*10^(-(A0+A1*T)) * sigma^(c0+c1*T) * t^(b0+b1*T)
!C1 = Ab  = 0.01*Aprime*10^(-(A0+A1*T) * (b0+b1*T)
!C2 = c   = c0+c1*T
!C3 = b-1 = b0+b1*T-1
!Aprime contains all the conversions from the original fields model to the units of this model
! time        : seconds
! Stress      : ksi
! Temperature : degrees C
! Strain      : natural units
TB,CREEP,1,,,2 ! creep model #2
TB,CREEP,1,10,,4,2 ! creep model #2,
TBTEMP,23
TBDATA,2,0,0,0,0
TBTEMP,400,
TBDATA,2,3.561852e-12,4.66,-0.7,0,
TBTEMP,450,
TBDATA,2,1.424203e-12,4.98,-0.525,0,
TBTEMP,500,
TBDATA,2,4.921699e-13,5.3,-0.35,0,
TBTEMP,550,
TBDATA,2,7.585412e-13,5.62,-0.175,0,
TBTEMP,600,
TBDATA,2,1.196324e-12,5.94,0,0,
TBTEMP,650,
TBDATA,2,1.828985e-12,6.26,0.175,0,
TBTEMP,700,
TBDATA,2,2.734196e-12,6.58,0.35,0,
TBTEMP,750,
TBDATA,2,4.018733e-12,6.9,0.525,0,
TBTEMP,800,
TBDATA,2,5.82897e-12,7.22,0.7,0,
```

Table E–7. ANSYS creep model for A 572 and CSA G4012 steels

```
!ANSYS creep model #2 for A572
!edot = c1*sigma^c2*t^c3
!NIST model: e = A *  sigma^n t^b
!strain = exp(ec0+ec1*T+ec2*T^2) * sigma^(n0+n1*T) * t^(b0+b1*T^b3)
!C1 = Ab  = exp(ec0+ec1*T+ec2*T^2) *  (b0+b1*T^b3)
!C2 = n   = n0+n1*T
!C3 = b   = b0+b1*T^b2
!Units
! time        : seconds
! Stress      : ksi
! Temperature : degrees C
! Strain      : natural units
TB,CREEP,1,10,,4,2 ! creep model #2,
TBTEMP,23
TBDATA,2,0,0,0,0
TBTEMP,400,
TBDATA,2,5.327526e-10,3.419601,-0.7223067,0,
TBTEMP,450,
TBDATA,2,8.514694e-10,3.569716,-0.6722258,0,
TBTEMP,500,
TBDATA,2,1.346261e-09,3.719831,-0.617346,0,
TBTEMP,550,
TBDATA,2,2.107694e-09,3.869946,-0.5577561,0,
TBTEMP,600,
TBDATA,2,3.270484e-09,4.020061,-0.4935354,0,
TBTEMP,650,
TBDATA,2,5.034164e-09,4.170176,-0.424755,0,
TBTEMP,700,
TBDATA,2,7.693152e-09,4.320291,-0.3514791,0,
TBTEMP,750,
TBDATA,2,1.168038e-08,4.470406,-0.2737666,0,
TBTEMP,800,
TBDATA,2,1.763044e-08,4.620521,-0.1916715,0,
```

The model file contains lines such as:

```
TBTEMP,400,
TBDATA,2,3.561852e-12,4.66,-0.7,0
```

The line that begins with TBTEMP defines the temperature, and TBDATA statement that follows it defines the creep parameters at that temperature. In the example above, the TBDATA statement defines material model 2 (time hardening) and $C_1 = 3.561852 \times 10^{-12}$, $C_2 = 4.66$, and $C_3 = -0.7$. The parameter C_4 is set identically to zero because the C_i are specified at individual temperatures. Note that the creep rate is also explicitly set to zero at room temperature. ANSYS interpolates the behavior between the designated model temperatures.

E.4 ELEVATED TEMPERATURE STRENGTH OF BOLTS

For the elevated temperature strength behavior of bolts, the analysis used the same models that the original WTC investigation used. Section 6.4.5 (p. 155) of NIST NCSTAR 1-3D documents these models. The models developed were technically for the steels from which the bolts were made, rather than for the bolts. Bolt failure is complex at both room- and elevated-temperature, and no methodology exists for modeling the failure of bolts, as distinct from the steels from which they are made, at elevated temperature.

The retained yield strength, Fy, and retained tensile strength, TS, were expressed as functions of temperature via:

$$f = \frac{F_y(T)}{F_y(23°\text{C})} = (1 - A_2)\exp\left(-\frac{1}{2}\left[\left(\frac{T}{s_1}\right)^{m_1} + \left(\frac{T}{s_2}\right)^{m_2}\right]\right) + A_2 \quad (13)$$

and

$$f = \frac{TS(T)}{TS(23°\text{C})} = (1 - A_2)\exp\left(-\frac{1}{2}\left[\left(\frac{T}{t_1}\right)^{n_1} + \left(\frac{T}{t_2}\right)^{n_2}\right]\right) + A_2 \quad (14)$$

These two equations are equations 6-1 and 6-2 of NIST NCSTAR-1-3D.

Table E–8 summarizes the values of the parameters in Equations 13 and 14, and originally appeared as Table 6-12 in NIST NCSTAR 1-3D.

Table E–8. Recommended values for the parameters in the strength reduction equations (Equations 13 and 14) for use with bolts.

Yield Strength Reduction parameters (Equation 13)	Tensile Strength Reduction parameters (Equation 14)
$A_2 =$ 0.07	$A_2 =$ 0.09
$m_1 =$ 6.8221	$n_1 =$ 5.0237
$m_2 =$ 1.0000	$n_2 =$ 5.0245
$s_1 =$ 491.0	$t_1 =$ 478.0
$s_2 =$ 810.0	$t_2 =$ 585.0

E.5 REFERENCES

Fields. B.A. and R.J. Fields. 1989. Elevated Temperature Deformation of Structural Steel. NISTIR 88-3899.

Williams-Leir, G. 1983. Creep of Structural Steel in Fire: Analytical Expressions. *Fire and Materials*. **7**[2] 73-78.

This page intentionally left blank.